CARBON DIOXIDE REACTION IN AQUEOUS AMINE SOLUTIONS

by

Phineas Machinga

Thesis presented in partial fulfilment
of the requirements for the Degree

of

MASTER OF SCIENCE IN ENGINEERING (CHEMICAL ENGINEERING)

in the Faculty of Engineering
at Stellenbosch University

Supervisors

Dr. L. Callanan
Prof. J. H. Knoetze

March 2012

DECLARATION

By submitting this thesis electronically, I declare that the entirety of the work contained therein is my own, original work, that I am the sole author thereof (save to the extent explicitly otherwise stated), that reproduction and publication thereof by Stellenbosch University will not infringe any third party rights and that I have not previously in its entirety or in part submitted it for obtaining any qualification.

……………………………
Signature

……………….
Date

i

ABSTRACT

The reaction kinetics of the reaction between aqueous solutions of carbon dioxide (CO_2) and monoethanolamine (MEA) were investigated over a temperature range of 298 to 313 K. The reaction kinetics experiments were conducted in a batch reactor and the experiments were divided into two series. The first series was for the ratio of MEA concentration to that of CO_2 greater than ten. This ensured pseudo-first-order conditions with respect to CO_2. The MEA concentrations ranged from 0.0199 to 0.261 mol/L. For the second seeries, the ratio of MEA concentration to that of CO_2 was maintained at approximately one and the MEA concentrations ranged from 0.0199 to 0.118 mol/L. Conductivity was used to follow the reaction kinetics of the reaction while conductometric titrations were used to determine the final extent of the reaction.

It was found that, for the experiments where MEA was in excess, the reaction between aqueous CO_2 and MEA occurred according to the zwitterion mechanism. The zwitterion deprotonation step was found to be faster than the zwitterion formation step thus making the zwitterion formation step the rate determining step. Water was found to deprotonate the zwitterion ion more than MEA.

For the experiments where MEA was in excess, the reaction orders with respect to MEA were found to be 1.22, 1.59, 1.15 and 0.91 at 298, 303, 308 and 313 K respectively. Reaction rate constants (k_f, k_w and k_a) were obtained by using the zwitterion mechanism where k_f is the forward second-order reaction rate constant for the formation of the zwitterion while $k_w = \dfrac{k_f k_{H_2O}}{k_r}$ and $k_a = \dfrac{k_f k_{MEA}}{k_r}$. The units of k_f are L/mol.s and the units of both k_w and k_a are L^2/mol^2.s. The respective Arrhenius equations for the reaction rate constants k_f, k_w and k_a were determined and they were found to be $k_f = 1.88 * 10^8 \exp\left(\dfrac{-4999}{T}\right)$, $k_w = 1.83 * 10^6 \exp\left(\dfrac{-3856}{T}\right)$ and $k_a = 1.36 * 10^8 \exp\left(\dfrac{-4812}{T}\right)$. From these Arrhenius equations, the activation energies for k_f, k_w and k_a were found to be 41.6, 32.1 and 40.0 kJ/mol respectively.

The orders of reaction with respect to both MEA and CO_2 for the experiments where CO_2 was in excess were determined. The orders of reaction with respect to MEA were 1.34, 1.65, 1.67 and 1.78 at 298, 303, 308 and 313 K respectively and the orders of reaction with respect to CO_2 were 1.35, 1.89, 1.59 and 1.60 at 298, 303, 308 and 313 K respectively.

Faster reaction rates were observed for the experiments where CO_2 was in excess than for the experiments where MEA was in excess. The orders of reaction with respect to MEA for the experiments where CO_2 was in excess were greater than those ones for the experiments where MEA was in excess at any particular temperature. The forward reaction rate constants for the reaction between MEA and CO_2 for the experiments where MEA was in excess were 11.5, 9.5, 17.4 and 23.6 L/mol.s at 298, 303, 308 and 313 K respectively while those ones for the experiments where CO_2 was in excess were 234, 6434, 2466 and 44 L/mol.s at 298, 303, 308 and 313 K respectively. The forward rate constants for the experiments where CO_2 was in excess were greater than the ones for the experiments where MEA was in excess at any particular temperature.

OPSOMMING

Die reaksiekinetika vir die reaksie van koolstofdioksied (CO_2) en mono-etanolamien (MEA) in water medium is in hierdie studie ondersoek. Die reaksie is uitgevoer in 'n enkelladingreaktor ("batch reactor") oor 'n temperatuurgebied van 298 tot 313 K by atmosferiese druk. Die verloop van die reaksie is bepaal deur die geleidingsvermoë van die reaksiemengsel deurgaans te monitor. Die finale omsetting bereik deur die reaksie is dan met 'n geleidingsvemoë-titrasie bepaal.

Die studie is opgedeel in twee reekse eksperimente. Die eerste reeks behels eksperimente by 'n MEA:CO_2 konsentrasieverhouding van meer as 10:1 by aanvang van die reaksie. Hierdie deel het ten doel om die pseudo-eerste orde reaksiekondisies met betrekking to CO_2 te ondersoek. Die MEA konsentrasiegebied vir die eerste deel strek van 0.0199 tot 0.261 mol/L. Die tweede reeks eksperimente het die konsentrasieverhouding van 1:1 ondersoek om 'n moontlike verandering in die reaksieorde te probeer uitwys. Vir die tweede reeks strek die MEA konsentrasies tussen 0.0199 en 0.118 mol/L.

Die resultate van die eerste reeks eksperimente het gewys dat die reaksie van CO_2 en MEA in water medium deur 'n zwitterioon (reaktiewe tussenproduk) meganisme beheer word. Die deprotonering van die zwitterioon ontaard in 'n kompetiesie tussen MEA en water, maar daar is gevind dat die deprotoneringsreaksie meer geredelik aan die hand van die H_2O molekuul geskied. Die deprotonering verloop vinniger as die vormingsreaksie van die zwitterioon en dus word die reaksietempo deur die vorming van die zwitterioon beheer.

Die eerste reeks eksperimente het tot die lig gebring dat die reaksieordes met betrekking tot MEA 1.22, 1.59, 1.15 en 0.91 by temperature van 298, 303, 308 en 313 K onderskeidelik was. Reaksietempokonstantes was verkry met behulp van die zwitterioonmeganisme waarin k_f die tweede-orde, voorwaartse reaksietempokonstante is vir die vorming van die zwitterioon, terwyl k_w en k_a (die konstantes vir die deprotonering van die zwitterioon deur onderskeidelik water en MEA) onderskeidelik deur die volgende vergelykings aangedui word: $k_w = \dfrac{k_f k_{H_2O}}{k_r}$ en $k_a = \dfrac{k_f k_{MEA}}{k_r}$. Die reaksietempokonstante k_f het eenhede van L/mol.s, terwyl beide k_w en k_a eenhede van L²/mol².s het. Die temperatuurafhanklikheid van die

reaksiekonstantes kan as volg deur hul onderskeidelike Arrhenius vergelykings beskryf word:

$$k_f = 1.88 * 10^8 \exp\left(\frac{-4999}{T}\right), \quad k_w = 1.83 * 10^6 \exp\left(\frac{-3856}{T}\right) \quad \text{en} \quad k_a = 1.36 * 10^8 \exp\left(\frac{-4812}{T}\right).$$

Die aktiveringsenergie wat gepaard gaan met elke vergelyking is 41.6, 32.1, 40.0 onderskeidelik.

Die reaksieorde met betrekking tot MEA en CO_2 is bepaal vir die tweede reeks eksperimente. Die ordes vir MEA is 1.34, 1.65, 1.67 en 1.78 by 298, 303, 308 en 313 K onderskeidelik en die ordes vir CO_2 is 1.35, 1.89, 1.59 en 1.60 by 298, 303, 308 en 313 K onderskeidelik.

'n Algehele vinniger reaksietempo is opgemerk vir die tweede reeks eksperimente in vergelyking met die eerste reeks. Die reaksieordes met betrekking tot MEA is groter vir die tweede reeks eksperimente. Bogenoemde word numeries gestaaf met die verskil in die reaksiekonstante vir die vormingsreaksie van die zwitterioon tussen die eerste en tweede reeks eksperimente. Vir die eerste reeks is k_f 11.5, 9.5, 17.4 en 23.6 L/mol.s by 298, 303, 308 en 313 K onderskeidelik terwyl k_f gestyg het na 234, 6434, 2466 en 44 L/mol.s by 298, 303, 308 en 313 K onderskeidelik. Die zwitterioon vormingsreaksie is dus vinniger vir die tweede reeks eksperimente oor die hele temperatuurgebied.

ACKNOWLEDGEMENTS

TABLE OF CONTENTS

LIST OF FIGURES

LIST OF TABLES

ABBREVIATIONS AND NOMENCLATURE

MEA	Monoethanolamine
DEA	Diethanolamine
MDEA	Methyl diethanolamine
CO_2	Carbon dioxide
SG	Specific gravity
NPT	NPT: National Pipe Thread
Cv	Flow Coefficient
MNPT	Male National Pipe Thread
FNPT	Female National Pipe Thread
In	Inch
g	grammes
Mol	Moles
Mol. Wt	Molecular weight
Psig	pound force per square inch gauge
lb/ft^3	pounds per cubic foot
^{o}C	degree Celsius
R_1R_2NH	Primary or secondary alkanolamine
$R_1R_2NH^{+}COO^{-}$	Zwitterion
$R_1R_2NCOO^{-}$	Carbamate
KCl	Potassium chloride
KI	Potassium iodide
CAL	Calibration
AR	Automatic read
DIN	Deutsches Institut für Normung
BIPM	International Bureau of Weights and Measures
IEC	International Electro technical Commission
ISO	International Organization for Standardization
IUPAP	International Union of Pure and Applied Physics
OIML	International Organization of Legal Metrology
rpm	Revolutions per minute
MSE	Mean of Squared Residuals
RMSE	Square Root of Mean of Squared Residuals

Symbol	Name	Units
k_{AM}	Forward second order reaction rate constant for an amine	L/mol.s
k_{H_2O}	Forward second order reaction rate constant for an water	L/mol.s
k_{OH^-}	Forward second order reaction rate constant for OH^-	L/mol.s
$k_{HCO_3^-}$	Forward second order reaction rate constant for HCO_3^-	L/mol.s
$k_{CO_3^-}$	Forward second order reaction rate constant for CO_3^-	L/mol.s
k_{ov}	Overall pseudo-first order reaction rate constant	s^{-1}
k_{obs}	Observed reaction rate constant	s^{-1}
k_{MEA}	Forward second order reaction rate constant for MEA	L/mol.s
k_{MDEA}	Forward second order reaction rate constant for MDEA	L/mol.s
k_{app}	Apparent pseudo-first order reaction rate constant	s^{-1}
T	Absolute temperature	K
C_A	Concentration of reactant A	mol/L
k_A	Reaction rate constant	Depends on order of reaction
α	Order of reaction with respect to A	-

β	Order of reaction with respect to B	-
A	Frequency factor	-
E	Activation energy	J/mol
R	Universal gas constant	J/mol.K
K_C	Equilibrium constant	-
D_i	Diffusivity of species i	m^2/s
P	Density	g/mL
V	Total molar volume	mL/mol
x_j	Mole fraction	-
M_j	Weight	G
μ	Viscosity	mPa.s
Ω	Mass percent	-
X	Conversion	-
M	Order of reaction with respect to MEA	-
N	Order of reaction with respect to CO_2	-
P	Order of reaction with respect to salt S	-
P_{H_2O}	Partial pressure of water vapour	Pa
P_{CO_2}	Partial pressure of CO_2	Pa
P_{total}	Total pressure	Pa
E_i	Infinite enhancement factor	-
Ha	Hatta number	-
D_{CO_2}	Diffusion coefficient of CO_2	m^2/s
D_{Am}	Diffusion coefficient of amine	m^2/s
m_{CO_2}	Solubility of CO_2 (m is dimensionless)	-

ν_{CO_2}	Stoichiometric coefficient	-
k_{ov}	Overall rate constant	s^{-1}
V_g	Gas volume	m^3
T	Time	s
k_l	First order reaction rate constant	s^{-1}
r_{CO_2}	Rate of reaction with respect to CO_2	mol/L.s
r_{MEA}	Rate of reaction with respect to MEA	mol/L.s
C_{Ae}	Concentration of reactant A at equilibrium	mol/L
k_f	Forward second-order reaction rate constant for the formation of the zwitterion	L/mol.s
k_w	$k_w = \dfrac{k_f k_{H_2O}}{k_r}$	$L^2/mol^2.s$
k_a	$k_a = \dfrac{k_f k_{MEA}}{k_r}$	$L^2/mol^2.s$
k_r	Backward first-order reaction rate constant	s^{-1}
k_b	Second-order reaction rate constant for a base	L/mol.s
k_B	$k_B = \dfrac{k_f k_B}{k_r}$	$L^2/mol^2.s$
ϑ	Initial molar ratio of MEA to CO_2	-
R^2	Coefficient of determination	-

K_{h*}	$K_{h*} = \dfrac{k_{-b}}{k_b K_{eqm}}$; where b is H_2O	-
K_{m*}	$K_{m*} = \dfrac{k_{-b}}{k_b K_{eqm}}$; where b is MEA	-
K_{eqm}	Equilibrium constant	-

$$K_{h*} = \frac{k_{-b}}{k_b K_{eqm}}$$

xvii

CHAPTER 1: INTRODUCTION

1.1 Background

Carbon dioxide is a greenhouse gas which contributes to global warming and its level in the atmosphere is increasing rapidly (Lin *and* Shyu, 1999; Li *et al.*, 2007). This has prompted several research groups in both industry and academia into developing interest in its capture. Most of the carbon dioxide emissions are from the combustion of fossil fuels from refineries, the energy and steel industries, and cement manufacturing industry (He *et al.*, 2003; Bonenfant *et al.*, 2007; Lin *and* Shyu, 1999). It is estimated by the International Energy Agency that the global energy consumption is expected to increase by 70% between 2000 and 2030 and that 90% of this energy has to come from fossil fuels (Amann *and* Bouallo, 2009). It is also projected that, by 2030, there will be an increase in carbon dioxide emissions of 63% from 2007 levels. This is 90% higher than the 1990 carbon dioxide emission levels (Li *et al.*, 2007).

Carbon dioxide has to be removed from the industrial exhaust gases so as to alleviate the problem of global warming. There has been development of technologies for the removal of carbon dioxide and these include cryogenic separation, adsorption and absorption using both physical and chemical solvents (Lin *and* Shyu, 1999; Masuda, 1995; Kimura *et al.*, 1995).

Absorption using chemical solvents relies on reaction of carbon with the solvent while absorption using a physical solvent depends on the solubility of carbon dioxide in the physical solvent (www.co2crc.co.au, 2011). The absorption process using physical solvents occurs at low temperatures and high carbon dioxide partial pressures (www.gcep.stanford.edu, 2005). Regeneration of the solvents can then be achieved by reducing pressure or by heating or by a combination of the two (www.gcep.stanford.edu, 2005; www.co2crc.co.au, 2011). The energy that is required for the regeneration process when using physical solvents is less than the energy that is required when using chemical solvents (www.gcep.stanford.edu, 2005). This is because of the interaction between carbon dioxide and a physical solvent is weak when compared to the interaction between carbon dioxide and a chemical solvent (www.gcep.stanford.edu, 2005). Examples of these physical solvents are selexol, methanol, N-methyl-2-pyrorolidone, dimethyl ethers of polyethylene

1

glycol and glycerol carbonate (Davison *et al.,* 2001; Kovvali and Sirkar, 2002; www.gcep.stanford.edu, 2005).

Use of chemical solvents has become an area of major focus for removal of carbon dioxide because they permit high recovery rates of carbon dioxide, even when its partial pressures are very low (Amann *and* Bouallo, 2009). These chemical solvents are mostly alkanolamines which will be discussed in detail in chapter 2. Apart from alkanolamines, other chemical solvents that are used for chemical absorption of carbon dioxide are potassium carbonate, ammonium carbonate and ammonia. Reactions (1.1), (1.2) and (1.3) are the reactions of potassium carbonate, ammonium carbonate and ammonia with carbon dioxide respectively.

$$CO_2 + K_2CO_3 + H_2O \leftrightarrow 2KHCO_3 \qquad\qquad (1.1)$$

$$CO_2 + (NH_4)2CO_3 + H_2O \leftrightarrow 2(NH_4)HCO_3 \qquad\qquad (1.2)$$

$$CO_2 + NH_3 + H_2O \leftrightarrow NH_4HCO_3 \qquad\qquad (1.3)$$
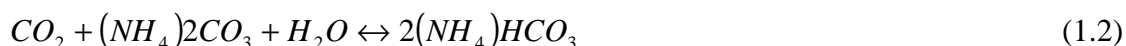
Reactions of alkanolamines with carbon dioxide are discussed in great detail in chapter 2.

1.2 Motivation

Much research work on the reaction kinetics of the reaction of CO_2 and MEA has been done. However, most of the previous work focussed on investigating the heterogeneous reaction kinetics. This is where researchers investigated the absorptive reaction kinetics of the reaction between MEA and CO_2. In this case, CO_2 was absorbed into aqueous or organic solutions of MEA. The aim of this project is to investigate the homogeneous reaction kinetics of the reaction between CO_2 and MEA in an aqueous medium. The reaction kinetics of the reaction will be followed by using conductivity.

This project also aims to report on the equilibrium conversions of both MEA and CO_2. Conductometric titrations will be used to determine the final extent of the reaction by finding the amount of the bound MEA. This bound MEA is that MEA that would have reacted with CO_2 at the end of the reaction. This will be discussed in greater detail in chapter 3.

1.3 Objectives

The aim of this project is to investigate the reaction kinetics of the reaction of CO_2 with MEA in aqueous medium as mentioned in section 1.2. The objectives of this project are as follows:

- To investigate if the reaction of CO_2 and MEA proceeds via the zwitterion mechanism or not. If it does, it will be determined whether the zwitterion formation step is faster or slower than the zwitterion deprotonation step. In other words, the rate determining step will be determined. The contribution of each of the bases present in the solution (MEA and water) to the overall deprotonation will be investigated.

- To determine the reaction rate constants and their respective activation energies.

- To investigate if the reaction of CO_2 and MEA follows second order reaction kinetics; first order in both MEA and CO_2.

- Determine the equilibrium conversion of both MEA and CO_2 using conductometric titrations.

- To test the various kinetic models that are being used for modelling the reaction between CO_2 and MEA.

1.4 Hypothesis

Two major hypotheses have been proposed for this project and these hypotheses are:

- The reaction between aqueous solutions of CO_2 and MEA proceeds via the zwitterion mechanism.
- The reaction between aqueous solutions of CO_2 and MEA follows second order reaction kinetics. The order of reaction with respect to both CO_2 and MEA is one.

Figure 1 shows the outline of the study. It shows the different aspects of the research project.

3
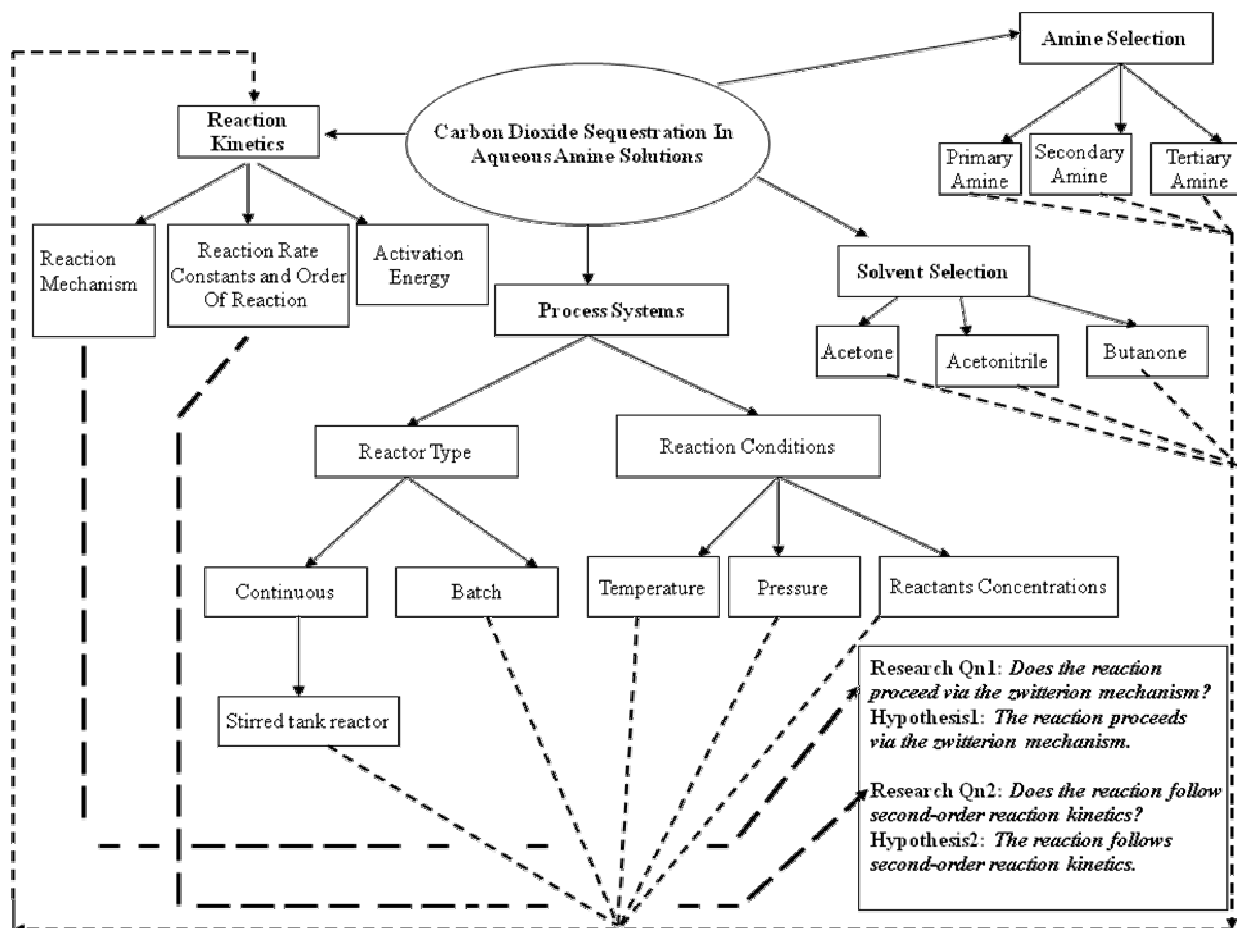
Figure 1: Mind map of the study

1.5 Thesis Structure

The second chapter will focus on the literature review of reaction kinetics of the reaction of CO_2 and MEA. The different types of alkanolamines will be discussed in this chapter. Also to be discussed are the reaction mechanisms through which these alkanolamines react with CO_2. These mechanisms are the zwitterion and termolecular mechanisms. The third chapter will give the details of the experimental procedure used in investigating the reaction kinetics of the reaction of CO_2 and MEA. The conductivity- and conversion-time profiles will be presented in the fourth chapter and the fifth chapter will present the modelling results and their discussion. In this chapter, the kinetic parameters will be presented. Conclusions and recommendations will be presented in the sixth chapter.

CHAPTER 2: LITERATURE REVIEW

2.1 Alkanolamines as Chemical Solvents for Carbon Dioxide Removal

Alkanolamines are being used as chemical solvents in the removal of carbon dioxide and hydrogen sulphide from industrial exhaust gases (Bavbek *and* Alper, 1999; Bonenfant *et al.*, 2007). These are chemical compounds that have two functional groups: the amino and the hydroxyl groups. The basicity of these alkanolamines is enhanced by the amino group while their solubility in water is enhanced by the hydroxyl group (Bavbek *and* Alper, 1999). The absorption capacities for carbon dioxide into alkanolamine solutions depend on factors such as alkanolamine structural characteristics, concentration and basicity (Bonenfant *et al.*, 2003).

Alkanolamines have been in use on a commercial scale for more than 75 years and the most commonly used ones are monoethanolamine (MEA), diethanolamine (DEA) and methyl diethanolamine (MDEA) as a primary, secondary and tertiary amine respectively (Li *et al.*, 2007). These alkanolamines are associated with very high rates of reaction (Ali *et al.*, 2002) Alkanolamines are being used for carbon dioxide capture in spray, packed and bubble column absorbers (Paul *et al.*, 2007). Chemical absorption using these alkanolamines is very efficient as 75 to 90% of carbon dioxide is captured when this technology is used (Rao *and* Rubin, 2002).

2.1.1 Primary and Secondary Alkanolamines

Aqueous solutions of primary and secondary alkanolamines react directly with carbon dioxide to form stable carbamates through the zwitterion reaction mechanism (Ramachandran *et al.*, 2006). The reaction is reversible and instantaneous. In theory, the capacity of the primary and secondary alkanolamines is 0.5 mol of carbon dioxide per mol of primary or secondary alkanolamine as shown by equation (2.0) (Bonenfant *et al.*, 2003; Amann *and* Bouallou, 2009). The carbon dioxide solubility into these solutions is high. Therefore, this carbon dioxide loading is achievable (Amann *and* Bouallou, 2009). The carbamate formation reaction is associated with high heat of absorption, thus, regeneration costs of the primary and secondary alkanolamines are very high (Ramachandran *et al.*, 2006).

5

$$CO_2 + 2RNH_2 \leftrightarrow RNHCOO^- + RNH_3^+ \qquad\qquad (2.0)$$

2.1.2 Tertiary Alkanolamines

Unlike primary and secondary alkanolamines, tertiary alkanolamines do not react directly to form stable carbamates since they do not have the nitrogen-hydrogen bond that is required for carbamate ion formation (Rinker *et al.*, 2000; Ramachandran *et al.*, 2006). They instead form bicarbonates and a protonated alkanolamine through hydrolysis of carbon dioxide (Rinker *et al.*, 2000; Ramachandran *et al.*, 2006). The tertiary alkanolamine selectivity towards carbon dioxide is poor since the hydrolysis reactions are slower, as compared to the primary and secondary alkanolamines reactions (Rinker *et al.*, 2000). The maximum loading of carbon dioxide is 1.0 mol of carbon dioxide per mol of alkanolamine (Rinker *et al.*, 2000; Ramachandran *et al.*, 2006; Amann *and* Bouallou, 2009). The reaction between tertiary alkanolamines and carbon dioxide is shown by equation (2.1). For low carbon dioxide partial pressures, this loading is not achievable as the solubility of carbon dioxide in tertiary alkanolamines is low (Amann *and* Bouallou, 2009). Tertiary alkanolamines also have low heats of regeneration thus resulting in low regeneration heat duty. (Rinker *et al.*, 2000; Ramachandran *et al.*, 2006).

$$CO_2 + RNH_2 + H_2O \leftrightarrow HCO_3^- + RNH_3^+ \qquad\qquad (2.1)$$

2.1.3 Sterically Hindered Alkanolamines

Other types of alkanolamines are the sterically hindered alkanolamines. Sterically hindered alkanolamines can be defined as primary alkanolamines where the amino group is on a tertiary carbon atom or it can be secondary alkanolamine where the amino group is on a tertiary or secondary carbon atom (Sartori *and* Savage, 1983). Sterically hindered alkanolamines have better carbon dioxide loading capacities than primary or secondary alkanolamines because they have lower carbamate stability constants, as compared to primary or secondary alkanolamines (Yih *and* Shen, 1988; Paul *et al.*, 2007). This means that sterically hindered alkanolamines have a low carbamate formation tendency. Yoon *et al.* (2002) reported that because of the low carbamate stability of sterically hindered

6

alkanolamines, their carbon dioxide absorption capacities might be high. In a sterically hindered alkanolamine, the size of the group attached to the secondary or tertiary carbon atom inhibits carbamate formation such that bicarbonate ions are formed instead (Yih *and* Shen, 1988). The formation of bicarbonates requires a relatively small amount of heat of reaction (Yoon *et al.*, 2002). This means that using sterically hindered amines results in great energy savings since less regeneration energy is required. The total operating costs of carbon dioxide absorption columns would be reduced (Yoon *et al.*, 2002). The stoichiometry of the reaction of a sterically hindered alkanolamine and carbon dioxide allows a high carbon dioxide loading of 1 mole per mole of the hindered alkanolamine (equation 2.1) (Sartori *and* Savage, 1983; Yih *and* Shen, 1988; Yoon *et al.*, 2002; Paul *et al.*, 2007; Paul *et al.*, 2009).

2.2 Reaction Kinetics Fundamentals

2.2.1 Reaction rate law

Considering a chemical reaction in which one of the reactants is species A, the rate at which A disappears is $-r_A$. This rate depends on temperature and composition. Thus, for many chemical reactions, the rate can be represented as follows:

$$-r_A = fn(\text{temperature, composition}) \tag{2.2}$$

$$-r_A = [k_A(T)][fn(C_A, C_B, ...)] \tag{2.3}$$

This is principally the product of a reaction rate constant k_A, sometimes called the specific rate constant, and a function of species activities, concentrations or partial pressures. The rate law can then be defined as the algebraic equation that relates the rate of disappearance of A, $-r_A$ to the concentration of all the chemical species taking part in the reaction (Levenspiel, 1972).

Experiments are used to determine the reliance of the reaction rate on the chemical species concentrations. One way in which this reliance can be represented, the power rate law, is given in the following mathematical form:

$$-r_A = k_A C_A^\alpha C_B^\beta \tag{2.4}$$

In this kinetic rate law, the powers to which the species concentrations are raised are called the order of the reaction. Where α and β are the orders with respect to reactants A and B respectively. The total of the orders will then be overall order of the reaction, n.

$$n = \alpha + \beta . \tag{2.5}$$

In the strictest sense, the reaction rate constant is not a constant. It is exponentially dependent on temperature, according to the Arrhenius law (equation 2.6), but independent of the chemical species concentrations. It can be assumed that the rate constant k_A depends on temperature for solid and liquid phase reactions and this assumption works well in industrial and laboratory reactions.

$$k_A(T) = A e^{-E/RT} \tag{2.6}$$

Where:

$A =$ Frequency factor

$E =$ Activation energy, J/mol

$R =$ Universal gas constant $= 8.314$ J/mol.K

$T =$ Absolute temperature, K

The natural logarithm of the Arrhenius equation can be taken to get:

$$\ln k_A = \ln A - \frac{E}{R}\left(\frac{1}{T}\right) \tag{2.7}$$

Carrying out the reaction at different temperatures enables the activation energy of the reaction to be determined by plotting $\ln k_A$ versus $1/T$. If the reaction mechanism does not change, this plot is a straight line whose gradient is proportional to the activation energy, E (Fogler, 1999).

8

2.2.2 Elementary reactions

An elementary reaction is one where the reaction occurs in a single step. The reaction order will match the stoichiometric coefficient, and be an integer, for an elementary reaction.

Considering the following general equation for a reversible reaction:

$$aA + bB \xleftrightarrow{K_C} cC + dD \tag{2.8}$$

The rate of formation of product C by the forward reaction is:

$$r_C = k_f C_A^a C_B^b \tag{2.9}$$

And the rate of its disappearance via the reverse reaction is:

$$-r_C = k_r C_C^c C_D^d \tag{2.10}$$

At equilibrium, the net rate of reaction for all the species is equal to zero.

$$-r_C = 0 \text{ or} \tag{2.11}$$

$$\frac{k_f}{k_r} = \frac{C_{Ce}^c C_{De}^d}{C_{Ae}^a C_{Be}^b} \tag{2.12}$$

$$K_C = \frac{C_{Ce}^c C_{De}^d}{C_{Ae}^a C_{Be}^b} \tag{2.13}$$

$$\therefore K_C = \frac{k_f}{k_r} = \frac{C_{Ce}^c C_{De}^d}{C_{Ae}^a C_{Be}^b} \tag{2.14}$$

2.2.3 Non-elementary reactions

A non-elementary reaction is one that occurs in more than one step. The kinetics of non-elementary reactions can be explained by assuming that elementary reactions occur sequentially or in parallel and that intermediates are formed but cannot be observed or measured due to the fact that they will be present in very small quantities. This leads to observing just the initial reactants and resulting products.

If the reaction kinetics show that the reaction is non-elementary, then the kinetics can be explained by postulating a sequence of elementary steps. It must then be seen whether there is correspondence between the predicted kinetic expression and experimental results so as to be able to test the postulated scheme. The intermediates that can be postulated can be in the form of molecules, free radicals, ions and polar substances (Levenspiel, 1972; Fogler, 1999).

It is not always possible to eliminate active intermediate concentration in the mole balance equations but an estimated solution can be obtained. The active intermediate can be considered to be present in low concentrations. It has a very high reactivity thus leading to its very short lifetime. Having these two conditions, the pseudo-steady state approximation can be assumed. It assumes that the rate at which the active intermediate is formed is equal to the rate at which it disappears. Consequently, its net rate of formation is equal to zero (Levenspiel, 1972; Fogler, 1999). The pseudo-steady state hypothesis is further discussed in section 2.3.2.

A reaction can proceed by a number of mechanisms thus making the search for a correct reaction mechanism difficult. Another factor that makes the search for a correct mechanism difficult is the fact that kinetic data can be consistent for more than one reaction mechanism. The chemistry of the species involved thus needs to be known so as to be able to overcome these difficulties. When the predicted rate expression is now matched with the experiment, the rate of change of active intermediates is small and these rates can be assumed to be zero without loss of accuracy. Also if one of the involved components takes part in more than one reaction, then its net rate of change is the summation of all the rates of change in all the elementary reactions (Levenspiel, 1972; Fogler, 1999).

2.3 Carbon Dioxide and Alkanolamines Reaction Kinetics

Primary and secondary amines react with carbon dioxide to form carbamates by two different reaction mechanisms, namely, the zwitterion and the termolecular mechanisms (Ramachandran *et al.*, 2006). These reaction mechanisms are described in sections 2.3.1 and 2.3.3. Carbon dioxide is an electron acceptor Lewis acid. The proton on the amino site is replaced by carbon dioxide.

$$2R_1R_2NH + CO_2 \xleftrightarrow{k_f,k_r} R_1R_2NH_2^+ + R_1R_2NCOO^- \qquad (2.15)$$

It is generally accepted that, for the reaction shown in (2.15), the reaction order is first order in carbon dioxide (Bavbek *and* Alper, 1999). It has been previously assumed that the reaction is a one-step carbamate formation and it is first order in the amine as well (Bavbek *and* Alper, 1999; Alper, 1990).

$$R_1R_2NH + CO_2 \xleftrightarrow{k_f,k_r} R_1R_2NCOO^- + H^+ \qquad (2.16)$$
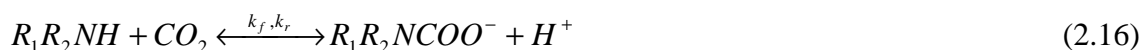
Another amine molecule reacts with the H^+ to stoichiometrically match the overall reaction equation (2.15).

2.3.1 Zwitterion mechanism

The zwitterion reaction mechanism was first proposed by Caplow (1968) and was later reintroduced by Danckwerts (1979). This mechanism is commonly accepted as the reaction mechanism for the reaction between carbon dioxide and primary and secondary alkanolamines to form carbamates (Horng *and* Li, 2002). The zwitterion mechanism has been successfully used in some aqueous alkanolamine solutions and also in some viscous and organic solutions (Blauwhoff *et al.*, 1984; Barth *et al.*, 1984; Alvarez-Fuster *et al.*, 1980; Alvarez-Fuster *et al.*, 1981; Sada *et al.*, 1985; Versteg *and* Swaaij, 1988).

The zwitterion mechanism consists of two steps which are the reaction of carbon dioxide and primary or secondary amines to form a zwitterion intermediate followed by the formation of the carbamate after the deprotonation of the intermediate zwitterion by a base (Li *et al.*, 2007;
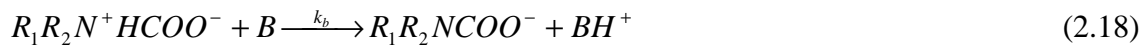
11

Littel *et al.*, 1992; Danckwerts, 1979). The bases in the reaction mixture all contribute to the deprotonation process and each base's overall contribution depends on its strength and its concentration (Ramachandran *et al.*, 2006; Hagewiesche *et al.*, 1995). The bases can be water, hydroxyl ions, amine or other solvents present in the solution. In aqueous solutions, water and the amine are the main bases responsible for the deprotonation process since the contribution of the hydroxyl ion is generally negligible in the dissociation of the zwitterion. The amine is regarded as the base in non-aqueous solutions. (Versteeg *and* van Swaaij, 1988; Versteeg *and* Oyevaar, 1989; Bosch *et al.*, 1990, Xu *et al.*, 1996; Bouhamra *et al.*, 1999).

In aqueous solutions, carbon dioxide reacts with primary and secondary alkanolamines to form carbamates as shown by equation (2.15). In equation (2.15), R_1 is an alkyl group and R_2 is a hydrogen atom for the primary alkanolamines and an alkyl group for secondary alkanolamines.
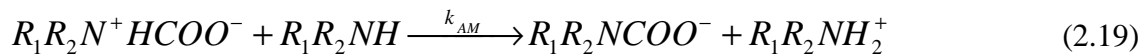
The two-step carbamate formation reaction is shown below:

$$CO_2 + R_1R_2NH \xleftrightarrow{k_f,k_r} R_1R_2N^+HCOO^- \tag{2.17}$$

Where $R_1R_2N^+HCOO^-$ is the zwitterion.

$$R_1R_2N^+HCOO^- + B \xrightarrow{k_b} R_1R_2NCOO^- + BH^+ \tag{2.18}$$

Where B represents any base molecule present. Based on this reaction mechanism, the deprotonation of the zwitterion can be represented by one of the following reactions:

$$R_1R_2N^+HCOO^- + R_1R_2NH \xrightarrow{k_{AM}} R_1R_2NCOO^- + R_1R_2NH_2^+ \tag{2.19}$$

$$R_1R_2N^+HCOO^- + H_2O \xrightarrow{k_{H_2O}} R_1R_2NCOO^- + H_3O^+ \tag{2.20}$$

$$R_1R_2N^+HCOO^- + OH^- \xrightarrow{k_{OH^-}} R_1R_2NCOO^- + H_2O \tag{2.21}$$

Reaction (2.17) is bimolecular and the product of this reaction is the zwitterion (da Silva *and* Svendsen, 2004). If the carbamate ion formed is not stable, the following reaction takes place subsequently (Alper, 1990):

$$R_1R_2NCOO^- + H_2O \leftrightarrow R_1R_2NH + HCO_3^- \qquad (2.22)$$

Apart from reactions (2.16), (2.17) and (2.18), the following reactions also occur:
Bicarbonate formation:

$$CO_2 + OH^- \xrightarrow{k_{OH^-}} HCO_3^- \qquad (2.23)$$

Carbonic acid formation:

$$CO_2 + H_2O \xrightarrow{k_{H_2O}} HCO_3^- + H^+ \qquad (2.24)$$

Alkyl carbonate formation:

$$CO_2 + R_1R_3C(OH)CNH + OH^- \leftrightarrow R_1R_3C(OCO_2^-)CNH + H_2O \qquad (2.25)$$
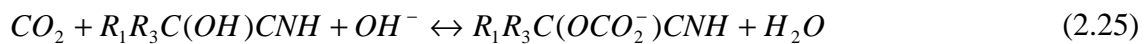
Each of the reactions from (2.23) to (2.25) and reaction (2.16) for primary and secondary alkanolamines contributes to the overall reaction rate constant. The reaction of carbon dioxide and water to form carbonic acid (reaction 2.24) is very slow ($k = 0.026$ sec^{-1} at 25°C (Pinsent *et al.*, 1956)) compared to reactions (2.22) and (2.23). For this reason, reaction (2.24) will not be incorporated in the overall reaction rate constant (Blauwhoff *et al.*, 1982). At pH<12, the alkylcarbonate reaction (2.25)'s contribution to the carbon dioxide absorption rate for MEA and DEA is negligible. Conversely, at low secondary amine concentrations, the bicarbonate formation reaction (2.23)'s contribution is significant (Blauwhoff *et al.*, 1982; Thomas, 1966).

2.3.2 Pseudo-steady state approximation

Following the zwitterion reaction mechanism proposed by Caplow (1968) and Danckwerts (1979), Bavbek *and* Alper, 1999 reported that the reaction rate for the reaction of carbon dioxide and a primary or secondary alkanolamine is:

$$r = k_f[R_1R_2NH][CO_2] - k_r[R_1R_2NH^+COO^-] \qquad (2.26)$$

Assuming pseudo-steady state conditions, the rate at which the zwitterion is formed is equal to the rate at which it is deprotonated.

$$r_{zwitterion} = r_z = 0 \qquad (2.27)$$

If $[R_1R_2NH^+COO^-]$ is the zwitterion concentration at pseudo-steady state conditions, then:

$$\frac{d[R_1R_2NH^+COO^-]}{dt} = k_f[R_1R_2NH][CO_2] - (k_r + \sum k_b[B])[R_1R_2NH^+COO^-] = 0$$
$$(2.28)$$

Where $\sum k_b[B]$ represents the contribution of all the bases present in the solution to the deprotonation of the zwitterion.

$$[R_1R_2NH^+COO^-] = \frac{k_f[R_1R_2NH][CO_2]}{k_r + \sum k_b[B]} \qquad (2.29)$$

Substituting equation (2.29) in equation (2.26) gives:

$$r = k_f[R_1R_2NH][CO_2] - \frac{k_f k_r[R_1R_2NH][CO_2]}{k_r + \sum k_b[B]} \qquad (2.30)$$

14

$$r = \frac{(k_r + \sum k_b[B])(k_f[R_1R_2NH][CO_2]) - k_f k_r[R_1R_2NH][CO_2]}{k_r + \sum k_b[B]}$$ (2.31)

$$r = k_f[R_1R_2NH][CO_2]\left\{\frac{\sum k_b[B]}{k_r + \sum k_b[B]}\right\}$$ (2.32)

Dividing both the denominator and numerator in equation (2.32) by $k_f \sum k_b[B]$ yields:

$$r = \frac{[R_1R_2NH][CO_2]}{\dfrac{k_r}{k_f \sum k_b[B]} + \dfrac{1}{k_f}}$$

$$r = \frac{[R_1R_2NH][CO_2]}{\dfrac{1}{k_f} + \dfrac{1}{\sum k_B[B]}}$$ (2.33)

Where $k_B = \dfrac{k_f k_b}{k_r}$ (Li *et al*., 2007; Henni *et al*., 2008)

If the alkanolamine concentration is always in great excess, compared to that of carbon dioxide, then the alkanolamine concentration will be essentially constant and the rate expression will simplify to an apparent irreversible first-order equation which can, therefore, be written as:

$$r = k_o[CO_2]$$ (2.34)

Where k_o is the observed pseudo-first-order reaction rate constant, with:

$$k_o = \frac{[R_1R_2NH]}{\dfrac{1}{k_f} + \dfrac{1}{\sum k_B[B]}}$$ (2.35)

There are two limiting cases that exist for equation (2.35) and these are:

1. If $\dfrac{1}{k_f} >>> \dfrac{1}{\sum k_B[B]}$, it means that the deprotonation of the zwitterion is relatively fast.

   Equation (2.35) then simplifies to:

$$k_o = k_f[R_1R_2NH] \tag{2.36}$$

2. If $\dfrac{1}{k_f} <<< \dfrac{1}{\sum k_B[B]}$, then equation (2.35) would simplify to:

$$k_o = [R_1R_2NH](\sum k_B[B]) \tag{2.37}$$

In summary, for the pseudo-steady state approximation, the reaction will always be first order in the amine.

According to Yoon *et al*. (2002), carbon dioxide hydration reactions must always be taken into account whenever considering the reaction of alkanolamines with carbon dioxide in aqueous solutions (equations 2.24 and 2.25). The reaction between carbon dioxide and water can be ignored since it proceeds slowly. The values of k_{H_2O} at 20 and 25$^{\text{o}}$C are 0.016 and 0.026 s^{-1} respectively (Blauwhoff *et al*., 1984; Astarita *et al*., 1983). On the contrary, the reaction of carbon dioxide and hydroxyl cannot be ignored since it is fast and can also improve mass transfer (Yoon *et al*., 2002). The reaction rate of the hydroxyl ion and carbon dioxide is thus represented as follows: (Yoon *et al*., 2002).

$$r_{co_2-OH^-} = k_{OH^-}[CO_2][OH^-] \tag{2.38}$$

The overall reaction rate constant can then be expressed as follows: (Yoon *et al*., 2002).

$$k_{ov} = k_{obs} + k_{OH^-}[OH^-] \tag{2.39}$$

2.3.3 Termolecular mechanism

An alternative reaction mechanism has been proposed by Crooks *and* Donnellan (1989). This is the termolecular mechanism which is to some extent similar to the zwitterion mechanism but does not involve any intermediate species. The mechanism assumes that the reaction proceeds in a single step, where the initial product is a loosely bound encounter complex and not a zwitterion. As the bond forms between the carbon dioxide and the alkanolamine's nitrogen atom, a proton is transferred from the alkanolamine nitrogen atom to a base molecule. Some reactant molecules form as the complex breaks up and ionic products are formed after the reaction between a small fraction of the complex and a second water or alkanolamine molecule (Crooks *and* Donnellan, 1989; Arstad *et al.*, 2006; Ramachandran *et al.*, 2006; Aboudheir *et al.*, 2003).

For the termolecular reaction mechanism, Crooks *and* Donnellan (1989) and Versteeg *et al.* (1996) presented the forward reaction rate as:

$$r_{CO_2} = (k_{H_2O}[H_2O] + k_{MEA}[MEA])[MEA][CO_2] \qquad (2.40)$$

Ramachandran *et al.* (2006) reported that, using the termolecular mechanism, the reaction rate expression for the reaction of carbon dioxide and mixed aqueous loaded solutions of MEA and MDEA is presented as:

$$r_{CO_2} = (k_{H_2O}[H_2O] + k_{MEA}[MEA] + k_{MDEA}[MDEA])[MEA][CO_2] \qquad (2.41)$$

Equation (2.41) is based on the analogy of the reported termolecular mechanism of a single alkanolamine (equation 2.40) (Ramachandran *et al.*, 2006)

2.4 Work Previously Done

2.4.1 Experimental Techniques

The focus of this section is on work that has been done previously on the reaction kinetics of carbon dioxide and alkanolamines, mainly monoethanolamine. Much attention will be paid on the various techniques that have been used to acquire the kinetic data. Also to be considered are the different temperatures at which the chemical reactions were taking place. Different concentrations or concentration ranges for both the alkanolamine and carbon dioxide will also be taken into account. The zwitterion and the termolecular mechanisms were used to interpret the reaction kinetics data.

There are different types of experimental techniques that can be used for studying the reaction kinetics of the reaction of carbon dioxide and alkanolamines. These experimental techniques include laminar jet absorbers, wetted wall columns, stirred cell reactors and stopped flow techniques.

2.4.1.1 Laminar jet absorber

Experimental techniques such as laminar jet absorbers, wetted wall columns and stirred cell reactors are usually used to obtain reaction kinetics of reactive absorption of gases into liquids (Aboudheir *et al*., 2004). However, laminar jet absorbers have proved to be the best experimental technique for fast chemical reactions between reactive liquids and absorbed gases (Aboudheir *et al*., 2004). An example is carbon dioxide being absorbed in solutions of monoethanolamine. Laminar jet absorbers can generate reliable absorption data because of the short contact time between the gas and the liquid and also because the interfacial area is known accurately (Danckwerts, 1970; Astarita *et al*., 1983). The schematic diagram of a laminar jet absorber is shown in figure 2.
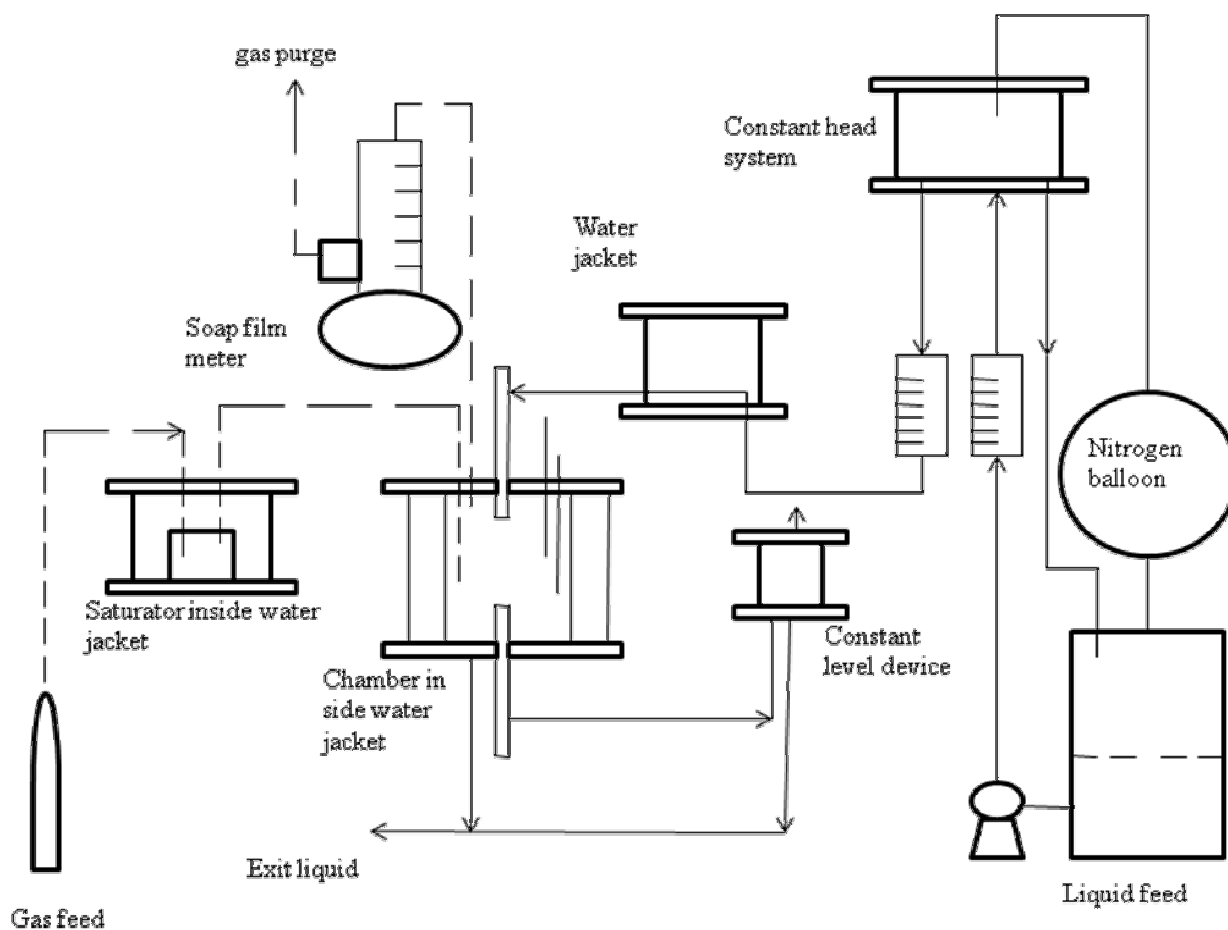
Figure 2: Schematic diagram of a laminar jet absorber.

This schematic diagram was redrawn from Aboudheir *et al*., 2004.

The following operating procedures and description of how the laminar jet absorber works are according to Aboudheir *et al*. (2004). The absorbing liquid, which can be an alkanolamine like monoethanolamine, was degassed and fed from a constant-head system to the jet chamber by gravity (see figure 2). The constant-head system was at a height of 3.0 m above the absorption chamber to ensure enough head for the required flow rate. The constant-head system had a capacity of 200 cm^3 and it had liquid-inlet and liquid-outlet ports on its bottom. When then constant-head system was being fed, the inlet flow rate was higher than the outlet one and the overflow was fed back to the feed tank. The liquid in the feed tank and the constant-head system was kept under nitrogen blanket and the nitrogen which was used to replace the used liquid was stored in a nitrogen balloon. This balloon was connected to the constant-head system and the feed tank.

The liquid flow rate was determined by measuring the mass of the discharged liquid at timed intervals and the level of the liquid in the receiver was adjusted by the constant-level device.

19

The level of the liquid was adjusted in such a way that there was no spill over of the liquid or entrainment of gas.

The gas from a gas cylinder was first saturated with water vapour before it entered the jet chamber. This saturation process was carried out at the experimental temperature. The temperature of both the gas and the liquid entering the jet chamber were measured and controlled to within $\pm$ 0.3 ^{o}C. The controlling of the temperature was achieved by having two separate heating or cooling circulator units. One circulator unit was for controlling the temperature of the liquid stream while the other one was for controlling the temperature of the gas stream.

2.4.1.2 Wetted wall column

Puxty *et al*. (2010) used a wetted wall column to investigate the absorption rate of carbon dioxide into aqueous solutions of monoethanolamine and ammonia. In the wetted wall column, the gas stream was contacted with a falling liquid in a counter-current manner (Puxty *et al*., 2010). The gas-liquid contacting in the wetted wall column was the same as that occurs in packed columns where the gas and the liquid streams enter at the bottom and at the top of the column respectively (Puxty *et al*., 2010).

The experimental procedures and the description of how the wetted wall column worked were according to Puxty *et al*. (2010). Figure 3 shows the diagram of a wetted wall column with a glass cover. Also shown in figure 3 is the position of the thermocouple and the thin liquid film. Figure 3 shows a full schematic diagram of a wetted wall column with all its associated equipment.
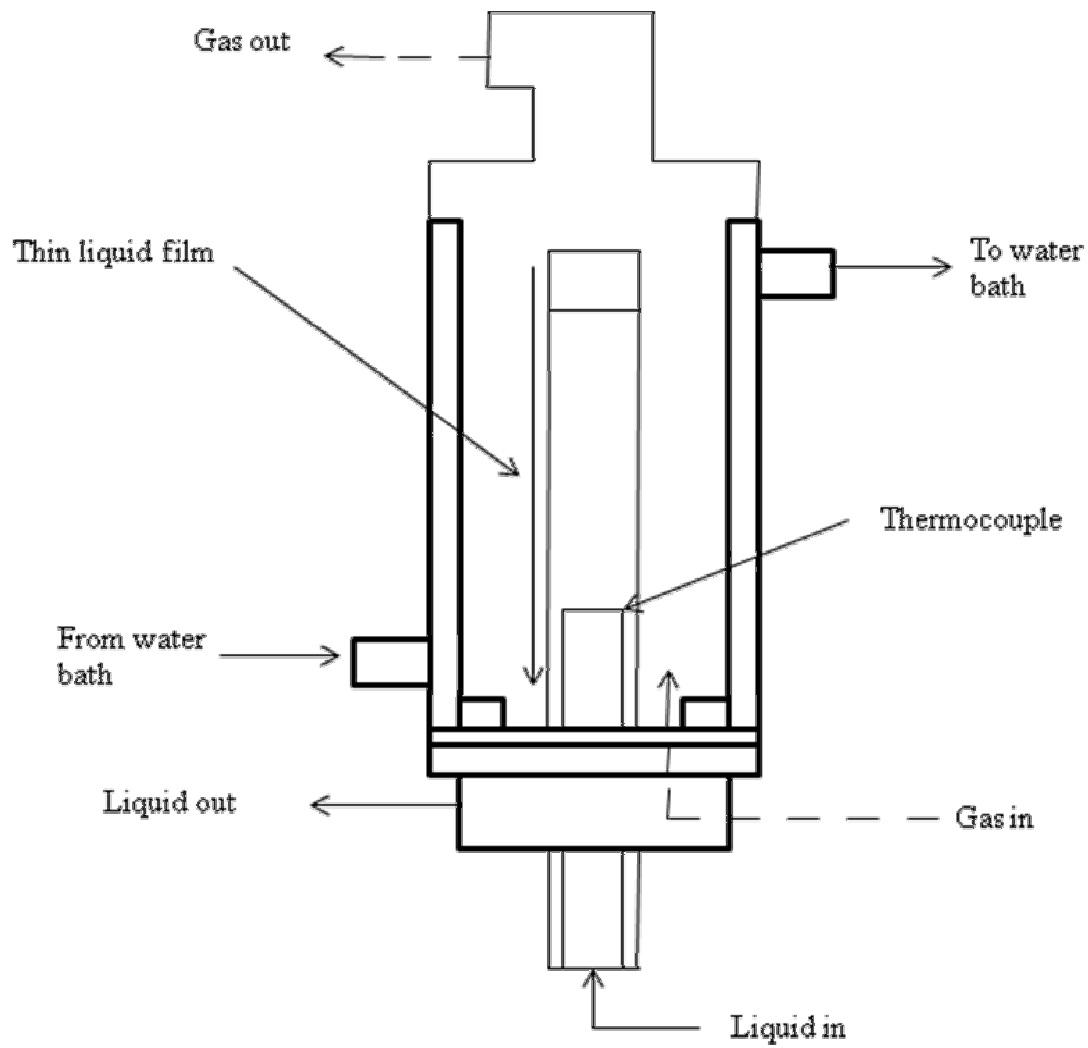
Figure 3: Schematic diagram of a wetted wall column.

Figure 3 was redrawn from Puxty *et al*. 2010.
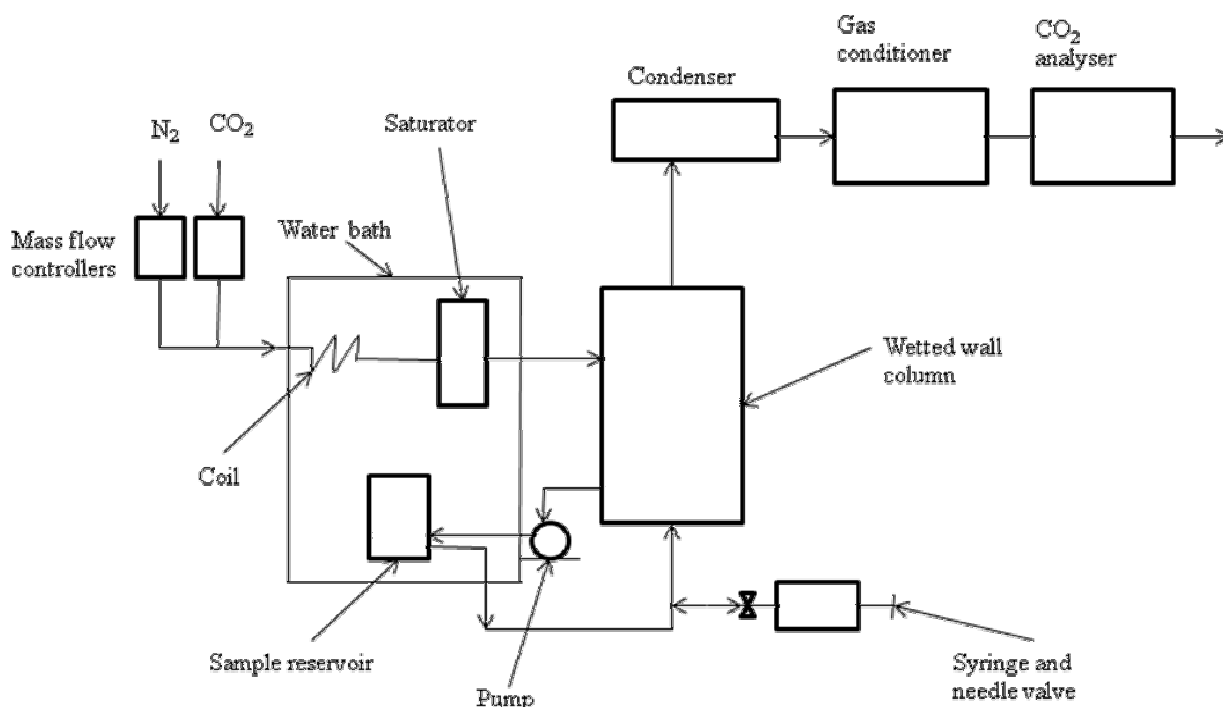
Figure 4: Full schematic diagram of a wetted wall column with its associated equipment

The schematic diagram shown in figure 4 was redrawn from Puxty *et al*. 2010.

Puxty *et al*. (2010) used a wetted wall column which was constructed using stainless steel and its effective height and diameter were 8.21 cm and 1.27 cm respectively. A thin liquid film flowed over the column under gravity. The liquid was pumped at a rate of 220 mL/min from a reservoir up the inside of the column and it then flowed out of the column at the top and flowed down on its sides. A flow rate of 220 mL/min was chosen so as to ensure that the formation of the film was ripple free and continuous. The liquid then returned to the reservoir. The liquid level in the system was controlled by using a needle valve and a syringe filled with extra liquid solution.

Carbon dioxide was mixed with nitrogen gas using two Bronkhurst mass flow controllers and the amounts of the gases in the gas flow were varied so as to have carbon dioxide partial pressures in the range of 0 to 20 kPa. The gas mixture then passed through a stainless steel coil and saturator after which it entered the column at its bottom. The mixture of the two gases then moved up the column and it was exhausted out of the column at its top. The exhaust gas then passed through a condenser and a gas conditioner before it entered a carbon dioxide analyser (see figure 4).

22

The column was contained in a jacketed glass cover which had water from a water bath flow through it (see figure 3). The water was used to control the temperature of the column. The temperature of the liquid inside the column was measured by a T-type thermocouple.

2.4.1.3 Stirred cell reactor

A schematic diagram of a stirred cell reactor is shown in figure 5.
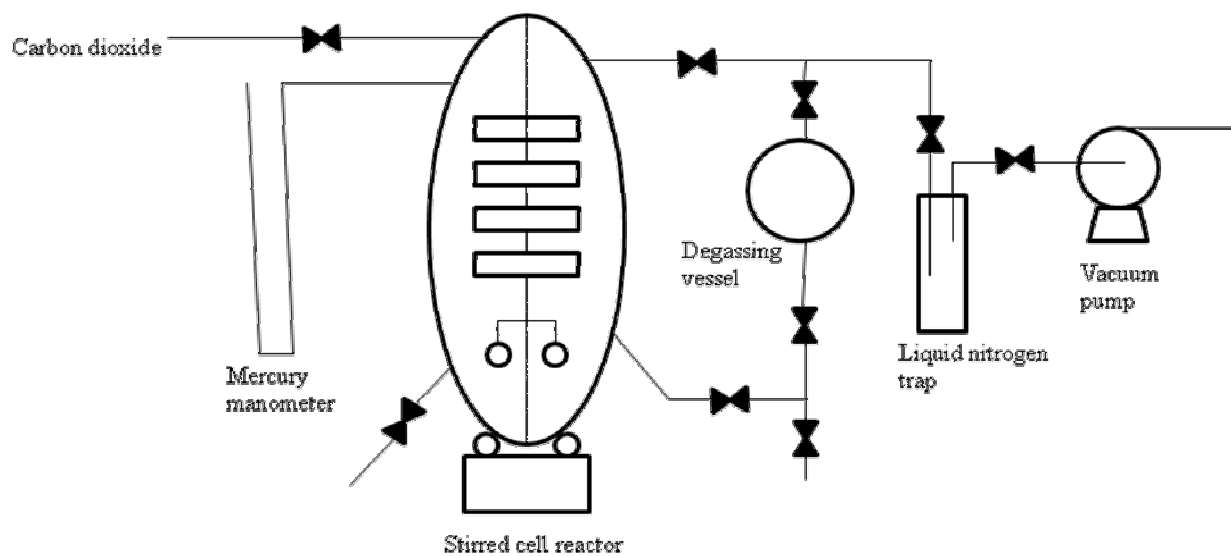
Figure 5: Schematic diagram of a stirred cell reactor.

This schematic diagram was redrawn from Blauwhoff *et al.* 1984.

Blauwhoff *et al.* (1984) measured the pressure decrease with time. The pressure decrease was due to the absorption of pure carbon dioxide by an amine (primary or secondary) at reduced absolute pressure and they used a closed stirred cell reactor. The reactor has an internal diameter of 10 cm and it was all glass. It was thermo-stated at 25 ^{o}C and it had a glass stirrer which was driven externally at 60 rpm. A mercury manometer was used to measure the absolute pressure in the reactor.

A degassing vessel was used to degas the freshly prepared solutions. The solutions were degassed under vacuum. After the degassing process, the solution was then fed into the reactor under vacuum. Establishment of vapour-liquid equilibrium was allowed for and the pressure reading was then taken. The measured pressure P_{H_2O} was used to get the actual P_{CO_2} by:

$$P_{CO_2} = P_{total} - P_{H_2O} \qquad (2.42)$$

During the experiment, the decrease in P_{CO_2} caused an increase in the infinite enhancement factor, E_i which is defined as follows:

$$E_i = \sqrt{\frac{D_{CO_2}}{D_{Am}}} + \sqrt{\frac{D_{Am}}{D_{CO_2}}} \left\{ \frac{[Am]RT}{v_{CO_2} P_{CO_2} m_{CO_2}} \right\} \qquad (2.43)$$

Pressure versus time readings in the region where $2 < Ha \ll E_i$ is met were used to obtain the overall reaction rate constant where Ha is the Hatta number which is defined as follows:

$$Ha = \frac{\sqrt{k_{ov}.D_{CO_2}}}{k_l} \qquad (2.44)$$

For a closed reactor with a gas volume of V_g, the pressure-time is as follow:

$$\ln P_{CO_2}(time = t) = -\frac{m_{CO_2}.A}{V_g}.\sqrt{k_{ov}D_{CO_2}}t + \ln P_{CO_2}(time = o) \qquad (2.45)$$

The overall reaction rate constant was then determined from the slope of the ln P_{CO_2} versus time graph in the region where $2 < Ha \ll E_i$.

2.4.1.4 Stopped-flow technique

A schematic diagram of a stopped-flow technique is shown in figure 6.

24
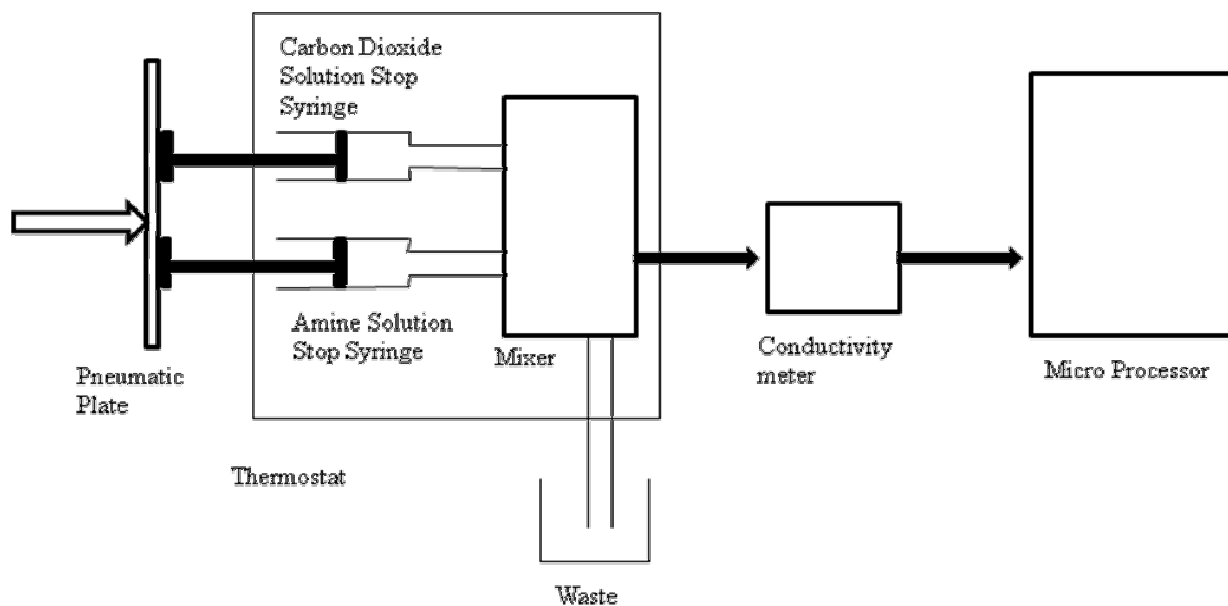
Figure 6: Schematic diagram of stopped-flow equipment

Figure 6 was redrawn from Henni *et al*. 2008.

The stopped flow technique is a direct method which does not involve gas absorption such that the experimental findings are fundamental homogeneous reaction rates of solutions (Li *et al.,* 2007; Henni *et al*., 2008). This direct method eliminates the errors that are usually caused by the depletion of the alkanolamine at the gas-liquid interface (Li *et al.,* 2007; Henni *et al*., 2008).

The following experimental procedure was according to Henni *et al*. (2008). This experimental setup consisted of a sample handling unit which was made of stainless steel, a conductivity-detection cell, an analogue to digital converter and a microprocessor. The sample handling unit provided support for the sample flow unit. There was a mode selector in the front panel of the sample handling unit. This mode selector included pneumatic push plates, a display for air pressure and temperature. Solutions of both the amine and CO_2 were pushed in equal volumes to the observation cell in sealed drive syringes. The pneumatic push plates were used to control waste or stop valve from the software. The valve moved to the waste position and emptied the stop syringe automatically when taking the sample measurement. This valve then returned to the drive position and the fresh solution was pushed by the pneumatic push plates to the observation cell. In this way, the old solution from the previous run was replaced.

As the reaction progressed, ion formation was monitored by the conductivity cell as a function of time. The ion formation initiated a change in voltage in the conductivity cell and this voltage output was directly proportional to the conductivity of the solution. Based on the output voltage readings, the microprocessor generated the observed pseudo-first-order constant.

2.4.2 Reaction kinetic data reported in literature

Table 1 shows the reaction kinetic data for the reaction of carbon dioxide and monoethanolamine available in literature. All the data in table 1 were obtained by using the laminar jet absorber. In the table 1, temperatures at which the experiments were conducted, and the concentrations or concentration ranges of the monoethanolamine are shown. The table also shows the various reaction-rate constants.

Table 1: Reaction kinetics of carbon dioxide and aqueous MEA obtained using a laminar jet absorber at different temperatures.

T (K)	[MEA] (mol/dm^3)	k (dm^3/mol.s)	Reference
294.5	0.25-2.0	5400	Astarita (1961)
298	1.6-4.8	7500	Clarke (1964)
298	1.0	6970	Sharma (1965)
303	1.0	9700	Sharma (1965)
291	1.0	5100	Danckwerts *and* Sharma (1966)
298	1.0	7600	Danckwerts *and* Sharma (1966)
308	1.0	13000	Danckwerts *and* Sharma (1966)
298	0.2-1.9	7140	Sada *et al.* (1976a)
298	0.2-1.9	8400	Sada *et al.* (1976a)
313	-	10090	Hagewiesche *et al.* (1995)

Data from Aboudheir et al, 2003.

Table 2 shows the reaction kinetics data obtained using the wetted wall column technique.

26

Table 2: Reaction kinetics of carbon dioxide and aqueous MEA obtained using a wetted wall column at different temperatures.

T (K)	[MEA] (mol/dm³)	k (dm³/mol.s)	Reference
298	0.1-2.0	5400	Emmert *and* Pigrord (1962)
293	0.2-2.0	4300	Alvarez-Fuster *et al.* (1980)
303	0.1-0.4	4774	Xiao *et al.* (2000)
308	0.1-0.4	7618	Xiao *et al.* (2000)
313	0.1-0.4	11743	Xiao *et al.* (2000)
303-313	0.1-0.5	$3.014 * 10^{11} \exp(-5376.2/T)$	Horng *and* Li (2002)

Data from Aboudheir et al., 2003.

Table 3 shows the reaction kinetics data obtained using the stirred cell reactor technique.

Table 3: Reaction kinetics of carbon dioxide and aqueous MEA obtained using a stirred cell reactor at different temperatures.

T (K)	[MEA] (mol/dm³)	k (dm³/mol.s)	Reference
353	-	90400	Leder (1971)
298	0.49-1.71	5870	Laddha *and* Danckwerts (1981)
303	0.5-2.0	7740	Sada *et al.* (1985)
318	0-3.2	10400	Little *et al.* (1992)
333	0-3.2	25700	Little *et al.* (1992)

Data from Aboudheir et al., 2003.

Table 4 shows the reaction kinetics data obtained using the stopped flow method.

Table 4: Reaction kinetics of carbon dioxide and aqueous MEA obtained using the stopped flow method at different temperatures.

T (K)	[MEA] (mol/dm^3)	k (dm^3/mol.s)	Reference
278-303	0-0.06	$1.23*10^{11}\exp(-5078/T)$	Penny *and* Ritter (1983)
293	0.02-0.05	3600	Barth *et al.* (1986)
298	0.02-0.05	4700	Barth *et al.* (1986)
298	0.02-0.06	3880	Crooks *and* Donnellan (1989)
278-298	0-0.45	$8.51*10^{11}\exp(-5617/T)$	Alper (1990)

Data from Aboudheir et al., 2003.

2.4.3 Comparison of Literature Data

It is worthwhile to note that Hagewiesche *et al.* (1995) in table 1 and Little *et al.* (1992) in table 3 carried out their kinetic studies and they were interpreted by using numerically solved absorption models. All the remaining absorptive reaction kinetic studies were analysed by utilising the gas absorption methodology with pseudo first-order reaction kinetics. This was used in conjunction with penetration theory equations that Danckwerts (1970) developed. Interpreting the reaction kinetics data by utilising a numerically solved absorption model is the best way for reliable reaction kinetics data to be obtained. (Littel *et al.*, 1992; Rinker *et al.*, 1996; Versteeg *et al.*, 1996; Aboudheir *et al.*, 2003).

Hikita *et al.* (1977, 1979) and Donaldson *and* Nguyen (1980) conducted their kinetics studies using the rapid mixing method and the membranes method respectively. Horng *and* Li (2002) carried out kinetic studies using a temperature range of 303-313 K while Hikita *et al.* (1977), Ritter (1983) *and* Alper (1990) carried out the kinetic studies in the temperature range of 278-308 K. All the other experimental works in tables 1 to 4 were carried out at a single temperature. Extrapolation for simple kinetic models cannot be done with assurance for concentration and temperature ranges that are outside where the kinetic data were acquired (Aboudheir *et al.*, 2003).

Figure 7 is a graph of the reported reaction rate constants (k) at different temperatures and for different experimental techniques that were used to obtain the reaction rate constants.
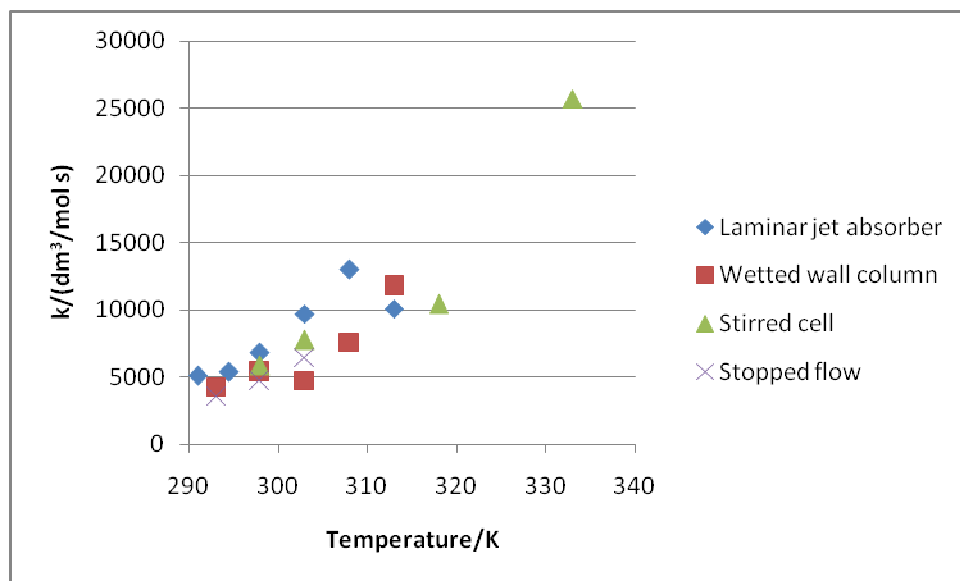
Figure 7: Literature data for reaction rate constants obtained at various temperatures and when using different experimental techniques.

At 298 K, the reported reaction rate constant (k) varies from 3880 dm^3/mol.s to 8400 dm^3/mol.s (tables 1 to 4 and figure 7). The wide range of the reaction rate constants can be explained by the pseudo-first order reaction assumption as well as the interfacial turbulence in some of the absorbers. Another possible explanation as to why the reaction rate constant range was very high is the existence of uncertainties in the physical properties (Aboudheir et al., 2003).

From figure 7, it can also be seen that the reaction rate constants generally increased with temperature as expected and that the reaction rate constants differed for each and every experimental technique that was used. The reported reaction rate constants obtained using the laminar jet absorber over a temperature range of 291 to 313 K are generally greater than the ones obtained using the wetted wall column, stirred cell reactor and stopped flow technique.

The kinetics experiments needed to be conducted within the typical temperature ranges of 293 to 333 K that are found in industrial absorbers. The experimental data would then be interpreted with the aid of numerically solved absorption model. This absorption model considers all the reversible reactions of monoethanolamine and carbon dioxide that could possibly take place. The system's chemical and physical properties have to be approximated

29

as functions of monoethanolamine concentration, temperature and carbon dioxide loading. These properties would then be used to interpret the absorption data (Aboudheir *et al.*, 2003).

2.4.3.1 Reaction kinetics according to the zwitterion mechanism

The experimental results of Aboudheir *et al.* (2003) of the apparent reaction-rate constants are in accord with literature (Littel *et al.*, 1992). They exhibit a defined temperature dependence of the overall reaction rate for all of the different temperatures studied. This shows that the rate determining step is likely to be the zwitterion formation step. The zwitterion mechanism was then used to interpret the experimental data considering all the bases' contribution to the zwitterion deprotonation. The zwitterion mechanism that was used was derived from the following general rate of zwitterion formation: (Aboudheir *et al..,* 2003)

$$r_{CO_2-MEA} = \frac{[CO_2][RNH_2] - k_r/k_f[RNHCOO^-](\sum k_{-b}[BH^+]/\sum k_b[B]}{1/k_f + (k_r/k_f \sum k_b[B]}$$
(2.46)

The reversibility of the deprotonation reactions was neglected since these reactions were instantaneous and fast. The apparent reaction rate constant expression of the zwitterion mechanism can then be represented as follows (Aboudheir *et al.,* 2003):

$$k_{app} = \frac{k_f[RNH_2]}{1 + (k_f/(k_{RNH_2}[RNH_2] + k_{H_2O}[H_2O] + k_{OH^-}[OH^-] + k_{HCO_{33}^-}[HCO_3^-] + k_{CO_3^-}[CO_3^-]))}$$
(2.47)

If the second term of the denominator $<< 1$, then:

$$k_{app} = k_f[RNH_2] \text{ And,}$$
(2.48)

$$r_{CO_2-MEA} = k_f[RNH_2][CO_2]$$
(2.49)

In the case for carbon dioxide and monoethanolamine system, this mechanism was previously assumed in literature (Blauwhoff *et al.*, 1984; Versteeg *et al.*, 1996; Aboudheir *et al.*, 2003).

30

The mechanism was proved to be valid for temperatures from 293 to 313 K and at low carbon dioxide and monoethanolamine concentrations.

If the second term of the denominator is >> 1, then:

$$k_{app} = (k_{RNH_2}[RNH_2] + k_{H_2O}[H_2O] + k_{OH^-}[OH^-] + k_{HCO_3^-}[HCO_3^-] + k_{CO_3^-}[CO_3^-])[RNH_2]$$

(2.50)

Linear regression analysis has been carried out to fit the experimentally found k_{app} values to the zwitterion mechanism and only k_{RNH_2} and k_{H_2O} fitted the experimental data optimally. This implies that only the alkanolamine and water were responsible for the completion of the zwitterion deprotonation. This also implies that the carbonate, hydroxyl and bicarbonate ions did not take part in the zwitterion deprotonation (Aboudheir *et al.*, 2003).

2.4.3.2 Reaction kinetics according to the termolecular mechanism

The termolecular reaction mechanism has the apparent reaction constant as follows:

$$k_{app} = k_{RNH_2}[RNH_2]^2 + k_{H_2O}[H_2O][RNH_2]$$

(2.51)

This termolecular mechanism expression was used to fit all the experimentally determined k_{app} values. The obtained values of k_{RNH_2} and k_{H_2O} for the different temperatures are tabulated in table 5.

Table 5: Reaction rate constants of monoethanolamine and water at different temperatures.

Temperature (K)	k_{RNH_2} (dm^6/mol^{2}s)	k_{H_2O} (dm^6/mol^{2}s)	AAD% in k_{app}
293	1372	56.3	16.8
303	2022	108.7	9.4
313	3542	129.7	12.6
323	5784	122.1	22.3
333	7767	287.1	15.5

Data from Aboudheir et al., 2003.

Also shown in table 5 are the average absolute deviation (AAD %) values between the fitted model and the experimental results. Aboudheir *et al.* (2003) reported that all the experimental kinetics data of their work were fitted and the ADD% was less than 22.3%. Based on the termolecular reaction mechanism, the following kinetic expressions were found from linear regression analysis of the data in table 5 (Aboudheir *et al.*, 2003):

$$k_{H_2O} = 4.55*10^6 \exp\left(\frac{-3287}{T}\right) \text{ and} \tag{2.52}$$

$$k_{RNH_2} = 4.61*10^9 \exp\left(\frac{-4412}{T}\right) \tag{2.53}$$

The reaction of the absorbed carbon dioxide into solutions of monoethanolamine can be represented by the following reversible reaction rate expression (Aboudheir *et al.*, 2003):

$$r_{CO_2-MEA} = -(k_{RNH_2}[RNH_2] + k_{H_2O}[H_2O]*([RNH_2][CO_2] + \frac{1}{K_{RNH_2}}[RNHCOO^-][H_3O^+])$$

$$\tag{2.54}$$

Where K_{RNH_2} is the carbamate formation reaction equilibrium constant. This expression is based on the found reaction-rate constants and the termolecular mechanism. Table 6 shows the values of k_{RNH_2} and k_{H_2O} that were obtained at 298 K for the absorption of carbon dioxide into solutions of monoethanolamine based on the termolecular reaction mechanism.

Table 6: Values of k_{RNH_2} and k_{H_2O} obtained at 298 based on the termolecular reaction mechanism.

k_{RNH_2} (dm^6/mol^{2}s)	k_{H_2O} (dm^6/mol^{2}s)	Reference
52600	24	Crooks *and* Donnellan (1989)
1713	73.7	Aboudheir *et al.* (2003)

Data from Aboudheir et al., 2003.

The values shown in table 6 are not comparable. The data reported by Crooks *and* Donnellan (1989) is believed to be incorrect because their experimental k_{app} data do not agree with the data that was published by Hikita *et al.* (1979) and Laddha *and* Danckwerts (1981). After applying regression analysis, the Crooks *and* Donnellan (1989) k_{app} data showed that the order of reaction in monoethanolamine concentration is 1.6. This value is not in agreement with the order of reaction with respect to monoethanolamine of 1 that has been published in literature for the concentration ranges shown in tables 1 to 4 and at a temperature of 298 K (Tables 1 to 4). Also, the k_{app} data could not be predicted by the model by Crooks *and* Donnellan (1989)'s model and its reaction rate parameters but these experimental data agreed with those predicted in the work of Aboudheir *et al.* (2003)

2.4.4 Conclusion

As has been discussed in section 2.4.3, there is a wide range of reported reaction rate constants in literature. For instance, the reported reaction rate constants at 298 K varied from 3880 to 8400 dm^3/mol.s. According to Aboudheir *et al.* (2003), these discrepancies might have been as a result of assuming pseudo-first order reaction kinetics and also that this was because of turbulence in some of the absorbers. They also reported that these discrepancies might have been caused by the inability to determine accurate contact areas between the liquid and the gas in the absorbers.

This work seeks to address these discrepancies. This will be achieved by studying the homogeneous reaction kinetics of the reaction between aqueous solutions of CO_2 and MEA. In this work, the CO_2 will first be dissolved in distilled water after degassing it by boiling it and bubbling nitrogen gas through it. This means there will not be absorptive reaction

kinetics in this work so there will not be inaccurate determination of the contact areas between the gas and liquid as was pointed out by Aboudheir *et al. (*2003).

Most of the kinetic data have been obtained at one temperature (table 1 to 4). The experimental work for this work will be carried out over a temperature range of 298 to 313 K. This is due to the fact that one cannot do extrapolation with confidence for simple kinetic models out of the temperature range in which the kinetic data were obtained.

The reaction between aqueous solutions CO_2 and MEA will be assumed to proceed via the zwitterion. This is because MEA is a primary alkanolamine and as has been discussed in section 2.1.1, primary and secondary alkanolamines react directly with CO_2 to form stable carbamates through the zwitterion mechanism (Ramachandran *et al.*, 2006; Horng and Li, 2002). This mechanism has been successfully used for aqueous alkanolamine solutions as well as in organic solutions (Blauwhoff *et al.*, 1984; Barth *et al.*, 1984; Alvarez-Fuster *et al.*, 1980; Alvarez-Fuster *et al.*, 1981; Sada *et al.*, 1985; Versteg *and* Swaaij, 1988).

CHAPTER 3: MATERIALS AND METHODS

This chapter describes the experimental methods and procedures used to study the reaction kinetics of the reaction between an aqueous solution of carbon dioxide (CO_2) and monoethanolamine (MEA) in detail. The first section of this chapter is dedicated to give full details of the experimental set-up and equipment that were used to carry out this research project. In this section, the reactor type, reactor feed system and analytical methods will be discussed. The second section is the materials section. All the materials that have been used in this project will be discussed in this section. The experimental procedures are fully described in the third section. This section shows how all the reactants were charged into the reactor. It also shows how the conductivity, mass and temperature measurements were done.

3.1 Experimental Set-up

The schematic diagram and the picture of the experimental set-up are shown in figure 8. The discussion of the experimental set-up is divided into three sections which are the reactor configuration, feed and analysis sections.
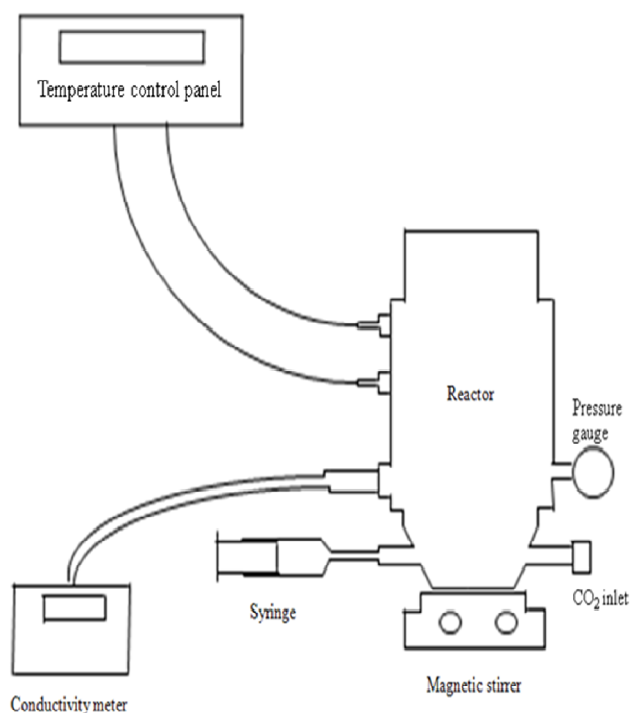
Figure 8: Schematic diagram and picture of the experimental set-up

35

3.1.1 Reactor configuration

This section consisted of a cylindrical batch reactor made of stainless steel grade 316 (see figure 8). Due to the corrosive nature of MEA, stainless steel was selected as the material of construction. The stainless steel was supplied by Macsteel VRN Cape Town, Republic of South Africa. The reactor had an internal diameter of 100 mm, a height of 200 mm and a wall thickness of 2 mm. The total volume of the reactor was 1L. The reactor had two inlets for feeding the MEA and CO_2.

The reactor had a piston that sat on top of the reacting solution. This piston was stopped from coming out of the reactor by a stopper that was screwed on top of the reactor. The piston was made of stainless steel, grade 316. A silicon rubber lip seal was tightly fitted around the piston so that no carbon dioxide could leak out of the reactor and no atmospheric air could enter the reactor. To test whether there was any carbon dioxide leakages water was poured on top of the reactor and no bubbles were noticed. This meant that no carbon dioxide escaped into the atmosphere. The silicon rubber lip seal had dimensions of 100 mm diameter and 10 mm depth. This silicon rubber lip seal was supplied by IMAC Hydraulics Somerset West, Republic of South Africa. There was a pressure relief valve fitted on top of the piston. This pressure relief valve could be opened to allow some of the carbon dioxide to escape into the atmosphere in case the pressure in the reactor built up. However, this pressure relief valve was never opened during the loading of carbon dioxide into the reactor. This is because carbon dioxide was fed into the reactor in very small amounts and as a result of this; there was no need to open the pressure relief. A pressure gauge was fitted on the reactor so as to measure and monitor the pressure inside the reactor.

The reaction mixture was stirred by a Stuart magnetic stirrer and a stirring rod which was 30 mm in length and 6 mm in diameter. The magnetic stirrer was always set at a stirring speed of 750 rpm for all experiments carried out. This magnetic stirrer was a model CB162 which had good temperature and chemical resistance.

A heating jacket that was fitted around the surface of the reactor was used to heat the reactor contents to the desired reaction temperature. This heating jacket had a power rating of 500 W and it had a diameter of 115 mm and it was 150 mm long. It was supplied by UNITEMP Cape Town, Republic of South Africa.

3.1.2 Feed section

The reactants were fed into the reactor through two inlets; one for MEA and the other one for CO_2. These two inlets were on the side walls of the reactor and they were directly opposite each other. They were positioned at the bottom of the reactor so that the reactants could be fed directly into the well mixed reaction zone. The MEA was fed into reactor using a 10 ml gas tight syringe which was supplied by Hamilton-Bonaduz, Schweiz, Switzerland.

The CO_2 gas was fed into the reactor using a gas bomb system (Figure 9). The picture of the gas bomb is also shown in figure 9. The procedure for filling the 50 ml CO_2 sample cylinder (304L-HDF4-50) is found in section 3.4.1.
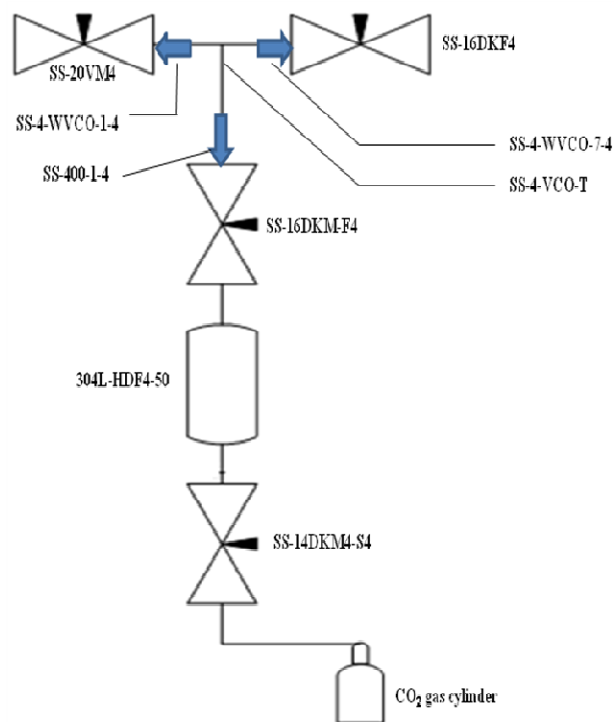
Figure 9: Schematic diagram and picture of CO_2 feed system

The CO_2 feed system comprised of four needle valves and fittings. The description of the types and specifications of the valves and fittings used are shown in appendix I. The rationale

behind the choice of the valves used and their respective positions is also shown in appendix I.

3.1.3 Analysis of reaction progression section

This section comprised a Pico Technology data logger, two conductivity meters (a Lab 960 laboratory conductivity meter and an EC 215 conductivity meter) with their standard conductivity cells and an electronic balance. The Pico Technology data logger was used to measure the conductivity and the temperature of the reaction solution while the Lab 960 conductivity meter and its standard conductivity cell were used to calibrate the Pico Technology data logger.

The Lab 960 conductivity meter was manufactured by Schott Instruments GmbH, Germany and its conductivity cell had a cell constant of 0.475 cm^{-1}. This conductivity meter (Lab 960) had a conductivity measuring range of 1 µS/cm to 2 S/cm and a temperature measuring range of -5 to 80 ^{o}C.

Conductivity was chosen as the analytical technique for this work because the progression of the reaction between aqueous solutions of CO_2 and MEA could be monitored with time. In other words, real time data could be generated using conductivity thus continuous concentration profiles of CO_2 and MEA could be generated. By using conductivity, both the concentrations of CO_2 and MEA could be determined at any particular instant.

Conductivity was also chosen because the Pico Technology data logger recorded the conductivity readings at a 10 ms interval. It was for this reason that the Pico Technology data logger was chosen since the reaction of between CO_2 and MEA is very fast and instantaneous.

It is also important to note that the kinetic data generated from conductivity measurements can be easily converted to CO_2 and MEA conversion data. The details of generating conversion data from conductivity measurements are shown in chapter 4. Once one has these conversion data, the reaction rate constants could be easily determined by utilising MATLAB as has been described in chapter 5.

3.1.3.1 Conductivity meter technical data

The technical data of the conductivity meter is presented in table 7. The conductivity and temperature measuring ranges as well as their resolution were shown in table 7.

Table 7: Technical data of the Lab 960 conductivity meter.

Variable	Measuring range	Resolution
Conductivity (µS/cm)	0.000 to 1.999	0.001
	0.00 to 19.99	0.01
	0.0 to 199.9	0.1
	0 to 1999	1
Conductivity (mS/cm)	0.00 to 19.99	0.01
	0.0 to 199.9	0.1
	0 to 500	1
Temperature (^{o}C)	-5.0 to +120.0	0.1

Data from Laboratory conductivity meter Lab 960 operating manual

3.1.3.2 Cell constant determination (Calibration)

The cell constant changes slightly due to aging and as a result of this, an inexact reading will be displayed on the meter. The conductivity meter was calibrated at regular intervals and the calibration process determined the up-to-date cell constant and this value was stored in the instrument. The cell constant could be set manually in the range of 0.250 to 2.500 cm^{-1} or 0.090 to 0.110 cm^{-1}. It could also be determined automatically in the following ranges: 0.450 to 0.500 cm^{-1}, 0.585 to 0.715 cm^{-1}, or 0.800 to 1.200 cm^{-1}. This was done by calibration using a 0.01mol/L KCl control standard. This method could only be used for measuring cells with cell constants in the above mentioned ranges. The conductivity cell had a cell constant of 0.475 cm^{-1} so the method of automatically determining the cell constant was used. The calibration procedure which was adapted from the manual of the Lab 960 conductivity meter is shown in appendix J.

3.1.3.3 Conductivity temperature compensation

A reference temperature of 25 ^{o}C was used as the basis for the calculation of the temperature compensation. One could choose between linear compensation with the coefficient being adjustable in the range of 0.001 to 3.000 %/K or nonlinear compensation according to DIN 38404 or EN 27888. According to the application tips shown in table 8, a linear temperature coefficient of 0.001 to 3.000 %/K was selected and set.

Table 8: Application tips for the Lab 960 conductivity meter.

Test sample	Temperature compensation
Ultrapure water	According to DIN 38404 EN 27 888
Natural water (surface, drinking, ground water)	According to DIN 38404 EN 27 888
Other aqueous solutions	Linear temperature coefficient (0.001 to 3.000 %/K)

Data from Laboratory conductivity meter Lab 960 operating manual

3.1.3.4 Calibration of the Pico Technology Data Logger

The data logger was calibrated using the Lab 960 laboratory conductivity meter. Aqueous solutions of potassium iodide (KI) were prepared. These solutions had different conductivities. The conductivity meter probe was connected to the Lab 960 laboratory conductivity meter. The probe was then dipped into each of the solutions and the respective conductivities of the solutions were recorded. The probe was then connected to the data logger and the conductivities of the solutions were measured. The conductivity meter probe was cleaned with degassed distilled water before a new conductivity reading was taken. All the conductivity readings were taken at the same temperature of 298 K. A water bath was used to maintain the temperatures of the solutions at 298 K. Table 9 shows the various conductivity readings that were recorded.

40

Table 9: Calibration data for the Pico Technology Data Logger

Solution	Actual conductivity/(μS/cm)	Measured conductivity/(μS/cm)
1	38	138
2	83	174
3	388	436
4	445	470
5	532	540
6	563	563
7	604	592
8	802	739
9	1195	975
10	1319	1027
11	1584	1213
12	1727	1236
13	1914	1321
14	2150	1457
15	2430	1556
16	2550	1565
17	2690	1618
18	2780	1664
19	2980	1742

The measured conductivity readings were plotted against the actual values and figure 10 shows the plot of measured values against the actual values.
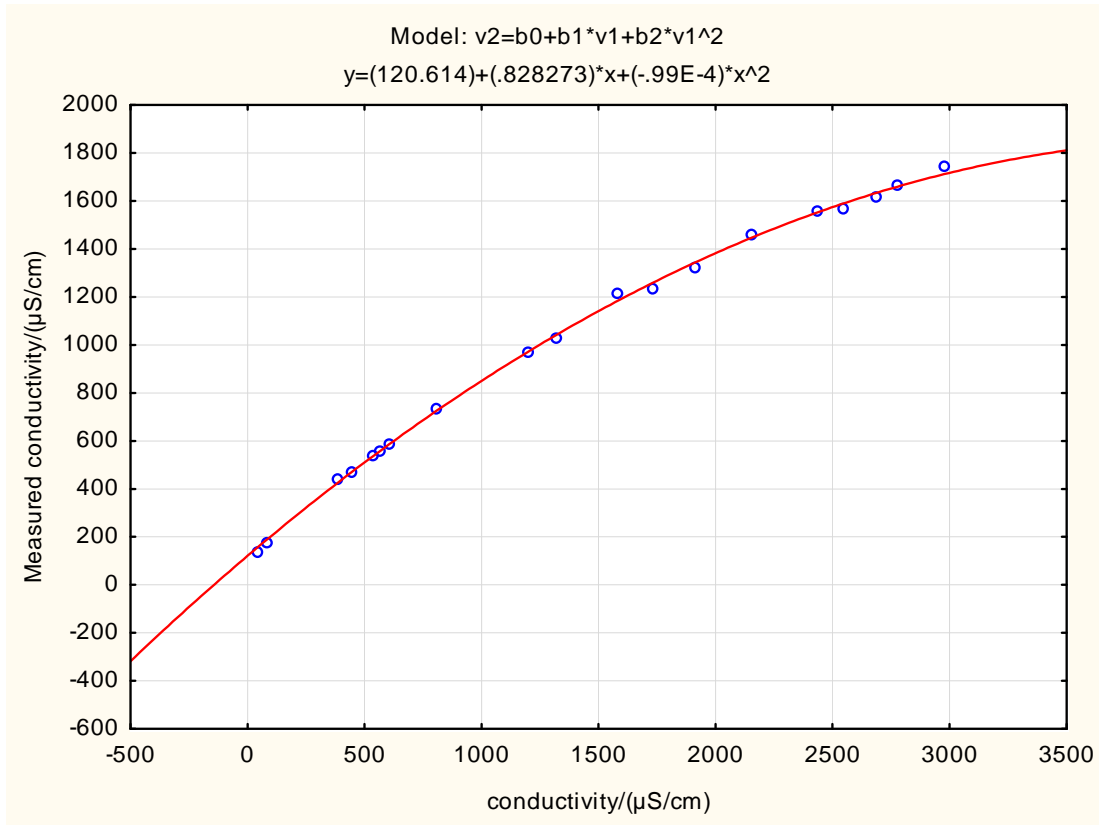
Figure 10: Calibration curve for the Pico Technology data logger

For fig 10, the root mean square errors (RMSE) for the regression were calculated and then bootstrap confidence intervals for the RMSE were determined. RMSE is the square root of the mean of the squared residuals. The MSE was found to be 16.14 and the confidence limits were found to be 13.47 and 22.47. This means that one can say with 95% confidence that the MSE lies between 13.47 and 22.47.

From figure 10, it can be seen that the conductivity readings that were read on the Lab 960 conductivity meter were almost the same as the ones read using the data logger. The data logger calibration process was necessary since a relationship between the conductivity readings obtained using the Lab 960 conductivity meter and the data logger had to be established. After the calibration process, the conductivity readings read on the Lab 960 conductivity meter were the same as the ones read on the data logger.

3.1.3.5 Mass measurement equipment

The mass of the gas bomb was measured using an electronic balance which was developed, manufactured and tested by Precisa Gravimetrics AG Dietikon, Switzerland. The electronic balance had the following specifications:

Make: Precisa

: 360 EP

Model: EP2220M

Capacity: 2220 g

Minimum: 0.1 g

Graduations: 0.001 g

3.1.3.6 Calibration of the electronic balance

The instrument calibration process was carried out using standards weights of known values and it was done at ambient conditions. These standard weights were traceable to the National Standard. The calibration results are presented in tables 10 and 11.

Table 10: Repeatability test for the electronic balance

Repeatability: Load Applied: 1000.00 g Settling Time: 4s	Accuracy and Linearity:		
	Load Applied/g	Before Adjustment/g	After Adjustment/g
999.992	2000.000	2000.777	2000.022
999.991	1500.000	1500.570	1500.005
999.990	1000.000	1000.372	999.996
999.990	500.000	500.187	500.000
999.989	200.000	200.076	199.997
999.990	100.000	100.039	99.998
Standard Deviation: 0.00103			

Table 11: Determination of eccentric error in mass measurements using the electronic balance

Eccentric Error:		
Applied Load: 700.000 g		

	Readings/g
2 3 1 4 5	1: 699.993
	2: 699.996
	3: 699.997
	4: 699.995
	5: 699.992
Maximum Error: 0.008 g	

Table 11 shows the value of the eccentric error that was obtained when a 700.000 g load was placed on the electronic balance. This eccentric error is the change in measurement readings when the 700.000 g load was placed on various positions (positions that are numbered 1, 2, 3, 4, and 5) on the weighing pan of the electronic balance. Also shown in table 11 are the different mass readings that were read for the various positions were the 700.000 g load was placed.

The uncertainty of measurement was +/-0.060 g. It was calculated and measured in accordance with the International Bureau of Weights and Measures (BIPM), International Electro technical Commission (IEC), International Organization for Standardization (ISO), International Union of Pure and Applied Physics (IUPAP), International Organization of Legal Metrology (OIML) document. This document is entitled "Guide to the Expression of Uncertainty in Measurement". The uncertainty of measurement was based on a standard uncertainty multiplied by a coverage factor $k = 2$ which, unless specifically stated otherwise, provided a level of confidence of approximately 95%.

The calibration values indicated in tables 10 and 11 were correct at the time of calibration. The accuracy depended on such factors as the care exercised in handling and the use of the balance as well as the frequency of use. The balance had to be re-calibrated after a period of six months to ensure that its accuracy remained within the desired limits.

3.2 Materials

The MEA that was used throughout all the experimental work was of a reagent grade with a purity of greater than 99%. It had a specific gravity and molecular weight of 1.012 and 61.08 g/mol respectively. It was purchased from Sigma-Aldrich CHEMIE GmbH, Steinheim, Germany. The MEA was used without any further purification. The CO_2 cylinder was supplied by African Oxygen Limited (Afrox) Cape Town, Republic of South Africa. Distilled water was used to prepare all the reaction solutions. The NaOH that was used in conductometric titrations was supplied by Merck (Pty) Ltd., Gauteng, South Africa. The physical and chemical properties of MEA, CO_2 and NaOH are shown in appendix A.

3.3 Experimental Plan

The experimental plan was prepared with the objective of highlighting the experimental work that was carried out. This experimental plan shows the different runs that were carried out as well as the process variables. The reaction kinetics experiments were carried out while varying the following process variables:

- MEA concentration
- CO_2 concentration
- Temperature

The experiments were carried out over a temperature range 298 to 313 K and the MEA concentrations were over the range of 0.0199 to 0.261 mol/L. The experiments were carried out for seven different MEA concentrations for each temperature setting. The experimental work was divided into two series. The first one was where the concentration of MEA was maintained in excess whereas CO_2 was in excess in the second series.

3.3.1 First Series of Experiments: Excess MEA

The ratio of MEA concentrations to that of CO_2 were always greater than 10 for any run. This ensured pseudo-first-order conditions with respect to carbon dioxide concentration.

45

Experiments were repeated three times at each temperature for all concentrations resulting in a total of 84 runs. Table 12 summarises all the first series runs that were carried out

Table 12: Experimental plan for [MEA]: [CO_2]>10

Temperature/(K)	[MEA]/(mol/L)						
	0.0199	0.0496	0.0792	0.118	0.158	0.197	0.261
298	3 replicates	3 replicates	3 replicates	3 replicates	3 replicates	3 replicates	3 replicates
303	3 replicates	3 replicates	3 replicates	3 replicates	3 replicates	3 replicates	3 replicates
308	3 replicates	3 replicates	3 replicates	3 replicates	3 replicates	3 replicates	3 replicates
313	3 replicates	3 replicates	3 replicates	3 replicates	3 replicates	3 replicates	3 replicates

3.3.2 Second Series of Experiments: Excess CO_2

The ratio of MEA concentration to that of CO_2 was maintained at approximately 1:1. For these runs, low MEA concentrations were used and the MEA concentration range was from 0.0199 to 0.118 mol/L. The total number of runs for this series was 48. Table 13 summarises all the second series runs that were carried out

Table 13: Experimental plan for [MEA]: [CO_2] ≈1

Temperature/(K)	[MEA]/(mol/L)			
	0.0199	**0.0496**	**0.0792**	**0.118**
298	3 replicates	3 replicates	3 replicates	3 replicates
303	3 replicates	3 replicates	3 replicates	3 replicates
308	3 replicates	3 replicates	3 replicates	3 replicates
313	3 replicates	3 replicates	3 replicates	3 replicates

3.4 Experimental Procedure

3.4.1 Loading of the reactor

The experimental procedure is described in detail in this section. This section shows how CO_2 was loaded into the gas bomb and later into the reactor. Feeding of the MEA into the reactor is also described. It also shows how conductivity was used to follow the reaction kinetics of the reaction between aqueous solutions of CO_2 and MEA.

The reactor was initially charged with 0.5 L of distilled water which was first degassed by boiling and bubbling nitrogen gas through it. The reactor was then closed by pushing down the piston. The piston was pushed down until it reached the surface of the water. The pressure relief valve was then closed and finally the piston stopper was screwed on top of the reactor to prevent the piston from moving upwards as the CO_2 was added.

The next step was to add CO_2 into the reactor using the gas bomb shown in figure 8. The mass of an empty gas bomb was measured on an electronic balance and its mass was recorded. It was then connected to the CO_2 gas cylinder keeping both its inlet (SS-14DKM4-S4) and outlet (SS-16DKM-F4) valves closed. The valve on the gas cylinder was opened followed by the flow regulator. The SS-14DKM4-S4 valve was opened allowing the gas to enter the gas bomb. The CO_2 gas was allowed to enter the gas bomb for about 20 to 30

seconds after which both the SS-14DKM4-S4 and SS-16DKM-F4 valves were closed starting off with SS-16DKM-F4. The flow regulator and the valve on the gas cylinder were then closed. The gas bomb was then disconnected from the gas cylinder and it was weighed on a balance. The mass of the loaded gas bomb was then recorded and it was connected to the reactor. The reactor contents were being stirred as the CO_2 was being added to it.

The SS-16DKM-F4 valve was opened slightly and then quickly closed to allow a little amount of CO_2 out of the gas bomb. The SS-20VM4 valve, which is the valve that led the CO_2 into the reactor, was also opened slightly and quickly closed to allow a little amount of CO_2 to enter the reactor. The gas bomb was then disconnected and weighed and the mass of the discharged carbon dioxide was recorded. The CO_2 loading procedure was repeated until the desired amount of CO_2 had been fed to the reactor. As the CO_2 was being fed to the reactor, the conductivity of the solution was measured by the Lab 960 conductivity meter. The CO_2 was allowed to dissolve for about an hour. At that point, the Lab 960 conductivity meter showed a constant conductivity reading and the pressure reading on the pressure gauge was 0 Pa. This showed that all the CO_2 had dissolved.

After allowing enough time for CO_2 dissolution, the conductivity probe was disconnected from the Lab 960 conductivity meter and was then connected to the Pico Technology data logger. A gas tight syringe was then used to draw known volumes of MEA from its container. The MEA was then quickly injected into the reactor and the conductivity, time and temperature were recorded as the reaction was proceeding. The conductivity reading was being measured at 10 ms intervals. The pressure in the reactor was measured by a pressure gauge which was mounted on the side wall of the reactor. The same experimental procedure was used for all experiments carried out.

It was important to ensure that there were no losses of CO_2 from the time the gas bomb was loaded to the time its mass was measured after feeding the CO_2 into the reactor. To ensure that there were no CO_2 losses, Teflon threading was used when connecting all the fittings of the gas bomb. This ensured that no CO_2 escaped out of the gas bomb feed system. Checks for CO_2 leakages on the gas bombs were done. To check for the leakages, the gas bomb was filled with CO_2 and with both SS-14DKM4-S4 and SS-16DKM-F4 closed, the gas bomb was immersed in a bucket full of water. No air bubbles were observed and this meant that there were no leakages on the gas bomb.

It was also ensured that before the gas bomb was disconnected from the reactor, the pressure reading on the pressure gauge was 0 Pa. The valve SS-20VM4 was repeatedly opened and closed until there were no pressure spikes. This meant that all the CO_2 between valves SS-16DKM-F4 and SS-20VM4 was fed into the reactor.

3.4.2 Bound MEA Determination

The final extent of the reaction was determined using conductometric titrations. This method of analysis was used to determine the amount of MEA that reacted with CO_2 by the end of the reaction. For this titration, the titrant was NaOH which was standardised by using potassium hydrogen phthalate (molecular weight 204.22 g/mol) as the standard. A radiometer TIM 856 autotitrator was used for standardising the NaOH. The procedure that was used for standardising NaOH was described in appendix K.

The standardised NaOH reacted with the bound MEA to form MEA, water and sodium cations as shown in equation (3.1). This method of using conductometric titrations was adopted from Cummings *et al*. (1990).

$$(HOCH_2CH_2NH_3^+) + NaOH = HOCH_2CH_2NH_2 + H_2O + Na^+ \qquad (3.1)$$

The titration procedure that follows describes how the titrations were carried out.

Titration procedure for bound MEA determination

- Pipette 40 ml of the reaction product into a 100 ml measuring cylinder and place the cylinder in a water bath which must be maintained at the same temperature as the reaction product.

- Immerse a conductivity meter probe in the measuring cylinder.

- Add standardised NaOH drop-wise from a dispenser while stirring.

- Allow the conductivity meter reading to stabilise before you take the reading.

- Plot conductivity values against volume of NaOH.

- Use the first and last points on the curve to draw two tangents and take a volume reading where these two tangents meet. This value is the titre value.

Titration curves for the runs carried out are shown in appendices F and G. After determining the amount of the reacted MEA, the conversions of the limiting reagents were then calculated. CO_2 was the limiting reagent for the first series of experiments where the MEA to CO_2 molar ratio was always maintained at greater than 10 while MEA was the limiting reagent for all the second series runs where the MEA to CO_2 molar ratio was approximately 1.

CHAPTER 4: RESULTS AND DISCUSSION

In this chapter, the results of the experimental work carried out will be presented. To be presented first are the results of the failed preliminary studies. The results that were obtained using conductivity to follow the reaction kinetics of the reaction between aqueous solutions of CO_2 and MEA will then be presented. The latter results will be presented in the form of conductivity- and conversion-time profiles. Effects of both the concentrations of MEA and CO_2 and temperature on both conductivity and conversion will be shown and discussed.

4.1 Preliminary Studies

The first phase of the experimental work was to find a suitable solvent for the reaction between aqueous solutions of CO_2 and MEA. Solvent selection experiments were then carried out with acetone, acetonitrile and butanone as candidate solvents. MEA was made to react with benzoyl chloride to form a white precipitate. To test for the suitable solvent, 10 ml of benzoyl chloride were added to four different beakers. 2.5 ml of MEA were added to one of the beakers and a precipitate was allowed to form for 15 minutes. 10 ml of acetone, acetonitrile and butanone were added to remaining three beakers respectively. 2.5 ml of MEA were added to the beakers with acetone, acetonitrile and butanone and 15 minutes were allowed for precipitates to form. The results of the solvent selection experiments are shown in table 14.

Table 14: Results of the solvent selection experiments

Sample	Mass of empty beaker/g	Mass of beaker and precipitate/g	Mass of precipitate/g
Pure	17.56	20.43	2.87
Acetone	18.36	20.41	2.05
Acetonitrile	16.76	19.30	2.54
Butanone	16.81	19.74	2.93

It can be seen from table 14 that the masses of the precipitates formed when acetone, acetonitrile and butanone were used are 2.05 g, 2.54 g and 2.93 g respectively. The mass of the precipitate formed with butanone was the only one that was closer to the mass formed

when there was no solvent (pure sample). This suggested that the butanone did not take part in the reaction between benzoyl chloride and MEA. Butanone was then selected as the solvent for the reaction between aqueous solutions of CO_2 and MEA.

After having selected butanone as the solvent for the reaction, reproducibility tests were carried out. The solvent selection experimental procedure has been carried out as before but now varying the volumes of butanone. The volumes of butanone used were 5 ml, 10 ml and 15 ml. The reproducibility tests were carried out to see if the same amount of the precipitate was formed in different volumes of butanone. Table 15 shows the results obtained for the different butanone volumes used.

Table 15: Reproducibility tests for butanone as a solvent

Sample	Mass of empty beaker/g	Mass of beaker and precipitate/g	Mass of precipitate/g
Pure	17.11	20.02	2.91
5ml Butanone	18.39	21.27	2.88
10ml Butanone	16.72	19.63	2.91
15ml Butanone	16.76	19.66	2.90

The masses of the precipitates formed for the pure sample, 5 ml butanone, 10 ml butanone and 15 ml butanone samples are 2.91, 2.88, 2.91 and 2.90 g respectively. It can be concluded that the experiment is reproducible since a 2.93 g precipitate was obtained for a pure sample during the previous run.

More tests had to be carried out by introducing water in the experimental procedure. This was done because the aim of the main kinetic experiments was to determine the reaction kinetics of the reaction between aqueous solutions of CO_2 and MEA. Therefore, the same experimental procedure was followed as before but now adding water to the system. Water was added to butanone in the proportions that are shown in table 16.

Table 16: Proportions of volumes of butanone to water

Volume of butanone/ml	Volume of water/ml	Total volume/ml
15	0	15
10	5	15
5	10	15
0	15	15

After MEA was added to all the three beakers that had water added to them, no precipitate was formed. This meant that amine scavenging using benzoyl chloride could not be used for an aqueous system. An alternative experimental setup and analytical technique had to be used to follow the reaction between aqueous solutions CO_2 and MEA. It was at this point that a batch reactor in conjunction with the conductivity was chosen to be used to investigate the reaction kinetics.

4.2 Conductivity-Time Profiles

A typical conductivity versus time profile obtained from the experimental work is shown in figure 11. The rest of the conductivity-time profiles are shown in appendices B and C. Appendix B is for the first series of runs and appendix C is for the second series of runs.
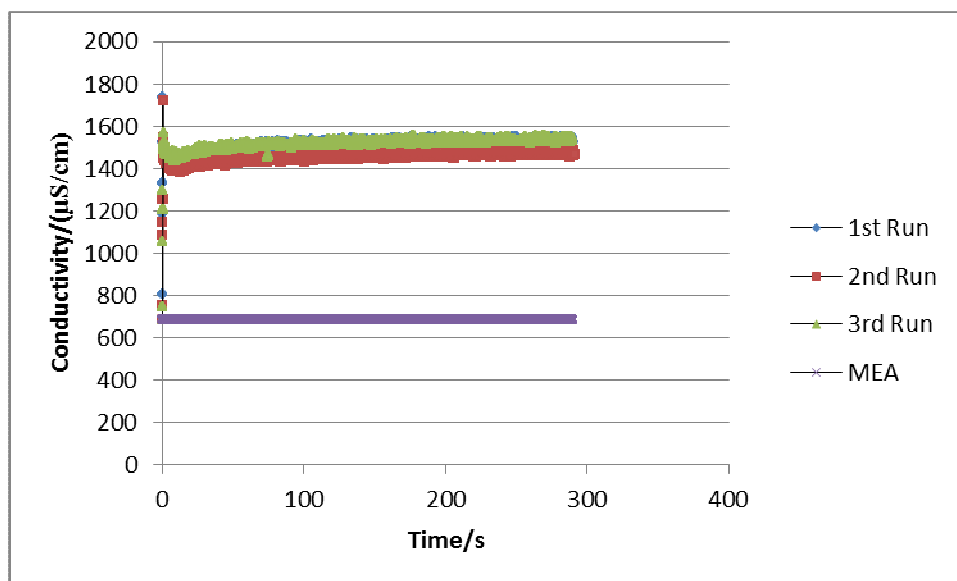
Figure 11: Conductivity-Time Profiles for [MEA] =0.207 mol/L, $[CO_2]_1$=0.0257 mol/L, $[CO_2]_2$=0.0245 mol/L and $[CO_2]_3$=0.0260 mol/L at 298 K

The conductivity of a 0.207 mol/L solution of MEA in distilled water is shown as the bottom curve in figure 11. This conductivity level was used as the reference point for the conductivity readings during the reaction. Also shown in figure 11 are the conductivity versus time curves for the three replicates of the experiment ([MEA] =0.207 mol/L; $[CO_2]$ =0.024 to 0.026 mol/L; T=298 K).

In figure 11 and in all the conductivity versus time profiles in appendices B and C, [MEA] =concentration of MEA, $[CO_2]_1$=concentration of CO_2 for the first replicate (that is shown as 1st run), $[CO_2]_2$= concentration of CO_2 for the second replicate (shown as 2nd run) and $[CO_2]_3$= concentration of CO_2 for the third replicate (shown as 3rd run).

In figure 11, the conductivity increases as the reaction is proceeding. This is because MEA reacts with CO_2 to form a carbamate, which is a salt. Salt solutions are known for having high conductivities due to the fact that they are ionic. The conductance of electric current is facilitated by the charge on the ions. As the reaction is taking place, more and more of the MEA and CO_2 react thus producing more ions that conduct electricity, thus resulting in the increase of the conductivity of the reaction mixture.

54

There are spikes in conductivity in the first 5 s of the conductivity-time profiles, as can be seen in figure 11 and all the graphs in appendices B and C. This might be due to the mixing time as the MEA was injected into the reactor. The MEA was injected close to the stirrer rod and this was also close to the conductivity meter probe. It could be that as the MEA was being added; perfect mixing was not achieved immediately at that particular time since MEA is a viscous liquid. As a result of this, there were some regions of high concentrations of MEA. This MEA then reacted with CO_2 thus resulting in the sharp increase in the conductivity readings. As the solution was becoming well mixed throughout the whole reactor, the conductivity decreased then started to increase with time as the overall reaction progressed until it flattens out. This flattening out showed that the reaction had reached equilibrium.

4.1.1 Effects of [MEA] and Temperature on Conductivity of MEA

The effects of the concentrations of both MEA and CO_2 and of temperature on conductivity will be shown in this section. First to be shown are the effects of temperature and MEA concentration on the conductivity of MEA in 0.5 L of distilled water. Lastly, the effects of temperature and effects of both MEA and CO_2 concentrations on the conductivity of the reaction solution will be presented.

Table 17 summarises the conductivities of MEA in 0.5 L for different MEA concentrations at different temperatures.

Table 17: MEA conductivities in µS/cm for different [MEA] and temperatures

[MEA]/(mol/L)	Temperature/(K)			
	298	303	308	313
0.0199	64	98	131	172
0.0496	210	261	301	357
0.0792	311	383	413	481
0.118	417	492	533	604
0.158	511	573	631	697
0.197	575	651	712	787
0.261	684	747	822	906

Figure 12 shows how the conductivity of MEA changes with changes in its concentration as well as with temperature changes.
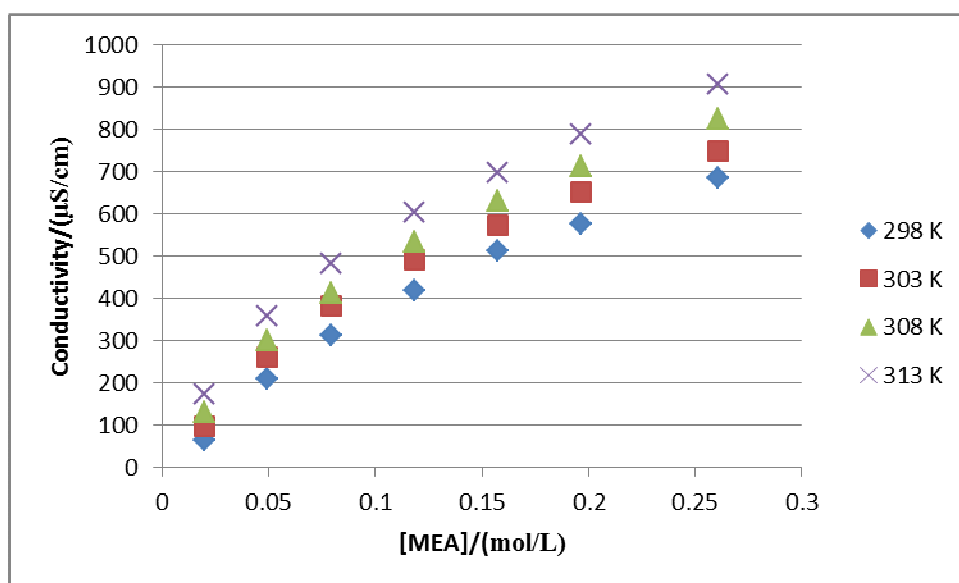
Figure 12: MEA conductivity for different [MEA] at different temperatures.

In table 17 and figure 12, it can be seen that the conductivity of MEA in 0.5 L of distilled water increases with increasing [MEA]. When a conductivity probe is immersed in a solution of MEA, a conductivity reading will be shown on the conductivity meter because of the lone

pair of electrons on the nitrogen atom of the MEA. As the concentration of MEA increases, the number of molecules of MEA also increases thus resulting in increased conductivity.

It can also be seen that the conductivity of MEA increases with increasing temperature. This is because as the temperature is increasing, the kinetic energy of the electrons also increases thus increasing the conductivity.

4.1.2 Effects of [MEA] and [CO_2] and Temperature on Conductivity

In this section, the effects of increasing the concentrations of both MEA and CO_2 will be shown. Figure 13 shows the conductivity-time profiles for [MEA] $=0.197$ mol/L, [CO_2]$_1$=0.0177 mol/L, [CO_2]$_2$=0.0189 mol/L and [CO_2]$_3$=0.0189 mol/L at 303 K.
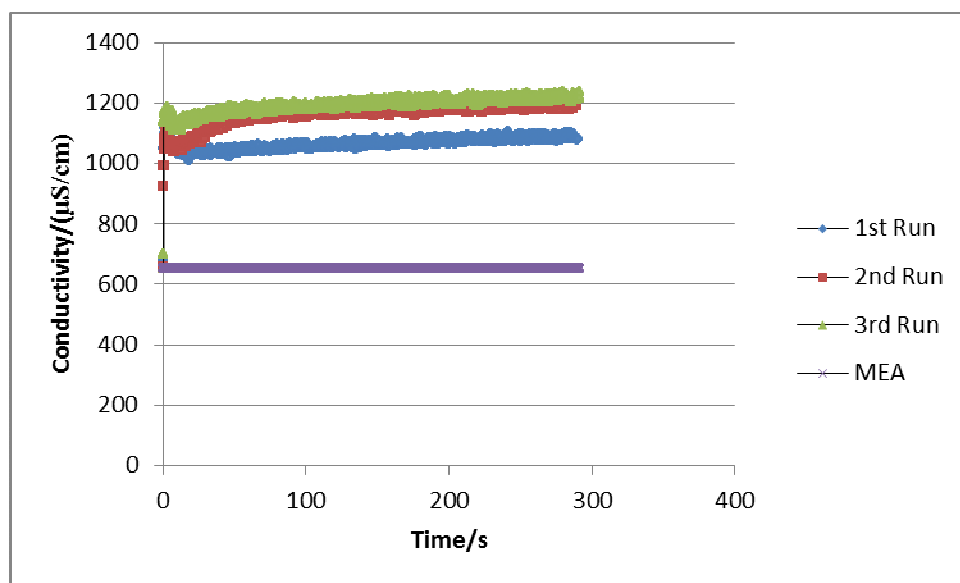
Figure 13: Conductivity-Time Profiles for [MEA] $=0.197$ mol/L, [CO_2]$_1$=0.0177 mol/L, [CO_2]$_2$=0.0189 mol/L and [CO_2]$_3$=0.0189 mol/L at 303 K.

Figure 14 shows the conductivity-time profiles for [MEA] $=0.261$ mol/L, [CO_2]$_1$=0.0232 mol/L, [CO_2]$_2$=0.0238 mol/L and [CO_2]$_3$=0.0238 mol/L at 303 K
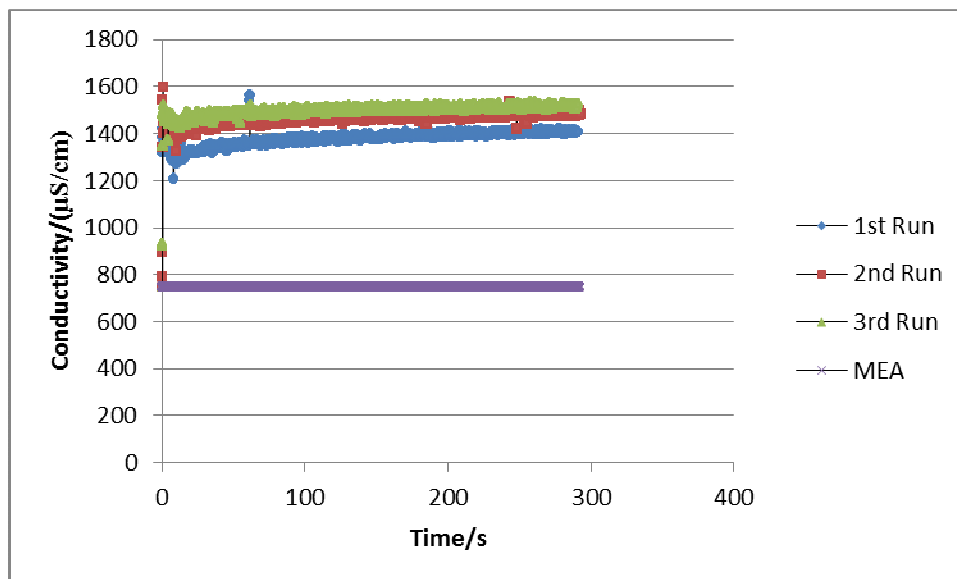
Figure 14: Conductivity-Time Profiles for [MEA] =0.261 mol/L, $[CO_2]_1$=0.0232 mol/L, $[CO_2]_2$=0.0238 mol/L and $[CO_2]_3$=0.0238 mol/L at 303 K.

From figures 13 and 14, it can be seen that increasing the concentrations of both MEA and CO_2 caused the conductivity to increase. This is because more carbamate ions were formed as a result of increasing [MEA] and $[CO_2]$. This in turn resulted in the increase of the conductivity of the solution. This increase in the conductivity of the reaction solution as entails fast reaction rates. It means that, as would be expected, faster reaction rates were observed at higher concentrations of both CO_2 and MEA than at lower concentrations.

From conductivity versus time profiles in appendices B and C, it can also be seen that increasing the temperature also caused the conductivity of the reaction solution to increase. This shows that at higher reaction temperature, faster reaction rates were observed than at lower temperatures.

4.3 Conversion-Time Profiles

In this section, a description on how CO_2 conversion data was generated from conductivity measurements is given. Table 18 shows the time, conductivity readings for the first replicate, conductivity of a 0.118 mol/L solution of MEA in distilled water, change in conductivity (ΔS) and CO_2 conversion (X). This conversion is the conversion of CO_2 at a particular time.

Table 18: Conversion of conductivity measurements to conversion data

Time/s	Conductivity of 1st replicate/(µS/cm)	MEA conductivity/(µS/cm)	ΔS/(µS/cm)	X
0.00	492.00	492	0.00	0.00
0.01	612.72	492	120.72	0.63
0.02	612.72	492	120.72	0.63
0.03	612.72	492	120.72	0.63
0.04	612.72	492	120.72	0.63
0.05	612.72	492	120.72	0.63
.	.	.	.	.
.	.	.	.	.
.	.	.	.	.
291.01	664.14	492	172.14	0.89
291.03	664.14	492	172.14	0.89
291.04	664.14	492	172.14	0.89
291.05	664.14	492	172.14	0.89
291.06	664.14	492	172.14	0.89
291.07	664.14	492	172.14	0.89

In table 18, the dots represent missing data points. Only the first six and last six points have been shown in the table. The change in conductivity (ΔS) is the difference between the conductivity readings for the first replicate and the MEA conductivity readings. This difference increased with time because as the reaction progressed, more and more of MEA and CO_2 reacted thus resulting in increased conductivity.

Conversion of CO_2 is shown as X in table 18. In calculating CO_2 conversion, an average of the last 100 conductivity readings for the first replicate was calculated. This average was calculated because the last conductivity reading for the first replicate and for all the runs was not necessarily the highest conductivity reading recorded. Therefore, conversion of CO_2 was calculated as follows:

$$X = \frac{\Delta S}{Average_{cond} - MEA_{cond}} * X_{eqm} \qquad (4.1)$$

Where $Average_{cond}$ is the average of the last conductivity readings, MEA_{cond} is the conductivity of a 0.118 mol/L MEA solution in 0.5 L of distilled water and X_{eqm} is the final equilibrium conversion. This conversion was found by using conductometric titrations that

were discussed in chapter 3. For the data shown in table 18, the average of the last 100 conductivity readings was 656.15µS/cm and the final CO_2 equilibrium conversion was 0.85. Now calculating the conversion of CO_2 after 0.02 s as an example:

$$X = \frac{120.72}{656.15 - 492} * 0.85 = 0.63$$

This is how all the conversion values were calculated from the conductivity readings.

Figure 15 shows typical conversion-time profiles that were obtained.
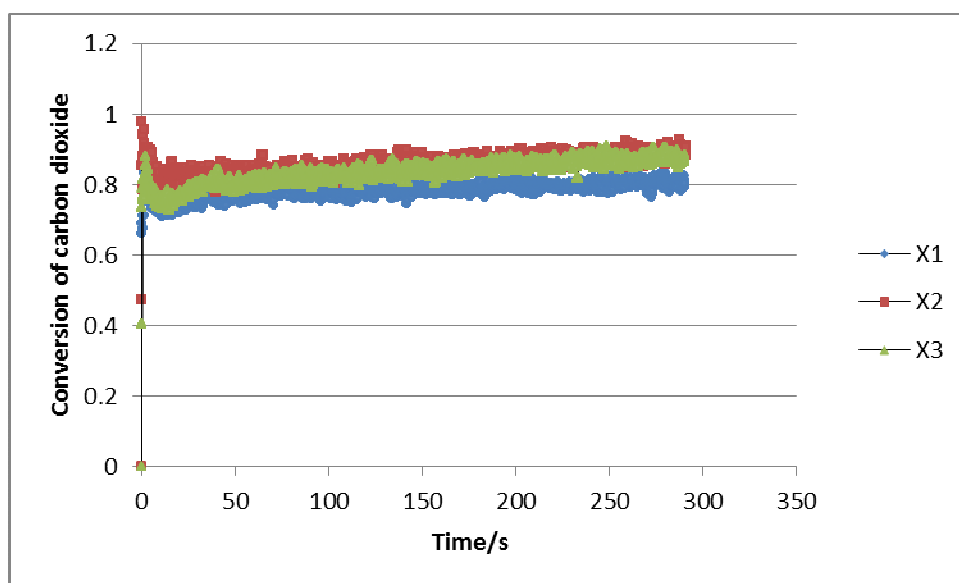
Figure 15: Conversion-Time Profiles for [MEA] =0.197 mol/L, $[CO_2]_1$=0.0180 mol/L, $[CO_2]_2$=0.0188 mol/L and $[CO_2]_3$=0.0183 mol/L at 308 K.

There are initial spikes in the conversion versus time profiles as were noticed in the conductivity-time profiles. This is because the conversion values were calculated directly from conductivity readings. In figure 15, the conversion values increase with time and the conversion versus time profiles level off showing that the reaction had reached equilibrium. Conversion values of less than one were obtained in this work. This shows that the reactions did not get to completion but reached equilibrium. Equilibrium conversion values have not been reported in literature. This might mean that previous researchers assumed that the reaction of CO_2 and MEA in aqueous solutions reached a conversion of one.

4.3.1 Effect of temperature on conversion

The effect of temperature on equilibrium conversion is shown in figure 16.
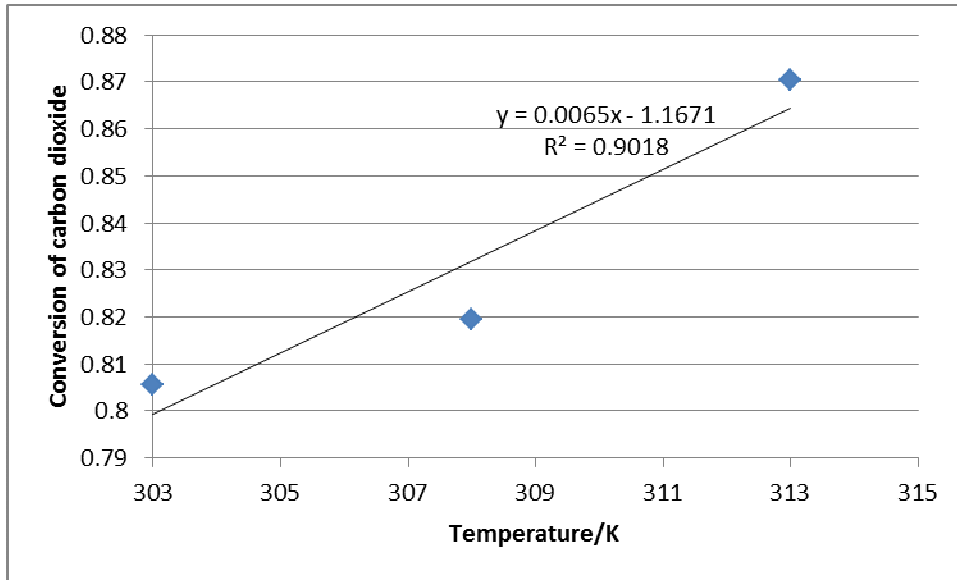
Figure 16: Effect of temperature on equilibrium conversion of CO_2.

From figure 16, it can be seen that the average equilibrium conversion of CO_2 increased with increased temperature. This is not what was expected since the reaction of CO_2 and MEA is an exothemic reaction. By Le Chatelier's principle, the equilibrium conversions should decrease with increase in temperature.

For figure 16, 95% confidence intervals were given for the regression parameters (the intercept and the gradient) as shown in table 19.

Table 19: Regression analysis for the regression parameters at 95% confidence interval (alpha= 0.05)

	Estimate	Standard Error	t-value d.f=2	p-value	Lower Confidence Limit	Upper Confidence Limit
Intercept	-1.17	0.66	-1.77	0.33	-9.55	7.22
Temperature/K	0.0065	0.0021	3.03	0.20	-0.021	0.034

From table 19, it can therefore be said with 95% confidence that the intercept lies between -9.55 and 7.22 and that the gradient lies between -0.021 and 0.034.

4.3.2 Summary of CO$_2$ equilibrium conversion data for different [MEA] and [CO$_2$] and at different temperatures

Table 20, 21 and 22 show summaries of the CO$_2$ equilibrium conversion data for different [MEA] and [CO$_2$] at 303, 308 and 313 K.

Table 20: A summary of CO$_2$ equilibrium conversion data for different [MEA] and [CO$_2$] at 303 K

Run	Temperature/K	[MEA]/(mol/L)	[CO$_2$]/(mol/L)	X$_{eq}$
1		0.0496	0.00453	0.95
2	303		0.00453	0.88
3			0.00435	0.91
1			0.00819	0.70
2			0.00810	0.62
3	303	0.0792	0.00832	0.72
4			0.00787	0.70
5			0.00728	0.80
1			0.00988	0.85
2	303	0.118	0.00830	0.67
3			0.00884	0.83
1			0.0144	0.78
2	303	0.158	0.0144	0.72
3			0.0137	0.80
1			0.0177	0.81
2	303	0.197	0.0189	0.77
3			0.0190	0.84
1			0.0238	0.93
2	303	0.261	0.0232	0.83
3			0.0232	0.81

62

Table 21: A summary of CO_2 equilibrium conversion data for different [MEA] and [CO_2] at 308 K

Run	Temperature/K	[MEA]/(mol/L)	[CO_2]/(mol/L)	X_{eq}
1			0.00231	0.93
2	308	0.0199	0.00281	0.64
3			0.00250	0.79
1			0.00430	0.98
2	308	0.0496	0.00444	0.95
3			0.00444	0.81
1			0.00823	0.89
2	308	0.0792	0.00620	0.79
3			0.00778	0.86
1			0.00943	0.79
2	308	0.118	0.0105	0.69
3			0.0102	0.92
1			0.0140	0.65
2	308	0.158	0.0139	0.71
3			0.0149	0.68
1			0.0188	0.81
2	308	0.197	0.0180	0.88
3			0.0183	0.87
1			0.0241	0.79
2	308	0.261	0.0238	0.83
3			0.0225	0.92

Table 22: A summary of CO_2 equilibrium conversion data for different [MEA] and [CO_2] at 313 K

Run	Temperature/K	[MEA]/(mol/L)	[CO_2]/(mol/L)	X_{eq}
1			0.00236	0.89
2	313	0.0199	0.00172	0.89
3			0.00168	0.99
1			0.00462	0.97
2	313	0.0496	0.00476	0.86
3			0.00503	0.86
1			0.00769	0.75
2	313	0.0792	0.00665	0.93
3			0.00638	0.95
1			0.0106	0.99
2	313	0.118	0.0102	0.98
3			0.0113	0.82
1			0.0141	0.79
2	313	0.158	0.0142	0.91
3			0.0151	0.98
1			0.0192	0.74
2	313	0.197	0.0193	0.97
3			0.0189	0.94
1			0.0248	0.73
2	313	0.261	0.0243	0.63
3			0.0255	0.78

4.4 Analysis of Errors and Repeatability in the Measurements

In this section, analysis of the errors associated with measuring the amount of CO_2 that was loaded into the reactor and conductivity will be presented. Also to be presented is the analysis repeatability of the CO_2 measurements as well as the repeatability of the conductivity measurements. To test the repeatability of CO_2 measurement results, 5 replicates of CO_2 measurements were carried out at a temperature of 303 K. Table 23 shows the results of the 5 replicates CO_2 measurements. Also shown in table 23 are the errors that were associated with these measurements.

Table 23: Error and repeatability analysis of CO_2 measurements at 303 K

Mass of CO_2/g	$[CO_2]$/mol/L	Error	Standard Deviation
0.181	0.0082	0.0052	
0.179	0.0081	0.0032	
0.184	0.0083	0.0082	0.0090
0.174	0.0079	-0.0018	
0.161	0.0073	-0.0148	

The standard error (standard deviation) of the masses of CO_2 in table 23 was 0.0090. It was very difficult to control the amount of CO_2 that was added into the reactor so this value of shows that the repeatability of adding CO_2 into the reactor was generally good. Also shown in table 23 are the errors that were associated with the measurements of CO_2. It can be seen that these errors are relatively small.

It was also necessary to determine the repeatability of the conductivity measurements using the data logger. This was done to see how repeatable the conductivity measurements were using the data logger. To test for this repeatability, the conductivity of an MEA solution was measured 5 times and each time before the measurements, the conductivity probe was thoroughly cleaned using degassed distilled water. The MEA solution had a concentration of 0.158 mol/L and these measurements were carried out at 303 K. The error and repeatability analysis of the conductivity measurements are shown in table 24.

Table 24: Error and repeatability analysis of conductivity measurements of a 0.158 mol/L MEA solution using the data logger at 303 K

Conductivity/(µS/cm)	Error	Deviation from mean conductivity/%
573	-0.2	-0.035
572	-0.2	-0.035
574	0.8	0.14
573	-0.2	-0.035
573	-0.2	-0.035

From table 24, it can be seen the errors in the measurement of conductivity of the MEA solution are very low and the deviation of the conductivity readings from the mean is within 0.14%. It can then be concluded the repeatability of the conductivity measurements was very good.

CHAPTER 5: MODELLING OF CO$_2$-MEA REACTION RATE EXPRESSON

In this section, the results of the reaction of CO$_2$ and MEA will be modelled using a rate expression which is based on the zwitterion mechanism. MATLAB programs that could estimate for the reaction rate constants were developed. The MATLAB programs that were used for modelling the results for series 1 and 2 will be described in detail in sections 5.2 and 5.3 respectively. Also to be presented in this chapter are the reaction orders with respect to CO$_2$ and MEA as well as Arrhenius plots and activation energies. The contribution of both MEA and water to the deprotonation of the zwitterion will be presented and discussed.

5.1 Selection of the Model that was Used for Modelling Series 1 Experimental Results

A model had to be selected from various models that were proposed for modelling series 1 experimental results. These models were basically the zwitterion and termolecular mechanisms that were modified. The selection of the model was based on using the bootstrap approach. This method was used to estimate measures of variability in the values of the generated reaction rate constants as well as variability in the predicted errors. The model that had the least variability in both the reaction rate constants and predicted errors was then selected. Also, the model with less number of outliers was selected.

The models that were tested are as follows:

Model 1:

$$r_{CO_2} = \frac{[CO_2][RNH_2] - \dfrac{k_r}{k_f}[RNHCOO^-][RNH_3^+]}{\dfrac{1}{k_f} + \dfrac{1}{\sum k_B[B]}}$$
(5.1)

Model 2:

$$r_{CO_2} = \cfrac{[CO_2][RNH_2] - \cfrac{k_r}{k_f}[RNHCOO^-]\cfrac{\sum k_{-b}[BH^+]}{\sum k_b[B]}}{\cfrac{1}{k_f} + \cfrac{1}{\sum k_B[B]}} \qquad (5.2)$$

Model 3:

$$r_{CO_2} = k_f[CO_2][RNH_2]^2 - k_r[RNHCOO^-]^2 \qquad (5.3)$$

Model 4:

$$r_{CO_2} = \cfrac{[CO_2][RNH_2] - \cfrac{k_r}{k_f}[RNHCOO^-]^{2.5}}{\cfrac{1}{k_f} + \cfrac{1}{\sum k_B[B]}} \qquad (5.4)$$

Model 5:

$$r_{CO_2} = \left(k_a[RNH_2] + k_w[H_2O]\right)[RNH_2][CO_2] - \frac{k_r}{k_f}[RNHCOO^-]^2 \qquad (5.5)$$

Models 1 to 4 are essentially based on the zwitterion mechanism while model 5 is the termolecular mechanism. The following figures (figures 17, 18, 19, 20 and 21) show the predicted profiles and actual data for [MEA] =0.118 mol/L and [CO_2] =0.0111 mol/L at 298 K using models 1, 2, 3, 4 and 5 respectively.
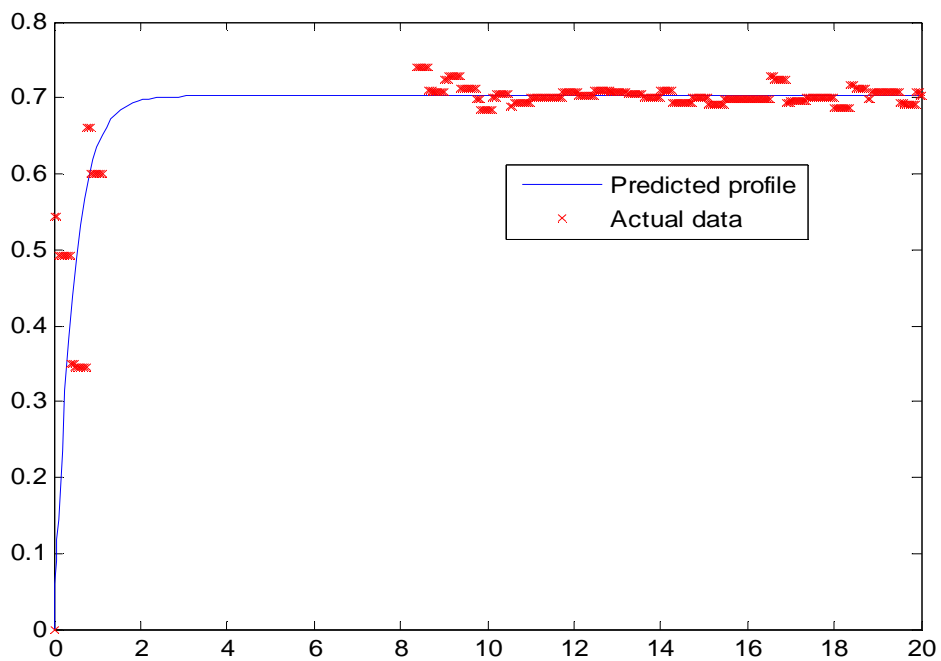
Figure 17: Predicted CO_2 conversion versus time profile using model 1 and actual data for [MEA] =0.118 mol/L and [CO_2] =0.0111 mol/L at 298 K.
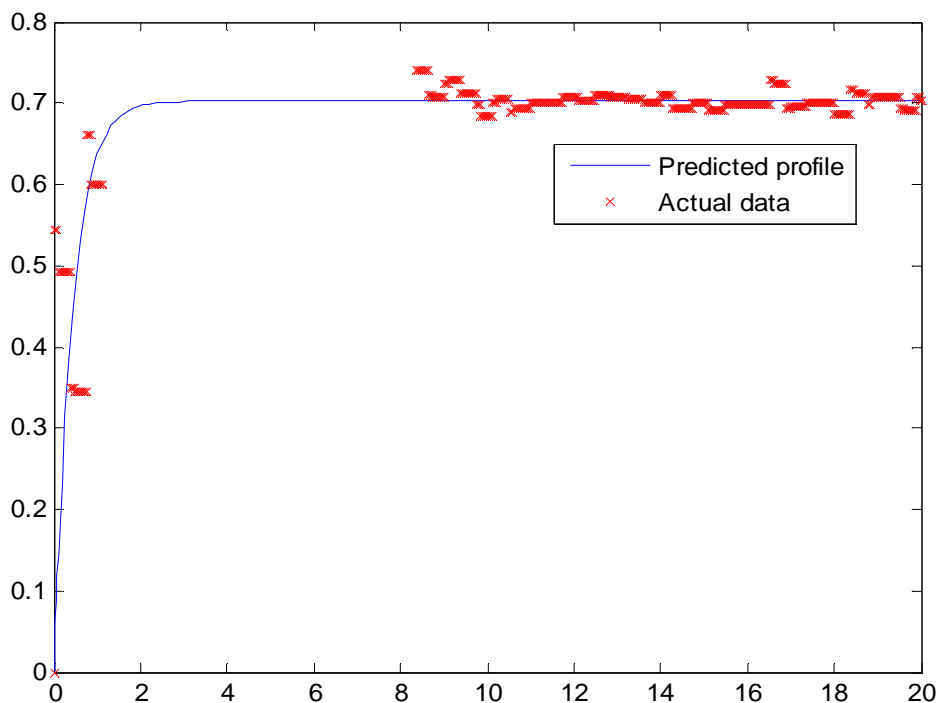
Figure 18: Predicted CO_2 conversion versus time profile using model 2 and actual data for [MEA] =0.118 mol/L and [CO_2] =0.0111 mol/L at 298 K.
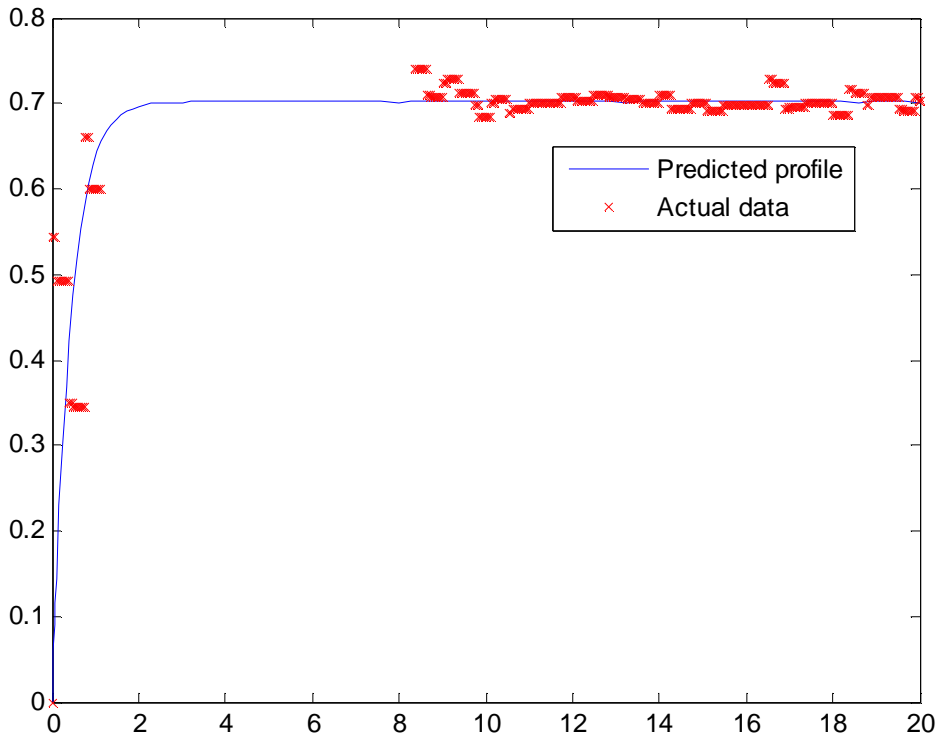
Figure 19: Predicted CO_2 conversion versus time profile using model 3 and actual data for [MEA] =0.118 mol/L and [CO_2] =0.0111 mol/L at 298 K.
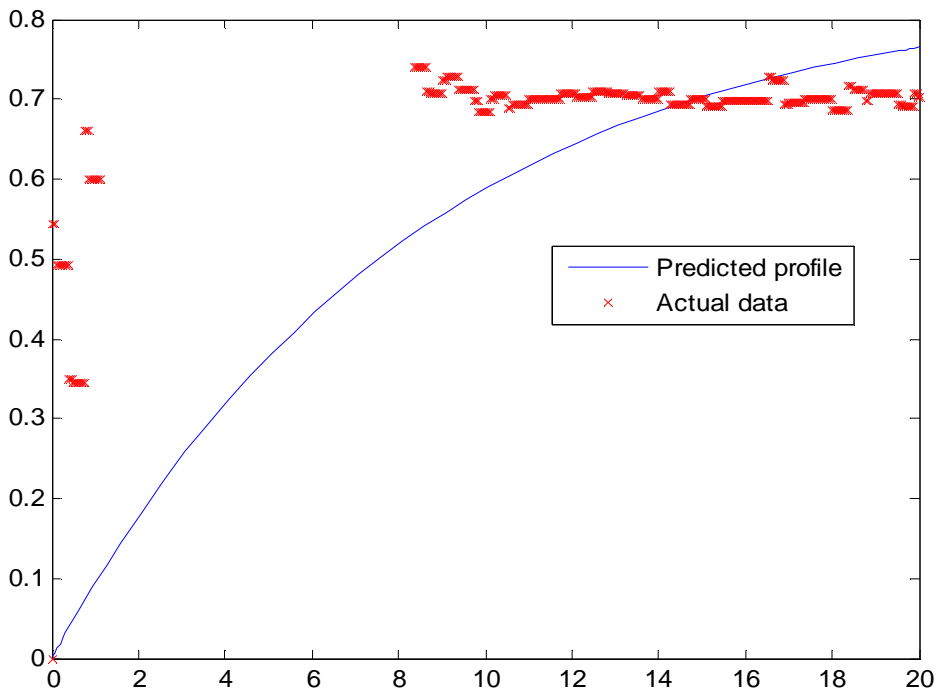
Figure 20: Predicted CO_2 conversion versus time profile using model 4 and actual data for [MEA] =0.118 mol/L and [CO_2] =0.0111 mol/L at 298 K.
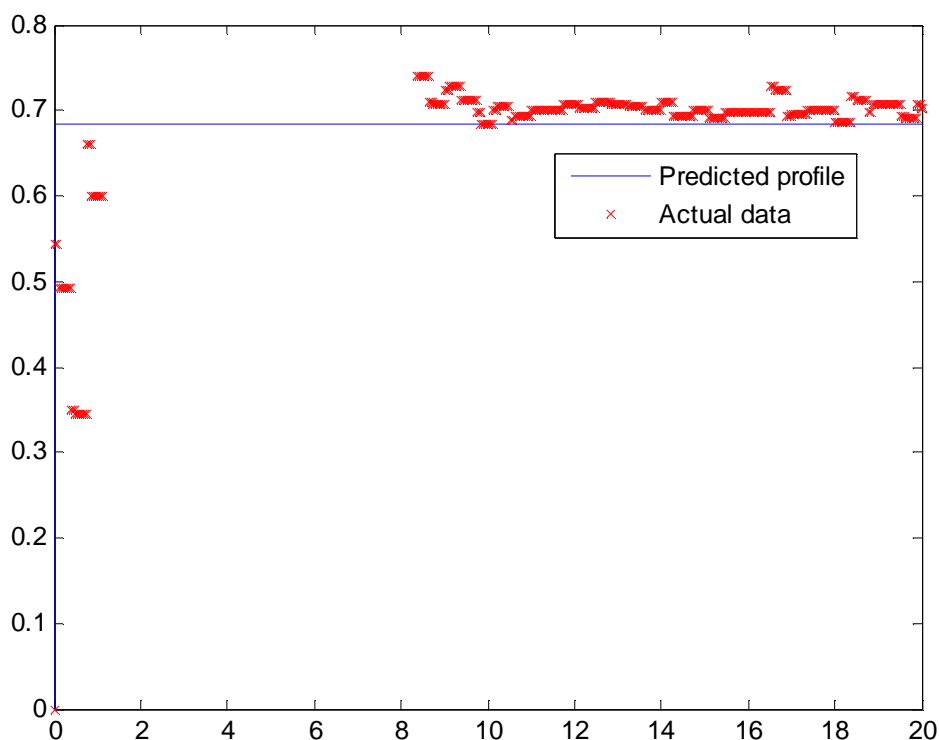
Figure 21: Predicted CO_2 conversion versus time profile using model 5 and actual data for [MEA] =0.118 mol/L and [CO_2] =0.0111 mol/L at 298 K.

The bootstrap approach was carried out in MATLAB. The MATLAB program that was used is shown in appendix M. A random split of conversion data was carried out and each sample had 75 % of total number of data points of a run. The data was then sorted so that the conversion-time relationship was enforced. This data was fitted on models 1 to 5. The variability in the generated reaction rate constants is shown in table 25 and figure 22 while the variability in the predicted errors is shown in table 26 and figure 23.

Table 25: Reaction rate constants for models 1 to 5 and for three different runs

Model 1

	First Run				Second Run				Third Run			
	k_f	$1/K_{eqm}$	k_w	k_a	k_f	$1/K_{eqm}$	k_w	k_a	k_f	$1/K_{eqm}$	k_w	k_a
	17.56-23.16	6.45-6.52	3.30-32.86	25.12-32.86	40.72-61.01	12.54-13.01	8.87-16.35	58.32-85.19	28.27-32.88	8.76-8.99	6.31-7.84	40.02-46.51

Model 2

	First Run					Second Run					Third Run				
	K_h*	K_{m*}	k_f	k_w	k_a	K_h*	K_{m*}	k_f	k_w	k_a	K_h*	K_{m*}	k_f	k_w	k_a
	3.38-3.74	1.84E-11-0.00066	12.07-18.04	0.72-3.84	12.07-18.04	2.48-2.49	3.73E-12-0.0049	28.40-4222	0.95-446.14	8.42-5790	0.00046-3.07	7.76E-11-6.10E-03	19.36-25.00	1.49-7.86	0.76-28.02

Model 3

	First Run		Second Run		Third Run	
	k_f	$1/k_r$	k_f	$1/k_r$	k_f	$1/k_r$
	0.85-1.08	1.10-1.40	1.90-2.83	0.77-9.51E-01	1.38-1.48	1.03-1.05

Model 4

	First Run				Second Run				Third Run			
	k_f	$1/K_{eqm}$	k_w	k_a	k_f	$1/K_{eqm}$	k_w	k_a	k_f	$1/K_{eqm}$	k_w	k_a
	1.19E06-2.09E08	0.0012-1.24E-03	4.20E-11-1.30E-06	90.41-120.39	3907-2.61E8	0.0020-2.02E-03	9.44E-11-6.23E-06	211.29-93013	34.47-1.46E07	0.0015-1.57E03	1.86E-14-3.52E06	147.43-305.59

Model 5

	First Run				Second Run				Third Run			
	k_f	$1/K_{eqm}$	k_w	k_a	k_f	$1/K_{eqm}$	k_w	k_a	k_f	$1/K_{eqm}$	k_w	k_a
	10.99-3.49E12	1.47E03-3.45E18	7.01E-18-2.32E01	7.03-3.43E04	26.44-1.28E11	2.28E-03-3.33E16	9.02E-15-1.02E01	0.28-219.90	3.15-9.59E10	1.80E-03-1.42E15	1.48E-15-0.40	9.16E-4-188.24

Table 26: Error variability for models 1 to 5 and for three different runs

	First Run	**Second Run**	**Third Run**
Model 1	2.73-3.81	3.03-5.06	1.05-1.26
Model 2	3.14-4.21	3.82-5.64	1.13-1.36
Model 3	2.93-4.42	3.96-6.04	1.06-1.35
Model 4	3.23-4.37	3.77-5.70	1.05-1.30
Model 5	3.35-24.87	4.16-54.83	1.08-31.81
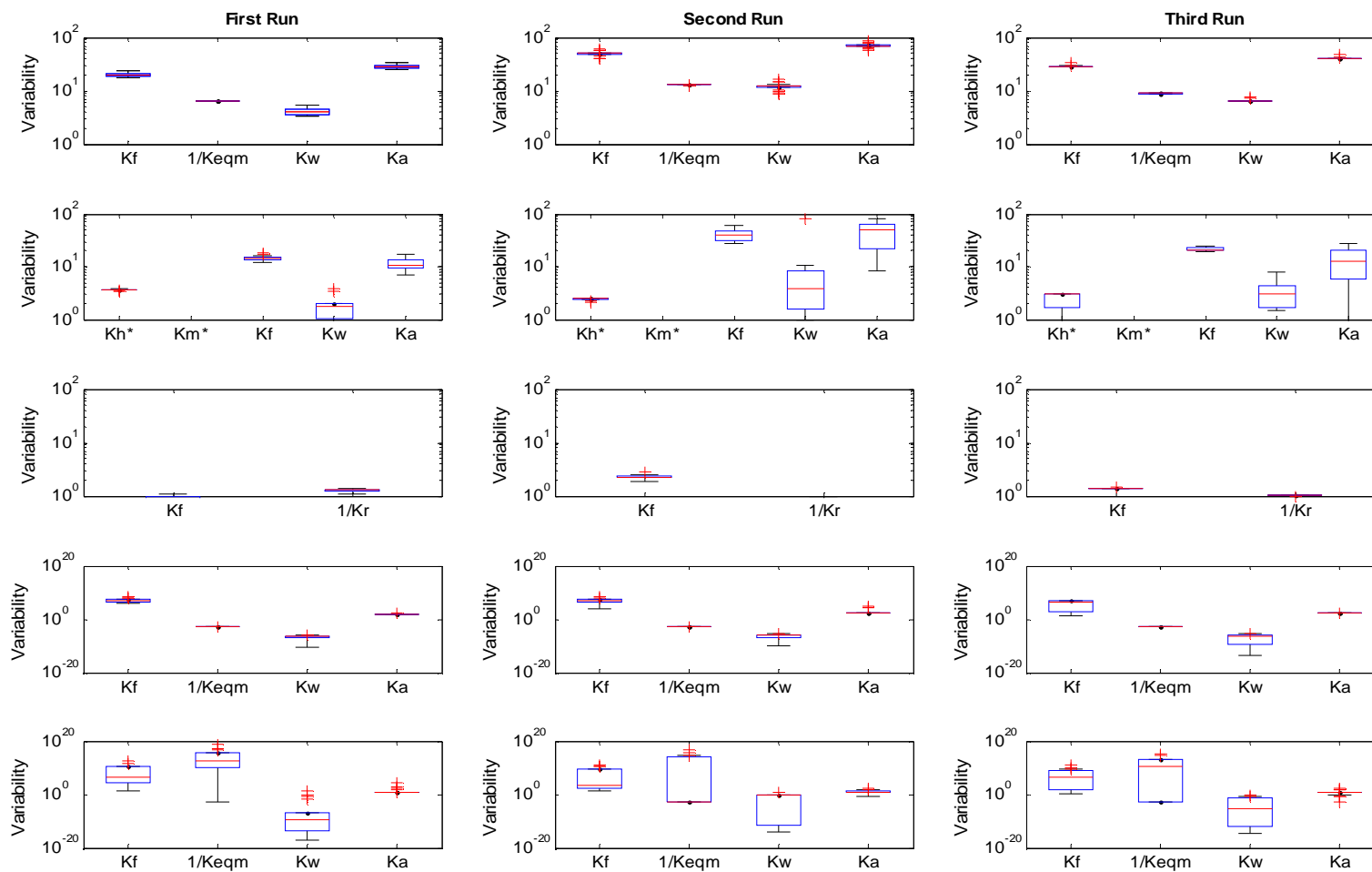
Figure 22: Variability in reaction rate constants for models 1 to 5 and for three different runs
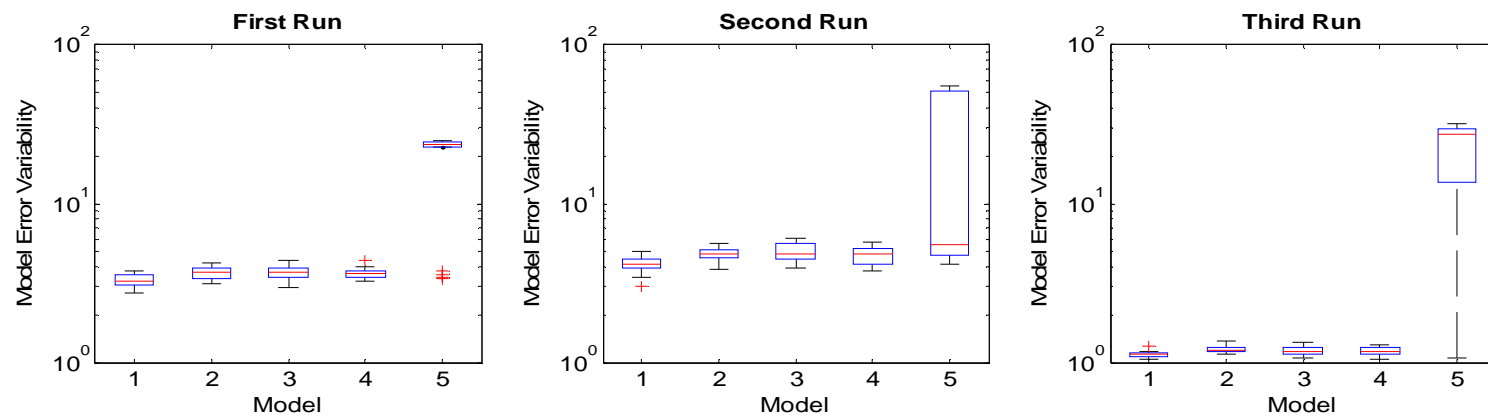
Figure 23: Variability in predicted errors for models 1 to 5 and for three different runs

In figure 22, the rows show the box plots for models 1 to 5 (from top to bottom) while the columns represent runs 1 to 3 (from left to right). It can be seen in table 26 and figure 23 that the distribution of the errors for models 1, 2 and 3 is narrower than for models 4 and 5. This shows that models 1, 2 and 3 fitted the data better than models 4 and 5.

By looking at box plots figure 22, it can be seen that there are more outliers in the box plots for models 4 and 5 than the ones in the box plots for models 1, 2 and 3. This again is an indication that models 1, 2 and 3 fitted the data better than models 4 and 5. This is also supported by the fact that there is a wider variability in the reaction rate constants for models 4 and 5 (especially for model 5) when compared to models 1, 2 and 3.

Although models 1, 2 and 3 fitted the data better than models 4 and 5, it was not possible to determine the best model among models 1, 2 and 3. This means that any of the three models could be selected so model 1 was chosen for modelling of the experimental results. Model 1 is discussed further in section 5.2.

5.2 Modelling of Experimental Results for Experiments with High [MEA] to [CO$_2$] (Series 1)

5.2.1 Model and MATLAB program development

5.2.1.1 Model development

The rate of reaction which was used was derived from the zwitterion mechanism as described in section 2.3.1. Now taking reversibility into consideration, equation (2.33) becomes:

$$r_{CO_2} = \frac{[CO_2][RNH_2] - \dfrac{k_r}{k_f}[RNHCOO^-][RNH_3^+]}{\dfrac{1}{k_f} + \dfrac{1}{\sum k_B[B]}}$$

This reaction is shown by equation (5.1) in section 5.1. Since the reaction product of the reaction between CO$_2$ and MEA is a salt, the concentrations of the cation and the anion are equal:

76

$$[RNHCOO^-] = [RNH_3^+] \tag{5.6}$$

As a result, equation (5.1) becomes:

$$r_{CO_2} = \frac{[CO_2][RNH_2] - \dfrac{k_r}{k_f}[RNHCOO^-]^2}{\dfrac{1}{k_f} + \dfrac{1}{\sum k_B[B]}} \tag{5.7}$$

Equation (5.7) was then modified so that it could be incorporated into the MATLAB program. The modification was done using the batch reactor design equation (equation 5.8) as the basis.

$$\frac{dX}{dt} = \frac{-r_{CO_2}}{[CO_2]_0} \tag{5.8}$$

$$-r_{CO_2} = [CO_2]_0 \frac{dX}{dt} = \frac{([CO_2]_0 - [CO_2]_0 * X_{CO_2})([RNH_2]_0 - [CO_2]_0 * X_{CO_2}) - \dfrac{k_r}{k_f}([CO_2]_0 * X_{CO_2})^2}{\dfrac{1}{k_f} + \dfrac{1}{k_w[H_2O]} + \dfrac{1}{k_a[RNH_2]}} \tag{5.9}$$

Letting $\theta = \dfrac{[RNH_2]_0}{[CO_2]_0}$ be the initial molar ratio of MEA to CO_2 and on dividing throughout by $[CO_2]_0$, equation (5.9) becomes:

$$\frac{dX}{dt} = \frac{[CO_2]_0((1 - X_{CO_2})(\theta - X_{CO_2}) - \dfrac{k_r}{k_f}(X_{CO_2})^2)}{\dfrac{1}{k_f} + \dfrac{1}{k_w[H_2O]} + \dfrac{1}{k_a[RNH_2]}} \tag{5.10}$$

Equation (5.10) is the differential equation that was used in generating the reaction rate constants k_f, k_w and k_a. The developed MATLAB program used the conversion-time data to fit the rate constants k_f, k_w and k_a.

5.2.1.1 MATLAB program

The MATLAB program that was used is in appendix H. This MATLAB program was a modification to a program that was used in previous work. It was modified so that it could be suitable for estimating the reaction rate constants using the zwitterion mechanism.

The reaction rate constants were determined by using the MATLAB function called fminsearchbnd. This function was used to find the minimum of the function shown in appendix H. This function is used exactly as the fminsearch function except that when using fminsearch function, one cannot set bound constraints for the variables. With fminsearchbnd function, bounds to the variables were applied. Therefore, the rate constants were searched for within certain bounds and these bounds were set as zero as the lower bound and infinity as the upper bound. The search for the reaction rate constants was therefore confined to values between zero and infinity because it is not practical to get negative reaction rate constants.

The MATLAB program was also used to predict the sum of squares of errors. These predicted sums of squares of errors were then used in the calculation of the coefficient of determination in section 5.2.

5.2.2 Analysis of the model for series 1

In this section, the quality of fit of the model is assessed. The coefficient of determination, R^2 will be used to measure the adequacy of the model. It shows how well the model fits the data. If $R^2 > 0.9$, then the model is said to fit the data well while R^2 values that are near to zero depict a poor fit (Vining, 1998). The residuals of the model are also used to determine the adequacy of a model. These residuals should have a normal distribution for a good model. The coefficient of determination is calculated as follows (Vining, 1998):

$$R^2 = \frac{SS_{reg}}{SS_{total}} = \frac{SS_{total} - SS_{res}}{SS_{total}} = 1 - \frac{SS_{res}}{SS_{total}} \qquad (5.11)$$

but $SS_{total} = SS_{reg} + SS_{res}$ \qquad (5.12)

and $SS_{res} = \sum_{i=1}^{n} \left(y_i - y_{ipred} \right)^2$ \qquad (5.13)

and $SS_{reg} = \sum_{i=1}^{n} \left(y_{ipred} - y_{imean} \right)^2$ \qquad (5.14)

where

y_i is the observed value

y_{ipred} is the predicted value

y_{imean} is the average of the observed values.

SS_{res} is the sum of squares of residuals and SS_{reg} is the sum of squares due to regression.

Figure 24 shows the predicted profile and actual data for [MEA] =0.261 mol/L and [CO$_2$] =0.0257 mol/L at 298 K.

79
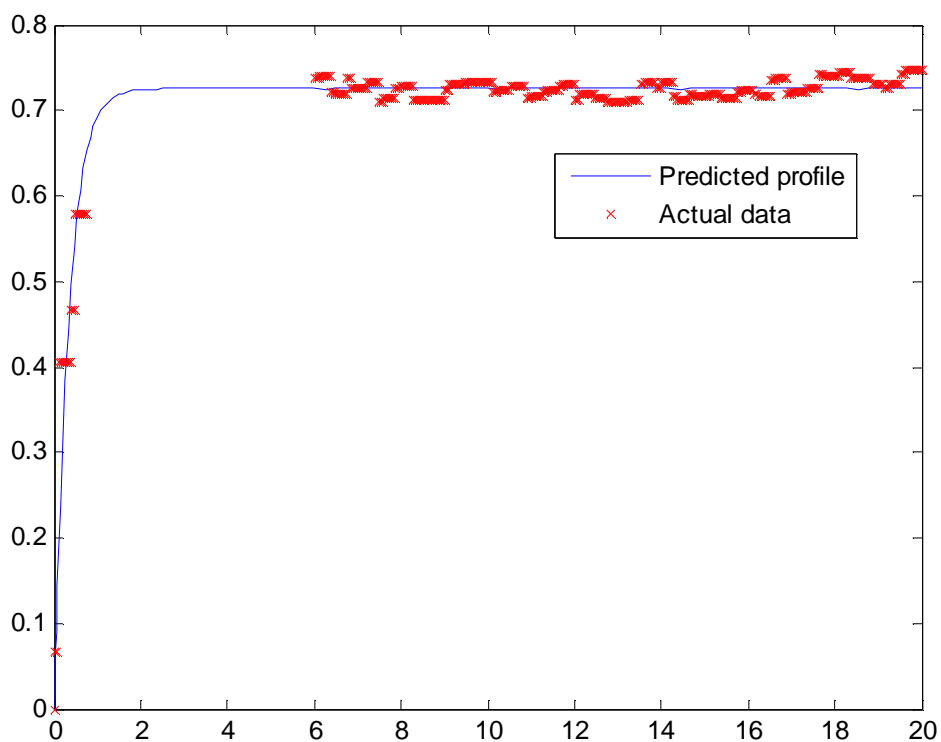
Figure 24: Predicted CO_2 conversion versus time profile and actual data for [MEA] =0.261 mol/L and [CO_2] =0.0257 mol/L at 298 K.

Figure 25 shows the predicted profile and actual data for [MEA] =0.261 mol/L and [CO_2] =0.0232 mol/L at 303 K.

80
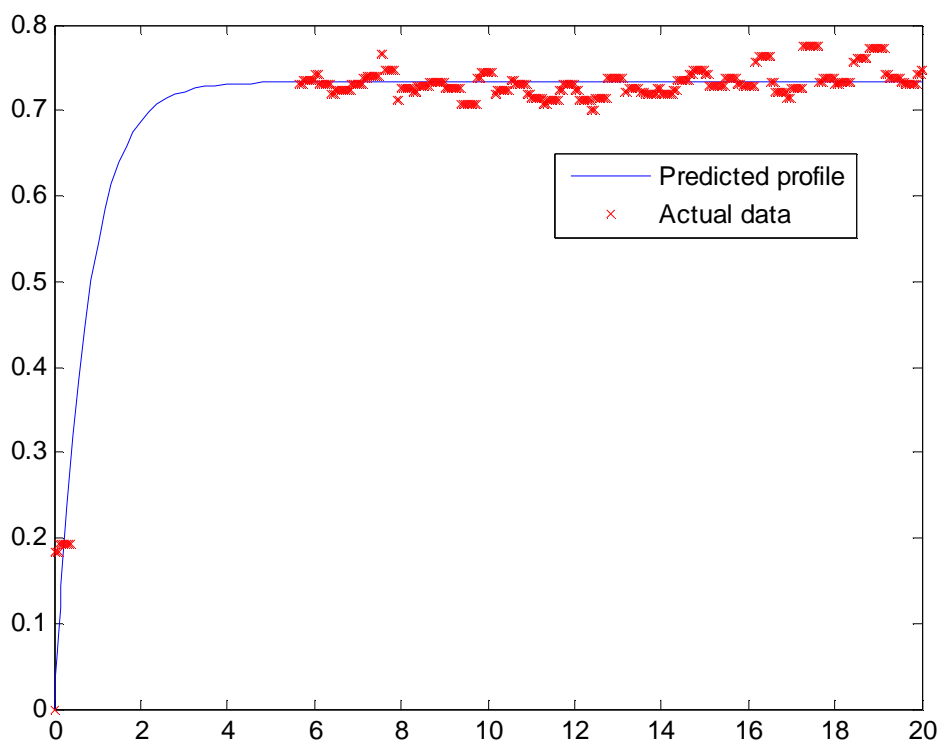
Figure 25: Predicted CO_2 conversion versus time profile and actual data for [MEA] =0.261 mol/L and [CO_2] =0.0232 mol/L at 303 K.

The quality of fit in both figures 24 and 25 are good. Their R^2 values are 0.9318 and 0.9465 respectively. This shows that the model fitted the data well. The R^2 values of 0.9318 and 0.9465 mean that the model could explain 93.18% and 94.65% of the total variability for the runs shown in figures 24 and 25 respectively.

The residuals plot for model 1 in figure 26 show that the residuals have a close to normal distribution. This further confirms that model 1 fitted the data well.
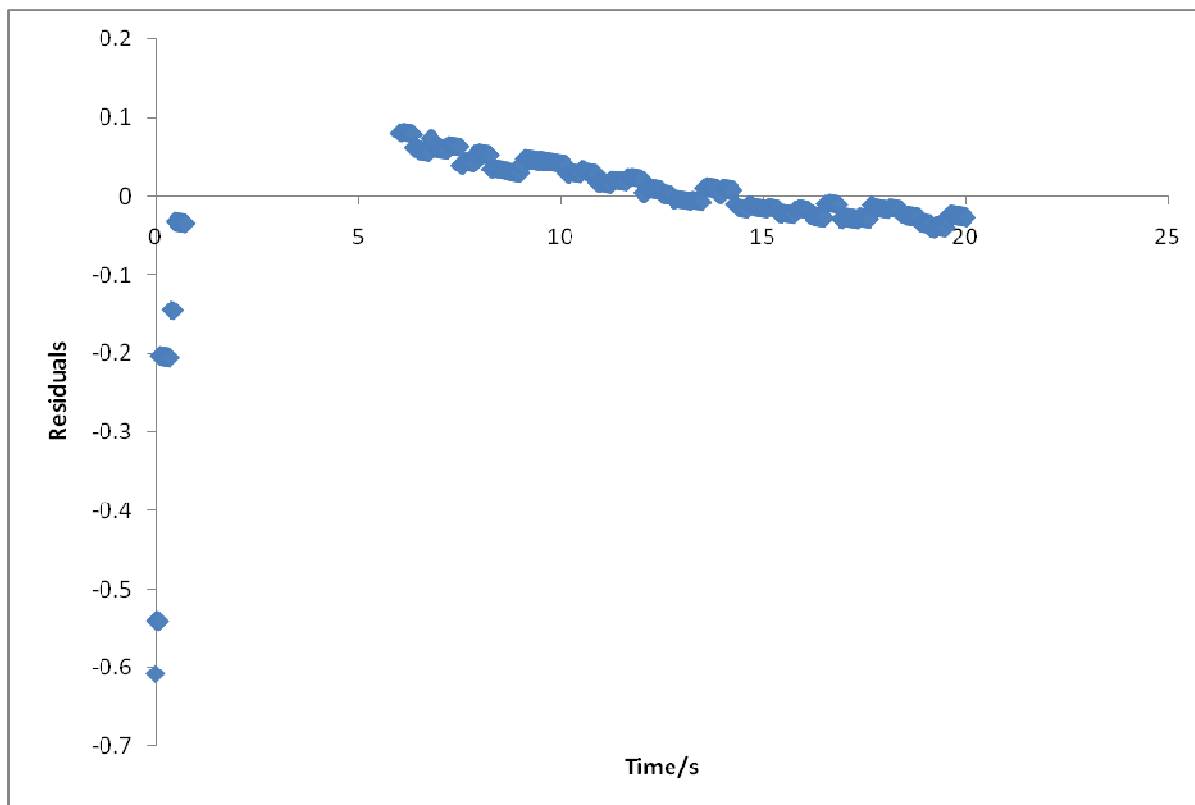
Figure 26: Residuals plot for model1

There are some gaps in the graphs in figures 24 and 25. This is because, as has been discussed in chapter 5, the conductivity profiles have initial spikes as a result of mixing time. Therefore, all the data points that constituted the spikes were removed since there is no model that can fit such a trend.

5.2.3 Reaction rate constants for the reaction of CO_2 with MEA

The experimentally determined reaction rate constants for the reaction of CO_2 and MEA are shown in table 27. These rate constants are k_f, k_w and k_a and k_r/k_f.

Table 27: Reaction Rate Constants for the Reaction of CO_2 with MEA at different temperatures.

Temperature/K	k_f/(L/mol.s)	k_r/k_f	k_w/(L^2/mol^2.s)	k_a/(L^2/mol^2.s)
298	11.5	0.20	5.1	15.0
303	9.5	0.17	4.1	13.9
308	17.4	0.22	7.2	22.5
313	23.6	0.42	8.7	30.8

It can be seen that the reaction rate constants k_f, k_w and k_a increase with temperature. This is in agreement with what is expected for the temperature dependence of the rate constants. As the reaction temperature increases, the rate at which molecular collisions occurs also increases thus leading to the increase in the rate constants.

The values of k_f obtained in this work are lower than the ones that have been reported in literature. The values that were reported in literature range from 3600 to 90400 L/mol.s. The literature k_f values and the different experimental techniques that were used are shown in chapter 2 (see tables 1 to 4 and figure 7). The difference in the literature k_f and the ones for this work might be because different experimental techniques were used to find the k_f values. Also shown in tables 1 to 4 and figure 7 are the concentrations of MEA that were used and the temperatures at which the kinetic experiments were carried out.

The ratio of k_r to k_f increases with increasing temperature. This shows that as one increases the temperature, the carbamate dissociates backs to CO_2 and MEA. This indicates that carbamates are not stable at high temperatures. This makes it easy to regenerate the MEA after CO_2 absorption in absorbers.

It is important to look at how each of the terms in the denominator of equation (5.1) compare to each other. This will give an indication of the relative significance of the reaction rate constants (k_f, k_w and k_a). Table 28 shows the values of the terms $1/k_f$, $1/(k_w[H_2O]+k_a[MEA])$, $k_w[H_2O]$ and $k_a[MEA]$ at four different temperatures

Table 28: Comparison of Reaction Rate Constants obtained at different temperatures.

Term	[MEA]/(mol/L)	Temperature/K			
		298	303	308	313
$1/k_f$/(mol.s/L)		0.0868	0.105	0.0576	0.0424
$1/(k_w[H_2O]+k_a[MEA])$/(mol.s/L)	0.0496	-	-	-	0.00298
	0.0792	0.00312	-	0.00245	0.00226
	0.118	0.00252	0.00611	0.00252	0.00343
	0.158	0.00273	0.00446	0.00617	0.00228
	0.197	0.00746	0.00459	0.00215	0.00374
	0.261	0.00666	0.0129	0.00511	0.00302
$k_w[H_2O]$/(L/mol.s)	0.0496	-	-	-	401.48
	0.0792	318.83	-	410.80	513.73
	0.118	404.27	335	663.29	293.27
	0.158	380.18	232	202.63	1042.88
	0.197	166.38	220	463.62	436.44
	0.261	180.02	79.1	210.13	325.34
$k_a[MEA]$/(L/mol.s)	0.0496	-	-	-	1.31
	0.0792	1.389	-	1.82	2.48
	0.118	2.34	2.009	4.64	2.39
	0.158	3.19	2.793	1.94	10.42
	0.197	1.66	2.519	5.15	4.89
	0.261	2.64	1.387	2.21	6.09

From table 28, it can be seen that the values of $1/k_f$ are always greater than those of $1/(k_w[H_2O]+k_a[MEA])$. This means that the deprotonation of the zwitterion was relatively fast when compared to the reversion rate of CO_2 and MEA. This also suggests that the zwitterion formation step is the rate determining step for this reaction since it is slower than the zwitterion deprotonation step. Although $1/k_f$ values are greater than the $1/(k_w[H_2O]+k_a[MEA])$ values, the term $1/(k_w[H_2O]+k_a[MEA])$ cannot be neglected. This shows that both the zwitterion formation and the deprotonation steps have significant roles in

84

the overall reaction. This is in agreement with what Li *et al* (2007) observed even though they were looking at the reaction kinetics of CO_2 in aqueous ethylenediamine, ethyl ethanolamine and diethyl monoethanolamine solutions. They used the stopped-flow technique and they carried their runs over a temperature range of 298 to 313 K.

After establishing that the term $1/(k_w[H_2O]+k_a[MEA])$ cannot be neglected and also that the zwitterion deprotonation was fast, it is therefore important to show which of the bases had a greater contribution to the deprotonation of the zwitterion than the other. This can be achieved by comparing the values of $k_w[H_2O]$ and $k_a[MEA]$. As shown in table 28, values of $k_w[H_2O]$ are always greater than those of $k_a[MEA]$. This indicates that the deprotonation of the zwitterion was mainly by water.

The contributions of MEA and water to the zwitterion deprotonation depend on their strengths and concentrations (Ramachandran *et al.*, 2006; Hagewiesche *et al.*, 1995). Although MEA is a stronger base than water, its concentration was much lower than that of water. This led to the deprotonation of the zwitterion being mainly by water.

Ali *et al* (2002) reported that water was found to deprotonate the zwitterion more than the 2-(methyl amino) ethanol (MMEA) and 2-(*n*-butyl amino) ethanol (NBAE). They said that the concentration of free amine was reduced because some of the amine might have reacted with atmospheric CO_2 when preparing the solvent and during experimentation. They also reported that the amine protonates to form hydroxides and ammonium ions. The hydroxide ions then deprotonated the zwitterion to a great extend thus leading to lower concentration of free amine available for deprotonating the zwitterion. However, this was not the case for this work.

5.2.4 Determination of activation energies

The second-order reaction rate constant (k_f) was fitted to the Arrhenius equation as shown below:

$$k_f = A\exp\left(\frac{-E_{act}}{RT}\right)$$ (5.15)

Where:

A is the Arrhenius constant, L/(mol.s).

E_{act} is the activation energy, J/mol

R is the universal gas constant which is equal to 8.314 J/mol.K

T is the absolute temperature, K.

On taking natural logarithm of equation (5.15), equation (5.15) becomes:

$$\ln k_f = \ln A - \frac{E_{act}}{R}\left(\frac{1}{T}\right) \qquad (5.16)$$

Plotting $\ln k_f$ versus $1/T$ should give a straight line whose gradient is proportional to the activation energy for the zwitterion formation step. Table 29 shows the values of $\ln k_f$, $\ln k_w$, $\ln k_a$ and $1/T$. These values were calculated using the k_f, k_w and k_a values that are shown in table 27. The k_f, k_w and k_a values that are shown in table 27 were calculated by taking the average of 18 individual data points.

Table 29: Values of $\ln k_f$, $\ln k_w$, $\ln k_a$ and $1/T$

Temperature/K	$\ln k_f$	$\ln k_w$	$\ln k_a$	1/T/(K^{-1})
298	2.45	1.64	2.71	0.00336
303	2.26	1.42	2.63	0.00330
308	2.85	1.97	3.11	0.00325
313	3.16	2.16	3.43	0.00320

The values of $\ln k_f$, $\ln k_w$, $\ln k_a$ were plotted against the values of $1/T$. Figure 27 shows the Arrhenius plot from which the activation energy for the zwitterion formation was obtained.
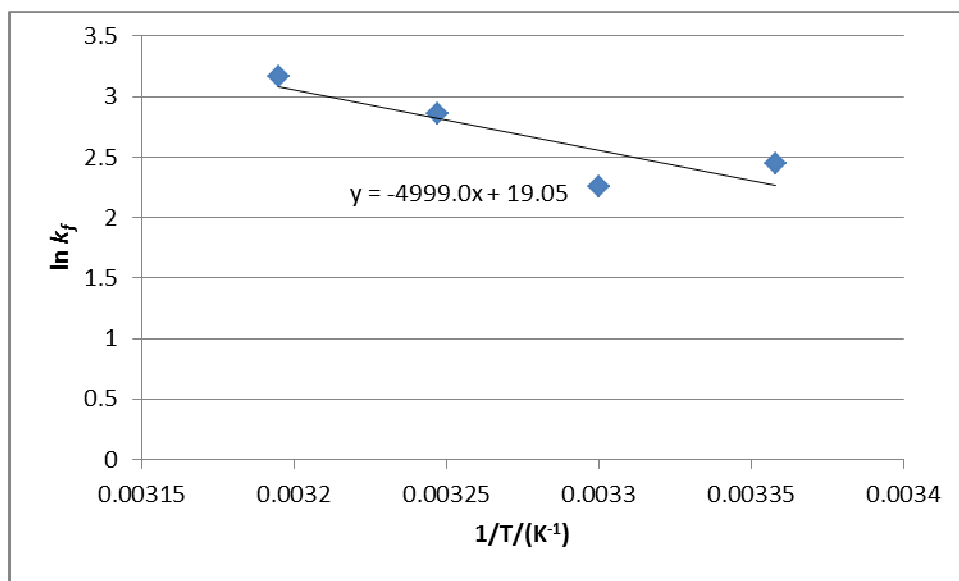
Figure 27: Arrhenius plot for the determination of the activation energy for the zwitterion formation.

From figure 27, the gradient, $\dfrac{E_{act}}{R}$ and the y-intercept, $ln\,A$ are -4999 and 19.05 respectively.

The Arrhenius equation can now be given as:

$$k_f = 1.88*10^8 \exp\left(\frac{-4999}{T}\right) \qquad (5.17)$$

The activation energy for the zwitterion formation step was determined to be 41.6 kJ/mol.

Table 30 shows some of the activation energy data that has been reported in literature.

Table 30: Activation energy literature data on the reaction of CO_2 and MEA

[MEA]/(mol/L)	Temp./K	E_{act}/(kJ/mol)	Experimental Technique	Reference
0.0152-0.177	278.6-308.4	41.2	Rapid mixing method	Hikita *et al* (1977)
1.0	291-308	41.8	Laminar jet	Danckwerts *and* Sharma (1966)
-	353	39.7	Stirred cell	Leder (1971)
1.0	291-308	41.8	Laminar jet	Sharma (1964)
0.04956-0.2609	298-313	41.6	Batch reactor	This work

It can be seen that this work's activation energy value for the zwitterion formation constant k_f falls right in between the values obtained by Hikita *et al* (1977) and Danckwerts *and* Sharma (1966) and Sharma (1964). This shows that the value obtained is in agreement with what has been reported in literature. It is important to note that the temperature ranges used by Danckwerts *and* Sharma (1966) and Sharma (1964) fall between the ranges used in this work. Also, the concentration ranges used in this work fall between the ranges used by Hikita *et al* (1977), Danckwerts *and* Sharma (1966) and Sharma (1964). This work's activation energy is also in good agreement with the value of Leder (1971).

The Arrhenius plots for the reaction rate constants k_w and k_a have also been plotted. Figures 28 and 29 show Arrhenius plots for k_w and k_a respectively.
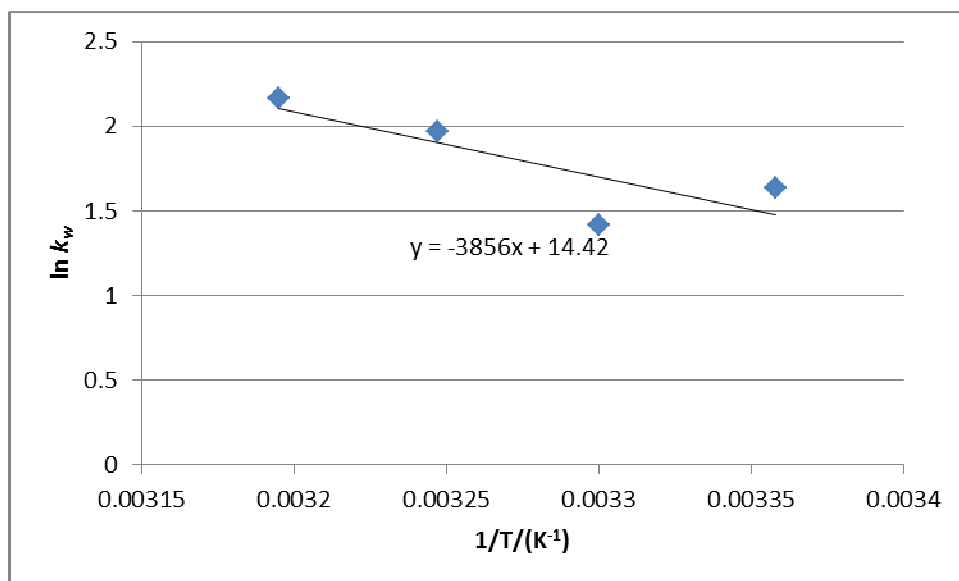
Figure 28: Arrhenius plot for the determination of activation energy of the reaction rate constant k_w.

From figure 28, the gradient, $\dfrac{E_{act}}{R}$ and the y-intercept, *ln A* are -3856 and 14.42 respectively.

The Arrhenius equation for the rate constant k_w can now be written as follows:

$$k_w = 1.83*10^6 \exp\left(\frac{-3856}{T}\right) \tag{5.18}$$

The activation energy for k_w was found to be 32.1 kJ/mol. This is activation energy was found by taking the average of 18 data points.

The activation energy was also determined by plotting Arrhenius plots using individual values k_w values and it was found that the activation energy ranged from 9.3 kJ/mol to 103 kJ/mol. An average of 54.8 kJ/mol was found by using this method. It can be seen that different activation energy values (32.1 kJ/mol and 54.8 kJ/mol) were obtained by using these two different methods. It is however important to note that there is not much difference between these two activation energy values and that 32.1 kJ/mol falls within the range found by using the second method.
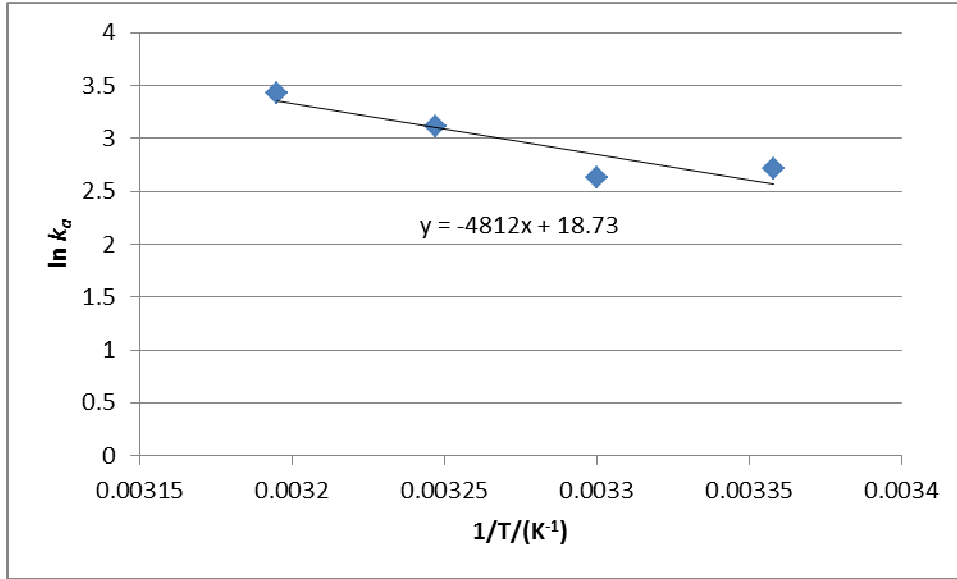
Figure 29: Arrhenius plot for the determination of activation energy of the reaction rate constant k_a

The gradient, $\dfrac{E_{act}}{R}$ and the y-intercept, *ln A* are -4812 and 18.73 respectively. The Arrhenius equation for k_a can be written as:

$$k_a = 1.36 * 10^8 \exp\left(\frac{-4812}{T}\right)$$ (5.19)

The activation energy for k_a was found to be 40.0 kJ/mol.

5.2.5 Estimation of the order of reaction with respect to MEA

The concentration of MEA was always in excess of that of CO_2. Taking the forward reaction of equation 5.1 and under the pseudo-first-order conditions, equation 5.1 becomes:

$$r_{CO_2} = k_o[CO_2]$$ (5.20)

Where k_o is an observed pseudo-first-order reaction rate constant.

$$k_o = \frac{[RNH_2]}{\dfrac{1}{k_f} + \dfrac{1}{\sum k_B[B]}}$$ (5.21)

90

Table 31 shows the pseudo-first-order rate constants, k_o for CO_2 reaction with MEA.

Table 31: Pseudo-first-order rate constants for CO_2 reaction with MEA

[MEA]/(mol/L)	ln[MEA]	Temperature/K	k_o/s^{-1}	lnk_o
0.0496	-3.00	298	-	-
		303	-	-
		308	-	-
		313	16.6	2.81
0.0792	-2.54	298	25.3	3.23
		303	-	-
		308	32.4	3.48
		313	35.0	3.56
0.118	-2.13	298	47.0	3.85
		303	19.4	2.96
		308	47.0	3.85
		313	34.5	3.54
0.158	-1.85	298	57.7	4.06
		303	35.3	3.56
		308	25.5	3.24
		313	69.2	4.24
0.197	-1.63	298	26.3	3.27
		303	42.8	3.76
		308	91.5	4.52
		313	52.6	3.96
0.261	-1.34	298	39.2	3.67
		303	20.2	3.01
		308	51.1	3.93
		313	86.4	4.46

In table 31, the pseudo-first-order rate constants were found to increase with temperature at each of the MEA concentrations studied. This means that the reaction rates increased with increasing both the concentration of MEA and the temperature.

The pseudo-first-order rate constants in table 31 were used to plot graphs of ln k_o versus ln ([MEA]) at different temperatures. Figures 30, 31, 32 and 33 show the graphs of ln k_o versus ln ([MEA]) at 298, 303, 308, and 313 K respectively.
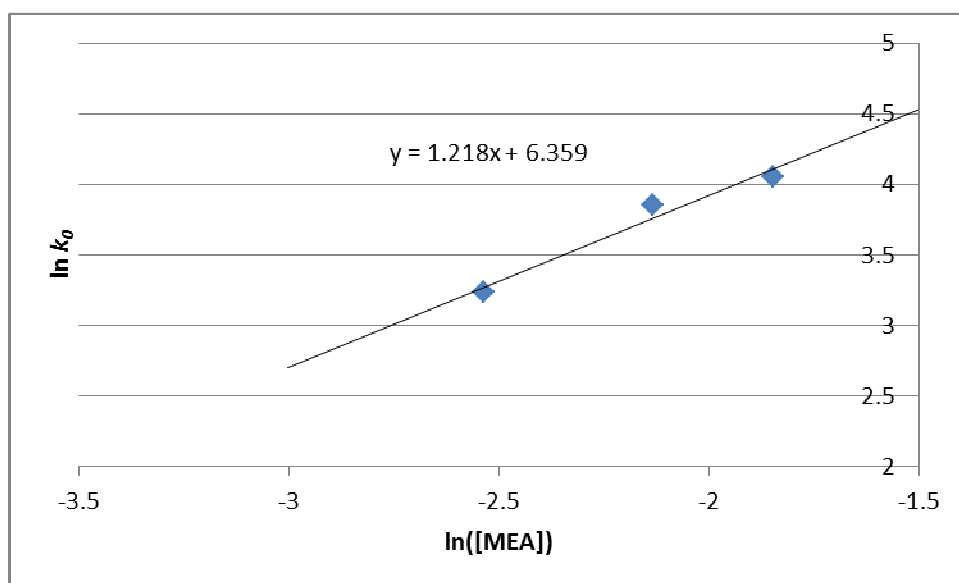
Figure 30: Graph of ln k_o versus ln([MEA]) for determining the order of reaction with respect to MEA at 298 K.
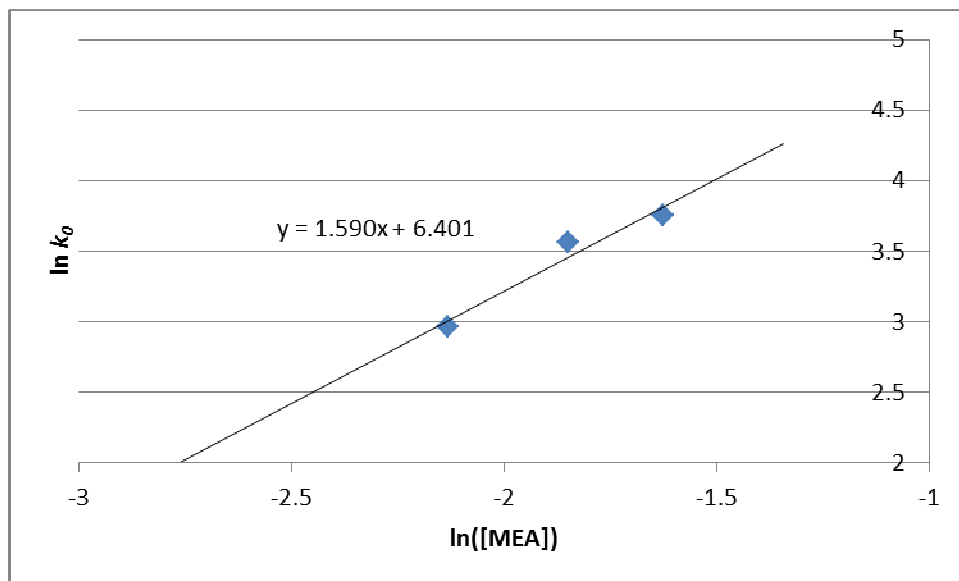
Figure 31: Graph of ln k_o versus ln([MEA]) for determining the order of reaction with respect MEA at 303 K.
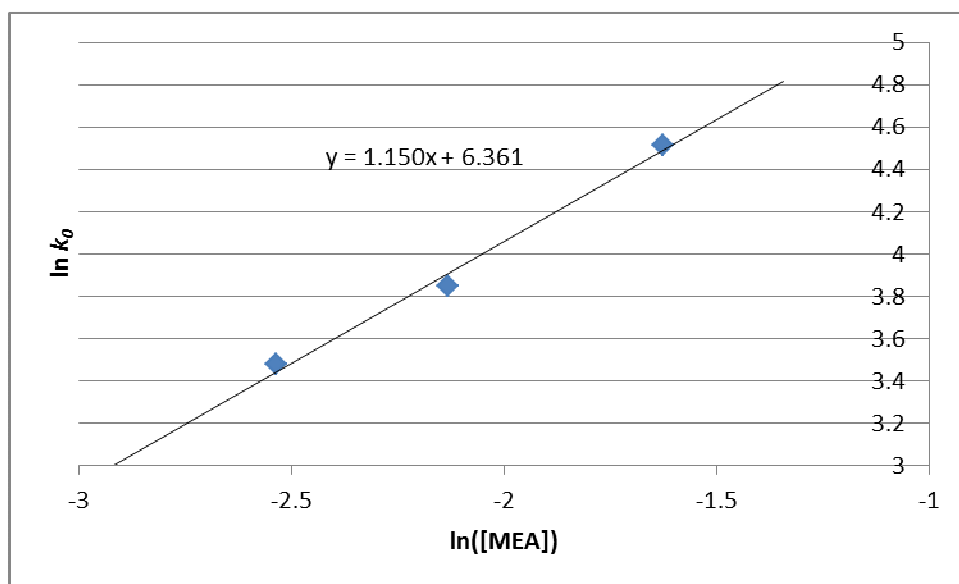
Figure 32: Graph of ln k_o versus ln([MEA]) for determining the order of reaction with respect MEA at 308 K.
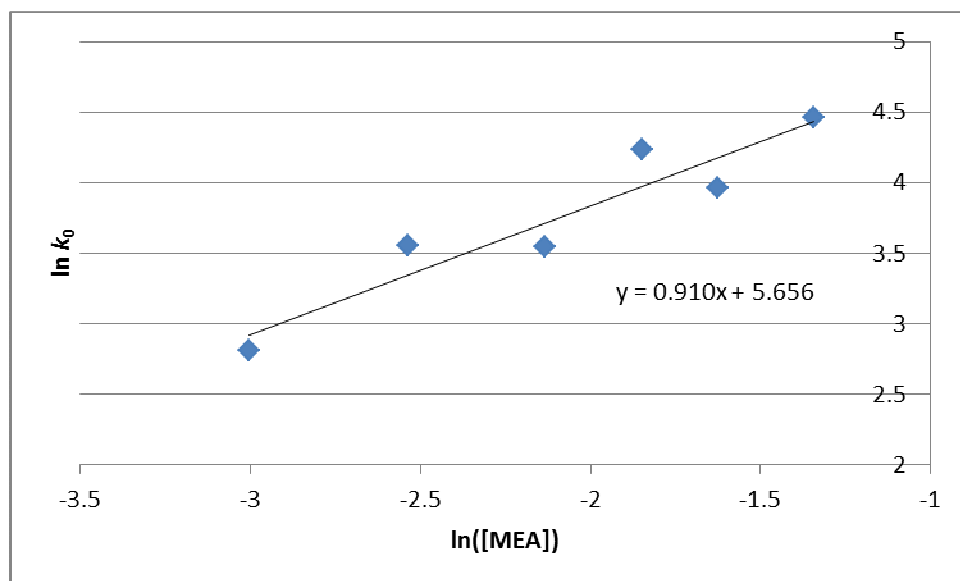
Figure 33: Graph of ln k_o versus ln([MEA]) for determining the order of reaction with respect MEA at 313 K.

From figures 30, 31, 32 and 33, it can be seen that the orders of reaction with respect to MEA are 1.22, 1.59, 1.15 and 0.91 at 298, 303, 308 and 313 K respectively. This is consistent with what has been reported in literature. Versteeg *et al*. (1996) and Bavbek and Alper (1999) reported that the order of reaction with respect to primary and secondary alkanolamines may change from 1 to 2. This change in the order of reaction depends on the concentration range and the rate constants of the alkanolamine. The orders of reaction with respect to MEA for this work are close to 1 and they also fall in the range of 1 to 2.

From this section (section 5.2), It can be concluded that the reaction between MEA and CO_2 follows the zwitterion mechanism. This zwitterion mechanism was first proposed by Caplow (1968) and it was later reintroduced by Danckwerts (1979). Blauwhoff *et al*. (1984), Barth *et al*. (1984), Alvarez-Fuster *et al*. (1980), Alvarez-Fuster *et al*. (1981), Sada *et al*. (1985) and Versteg *and* Swaaij (1988) also reported that reaction of CO_2 and MEA in aqueous medium is according to the zwitterion mechanism.

5.3 Modelling of Experimental Results for Experiments with High [CO₂] to [MEA] (Series 2)

Modelling results of the second series of experiments are presented in this section. A different model was used for modelling the second series results and this model is shown in section 5.3.1.

5.3.1 Model development

The reaction rate equation used for this series is shown by equation (5.22).

$$r_{RNH_2} = k_f [RNH_2]^m [CO_2]^n - k_r [S]^p \tag{5.22}$$

Where:

m is the reaction order with respect to MEA.

n is the reaction order with respect to CO_2.

p is the reaction order with respect to the salt S.

Equation (5.22) just considered the overall reaction of MEA and CO_2. It just focussed on the forward reaction which is the formation of the salt and the backward reaction which the dissociation of the salt back to MEA and CO_2. The deprotonation term was not incorporated in equation (5.22) since equation (5.22) has five parameters that needed to be fitted. Including the deprotonation term could have made the MATLAB program very slow since a total of seven parameters would have been fitted.

For equation (5.22) to be incorporated in the MATLAB program, it was modified using the batch reactor equation as a basis as follows:

$$\frac{dX}{dt} = \frac{-r_{RNH_2}}{C_{RNH_{2,0}}} \tag{5.23}$$

$$-r_{RNH_2} = C_{RNH_{2,0}} \frac{dX}{dt} = k_f [RNH_2]^m [CO_2]^n - k_r [S]^p \tag{5.24}$$

95

$$C_{RNH_{2,0}} \frac{dX}{dt} = k_f (C_{RNH_{2,0}} - C_{RNH_{2,0}} * X_{RNH_{2,0}})^m (C_{CO_2} - C_{RNH_{2,0}} * X_{RNH_{2,0}})^n - k_r (C_{RNH_{2,0}} * X_{RNH_{2,0}})^p$$

(5.25)

Letting $\theta = \dfrac{C_{CO_{2,0}}}{C_{RNH_{2,0}}}$ be the initial molar ratio of CO_2 to MEA, equation (5.25) becomes:

$$C_{RNH_{2,0}} \frac{dX}{dt} = k_f (C_{RNH_{2,0}})^m (1 - X_{RNH_{2,0}})^m (C_{RNH_{2,0}})^n (\theta - X_{RNH_{2,0}})^n - k_r (C_{RNH_{2,0}} * X_{RNH_{2,0}})^p$$

(5.26)

Dividing equation (5.26) throughout by $C_{RNH_{2,0}}$ gives:

$$\frac{dX}{dt} = \frac{k_f (C_{RNH_{2,0}})^m}{C_{RNH_{2,0}}} (1 - X_{RNH_{2,0}})^m \frac{(C_{RNH_{2,0}})^n}{C_{RNH_{2,0}}} (\theta - X_{RNH_{2,0}})^n - \frac{k_r}{C_{RNH_{2,0}}} (C_{RNH_{2,0}} * X_{RNH_{2,0}})^p$$

(5.27)

$$\frac{dX}{dt} = \frac{k_f (C_{RNH_{2,0}})^m (C_{CO_{2,0}})^n}{(C_{RNH_{2,0}})^2} (1 - X_{RNH_{2,0}})^m (\theta - X_{RNH_{2,0}})^n - \frac{k_r}{C_{RNH_{2,0}}} (C_{RNH_{2,0}} * X_{RNH_{2,0}})^p$$

(5.28)

Equation (5.28) is the differential equation that was used to generate both the forward and reverse reaction rate constants (k_f and k_r respectively). Also generated were the orders of reaction with respect to MEA, CO_2 and the salt (m, n and p respectively). The developed MATLAB program used conversion-time to fit these reaction rate constants and these orders of reaction.

The MATLAB function, fminsearchbnd was also used for the modelling of the second series results. The only difference now was that for the second series, the MATLAB program was used to fit the orders of reaction with respect to MEA, CO_2 and the salt apart from fitting the reaction rate constants. The search for the optimum k_f and k_r values was achieved within certain bounds and these bounds were set as zero as the lower bound and infinity as the upper bound. Bounds were also applied when fitting m, n and p and they were set as zero as the

96

lower bound and two as the upper one. The MATLAB program that was used for the second series is shown in appendix L.

5.3.2 Analysis of model for series 2

The MATLAB program that was used for the second series was also used to predict the sum of squares of errors and these errors were then used in determining the coefficient of determination.

Figure 34 shows the graph of the predicted profile of MEA conversion versus time and the actual data for [MEA] ≈ [CO_2] ≈0.0496 mol/L at 298 K while figure 35 shows the graph of the predicted profile of MEA conversion versus time and the actual data for [MEA] ≈ [CO_2] ≈0.0199 mol/L at 303 K.
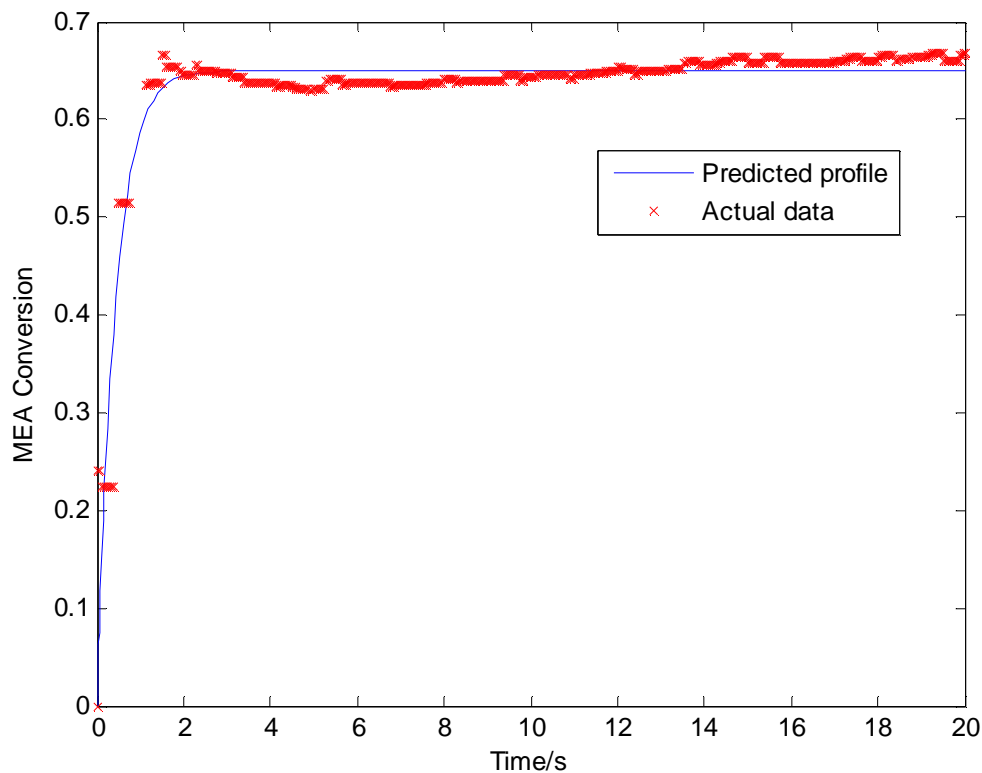
Figure 34: Predicted MEA conversion versus time profile and actual data for [MEA] ≈ [CO_2] ≈0.0496 mol/L at 298 K

97
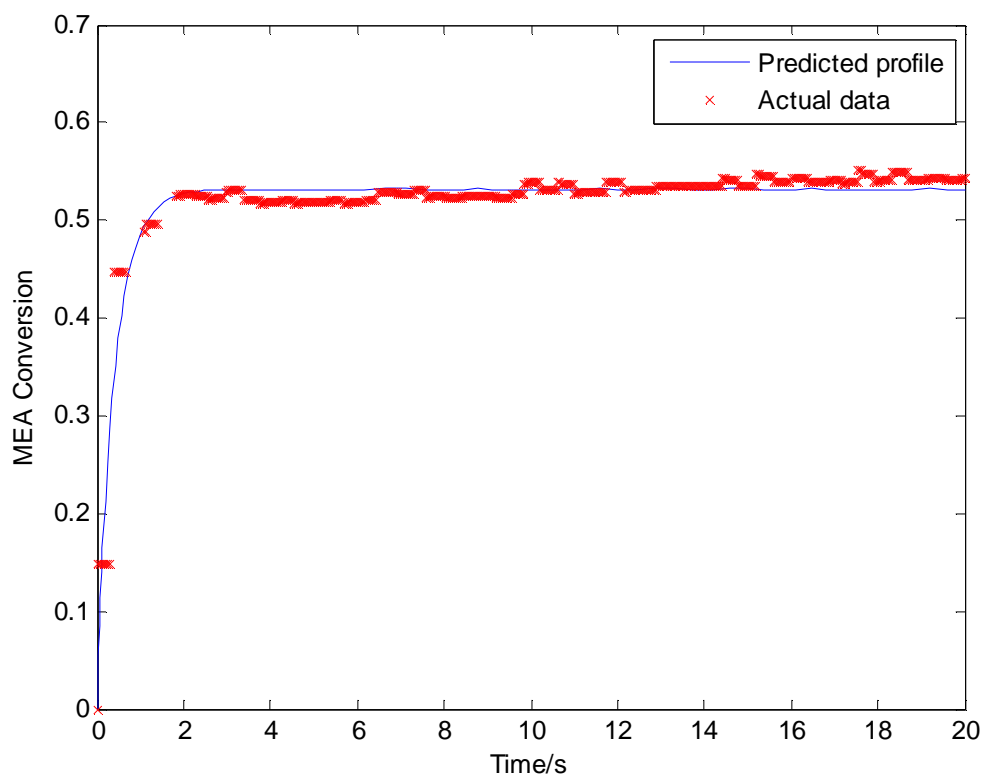
Figure 35: Predicted MEA conversion versus time profile and actual data for [MEA] ≈ [CO$_2$] ≈0.0199 mol/L at 303 K.

It can be seen from both figures 34 and 35 that the quality of fit is good. The calculated determination of coefficient (R^2) values for figures 34 and 35 are 0.9016 and 0.9051 respectively. This means that the model fitted the data very well.

5.3.3 Reaction rate constants for the reaction between CO$_2$ and MEA

The experimentally determined reaction rate constants for the second series of experiments for the reaction between CO$_2$ and MEA are shown in table 32. These reaction rate constants are the forward and reverse rate constants (k_f and k_r respectively) for the reaction of CO$_2$ and MEA.

Table 32: Reaction rate constants for the second series of experiments for the reaction of CO_2 and MEA

Temperature/K	k_f/(L/mol.s)	k_r/(L/mol.s)
298	234	2.81
303	6434	24.7
308	2466	3.59
313	44	0.36

It can also be seen from table 32 that the k_f are always greater than k_r values. This shows that the forward reaction was more favourable than the reverse one. This means that more carbamate ions were formed from the forward reaction of CO_2 and MEA and less of the carbamate ions dissociated back to CO_2 and MEA in reverse reaction.

Table 33 shows the forward reaction rate constant obtained at 303 K. The table also shows the rate constants that have been reported in literature and the experimental techniques that have been used.

Table 33: Comparison of the forward reaction rate constant obtained at 303 K with literature data.

[MEA]/(mol/L)	k_f/(L/mol.s)	Experimental technique	Reference
0-0.06	6479	Stopped flow	Penny and Ritter (1983)
0.1-0.4	4774	Wetted wall column	Xiao *et al.* (2000)
0.5-2.0	7740	Stirred cell reactor	Sada *et al.* (1985)
0.02-0.26	6434	Batch reactor	This work

The k_f value that was obtained at 303 K for this work is 6434 L/mol.s. This value is in agreement with what has been reported in literature. As shown in table 31, this value is very close to the one obtained by Penny and Ritter (1983). The value obtained in this work falls in between the values obtained by Xiao *et al.* (2000) and Sada *et al.* (1985).

5.3.4 Orders of reaction with respect to MEA and CO_2 that were obtained for series two

Apart from fitting the forward and backward reaction rate constants, the MATLAB program that was used for modelling second series results was also used to generate the reaction orders with respect to MEA and CO_2. The orders of reaction that were obtained for the second series experiments are shown in table 34. These orders of reaction were obtained at different reaction temperatures as also shown in table 34.

Table 34: Orders of reaction with respect to MEA and CO_2 obtained for series two.

Temperature/K	Reaction order with respect to MEA (m)	Reaction order with respect to CO_2 (n)
298	1.34	1.35
303	1.65	1.89
308	1.67	1.59
313	1.78	1.60

It can be seen from table 34 that the reaction orders with respect MEA are 1.34, 1.65, 1.67 and 1.78 at 298, 303, 308 and 313 K respectively. This is consistent with what has been reported in literature. Versteeg *et al*. (1996) and Bavbek and Alper (1999) reported that the order of reaction with respect to primary and secondary alkanolamines may change from 1 to 2. This change in the order of reaction depends on the concentration range and the rate constants of the alkanolamine.

In table 34, the orders of reaction with respect to carbon dioxide are 1.35, 1.89, 1.59 and 1.60 at 298, 303, 308 and 313 K respectively. Bavbek and Alper (1999) reported that it is universally accepted that the order of reaction with respect to carbon dioxide is 1. This is not in agreement with the results obtained in this work. It means that for the [MEA] and [CO_2] used in the second series of experiments, one cannot assume the order of reaction with respect to CO_2 to be 1. It can also be seen that the orders of reaction with respect to both MEA and CO_2 increase with increasing temperature. This shows that the reaction rate between MEA and CO_2 increases with increasing temperature.

Semi-empirical models have been used in modelling experimental results of the reaction between MEA and CO_2. This is because the reaction between MEA and CO_2 in aqueous

medium is a very complex reaction. Due to this complexity of the reaction kinetics of the reaction, fundamental models could not be used for modelling the results of these reactions thus leading to the change from the fundamental approach to semi-empirical approach.

CHAPTER 6: CONCLUSIONS AND RECOMMENDATIONS

In this chapter, the conclusions that were arrived at will be presented. Based on the results of the investigation of the reaction kinetics, some recommendations were be made.

6.1 Conclusions

It was found that for the first series of experiments, where ratio of MEA concentration to that of CO_2 was greater than ten, CO_2 reacts with MEA in aqueous medium according to the zwitterion intermediate mechanism. The reaction orders with respect to MEA were 1.22, 1.59, 1.15 and 0.91 at 298, 303, 308 and 313 K respectively. Having established that CO_2 reacts with MEA in aqueous medium according the zwitterion intermediate mechanism, the zwitterion formation step was found to be the rate determining step and that it was also found that the deprotonation of the zwitterion was mainly by water.

The respective Arrhenius equations for the reaction rate constants k_f, k_w and k_a were determined and they were found to be $k_f = 1.88*10^8 \exp\left(\dfrac{-4999}{T}\right)$, $k_w = 1.83*10^6 \exp\left(\dfrac{-3856}{T}\right)$ and $k_a = 1.36*10^8 \exp\left(\dfrac{-4812}{T}\right)$. From these Arrhenius equations, the activation energies for k_f, k_w and k_a were found to be 41.6, 32.1 and 40.0 kJ/mol respectively.

For the second series of experiments, where the ratio of MEA concentration to that of CO_2 was maintained at approximately one, the orders of reaction with respect to both MEA and CO_2 were determined. The orders of reaction with respect to MEA were 1.34, 1.65, 1.67 and 1.78 at 298, 303, 308 and 313 K respectively and the orders of reaction with respect to CO_2 were 1.35, 1.89, 1.59 and 1.60 at 298, 303, 308 and 313 K respectively.

The orders of reaction with respect to both MEA and CO_2 that were found in this work show that the rate of reaction for the reaction between MEA and CO_2 depends on the

concentrations of both MEA and CO_2. Increasing the concentration of either MEA or that of CO_2 or increasing the concentrations of both results in the increase in the rate of reaction.

The orders of reaction with respect to MEA for the second series are greater than those ones for the first series at any particular temperature. This shows that faster reaction rates were observed for the second series of experiments than for the first series of experiments. The forward reaction rate constants for the reaction between MEA and CO_2 for the first series were 11.5, 9.5, 17.4 and 23.6 L/mol.s at 298, 303, 308 and 313 K respectively while those ones for the second series were 234, 6434, 2466 and 44 L/mol.s at 298, 303, 308 and 313 K respectively. The forward rate constants for the second series were greater than the ones for the first series at any particular temperature thus showing faster reaction rates for the second of experiments.

It was also found that the conductivity of the carbamate formed from the reaction of CO_2 and MEA increased with increasing both the concentrations of CO_2 and MEA. The conductivity also increased with increasing temperature. This means that the rate of the reaction between MEA and CO_2 increased with increasing temperature as well and concentrations of CO_2 and MEA.

The main conclusion for this work is that the reaction kinetics of the reaction between MEA and CO_2 in aqueous medium is more complicated than the simplistic models reported in literature.

The results of this reaction kinetics study were significant. This work's results showed that for one to increase the reaction rate for the reaction between MEA and CO_2, the concentrations of both MEA and CO_2 have to be increased. It was also shown that increasing the reaction temperature results in increased reaction rates. The results of this work also help in the designing of CO_2 absorbers. For one to design a CO_2 absorption column, the reaction mechanism of the reaction has to be known. The rates of reaction also have to be known. These factors enable economic designs of CO_2 absorption columns to be carried out.

6.2 Recommendations

The conductivity-time profiles in appendices B and C have an initial spike which might have been as a result of mixing time as discussed in chapter 4. Using a semi-batch operation for the reaction of MEA and CO_2 would slow down the reaction significantly such that the kinetic activity that happens during the first five seconds of the reaction could be studied (Du Preez, 2012). This will be possible since the data points of the reaction will be clearer. It is therefore suggested that a semi-batch system be used as part of future work for the reactor set-up of this study.

In this work, it was assumed that all the CO_2 that was released from the gas bomb was all fed into the reactor. There might be some small amounts of CO_2 that might not get into the reactor and remain in the space between the reactor and where the gas bomb is connected. As a result of this; the initial concentrations of CO_2 could be inflated. Having said this, there has to be a technique of determining or measuring the initial concentration of CO_2 more accurately. Such a technique can be gas chromatography. This means that the CO_2 solution will have to be prepared by premixing the CO_2 with water. Its initial concentration will be determined before it is fed into the reactor. Degassed distilled water can be used to adjust the initial concentration of the CO_2 accordingly.

REFERENCES

Aboudheir, A; Tontiwachwuthikul, P; Chakma, A; Idem, R.: *"Kinetics of the Absorption of Carbon Dioxide in High Carbon Dioxide-Loaded Concentrated Aqueous Monoethanolamine Solutions." Chemical Engineering Science*. 2003, *58*, 5195-5210.

Aboudheir, A; Tontiwachwuthikul, P; Chakma, A; Idem, R.: *"On the Numerical Modelling of Gas Absorption into Reactive Liquids in a Laminar Jet Absorber." Canadian Journal of Chemical Engineering*. 2003, *81(3/4)*, 604-612.

Aboudheir, A; Tontiwachwuthikul, P; Chakma, A; Idem, R.: *"Novel Design for the Nozzle of a Laminar Jet Absorber."Industrial and Engineering Chemistry Research.* 2004, *43*, 2568-2574.

Ali, S.H.; Merchant, S.Q.; Fahim, M.A.: *"Reaction Kinetics of Some Secondary Alkanolamines with Carbon Dioxide in Aqueous Solutions by Stopped Flow Technique." Separation and Purification Technology.* 2002, *27*, 120-136.

Alper, E.: *"Reaction Mechanism and Kinetics of Aqueous Solutions of 2-Amino-2-methyl-1-propanol and Carbon Dioxide." Industrial and Engineering Chemistry Research.* 1990, *29*, 1725-1728.

Alvarez-Fuster, C.; Midoux N.; Laurent A.; Charpentier J. C.: *"Chemical Kinetics of the Reaction of Carbon Dioxide with Amines in Pseudo-m-nth Order Conditions in Aqueous and Organic Solutions." Chemical Engineering Science.* 1980, *35*, 1717-1723.

Alvarez-Fuster, C.; Midoux N.; Laurent A.; Charpentier J. C.: *"Chemical Kinetics of the Reaction of Carbon Dioxide with Amines in Pseudo-m-nth Order Conditions in Polar and Viscous Organic Solutions." Chemical Engineering Science*. 1981, *36*, 1513-1518.

Amann, J. G.; Bouallou, C.: *"Kinetics of the Absorption of Carbon Dioxide in Aqueous Solutions of N-Methyldiethanolamine + Triethylene Tetramine." Industrial and Engineering Chemistry Research.* 2009, *48*, 3761-3770.

Arstad, B.; Blom, R.; Swang, O.: *"Carbon Dioxide Absorption in Aqueous Solutions of Alkanolamines: Mechanistic Insight from Quantum Chemical Calculations." Journal of Physical Chemistry A.* 2007, *111*, 1222-1228.

Astarita, G.; Savage, D. W.; Bisio, A.: *"Gas Treating with Chemical Solvents" John Wiley and Sons,* 1983, New York.

Astarita, G.: *"Carbon Dioxide Absorption in Aqueous Monoethanolamine Solutions." Chemical Engineering Science.* 1961, *16*, 202-207.

Blauwhoff, P. M. M.; Versteeg, G. F.; Van Swaaij, W. P. M.: *"A study on the Reaction between Carbon Dioxide and Alkanolamines in Aqueous Solutions." Chemical Engineering Science.* 1984, *39*, 207-225.

Barth, D.; Tondre, C.; Delpuech, J.-J.: *"Kinetics and Mechanism of the Reactions of Carbon Dioxide with Alkanolamines: A Discussion Concerning the Cases of MDEA and DEA." Chemical Engineering Science.* 1984, *39*, 1753-1757.

Barth, D.; Tondre, C.; Delpuech, J.: *"Stopped-flow Investigations of the Reaction Kinetics of Carbon Dioxide with Some Primary and Secondary Alkanolamines in Aqueous Solutions." International Journal of Chemical Kinetics.* 1986, *18*, 445-457.

Bavbek, O.; Alper, E.: *"Reaction Mechanism and Kinetics of Aqueous Solutions of Primary and Secondary Alkanolamines and Carbon Dioxide." Turkish Journal of Chemistry.* 1999, *23*, 293-300.

Bonenfant, D.; Mimeault, M.; Hausler, R.: *"Determination of the Structural Features of Distinct Amines Important for the Absorption of Carbon Dioxide and Regeneration in Aqueous Solution." Industrial and Engineering Chemistry Research.* 2003, *42*, 3179-3184.

Bonenfant, D.; Mimeault, M.; Hausler, R.: *"Estimation of the Carbon Dioxide Absorption Capacities in Aqueous 2-(2-Aminoethylamino)ethanol and Its Blends with MDEA and TEA in the Presence of Sulphur Dioxide." Industrial Engineering Chemistry Research.* 2007, *46*, 8968-8971.

Bouhamra, W.; Bavbek, O.; Alper, E.: *"Reaction Mechanism and Kinetics of Aqueous Solutions of 2-Amino-2-Methyl-1,3-Propandiol and Carbon Dioxide." Chemical Engineering Journal.* 1999, *73*, 67-70.

Bosch, H.; Versteeg, G. F.; Van Swaaij, P. M.: *"Kinetics of the Reaction of Carbon Dioxide with the Sterically Hindered Amine 2- Amino-2-Methylpropanol at 298 K." Chemical Engineering Science.* 1990, *45*, 1167.

Caplow, M.: *"Kinetics of Carbamate Formation and Breakdown." Journal of the American Chemical Society.* 1968, *90*, 6795.

Clarke, J. K. A.: "*Kinetics of Absorption on Carbon Dioxide in Monoethanolamine Solutions at Short Contact Times.*" *Industrial and Chemical Engineering Fundamentals*, 1964, *3(3)*, 239-245.

Crooks, J. E.; Donnellan, J. P.: "*Kinetics and Mechanism of the Reaction between Carbon Dioxide and Amines in Aqueous Solution.*" *Journal of the Chemical Society, Perkin Transactions.* 1989, *2*, 331-333.

Cummings, A. L.; Veatch, F. C.; Keller, A. E.; Mecum, S. M.; Kammiller, R. M.: "*An Analytical Method for Determining Bound and Free Alkanolamines in Heat Stable Salt Contaminated Solutions. Unpublished Paper Prepared for Presentation at AICHE 1990 Summer National Meeting Symposium on Gas Processing*. 21 August, Ponca City.

Danckwerts, P. V.: "*Gas Liquid Reactions.*" *McGraw-Hill*, 1970, New York.

Danckwerts, P. V.: "*The Reaction of Carbon Dioxide with Ethanolamines.*" *Chemical Engineering Science.* 1979, *34*, 443-446.

Danckwerts, P. V.; Sharma, M. M.: "*Absorption of Carbon Dioxide into Solutions of Alkalis and Amines (with Some Notes on Hydrogen Sulphide and Carbonyl Sulphide).*" *Institution of Chemical Engineers. Review , No.2 Chemical Engineering, October*, 1966, CE244-CE280.

da Silva, E. F.; Svendsen, H. F.: "*Ab Initio Study of the Reaction of Carbamate Formation from Carbon Dioxide and Alkanolamines.*" *Industrial and Engineering Chemistry Research.* 2004, *43*, 3413-3418.

Davison, J., Freund, P., and Smith, A.: "*Putting Carbon Back Into the Ground.*" *IEA Greenhouse Gas R&D Programme*, 2001.

Du Preez, L. J. 2012; Personal Communication. 5 March, Stellenbosch.

Emmert, R. E.; Pigrord, R.L.: "*Gas Absorption Accompanied by Chemical Reaction: A Study of the Absorption of Carbon Dioxide in Aqueous Solutions of Monoethanolamine.*" *American Institute of Chemical Engineers Journal.* 1962, *8(2)*, 171-175.

Fogler, H. S.: "*Elements of Chemical Reaction Engineering.*" *Third Edition, Chapter 3, Prentice-Hall International, Inc. New Jersey*, 1999.

Hagewiesche, D. P.; Ashour, S. S.; Al-Ghawas, H. A.; Sandall, O. C.: "*Absorption of Carbon Dioxide into Aqueous Blends of Monoethanolamine and N-Methyldiethanolamine.*" *Chemical Engineering Science.* 1995, *50(7)*, 1071-1079.

He, B.; Zheng, X.; Wen, Y.; Tong, H.; Chen, M.; Chen, C.: "*Temperature Impact on Sulphur Dioxide Removal Efficiency by Ammonia Gas Scrubbing.*" *Energy Conversion and Management.* 2003, *44*, 2175-2188.

Henni, A; Li, J; Tontiwachwuthikul, P.: "*Reaction Kinetics of CO_2 in Aqueous 1-Amino-2-Propanol, 3-Amino-1-Propanol, and Dimethylmonoethanolamine Solutions in the Temperature Range of 298-313 K Using the Stopped-Flow Technique.*" *Industrial and Engineering Chemistry Research.* 2008, *47*, 2213-2220.

Hikita, H.; Asai, S.; Ishikawa, H.; Honda, M.: "*The Kinetics of Reaction of Carbon Dioxide with Monoethanolamine, Diethanolamine and Triethanoamine by a Rapid Mixing Method.*" *Chemical Engineering Journal.* 1977, *13,* 7-12.

Hikita, H.; Asai, S.; Katsu, Y.; Ikuno, S.: "*Absorption of Carbon Dioxide into Aqueous Monoethanolamine Solutions.*" *American Institute of Chemical Engineers Journal.* 1979, *25(5)*, 793-800.

Horng, S-Y.; Li, M-H.: "*Kinetics of Absorption of Carbon Dioxide into Aqueous Solutions of Monoethanolamine and Triethanolamine.*" *Industrial and Engineering Chemistry Research.* 2002, *41*, 257-266.

Kimura, N.; Omata, K.; Kiga, T.; Takano, S.; Shikisima, S.: "*The Characteristics of Pulverised Coal Combustion in Oxygen/Carbon Dioxide Mixture for Recovery.*" *Energy Conservation Management.* 1995, *36*, 805-808.

Ko, J-J.; Tsai, T-C.; Lin, C-Y.; Wang, H-M.; Li, M-H.: "*Diffusivity of Nitrous Oxide* in *Aqueous Alkanolamine Solutions.*" *Journal of Chemical and Engineering Data.* 2001, *46*, 160-165.

Kovvali, A.S.; Sirkar, K.K.: "*Carbon Dioxide Separation with Novel Solvents as Liquid Membranes.*" *Ind. Eng. Chem. Research.* 2002, *41*, 2287-2295.

Laddha, S. S.; Danckwerts, P. V.: "*Reaction of Carbon Dioxide with Ethanolamines: Kinetics from Gas Absorption.*" *Chemical Engineering Science.* 1981, *36*, 479-482.

Leder, F.: "*The Absorption of Carbon Dioxide into Chemically Reactive Solutions at High Temperature.*" *Chemical Engineering Science.* 1971, *26*, 1381-1390.

Levenspiel, O.: "*Chemical Reaction Engineering.*" *Second Edition, Chapter 2, Wiley International Edition*, 1972.

Li, J.; Henni, A.; Tontiwachwuthikul, P.: "*Reaction Kinetics of Carbon Dioxide in Aqueous Ethylenediamine, Ethyl Ethanolamine, and Diethyl Monoethanolamine Solutions in the Temperature Range of 298-313K, Using the Stopped-Flow Technique.*" *Industrial and Engineering Chemistry Research.* 2007, *46*, 4426-4434.

Lin, S. H.; Shyu, C. T.: "*Performance Characteristics and Modelling of Carbon Dioxide Absorption by Amines in a Packed Column.*" *Waste Management*, 1999, *19*, 255-262.

Littel, R. J.; Versteeg, G. F.; Van Swaaij, W. P. M.: "*Kinetics of Carbon Dioxide and Secondary Amines in Aqueous Solutions. Influence of Temperature on Zwitterion Formation and Deprotonation Rates.*" *Chemical Engineering Science.* 1992, *47(8)*, 2037-2045.

Masuda, S.: "*Chemical Carbon Dioxide Fixation Technology-RITE Projects.*" *Energy Conservation Management.* 1995, *36*, 567-572.

Paul, S.; Ghoshal, A. K.; Mandal, B.: "*Removal of Carbon Dioxide by Single and Blended Aqueous Alkanolamine Solvents in Hollow-Fiber Membrane Contactor: Modelling and Simulation.*" *Industrial and Engineering Chemistry Research.* 2007, *46*, 2576-2588.

Paul, S.; Ghoshal, A. K.; Mandal, B.: "*Absorption of Carbon Dioxide into Aqueous Solutions of 2-Piperidineethanol: Kinetics Analysis.*" *Industrial and Engineering Chemistry Research.* 2009, *48*, 1414-1419.

Penny, D.; Ritter, T.: "*Kinetic Study of Reaction between Carbon Dioxide and Primary Amines.*" *Journal of Chemical Society Faraday Transactions.* 1983, *79*, 2103-2109.

Pinsent, B. R. W.; Pearson, L.; Roughton F. J. W.: "*The Kinetics of Combination of Carbon Dioxide with Hydroxide Ions.*" *Transactions of the Faraday Society*. 1956, *52*, 1512-1520.

Puxty, G.; Rowland, R.; Attalla, M.: "*Comparison of the Rate of Carbon Dioxide Absorption into Aqueous Ammonia and Monoethanolamine.*" *Chemical Engineering Science.* 2010, *65*, 915-922.

Ramachandran, N.; Aboudheir, A.; Idem, R.; Tontiwachwuthikul, P.: "*Kinetics of the Absorption of Carbon Dioxide into Mixed Aqueous Loaded Solutions of Monoethanolamine and Methyldiethanolamine.*" *Industrial and Engineering Chemistry Research.* 2006, *45*, 2608-2616.

Rao, A. B.; Rubin, E. S.: "*A Technical, Economic, and Environmental Assessment of Amine-Based Carbon Dioxide Capture Technology for Power Plant Greenhouse Gas Control.*" *Environmental Science and Technology*. 2002, *36*, 4467- 4475.

Rinker, E. B.; Ashour, S. S.; Sandall, O. C.: "*Kinetics and Modelling of Carbon Dioxide Absorption into Aqueous Solutions of Diethanolamine.*" *Industrial and Engineering Chemistry Research.* 1996, *35*, 1107-1114.

Rinker, E. B.; Ashour, S. S.; Sandall, O. C.: "*Absorption of Carbon Dioxide into Aqueous Blends of Diethanolamine and Methyldiethanolamine.*" *Industrial and Engineering Chemistry Research.* 2000, *39*, 4346-4356.

Sada, E.; Kumazawa, H.; Butt, M. A.: "*Gas Absorption with Consecutive Chemical Reaction: Absorption of Carbon Dioxide into Aqueous Amine Solutions.*" *Canadian Journal of Chemical Engineering*, 1976a, *54*, 421-424.

Sada, E.; Kumazawa, H.; Butt, M. A.; Hayashi, D.: "*Simultaneous Absorption of Carbon Dioxide and Hydrogen Sulphide into Aqueous Monoethanolamine Solutions.*" *Chemical Engineering Science*, 1976b, *31*, 839-841.

Sada, E.; Kumazawa, H.; Han, Z. Q.; Matsuyama, H.: "*Chemical Kinetics of the Reaction of Carbon Dioxide with Ethanolamines in Non-aqueous Solvents.*" *American Institute of Chemical Engineers.* 1985, *31(8)*, 1297-1303.

Sartori, G.; Savage, D. W.: "*Sterically Hindered Amines for Carbon Dioxide Removal from Gases.*" *Industrial and Engineering Chemistry Fundamentals.* 1983, *22*, 239-249.

Sharma, M. M.: *Thesis. Cambridge: University of Cambridge*. 1964.

Sharma, M. M.: "*Kinetics of Reactions of Carbonyl Sulphide and Carbon Dioxide with Amines and Catalysis by Bronsted Bases of the Hydrolysis of Carbonyl Sulphide.*" *Transactions of Faraday Society*, 1965, *61*, 681-688.

Thomas, W. J.: *American Institute of Chemical Engineers Journal*. 1966, *12*, 1051.

Versteeg, G. F.; Oyevaar, M. H.: "*The Reaction of Carbon Dioxide and Diethanolamine at 298 K.*" *Chemical Engineering Science.* 1989, *44*, 1264.

Versteeg, G. F.; van Swaaij, W. P. M.: "*On the Kinetics between Carbon Dioxide and Alkanolamines both in Aqueous and Non-aqueous Solutions -1. Primary and Secondary Amines.*" *Chemical Engineering Science.* 1988, *43*, 573-585.

Versteeg, G. F.; van Swaaij, W. P. M.: "*Solubility and Diffusivity of Acid Gases (CO_2, N_2O) in Aqueous Alkanolamine Solutions.*" *Journal of Chemical and Engineering Data.* 1988, *33*, 29-34.

Versteeg, G. F; van Dijck, L. A.; van Swaaij, P. M.: "*On the Kinetics between Carbon Dioxide and Alkanolamines both in Aqueous and Non-aqueous Solutions, An Overview.*" *Chemical Engineering Communications.* 1996, *144*, 113-158.

Vining, G. G.: "*Statistical Methods for Engineers.*" *Cole Publishing Company,* 1998, Pacific Groove. Chapter 6.

Weiland, R., Dingman, J., Cronin, D., Browning, G.: "*Density and Viscosity of Some Partially Carbonated Aqueous Alkanolamine Solutions and their Blends.*" *Journal of Chemical and Engineering Data.* 1998, *43*, 378-382.

Xiao, J.; Li, C.; Li, M.: "*Kinetics of Absorption of Carbon Dioxide into Aqueous Solutions of 2-Amino-2-Methyl-1-Propanol and Monoethanolamine.*" *Chemical Engineering Science.* 2000, *55*, 161-175.

Xu, S.; Wang, Y. W.; Otto, F.D.; Mather, A. E.: "*Kinetics of the Reaction of Carbon Dioxide with 2-Amino-2-Methylpropanol Solutions.*" *Chemical Engineering Science.* 1996, *51*, 841.

Yih, S-M.; Shen, K-P.: "*Kinetics of Carbon Dioxide Reaction with Sterically Hindered 2-Amino-2-Methyl-1-Propanol Aqueous Solutions.*" *Industrial and Engineering Chemical Research.* 1988, *27*, 2237-2241.

Yoon, J-H.; Shim, J-G.; Lee, J. K.; Min, B-Y.; Eum, H-M.: "*Kinetics of Absorption of Carbon Dioxide into Aqueous 2-Amino-2-Ethyl-1, 3-Propanediol Solutions.*" *Industrial and Engineering Chemistry Research.* 2002, *41*, 3651-3656.

http://www.vizavalve.com/downloads/butterfly-Data5.pdf [2011, December 9].

http://www.co2crc.com.au/dls/factsheets/CO2CRC_factSheet_17.pdf [2012, January 11].
http://gcep.stanford.edu/pdfs/assessments/carbon_capture_assessment.pdf [2012, January 11].

APPENDICES

APPENDIX A: PHYSICAL AND CHEMICAL PROPERTIES

A1: Physical and Chemical Properties of MEA (www.sciencelab.com)

Physical State	Liquid
Molecular Weight	61.08g/mol
Specific Density	1.018
Vapour Density	2.1
Vapour Pressure	0.1kPa (at 20°C)
Solubility	Soluble in both hot and cold water
Colour	Colourless
pH(1% solution/water)	10
Melting Point	10.3^{o}C
Boiling Point	170.8^{o}C
Critical Temperature	341°C

A2: Physical and Chemical Properties of CO$_2$ (www.airgas.com)

Molecular Weight	44.01g/mol
Specific Volume	8.77193
Vapour Density	1.53 (ft^3/lb)
Vapour Pressure	830 psig
Melting Point	-78.5^{o}C
Boiling Point	-78.55^{o}C
Critical Temperature	30.9^{o}C
Gas Density	0.114 (lb/ft^3)

A3: Physical and Chemical Properties of NaOH

Physical State	Liquid
Vapour Density	0.62
Vapour Pressure	2.3kPa (at 20°C) (water)
Solubility	Soluble in cold water
Colour	Colourless
pH(1% solution/water)	Basic
Melting Point	12°C
Boiling Point	140°C
Specific Gravity	1.53

APPENDIX B: CONDUCTIVITY-TIME PROFILES FOR FIRST SERIES RUNS
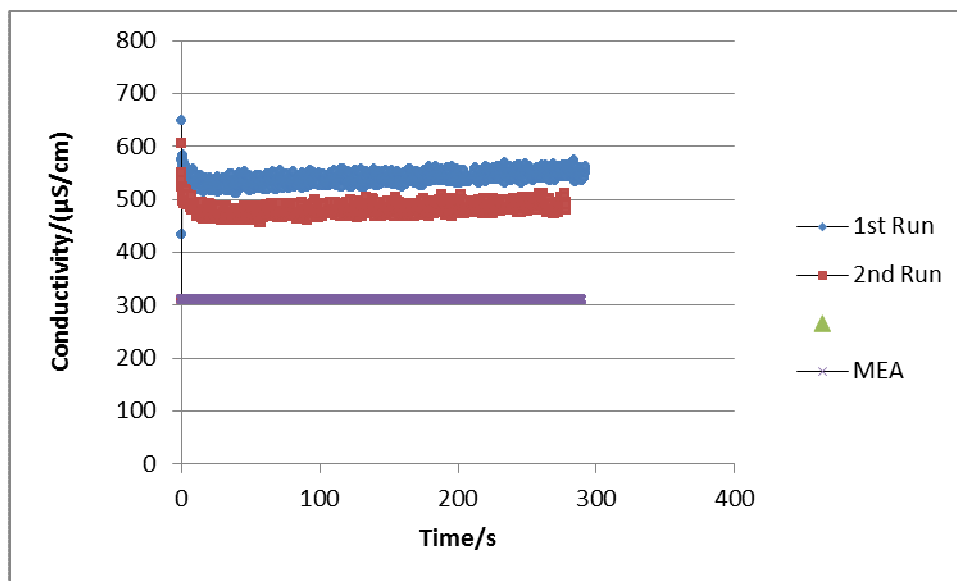
Figure B1: Conductivity-Time Profiles for [MEA] =0.07915 mol/L, $[CO_2]_1$=0.01004 mol/L, $[CO_2]_2$=0.009633 mol/L at 298 K.
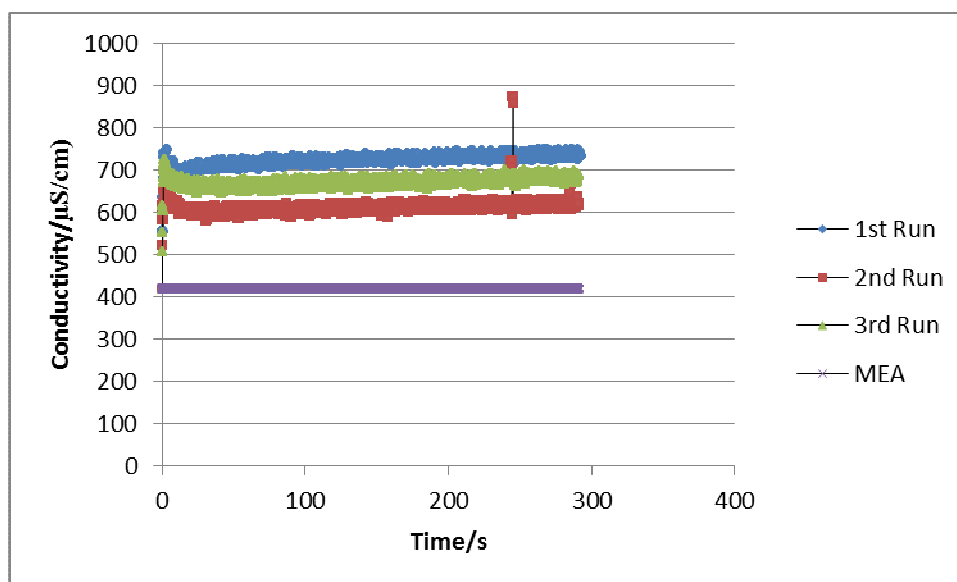
Figure B2: Conductivity-Time Profiles for [MEA] =0.1184 mol/L, $[CO_2]_1$=0.01114 mol/L, $[CO_2]_2$=0.01038 mol/L and $[CO_2]_3$=0.01083 mol/L at298 K.

115
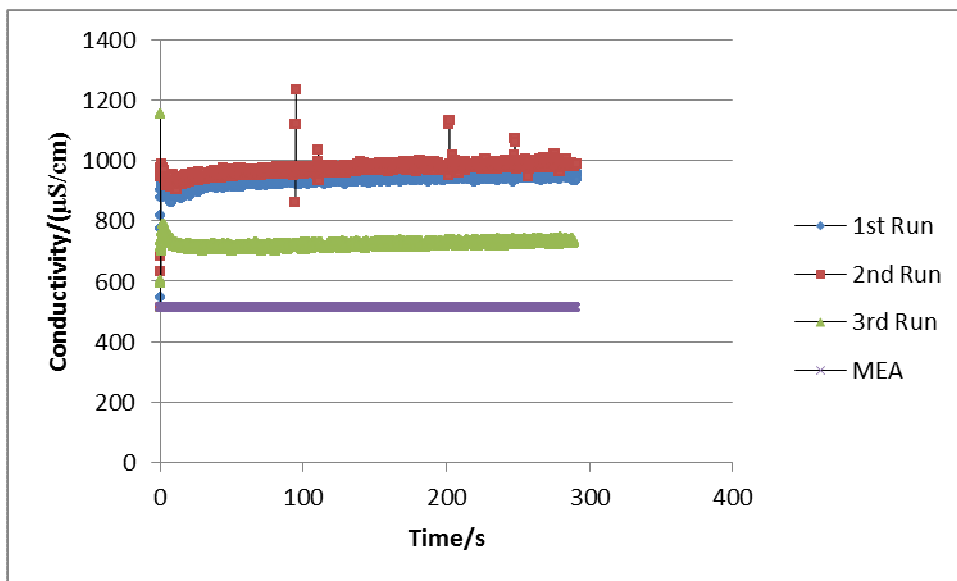
Figure B3: Conductivity-Time Profiles for [MEA] =0.1575 mol/L, $[CO_2]_1$=0.01548 mol/L, $[CO_2]_2$=0.01571 mol/L and $[CO_2]_3$=0.01490 mol/L at 298 K.
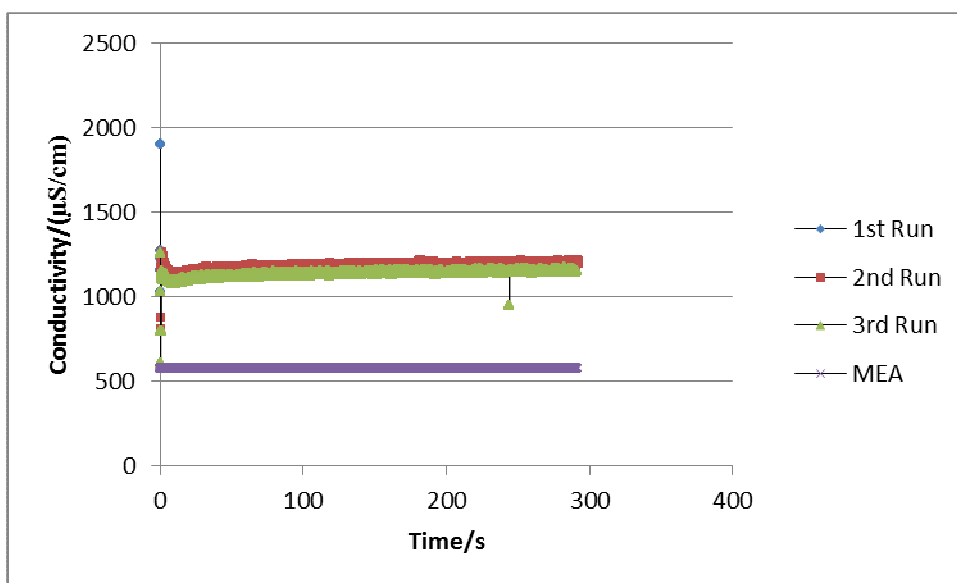
Figure B4: Conductivity-Time Profiles for [MEA] =0.1913 mol/L, $[CO_2]_1$=0.01913 mol/L, $[CO_2]_2$=0.01900 mol/L and $[CO_2]_3$=0.01864 mol/L at 298 K.
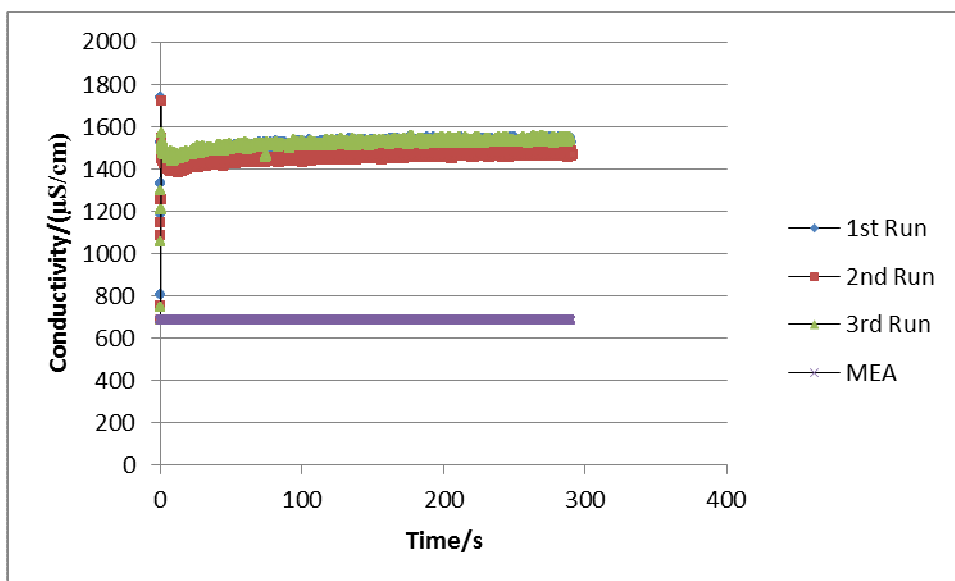
Figure B5: Conductivity-Time Profiles for [MEA] =0.2609 mol/L, $[CO_2]_1$=0.02572 mol/L, $[CO_2]_2$=0.02447 mol/L and $[CO_2]_3$=0.02599 mol/L at 298 K.
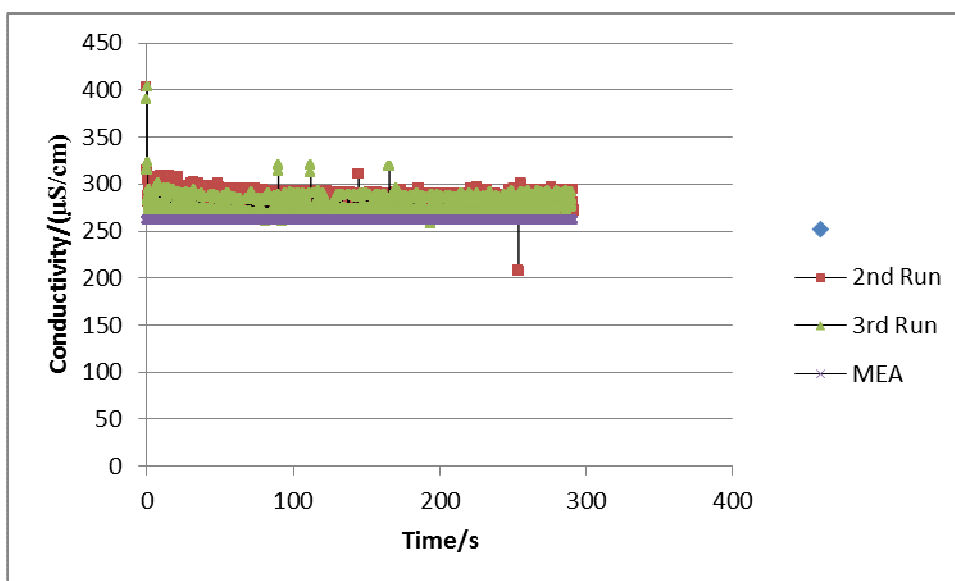
Figure B6: Conductivity-Time Profiles for [MEA] =0.04956 mol/L, $[CO_2]_2$=0.004531 mol/L and $[CO_2]_3$=0.004350 mol/L at 303 K.

117
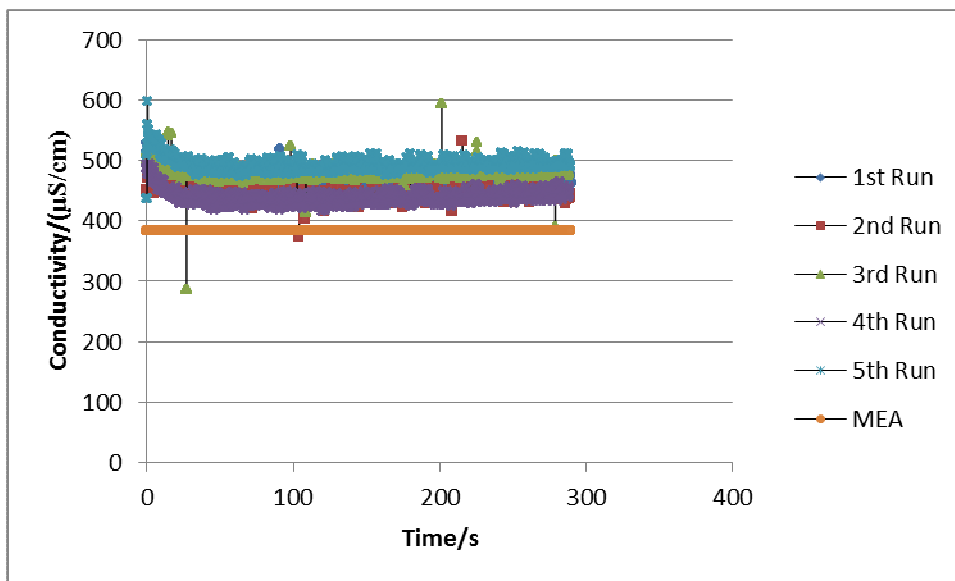
Figure B7: Conductivity-Time Profiles for [MEA] =0.07915 mol/L, $[CO_2]_1$=0.008322 mol/L, $[CO_2]_2$=0.008186mol/L and $[CO_2]_3$=0.008096 mol/L, $[CO_2]_4$=0.007282 mol/L and $[CO_2]_5$=0.007870 mol/L at 303 K.
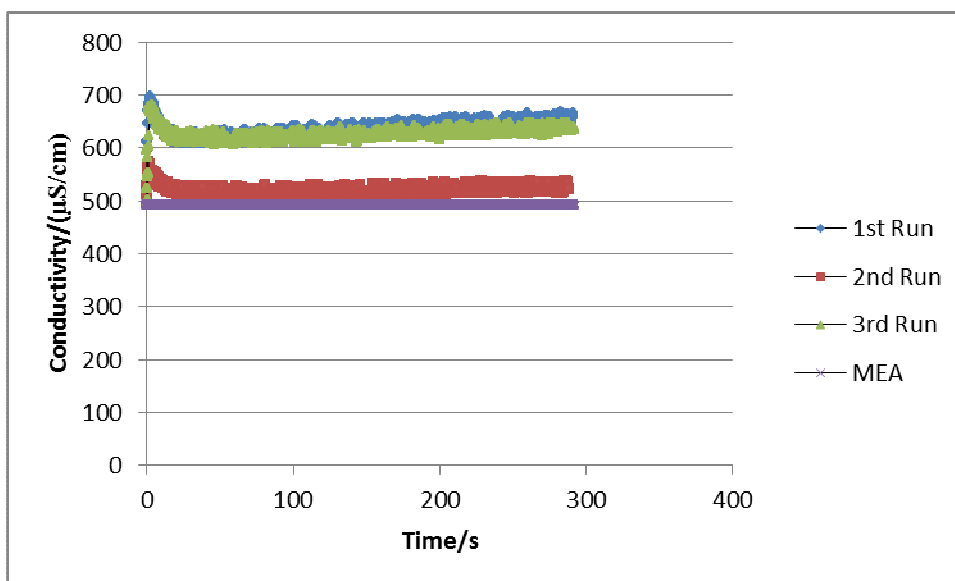
Figure B8: Conductivity-Time Profiles for [MEA] =0.1184 mol/L, $[CO_2]_1$=0.009881 mol/L, $[CO_2]_2$=0.008302 mol/L and $[CO_2]_3$=0.008843 mol/L at 303 K.

118
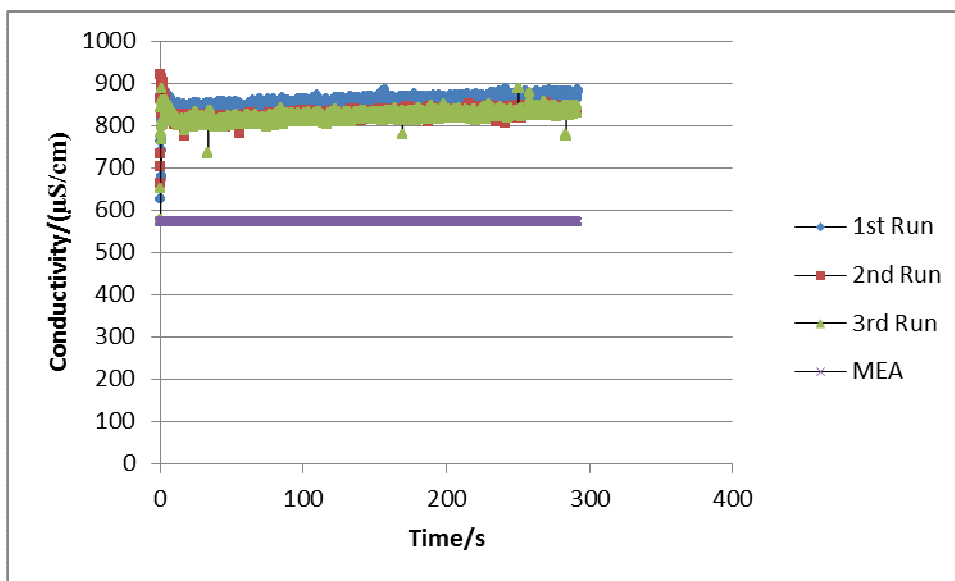
Figure B9: Conductivity-Time Profiles for [MEA] =0.1575 mol/L, $[CO_2]_1$=0.01445 mol/L, $[CO_2]_2$=0.01440 mol/L and $[CO_2]_3$=0.01373 mol/L at303 K .
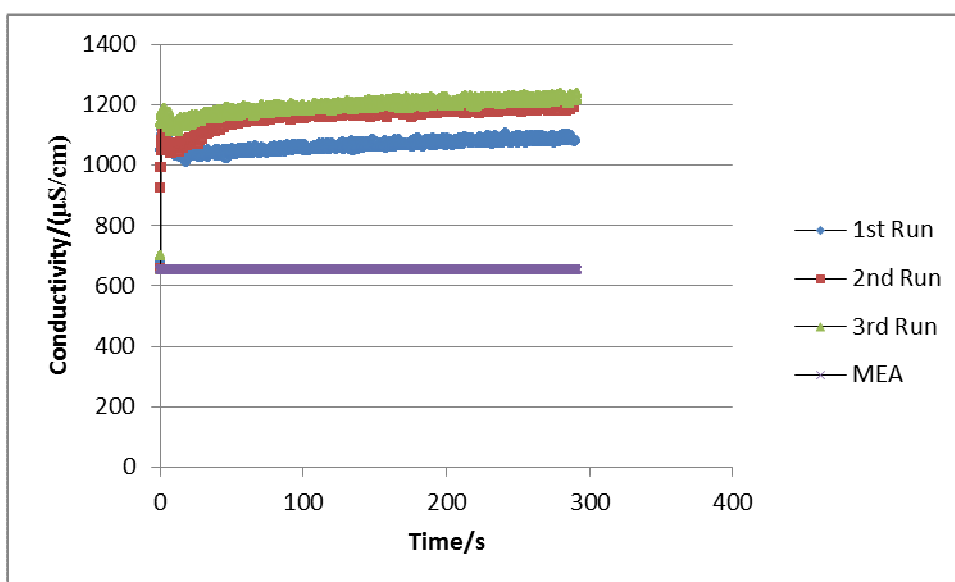
Figure B10: Conductivity-Time Profiles for [MEA] =0.1965 mol/L, $[CO_2]_1$=0.01769 mol/L, $[CO_2]_2$=0.01891 mol/L and $[CO_2]_3$=0.01899 mol/L at 303 K.

119
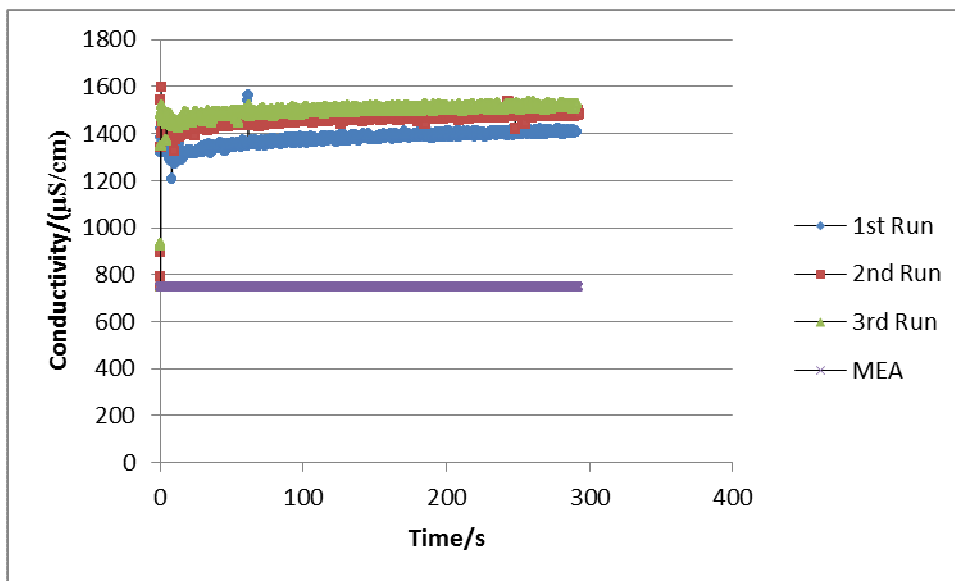
Figure B11: Conductivity-Time Profiles for [MEA] =0.2609 mol/L, $[CO_2]_1$=0.02317 mol/L, $[CO_2]_2$=0.02384 mol/L and $[CO_2]_3$=0.02384 mol/L at 303 K.
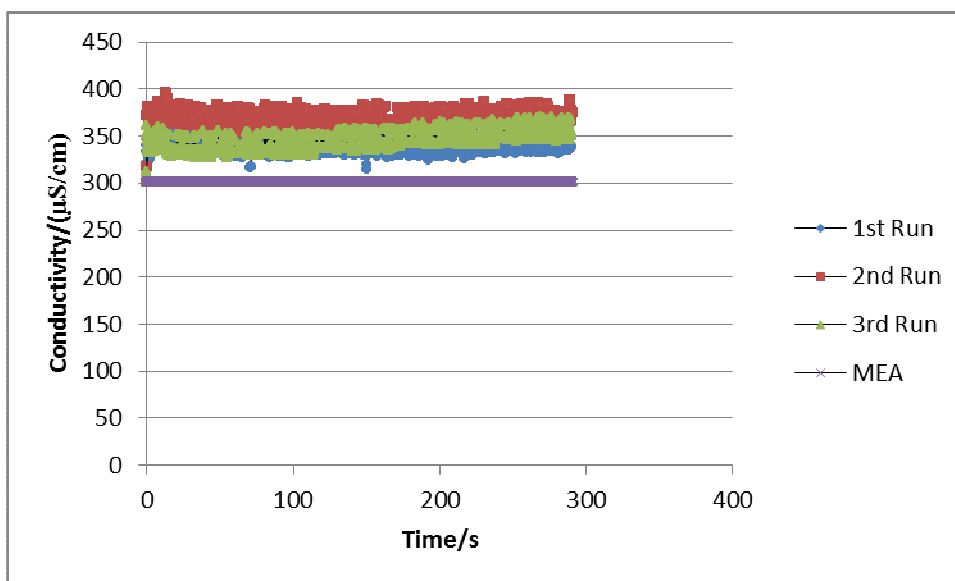
Figure B12: Conductivity-Time Profiles for [MEA] =0.04956 mol/L, $[CO_2]_1$=0.004303 mol/L, $[CO_2]_2$=0.004440 mol/L and $[CO_2]_3$=0.004440 mol/L at 308 K.
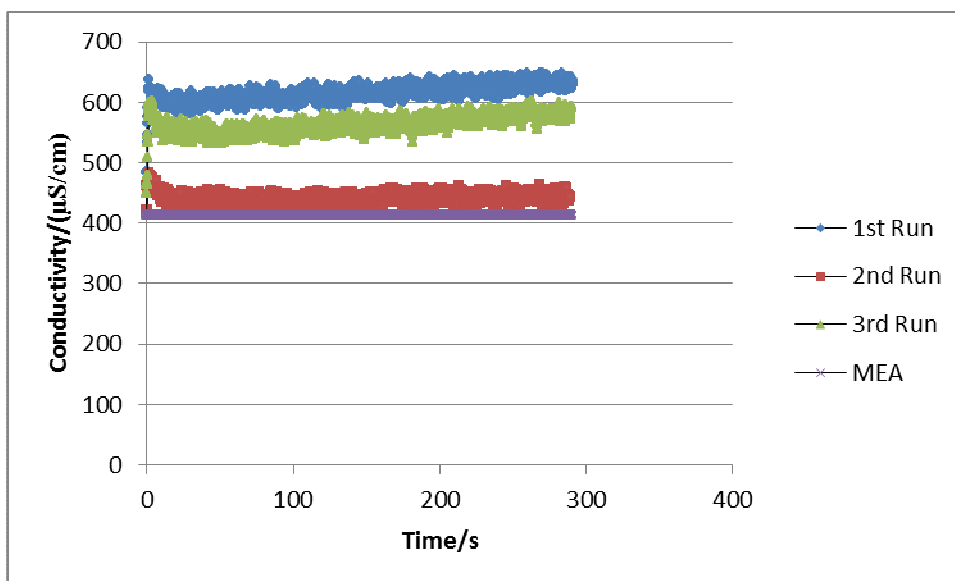
Figure B13: Conductivity-Time Profiles for [MEA] =0.07915 mol/L, $[CO_2]_1$=0.008231 mol/L, $[CO_2]_2$=0.006196 mol/L and $[CO_2]_3$=0.007779 mol/L at 308 K.
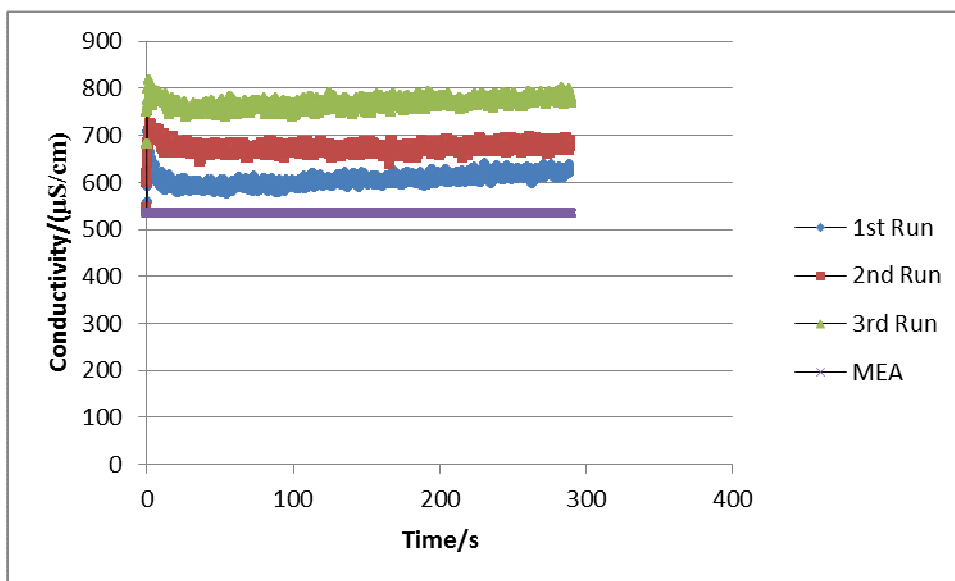
Figure B14: Conductivity-Time Profiles for [MEA] =0.1184 mol/L, $[CO_2]_1$=0.009430 mol/L, $[CO_2]_2$=0.01015 mol/L and $[CO_2]_3$=0.01047 mol/L at 308 K.
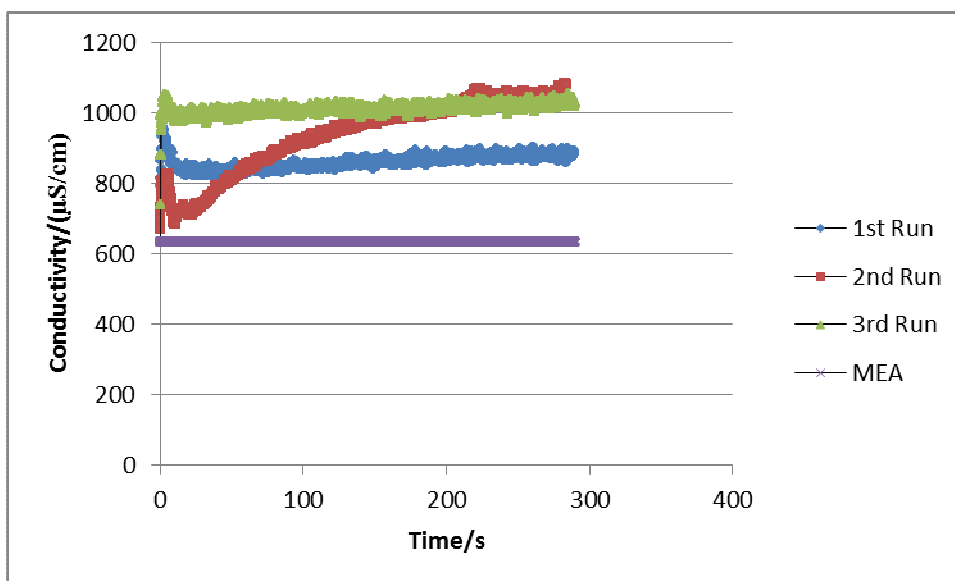
Figure B15: Conductivity-Time Profiles for [MEA] =0.1575 mol/L, $[CO_2]_1$=0.01391 mol/L, $[CO_2]_2$=0.01400 mol/L and $[CO_2]_3$=0.01490 mol/L at 308 K.
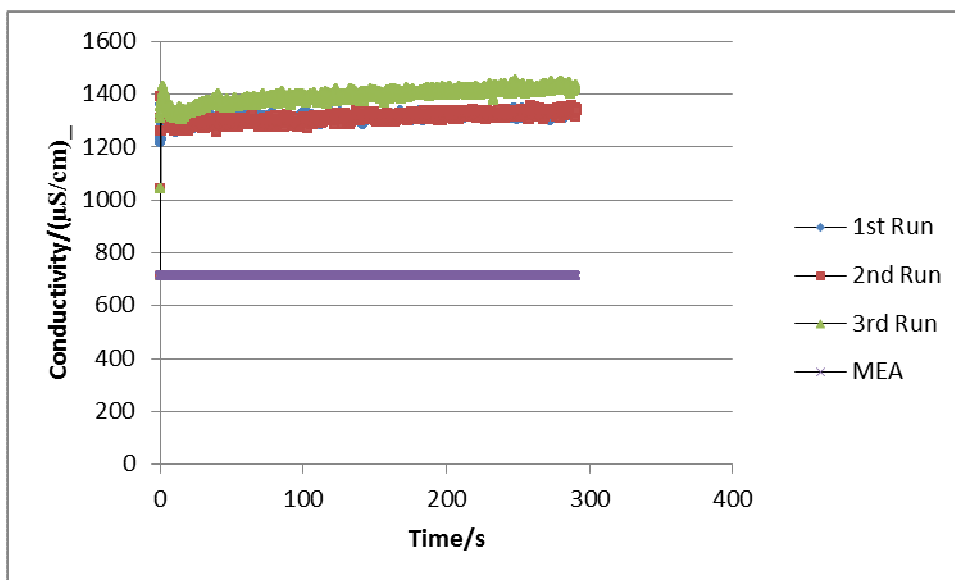
Figure B16: Conductivity-Time Profiles for [MEA] =0.1965 mol/L, $[CO_2]_1$=0.01877 mol/L, $[CO_2]_2$=0.01801 mol/L and $[CO_2]_3$=0.01832 mol/L at 308 K.

122
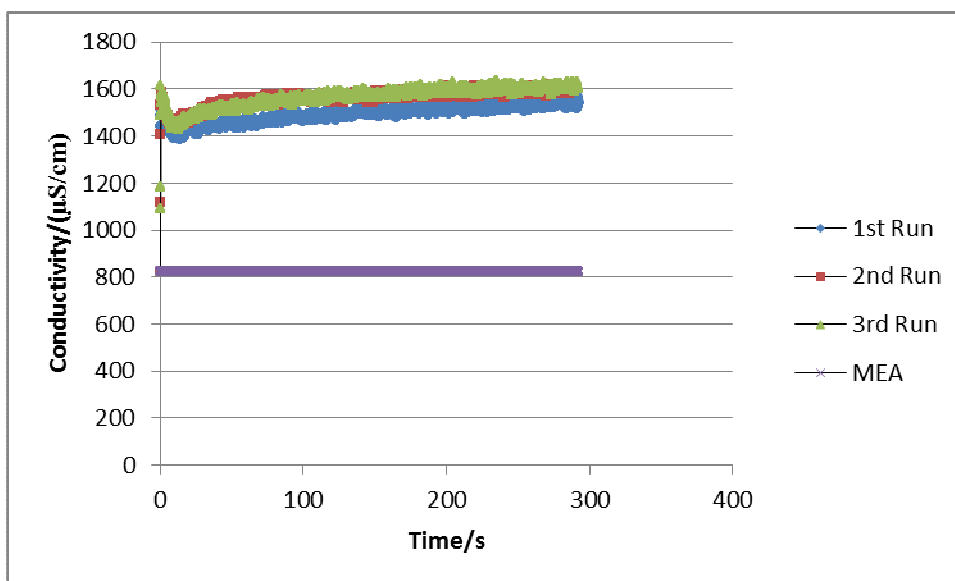
Figure B17: Conductivity-Time Profiles for [MEA] =0.2609 mol/L, $[CO_2]_1$=0.02245 mol/L, $[CO_2]_2$=0.02375 mol/L and $[CO_2]_3$=0.02411 mol/L at 308 K.
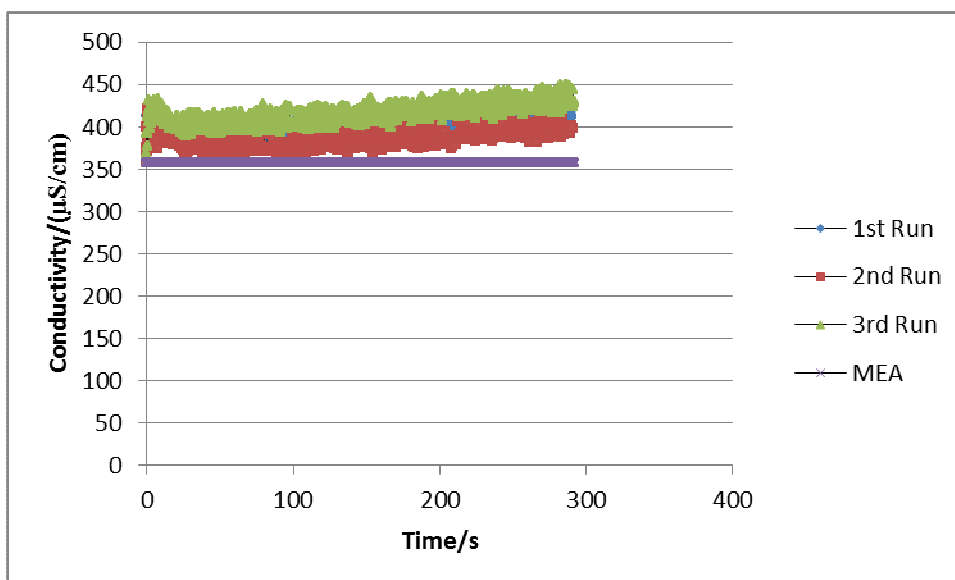
Figure B18: Conductivity-Time Profiles for [MEA] =0.04956 mol/L, $[CO_2]_1$=0.004757 mol/L, $[CO_2]_2$=0.004621 mol/L and $[CO_2]_3$=0.005029 mol/L at 313 K.
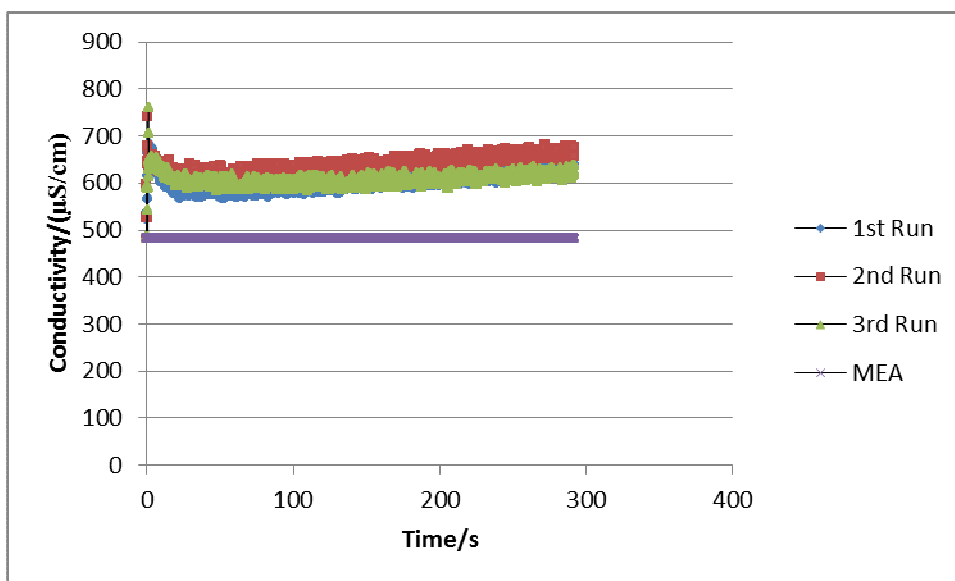
Figure B19: Conductivity-Time Profiles for [MEA] =0.07915 mol/L, $[CO_2]_1$=0.006377 mol/L, $[CO_2]_2$=0.007689 mol/L and $[CO_2]_3$=0.006648 mol/L at 313 K.
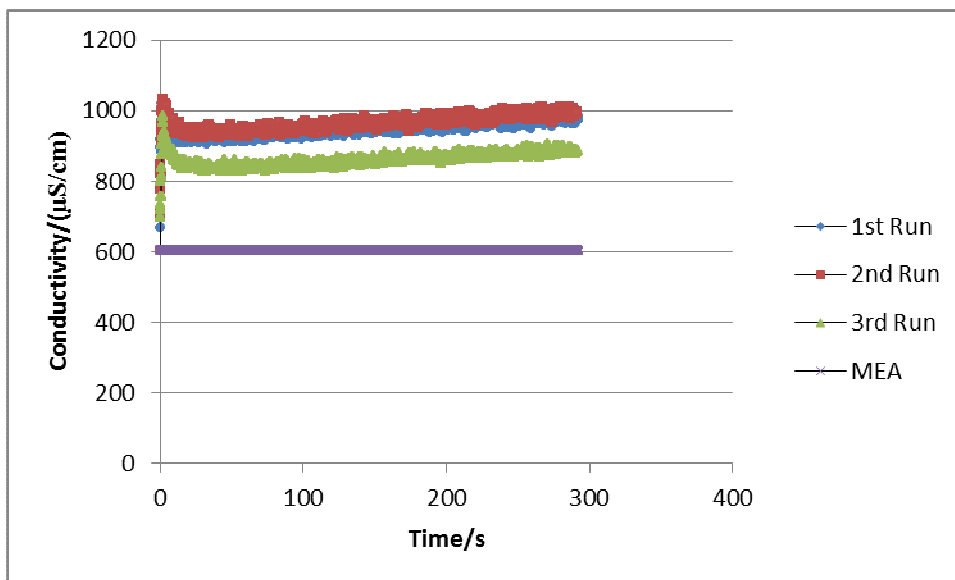
Figure B20: Conductivity-Time Profiles for [MEA] =0.1184 mol/L, $[CO_2]_1$=0.01060 mol/L, $[CO_2]_2$=0.01128 mol/L and $[CO_2]_3$=0.01020 mol/L at 313 K.

124
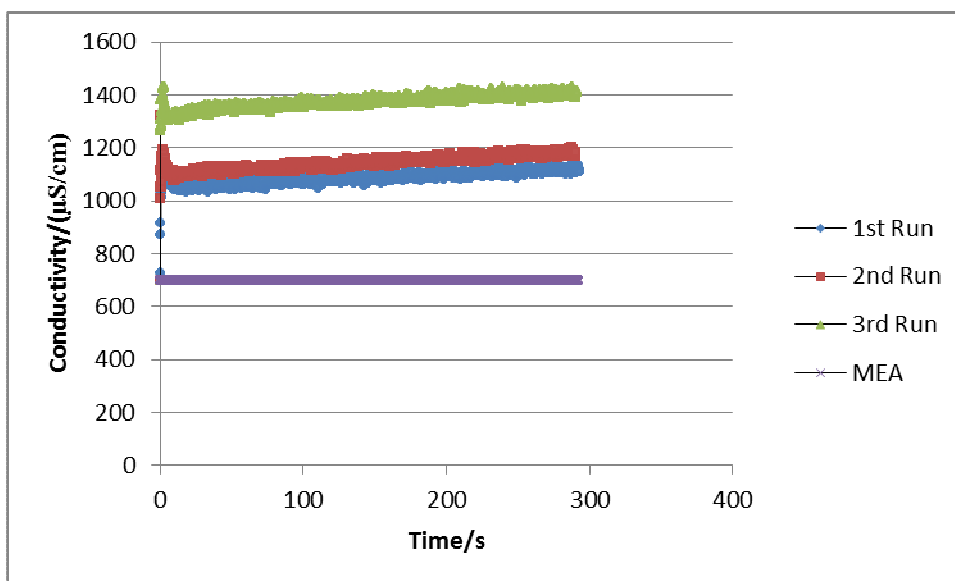
Figure B21: Conductivity-Time Profiles for [MEA] =0.1575 mol/L, $[CO_2]_1$=0.01413 mol/L, $[CO_2]_2$=0.01422 mol/L and $[CO_2]_3$=0.01512 mol/L at 313 K.
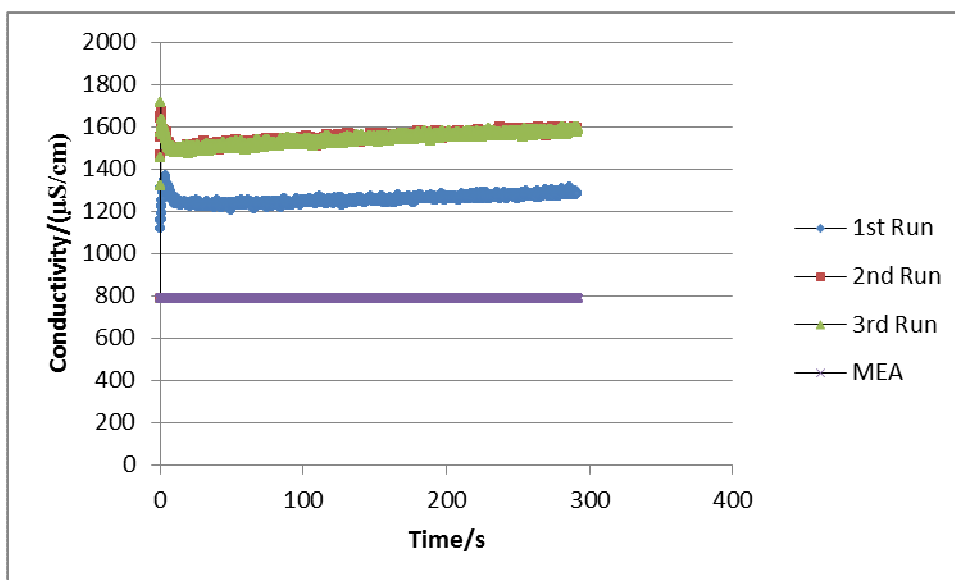
Figure B22: Conductivity-Time Profiles for [MEA] =0.1965 mol/L, $[CO_2]_1$=0.01891 mol/L, $[CO_2]_2$=0.01931mol/L and $[CO_2]_3$=0.01918 mol/L at 313 K.
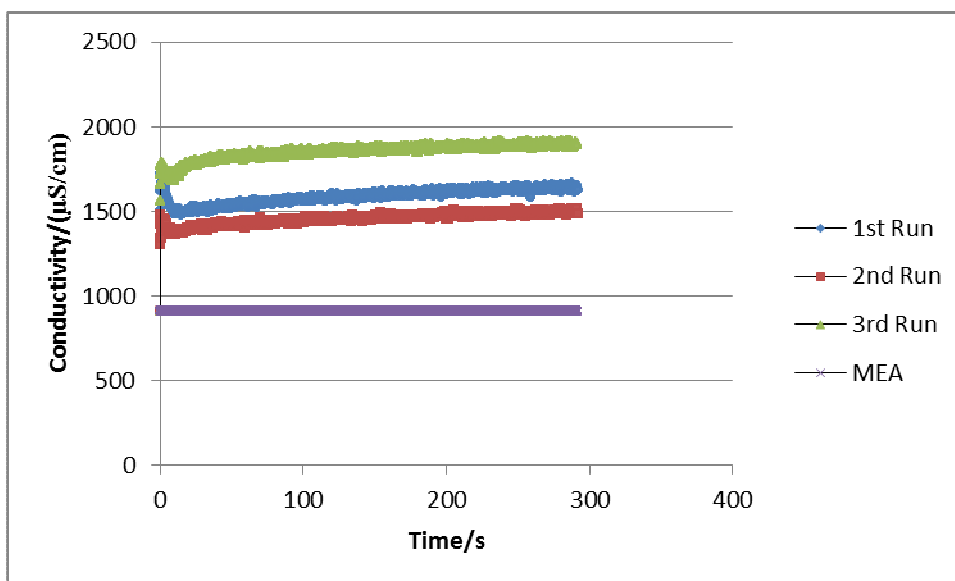
Figure B23: Conductivity-Time Profiles for [MEA] =0.2609 mol/L, $[CO_2]_1$=0.02478 mol/L, $[CO_2]_2$=0.02429 mol/L and $[CO_2]_3$=0.02545 mol/L at 313 K.

APPENDIX C: CONDUCTIVITY-TIME PROFILES FOR SECOND SERIES RUNS
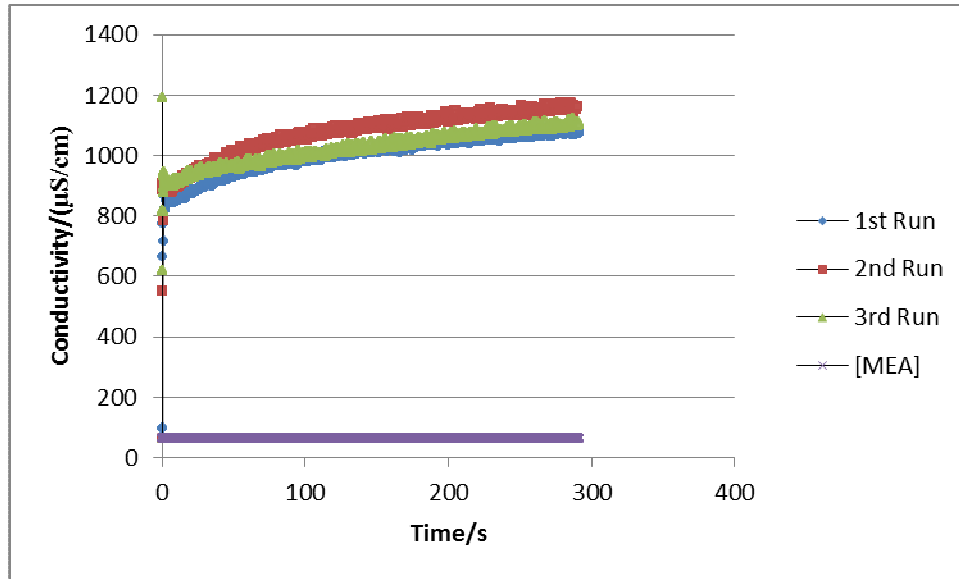
Figure C1: Conductivity-Time Profiles for [MEA] =0.01986 mol/L, $[CO_2]_1$=0.01993 mol/L, $[CO_2]_2$=0.01938 mol/L and $[CO_2]_3$=0.01938 mol/L at 298 K.
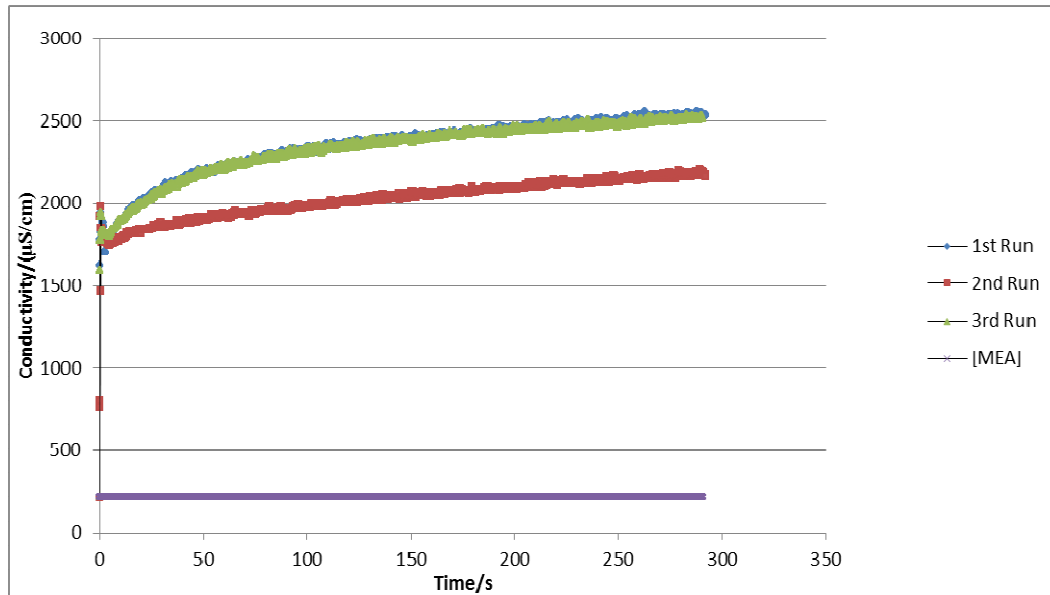
Figure C2: Conductivity-Time Profiles for [MEA] =0.04956 mol/L, $[CO_2]_1$=0.05147 mol/L, $[CO_2]_2$=0.04721 mol/L and $[CO_2]_3$=0.05269 mol/L at298 K.
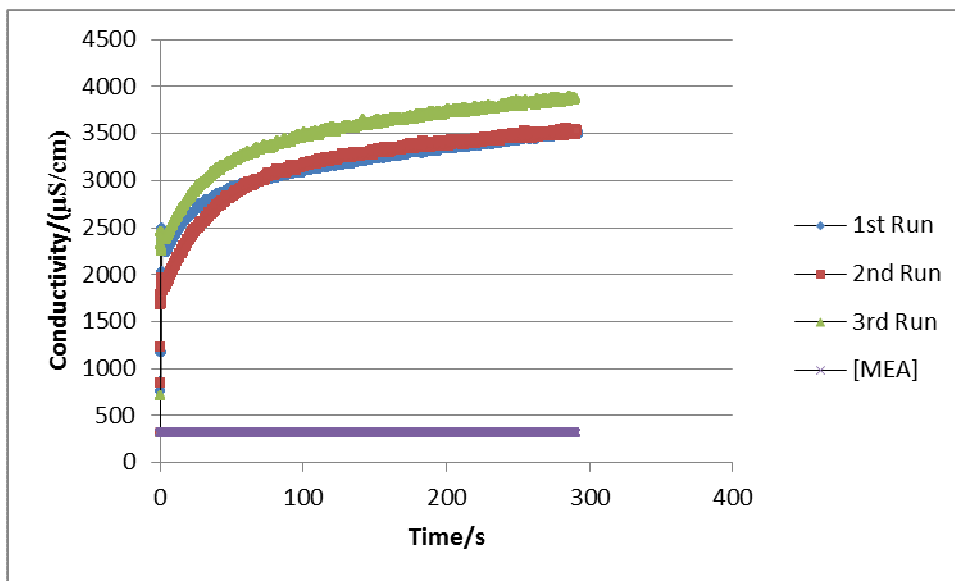
Figure C3: Conductivity-Time Profiles for [MEA] =0.07915 mol/L, $[CO2]_1$=0.07761 mol/L, $[CO2]_2$=0.07761 mol/L and $[CO2]_3$=0.07996 mol/L at 298 K.
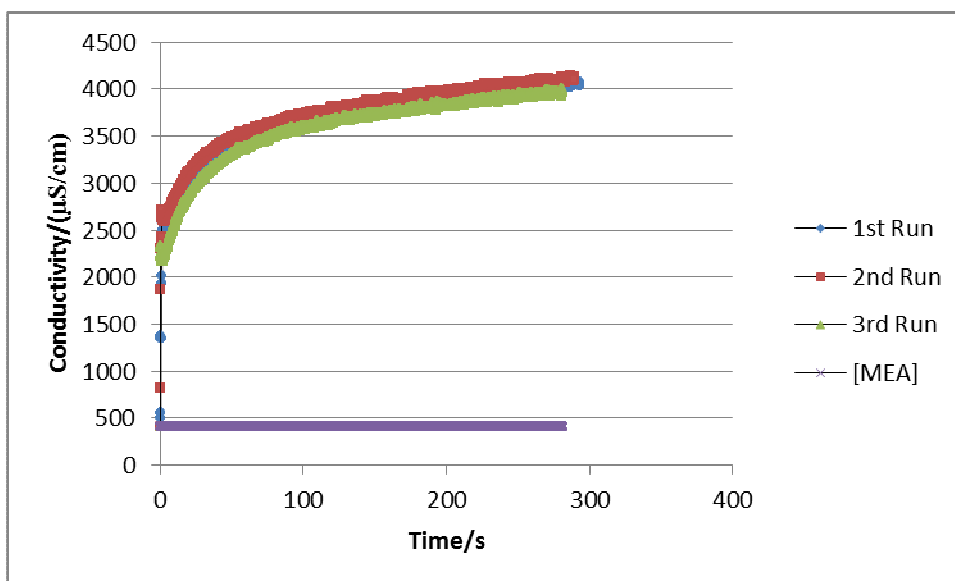
Figure C4: Conductivity-Time Profiles for [MEA] =0.1184 mol/L, $[CO_2]_1$=0.1173 mol/L, $[CO_2]_2$=0.1183 mol/L and $[CO_2]_3$=0.1169 mol/L at 298 K.
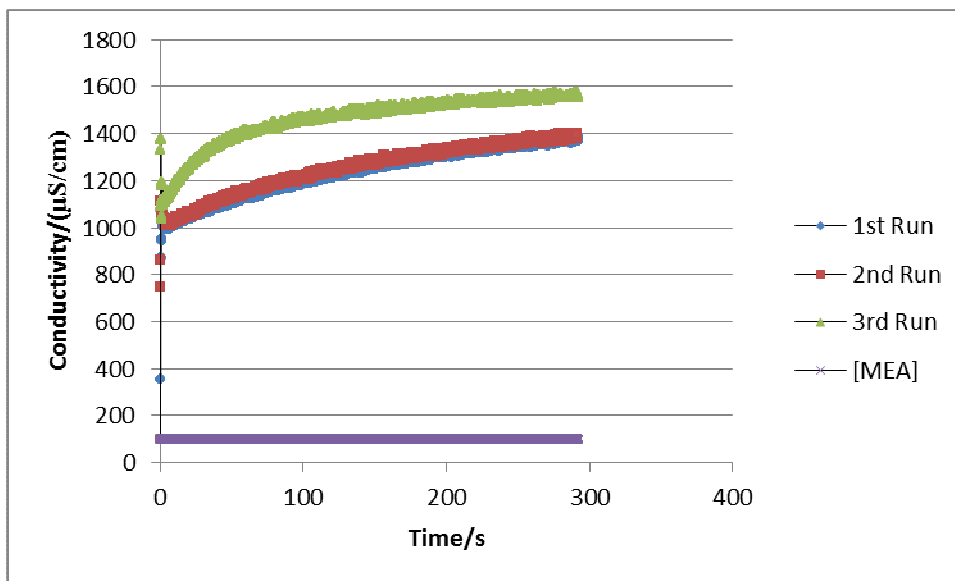
Figure C5: Conductivity-Time Profiles for [MEA] =0.01986 mol/L, $[CO_2]_1$=0.01943 mol/L, $[CO_2]_2$=0.01938 mol/L and $[CO_2]_3$=0.02111 mol/L at 303K.
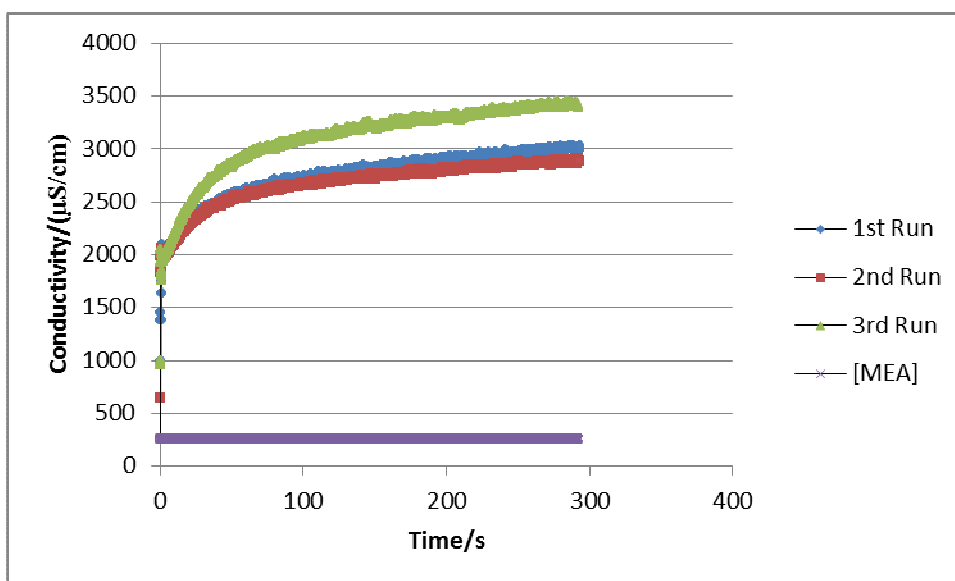
Figure C6: Conductivity-Time Profiles for [MEA] =0.04956 mol/L, $[CO_2]_1$=0.04834 mol/L, $[CO_2]_2$=0.04948 mol/L and $[CO_2]_3$=0.05034 mol/L at 303K.
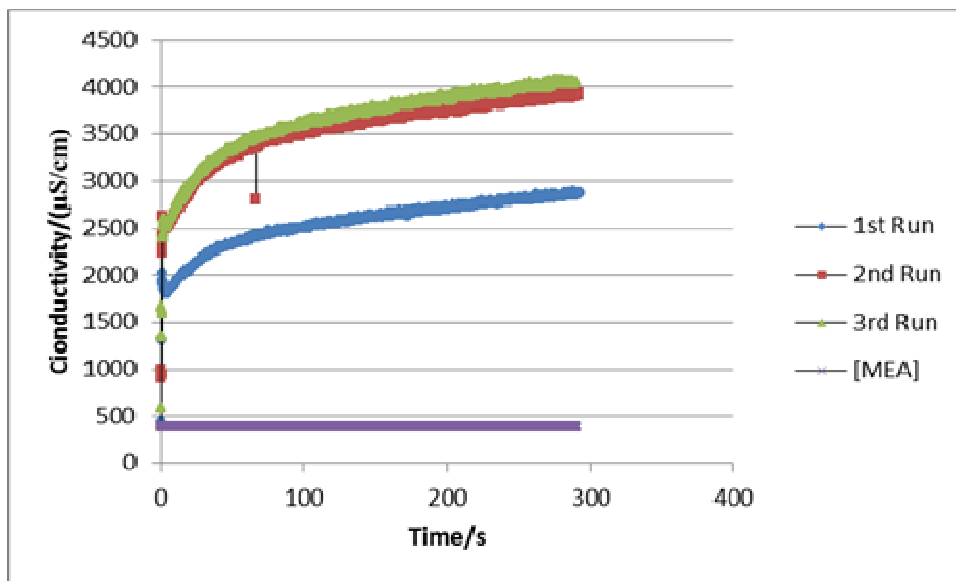
Figure C7: Conductivity-Time Profiles for [MEA] =0.0791 5mol/L, $[CO_2]_1$=0.07928 mol/L, $[CO_2]_2$=0.07956 mol/L and $[CO_2]_3$=0.07983 mol/L at 303K.
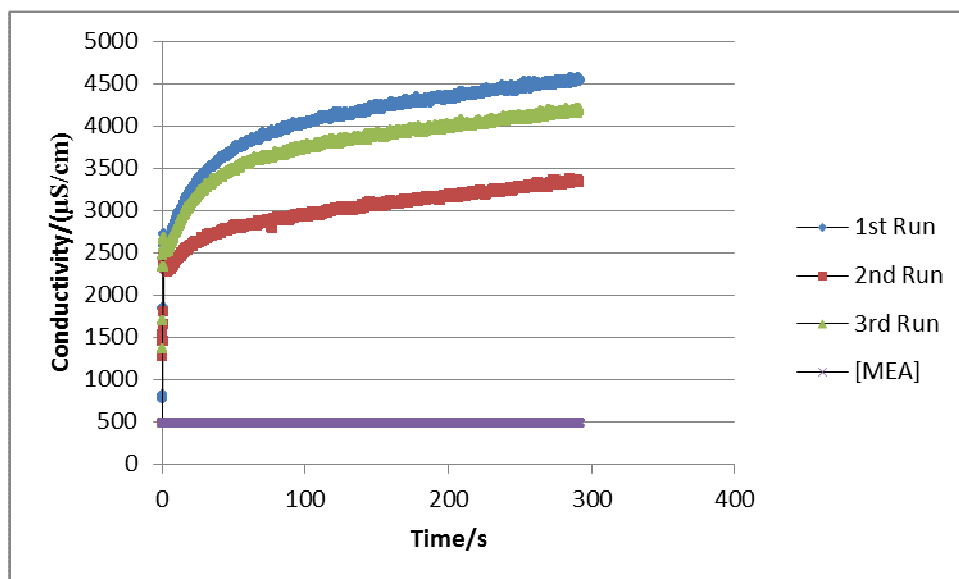
Figure C8: Conductivity-Time Profiles for [MEA] =0.1184 mol/L, $[CO_2]_1$=0.1185 mol/L, $[CO_2]_2$=0.1164 mol/L and $[CO_2]_3$=0.1171 mol/L at 303K.
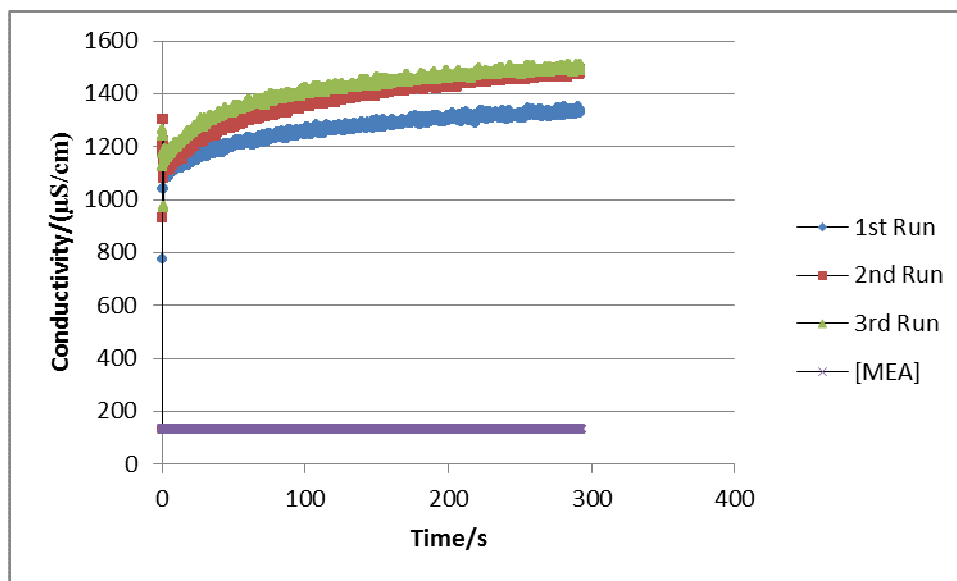
Figure C9: Conductivity-Time Profiles for [MEA] =0.01986 mol/L, $[CO_2]_1$=0.01834 mol/L, $[CO_2]_2$=0.01897 mol/L and $[CO_2]_3$=0.02015 mol/L at 308 K.
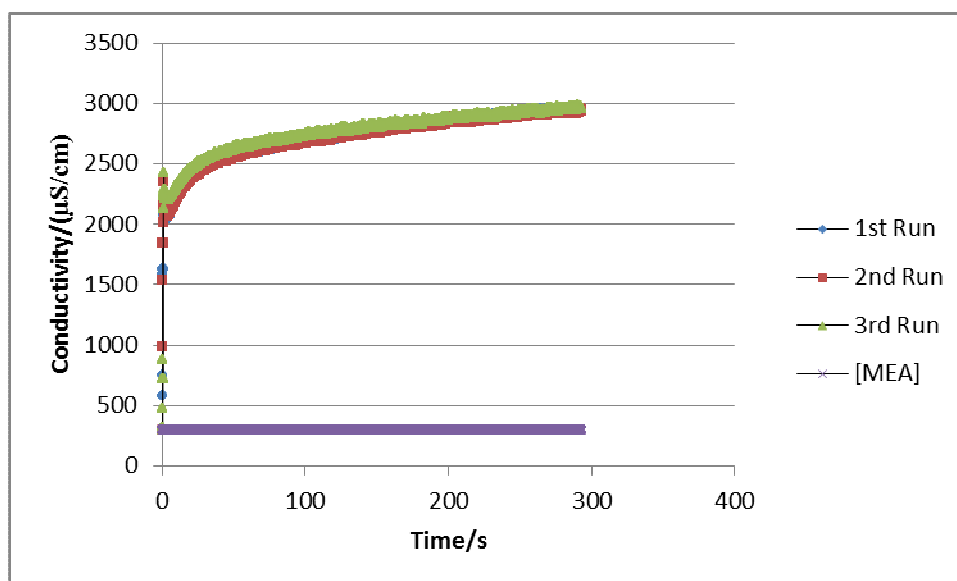
Figure C10: Conductivity-Time Profiles for [MEA] =0.04956 mol/L, $[CO2]_1$=0.04807 mol/L, $[CO2]_2$=0.04776 mol/L and $[CO2]_3$=0.04907 mol/L at 308 K.

131
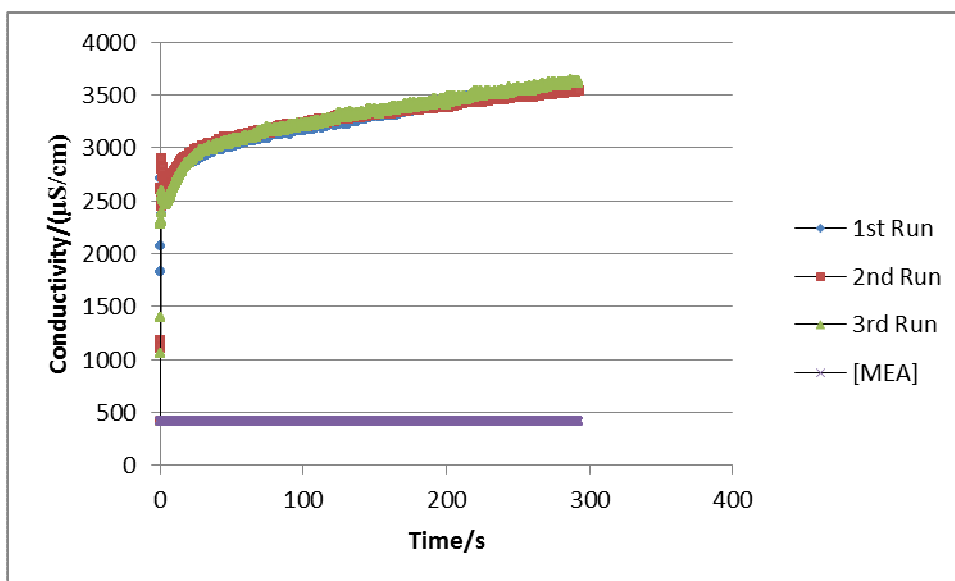
Figure C11: Conductivity-Time Profiles for [MEA] =0.07915 mol/L, $[CO2]_1$=0.07743 mol/L, $[CO2]_2$=0.07666 mol/L and $[CO2]_3$=0.07702 mol/L at 308 K.
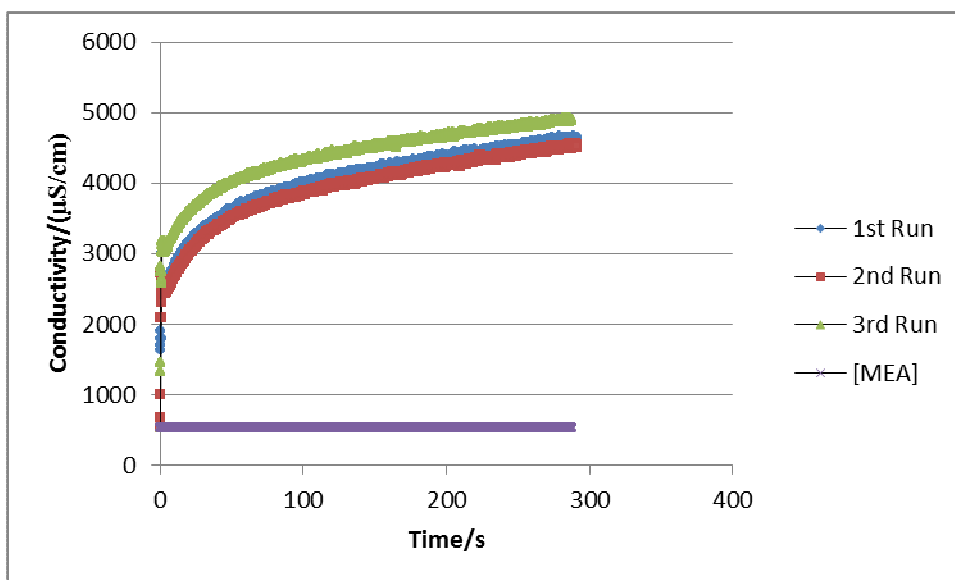
Figure C12: Conductivity-Time Profiles for [MEA] =0.1184 mol/L, $[CO_2]_1$=0.1177 mol/L, $[CO_2]_2$=0.1165 mol/L and $[CO_2]_3$=0.1193 mol/L at 308 K.

132
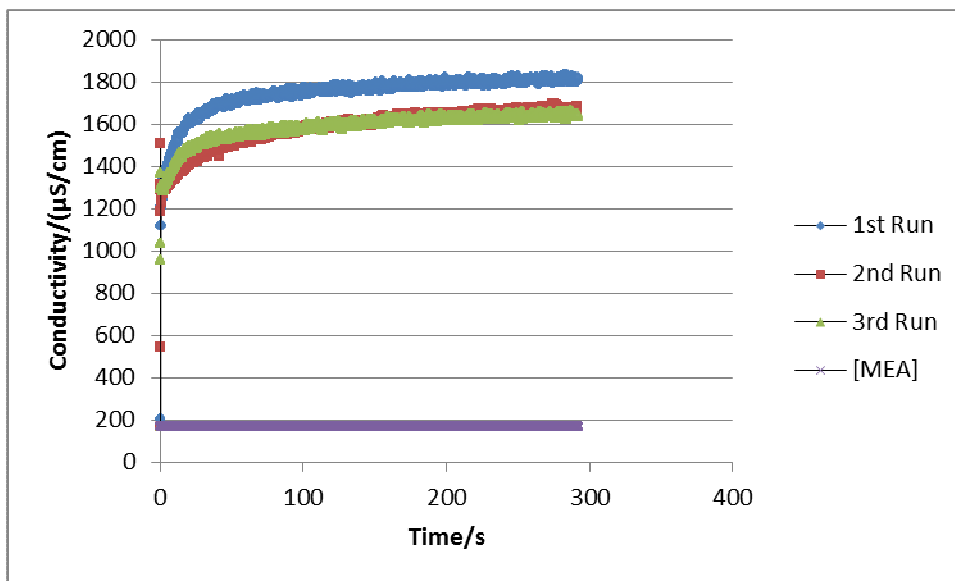
Figure C11: Conductivity-Time Profiles for [MEA] =0.01986 mol/L, $[CO_2]_1$=0.02043 mol/L, $[CO_2]_2$=0.01938 mol/L and $[CO_2]_3$=0.01888 mol/L at 313 K.
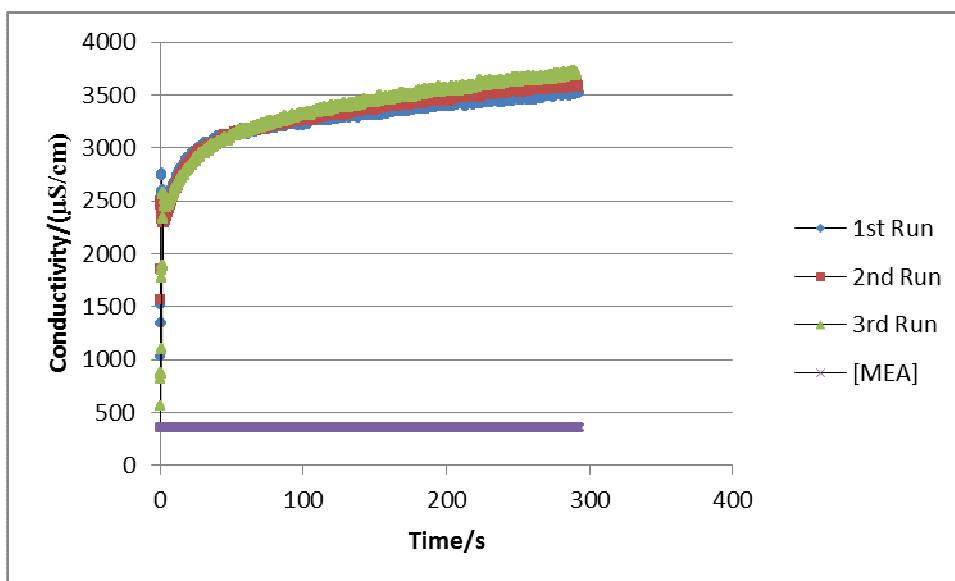
Figure C12: Conductivity-Time Profiles for [MEA] =0.04956 mol/L, $[CO_2]_1$=0.04979 mol/L, $[CO_2]_2$=0.04998 mol/L and $[CO_2]_3$=0.05029 mol/L at313 K.
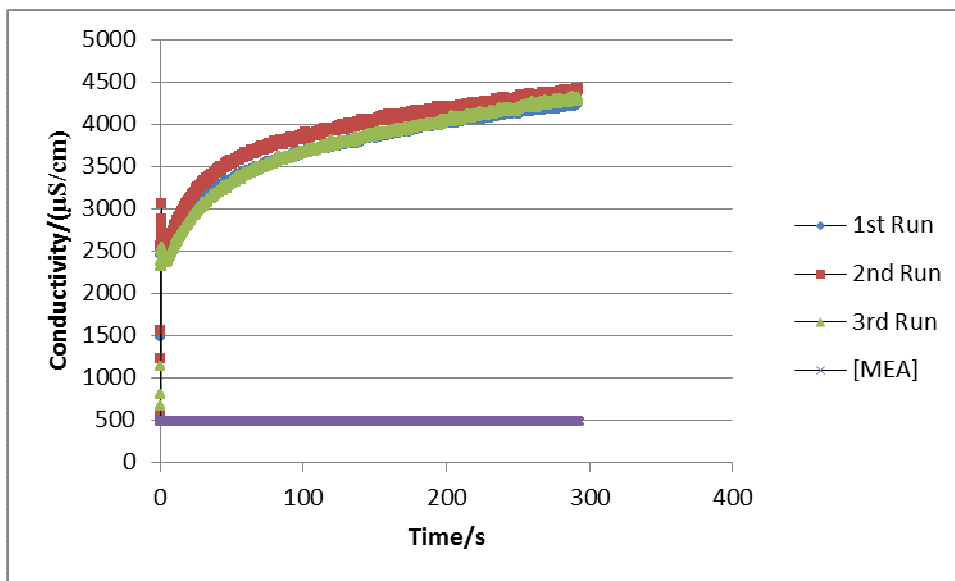
Figure C13: Conductivity-Time Profiles for [MEA] =0.07915 mol/L, $[CO_2]_1$=0.07765 mol/L, $[CO_2]_2$=0.07978 mol/L and $[CO_2]_3$=0.07892 mol/L at 313 K.
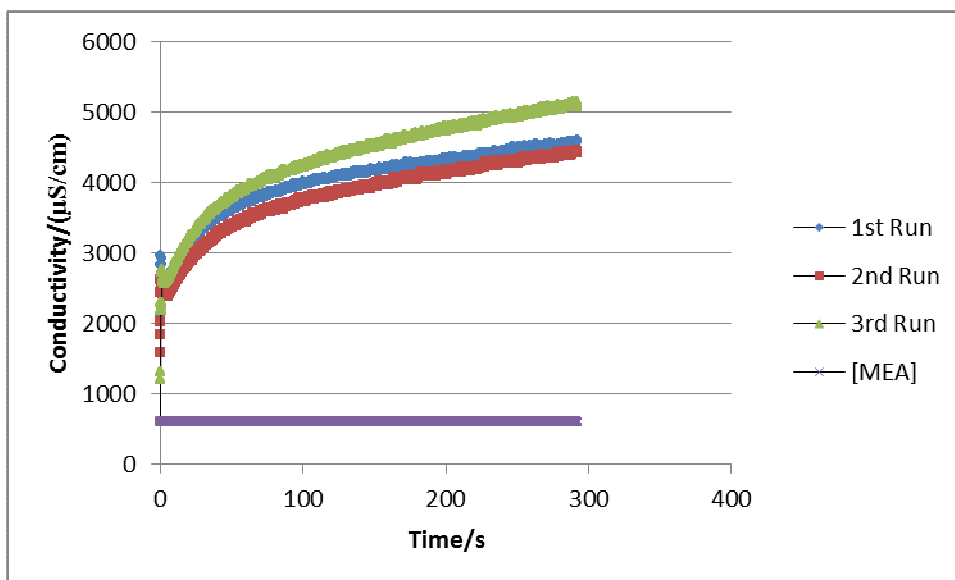
Figure C14: Conductivity-Time Profiles for [MEA] =0.1184 mol/L, $[CO_2]_1$=0.1194 mol/L, $[CO_2]_2$=0.1182 mol/L and $[CO_2]_3$=0.1235 mol/L at 313 K.

APPENDIX D: CONVERSION-TIME PROFILES FOR FIRST SERIES RUNS
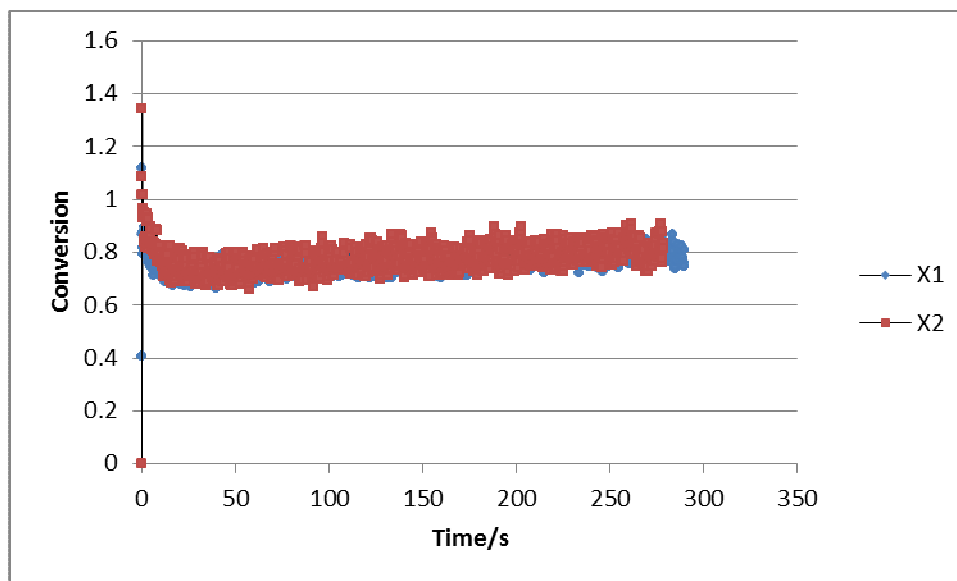
Figure D1: Conversion-Time Profiles for [MEA] =0.07915 mol/L, $[CO_2]_1$=0.01004 mol/L, $[CO_2]_2$=0.009633 mol/L at 298 K.
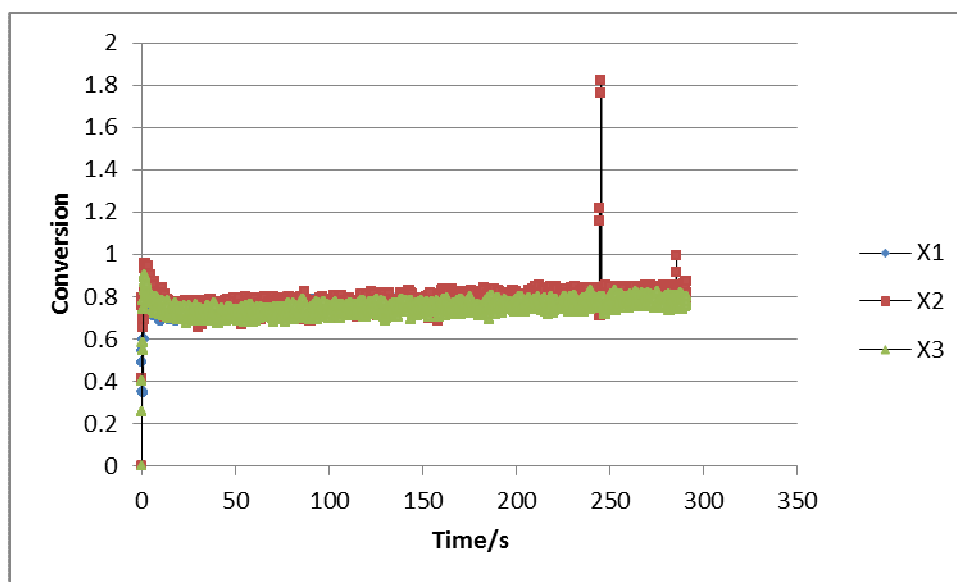
Figure D2: Conversion-Time Profiles for [MEA] =0.1184 mol/L, $[CO_2]_1$=0.01114 mol/L, $[CO_2]_2$=0.01038 mol/L and $[CO_2]_3$=0.01083 mol/L at298 K.
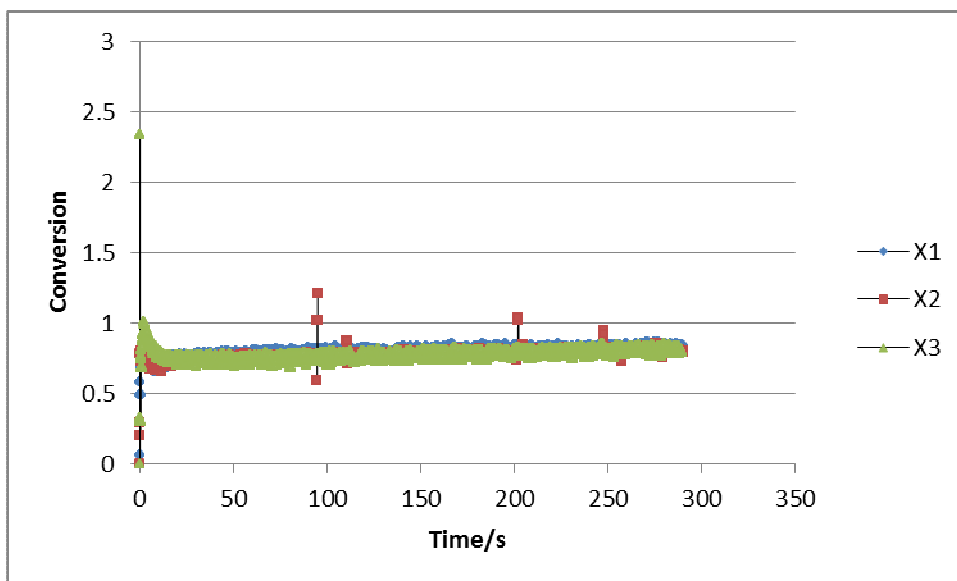
Figure D3: Conversion-Time Profiles for [MEA] =0.1575 mol/L, $[CO_2]_1$=0.01548 mol/L, $[CO_2]_2$=0.01571 mol/L and $[CO_2]_3$=0.01490 mol/L at 298 K.
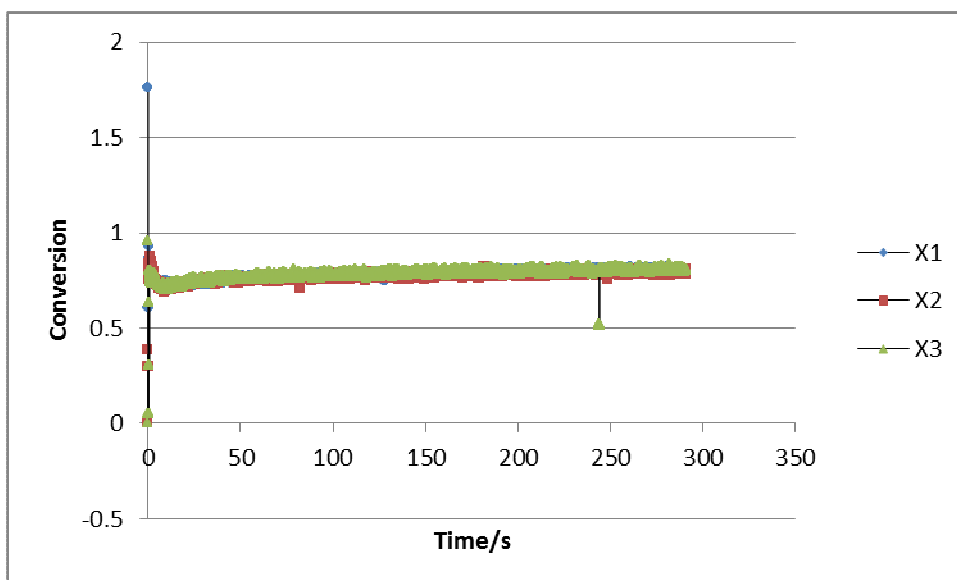
Figure D4: Conversion-Time Profiles for [MEA] =0.1913 mol/L, $[CO_2]_1$=0.01913 mol/L, $[CO_2]_2$=0.01900 mol/L and $[CO_2]_3$=0.01864 mol/L at 298 K.

136
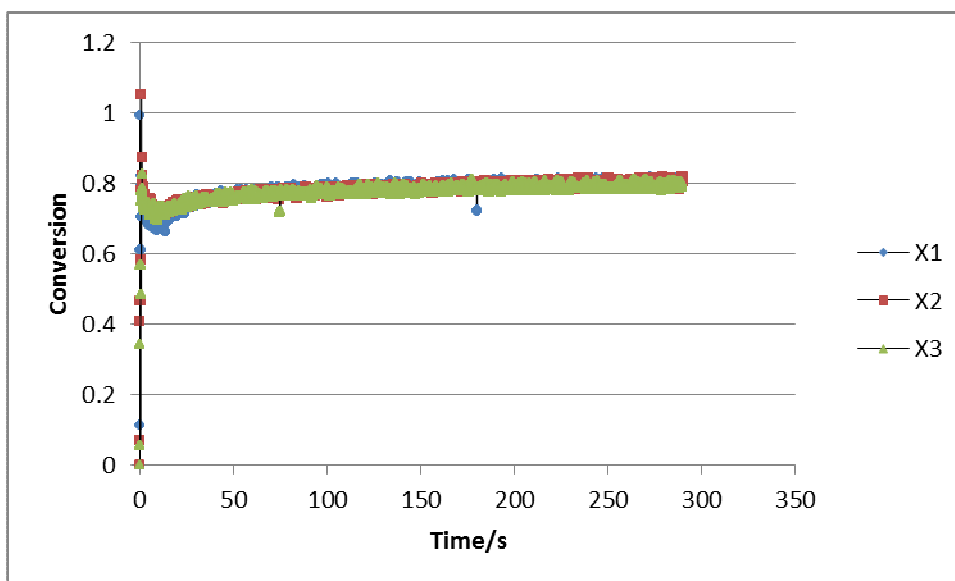
Figure D5: Conversion-Time Profiles for [MEA] =0.2609 mol/L, $[CO_2]_1$=0.02572 mol/L, $[CO_2]_2$=0.02447 mol/L and $[CO_2]_3$=0.02599 mol/L at 298 K.
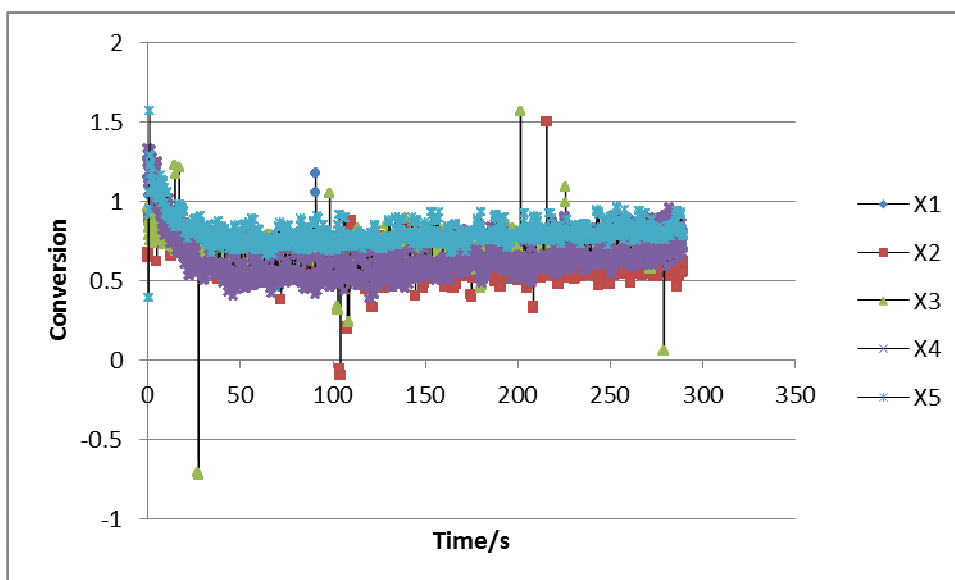
Figure D7: Conversion-Time Profiles for [MEA] =0.07915 mol/L, $[CO_2]_1$=0.008322 mol/L, $[CO_2]_2$=0.008186 mol/L and $[CO_2]_3$=0.008096 mol/L, $[CO_2]_4$=0.007282 mol/L and $[CO_2]_5$=0.007870 mol/L at 303 K.
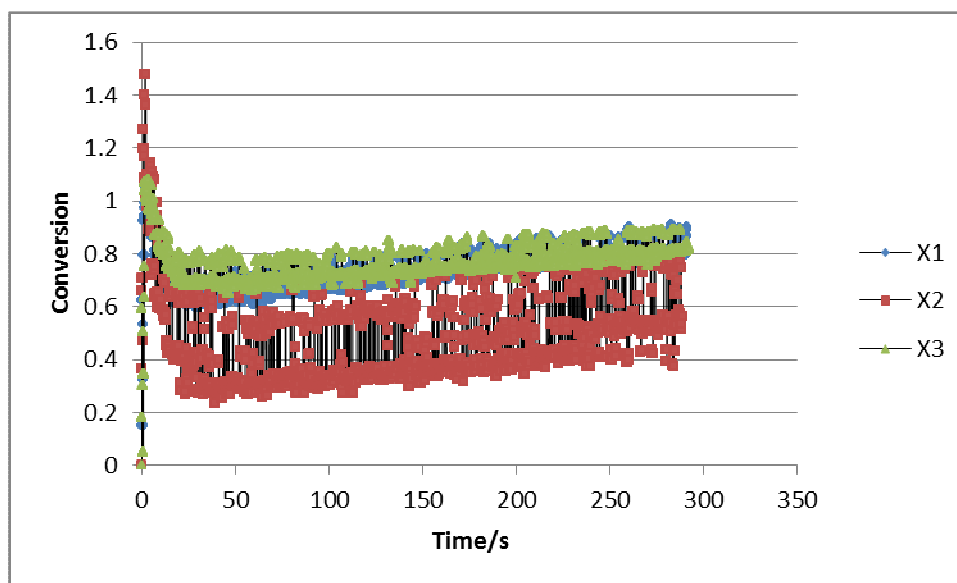
Figure D8: Conversion-Time Profiles for [MEA] =0.1184 mol/L, $[CO_2]_1$=0.009881 mol/L, $[CO_2]_2$=0.008302 mol/L and $[CO_2]_3$=0.008843 mol/L at303 K.
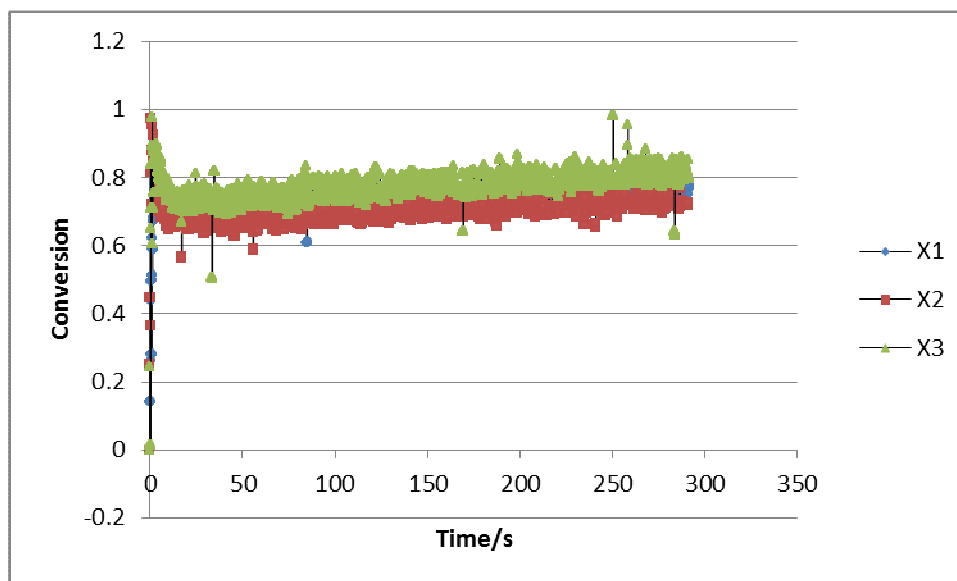
Figure D9: Conversion-Time Profiles for [MEA] =0.1575 mol/L, $[CO_2]_1$=0.01445 mol/L, $[CO_2]_2$=0.01440 mol/L and $[CO_2]_3$=0.01373 mol/L at 303 K.

138
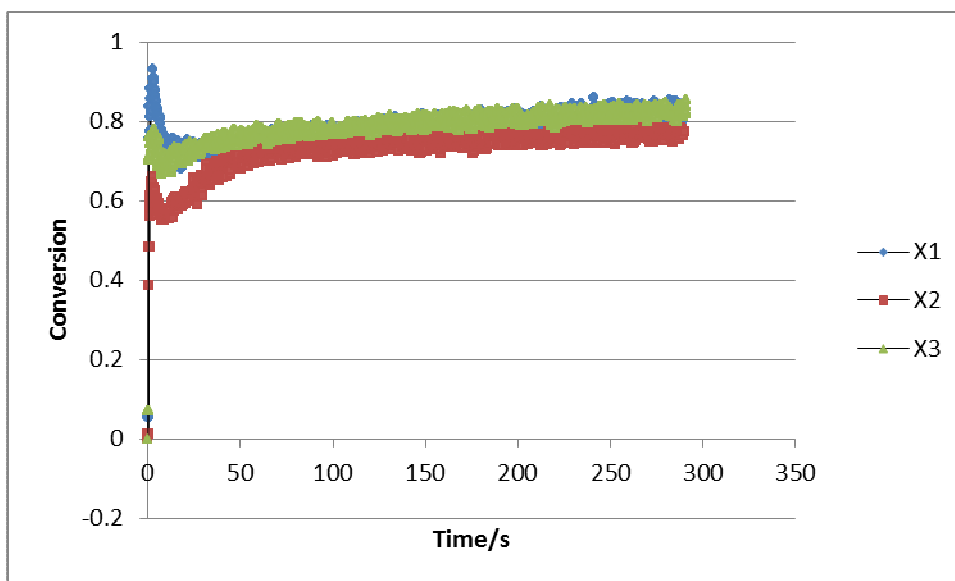
Figure D10: Conversion-Time Profiles for [MEA] =0.1965 mol/L, $[CO_2]_1$=0.01769 mol/L, $[CO_2]_2$=0.01891 mol/L and $[CO_2]_3$=0.01899 mol/L at 303 K.
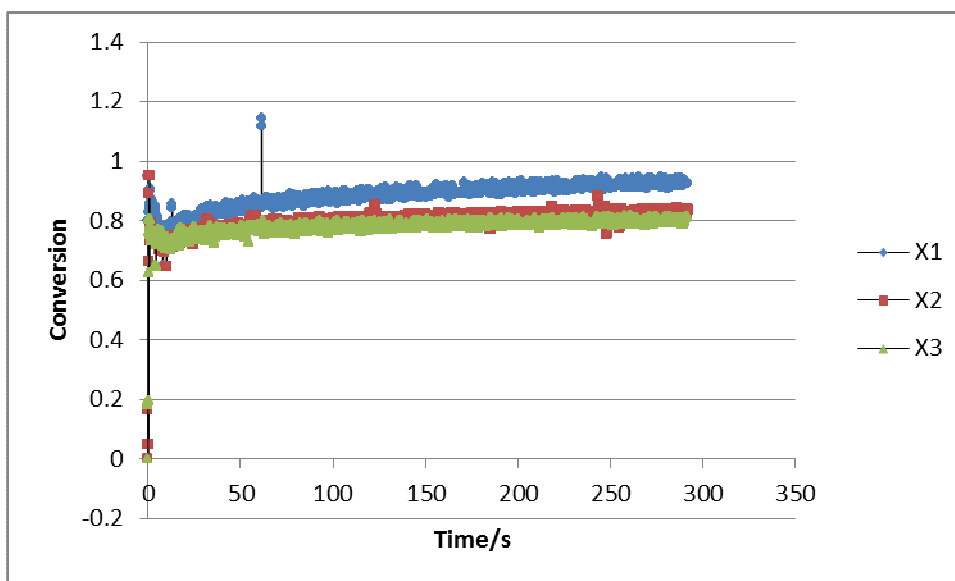
Figure D11: Conversion-Time Profiles for [MEA] =0.2609 mol/L, $[CO_2]_1$=0.02317 mol/L, $[CO_2]_2$=0.02384 mol/L and $[CO_2]_3$=0.02384 mol/L at 303 K.
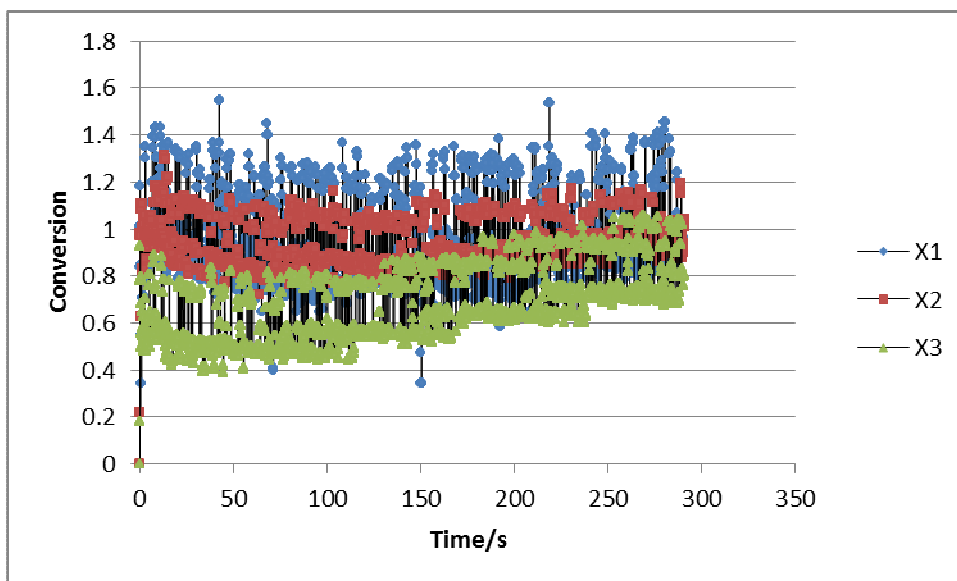
Figure D12: Conversion-Time Profiles for [MEA] =0.04956 mol/L, $[CO_2]_1$=0.004303 mol/L, $[CO_2]_2$=0.004440 mol/L and $[CO_2]_3$=0.004440 mol/L at 308 K.
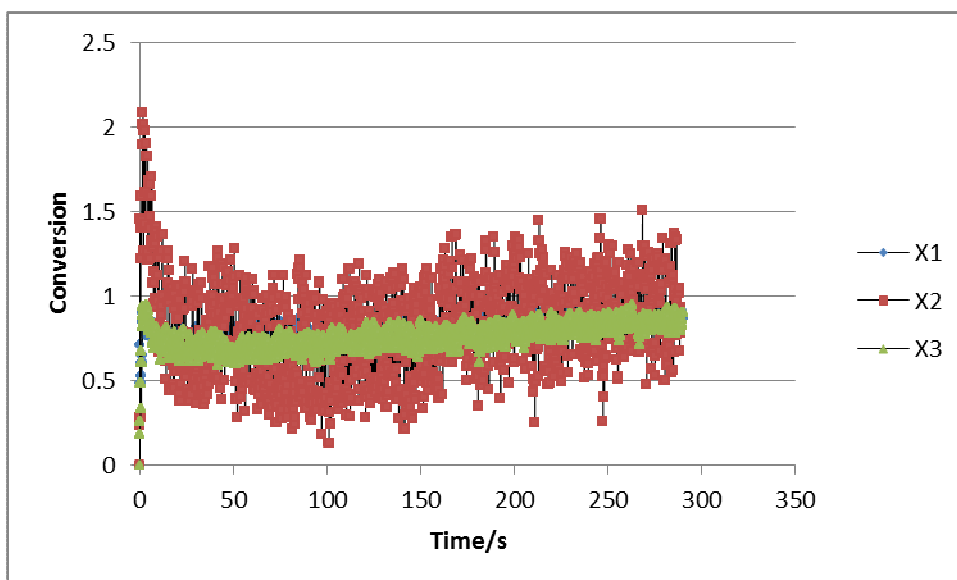
Figure D13: Conversion-Time Profiles for [MEA] =0.07915 mol/L, $[CO_2]_1$=0.008231 mol/L, $[CO_2]_2$=0.006196 mol/L and $[CO_2]_3$=0.007779 mol/L at 308 K.
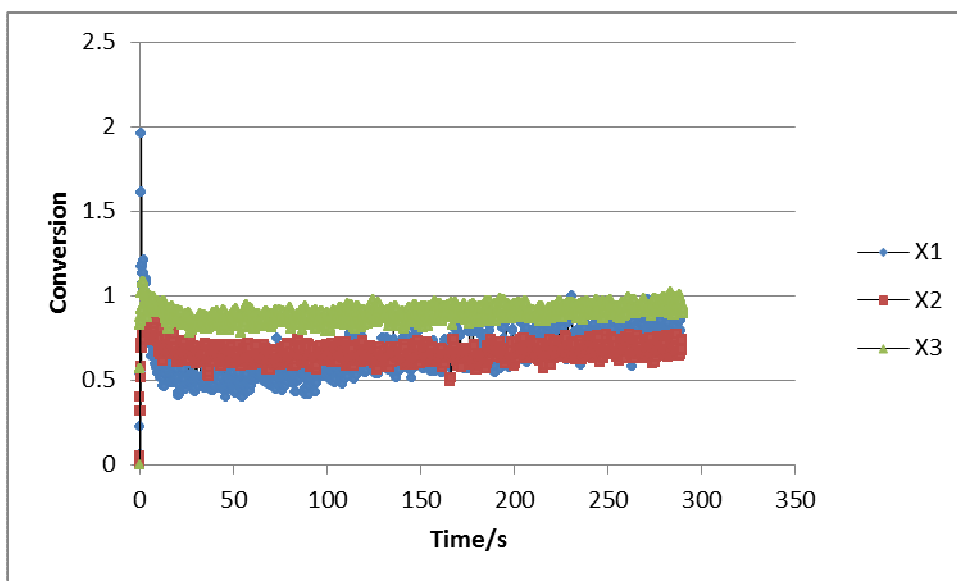
Figure D14: Conversion-Time Profiles for [MEA] =0.118 4mol/L, $[CO_2]_1$=0.009430 mol/L, $[CO_2]_2$=0.01015 mol/L and $[CO_2]_3$=0.01047 mol/L at 308 K.
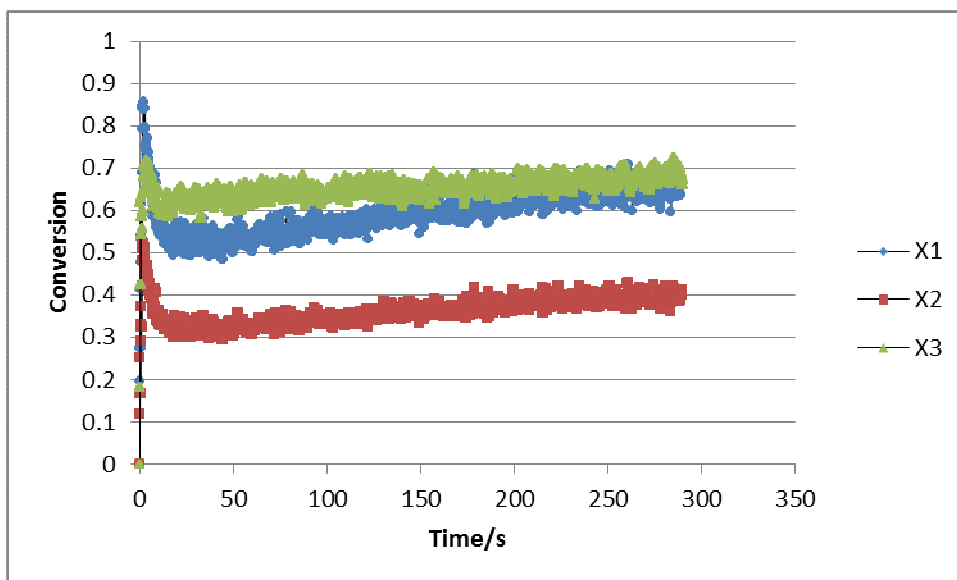
Figure D15: Conversion-Time Profiles for [MEA] =0.1575 mol/L, $[CO_2]_1$=0.01391 mol/L, $[CO_2]_2$=0.01400 mol/L and $[CO_2]_3$=0.01490 mol/L at 308 K.
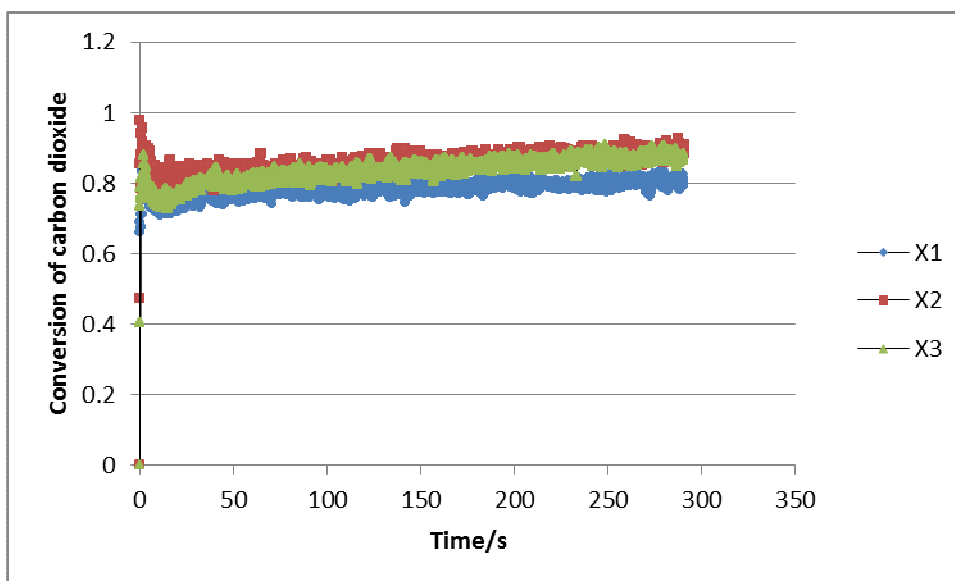
Figure D16: Conversion-Time Profiles for [MEA] =0.1965 mol/L, $[CO_2]_1$=0.01877 mol/L, $[CO_2]_2$=0.01801 mol/L and $[CO_2]_3$=0.01832 mol/L at 308 K.
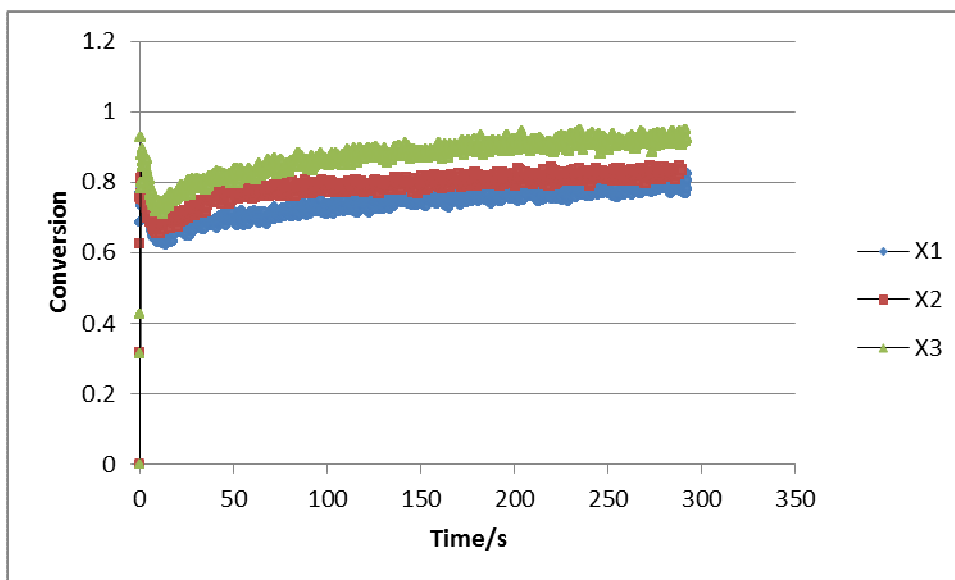
Figure D17: Conversion-Time Profiles for [MEA] =0.2609 mol/L, $[CO_2]_1$=0.02245 mol/L, $[CO_2]_2$=0.02375 mol/L and $[CO_2]_3$=0.02411 mol/L at 308 K.

142
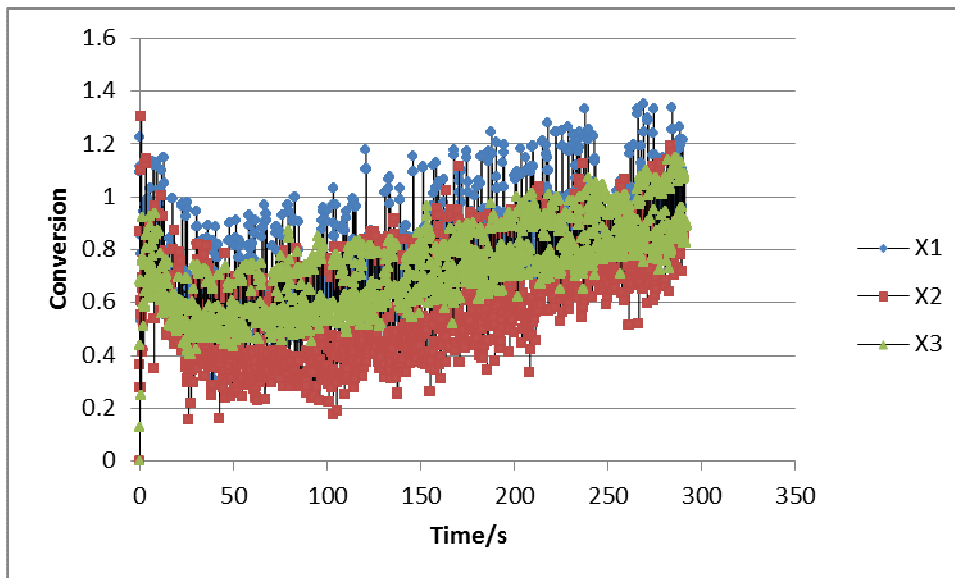
Figure D18: Conversion-Time Profiles for [MEA] =0.04956 mol/L, $[CO_2]_1$=0.004757 mol/L, $[CO_2]_2$=0.004621 mol/L and $[CO_2]_3$=0.005029 mol/L at 313 K.
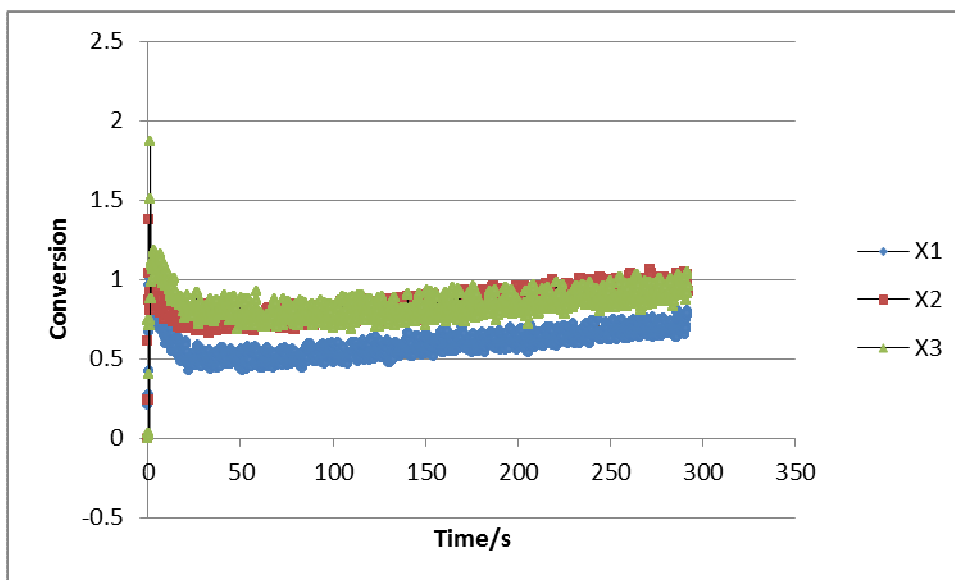
Figure D19: Conversion-Time Profiles for [MEA] =0.07915 mol/L, $[CO_2]_1$=0.006377 mol/L, $[CO_2]_2$=0.007689 mol/L and $[CO_2]_3$=0.006648 mol/L at 313 K

143
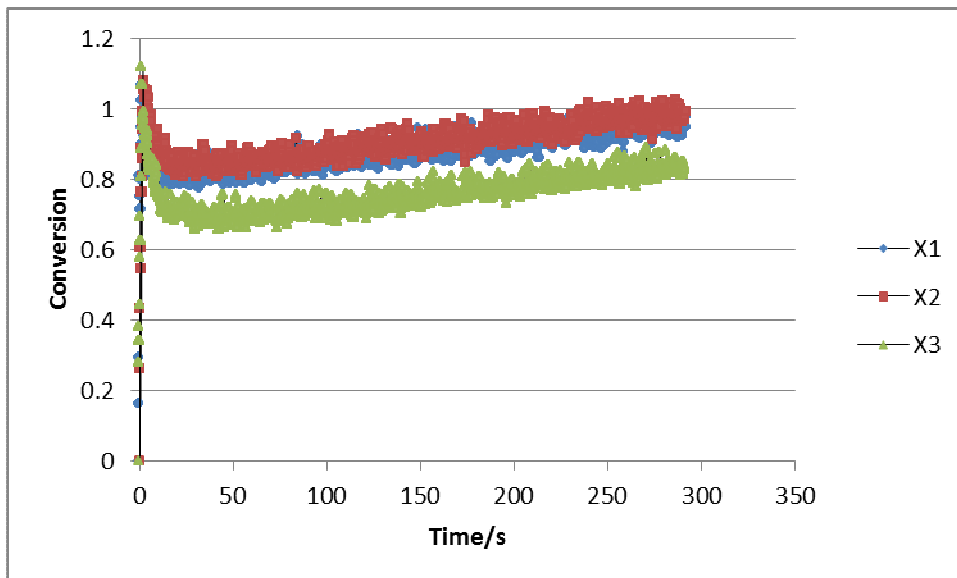
Figure D20: Conversion-Time Profiles for [MEA] =0.1184 mol/L, $[CO_2]_1$=0.01060 mol/L, $[CO_2]_2$=0.01128 mol/L and $[CO_2]_3$=0.01020 mol/L at 313 K.
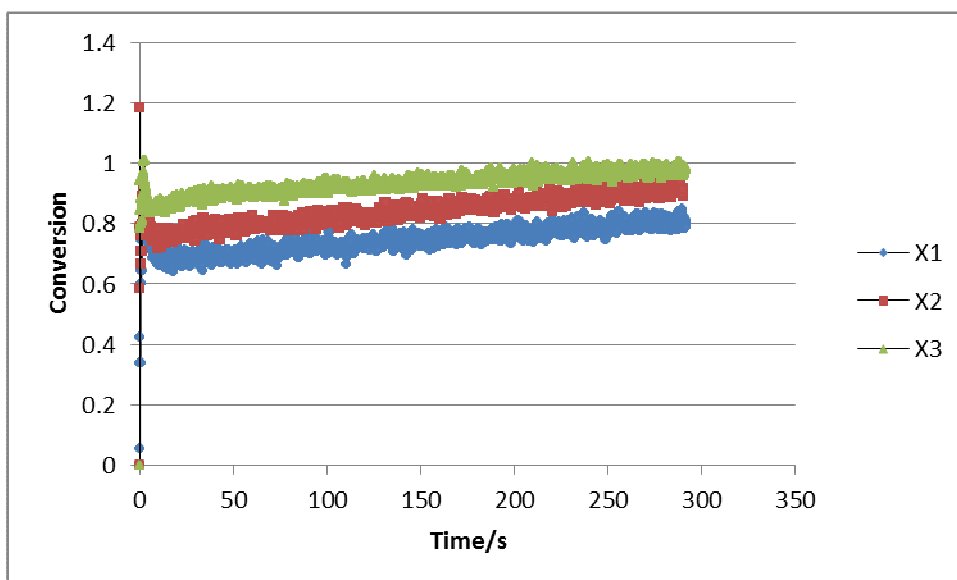
Figure D21: Conversion-Time Profiles for [MEA] =0.1575 mol/L, $[CO_2]_1$=0.01413 mol/L, $[CO_2]_2$=0.01422 mol/L and $[CO_2]_3$=0.01512 mol/L at 313 K.

144
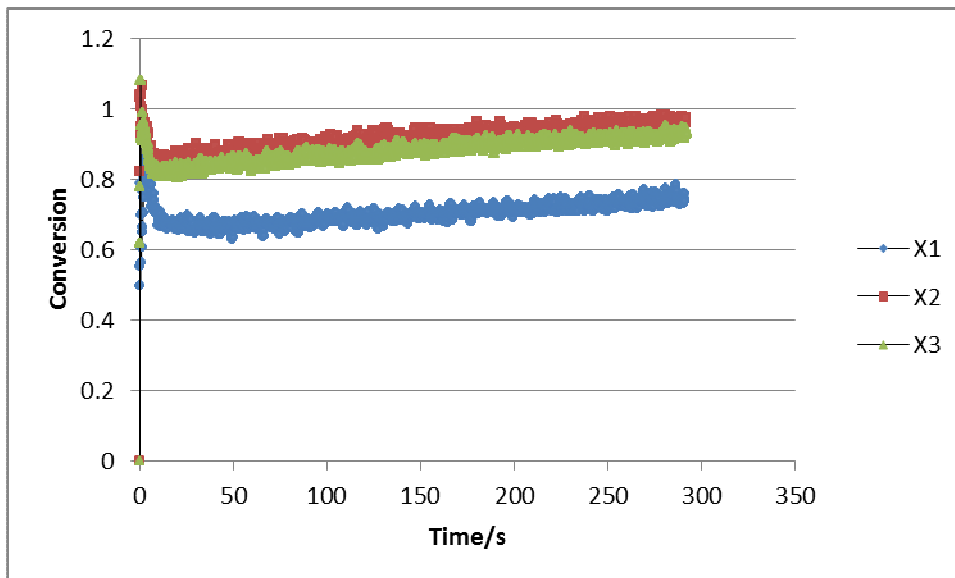
Figure D22: Conversion-Time Profiles for [MEA] =0.1965 mol/L, $[CO_2]_1$=0.01891 mol/L, $[CO_2]_2$=0.01931 mol/L and $[CO_2]_3$=0.01918 mol/L at 313 K.
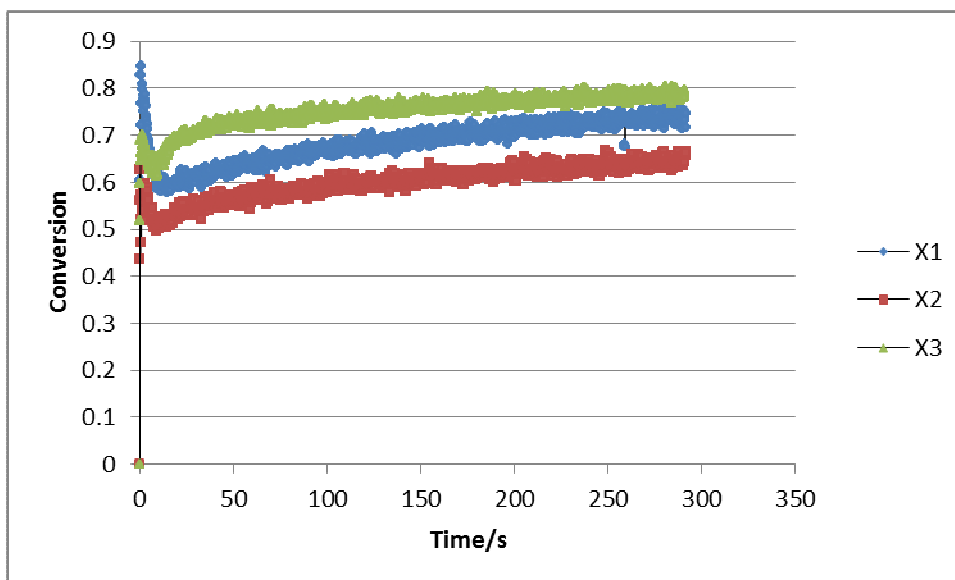
Figure D23: Conversion-Time Profiles for [MEA] =0.2609 mol/L, $[CO_2]_1$=0.02478 mol/L, $[CO_2]_2$=0.02429 mol/L and $[CO_2]_3$=0.02545 mol/L at 313 K.

APPENDIX E: CONVERSION-TIME PROFILES FOR SECOND SERIES RUNS
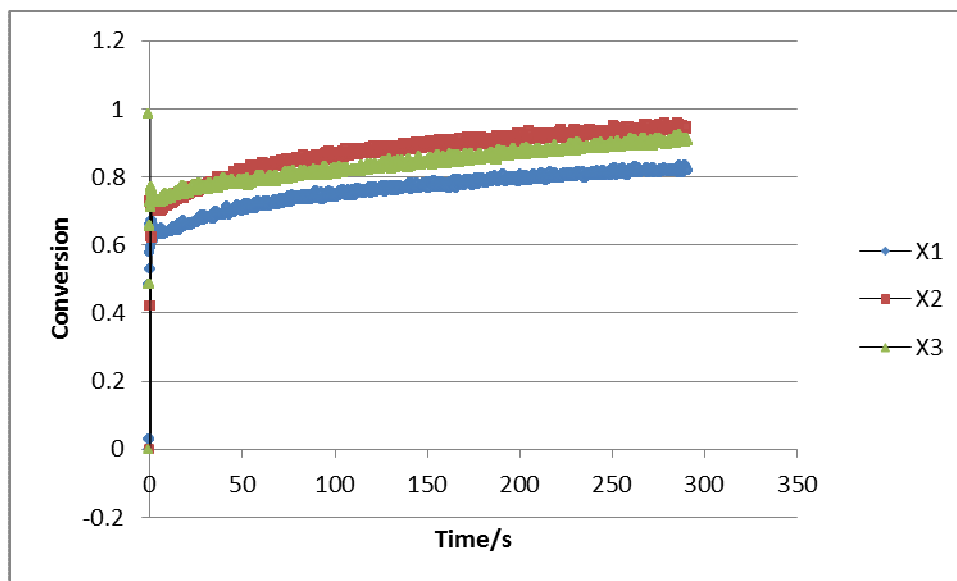
Figure E1: Conversion-Time Profiles for [MEA] =0.01986 mol/L, $[CO_2]_1$=0.01993 mol/L, $[CO_2]_2$=0.01938 mol/L and $[CO_2]_3$=0.01938 mol/L at 298 K.
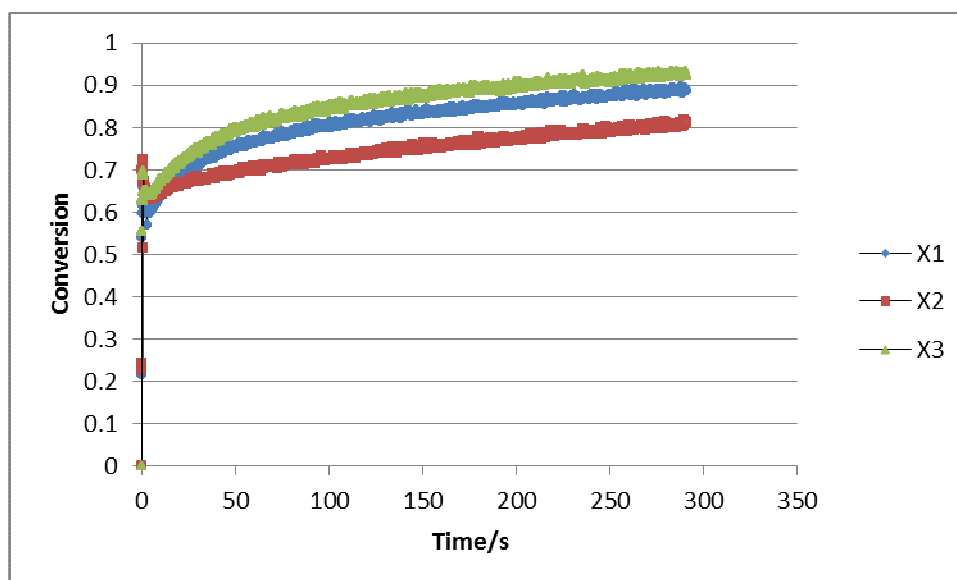
Figure E2: Conversion-Time Profiles for [MEA] =0.04956 mol/L, $[CO_2]_1$=0.05147 mol/L, $[CO_2]_2$=0.04721 mol/L and $[CO_2]_3$=0.05269 mol/L at 298 K.
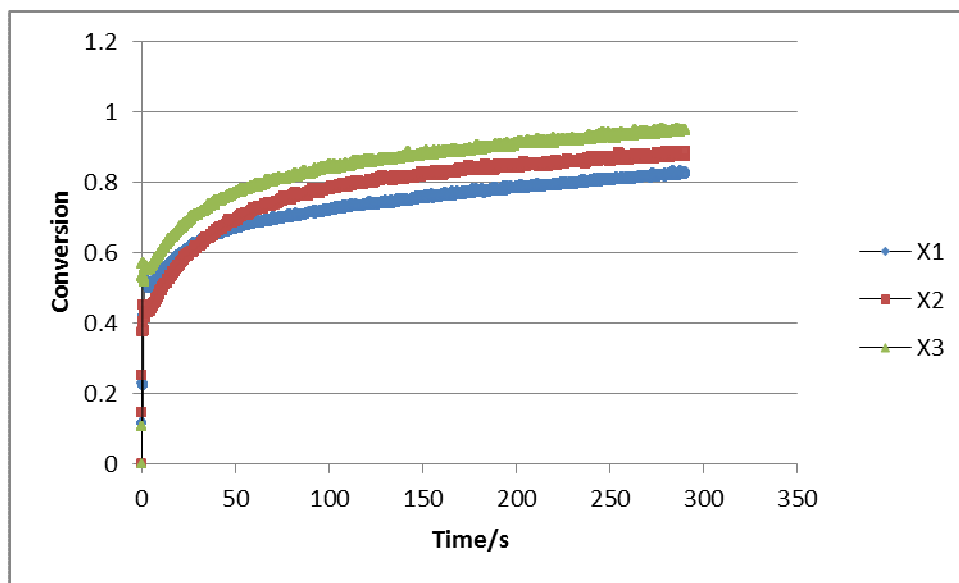
Figure E4: Conversion-Time Profiles for [MEA] =0.1184 mol/L, $[CO_2]_1$=0.1173 mol/L, $[CO_2]_2$=0.1183 mol/L and $[CO_2]_3$=0.1169 mol/L at 298 K.
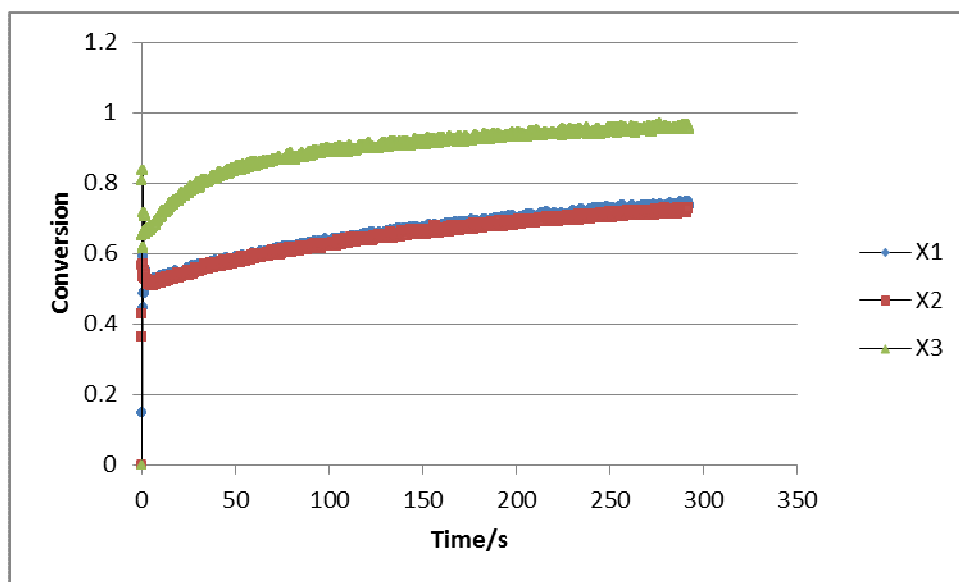
Figure E5: Conversion-Time Profiles for [MEA] =0.01986 mol/L, $[CO_2]_1$=0.01943 mol/L, $[CO_2]_2$=0.01938 mol/L and $[CO_2]_3$=0.02111 mol/L at 298 K.
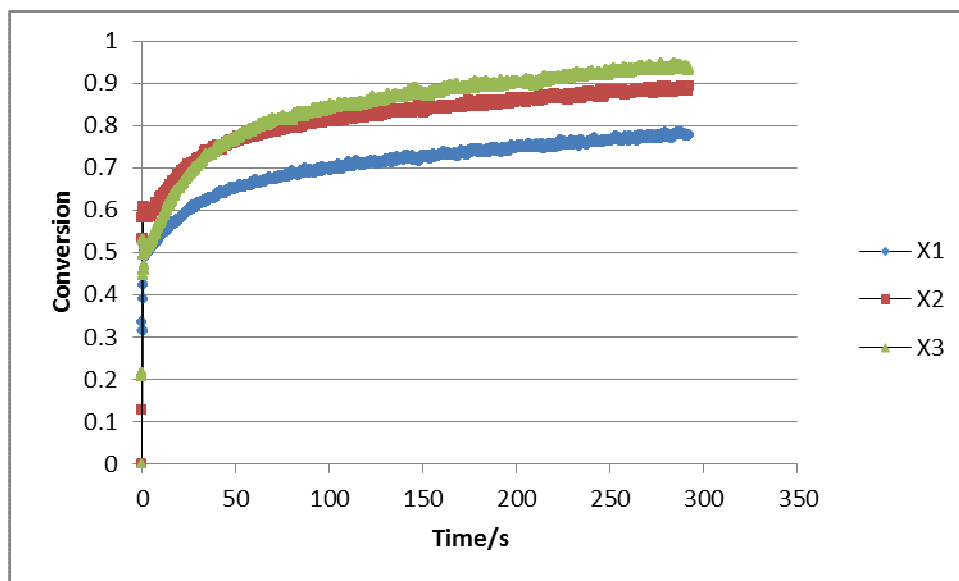
Figure E6: Conversion-Time Profiles for [MEA] =0.04956 mol/L, $[CO_2]_1$=0.04834 mol/L, $[CO_2]_2$=0.04948 mol/L and $[CO_2]_3$=0.05034 mol/L at 303 K.
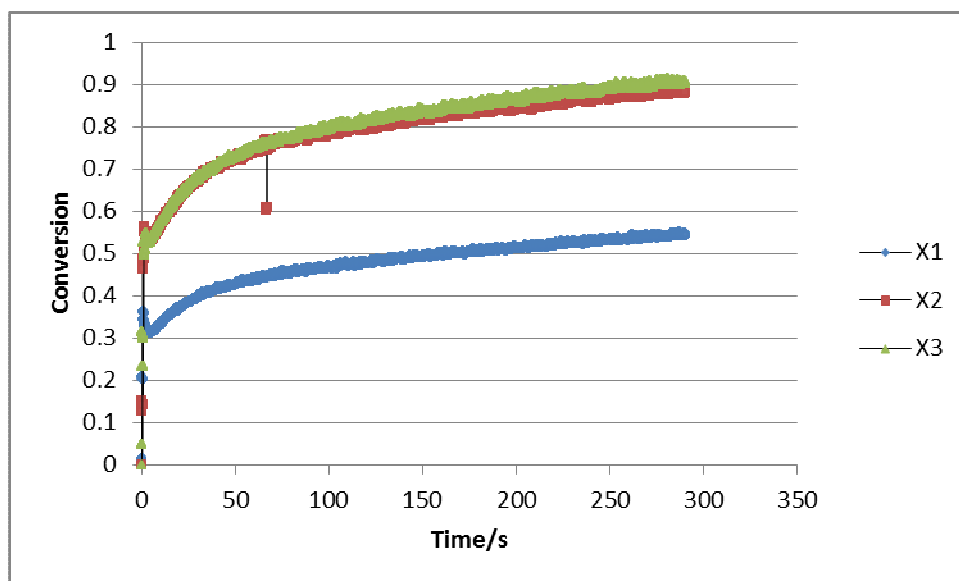
Figure E7: Conversion-Time Profiles for [MEA] =0.07915 mol/L, $[CO_2]_1$=0.07928 mol/L, $[CO_2]_2$=0.07956 mol/L and $[CO_2]_3$=0.07983 mol/L at 303 K.
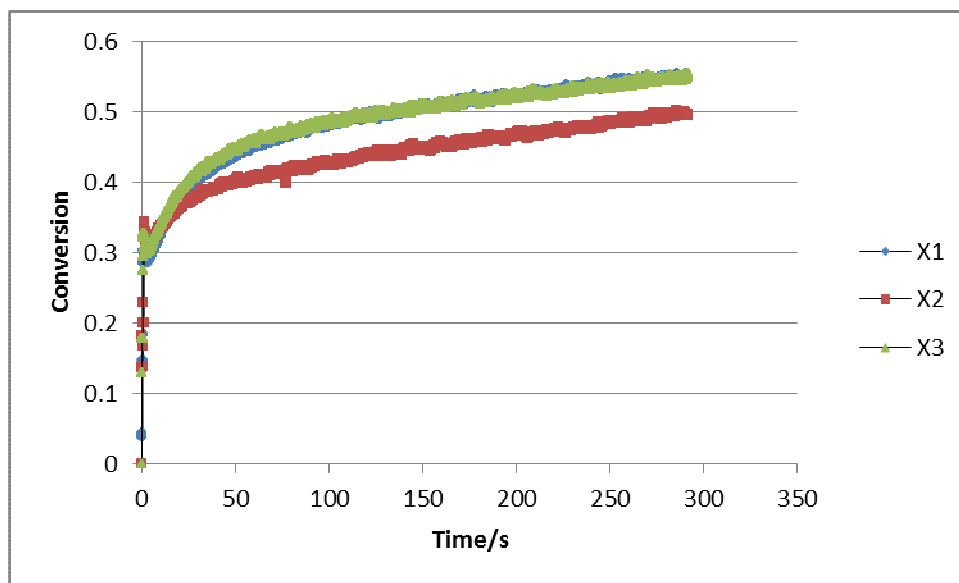
Figure E8: Conversion-Time Profiles for [MEA] =0.1184 mol/L, $[CO_2]_1$=0.1185 mol/L, $[CO_2]_2$=0.1164 mol/L and $[CO_2]_3$=0.1171 mol/L at 303 K.
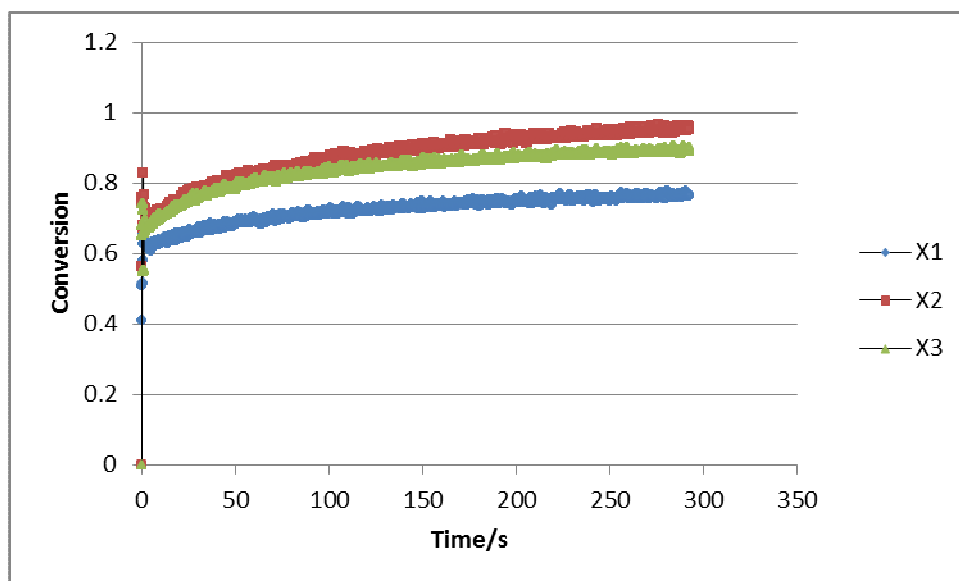
Figure E9: Conversion-Time Profiles for [MEA] =0.01986 mol/L, $[CO_2]_1$=0.01834 mol/L, $[CO_2]_2$=0.01897 mol/L and $[CO_2]_3$=0.02015 mol/L at 308 K.

149
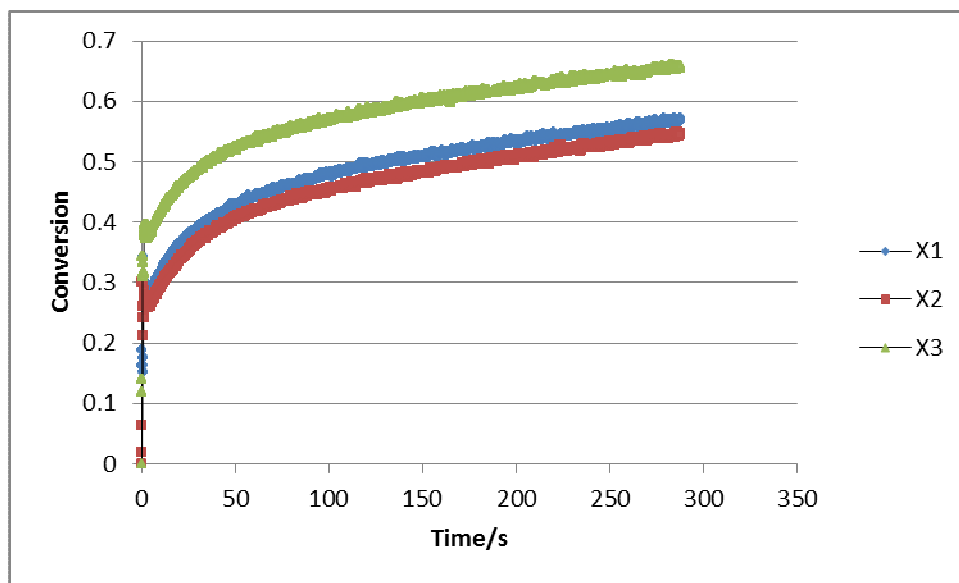
Figure E10: Conversion-Time Profiles for [MEA] =0.1184 mol/L, $[CO_2]_1$=0.1177 mol/L, $[CO_2]_2$=0.1165 mol/L and $[CO_2]_3$=0.1193 mol/L at 308 K.
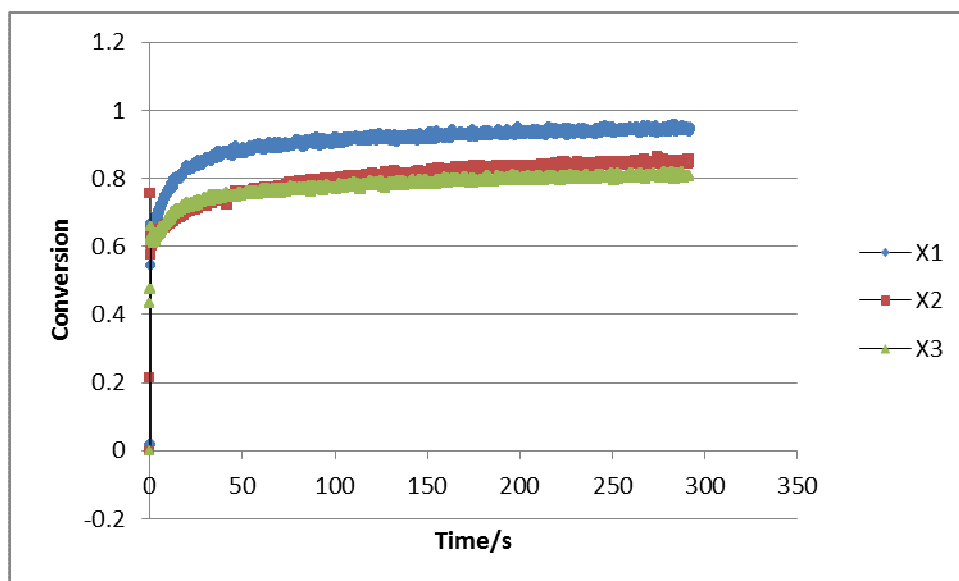
Figure E11: Conversion-Time Profiles for [MEA] =0.01986 mol/L, $[CO_2]_1$=0.02043 mol/L, $[CO_2]_2$=0.01938 mol/L and $[CO_2]_3$=0.01888 mol/L at 313 K.
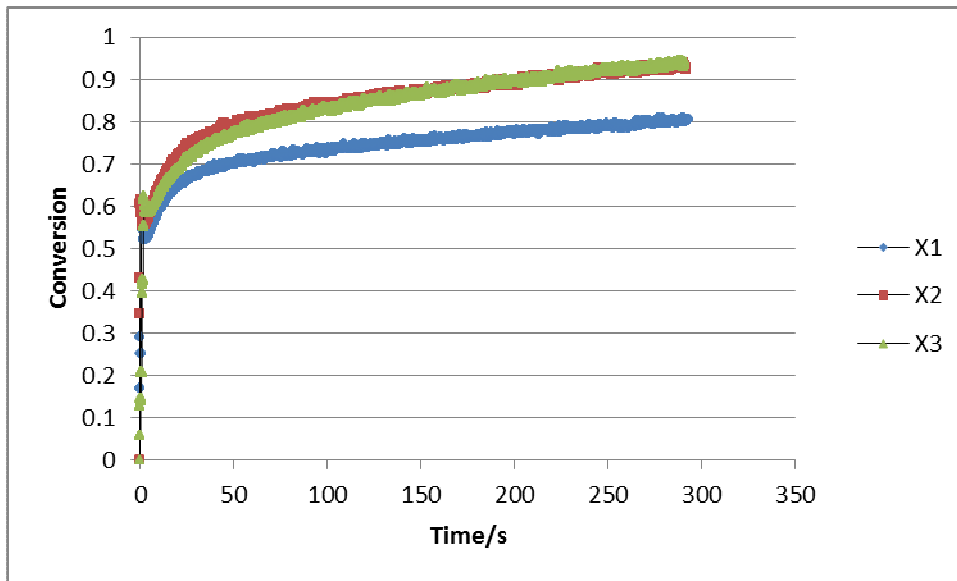
Figure E12: Conversion-Time Profiles for [MEA] =0.04956mol/L, $[CO_2]_1$=0.04979mol/L, $[CO_2]_2$=0.04998mol/L and $[CO_2]_3$=0.05029mol/L at 313 K.
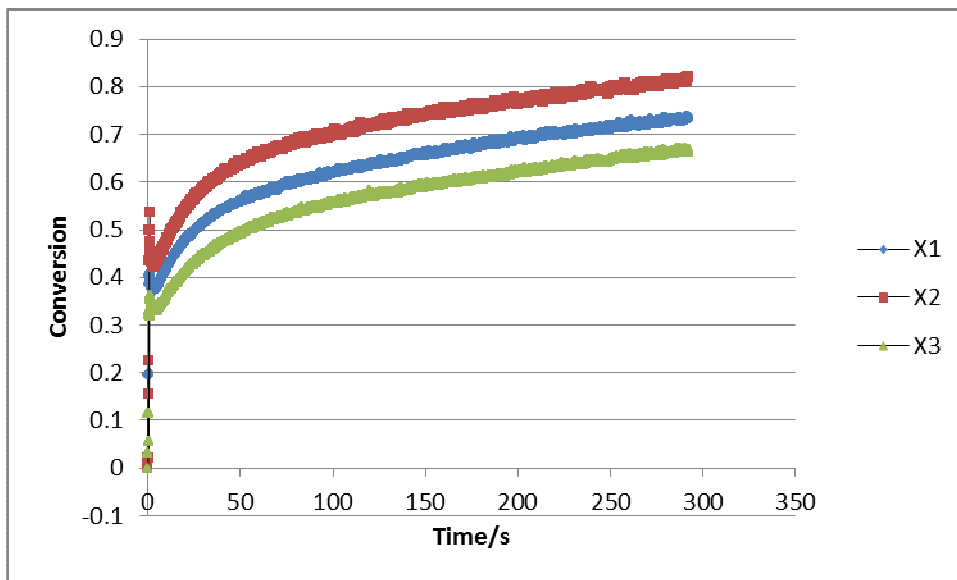
Figure E13: Conversion-Time Profiles for [MEA] =0.07915 mol/L, $[CO_2]_1$=0.07765 mol/L, $[CO_2]_2$=0.07978 mol/L and $[CO_2]_3$=0.07892 mol/L at 313 K.
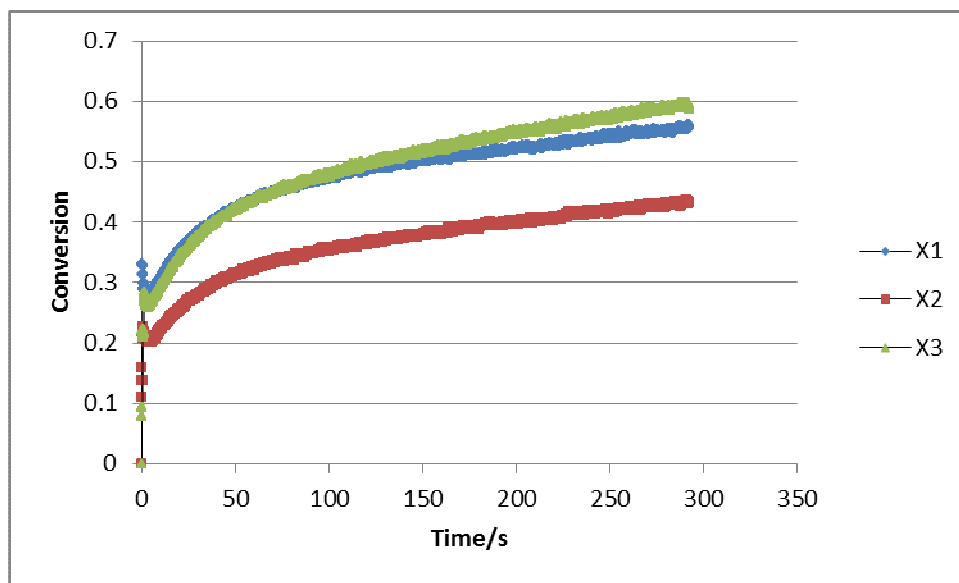
Figure E14: Conversion-Time Profiles for [MEA] =0.1184 mol/L, $[CO_2]_1$=0.1194 mol/L, $[CO_2]_2$=0.1182 mol/L and $[CO_2]_3$=0.1235 mol/L at 313 K.

APPENDIX F: TITRATION CURVES FOR FIRST SERIES RUNS

F1: Titration Curves for 0.04956 mol/L MEA First Run at 303 K
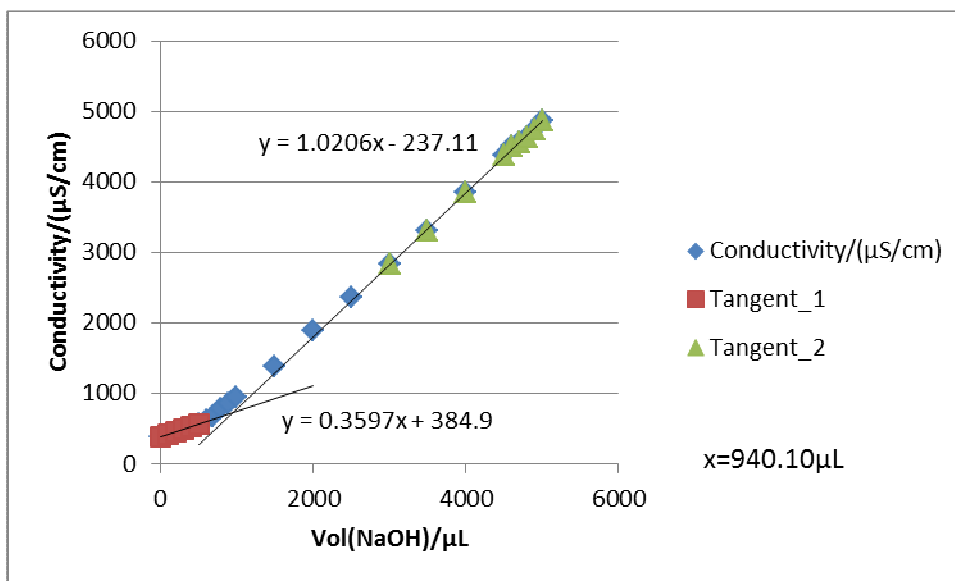
Figure F1-1: Titration 1 for 0.04956 mol/L MEA First Run
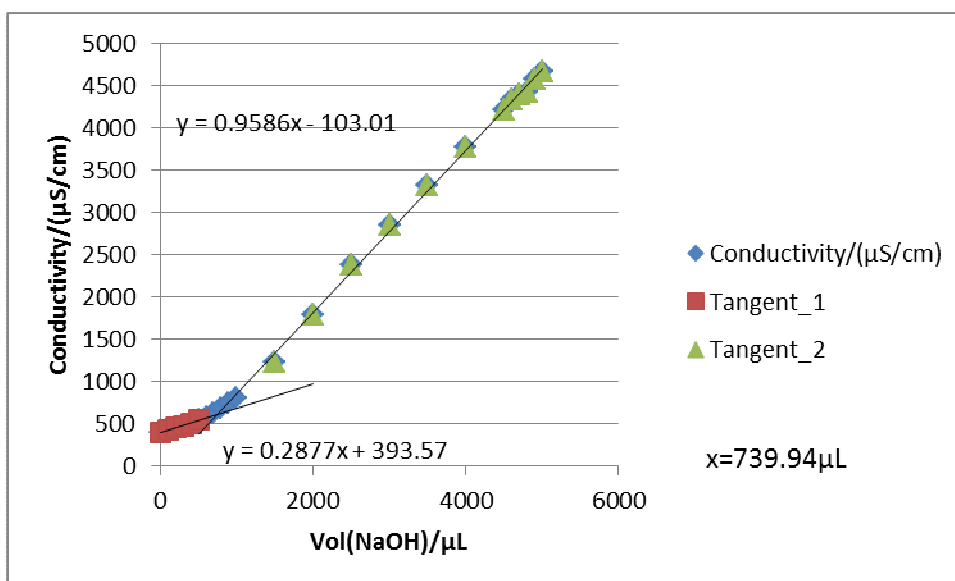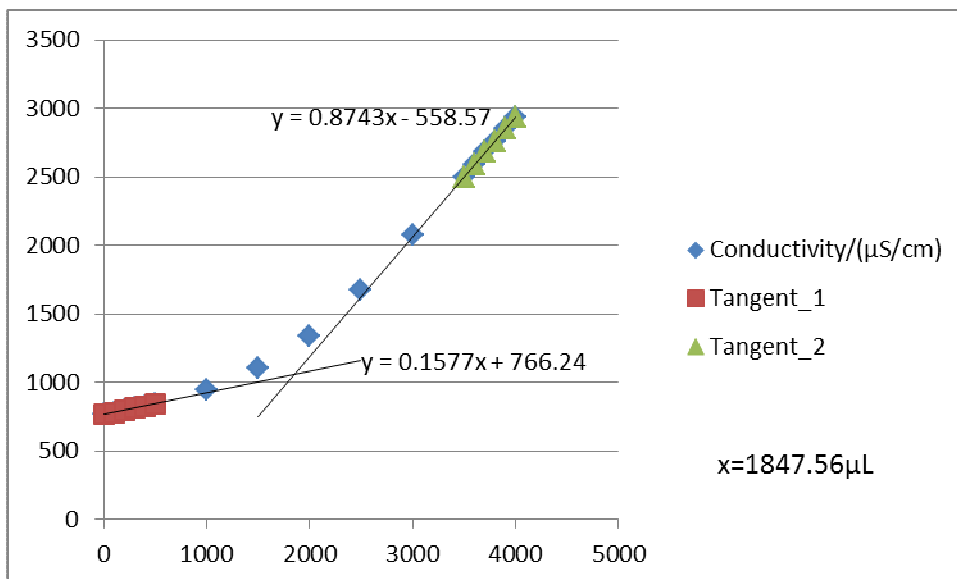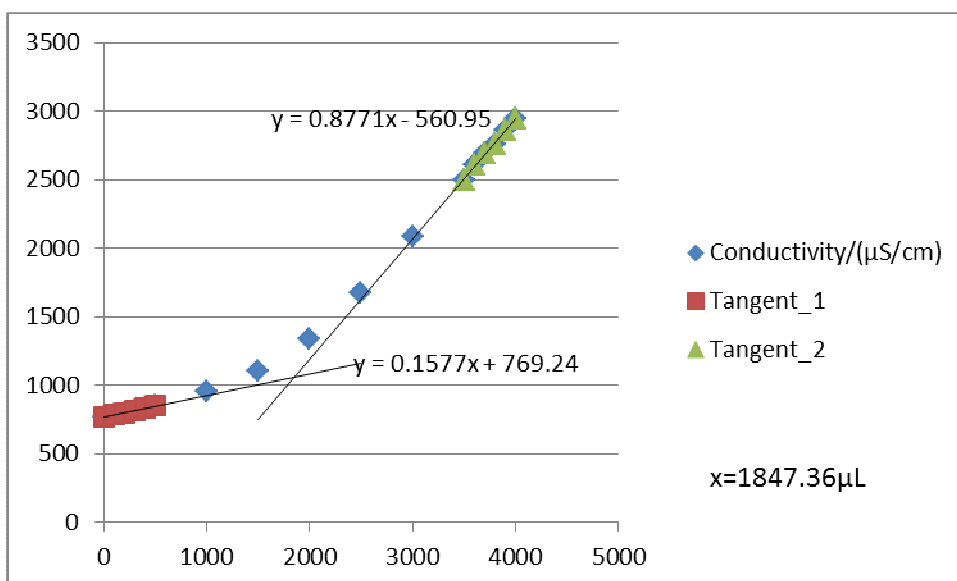

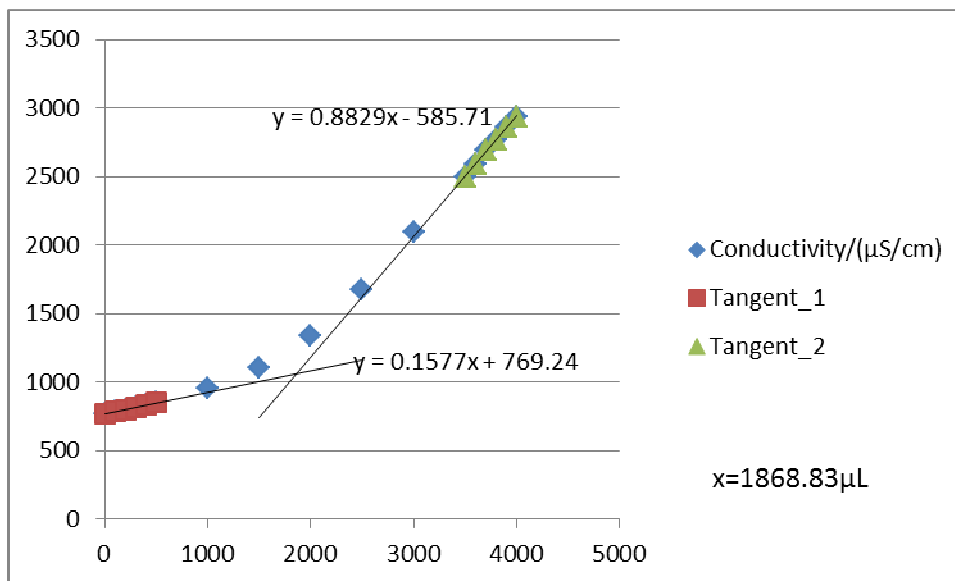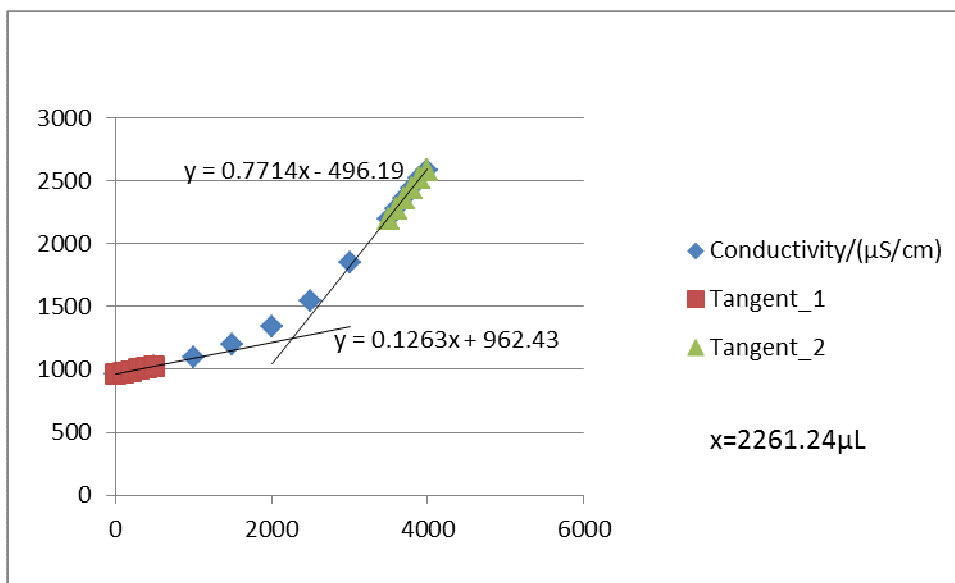Figure F1-2: Titration 2 for 0.04956 mol/L MEA First Run

153
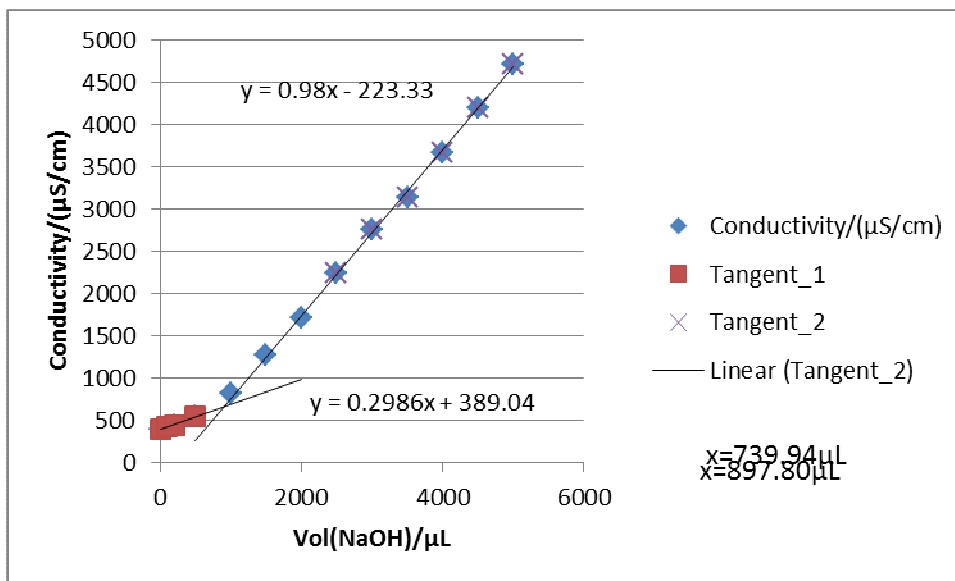
Figure F1-3: Titration 3 for 0.04956 mol/L MEA First Run

F2: Titration Curves for 0.04956 mol/L MEA Second Run at 303 K
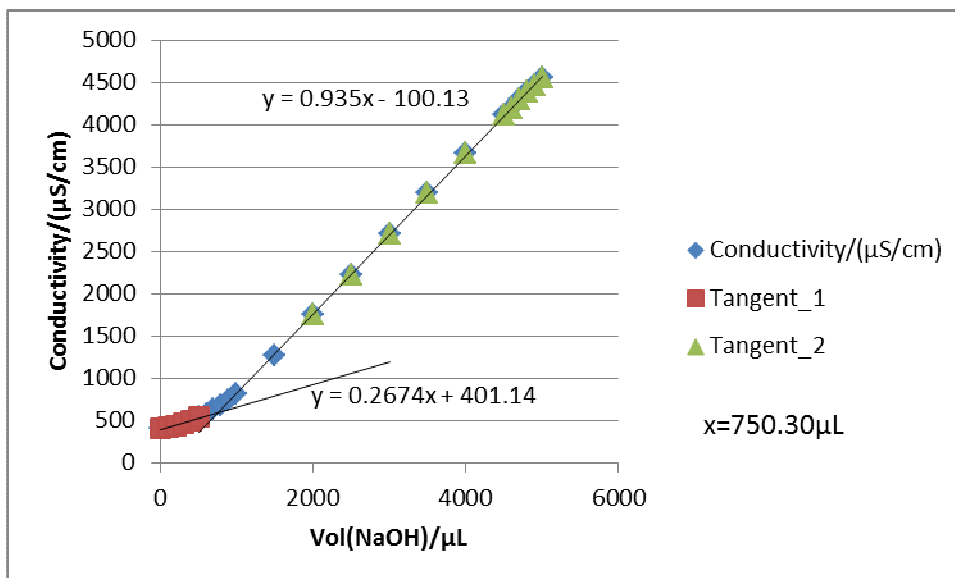
Figure F2-1: Titration 1 for 0.04956 mol/L MEA Second Run

154
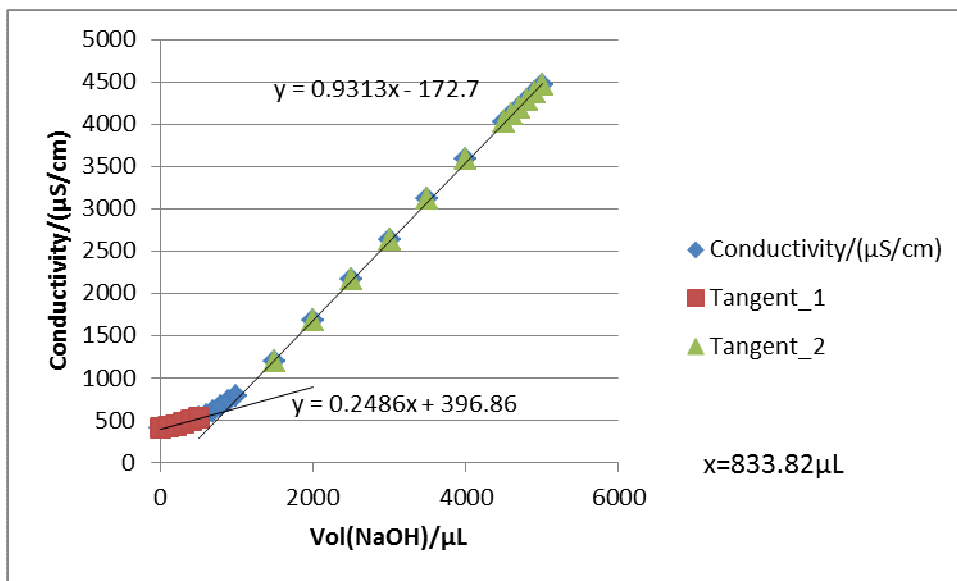
Figure F2-3: Titration 2 for 0.04956 mol/L MEA Second Run
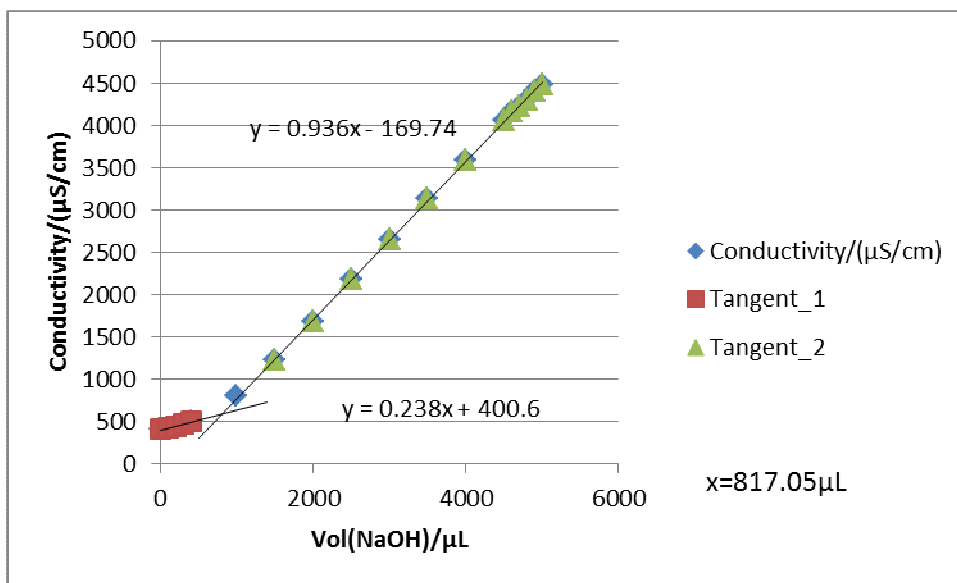
Figure F2-3: Titration 3 for 0.04956 mol/L MEA Second Run

F3: Titration Curves for 0.04956 mol/L MEA Third Run at 303 K
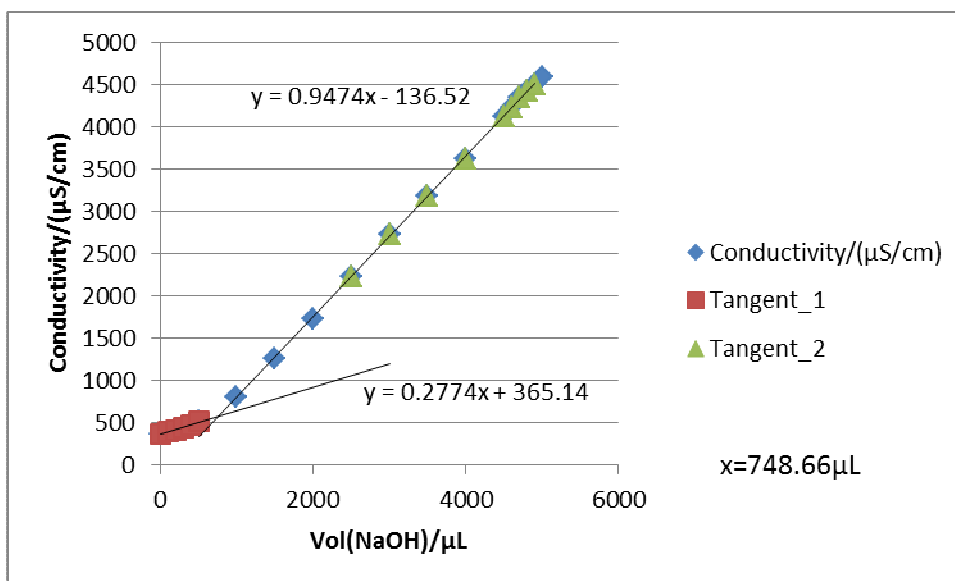
Figure F3-1: Titration 1 for 0.04956 mol/L MEA Third Run
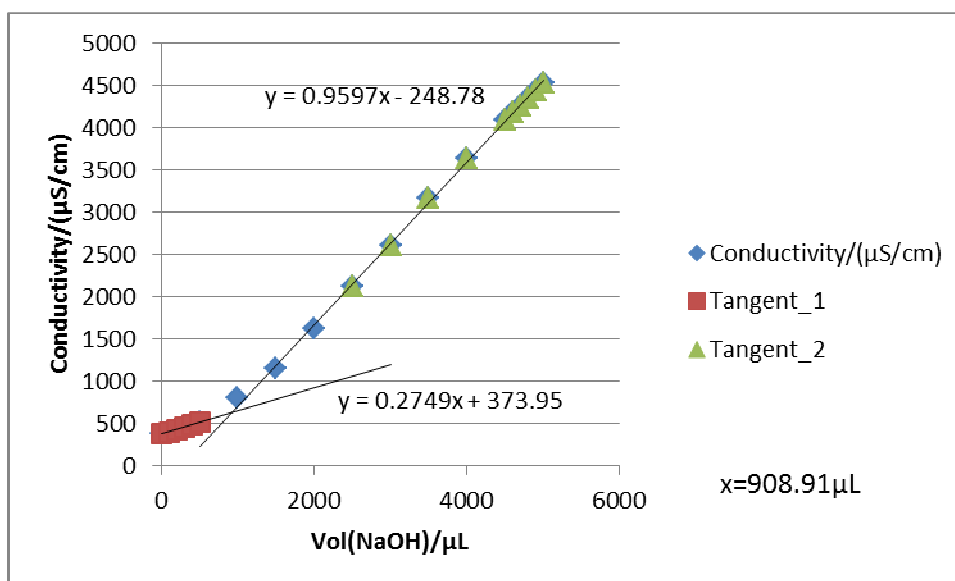
Figure F3-2: Titration 2 for 0.04956 mol/L MEA Third Run

156
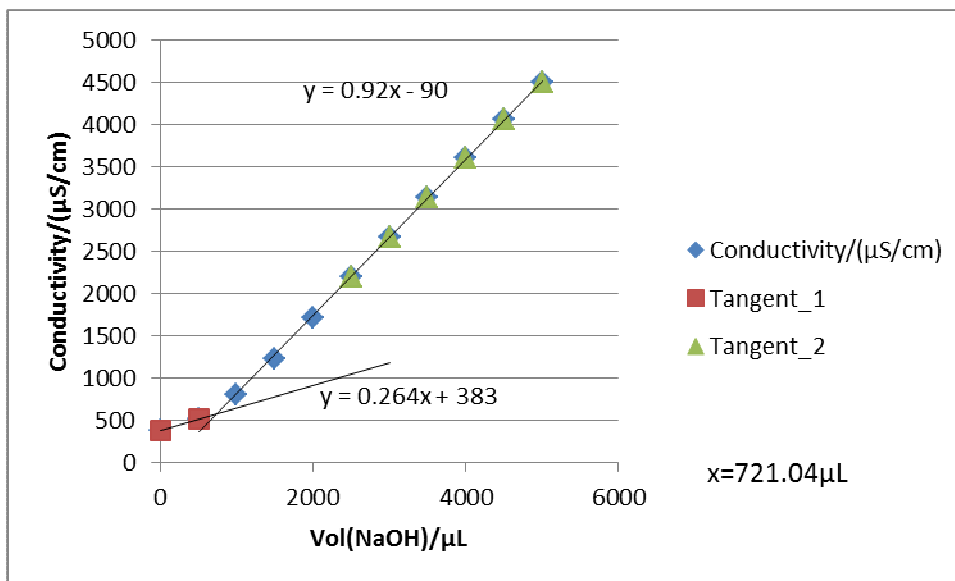
Figure F3-3: Titration 3 for 0.04956 mol/L MEA Third Run

F4: Titration Curves for 0.07915 mol/L MEA First Run at 303 K
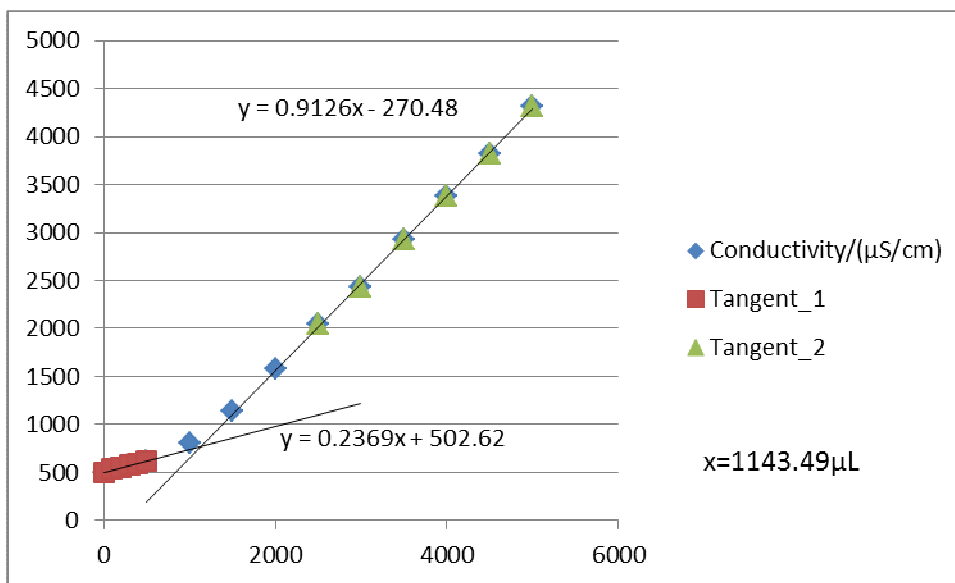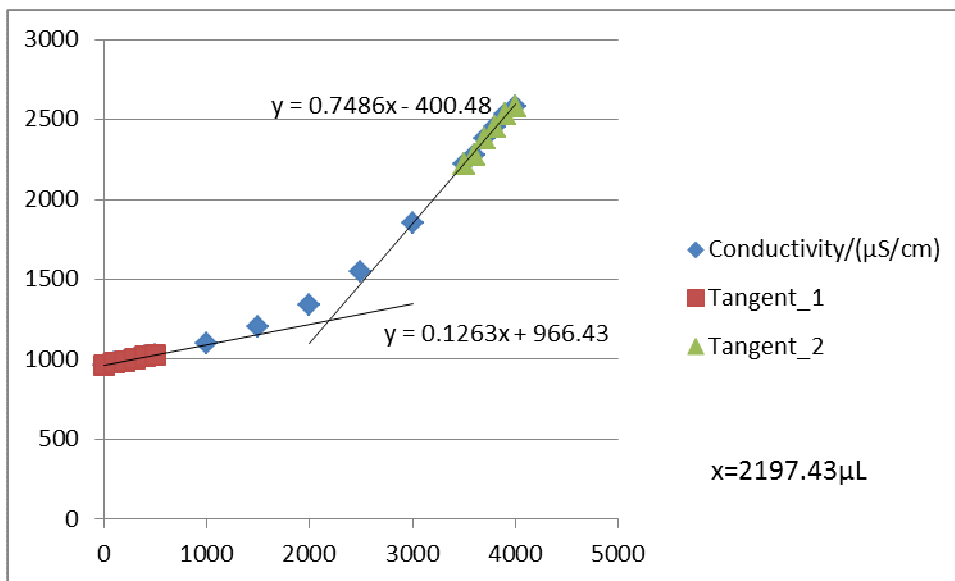

Figure F4-1: Titration 1 for 0.07915 mol/L MEA First Run
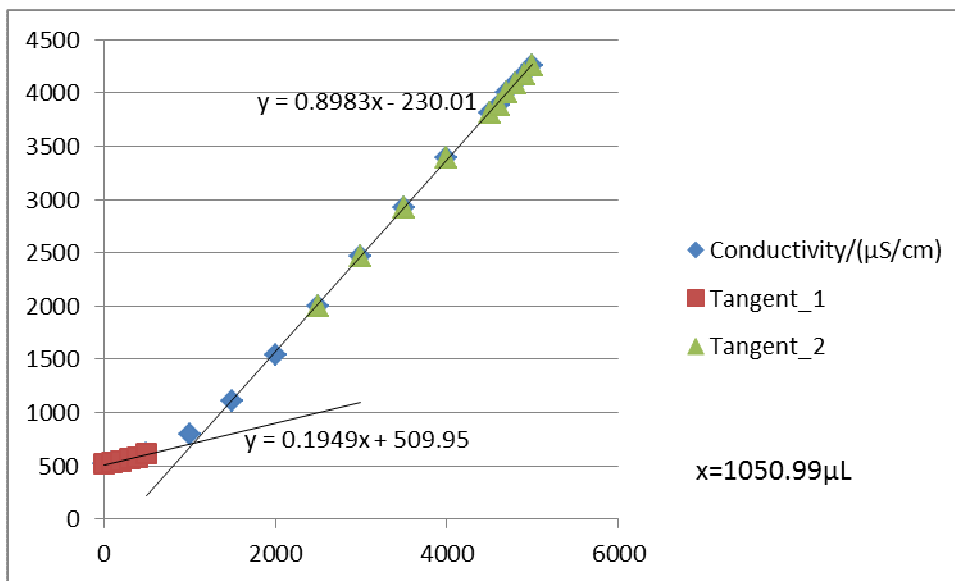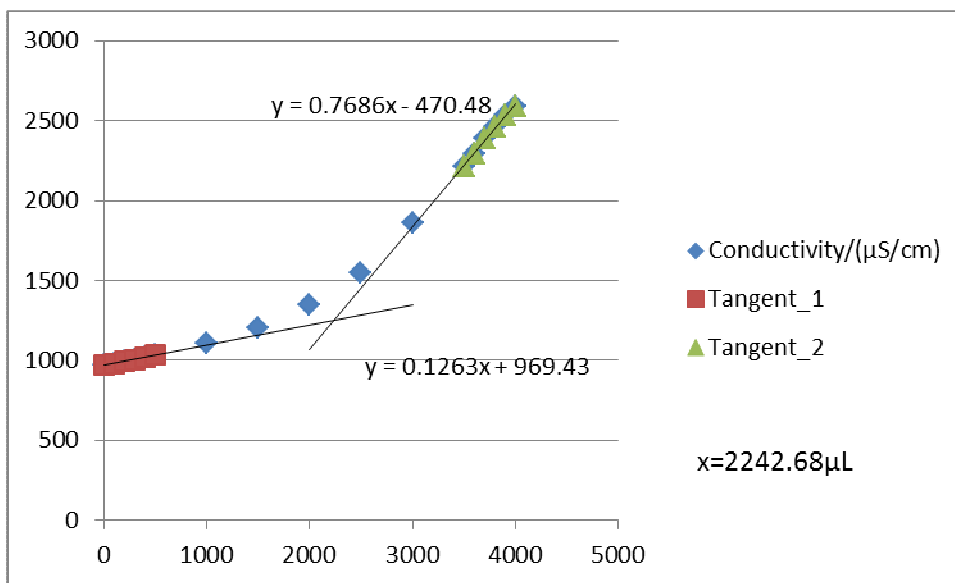
Figure F4-2: Titration 2 for 0.07915 mol/L MEA First Run
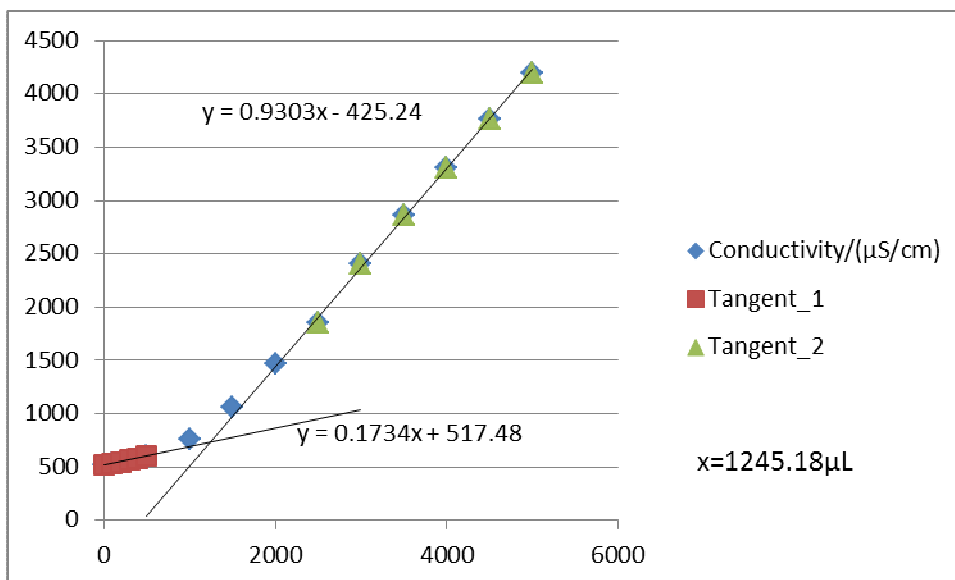
Figure F4-3: Titration 3 for 0.07915 mol/L MEA First Run

158

F5: Titration Curves for 0.07915 mol/L MEA Second Run at 303 K
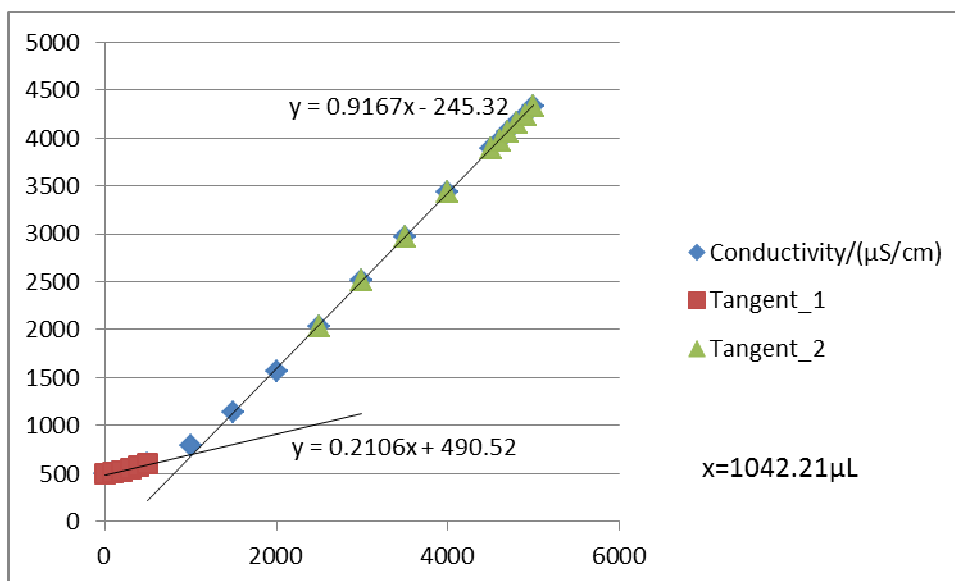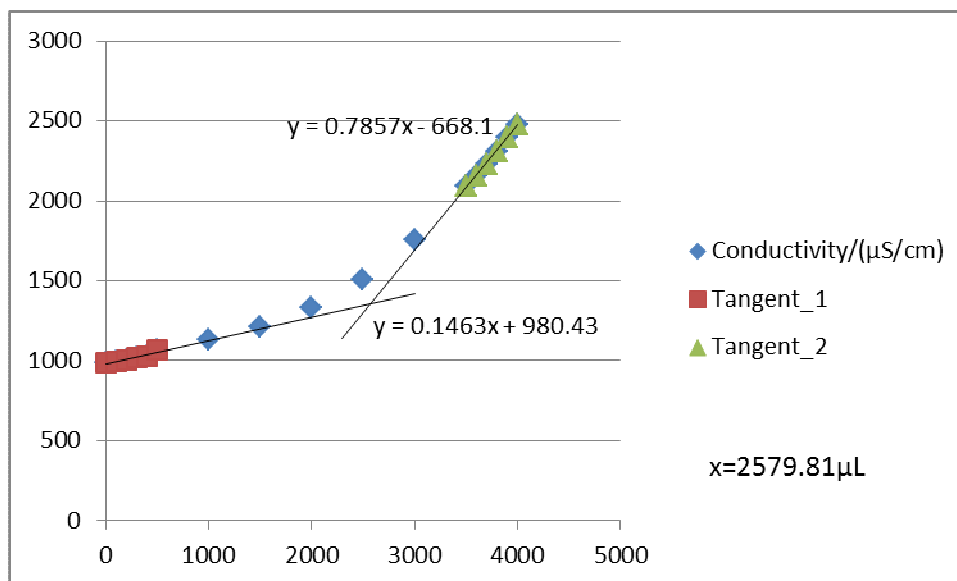

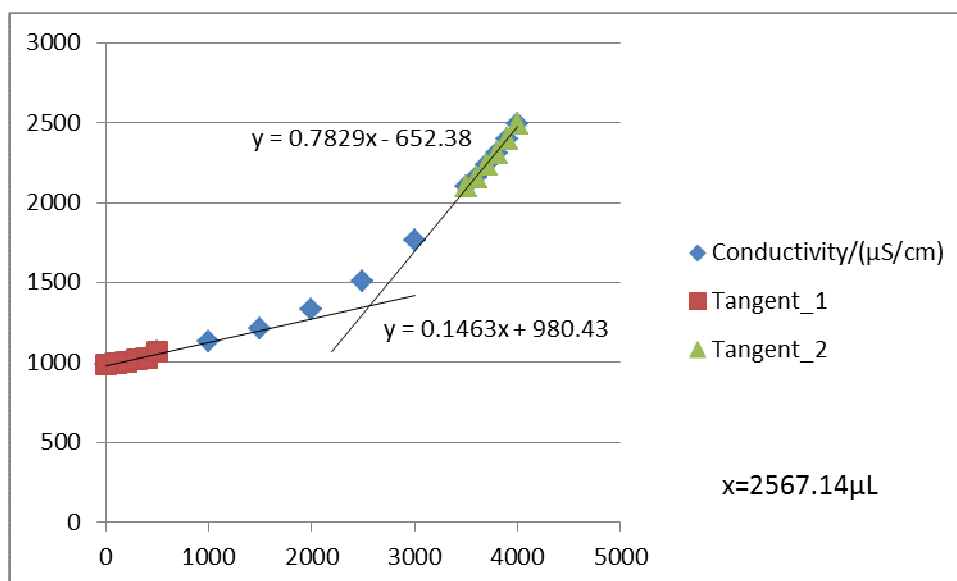Figure F5-1: Titration 1 for 0.07915 mol/L MEA Second Run
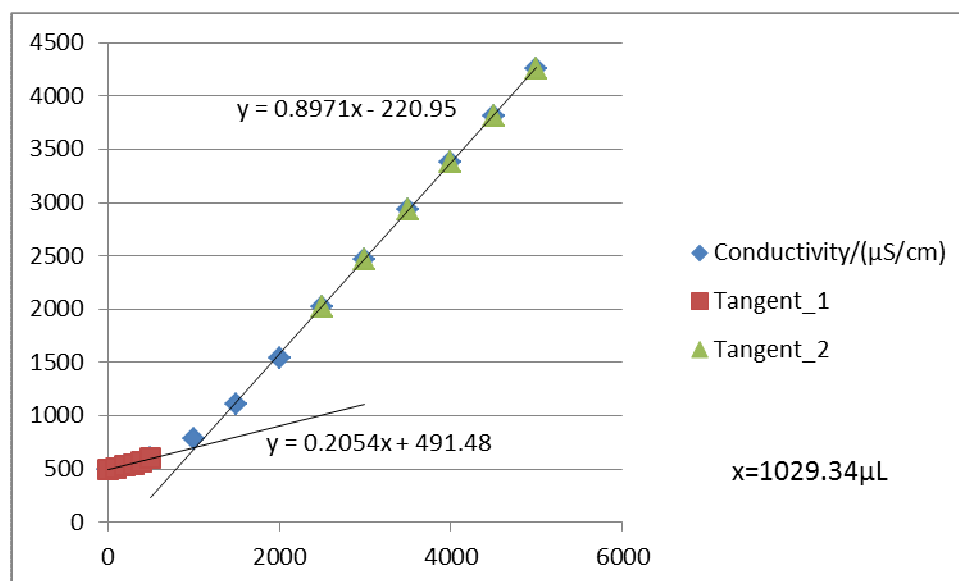
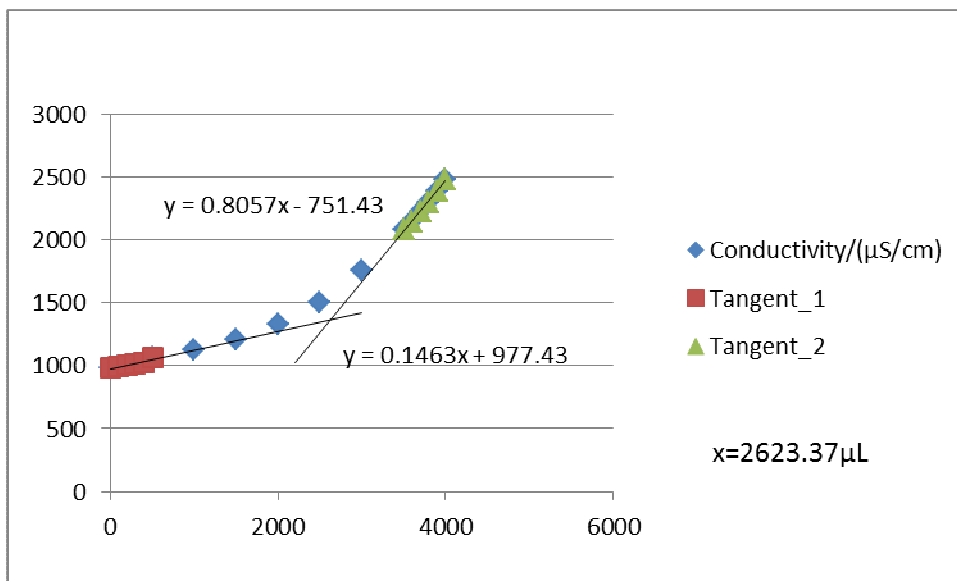

Figure F5-2: Titration 2 for 0.07915 mol/L MEA Second Run
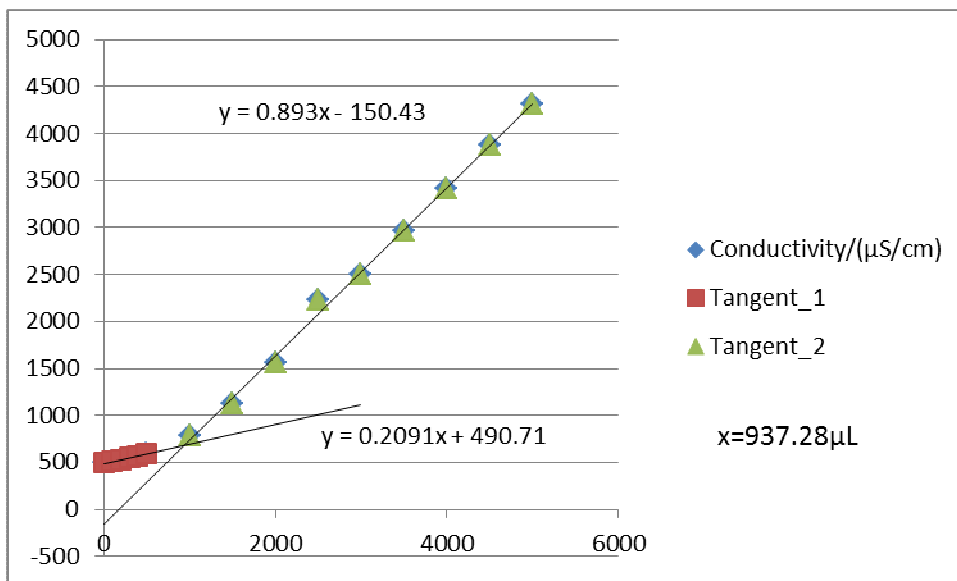
Figure F-3: Titration 3 for 0.07915 mol/L MEA Second Run

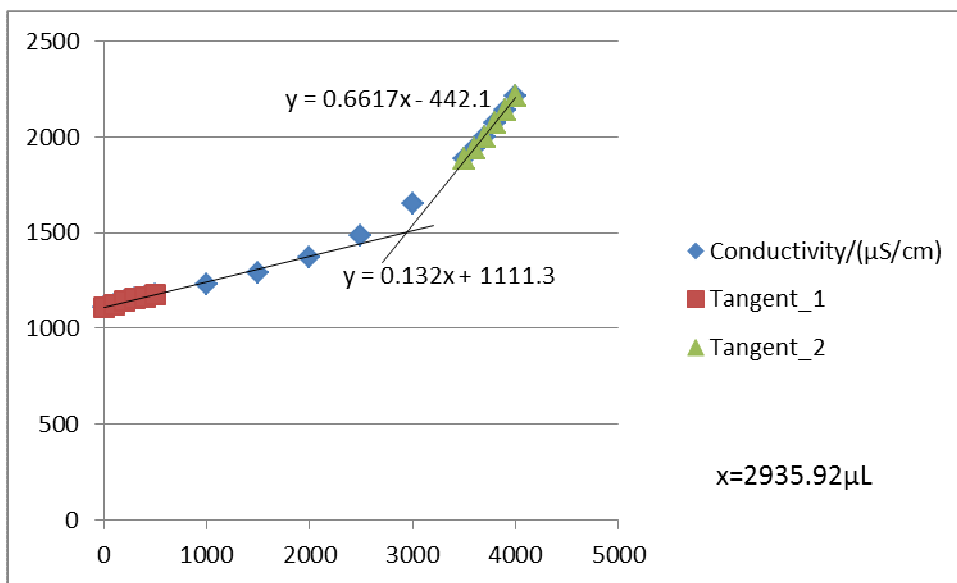## F6: Titration Curves for 0.07915 mol/L MEA Third Run at 303 K
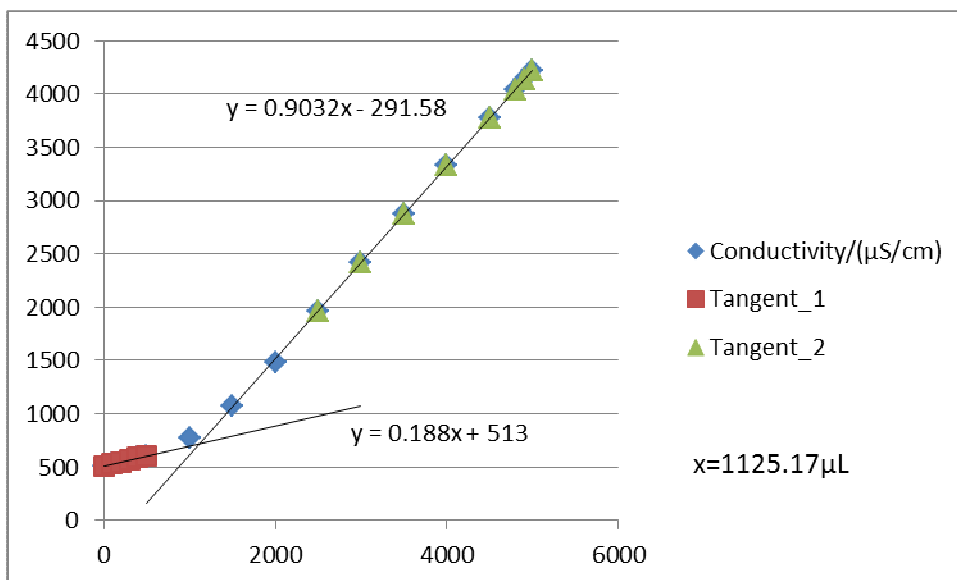
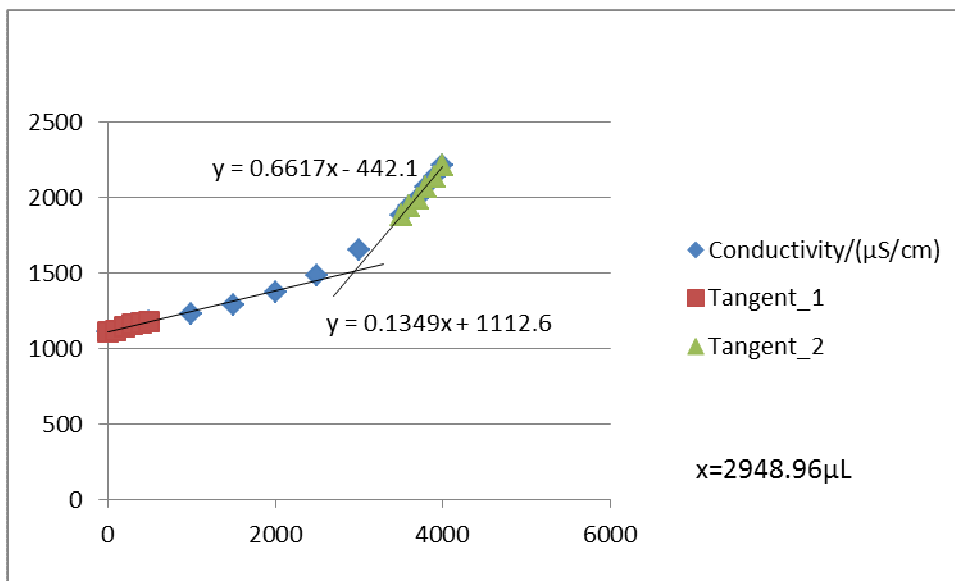Figure F6-1: Titration 1 for 0.07915 mol/L MEA Third Run

160
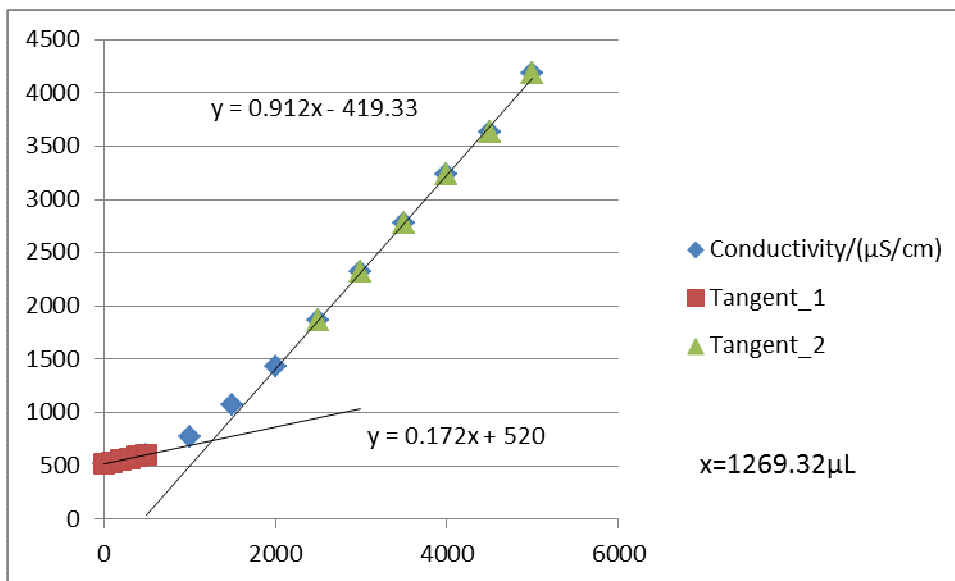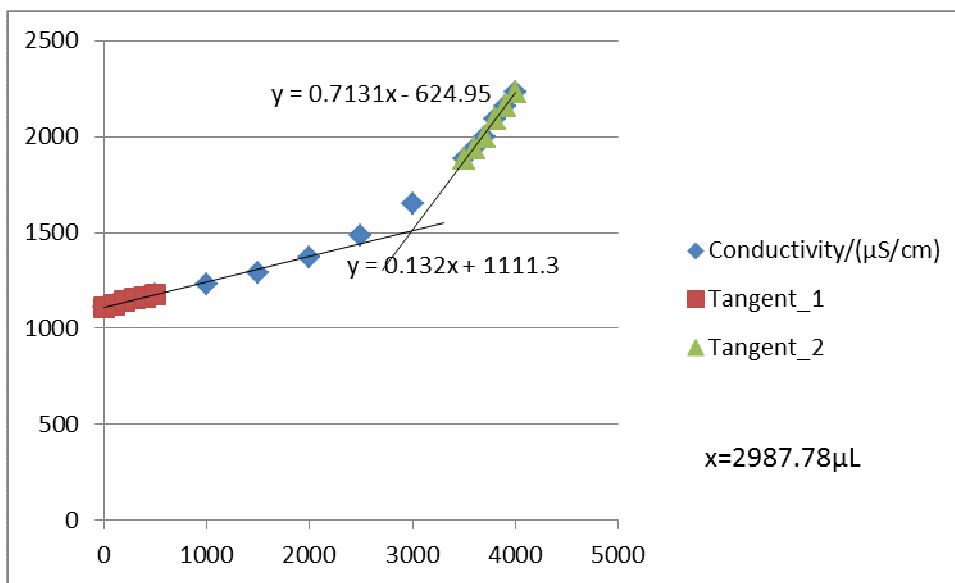
Figure F6-2: Titration 2 for 0.07915 mol/L MEA Third Run
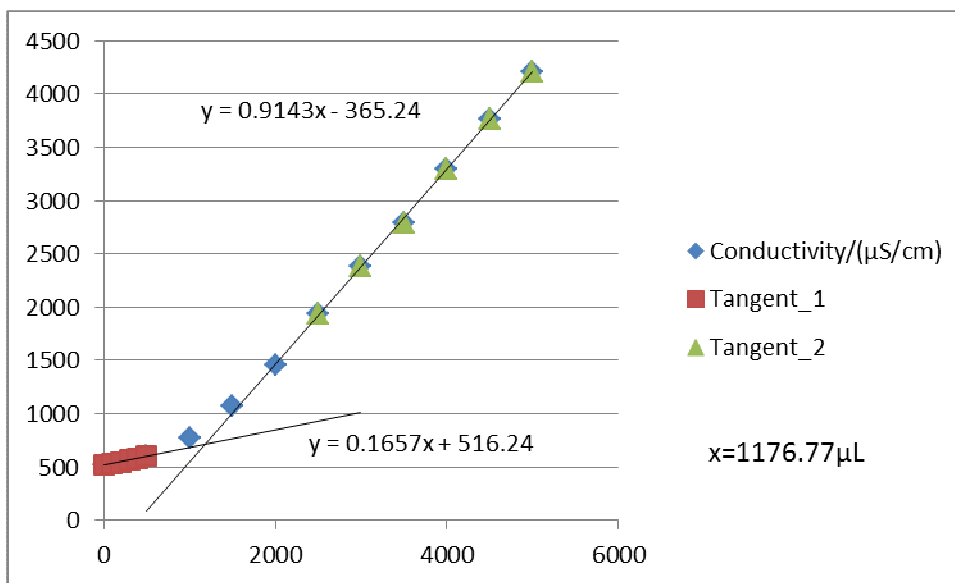
Figure F6-3: Titration 3 for 0.07915 mol/L MEA Third Run

F7: Titration Curves for 0.1184 mol/L MEA First Run at 303 K

$y = 0.8777x - 528.27$

$y = 0.1303x + 719.1$

x=1669.75µL
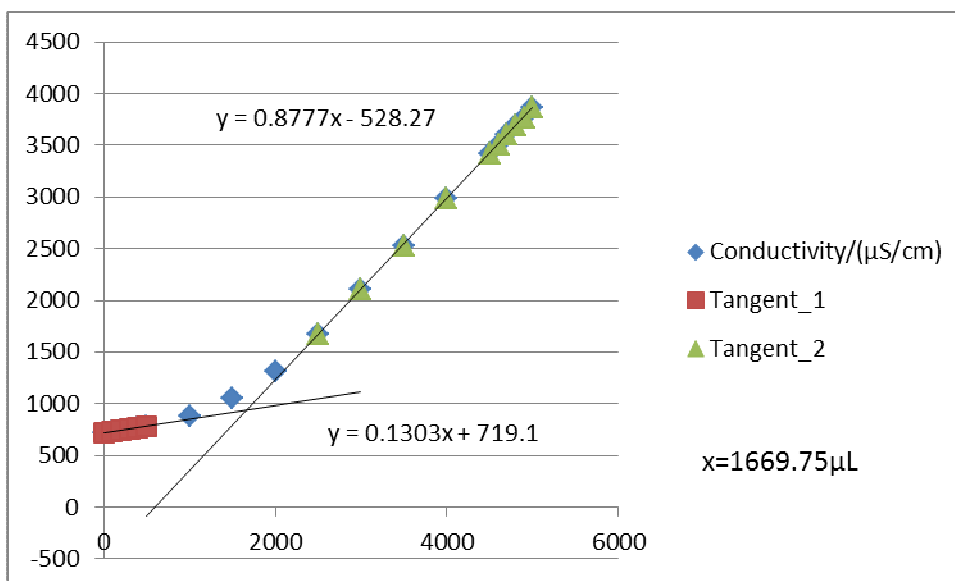
Figure F7-1: Titration 1 for 0.1184 mol/L MEA First Run

$y = 0.8721x - 503.55$

$y = 0.1374x + 710.48$

x=1651.56µL
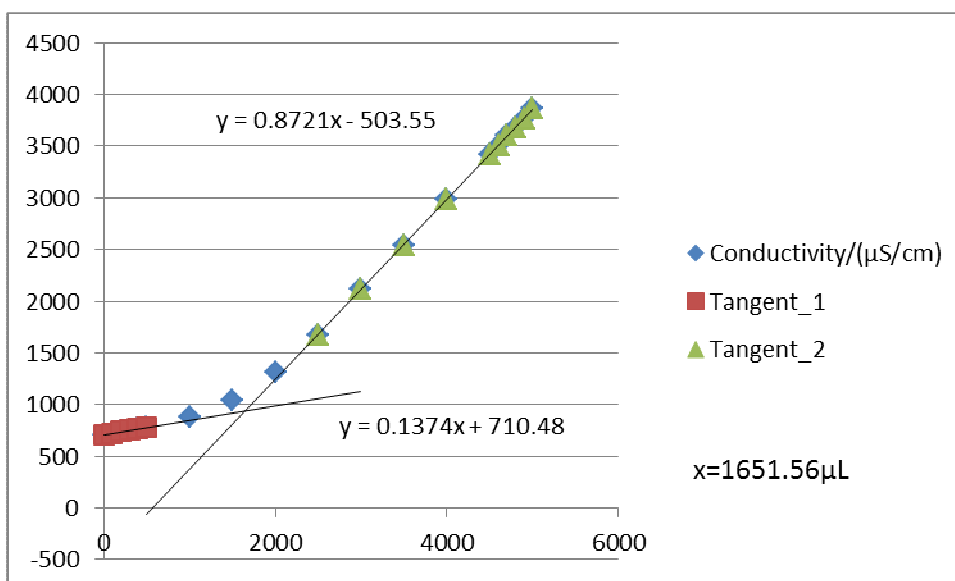
Figure F7-2: Titration 2 for 0.1184 mol/L MEA First Run

162
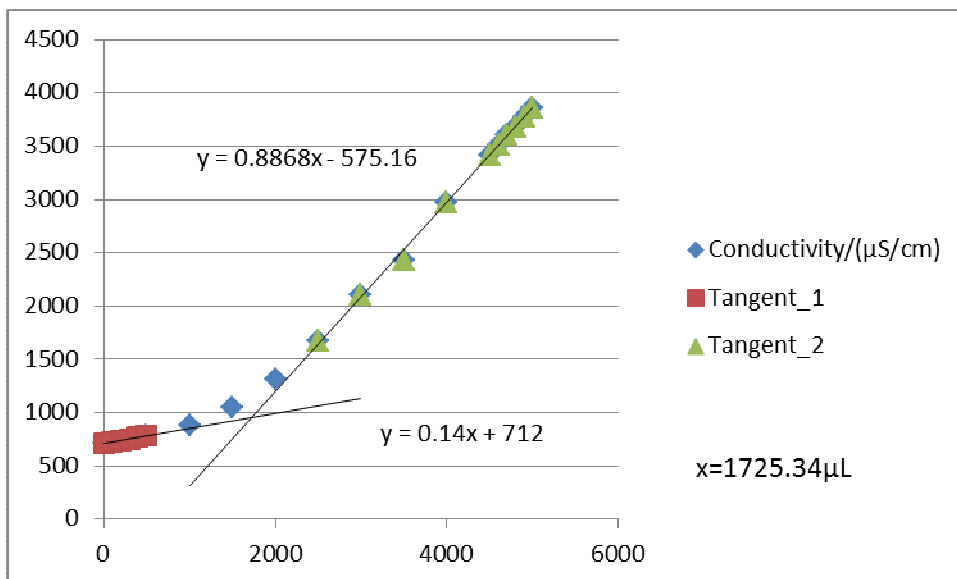
Figure F7-3: Titration 3 for 0.1184 mol/L MEA First Run

F8: Titration Curves for 0.1184 mol/L MEA Second Run at 303 K
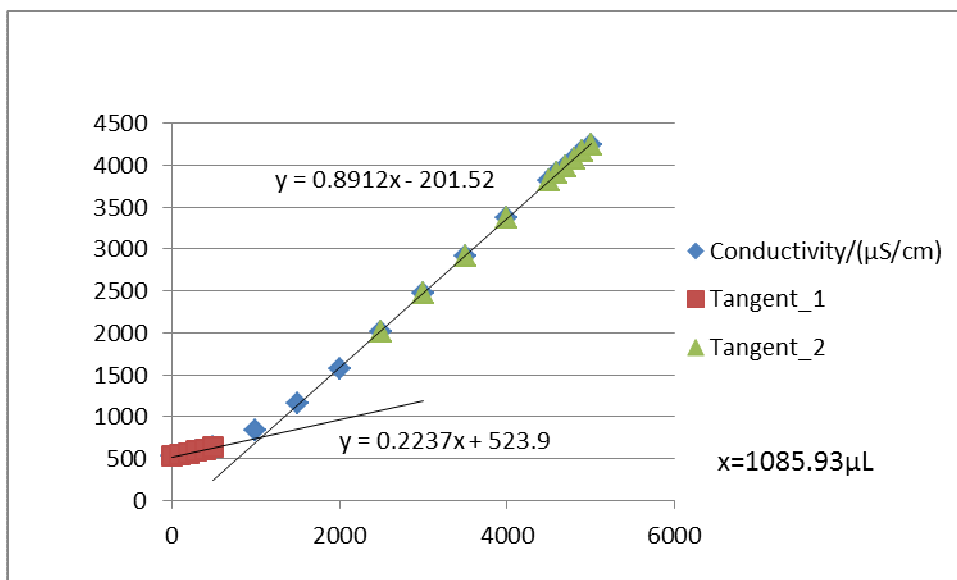
Figure F8-1: Titration 1 for 0.1184 mol/L MEA Second Run

163
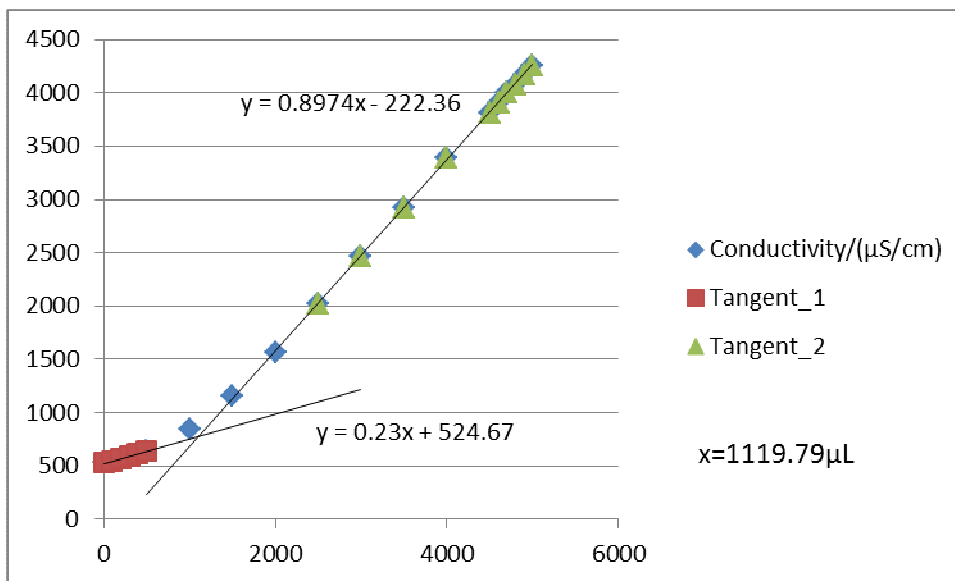
Figure F8-2: Titration 2 for 0.1184 mol/L MEA Second Run
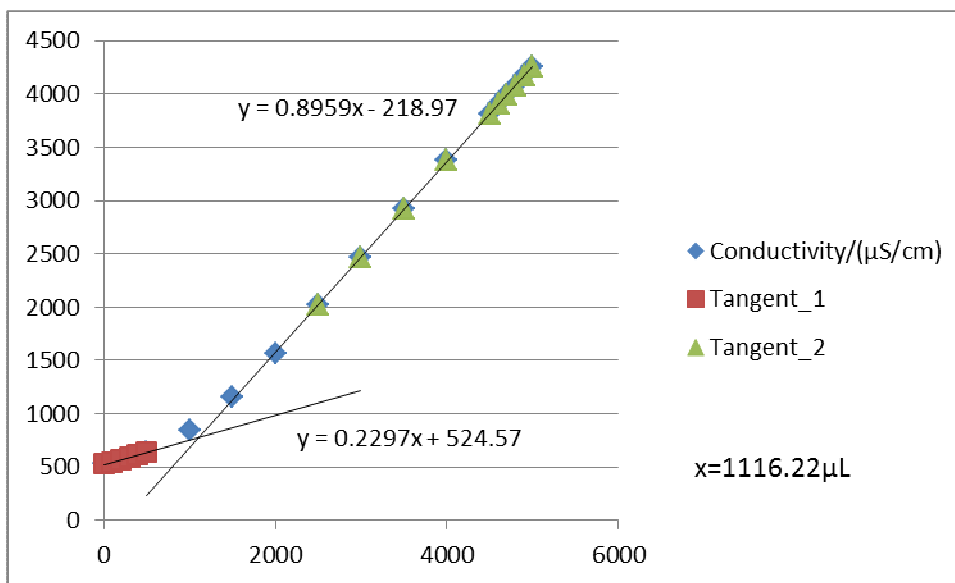
Figure F8-3: Titration 3 for 0.1184 mol/L MEA Second Run

164

F9: Titration Curves for 0.1184 mol/L MEA Third Run at 303 K
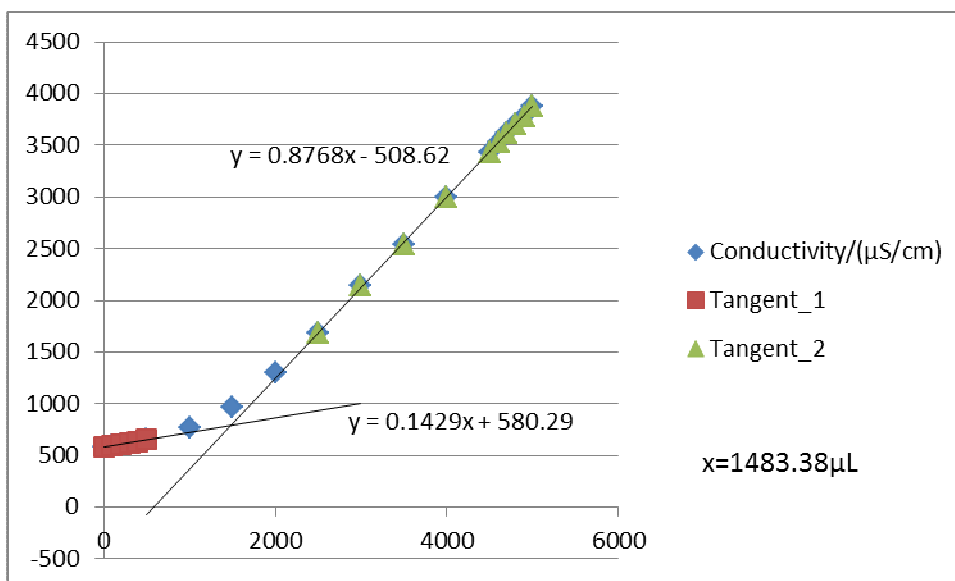
Figure F9-1: Titration 1 for 0.1184 mol/L MEA Third Run
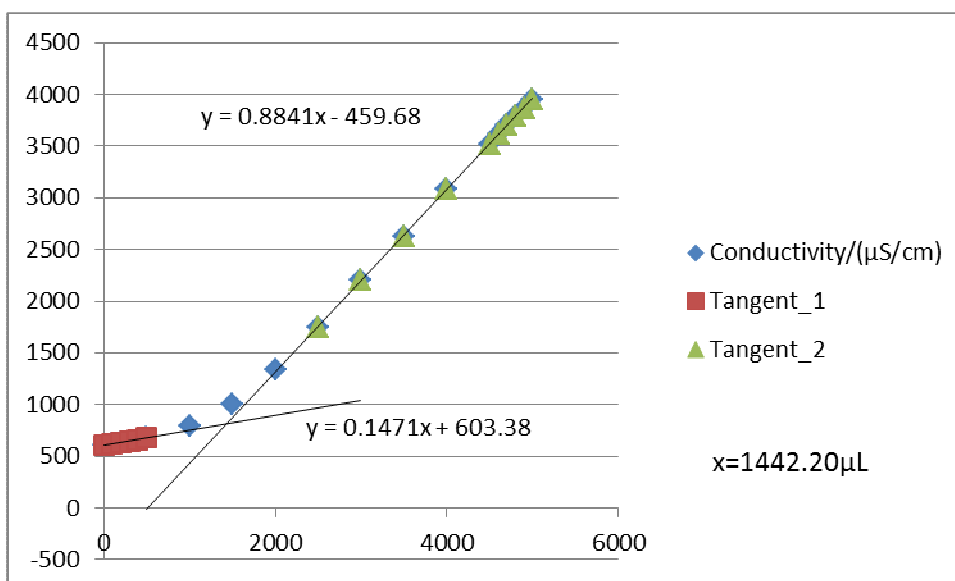
Figure F9-2: Titration 2 for 0.1184 mol/L MEA Third Run
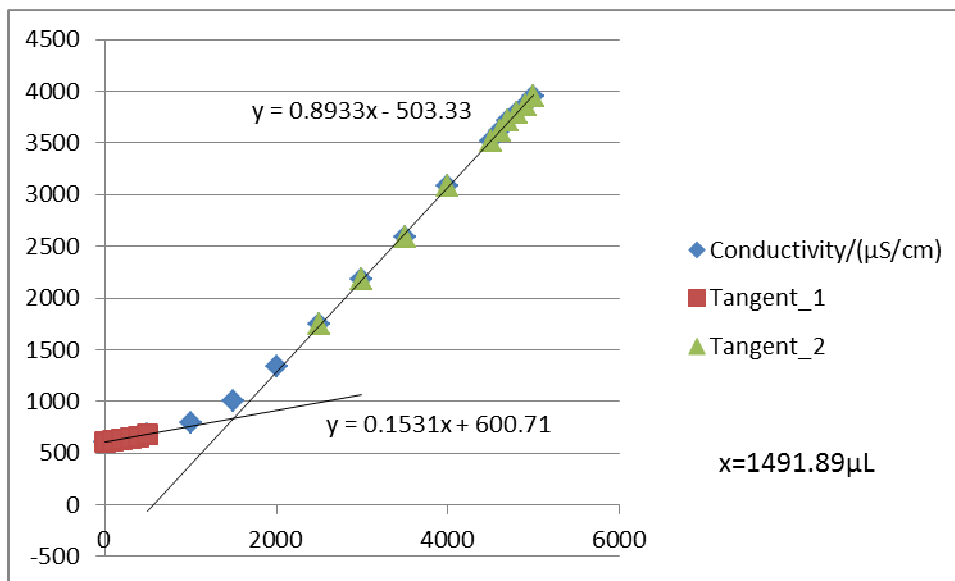
Figure F9-3: Titration 3 for 0.1184 mol/L MEA Third Run

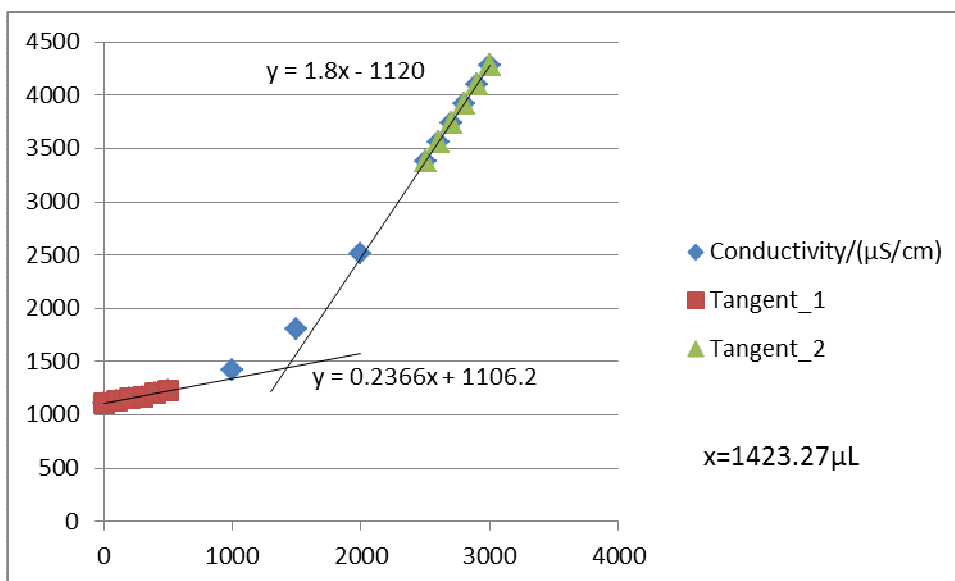**F10: Titration Curves for 0.1575 mol/L MEA First Run at 303 K**
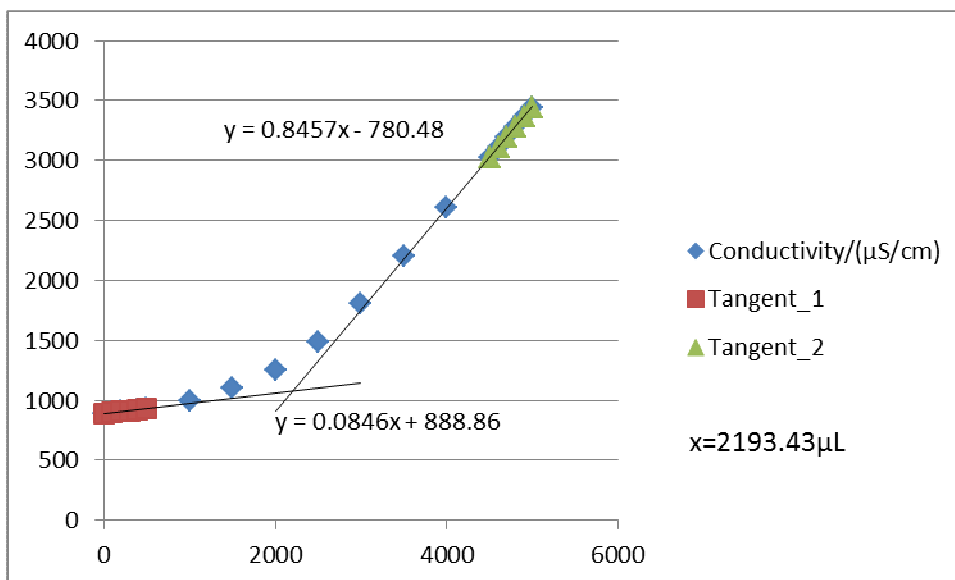
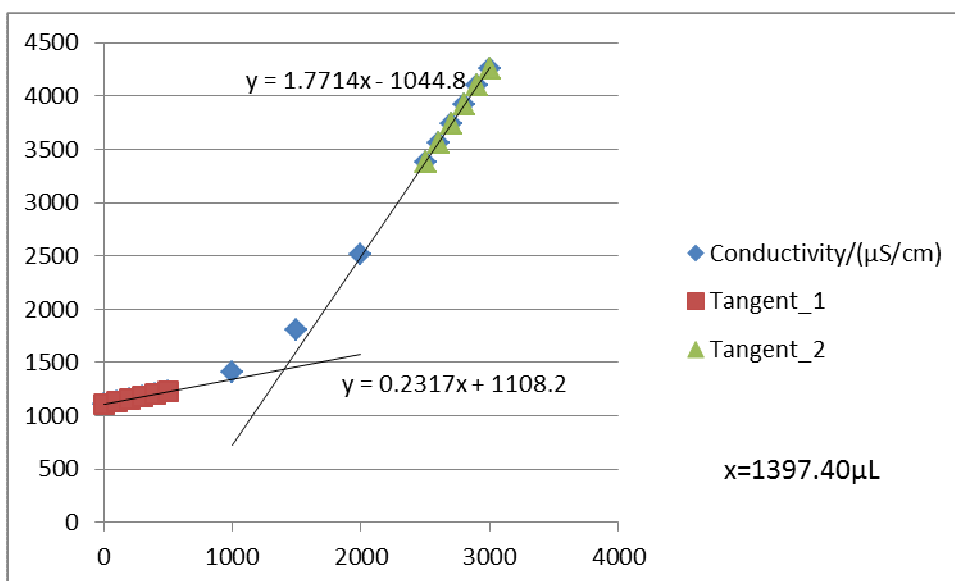Figure F10-1: Titration 1 for 0.1575 mol/L MEA First Run

166
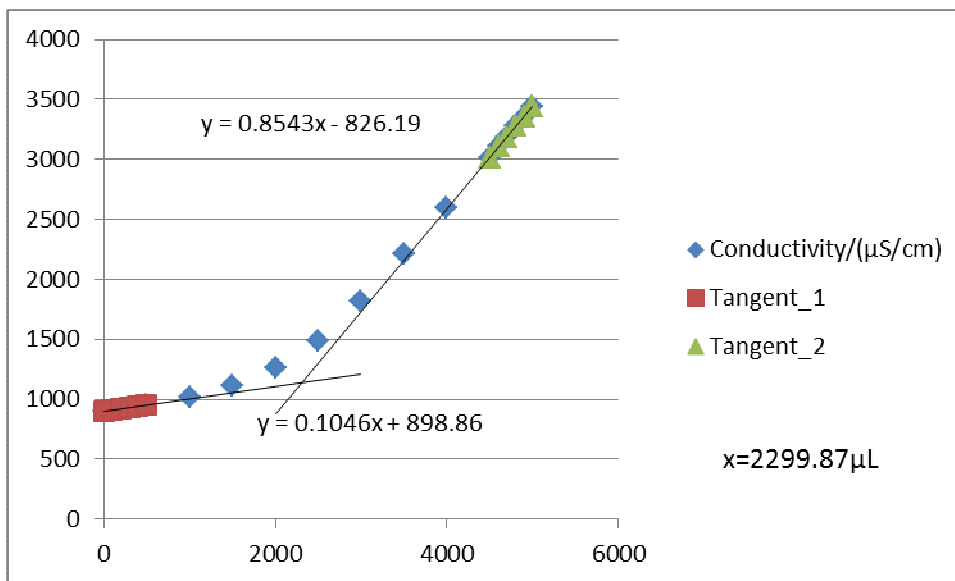
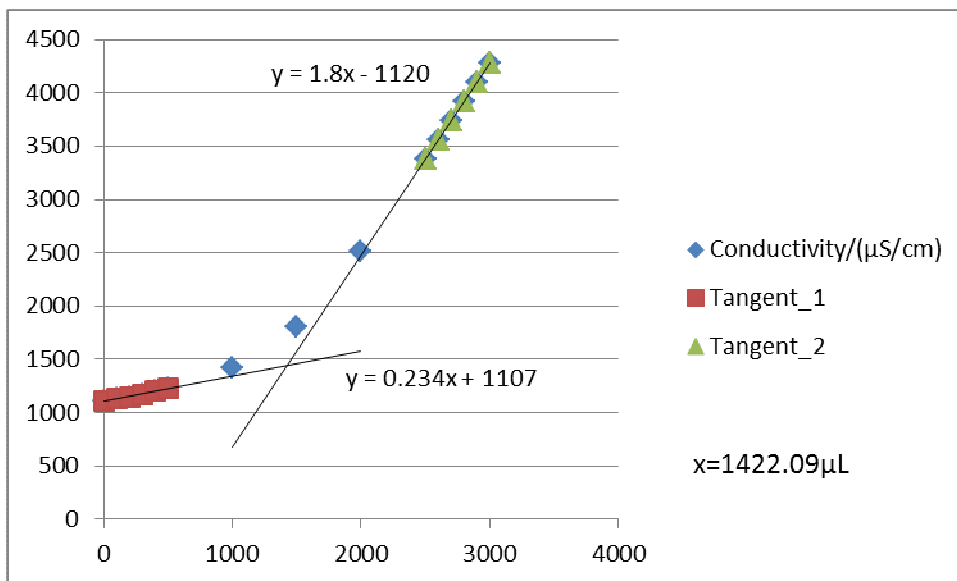Figure F10-2: Titration 2 for 0.1575 mol/L MEA First Run
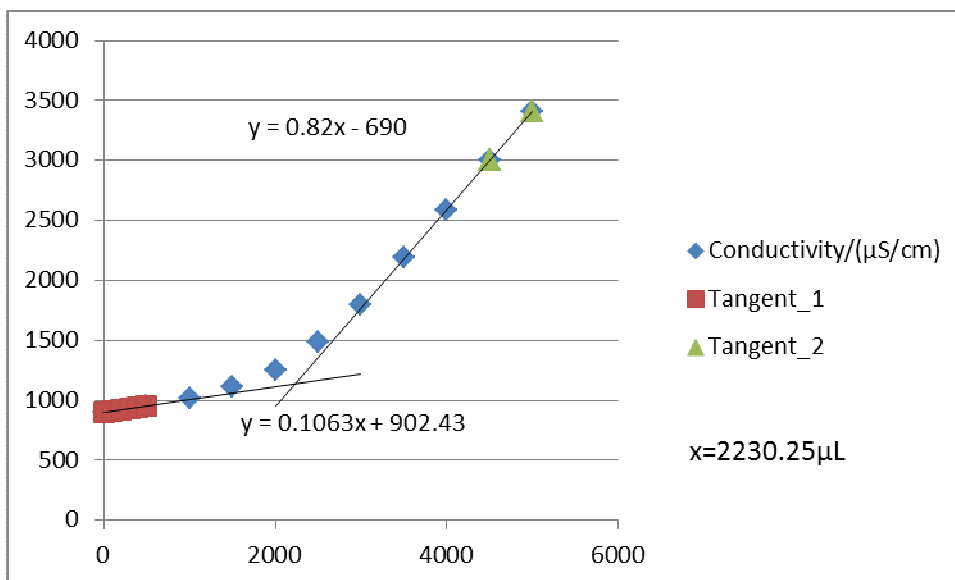
Figure F10-3: Titration 3 for 0.1575 mol/L MEA First Run

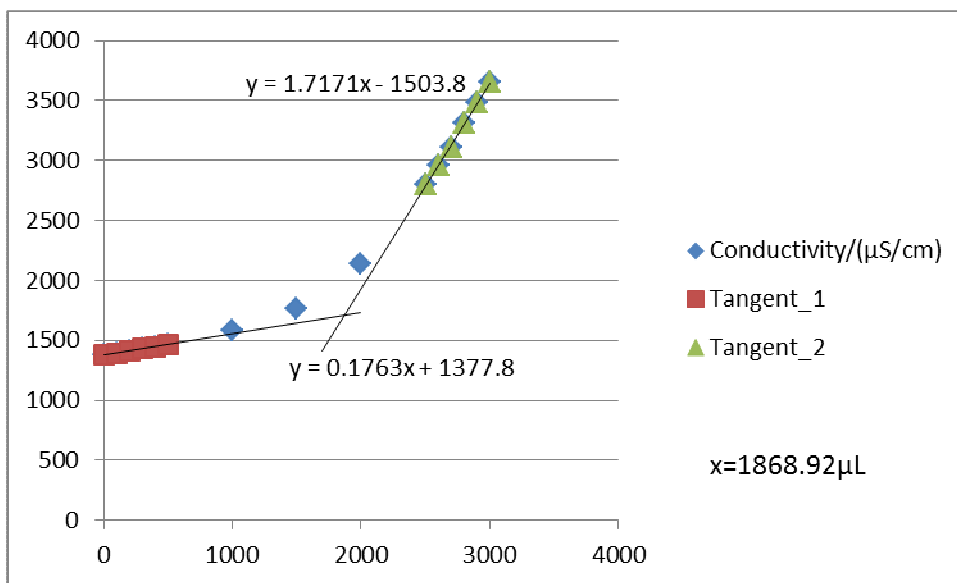**F11: Titration Curves for 0.1575 mol/L MEA Second Run at 303 K**
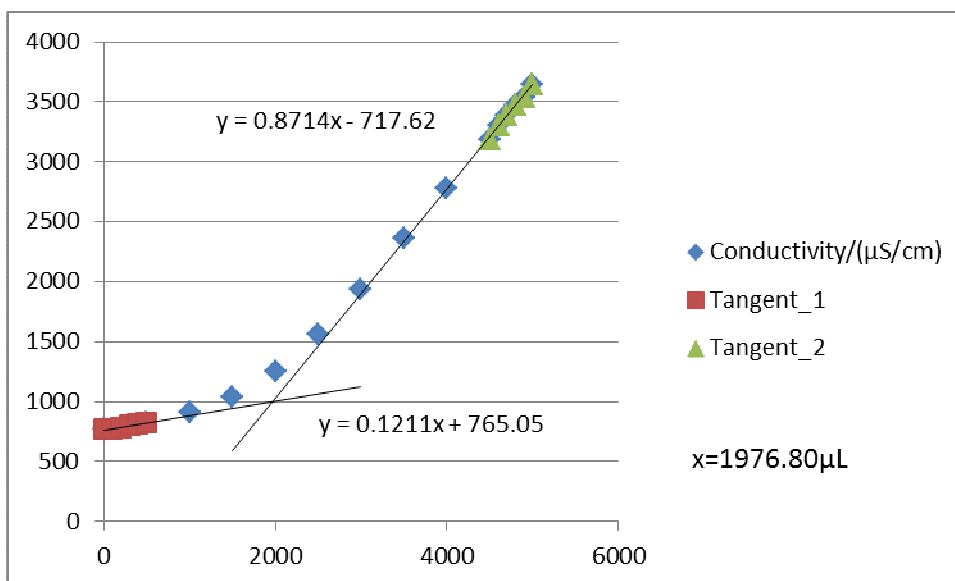
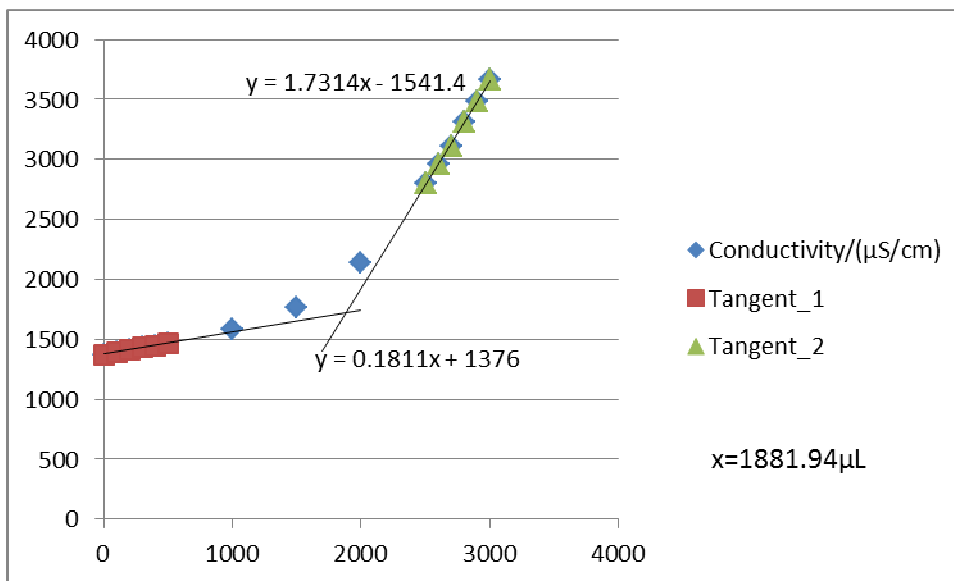Figure F11-1: Titration 1 for 0.1575 mol/L MEA Second Run
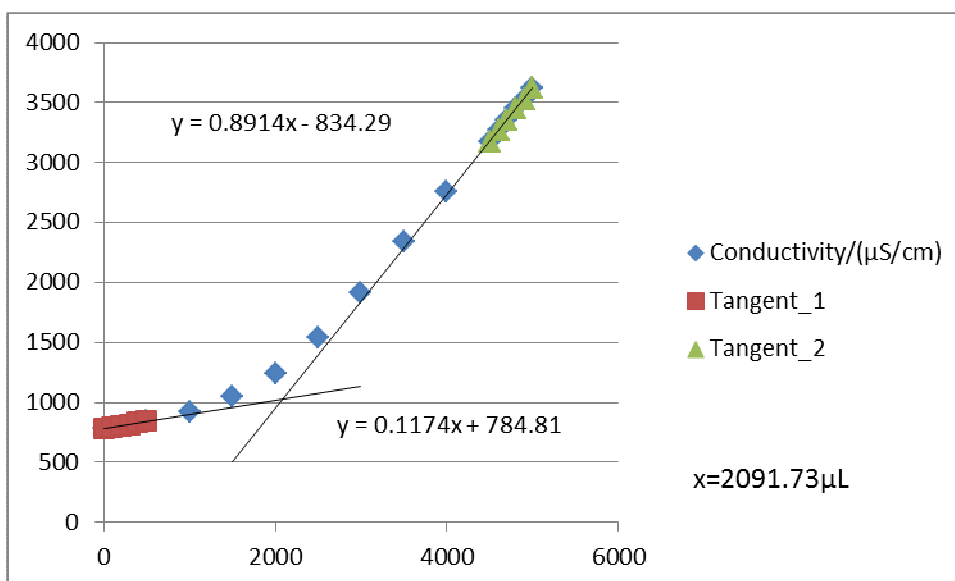
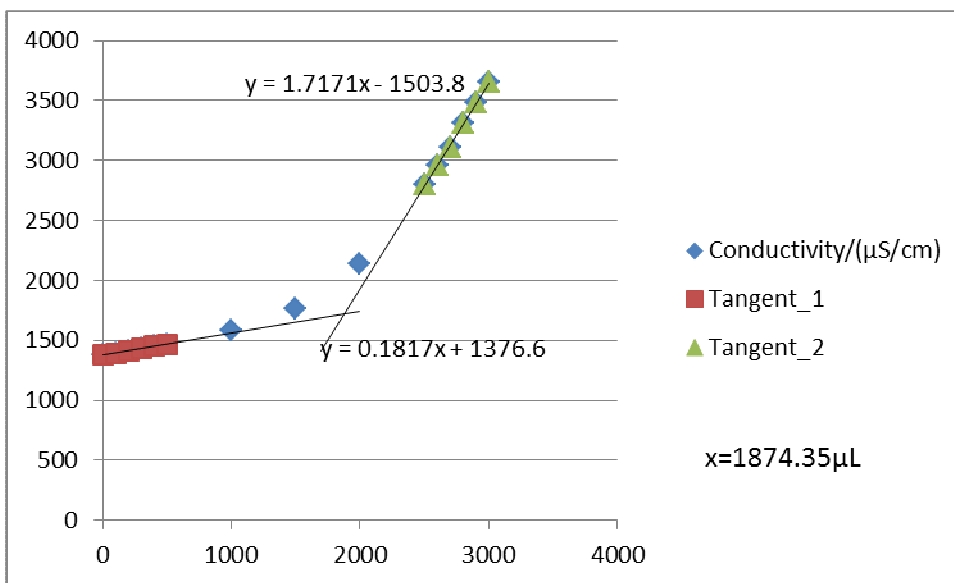

Figure F11-2: Titration 2 for 0.1575 mol/L MEA Second Run

168
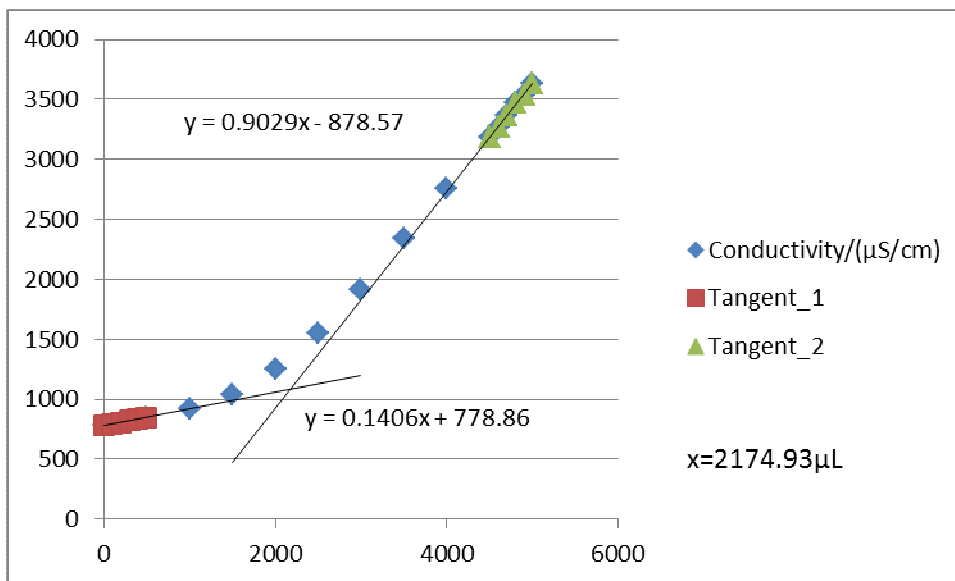
Figure F11-3: Titration 3 for 0.1575 mol/L MEA Second Run

F12: Titration Curves for 0.1575 mol/L MEA Third Run at 303 K
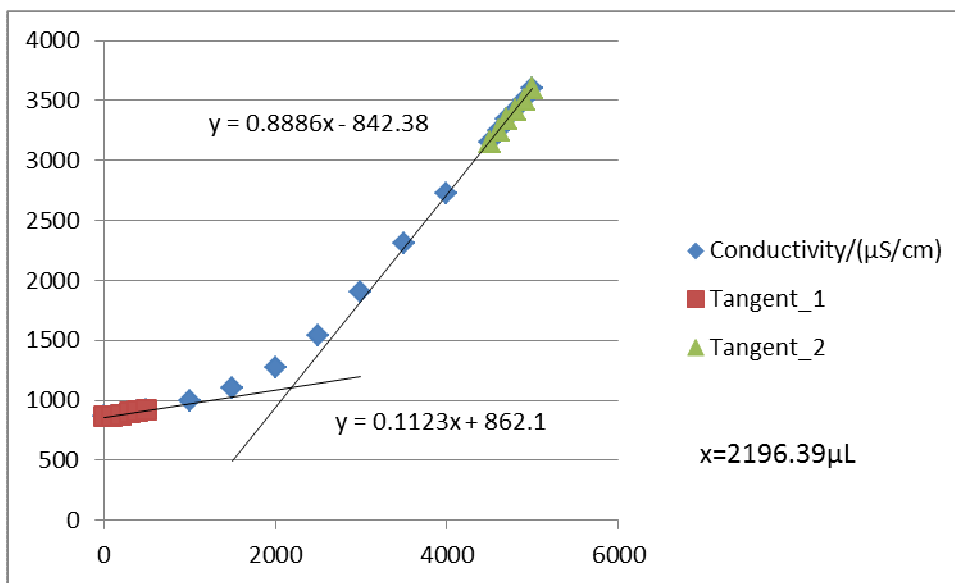
Figure F12-1: Titration 1 for 0.1575 mol/L MEA Third Run
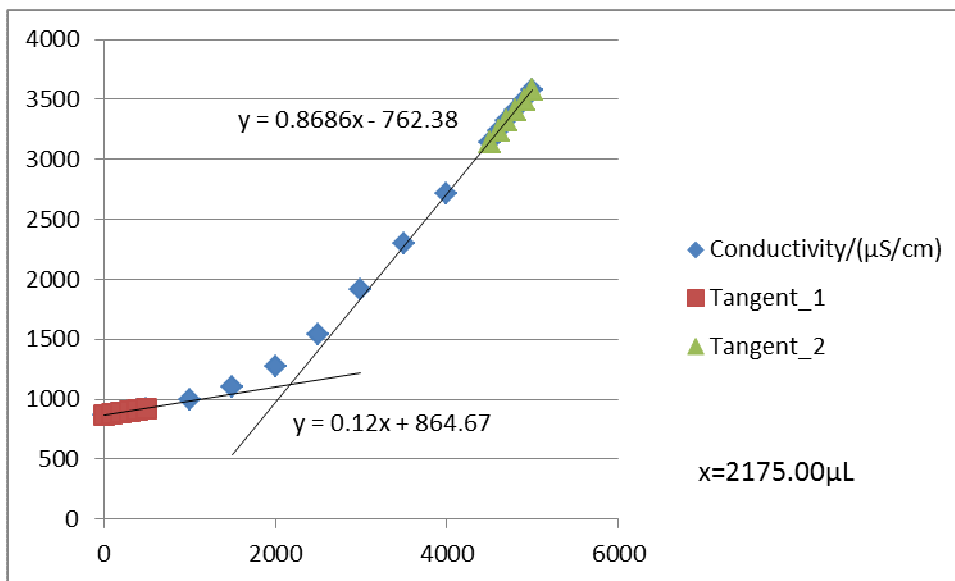
Figure F12-2: Titration 2 for 0.1575 mol/L MEA Third Run
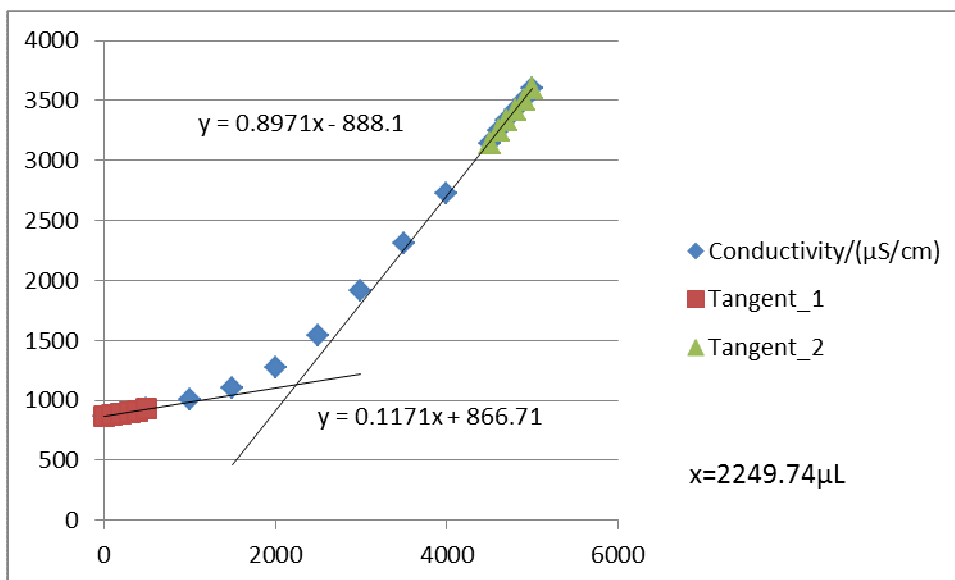
Figure F12-3: Titration 3 for 0.1575 mol/L MEA Third Run

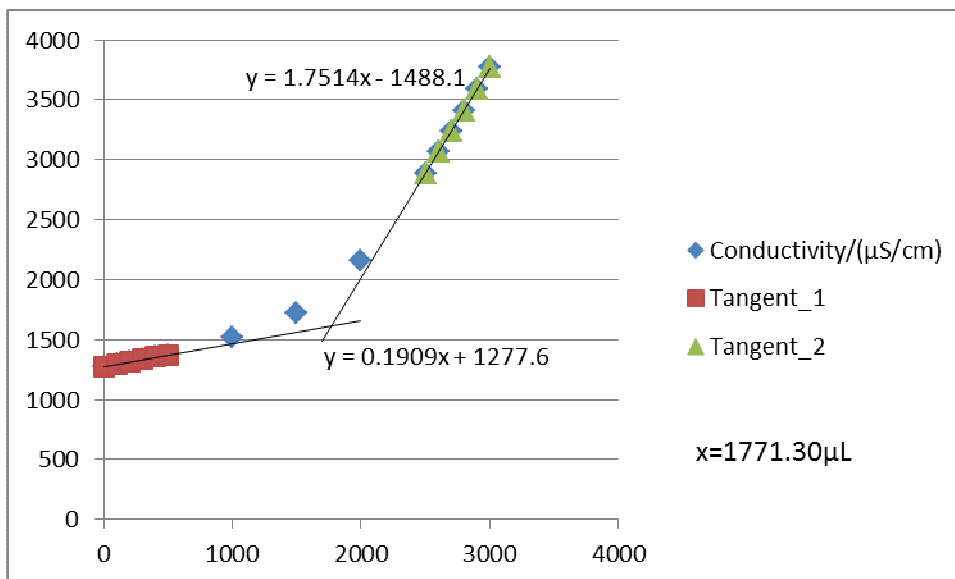**F13: Titration Curves for 0.1965 mol/L MEA First Run at 308 K**
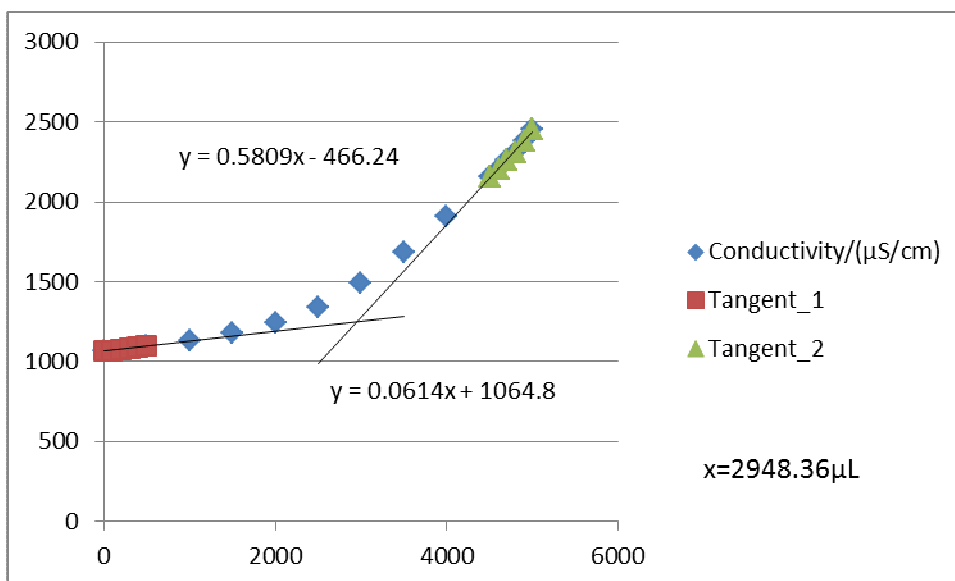
Figure F13-1: Titration 1 for 0.1965 mol/L MEA First Run
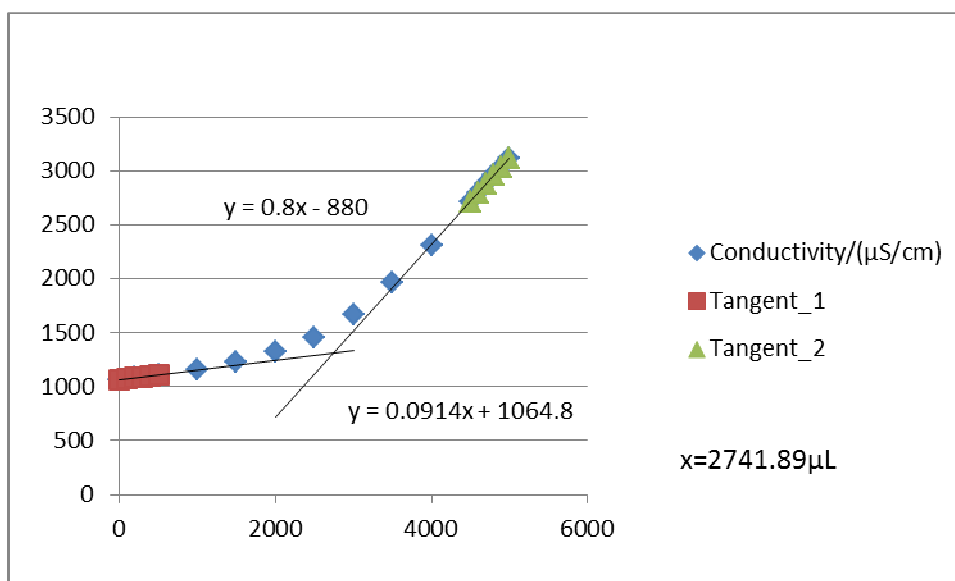
Figure F13-2: Titration 2 for 0.1965 mol/L MEA First Run

171
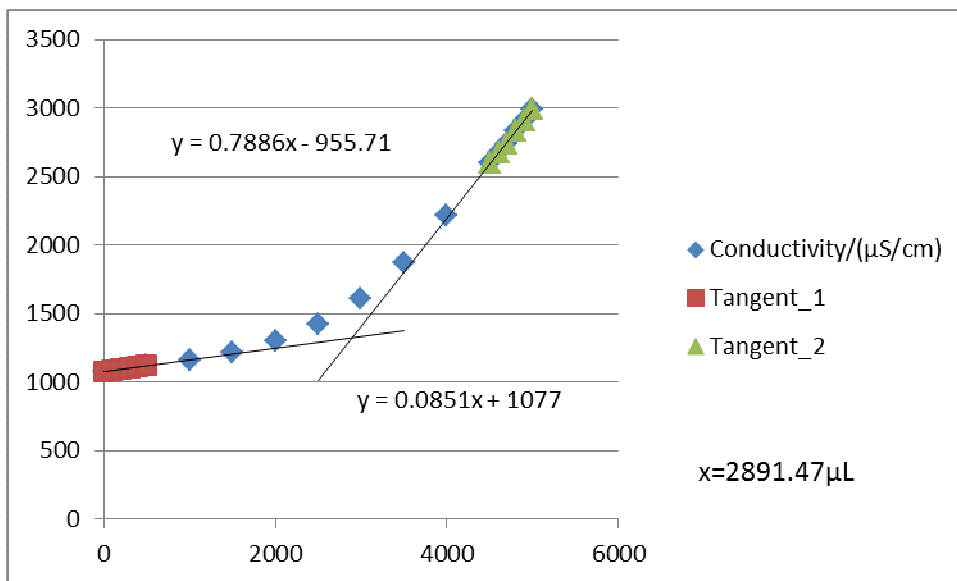
Figure F13-3: Titration 3 for 0.1965 mol/L MEA First Run

F14: Titration Curves for 6.0ml MEA Second Run at 303 K
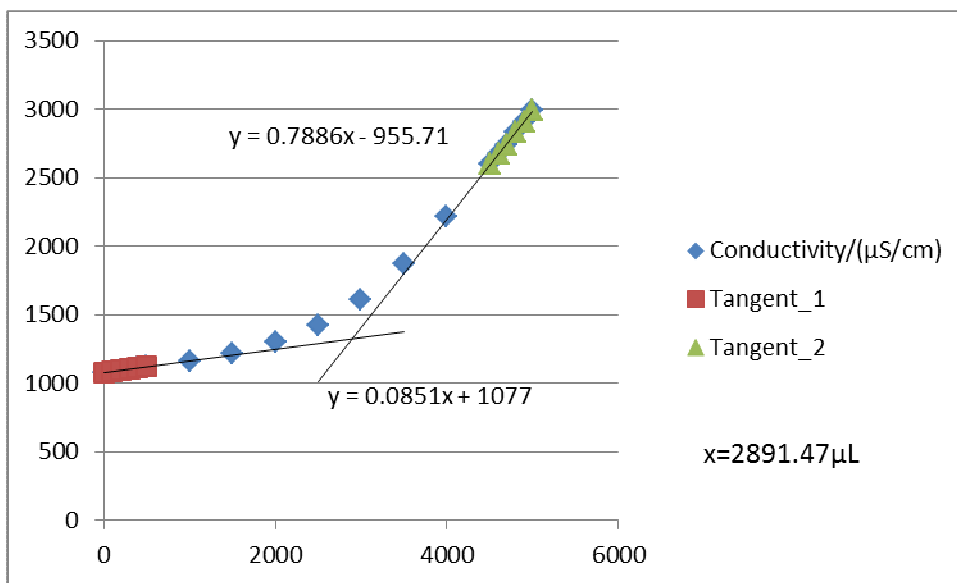
Figure F14-1: Titration 1 for 0.1965 mol/L MEA Second Run
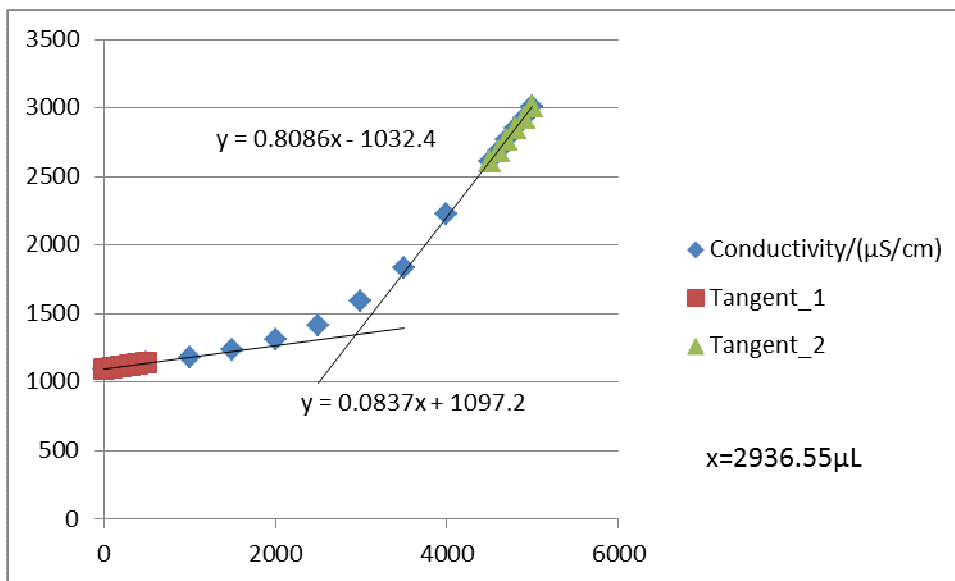
Figure F14-2: Titration 2 for 0.1965 mol/L MEA Second Run
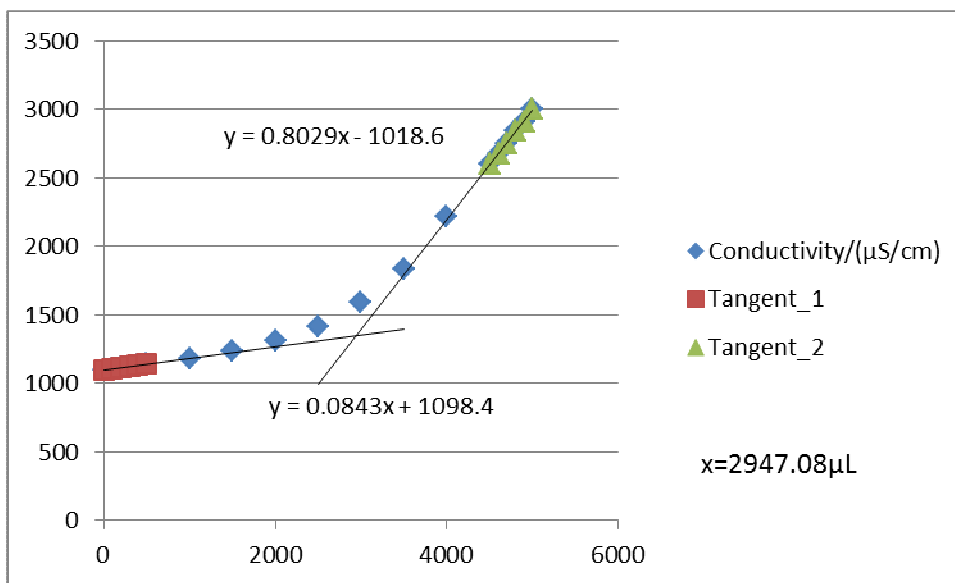
Figure F14-3: Titration 3 for 0.1965 mol/L MEA Second Run

F15: Titration Curves for 0.1965 mol/L MEA Third Run at 303 K
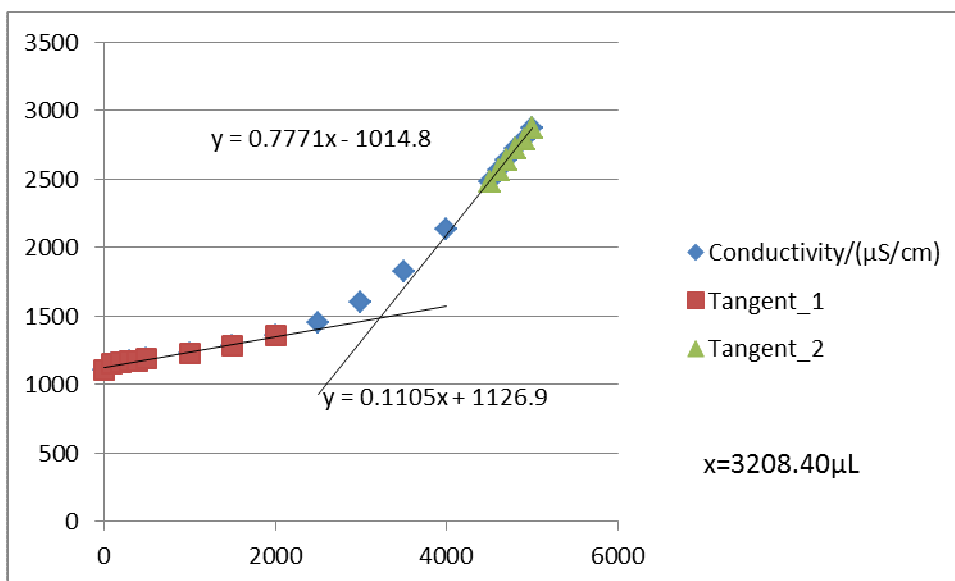
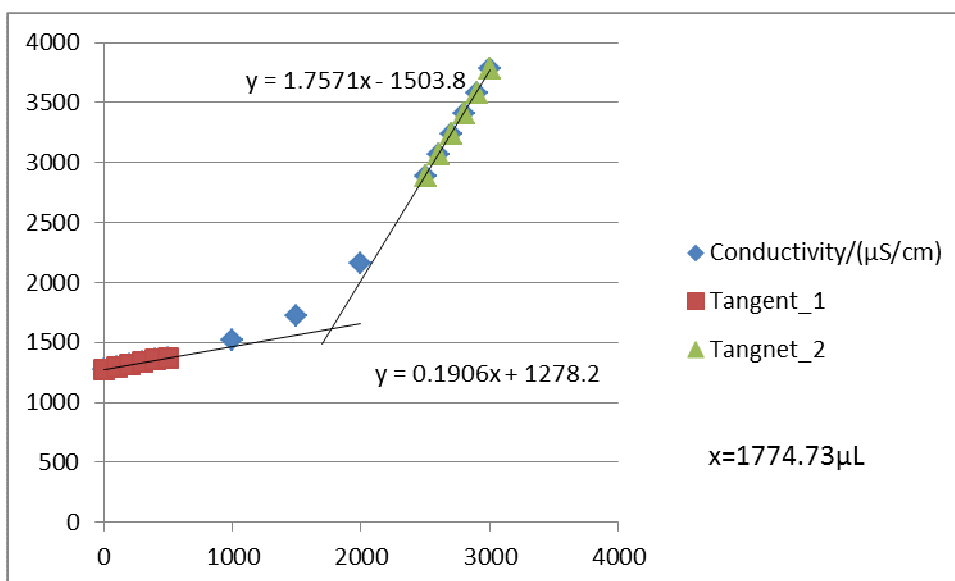Figure F15-1: Titration 1 for 0.1965 mol/L MEA Third Run
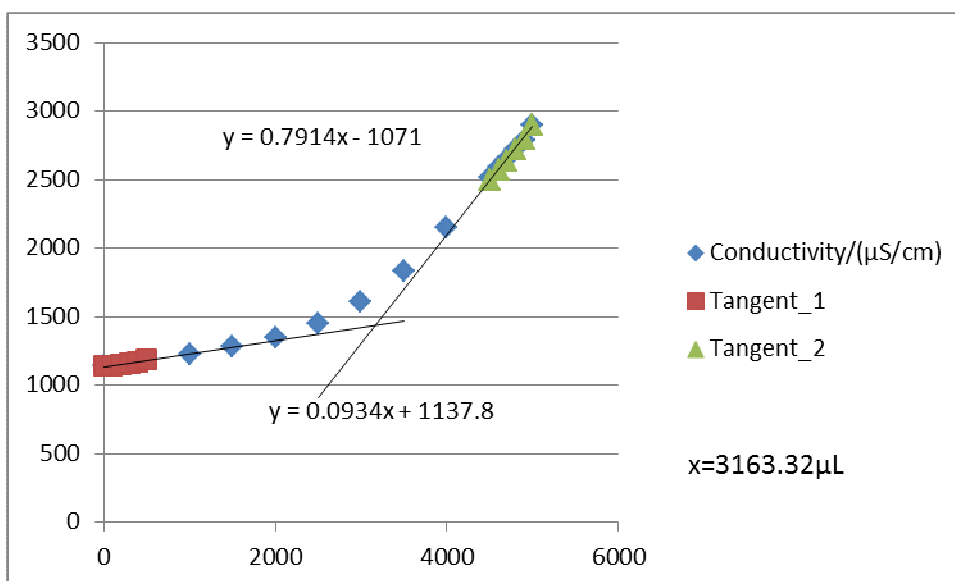
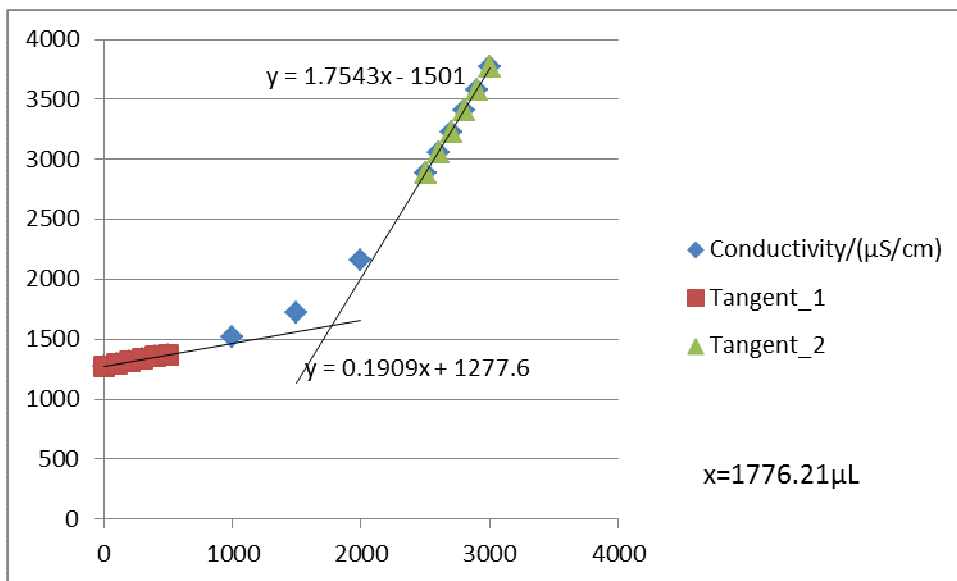Figure F15-2: Titration 2 for 0.1965 mol/L MEA Third Run

174
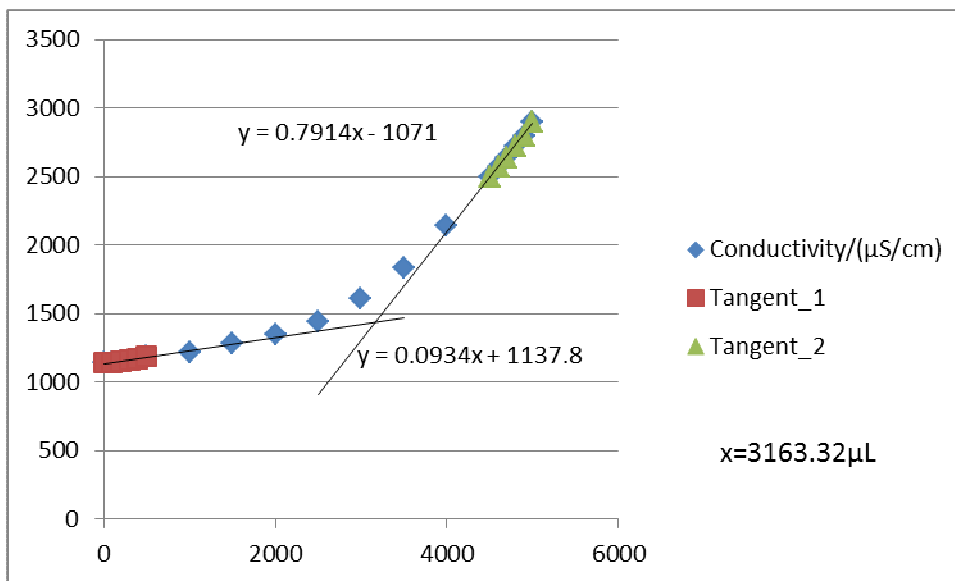
Figure F15-3: Titration 3 for 0.1965 mol/L MEA Third Run

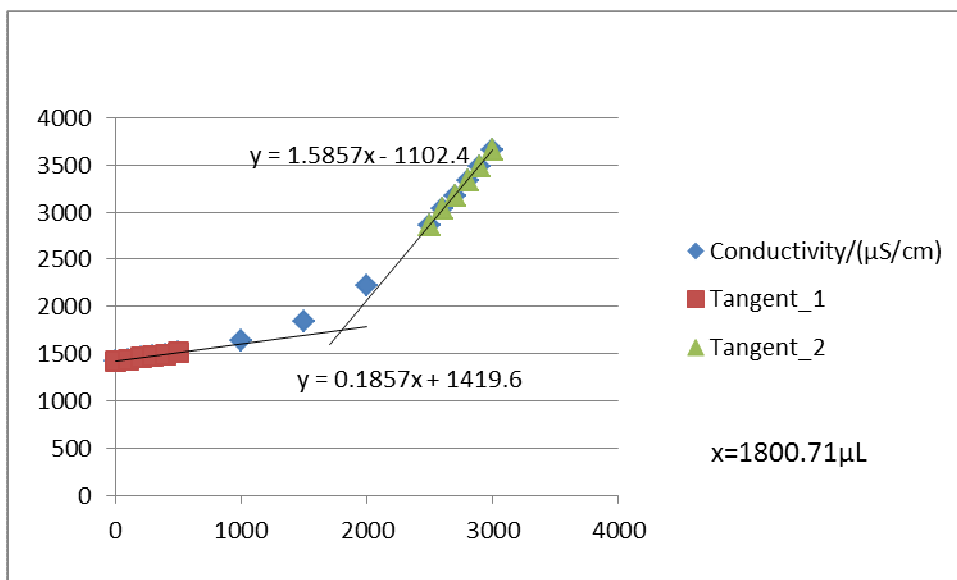**F16: Titration Curves for 0.2609 mol/L MEA First Run at 303 K**
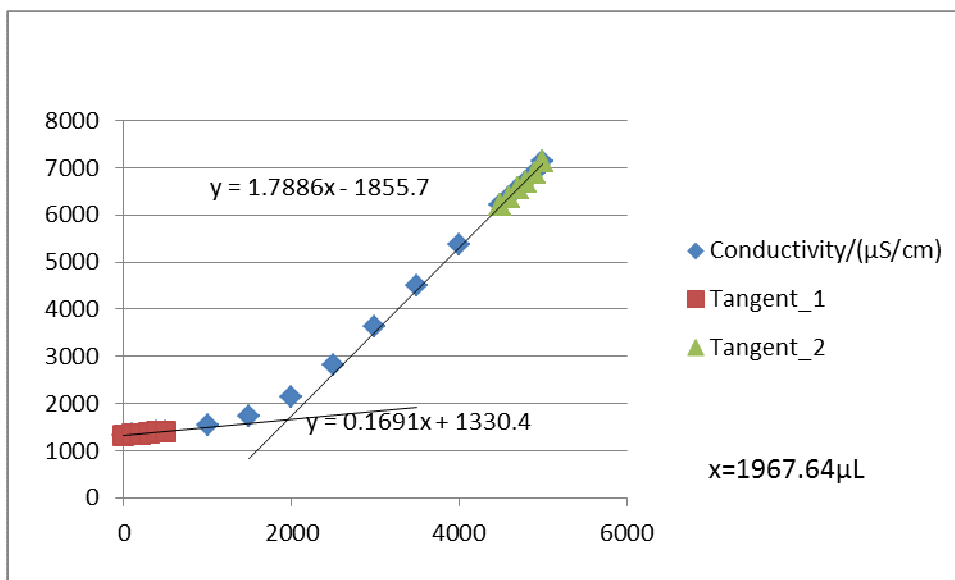
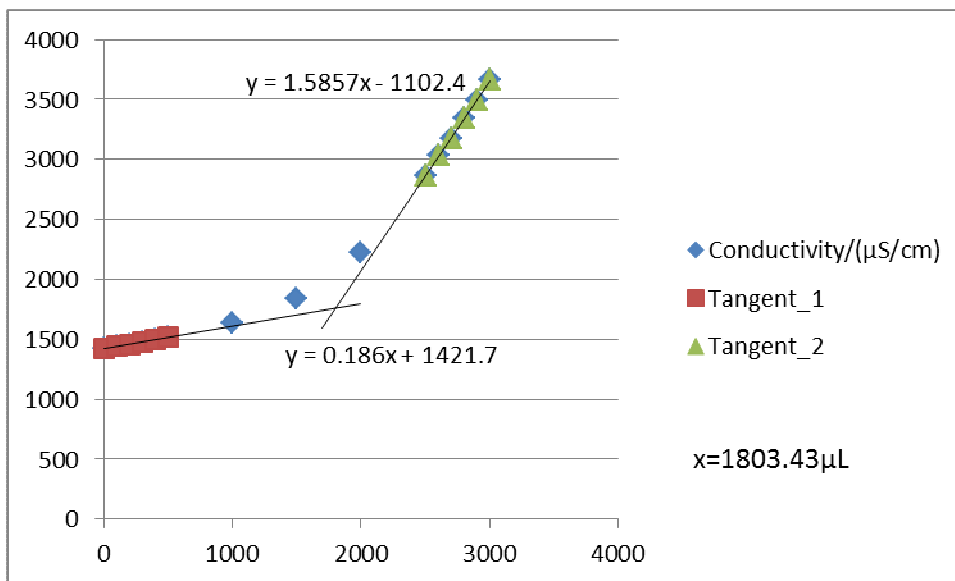Figure F16-1: Titration 1 for 0.2609 mol/L MEA First Run

175
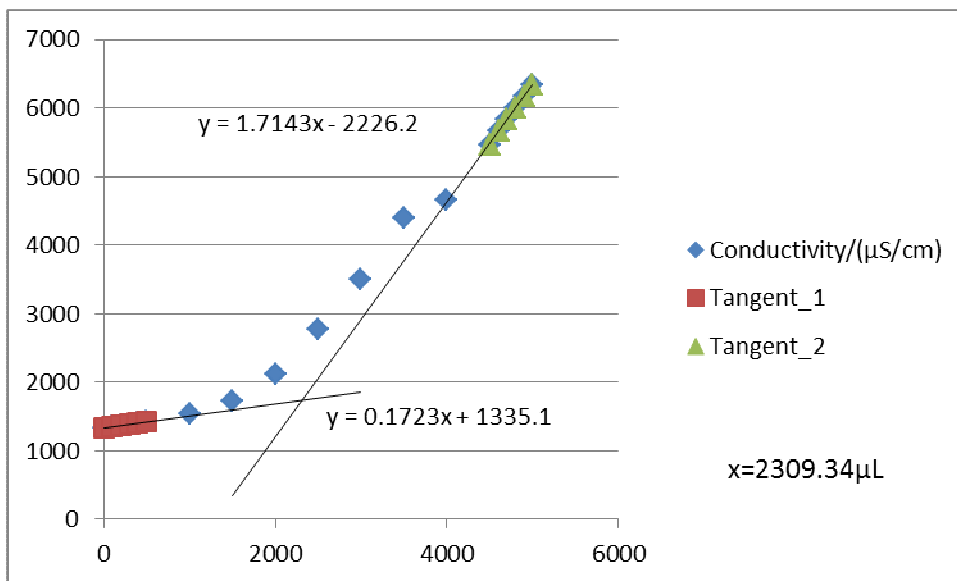
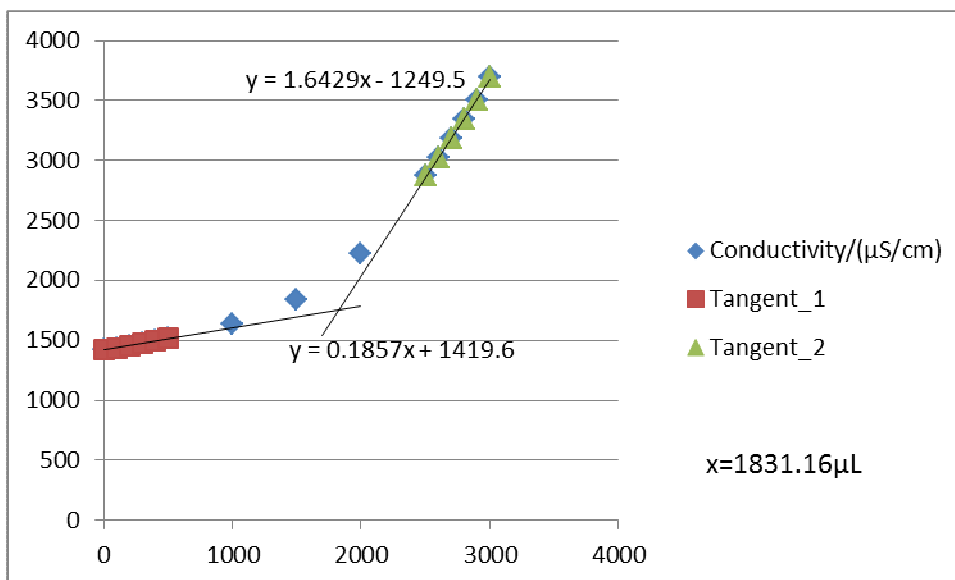Figure F16-2: Titration 2 for 0.2609 mol/L MEA First Run
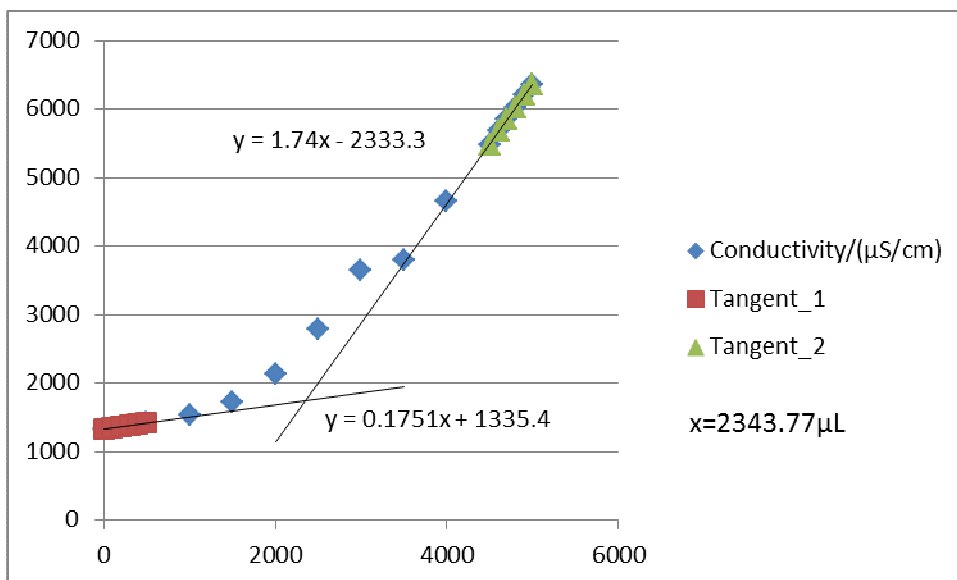
Figure F16-3: Titration 3 for 0.2609 mol/L MEA First Run

176

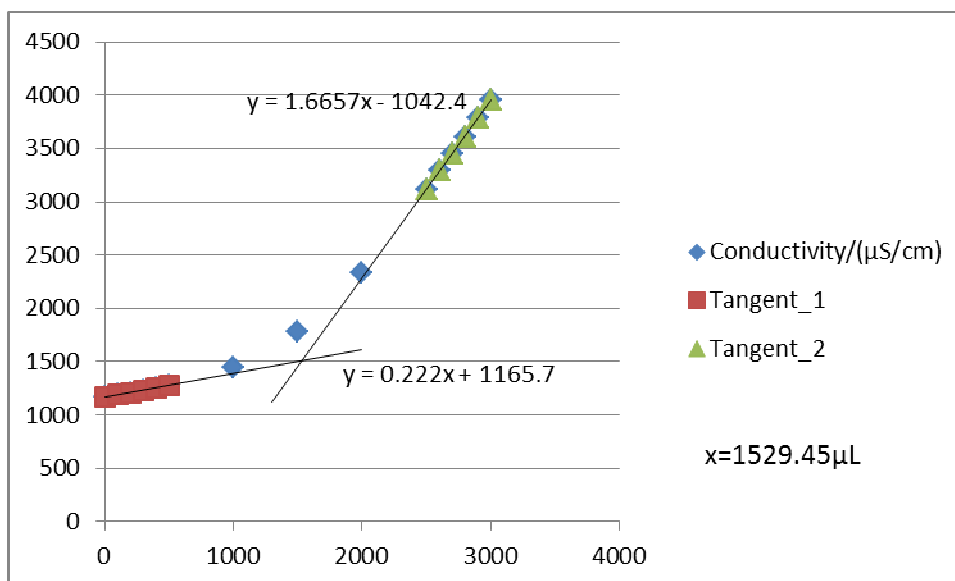**F17: Titration Curves for 0.2609 mol/L MEA Second Run at 303**
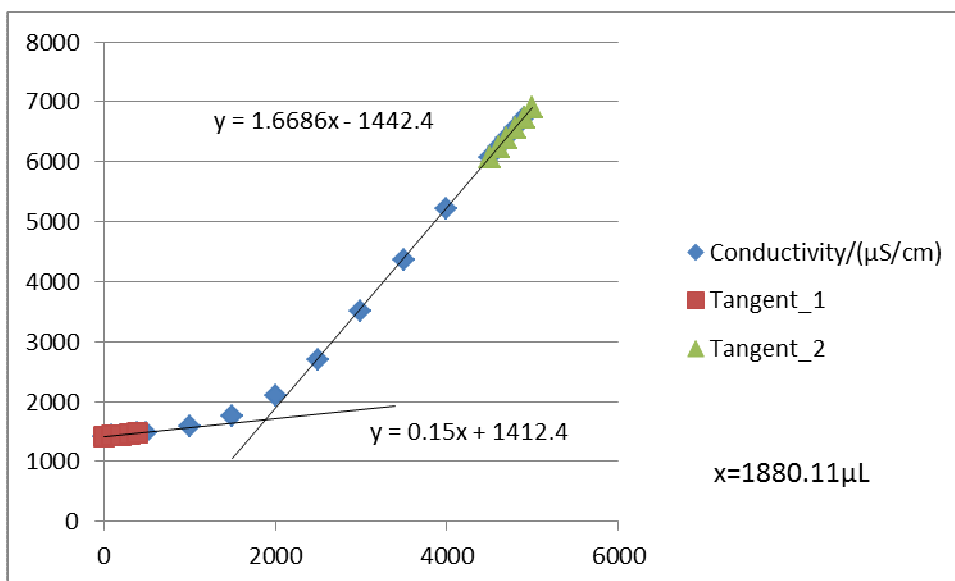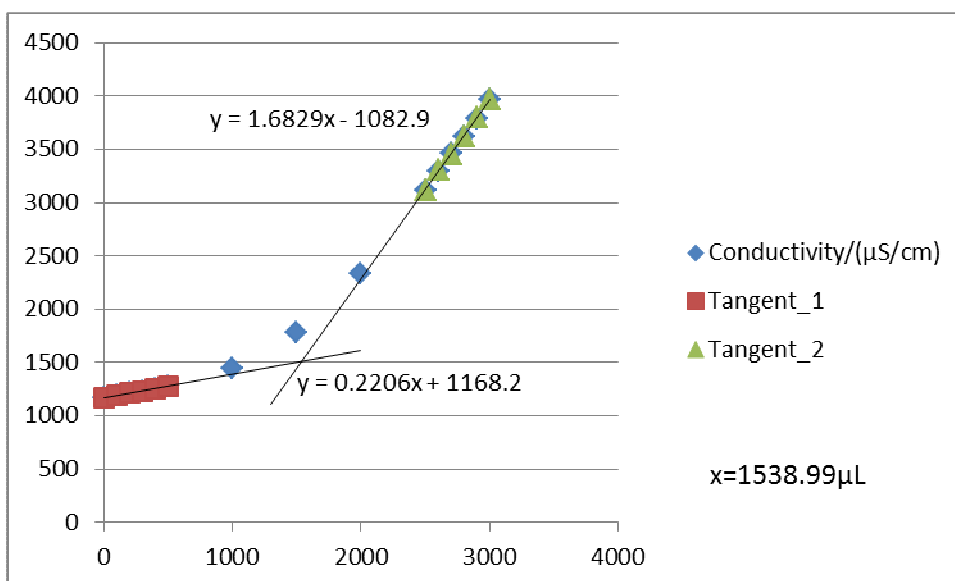

Figure F17-1: Titration 1 for 0.2609 mol/L MEA Second Run
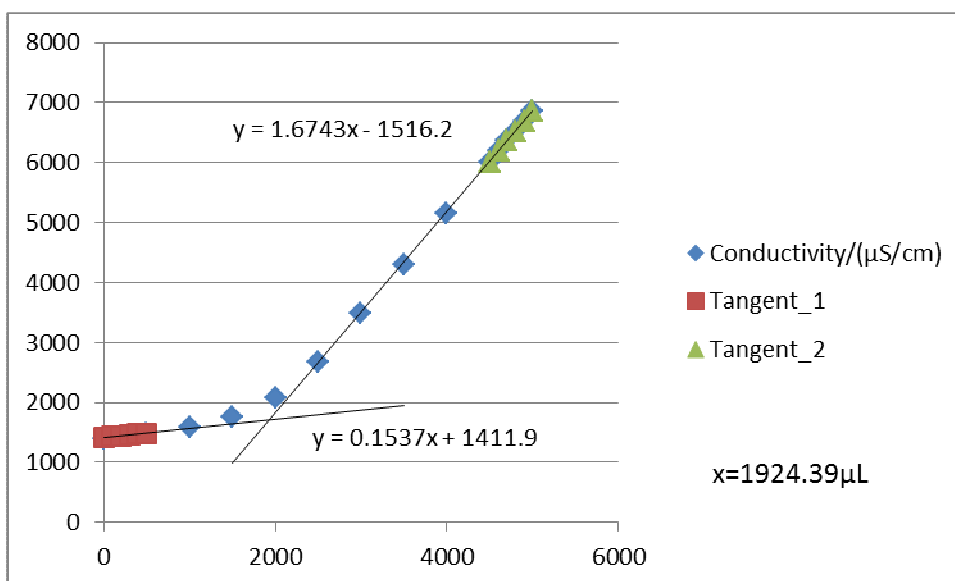
Figure F17-2: Titration 2 for 0.2609 mol/L MEA Second Run
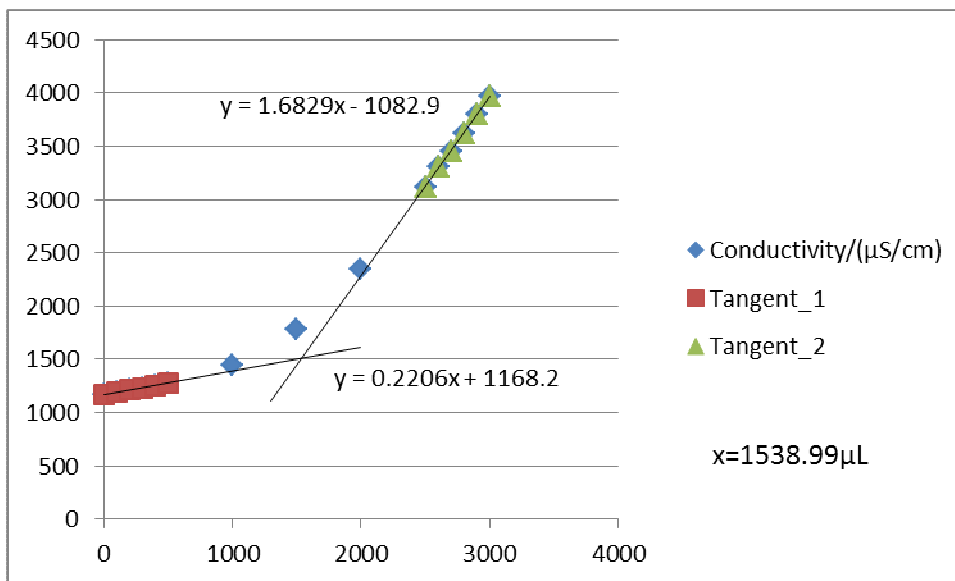
177
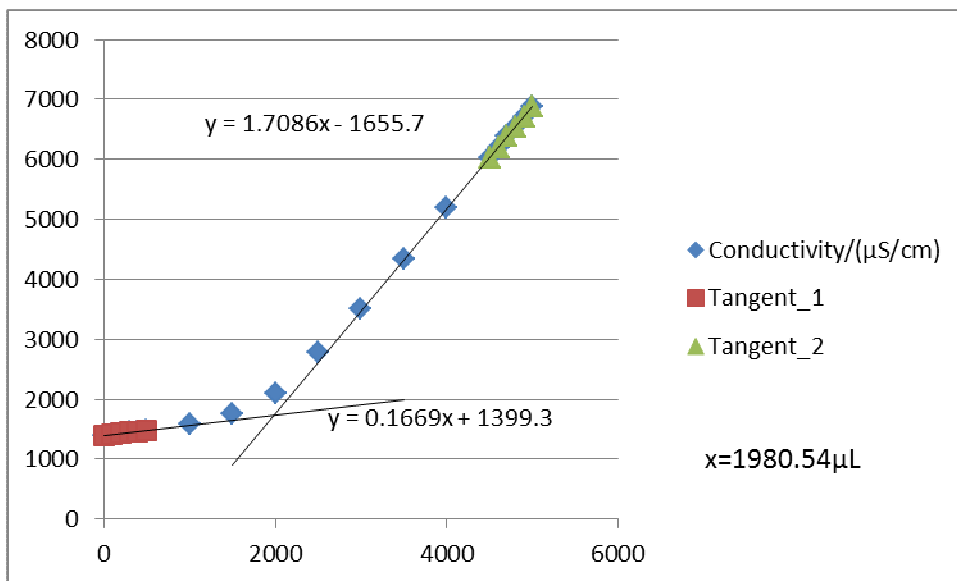
Figure F17-3: Titration 3 for 0.2609 mol/L MEA Second Run

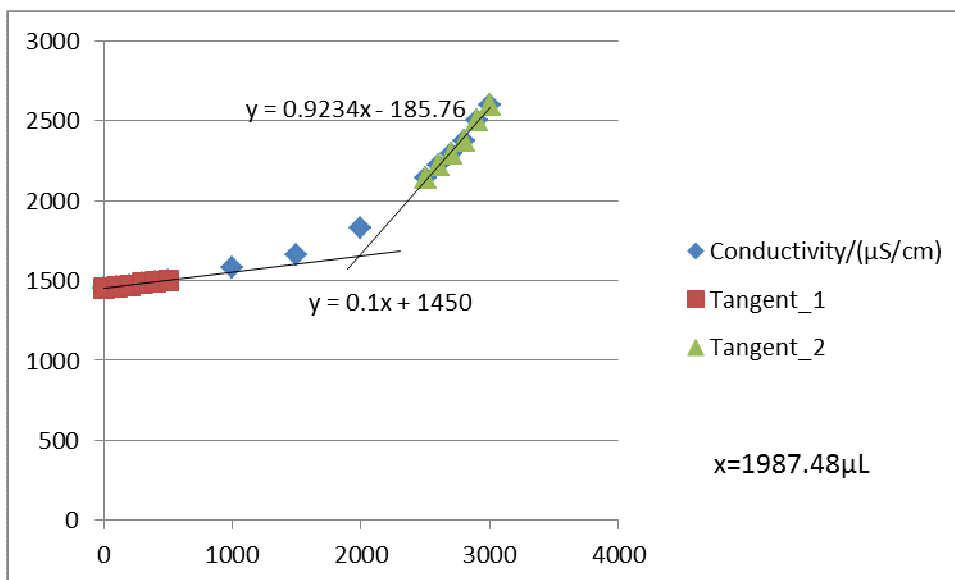**F18: Titration Curves for 0.2609 mol/L MEA Third Run at 303 K**
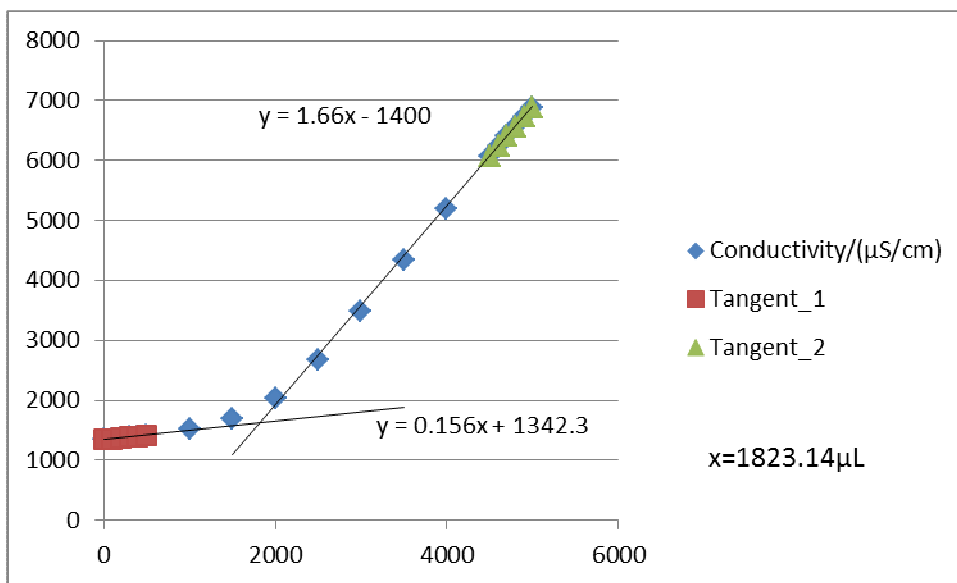
Figure F18-1: Titration 1 for 0.2609 mol/L MEA Third Run

178
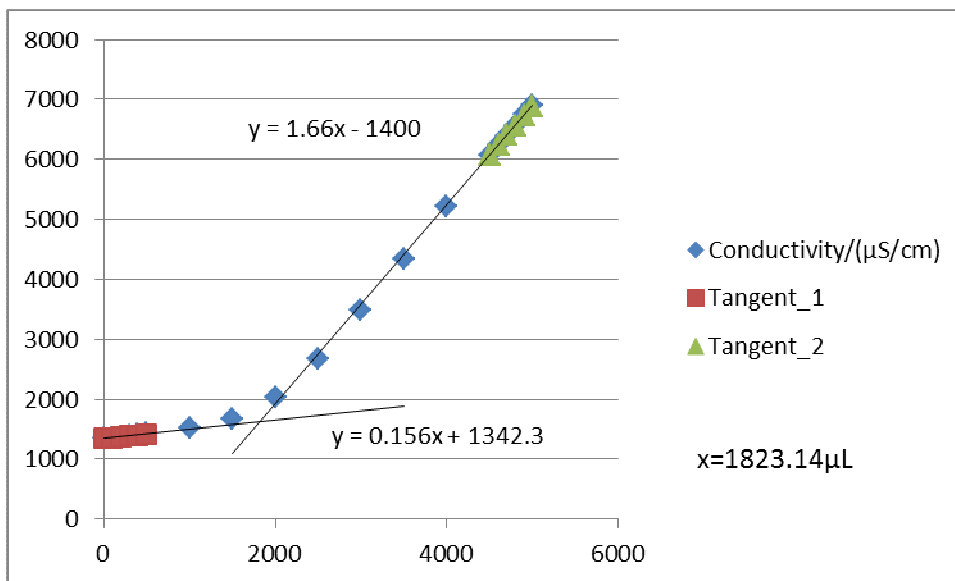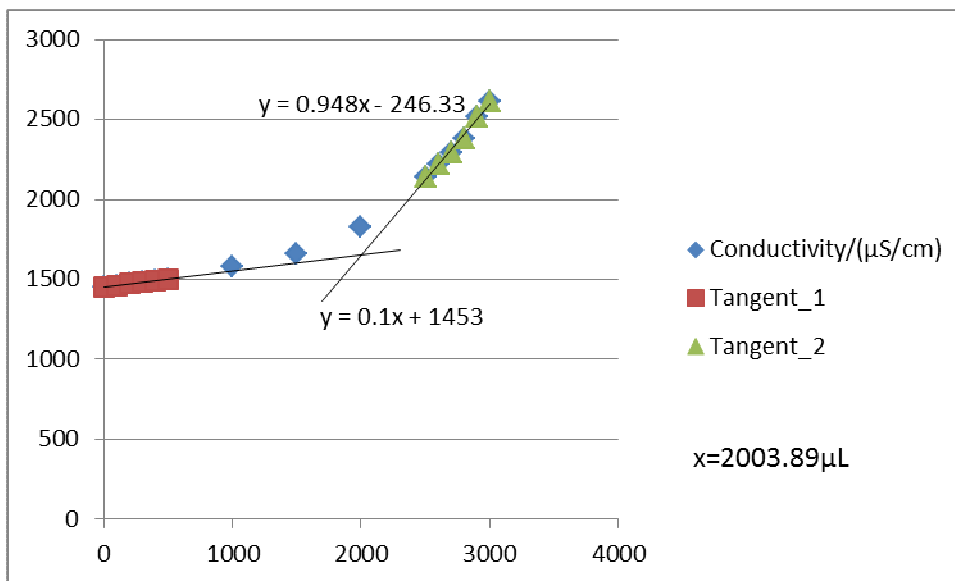
Figure F18-2: Titration 2 for 0.2609 mol/L MEA Third Run
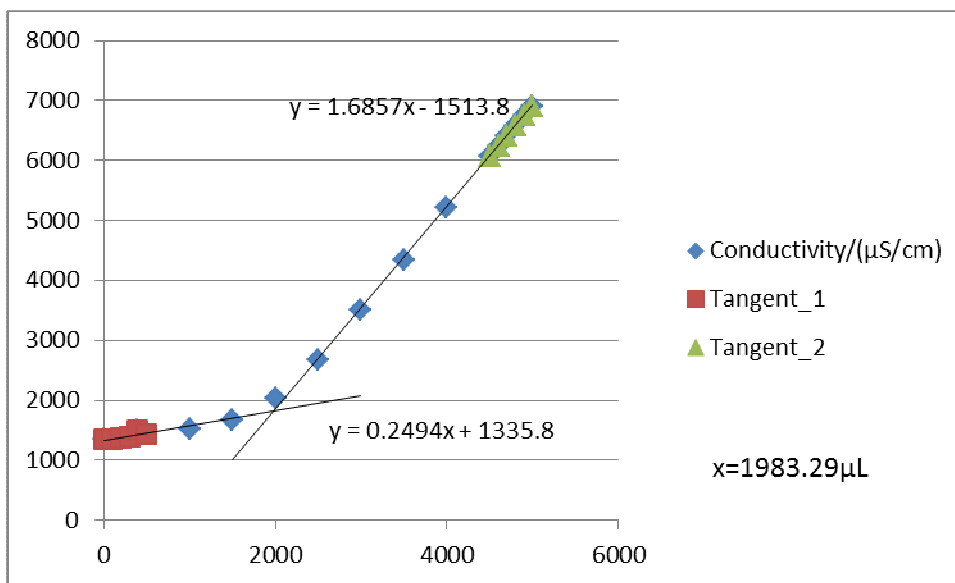
Figure F18-3: Titration 3 for 0.2609 mol/L MEA Third Run

F19: Titration Curves for 0.01986 mol/L MEA First Run at 308 K
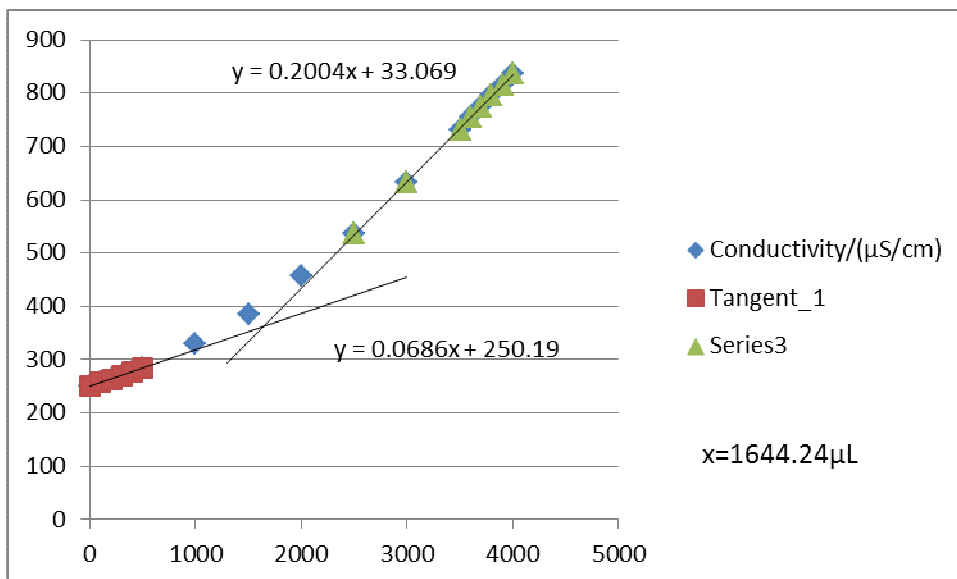
Figure F19-1: Titration 1 for 0.01986 mol/L MEA First Run
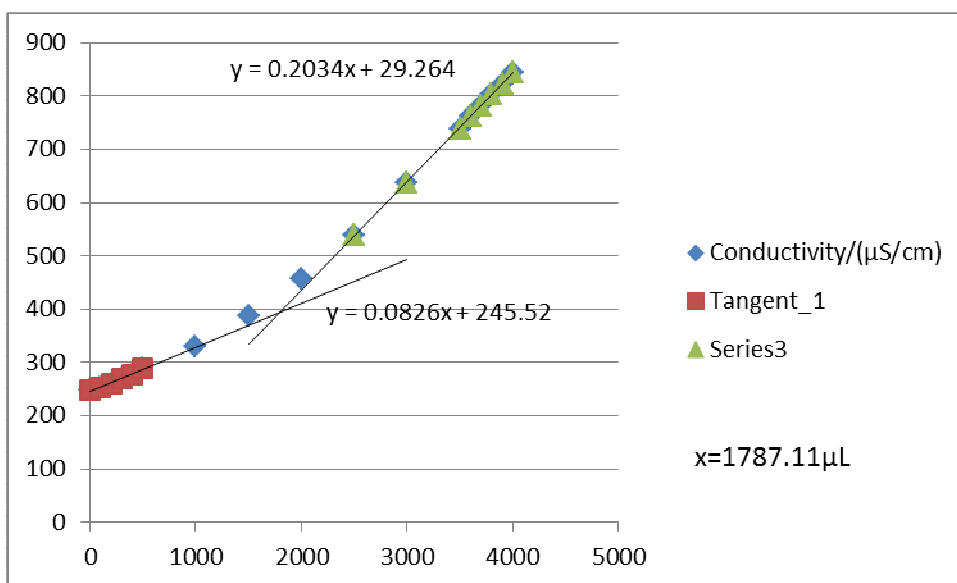
Figure F19-2: Titration 2 for 0.01986 mol/L MEA First Run
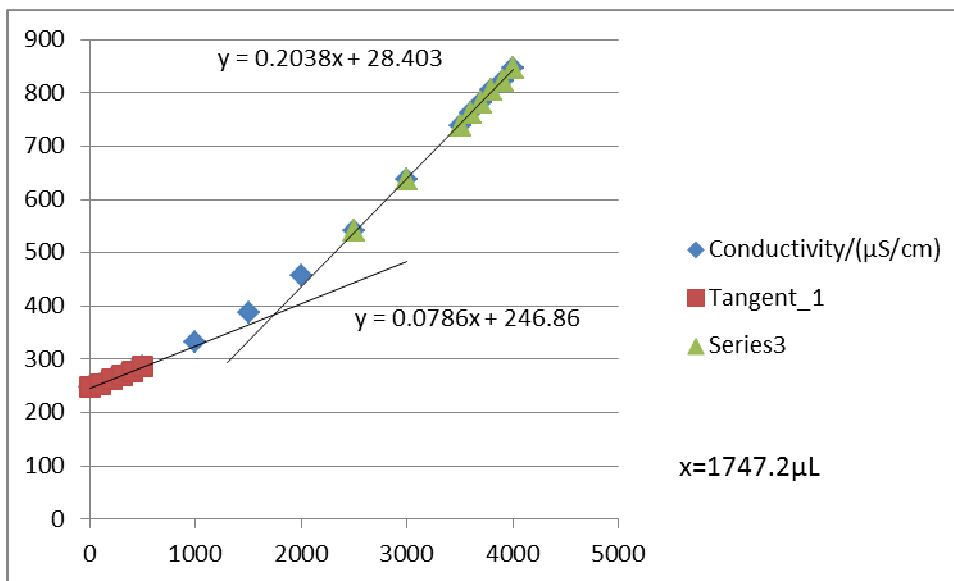
Figure F19-3: Titration 3 for 0.01986 mol/L MEA First Run

F20: Titration Curves for 0.01986 mol/L MEA Second Run at 35°C
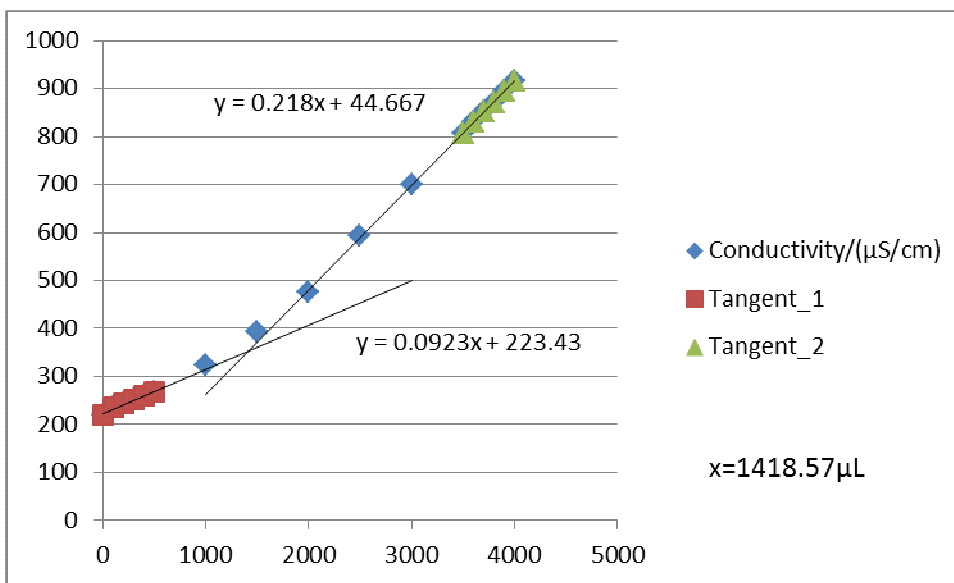
Figure F20-1: Titration 1 for 0.01986 mol/L MEA Second Run

181
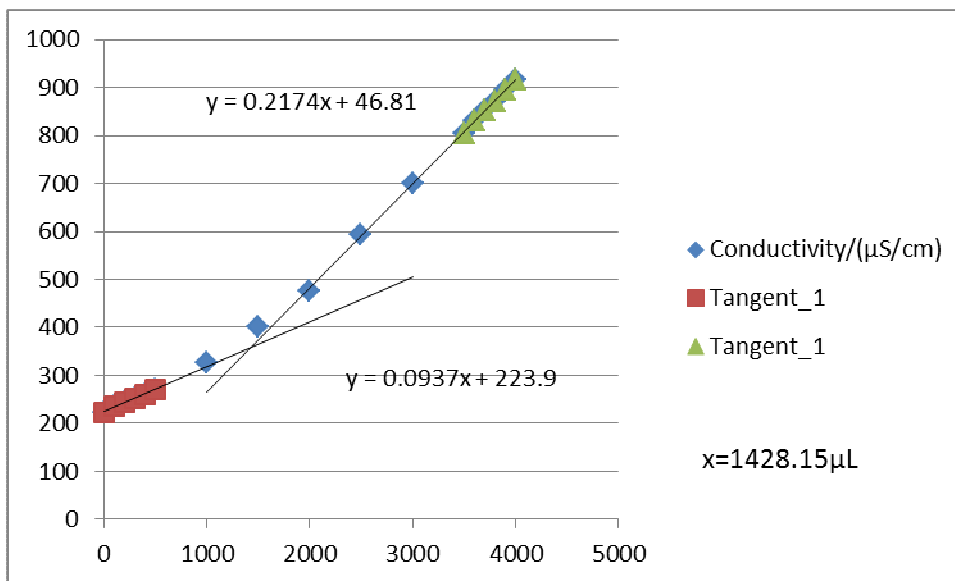
Figure F20-2: Titration 2 for 0.01986 mol/L MEA Second Run
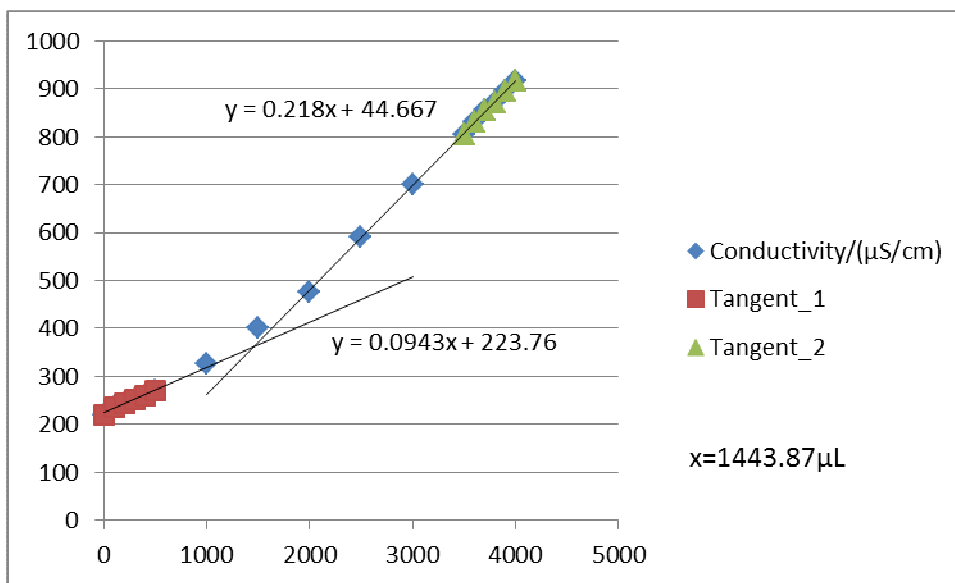
Figure F20-3: Titration 3 for 0.01986 mol/L MEA Second Run

182

F21: Titration Curves for 0.01986 mol/L MEA Third Run at 308 K
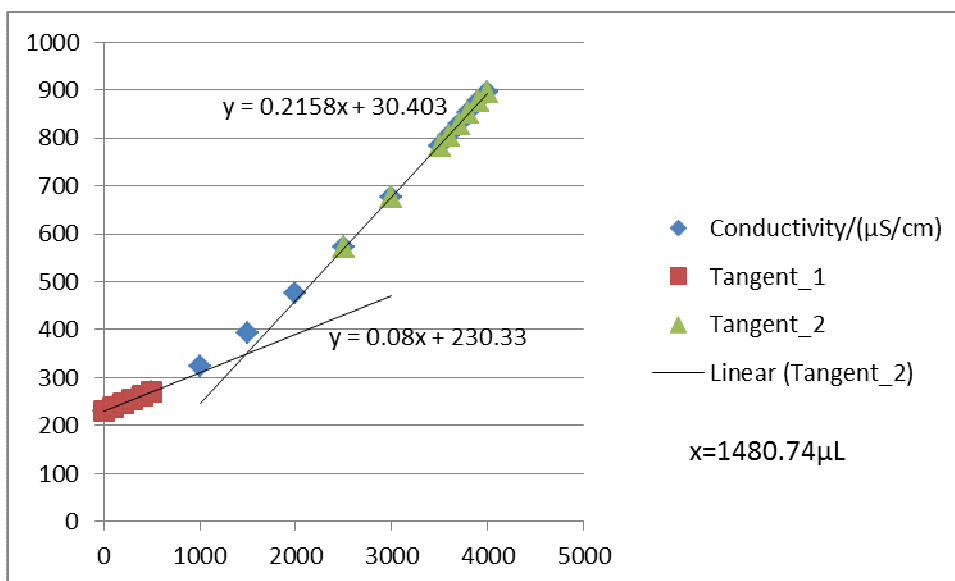
Figure F21-1: Titration 1 for 0.01986 mol/L MEA Third Run
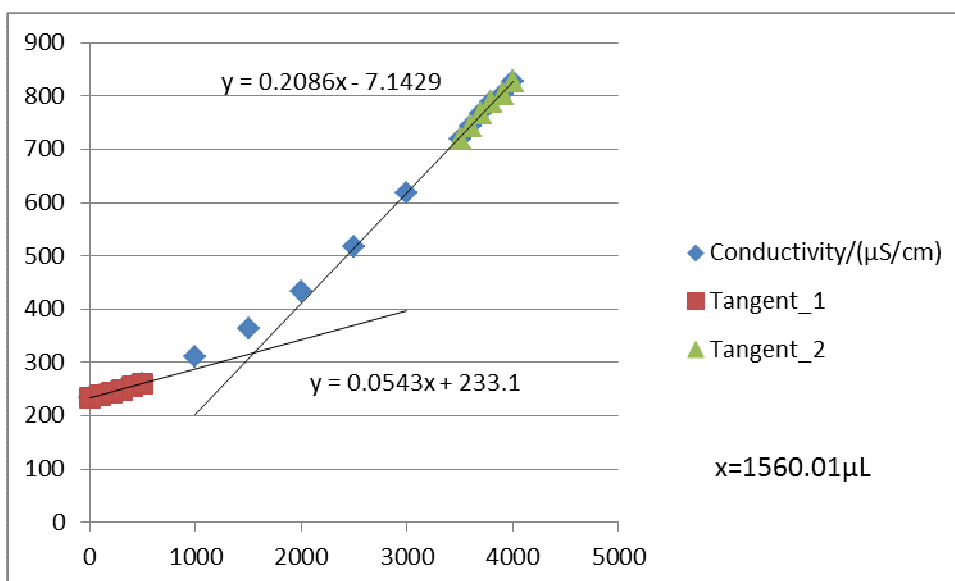
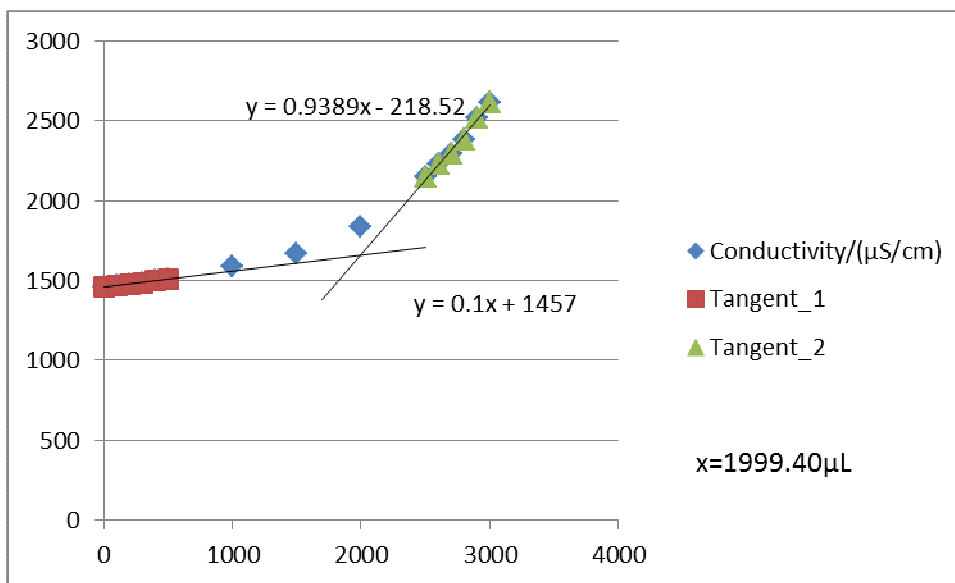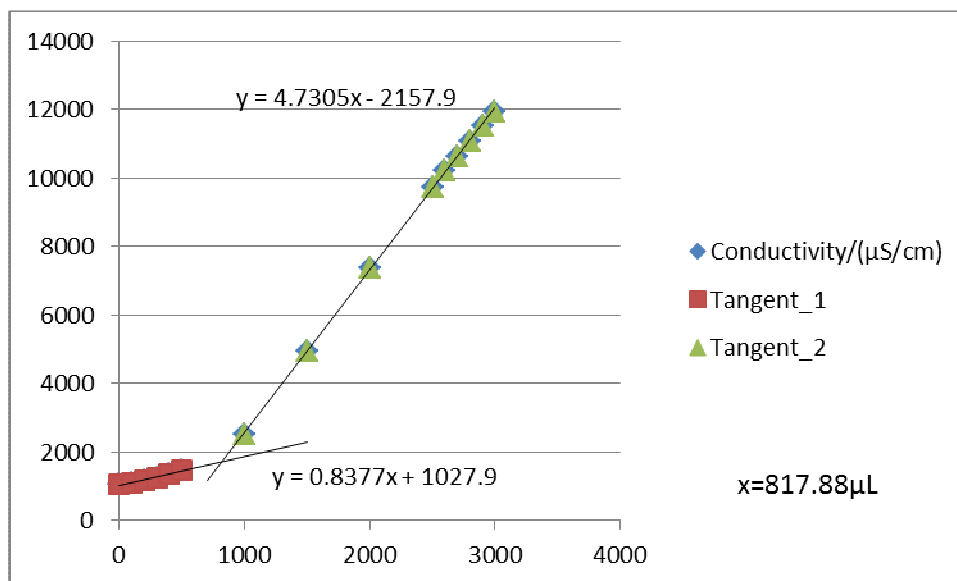

Figure F21-2: Titration 2 for 0.01986 mol/L MEA Third Run

183
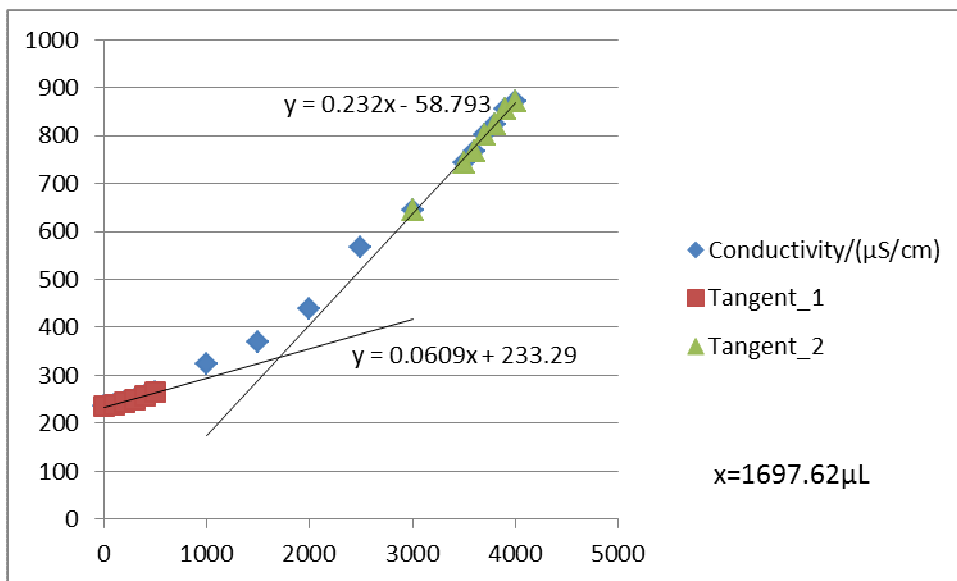
Figure F21-3: Titration 3 for 0.01986 mol/L MEA Third Run

F22: Titration Curves for 0.04956 mol/L MEA First Run at 308 K
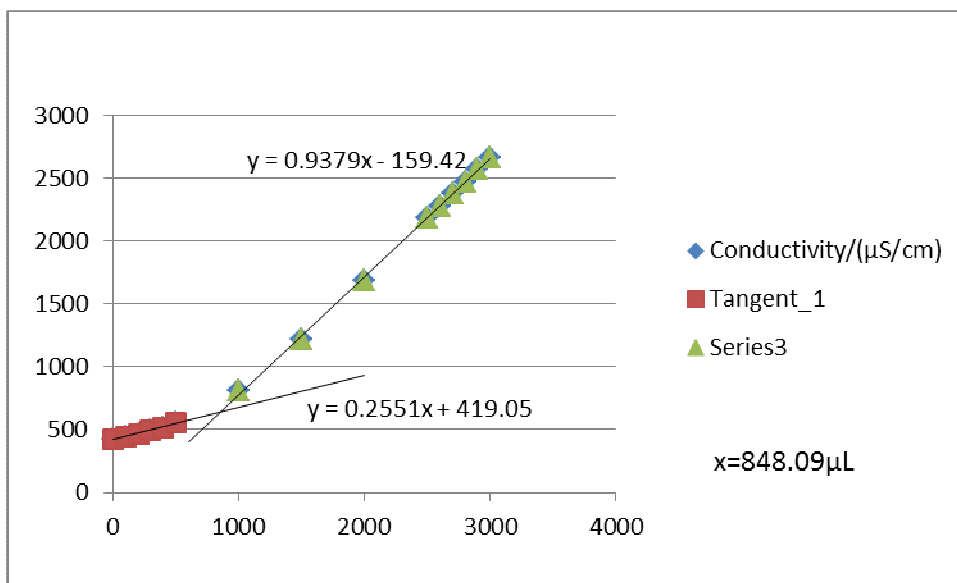
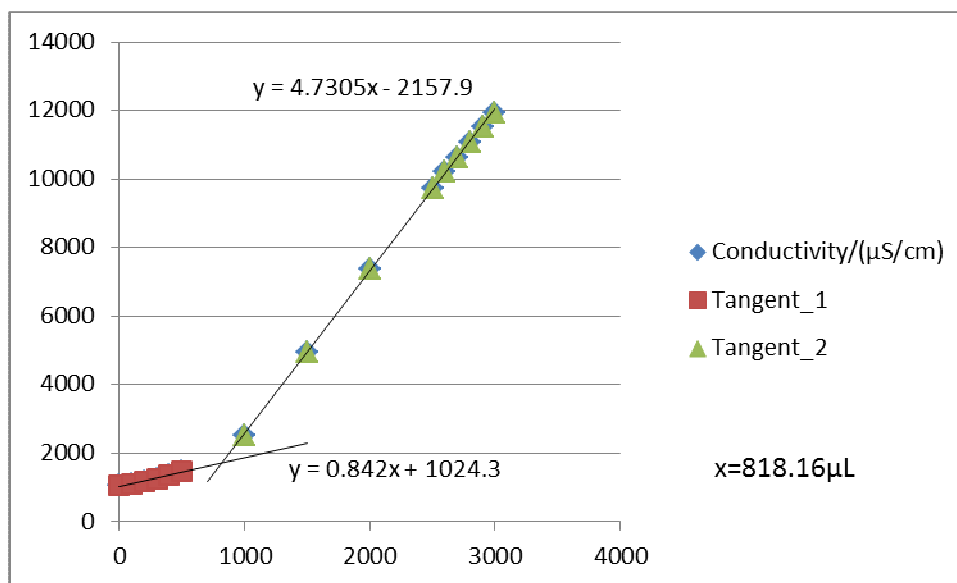Figure F22-1: Titration 1 for 0.04956 mol/L MEA First Run

184
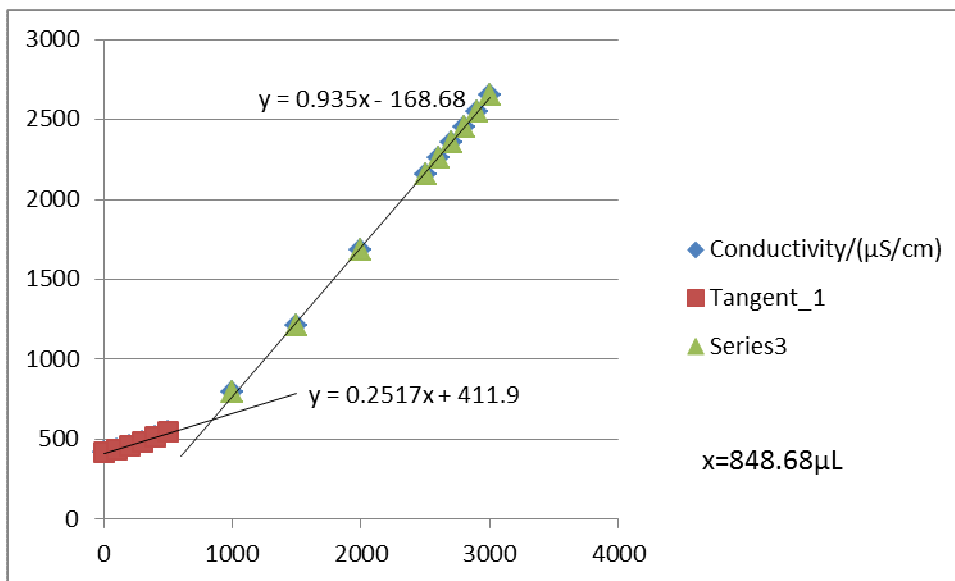
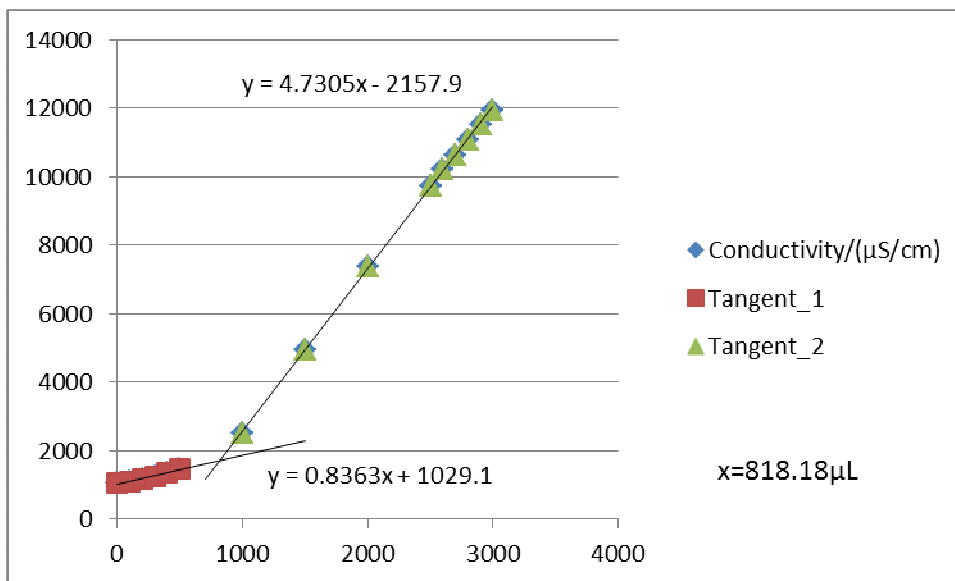Figure F22-2: Titration 2 for 0.04956 mol/L MEA First Run
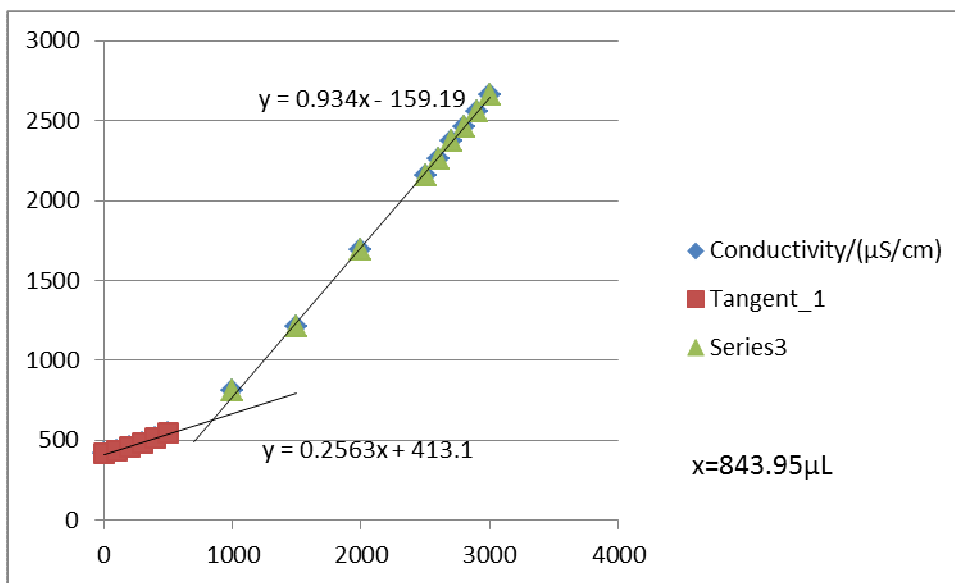
Figure F22-3: Titration 3 for 0.04956 mol/L MEA First Run

185

F23: Titration Curves for 0.04956 mol/L MEA Second Run at 308 K
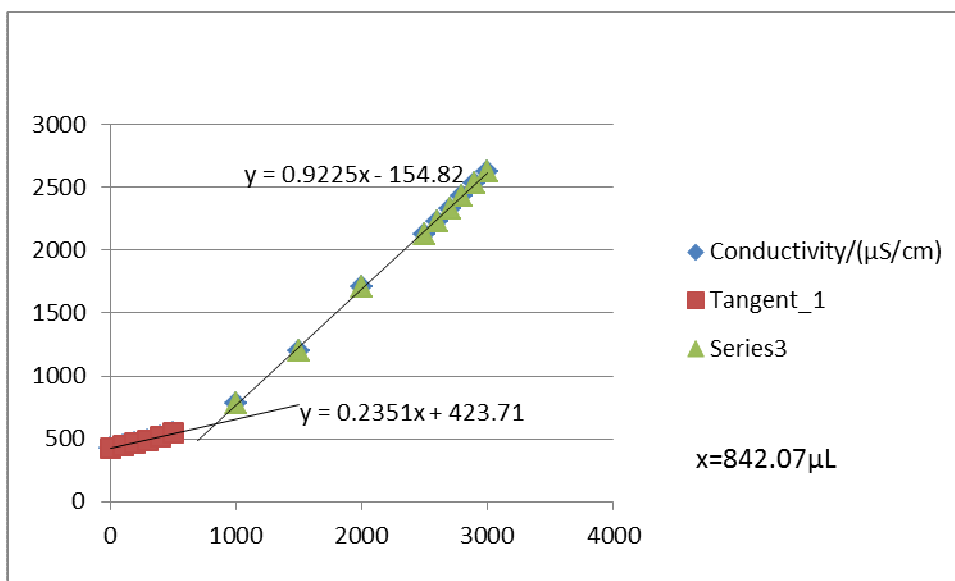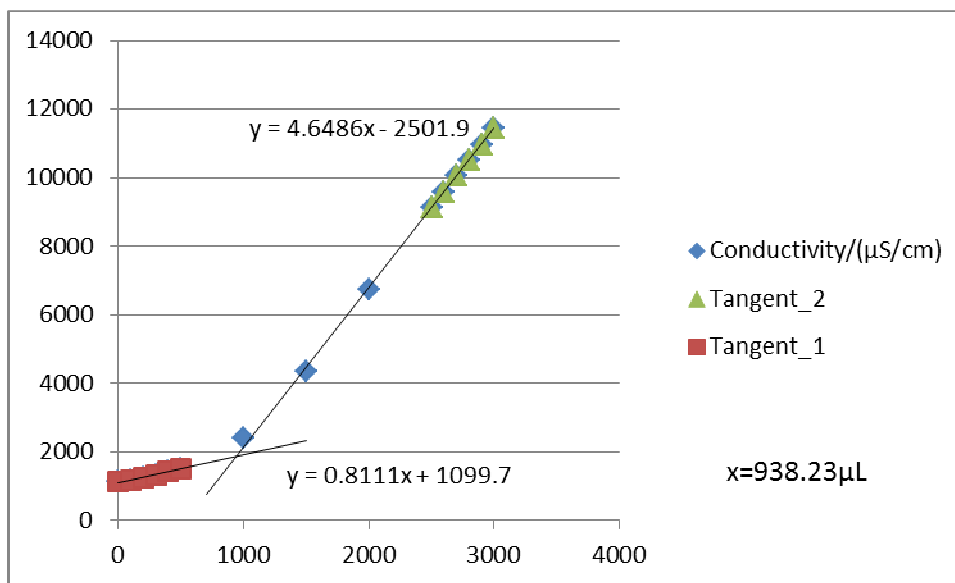

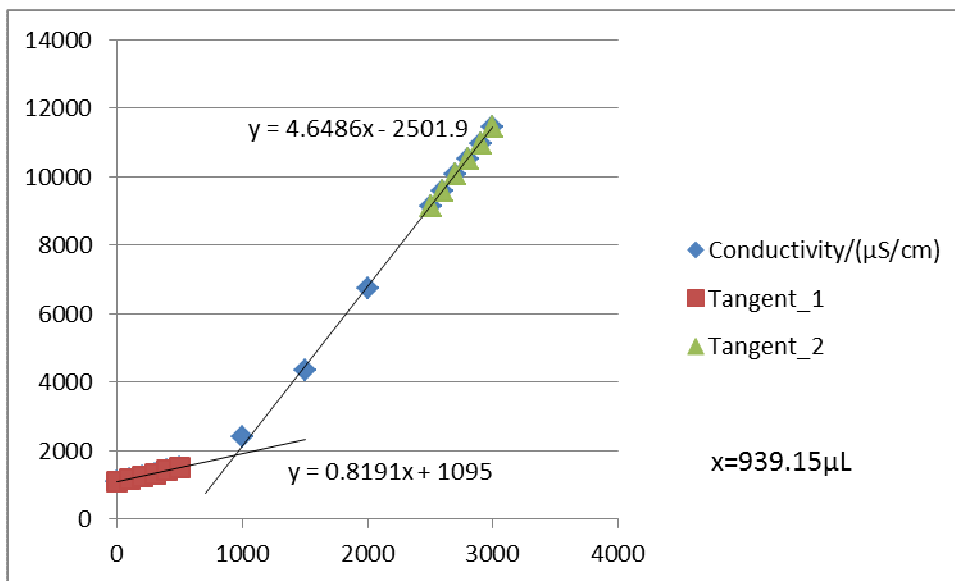Figure F23-1: Titration 1 for 0.04956 mol/L MEA Second Run
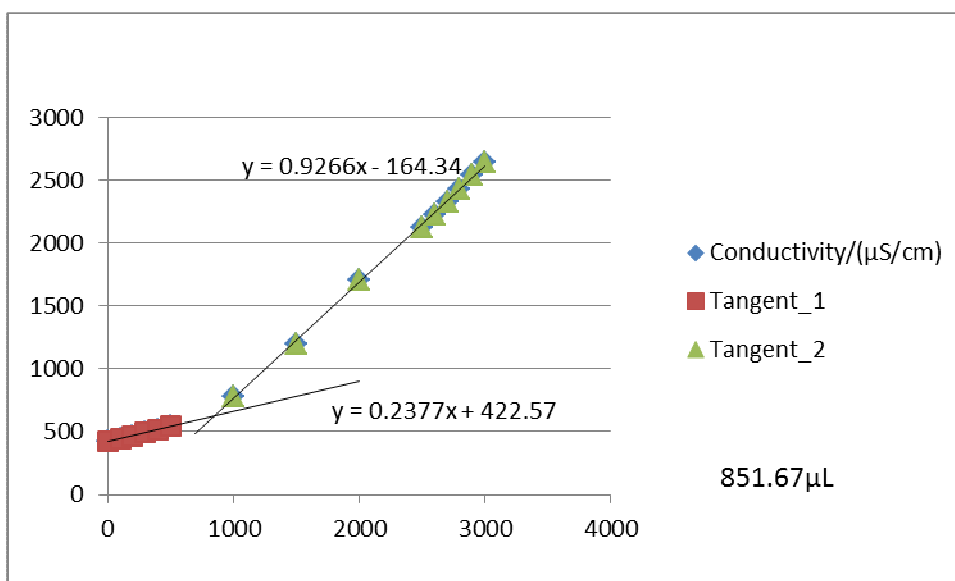
Figure F23-2: Titration 2 for 0.04956 mol/L MEA Second Run
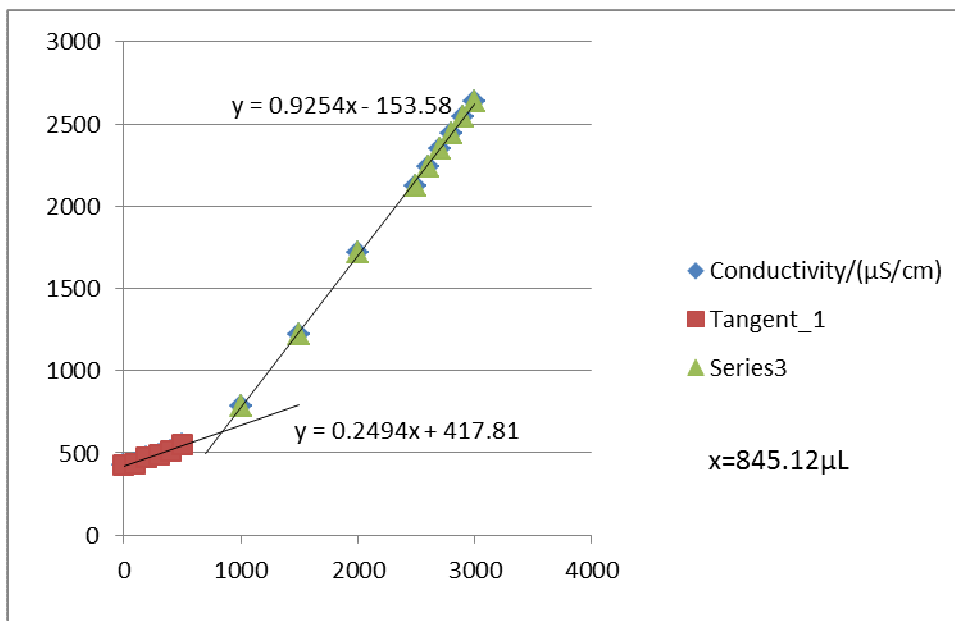
Figure F23-3: Titration 3 for 0.04956 mol/L MEA Second Run

F24: Titration Curves for 0.04956 mol/L MEA Third Run at 308 K
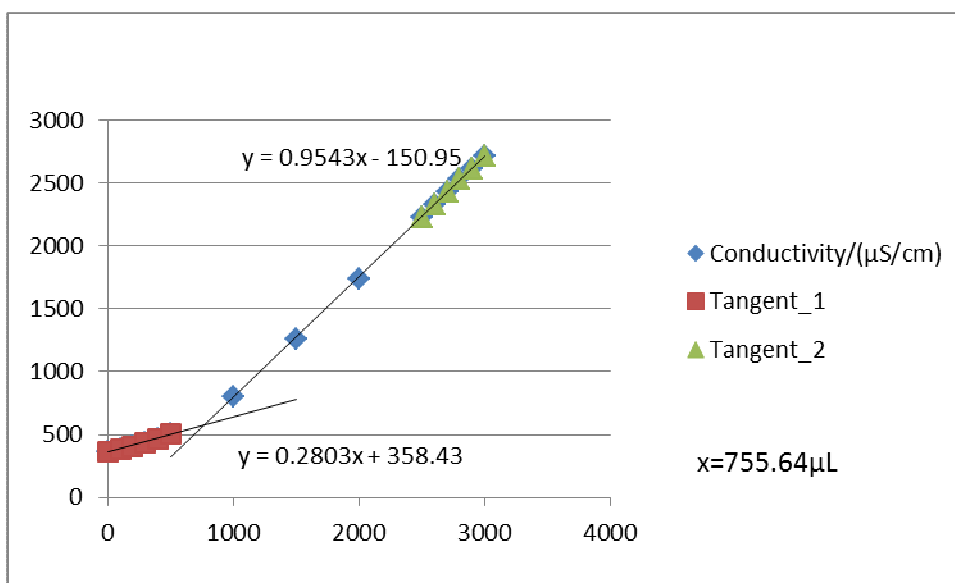
Figure F24-1: Titration 1 for 0.04956 mol/L MEA Third Run

187
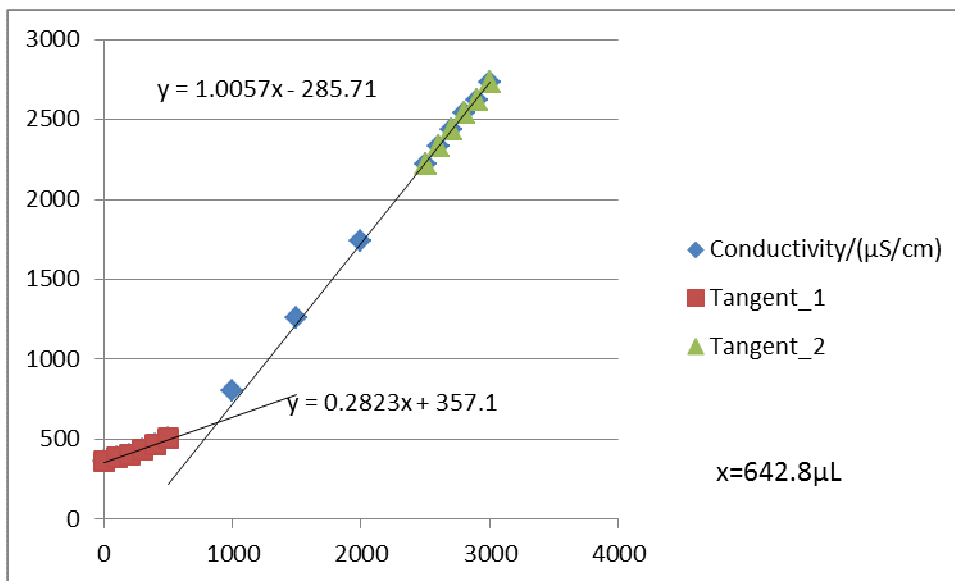
Figure F24-2: Titration 2 for 0.04956 mol/L MEA Third Run
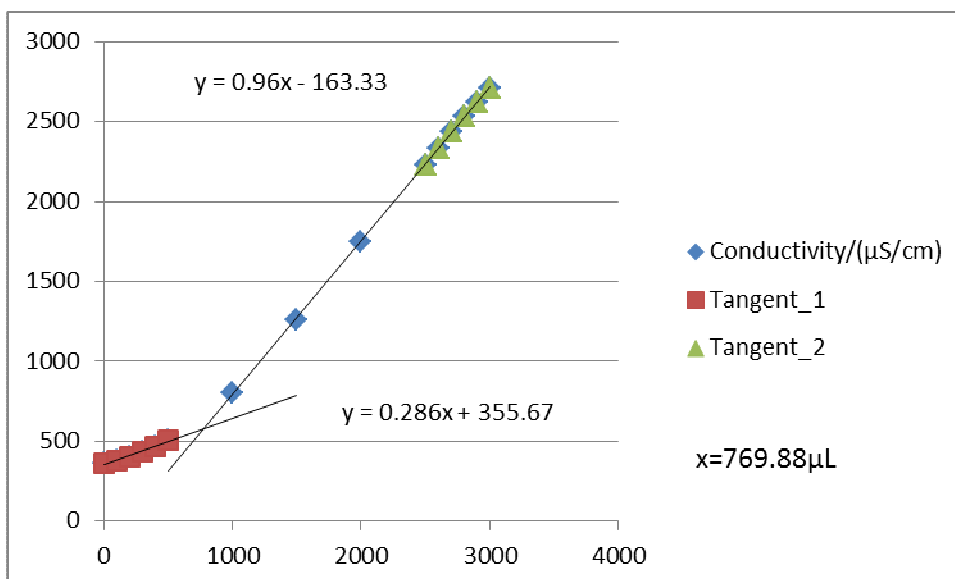
Figure F24-3: Titration 3 for 0.04956 mol/L MEA Third Run

F25: Titration Curves for 0.07915 mol/L MEA First Run at 308 K
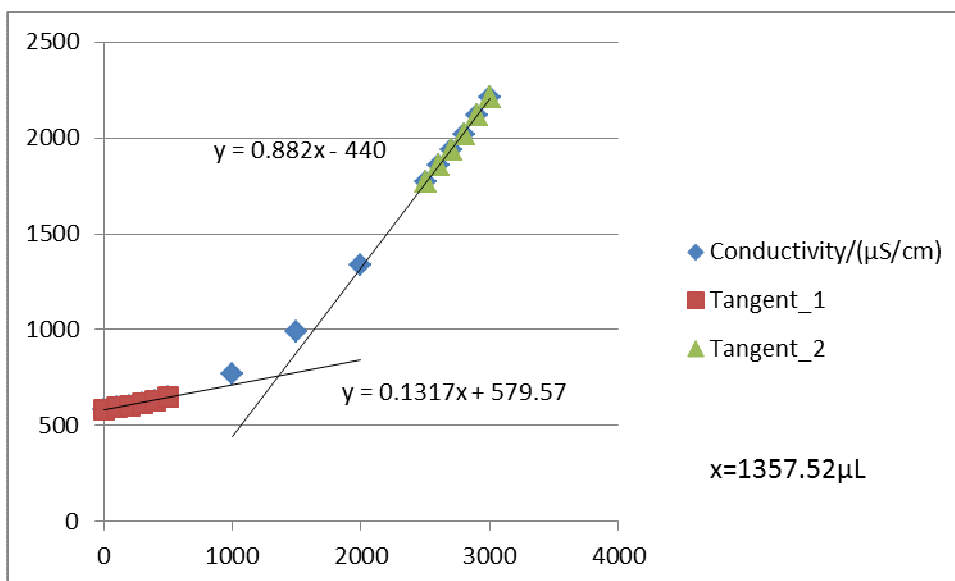
Figure F25-1: Titration 1 for 0.07915 mol/L MEA First Run
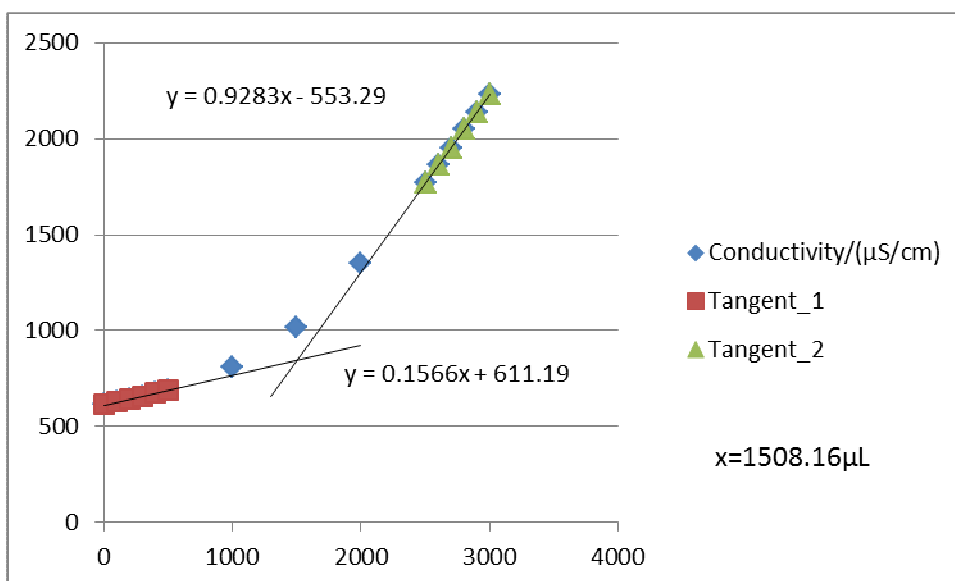
Figure F25-2: Titration 2 for 0.07915 mol/L MEA First Run

189
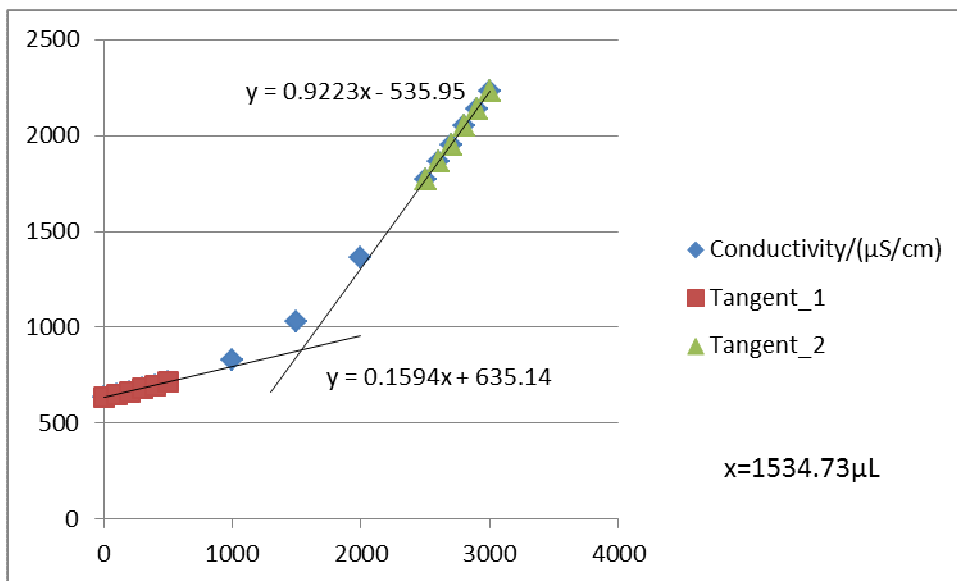
Figure F25-3: Titration 3 for 0.07915 mol/L MEA First Run

F26: Titration Curves for 0.07915 mol/L MEA Second Run at 308 K
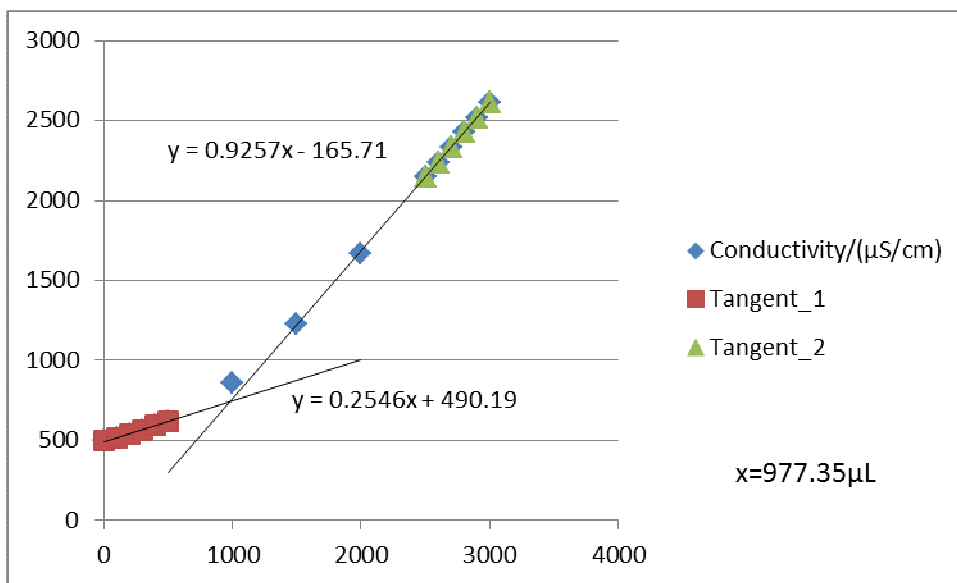
Figure F26-1: Titration 1 for 0.07915 mol/L MEA Second Run

190
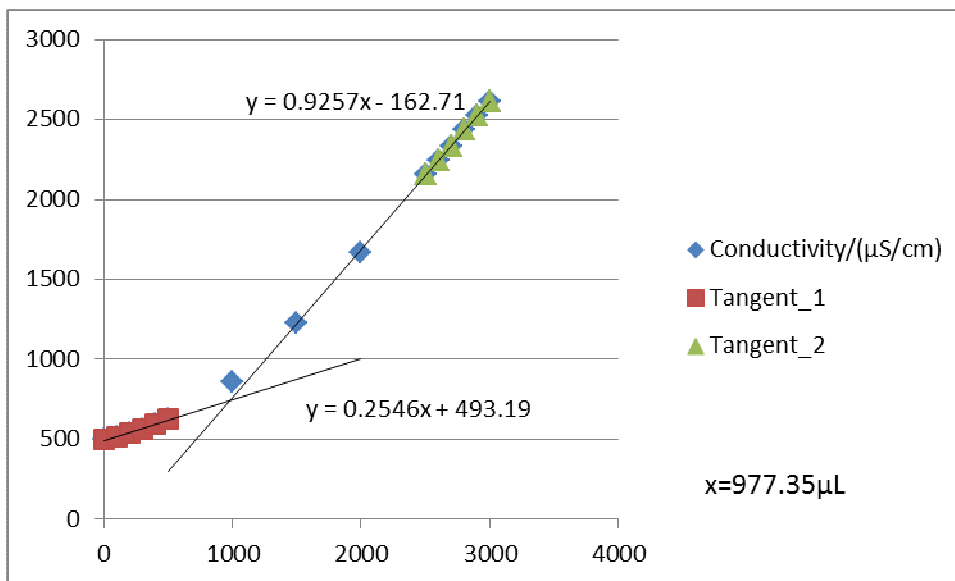
Figure F26-2: Titration 2 for 0.07915 mol/L Second Run
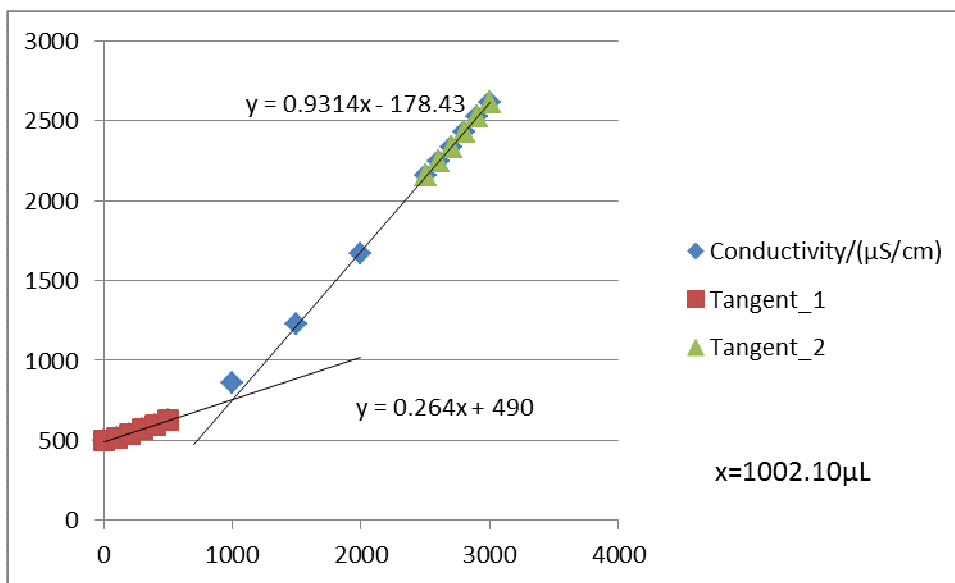
Figure F26-3: Titration 3 for 0.07915 mol/L MEA Second Run

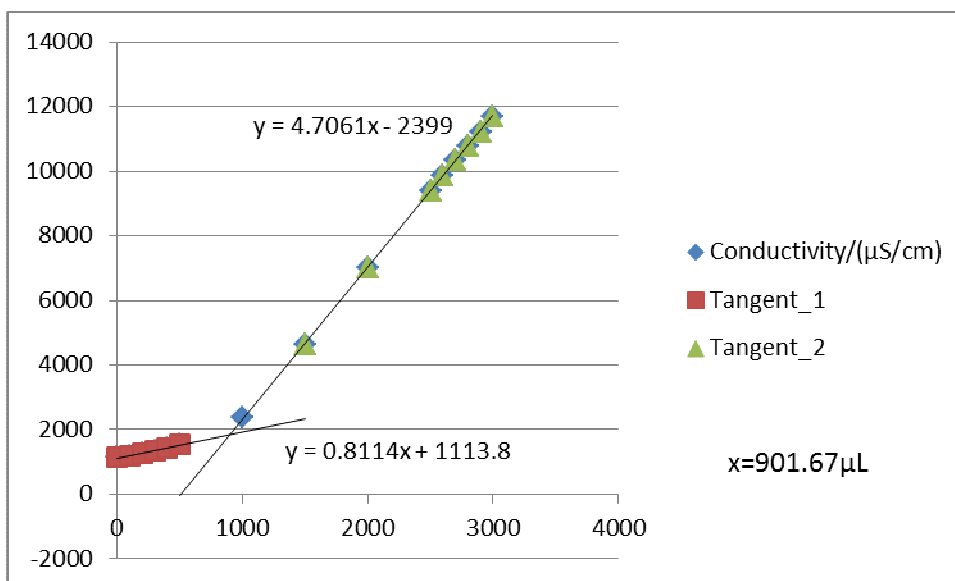**F27: Titration Curves for 0.07915 mol/L MEA Third Run at 308 K**
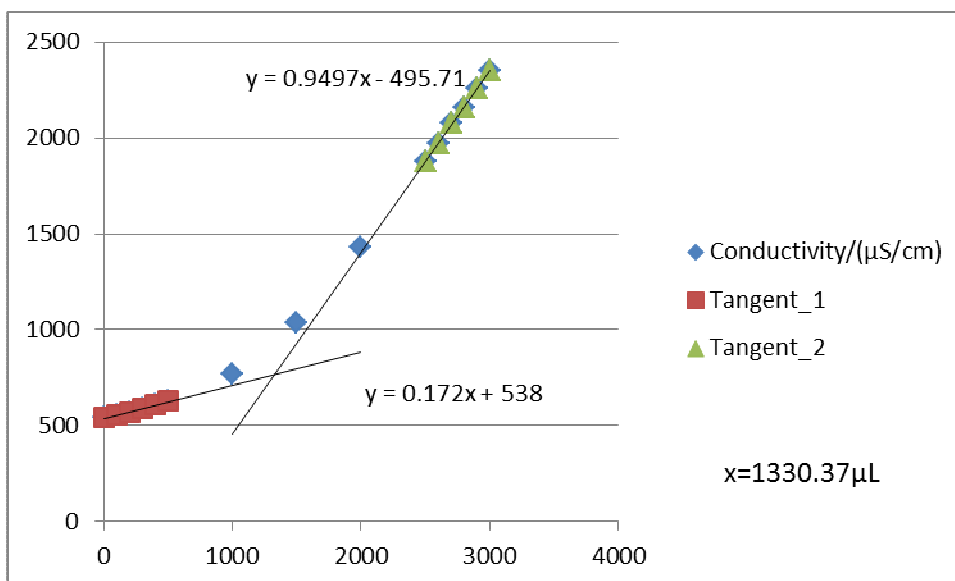
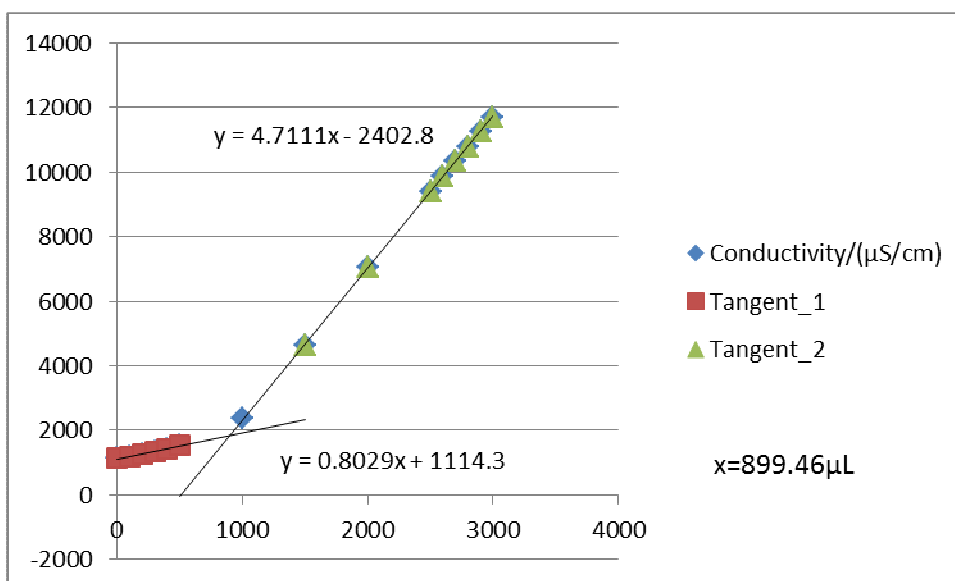

Figure F27-1: Titration 1 for 0.07915 mol/L MEA Third Run
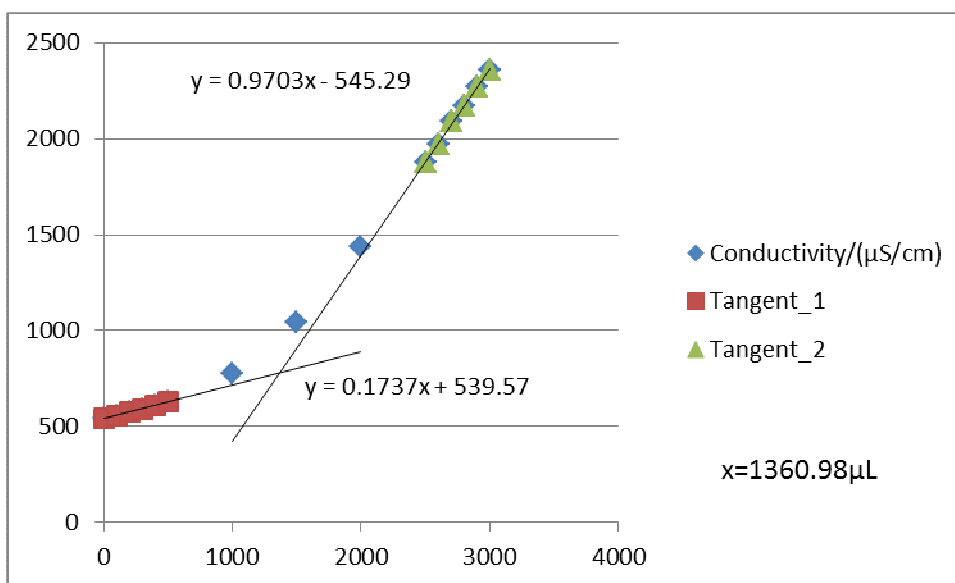
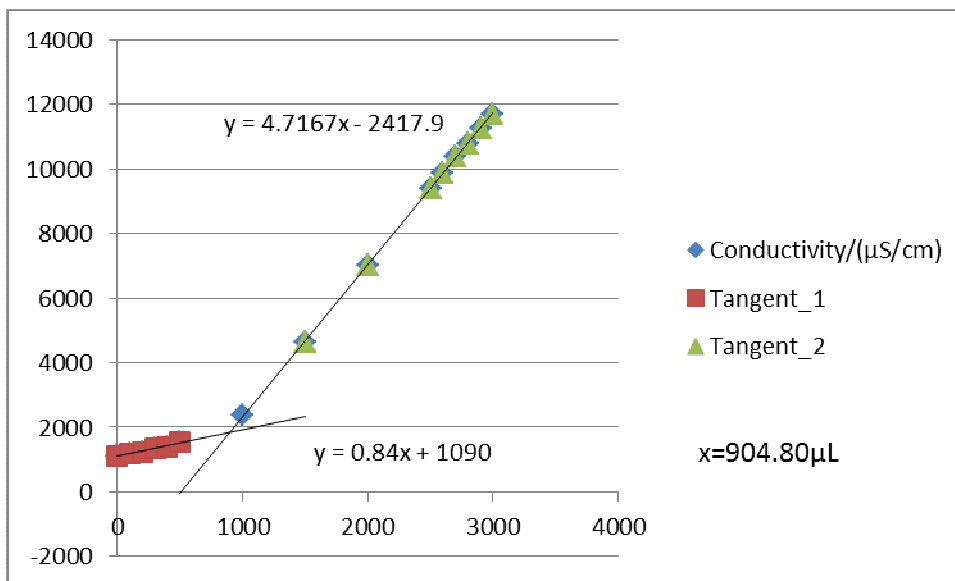

Figure F27-2: Titration 2 for 0.07915 mol/L MEA Third Run

192
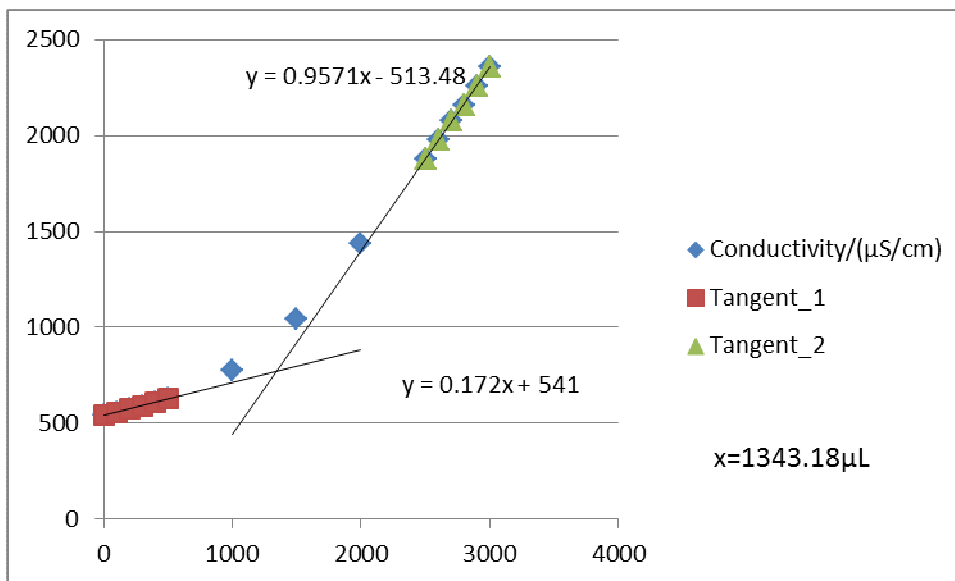
Figure F27-3: Titration 3 for 0.07915 mol/L MEA Third Run

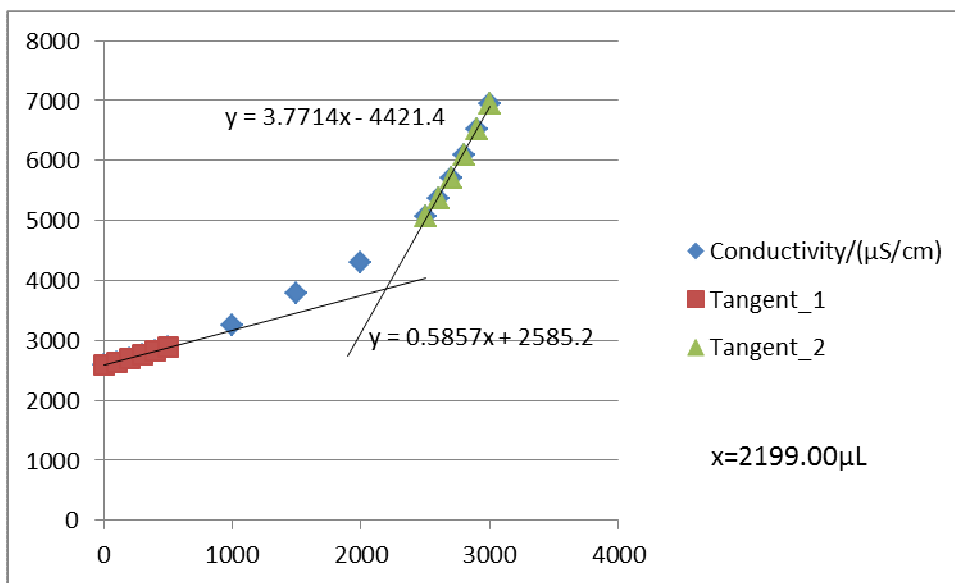**F28: Titration Curves for 0.1184 mol/L MEA First Run at 308 K**
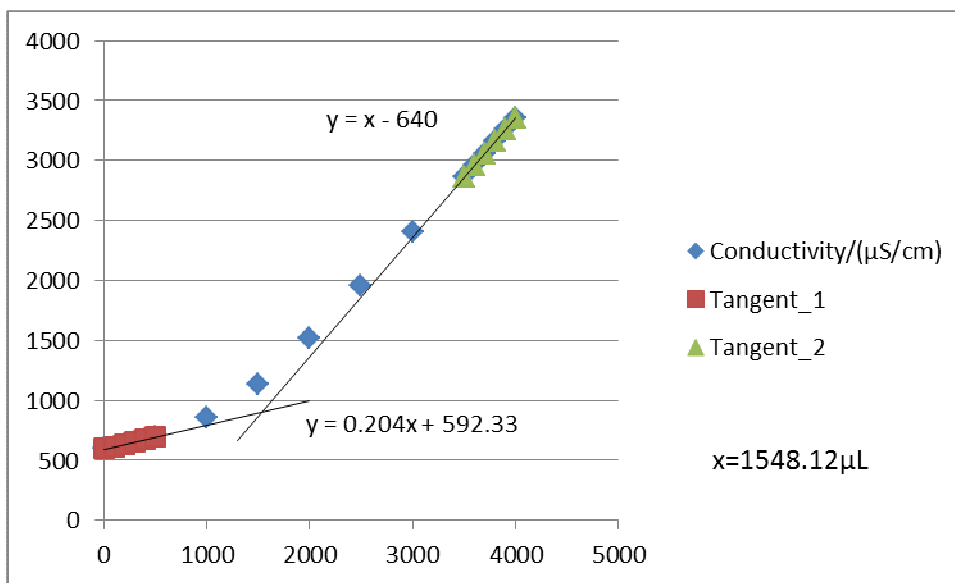
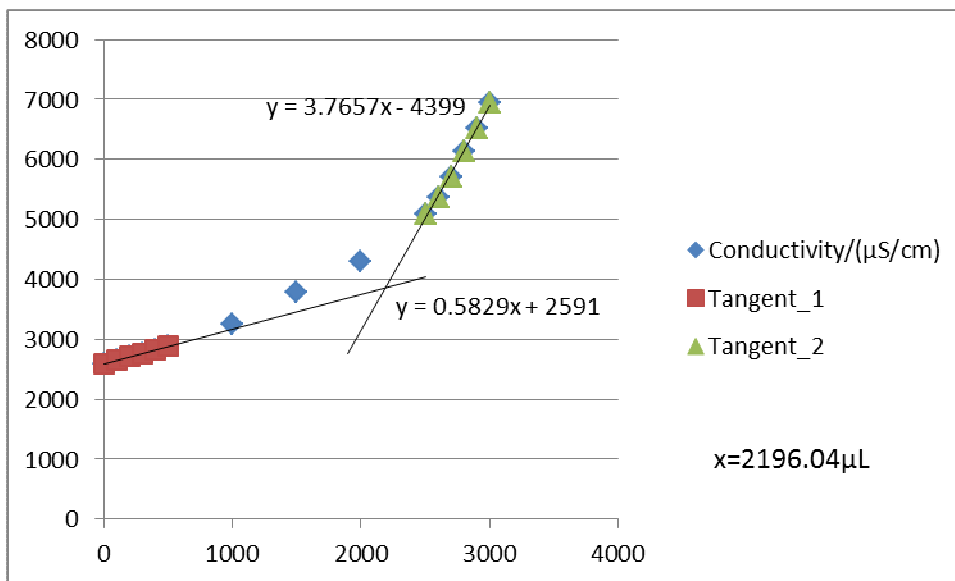Figure F28-1: Titration 1 for 0.1184 mol/L MEA First Run
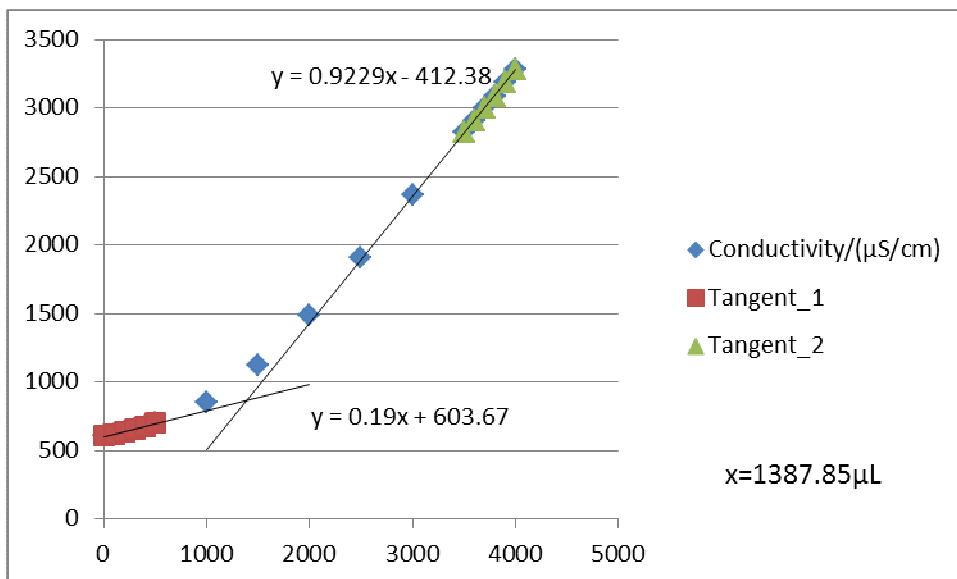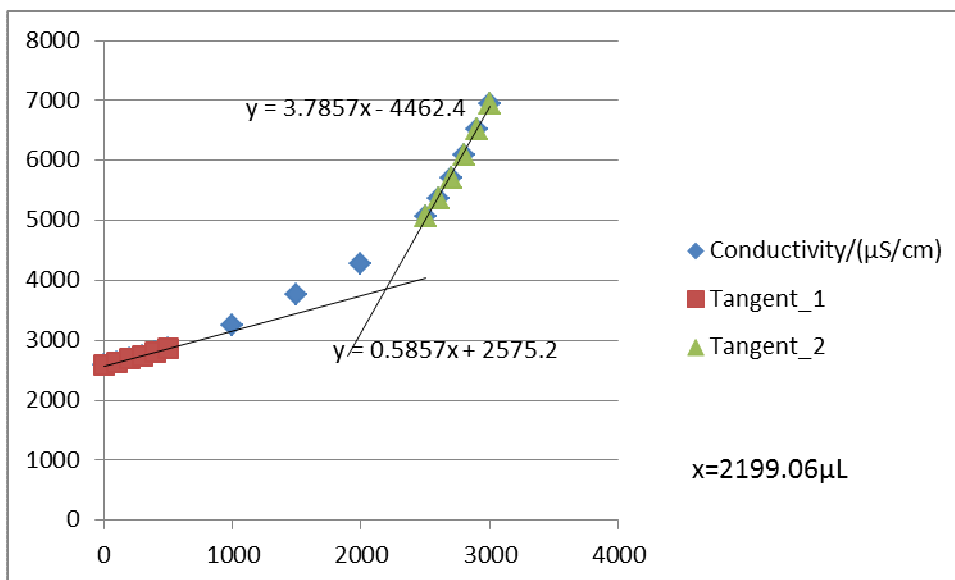
Figure F28-2: Titration 2 for 0.1184 mol/L MEA First Run
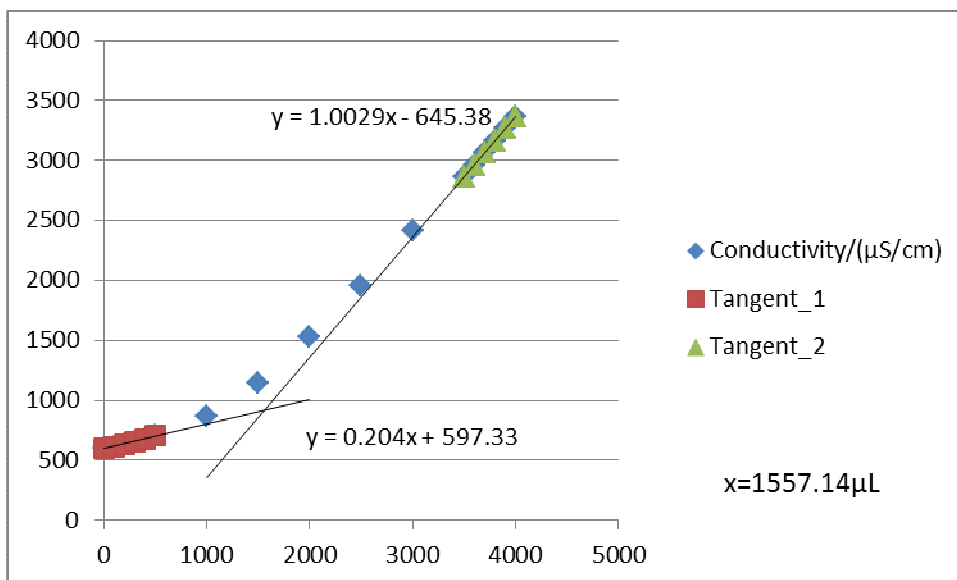
Figure F28-3: Titration 3 for 0.1184 mol/L MEA First Run

F29: Titration Curves for 0.1184 mol/L MEA Second Run at 308 K
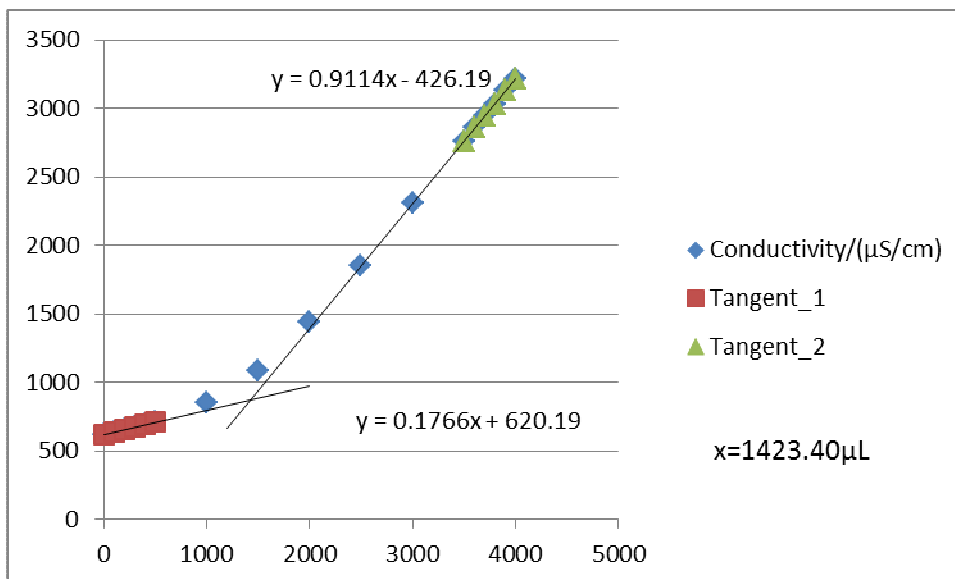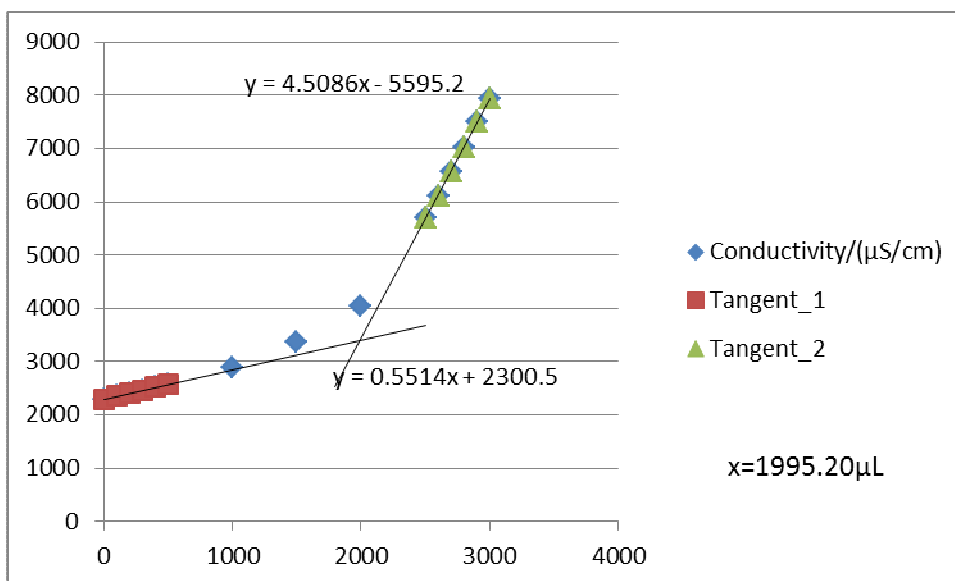

Figure F29-1: Titration 1 for 0.1184 mol/L MEA Second Run
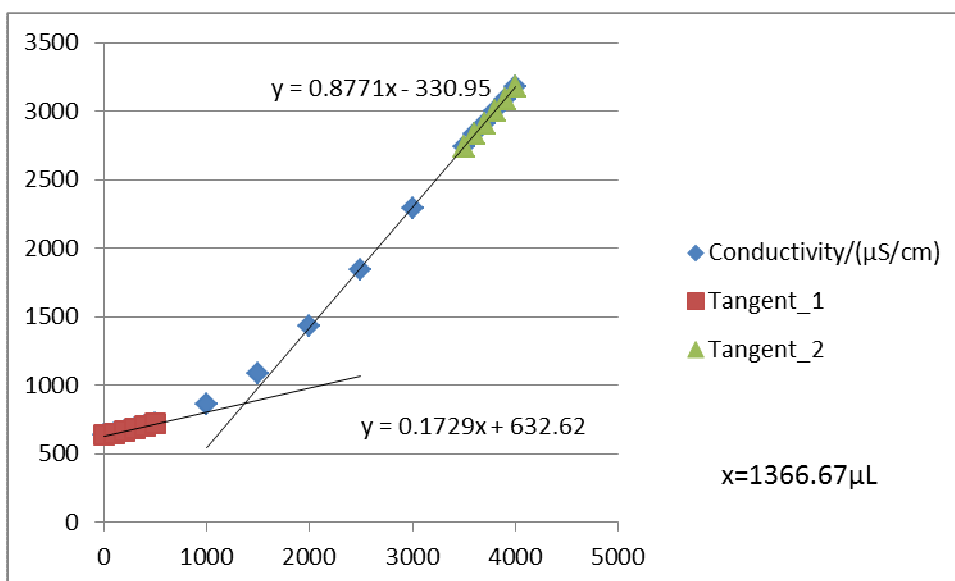
Figure F29-2: Titration 2 for 0.1184 mol/L MEA Second Run

195
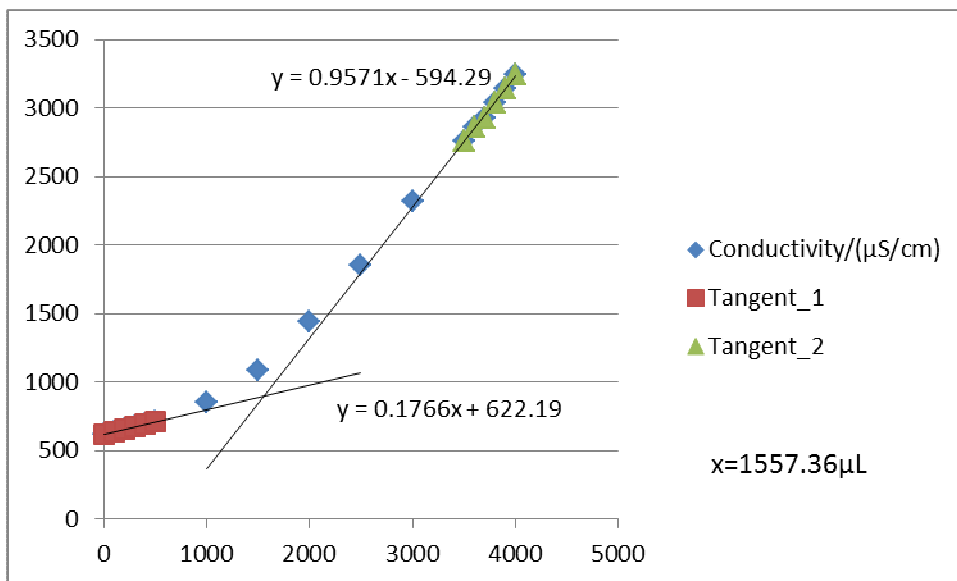
Figure F29-3: Titration 3 for 0.1184 mol/L MEA Second Run

F30: Titration Curves for 0.1184 mol/L MEA Third Run at 308 K
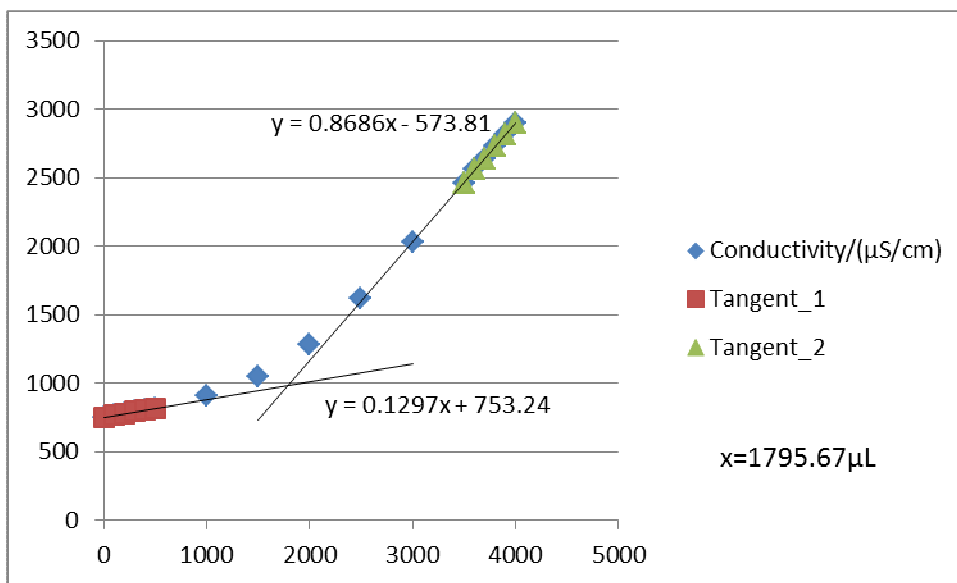
Figure F30-1: Titration 1 for 0.1184 mol/L MEA Third Run

196
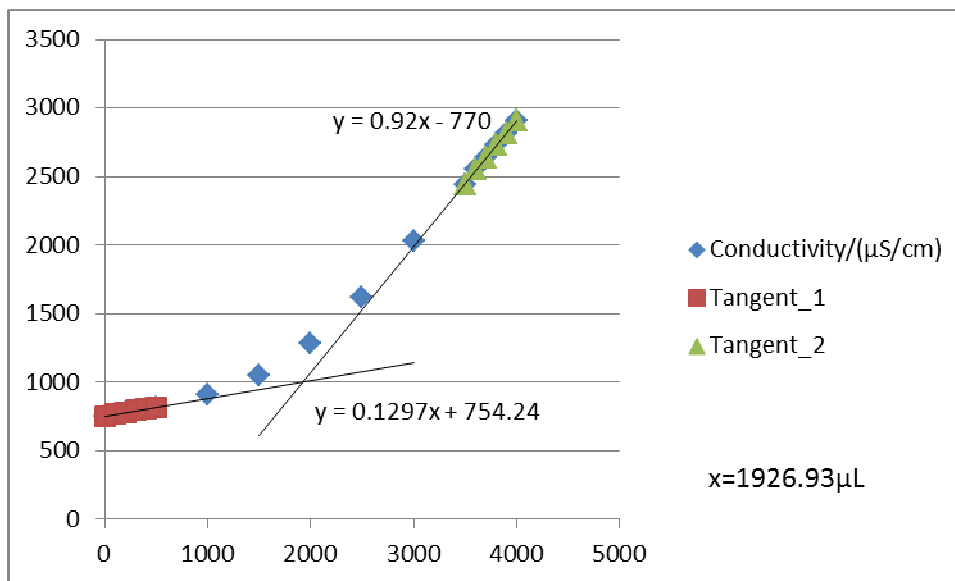
Figure F30-2: Titration 2 for 0.1184 mol/L MEA Third Run
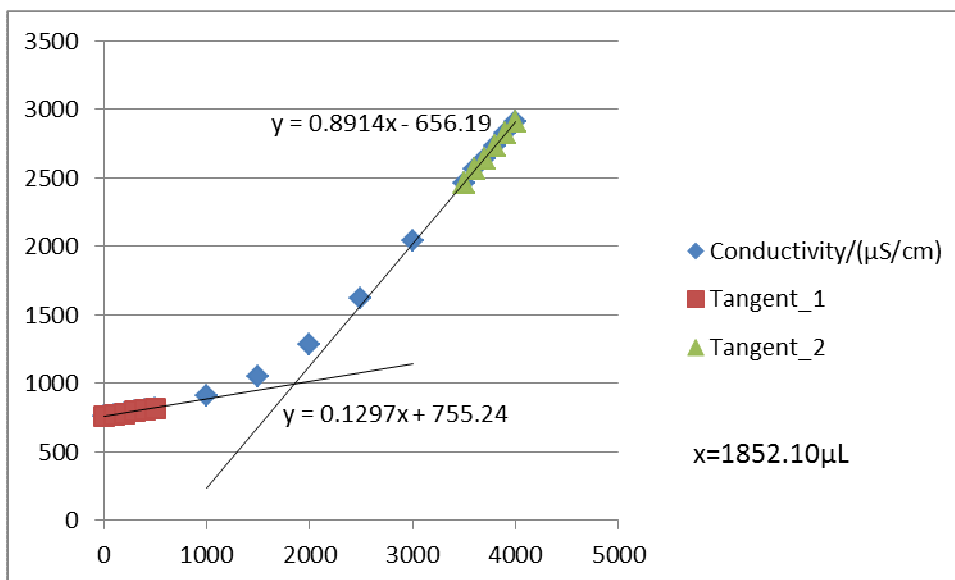
Figure F30-3: Titration 3 for 0.1184 mol/L MEA Third Run

F31: Titration Curves for 0.1575 mol/L MEA First Run at 308 K
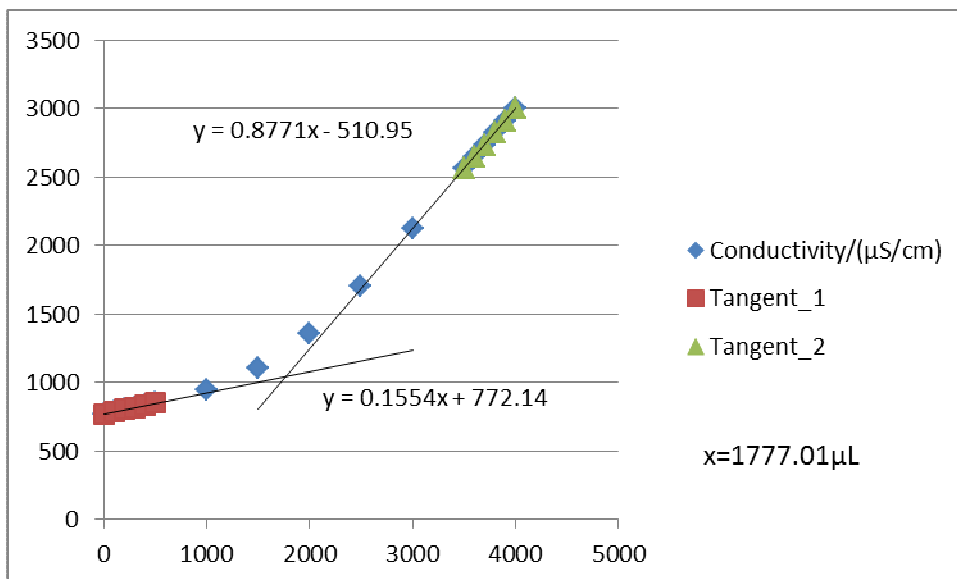
Figure F31-1: Titration 1 for 0.1575 mol/L MEA First Run
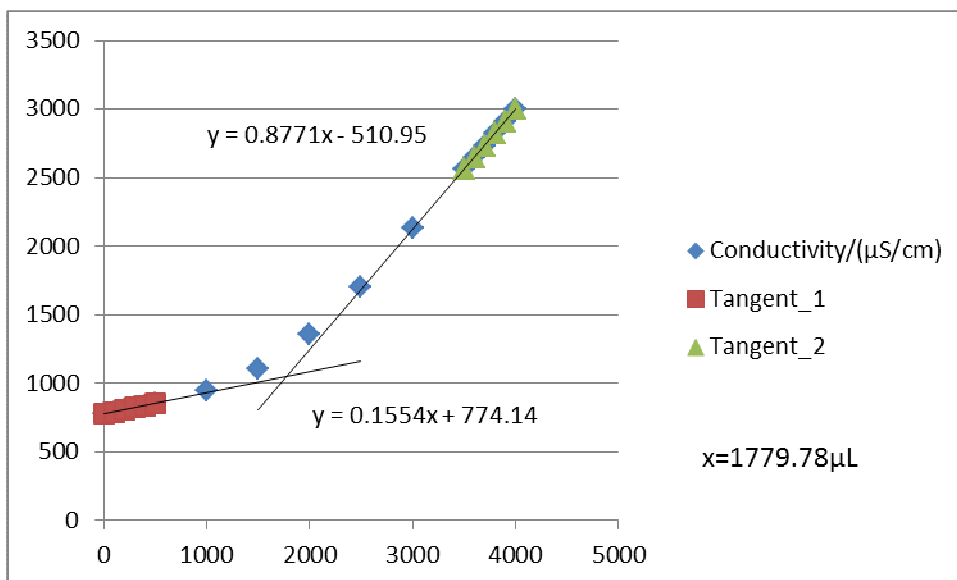
Figure F31-2: Titration 2 for 0.1575 mol/L MEA First Run

198
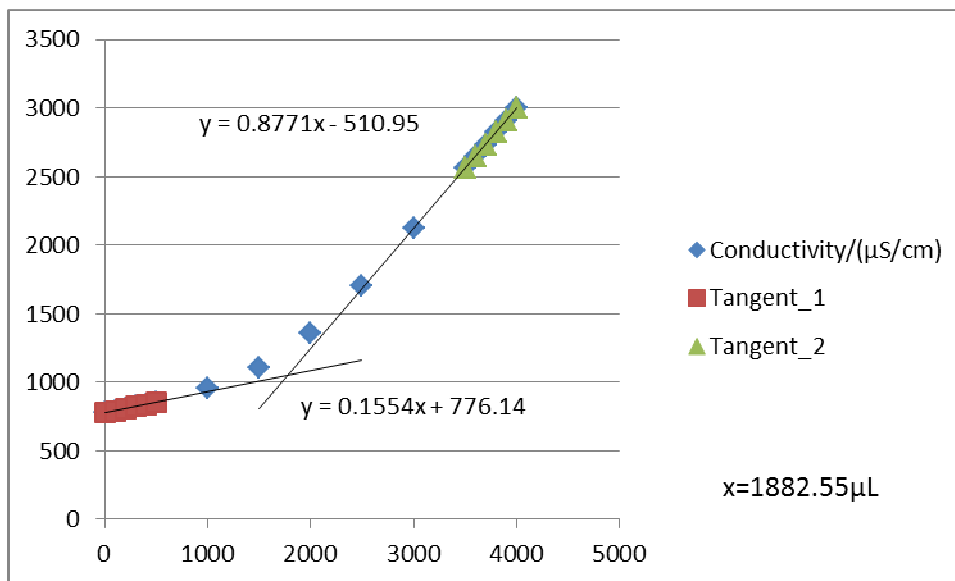
Figure F31-3: Titration 3 for 0.1575 mol/L MEA First Run

F32: Titration Curves for 0.1575 mol/L MEA Second Run at 308 K
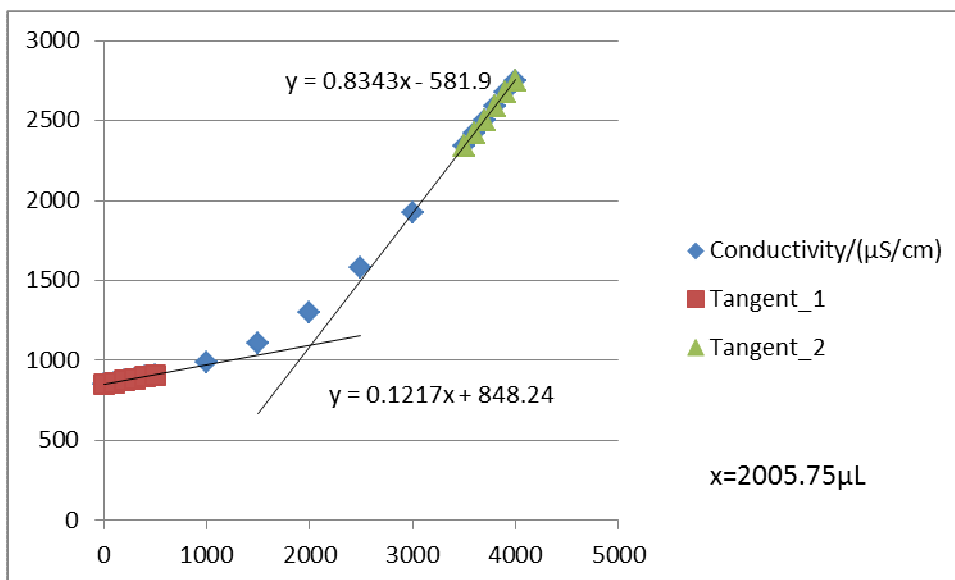
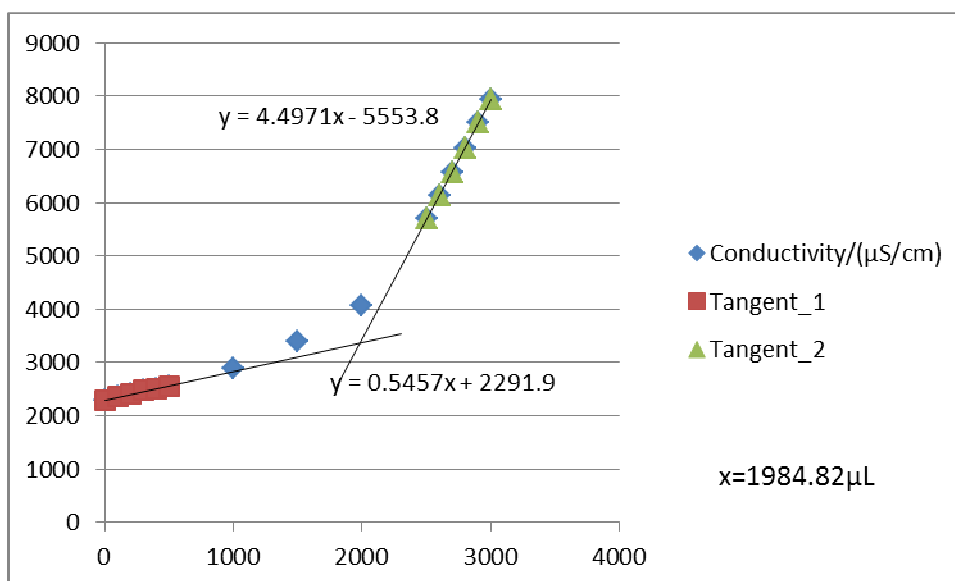Figure F32-1: Titration 1 for 0.1575 mol/L MEA Second Run

199
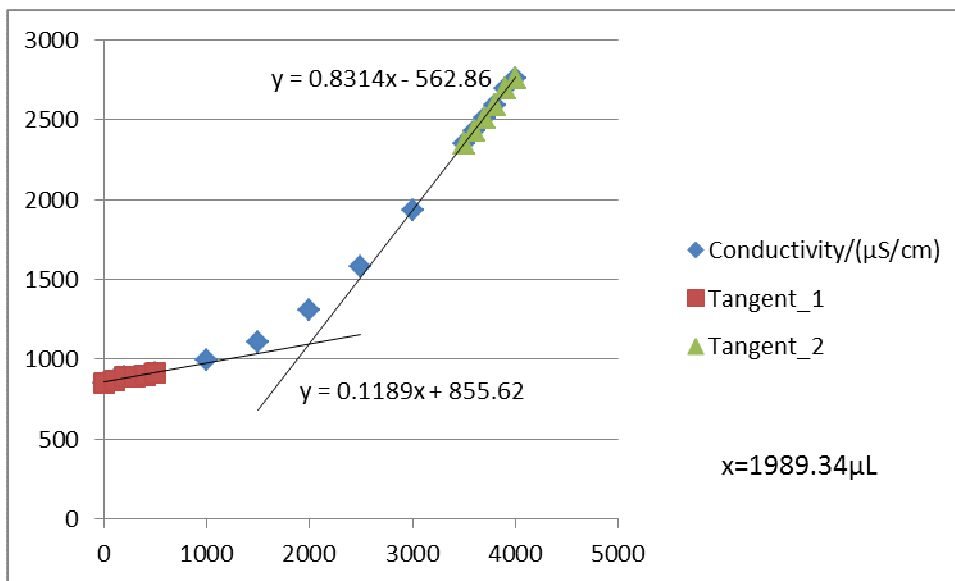
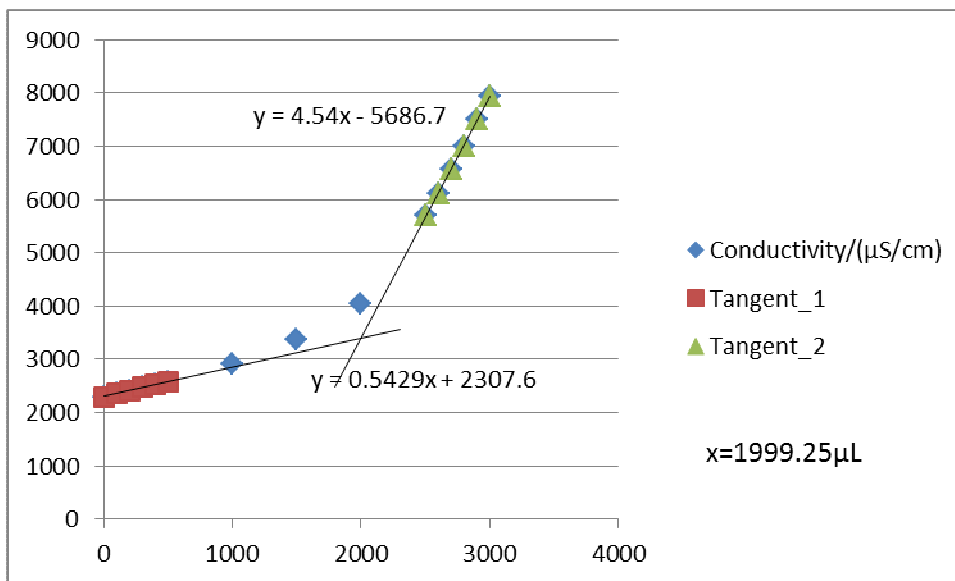Figure F32-2: Titration 2 for 0.1575 mol/L MEA Second Run
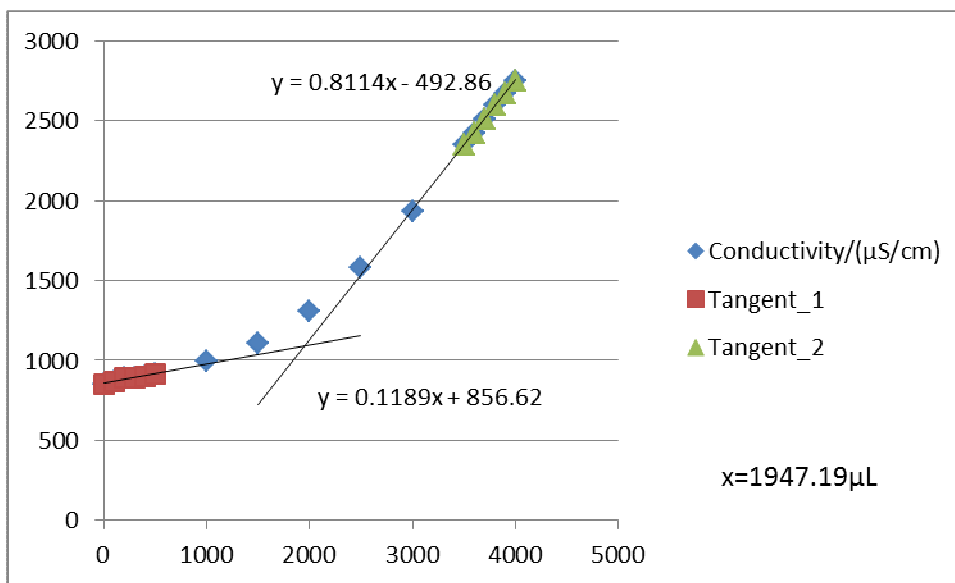
Figure F32-3: Titration 3 for 0.1575 mol/L MEA Second Run

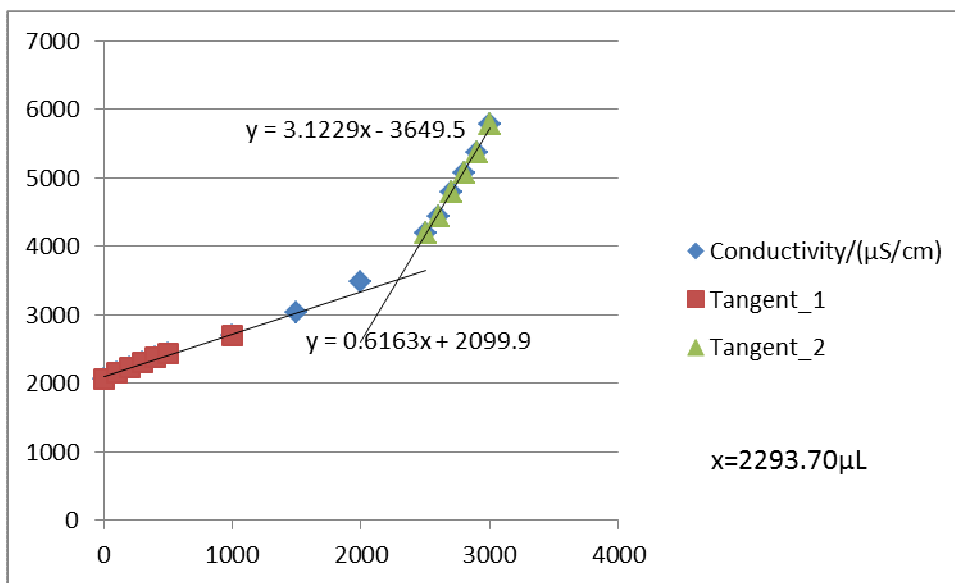**F33: Titration Curves for 0.1575 mol/L MEA Third Run at 308 K**
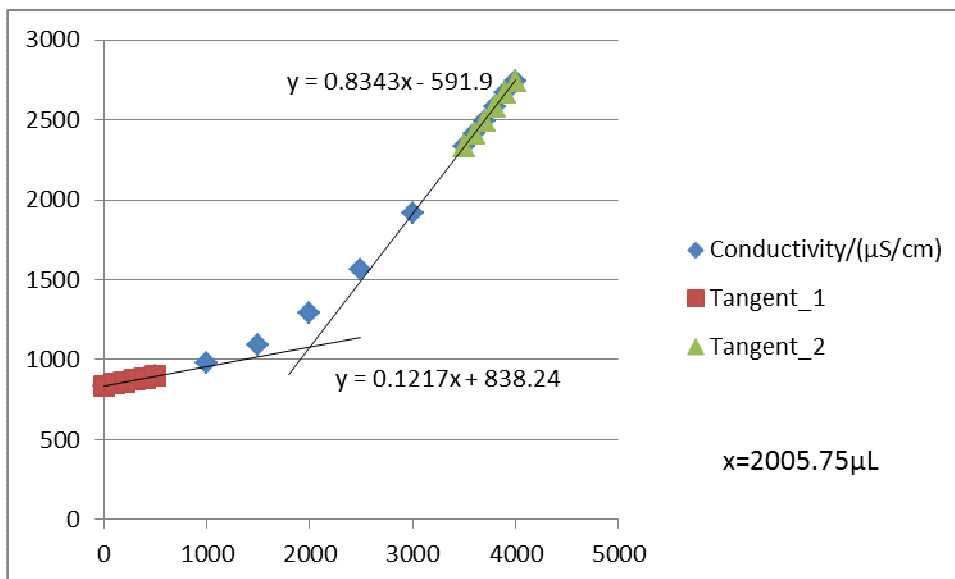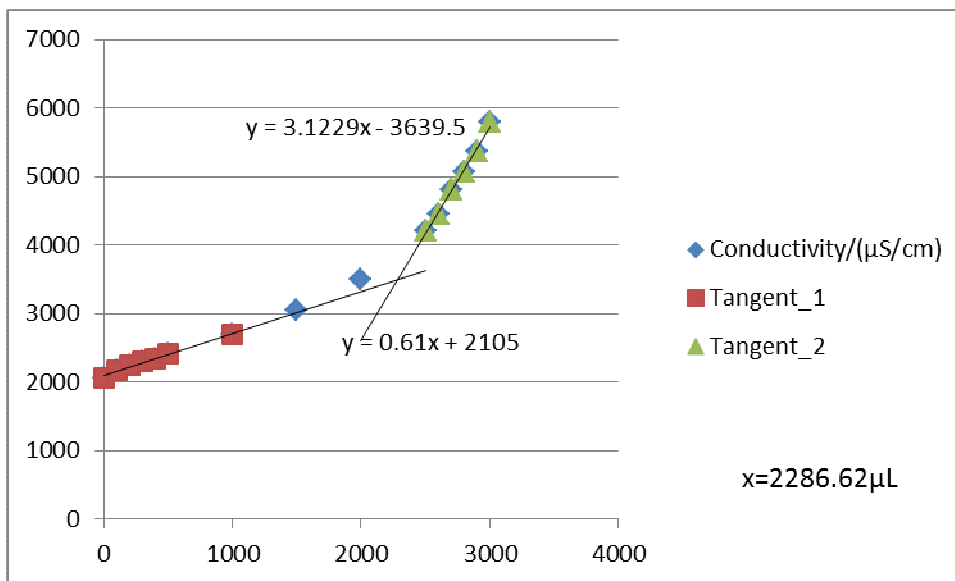

Figure F33-1: Titration 1 for 0.1575 mol/L MEA Third Run
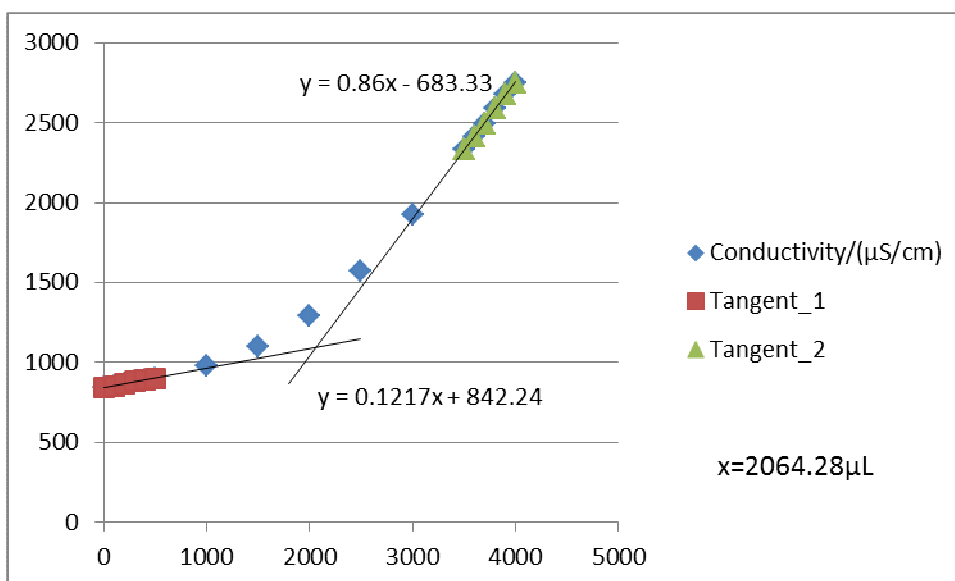
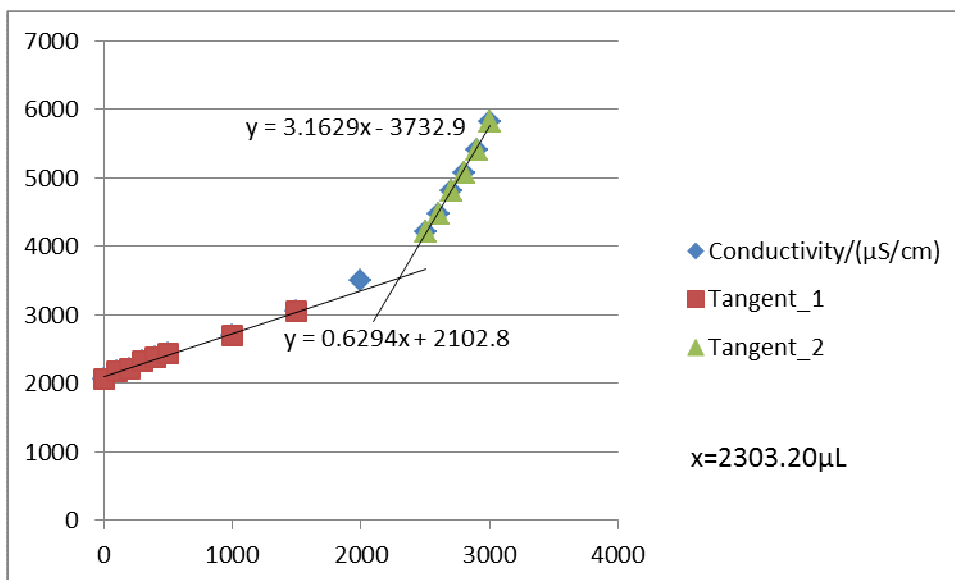Figure F33-2: Titration 2 for 0.1575 mol/L MEA Third Run

201
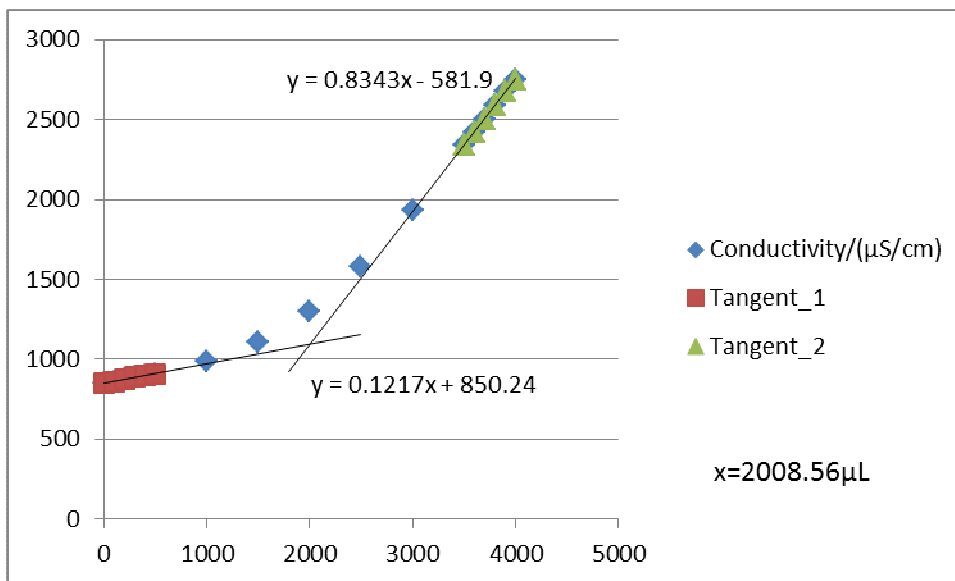
Figure F33-3: Titration 3 for 0.1575 mol/L MEA Third Run

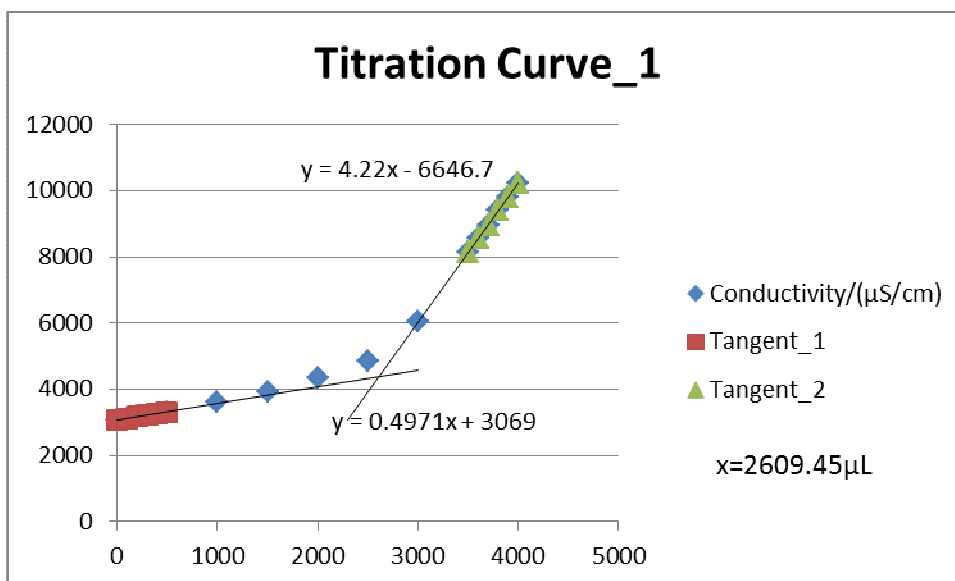**F34: Titration Curves for 0.1965 mol/L MEA First Run at 308 K**
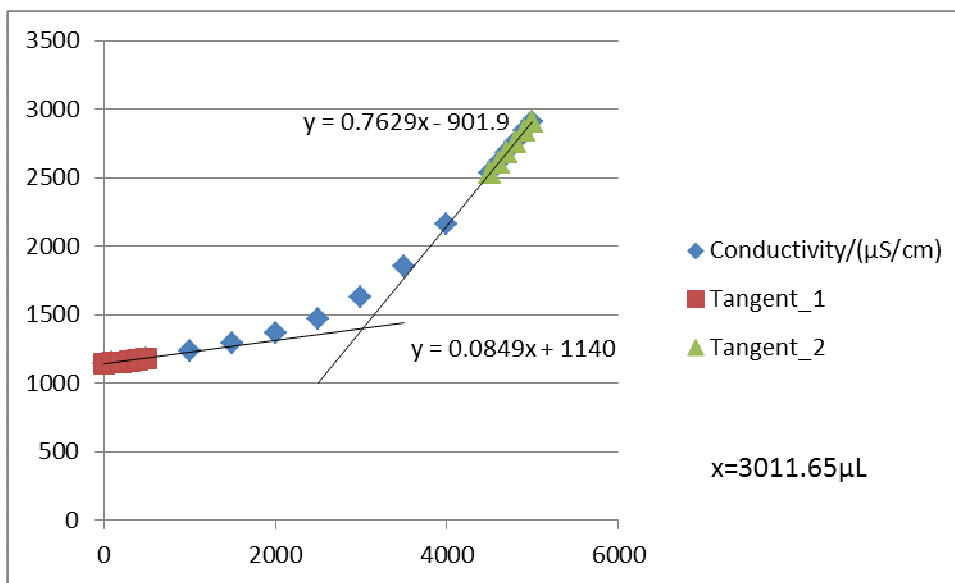
Figure F34-1: Titration 1 for 0.1965 mol/L MEA First Run

202
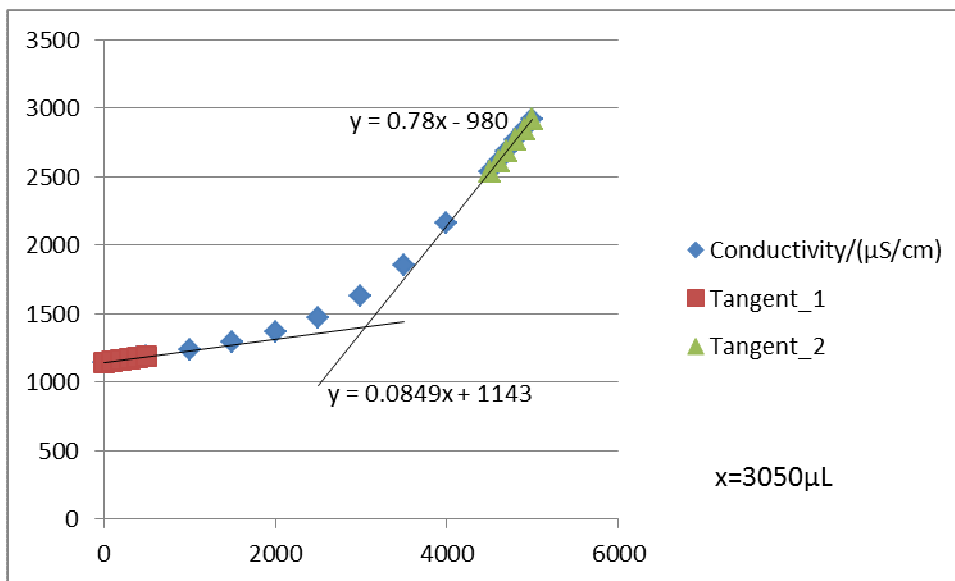
Figure F34-2: Titration 2 for 0.1965 mol/L MEA First Run
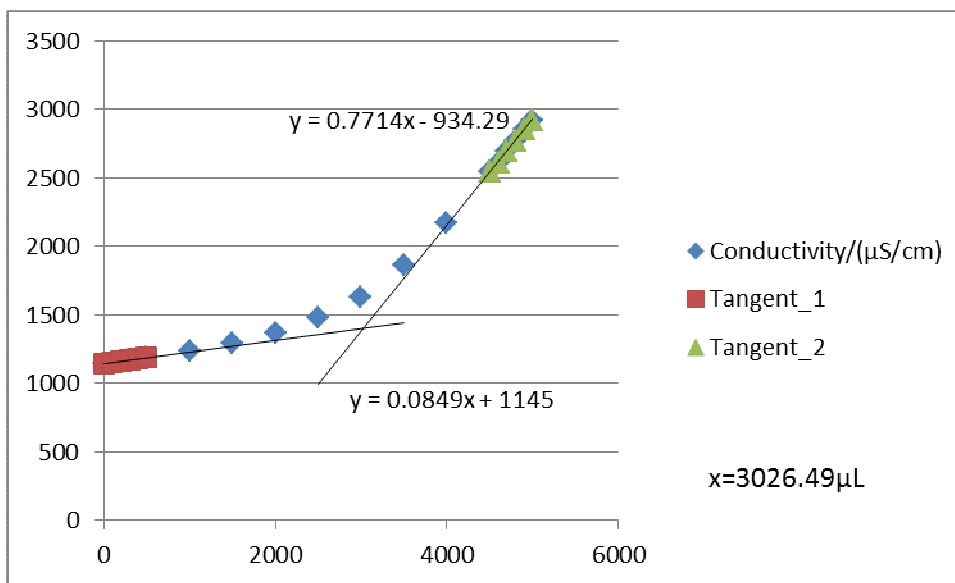
Figure F34-3: Titration 3 for 0.1965 mol/L MEA First Run

F35: Titration Curves for 0.1965 mol/L MEA Second Run at 308 K
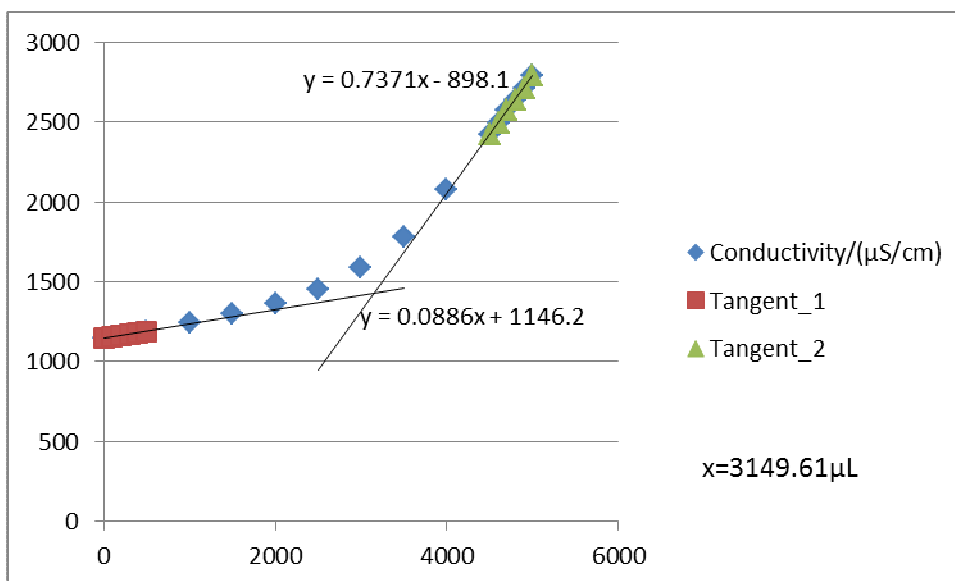
Figure F35-1: Titration 1 for 0.1965 mol/L MEA Second Run
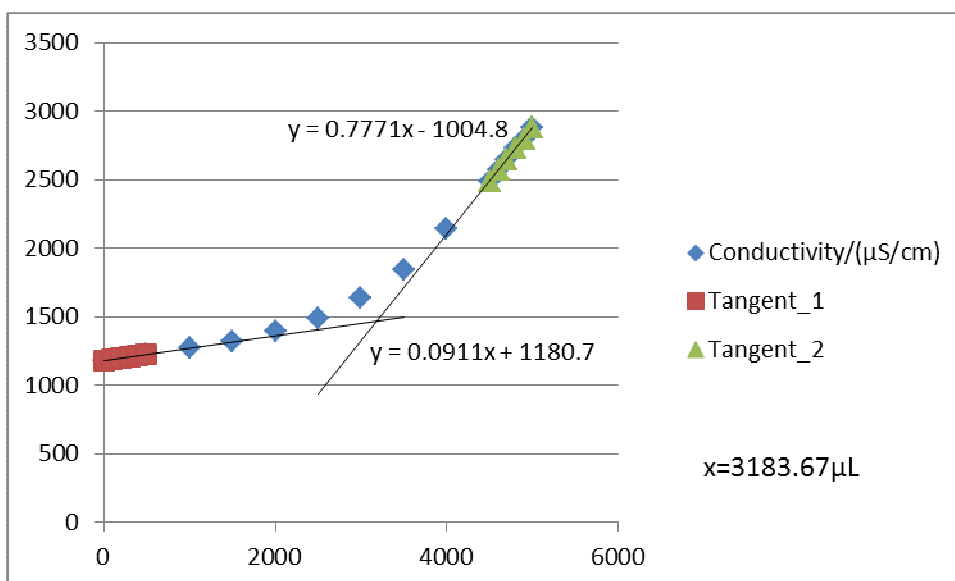
Figure F35-2: Titration 2 for 0.1965 mol/L MEA Second Run

204
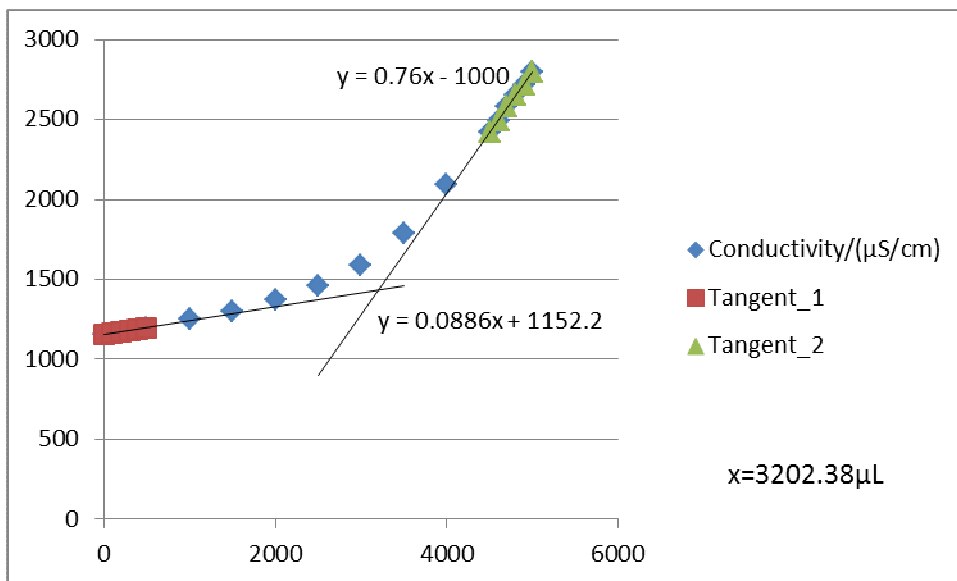
Figure F35-3: Titration 3 for 0.1965 mol/L MEA Second Run

F36: Titration Curves for 0.1965 mol/L MEA Third Run at 308 K
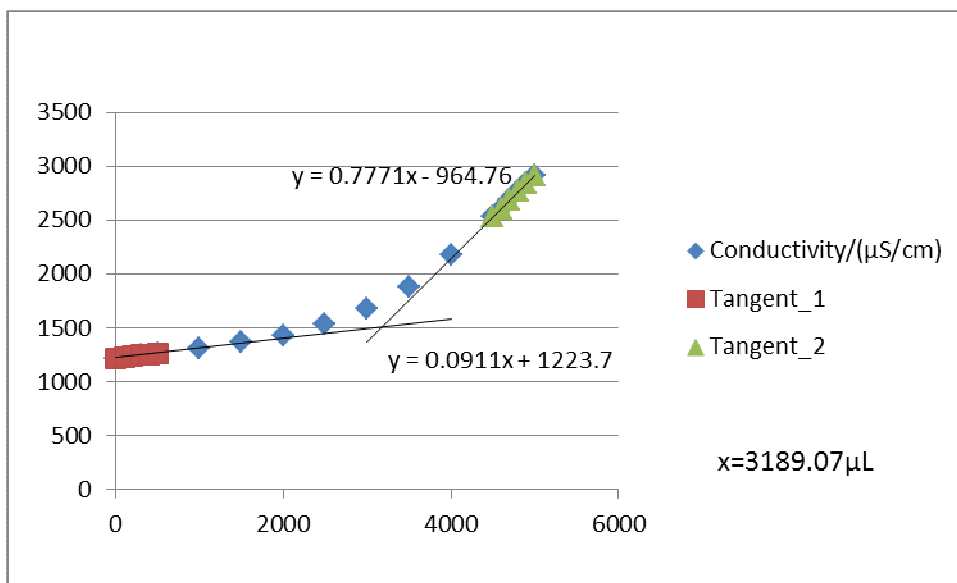
Figure F36-1: Titration 1 for 0.1965 mol/L MEA Third Run
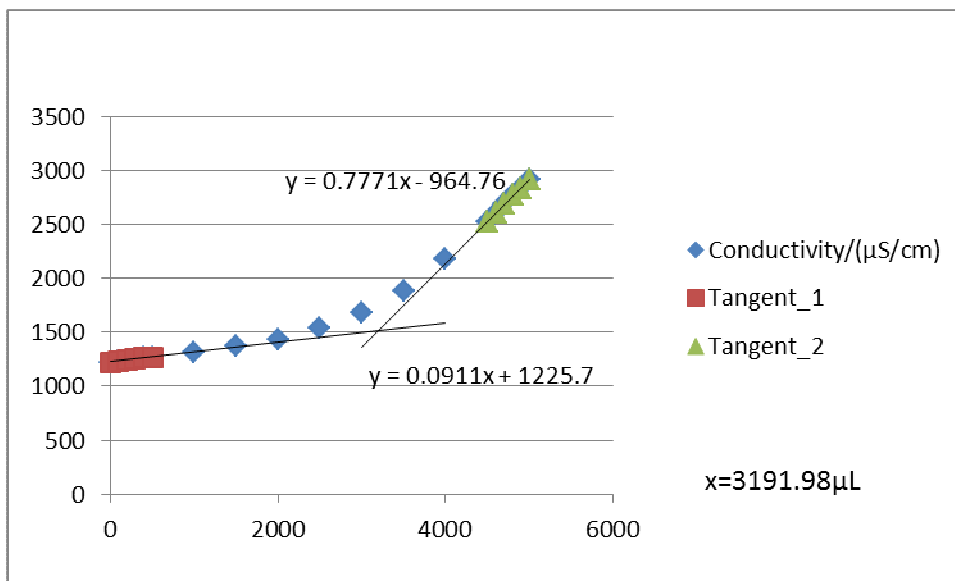
Figure F36-2: Titration 2 for 0.1965 mol/L MEA Third Run
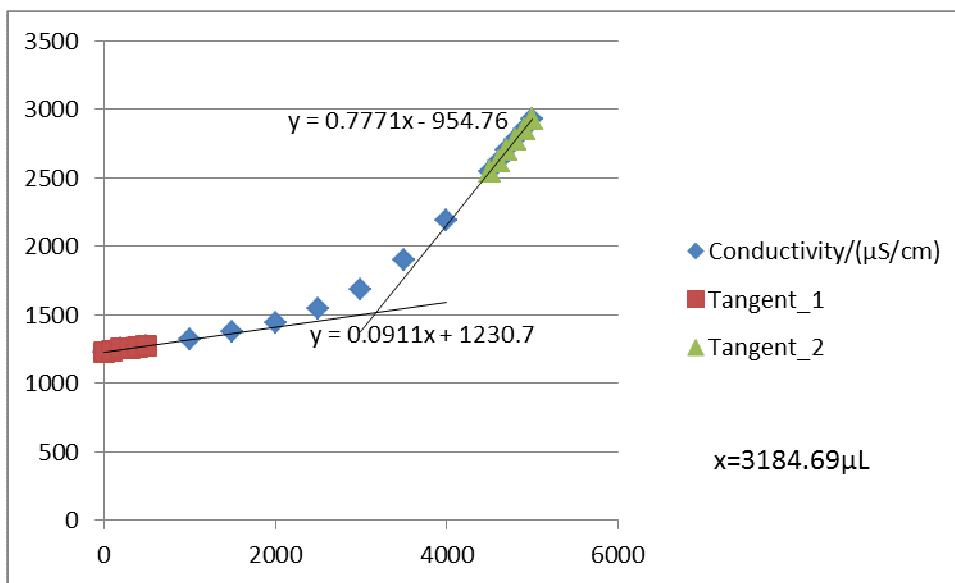
Figure F36-3: Titration 3 for 0.1965 mol/L MEA Third Run

F37: Titration Curves for 0.2609 mol/L MEA First Run at 308 K
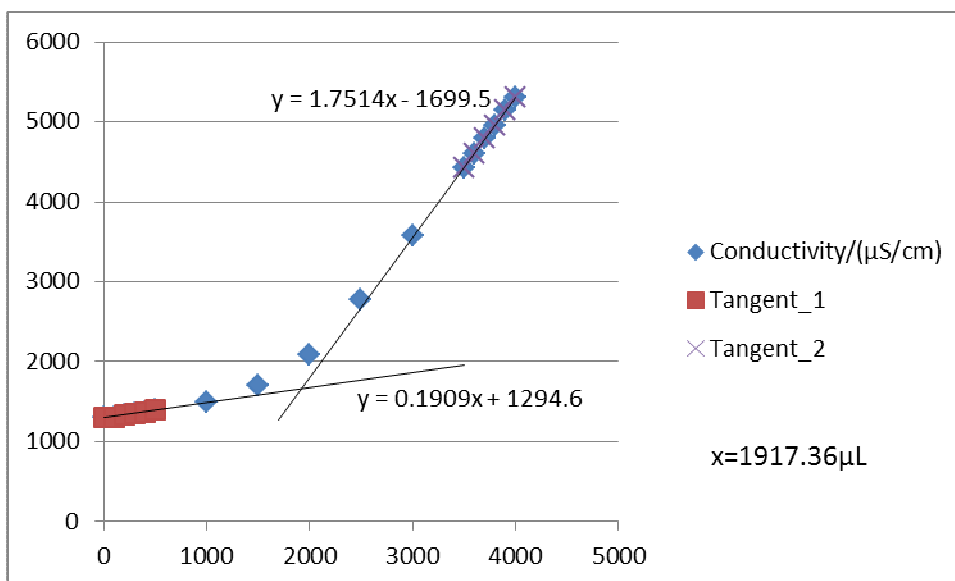
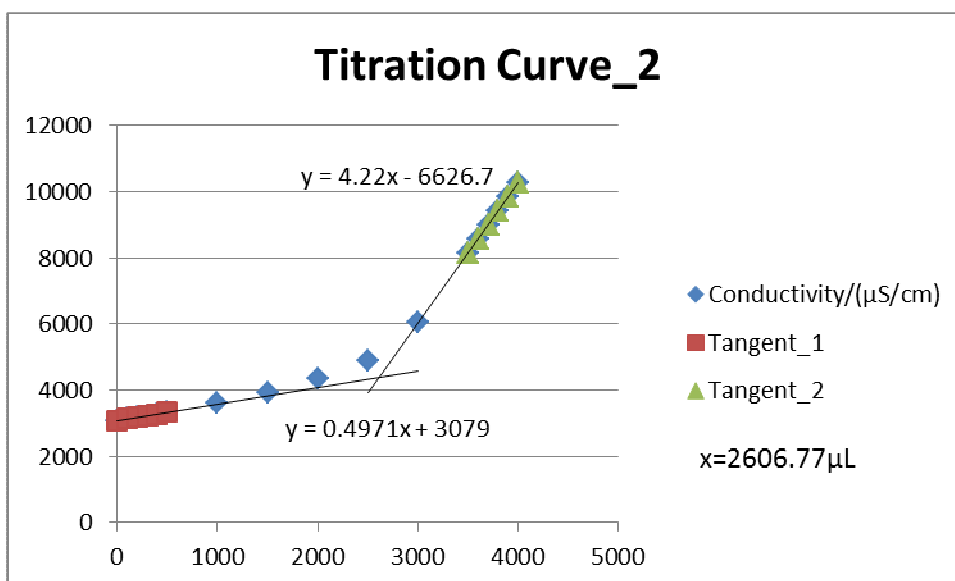Figure F37-1: Titration 1 for 0.2609 mol/L MEA First Run
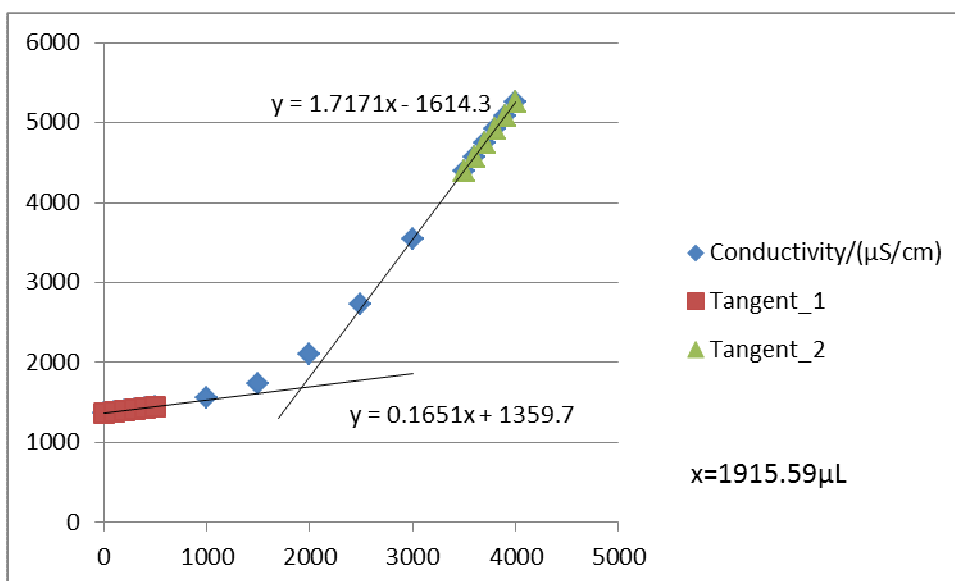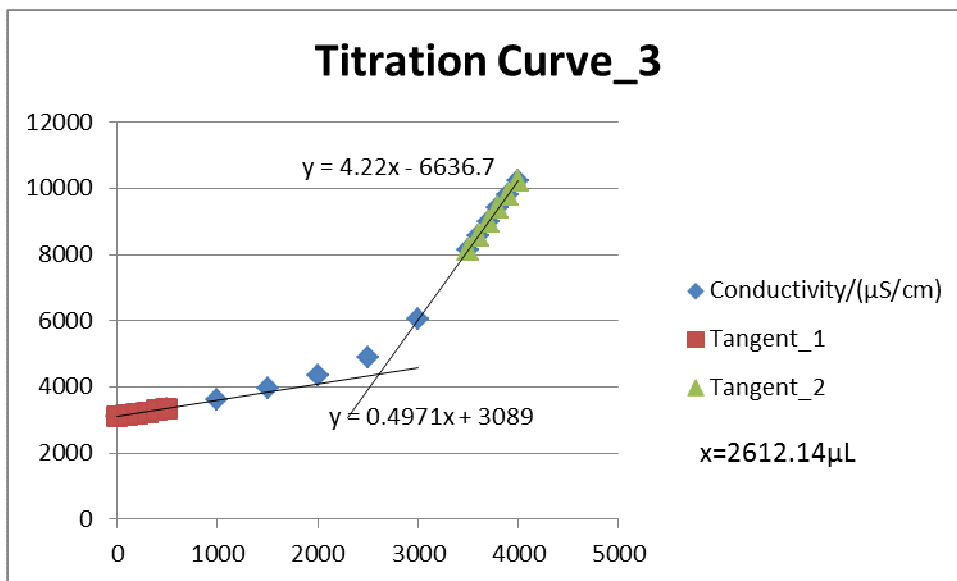

Figure F37-2: Titration 2 for 0.2609 mol/L MEA First Run

207
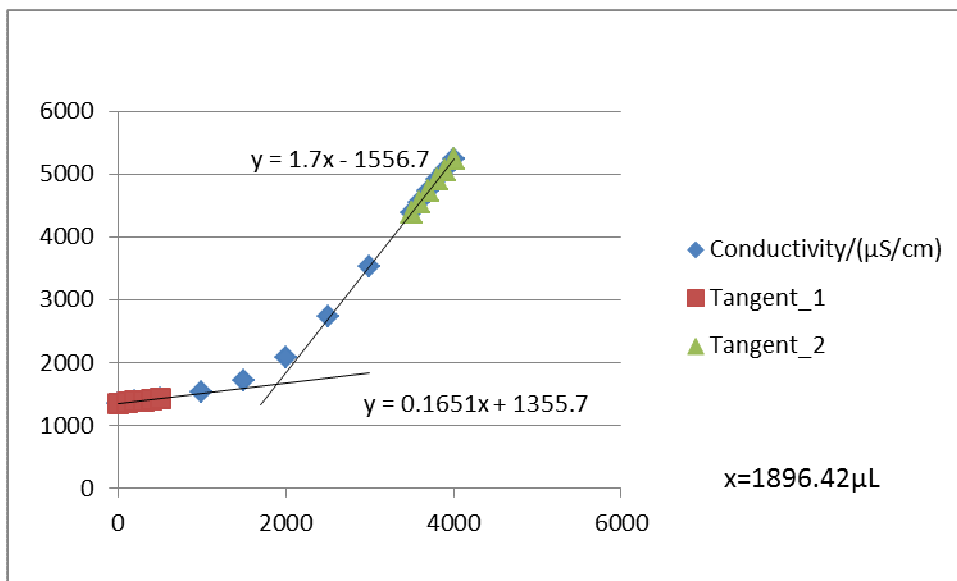
Figure F37-3: Titration 3 for 0.2609 mol/L MEA First Run

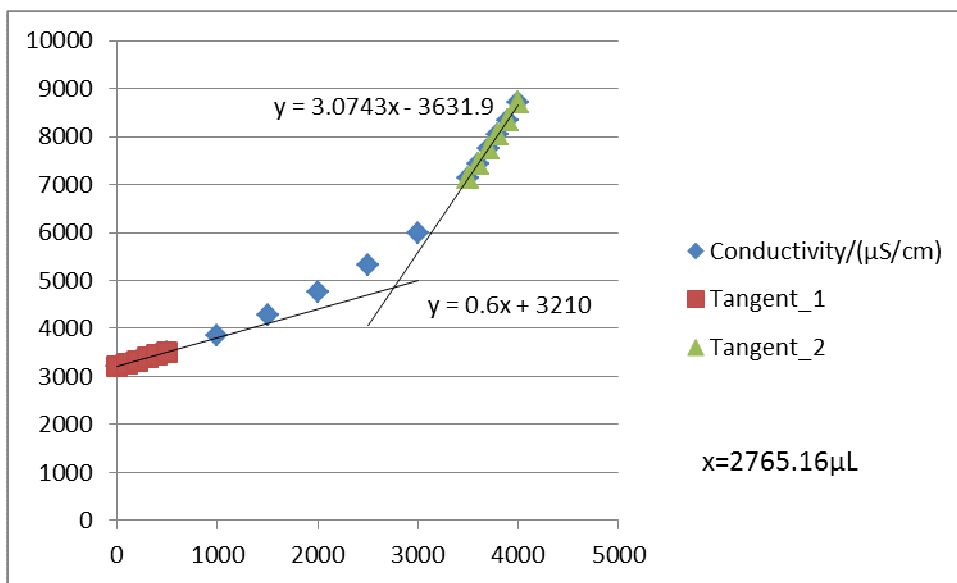**F38: Titration Curves for 0.2609 mol/L MEA Second Run at 308 K**
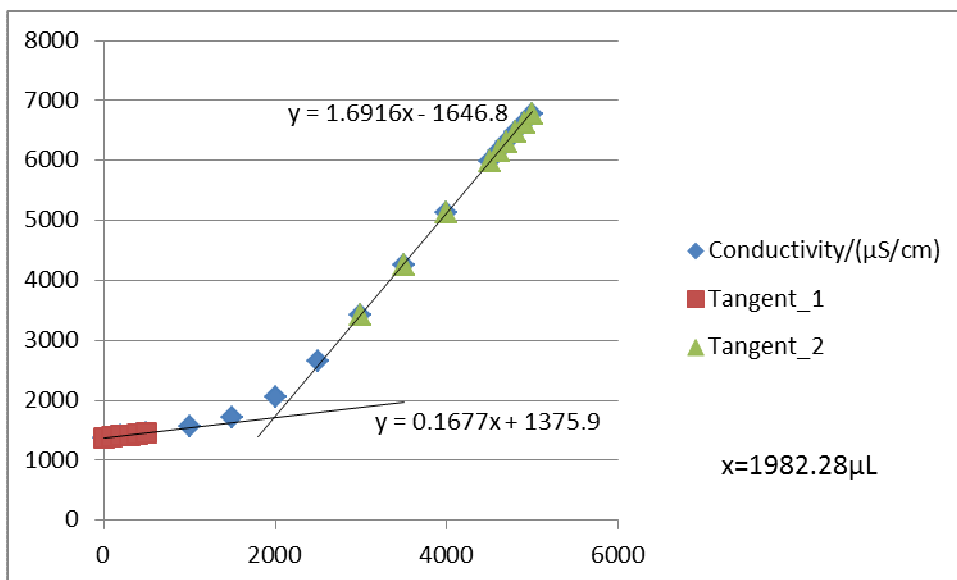
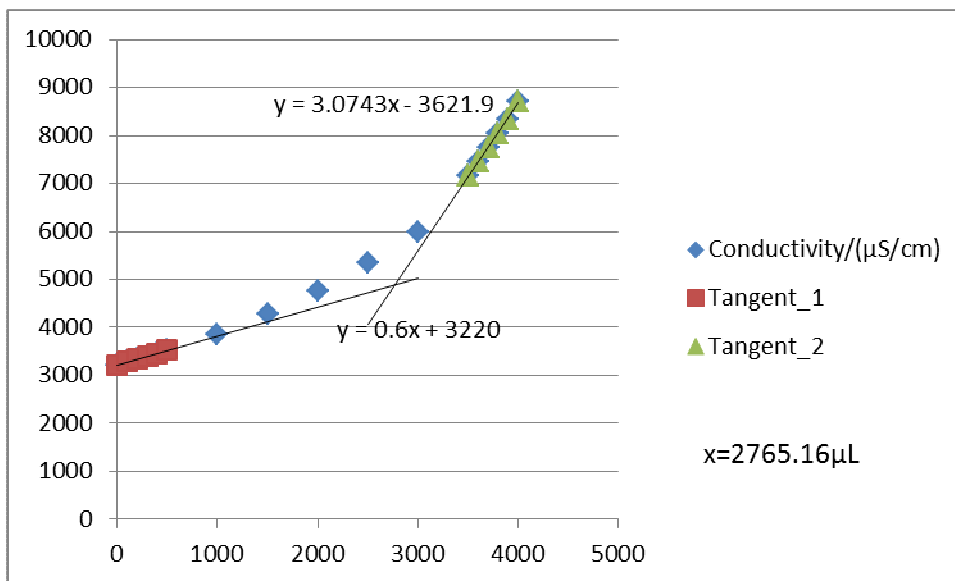

Figure F38-1: Titration 1 for 0.2609 mol/L MEA Second Run
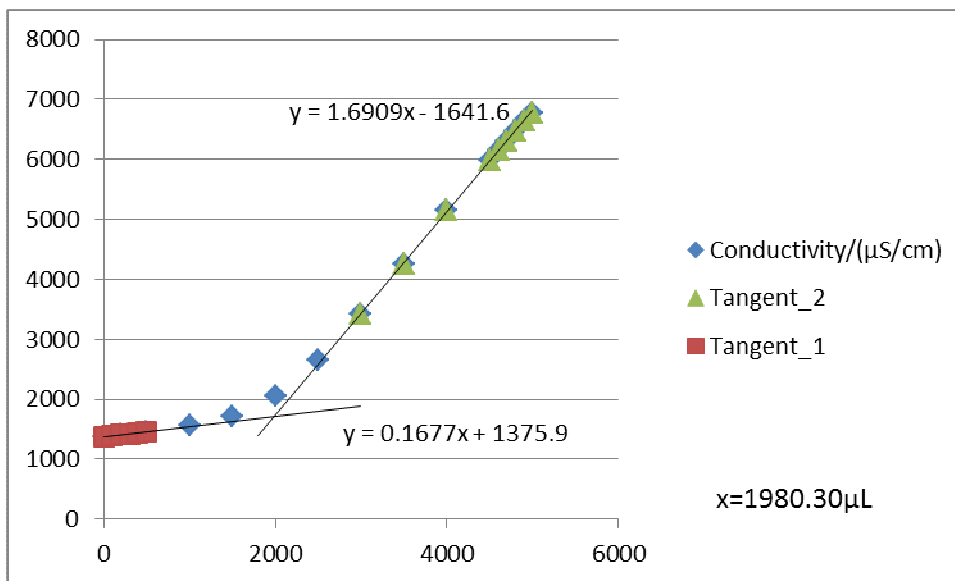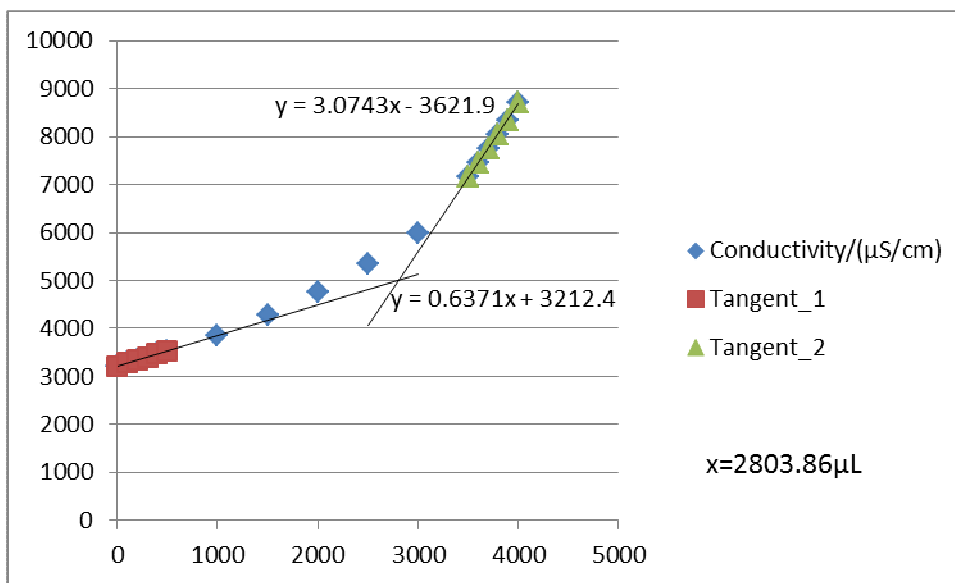
Figure F38-2: Titration 2 for 0.2609 mol/L MEA Second Run
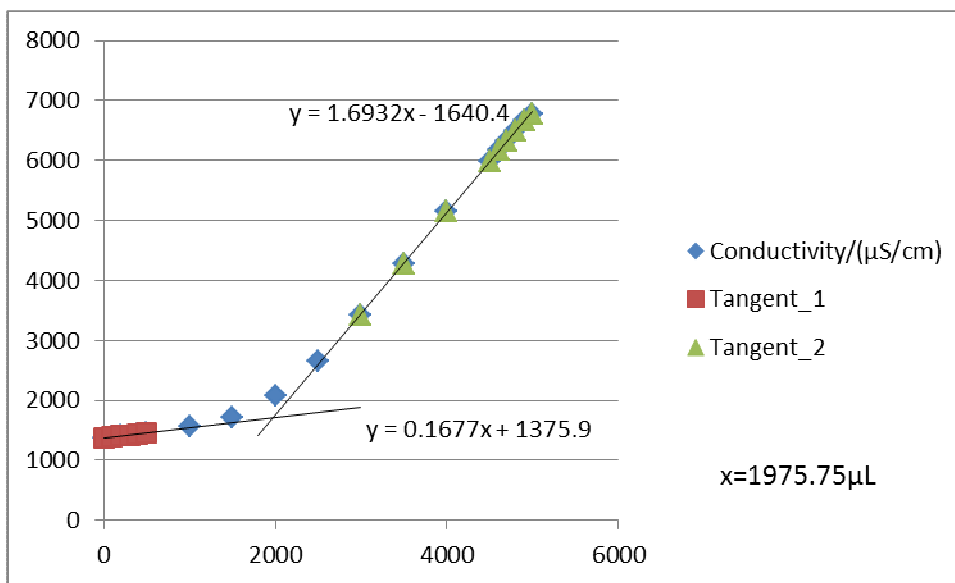
Figure F38-3: Titration 3 for 0.2609 mol/L MEA Second Run

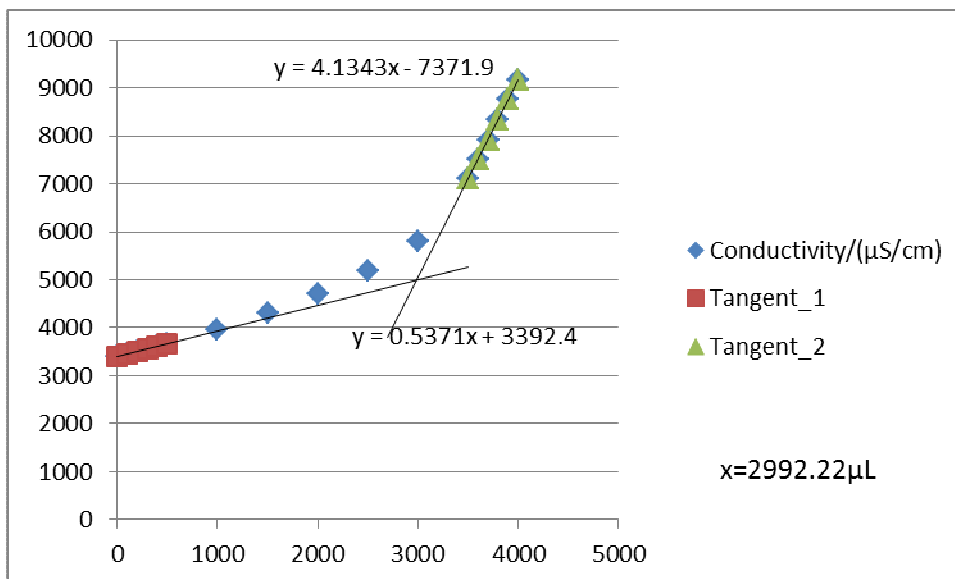**F39: Titration Curves for 0.2609 mol/L MEA Third Run at 308 K**
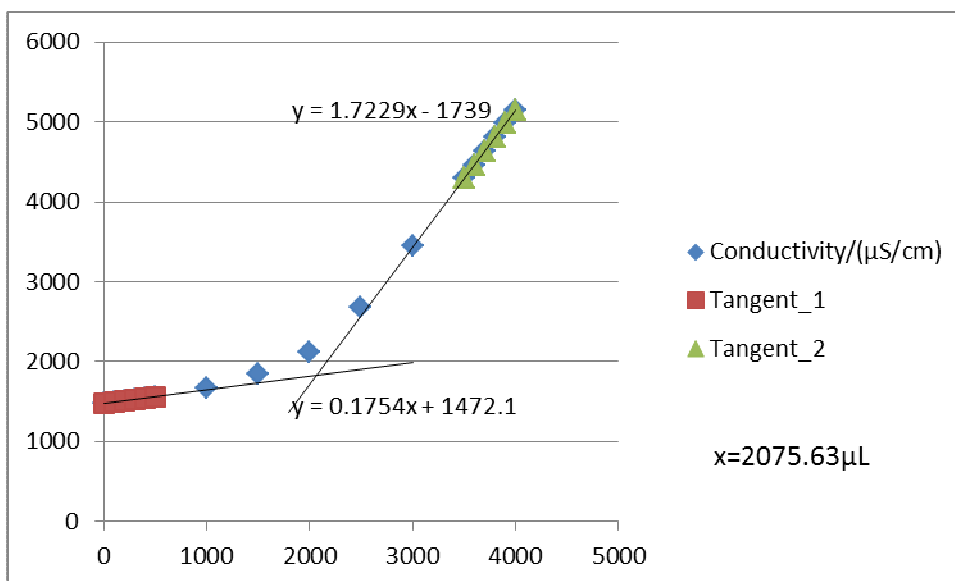
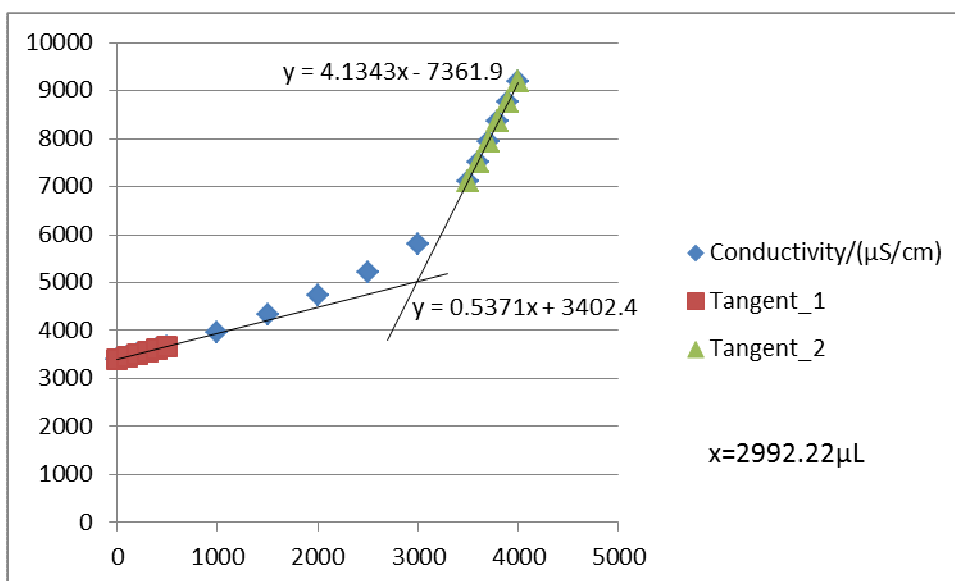Figure F39-1: Titration 1 for 0.2609 mol/L MEA Third Run
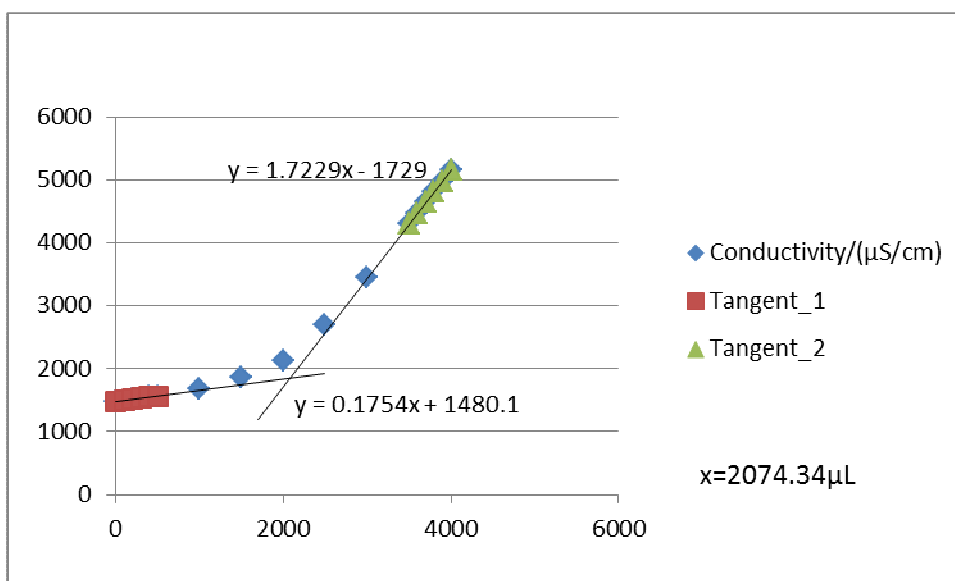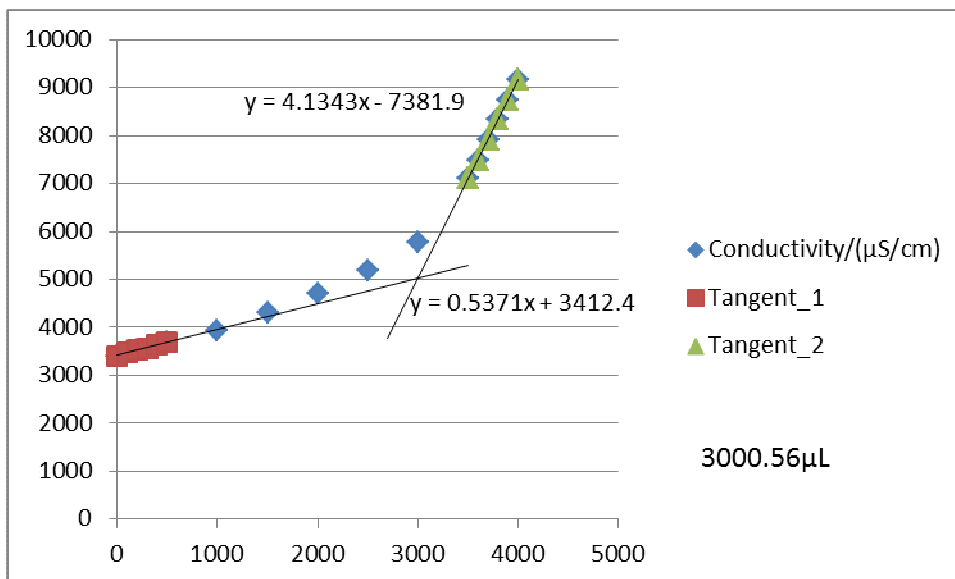

Figure F39-2: Titration 2 for 0.2609 mol/L MEA Third Run
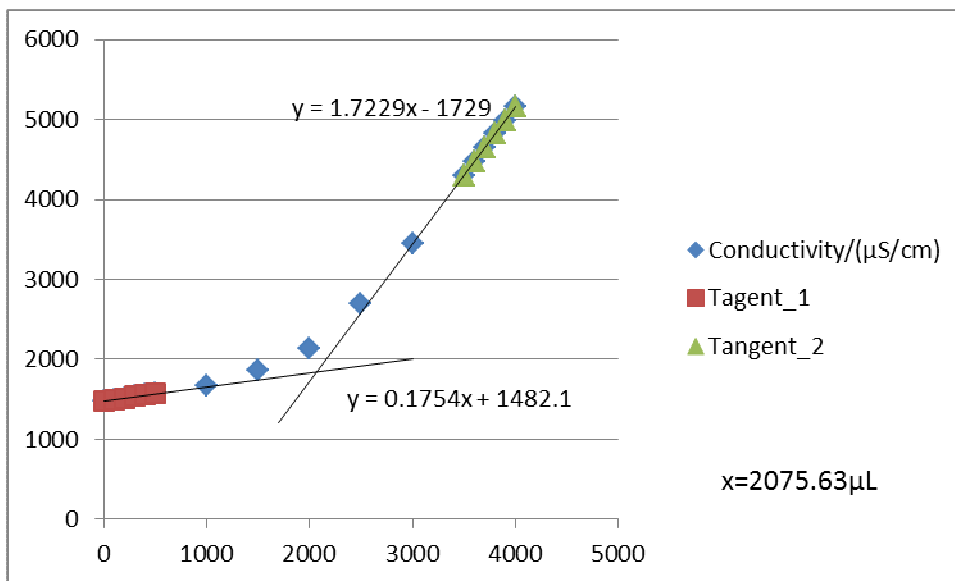
Figure F39-3: Titration 3 for 0.2609 mol/L MEA Third Run

F40: Titration Curves for 0.01986 mol/L MEA First Run at 313 K
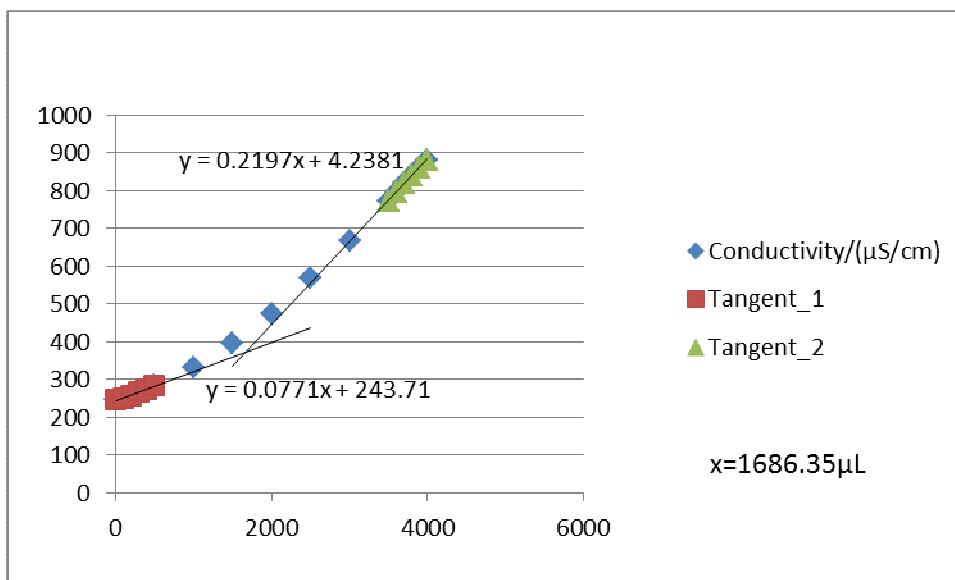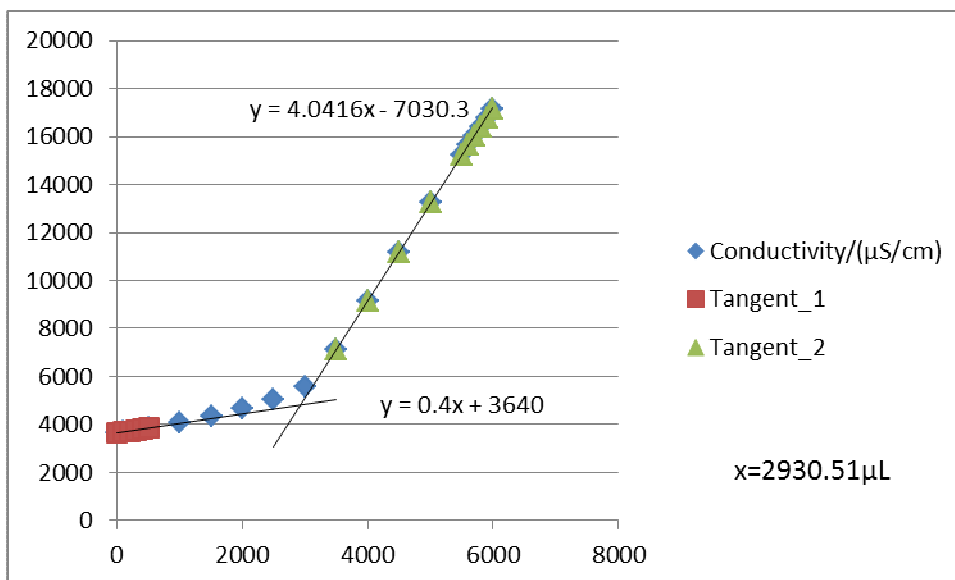

Figure F40-1: Titration 1 for 0.01986 mol/L MEA First Run

211
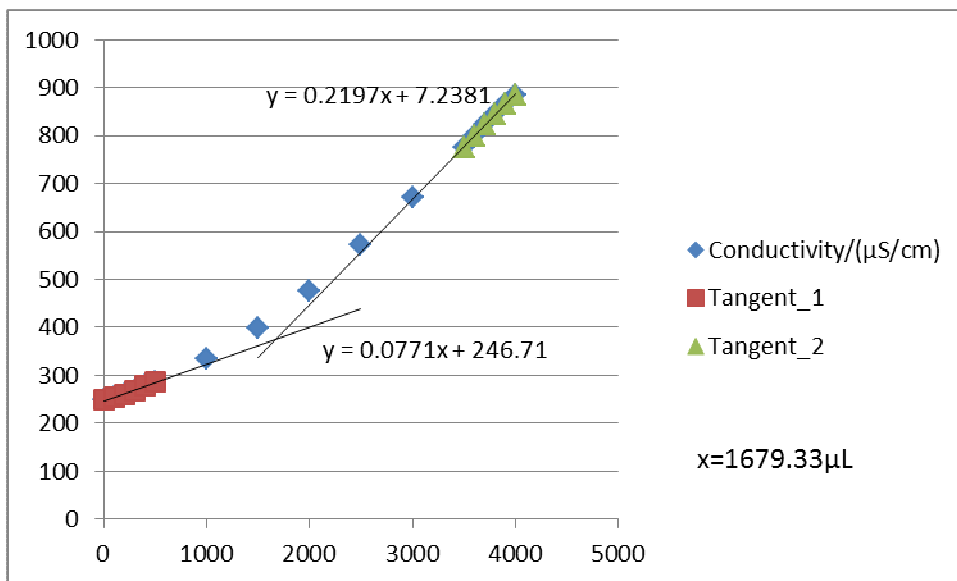
Figure F40-2: Titration 2 for 0.01986 mol/L MEA First Run
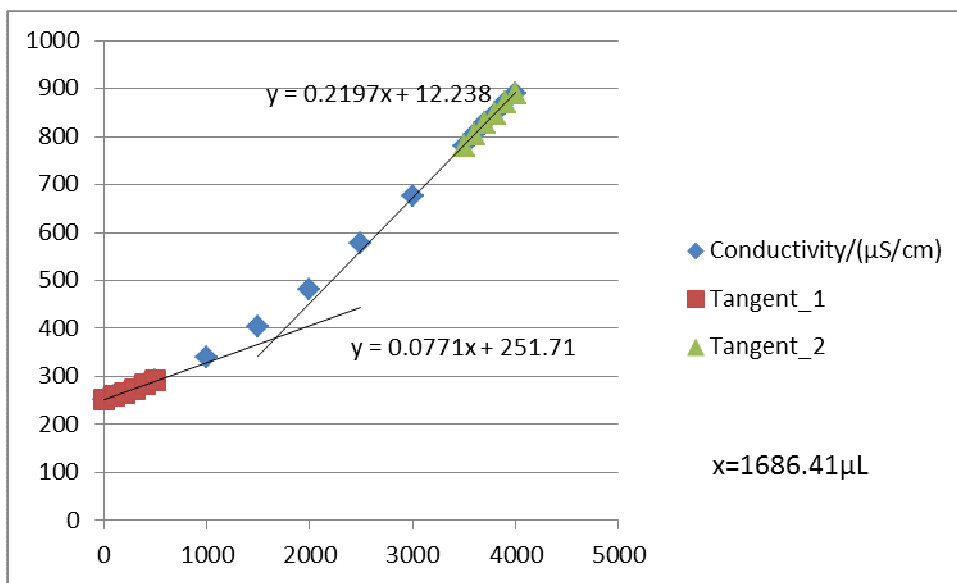
Figure F40-3: Titration 3 for 0.01986 mol/L MEA First Run

F41: Titration Curves for 0.01986 mol/L MEA Second Run at 313 K
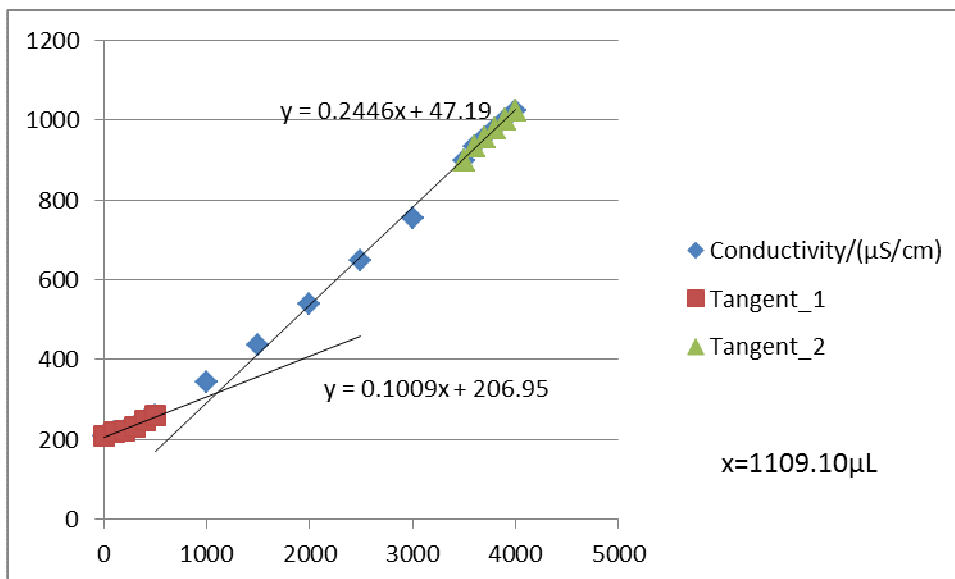
Figure F41-1: Titration 1 for 0.01986 mol/L MEA Second Run
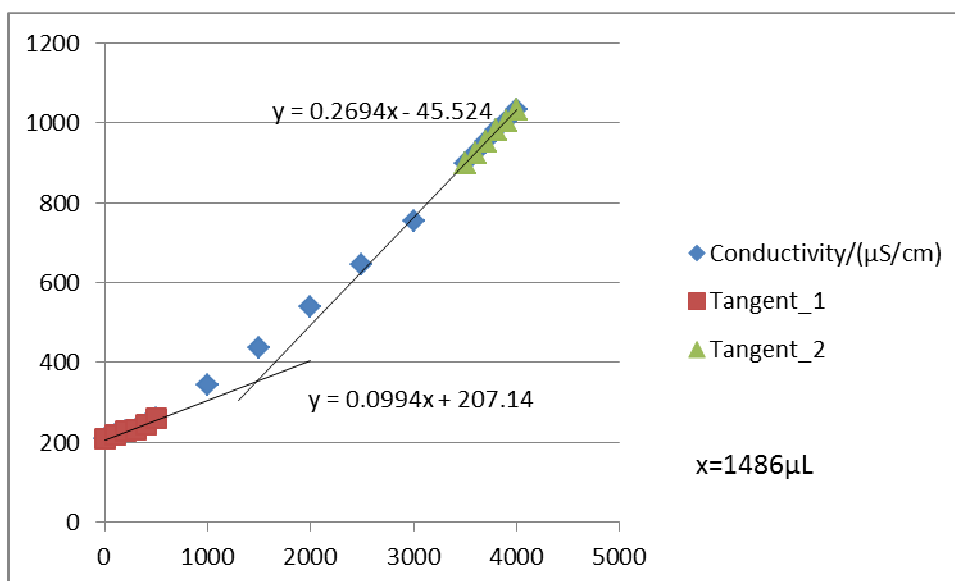
Figure F41-2: Titration 2 for 0.01986 mol/L MEA Second Run

213
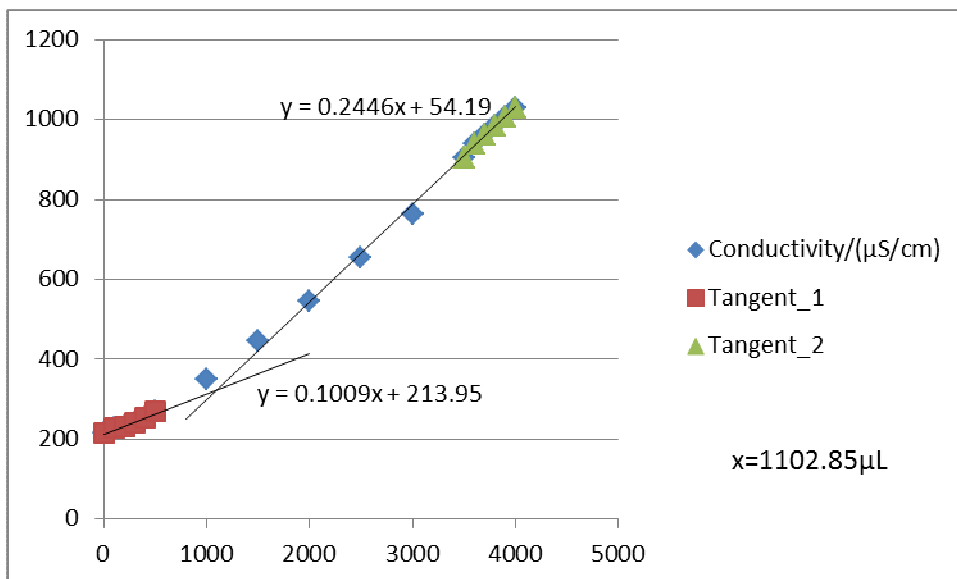
Figure F41-3: Titration 3 for 0.01986 mol/L MEA Second Run

F42: Titration Curves for 0.01986 mol/L MEA Third Run at 313 K
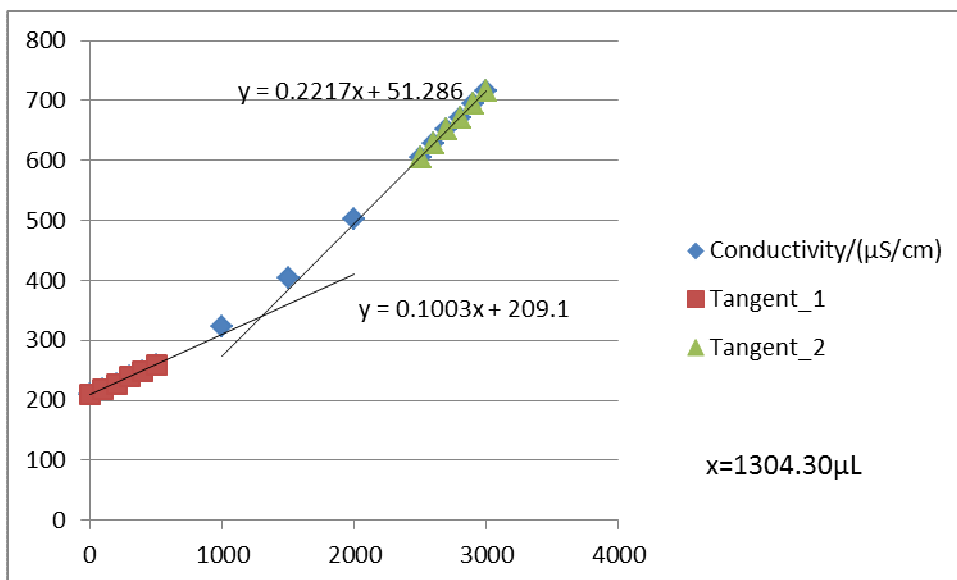
Figure F42-1: Titration 1 for 0.01986 mol/L MEA Third Run

214
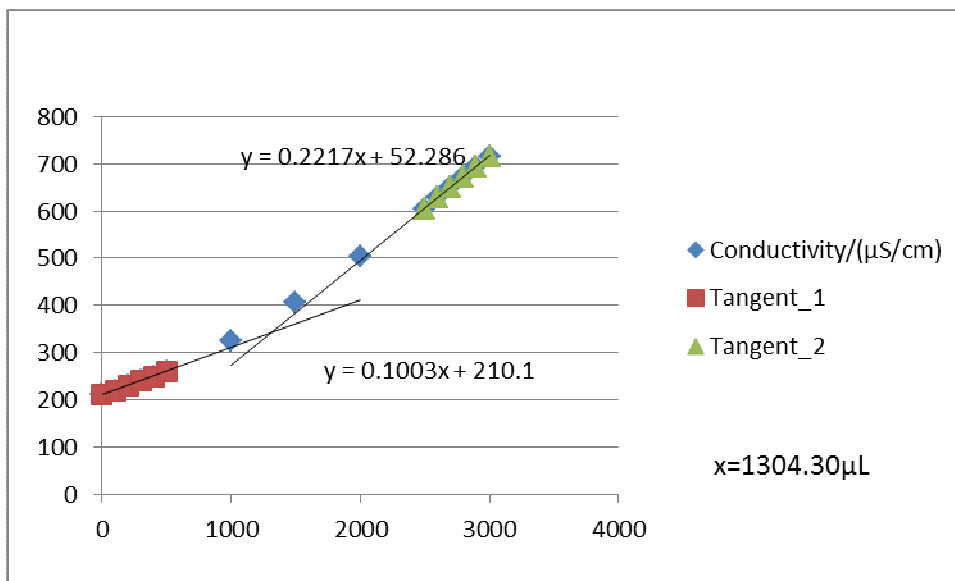
Figure F42-2: Titration 2 for 0.01986 mol/L MEA Third Run
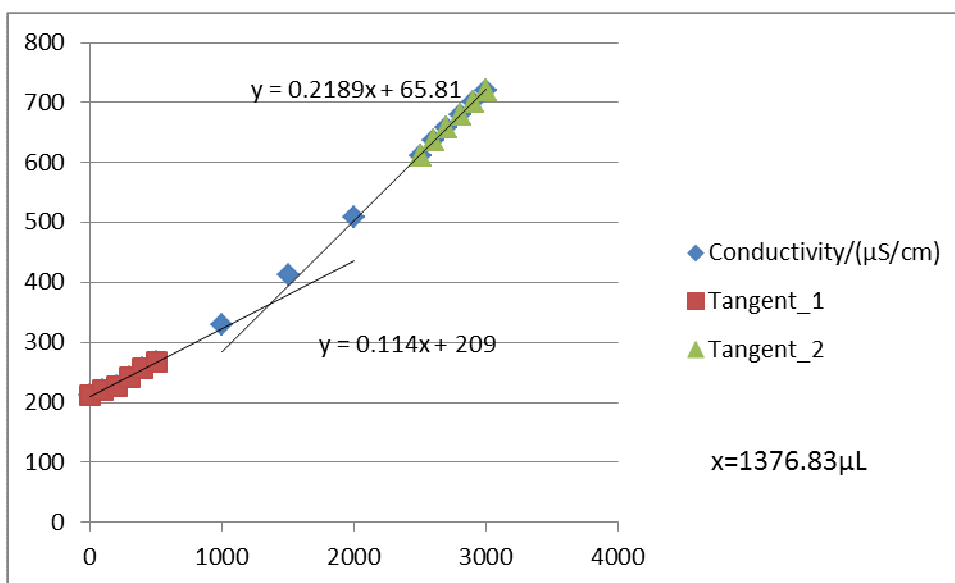
Figure F42-3: Titration 3 for 0.01986 mol/L MEA Third Run

215

F43: Titration Curves for 0.04956 mol/L MEA First Run at 313 K
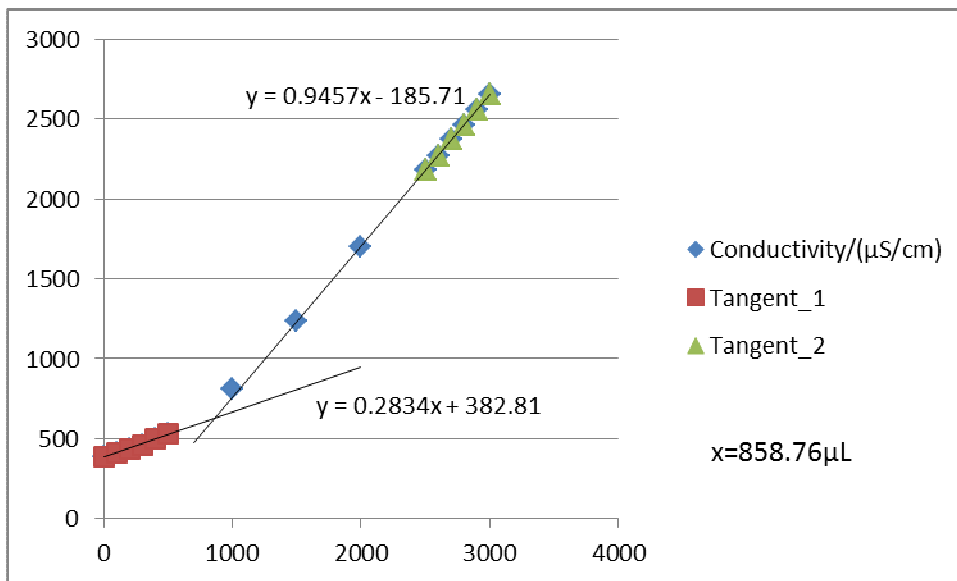
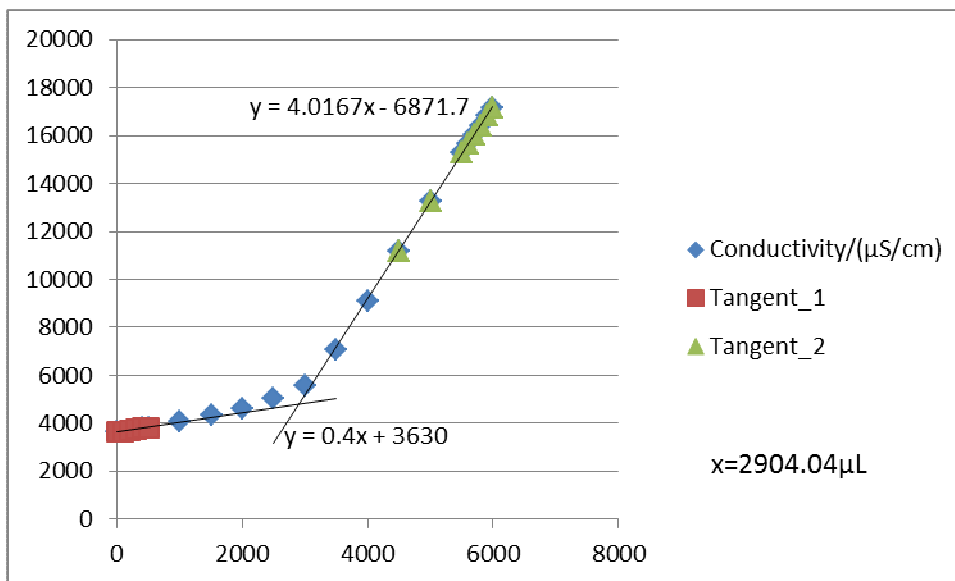Figure F43-1: Titration 1 for 0.04956 mol/L MEA First Run
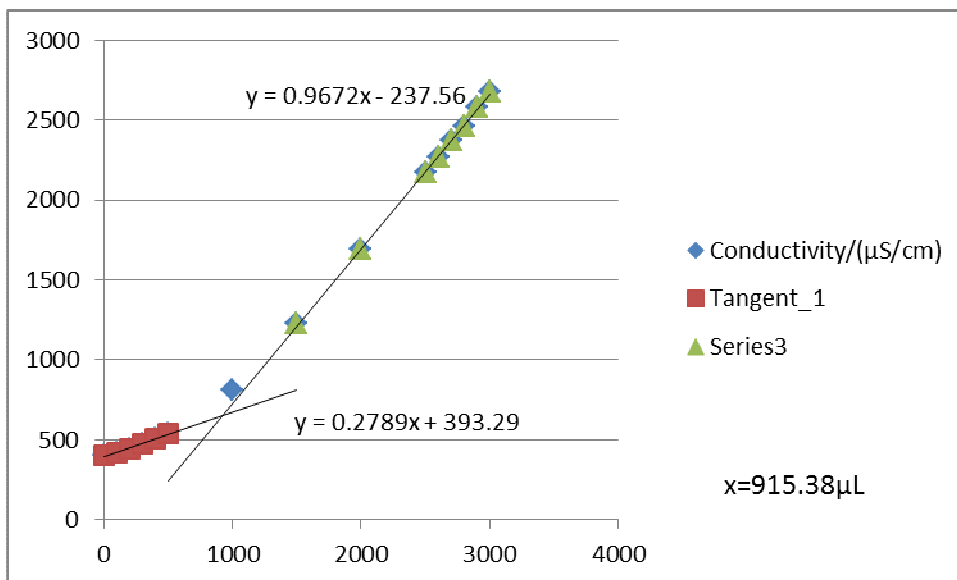
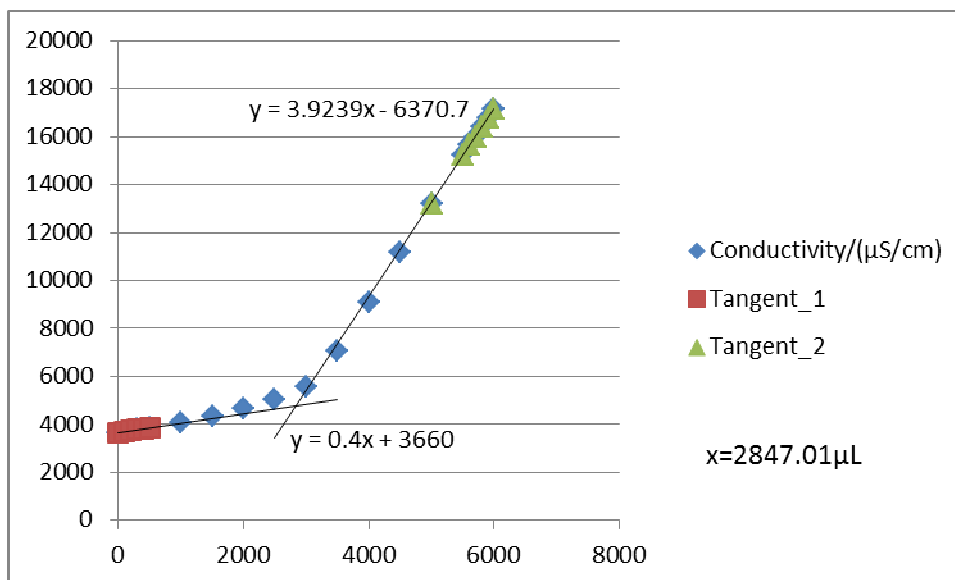

Figure F43-2: Titration 2 for 0.04956 mol/L MEA First Run
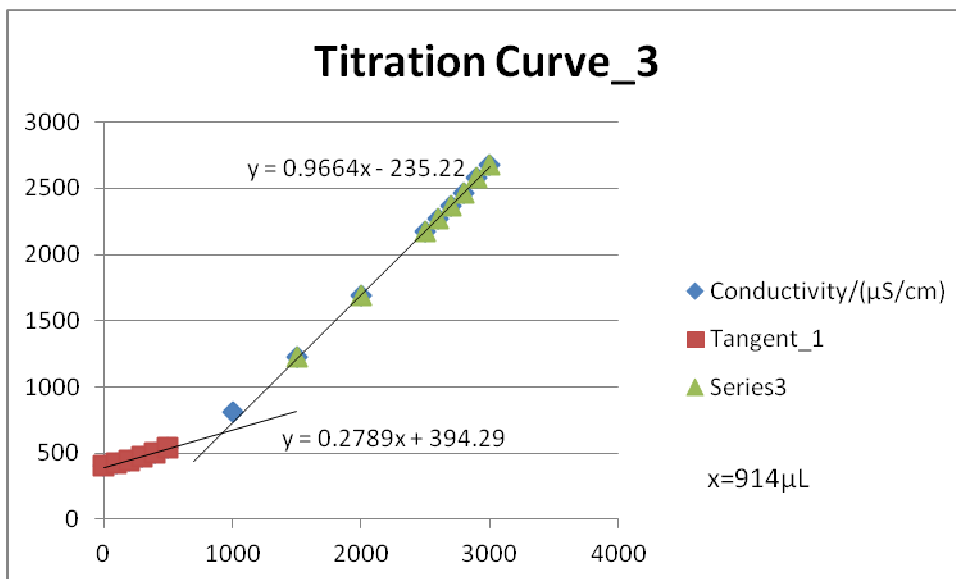
Figure F43-3: Titration 3 for 0.04956 mol/L MEA First Run

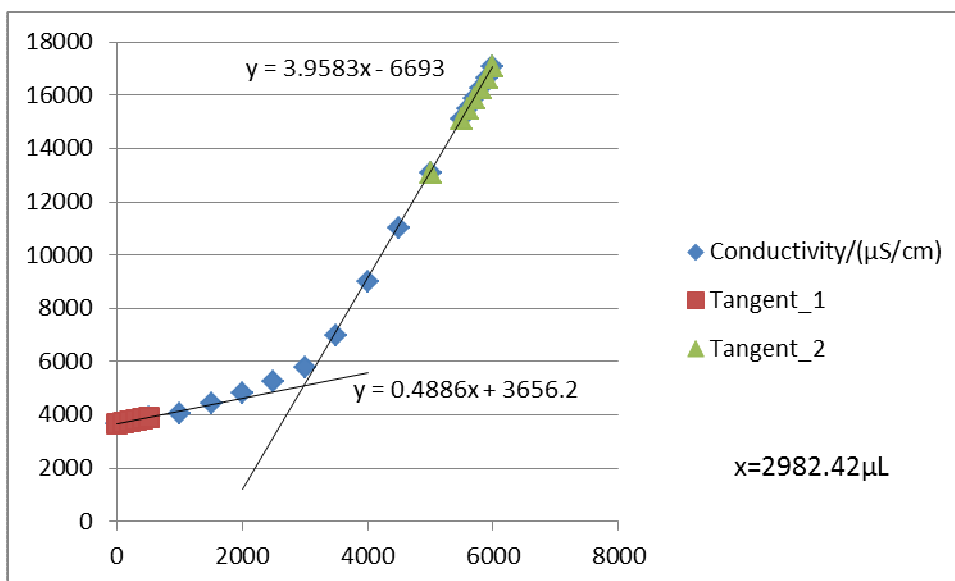**F44: Titration Curves for 0.04956 mol/L MEA Second Run at 313 K**
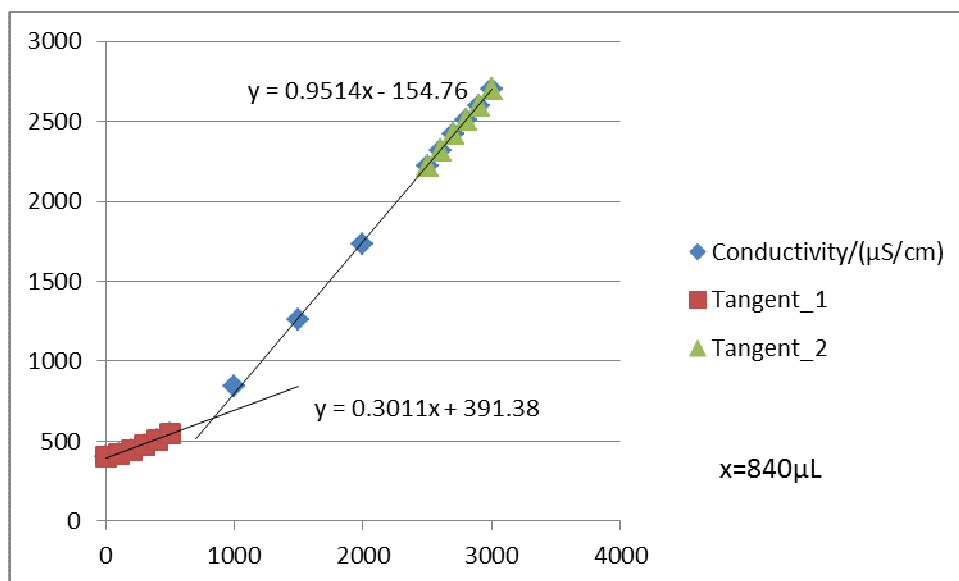
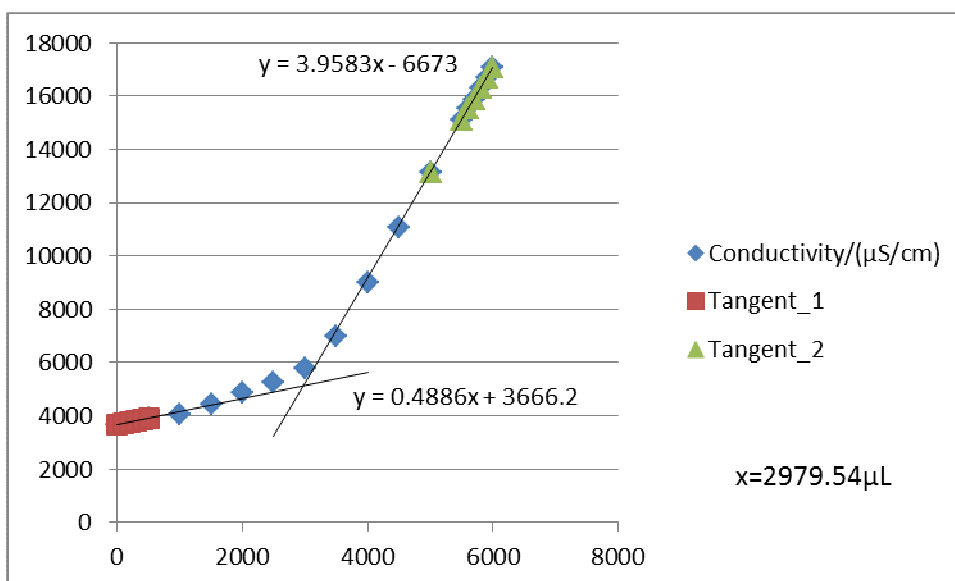
Figure F44-1: Titration 1 for 0.04956 mol/L MEA Second Run

217
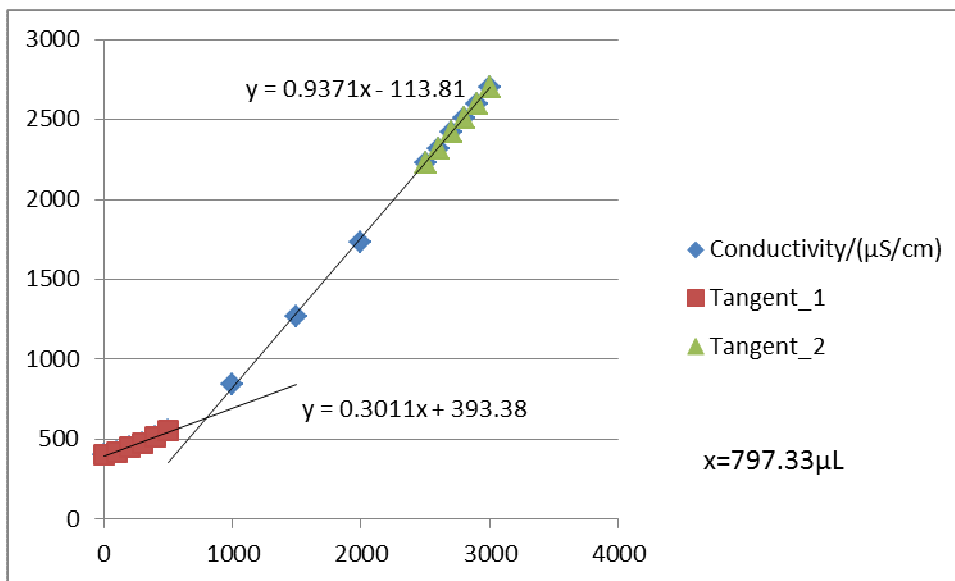
Figure F44-2: Titration 2 for 0.04956 mol/L MEA Second Run
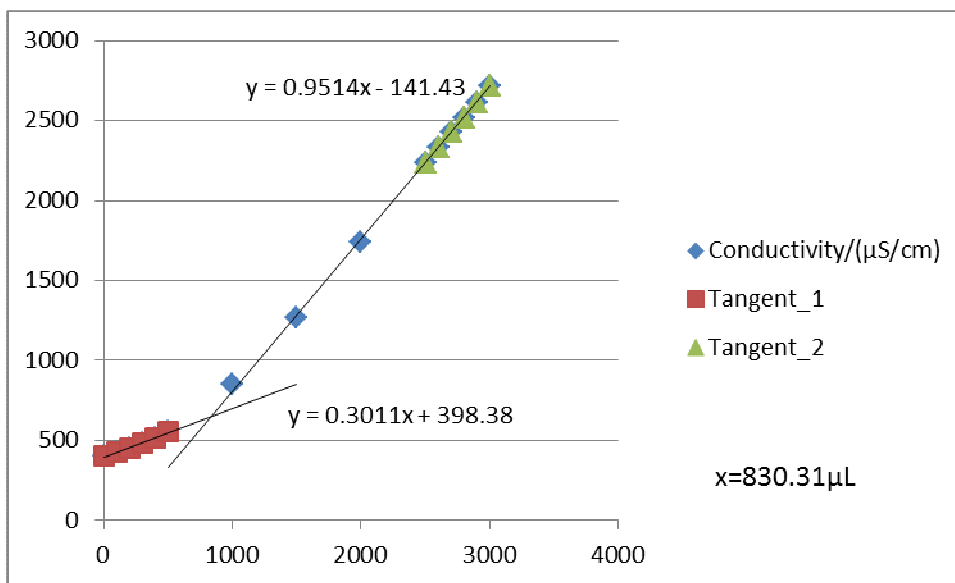
Figure F44-3: Titration 3 for 0.04956 mol/L MEA Second Run

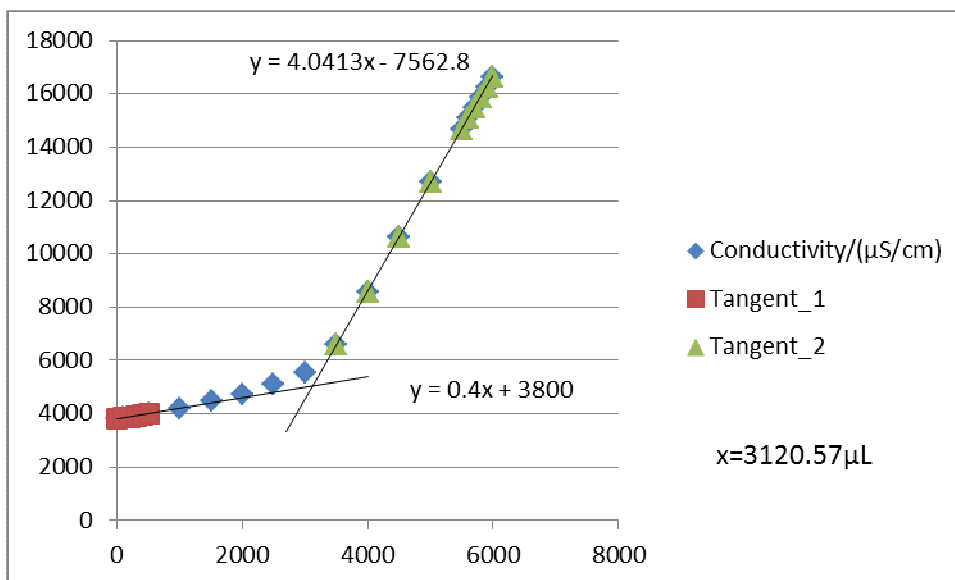**F45: Titration Curves for 0.04956 mol/L MEA Third Run at 313 K**

$y = 0.9514x - 224.76$

$y = 0.2834x + 365.81$

x=883.98µL
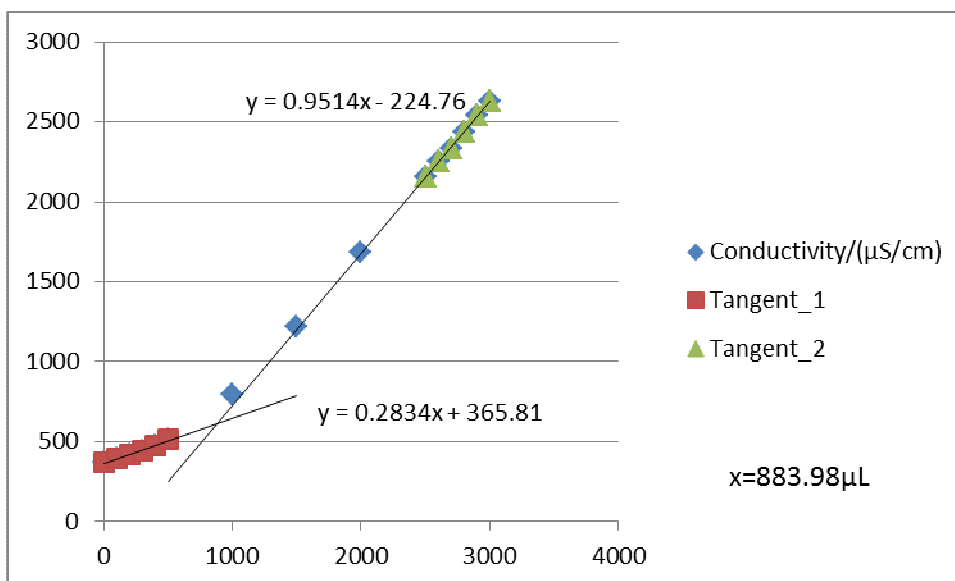
Figure F45-1: Titration 1 for 0.04956 mol/L MEA Third Run

$y = 0.9371x - 167.14$

$y = 0.2834x + 369.81$

x=820.95µL
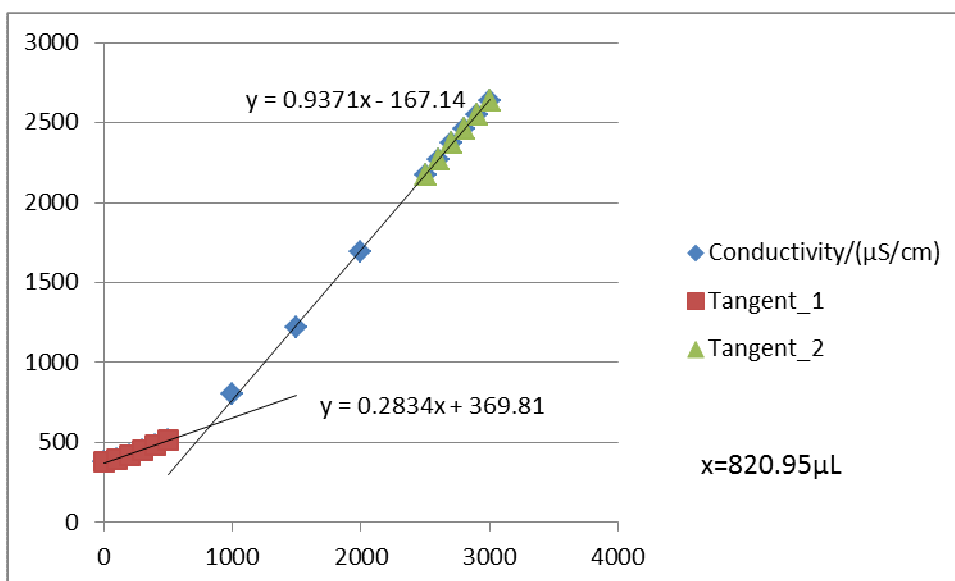
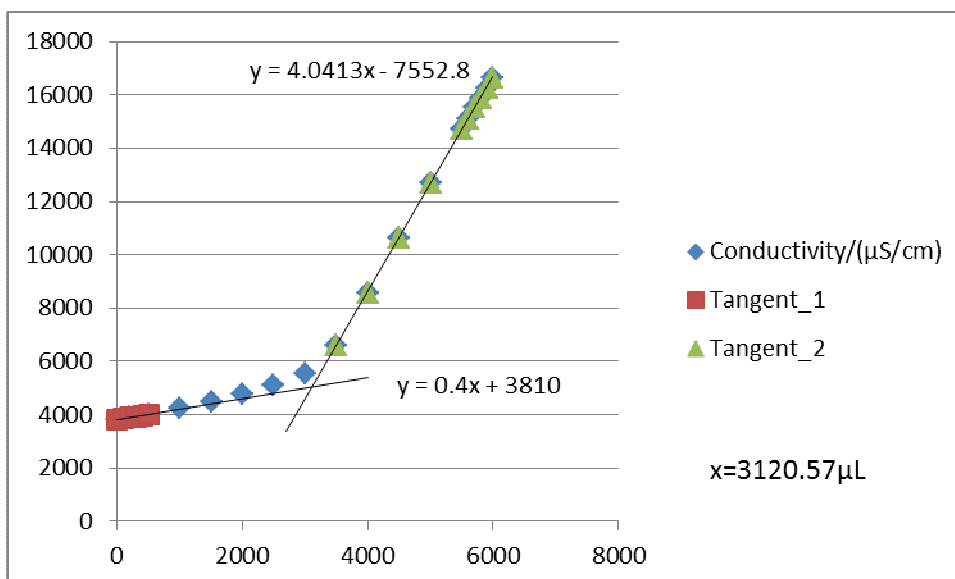Figure F45-2: Titration 2 for 0.04956 mol/L MEA Third Run
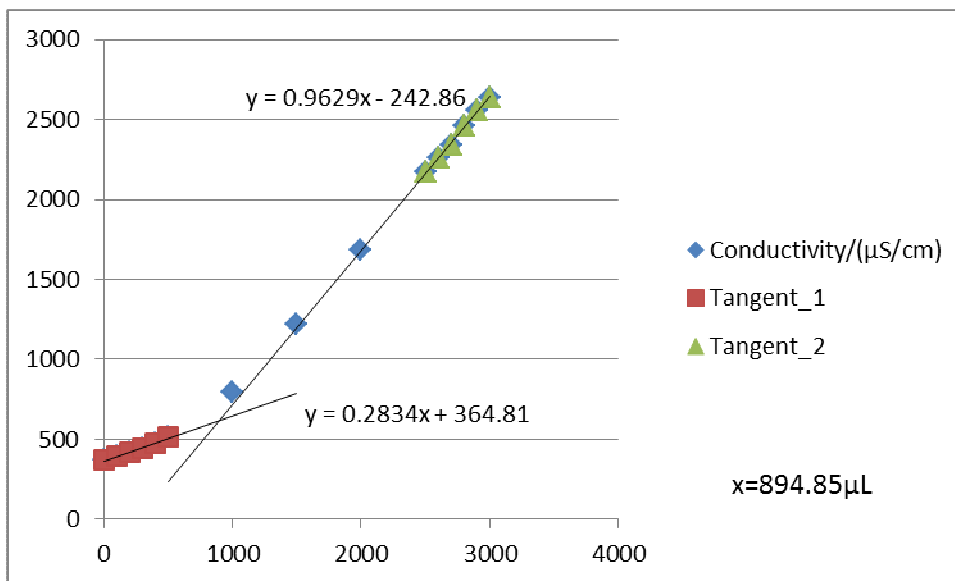
Figure F45-3: Titration 3 for 0.04956 mol/L MEA Third Run

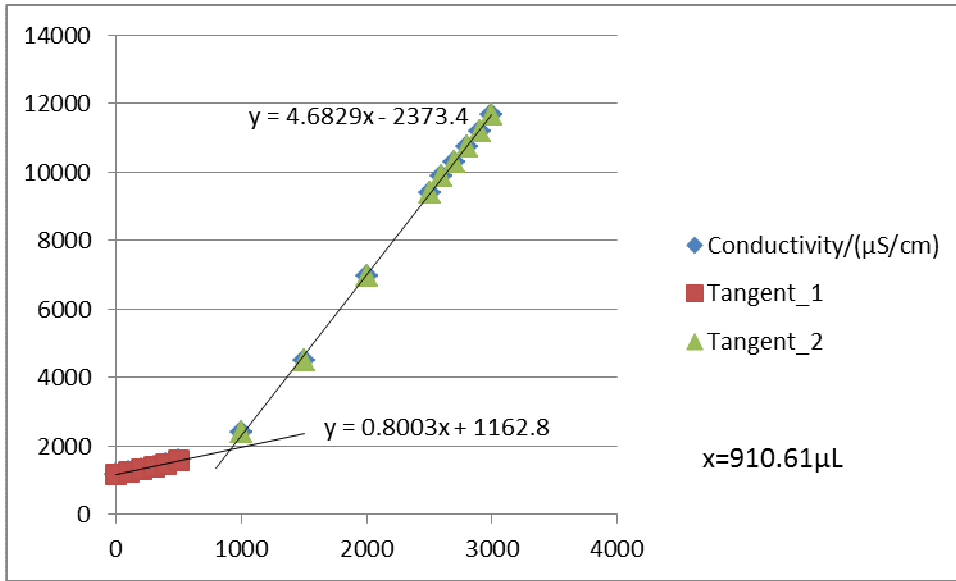**F46: Titration Curves for 0.07915 mol/L MEA First Run at 313 K**
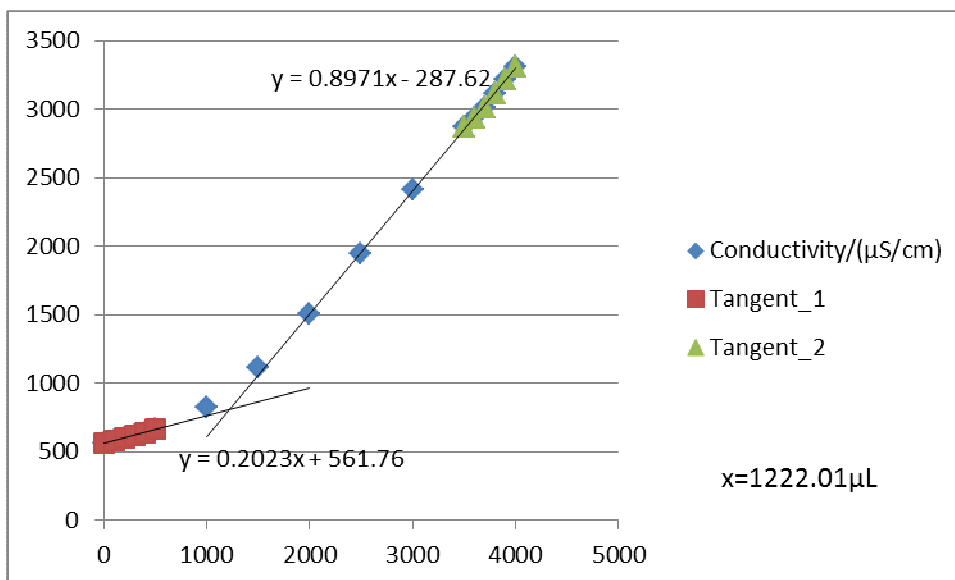
Figure F46-1: Titration 1 for 0.07915 mol/L MEA First Run

220
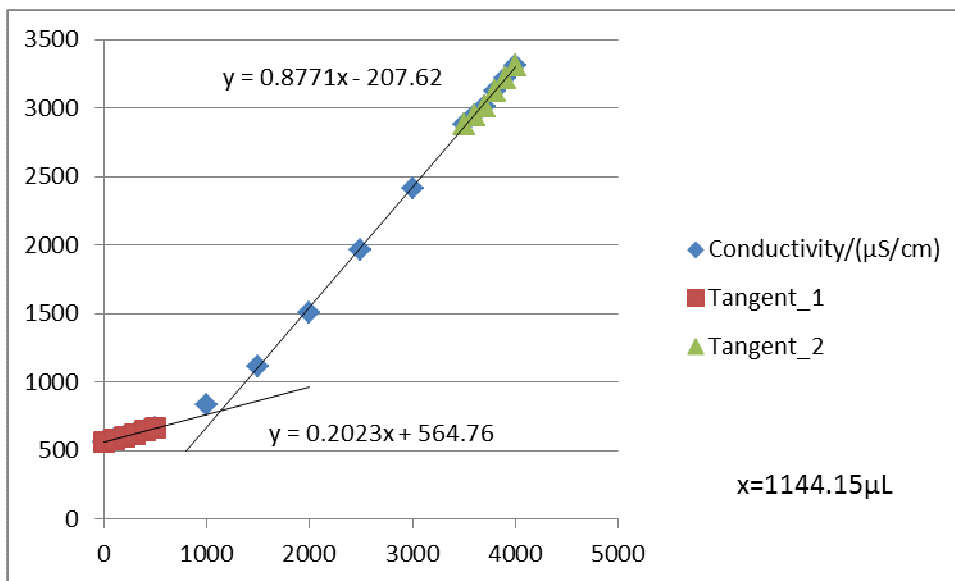
Figure F46-2: Titration 2 for 0.07915 mol/L MEA First Run
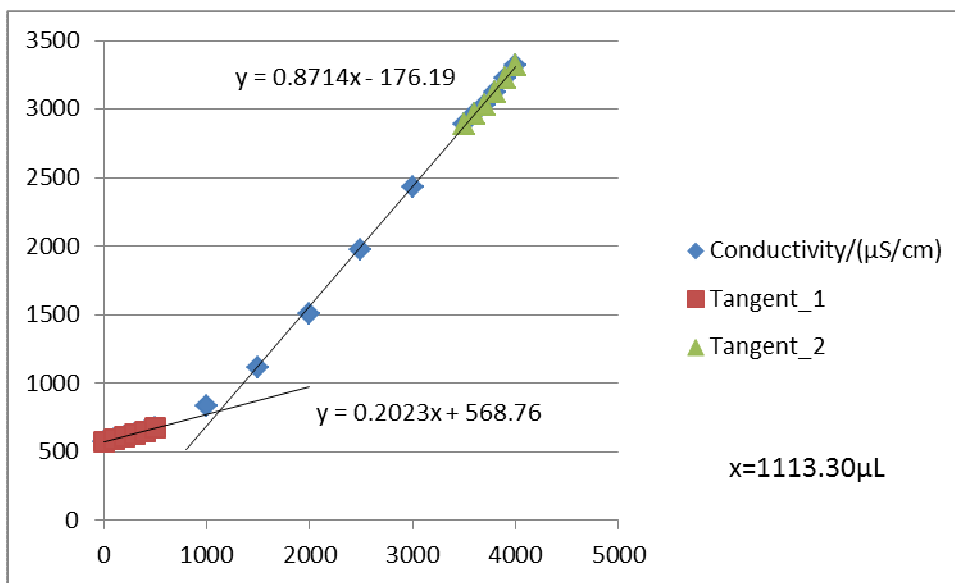
Figure F46-3: Titration 3 for 0.07915 mol/L MEA First Run

221

F47: Titration Curves for 0.07915 mol/L MEA Second Run at 313 K
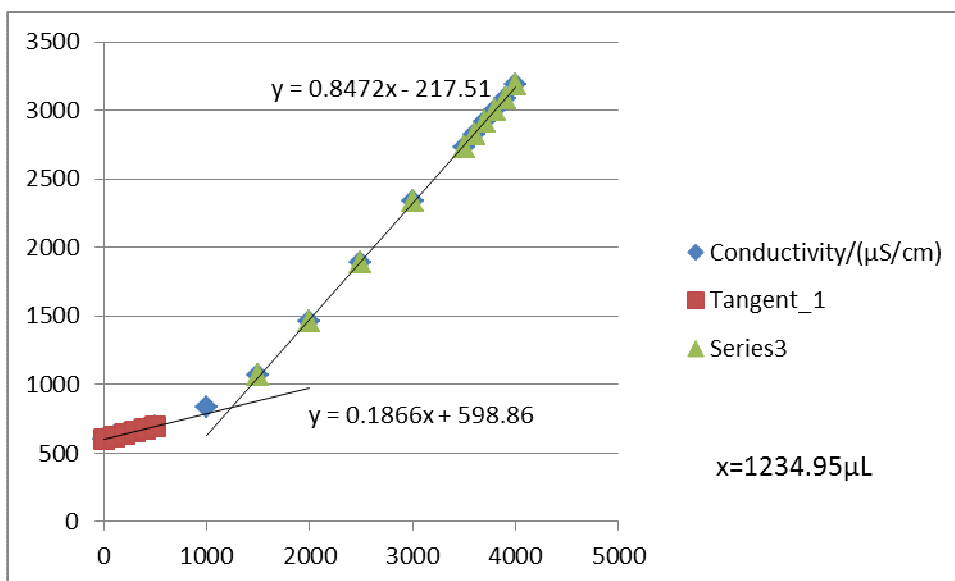
Figure F47-1: Titration 1 for 0.07915 mol/L MEA Second Run
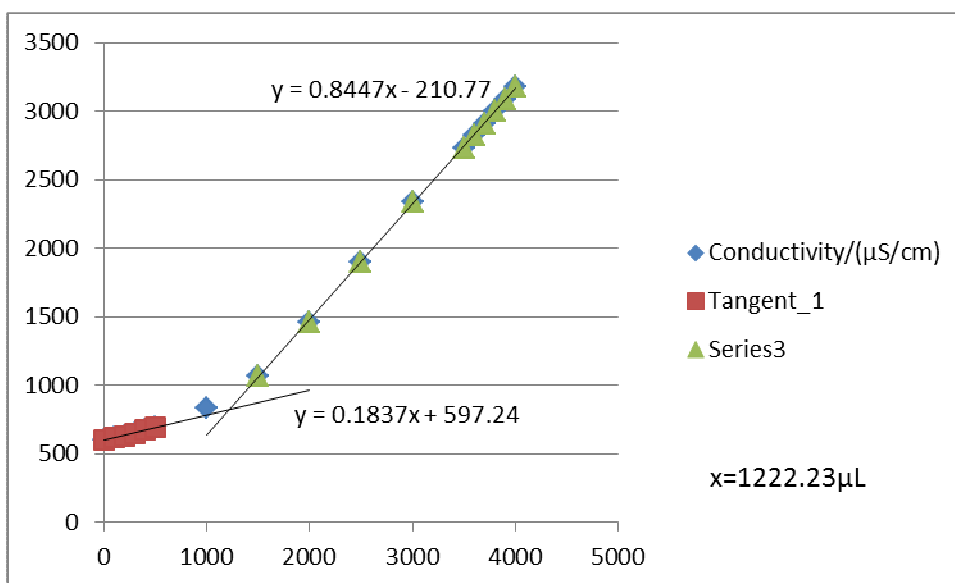
Figure F47-2: Titration 2 for 0.07915 mol/L MEA Second Run

$y = 0.8501x - 225.57$

$y = 0.1866x + 599.86$

x=1242.92µL
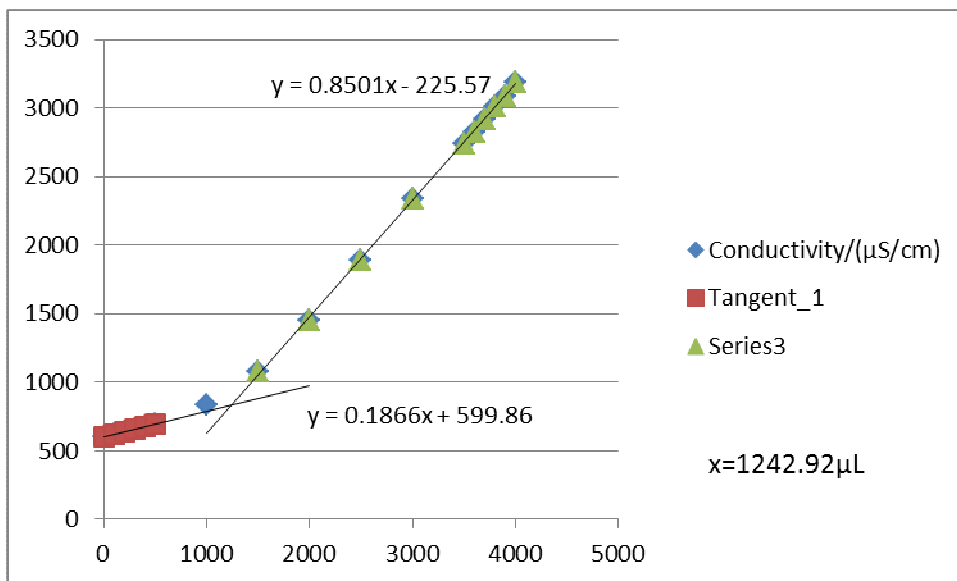
Figure F47-3: Titration 3 for 0.07915 mol/L MEA Second Run

F48: Titration Curves for 0.07915 mol/L MEA Third Run at 313 K

$y = 0.9042x - 301.15$

$y = 0.1949x + 558.95$

x=1211.27µL
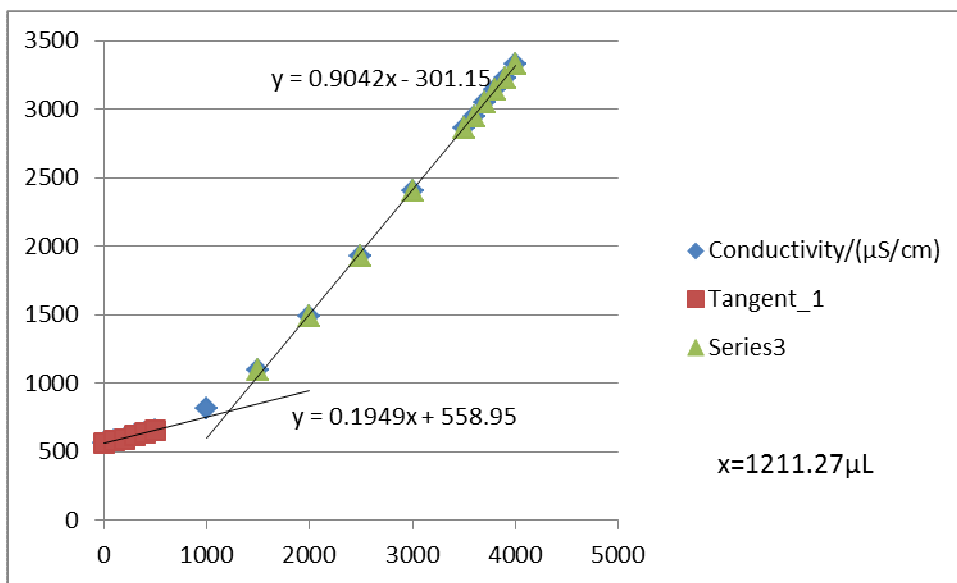
Figure F48-1: Titration 1 for 0.07915 mol/L MEA Third Run
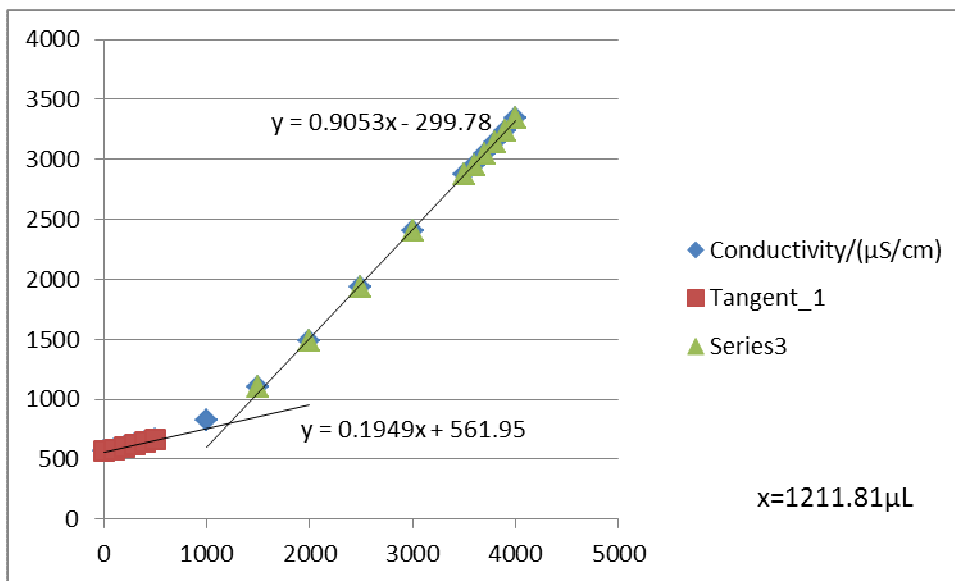
Figure F48-2: Titration 2 for 0.07915 mol/L MEA Third Run
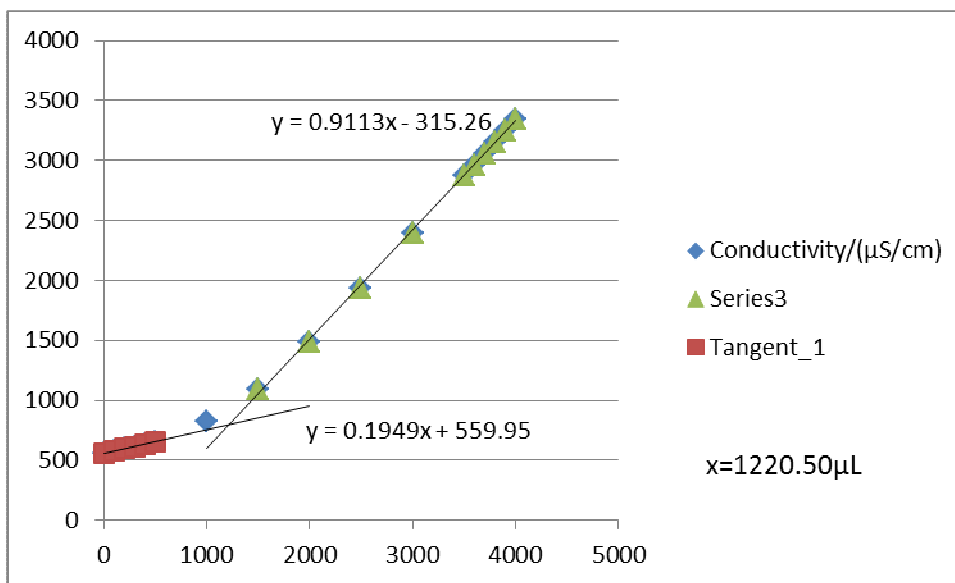
Figure F48-3: Titration 3 for 0.07915 mol/L MEA Third Run

224

F49: Titration Curves for 0.1184 mol/L MEA First Run at 313 K
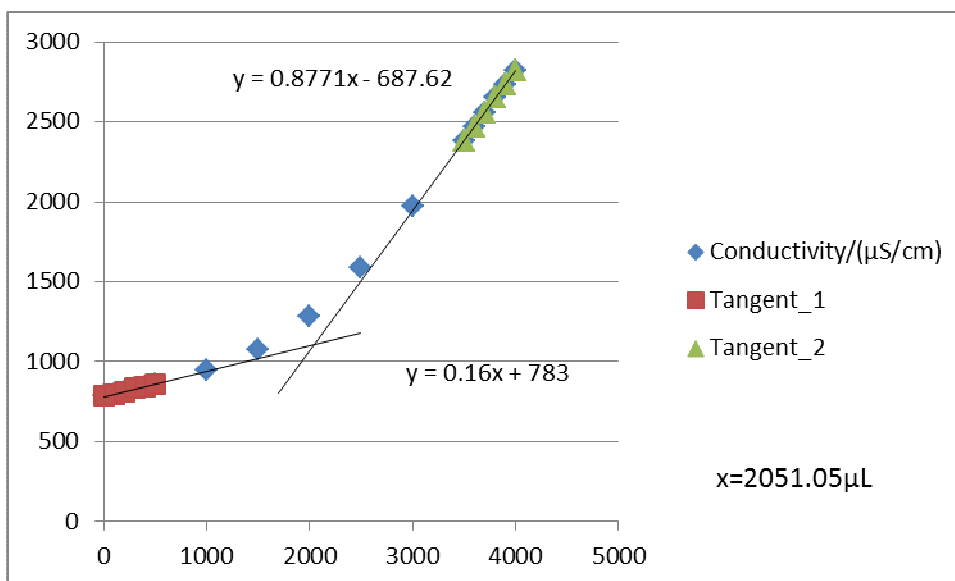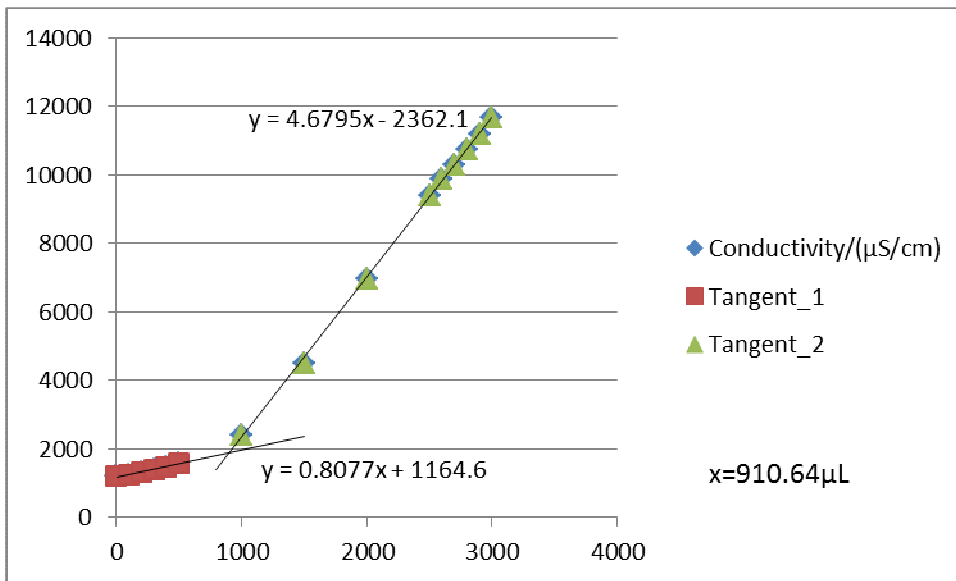

Figure F49-1: Titration 1 for 0.1184 mol/L MEA First Run
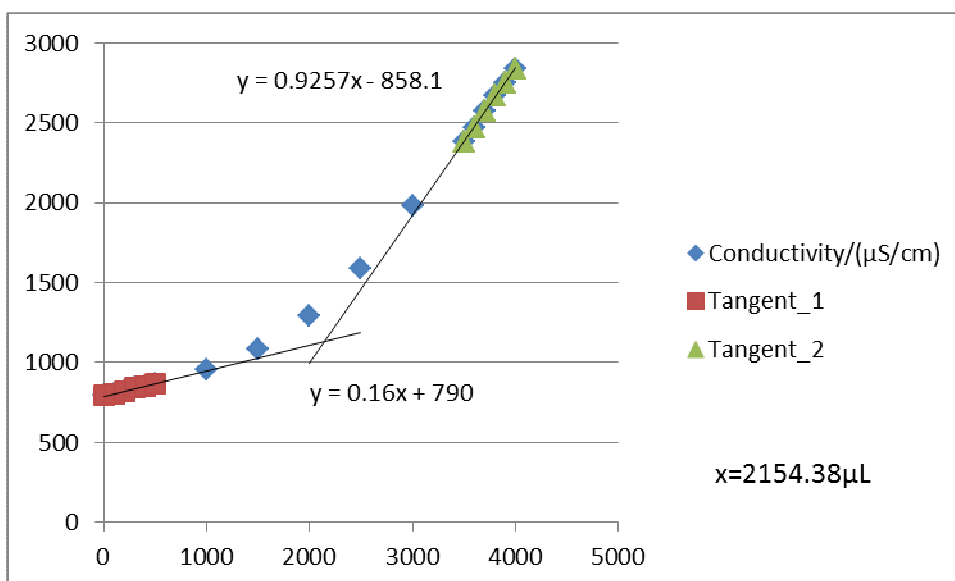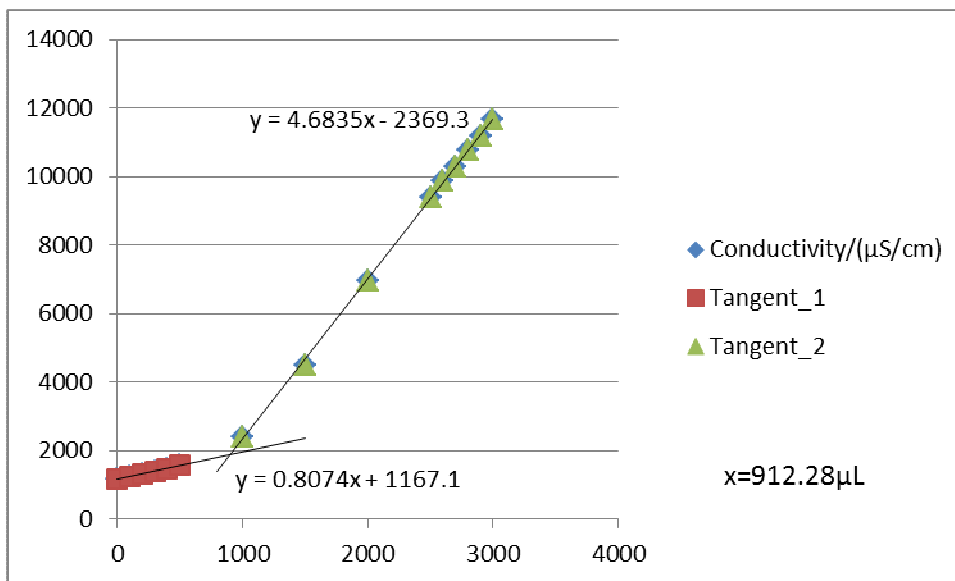

Figure F49-2: Titration 2 for 0.1184 mol/L MEA First Run

225
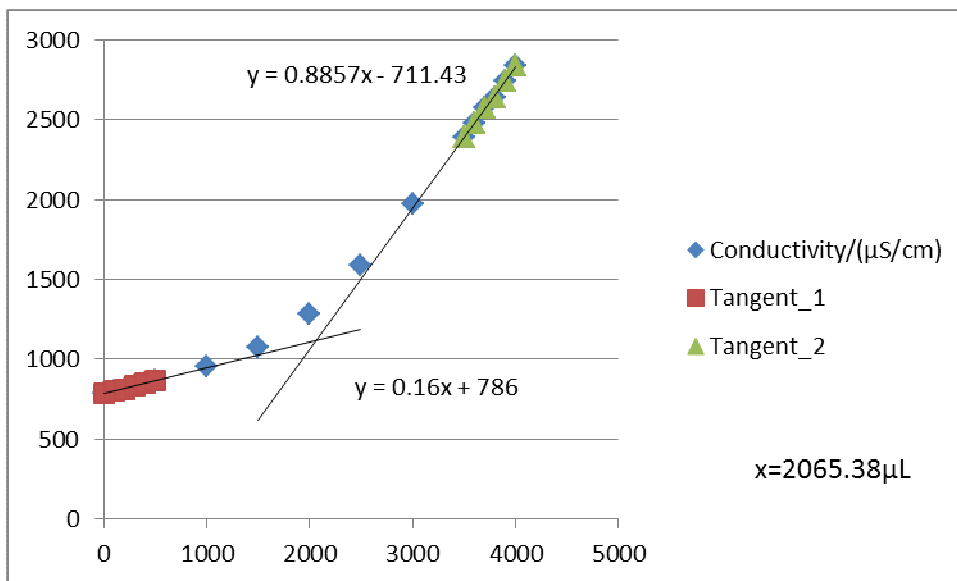
Figure F49-3: Titration 3 for 0.1184 mol/L MEA First Run

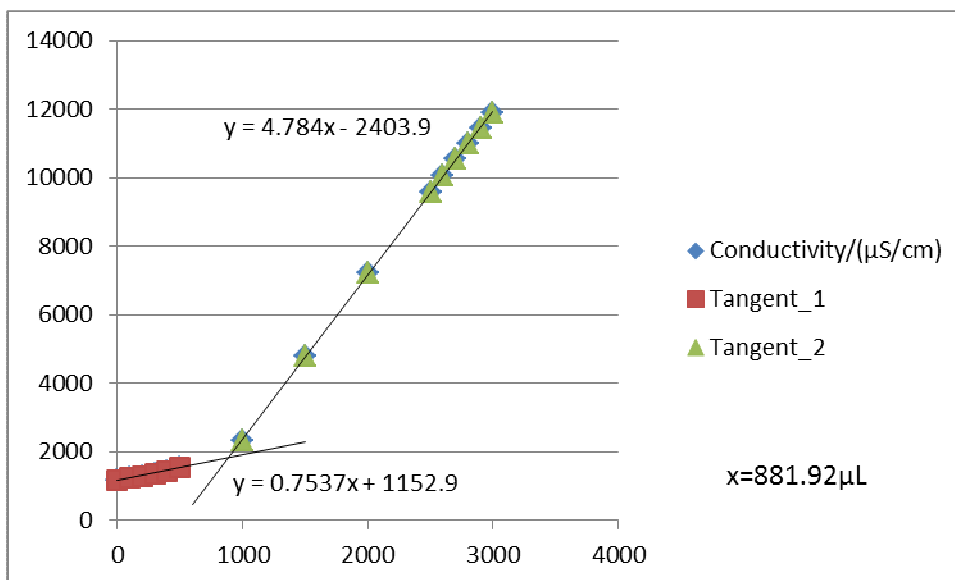## F50: Titration Curves for 0.1184 mol/L MEA Second Run at 313 K
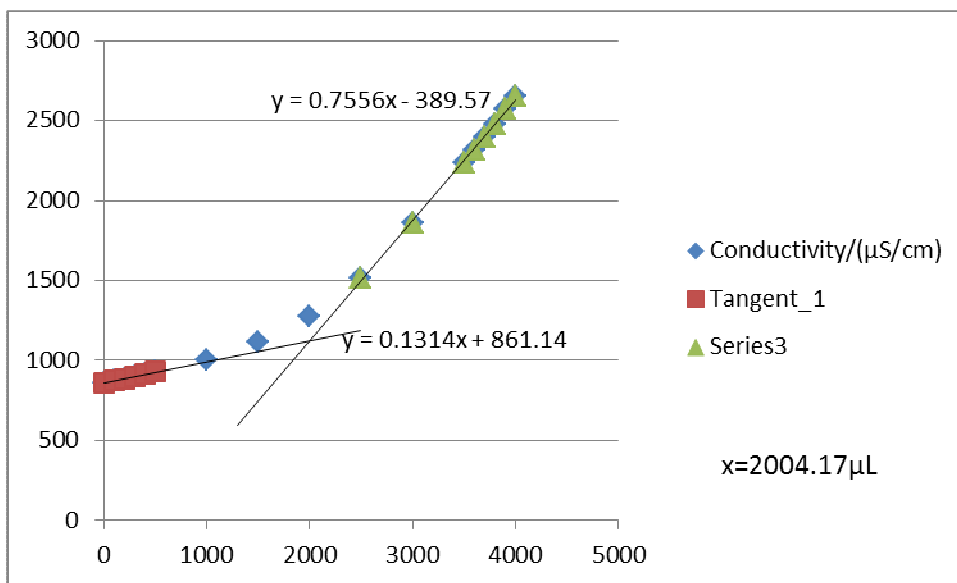
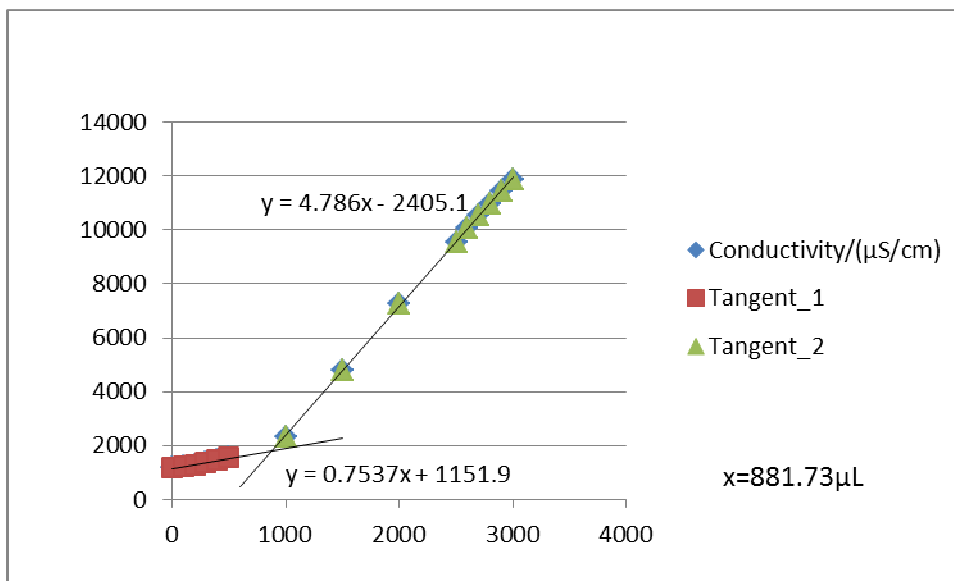Figure F50-1: Titration 1 for 0.1184 mol/L MEA Second Run
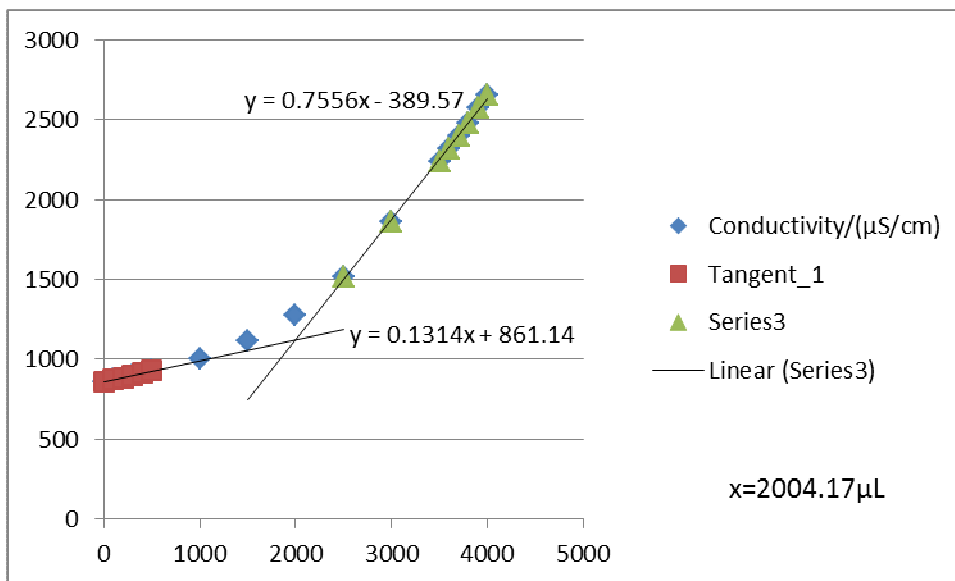
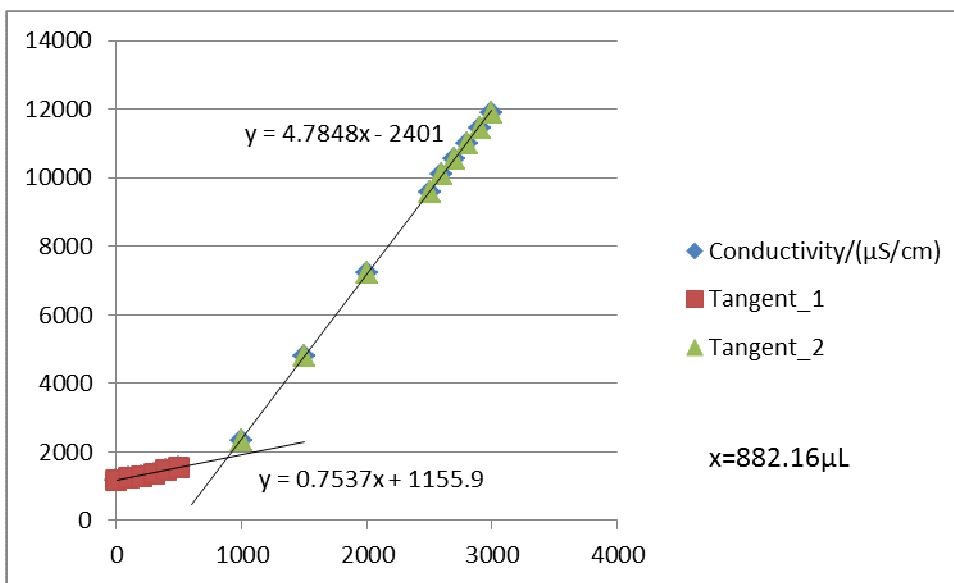Figure F50-2: Titration 2 for 0.1184 mol/L MEA Second Run
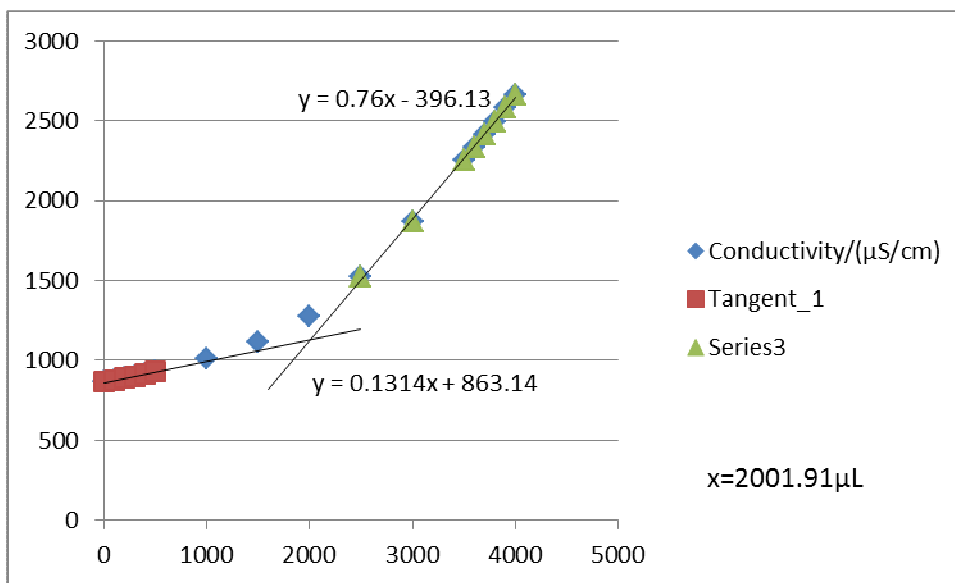
Figure F50-3: Titration 3 for 0.1184 mol/L MEA Second Run

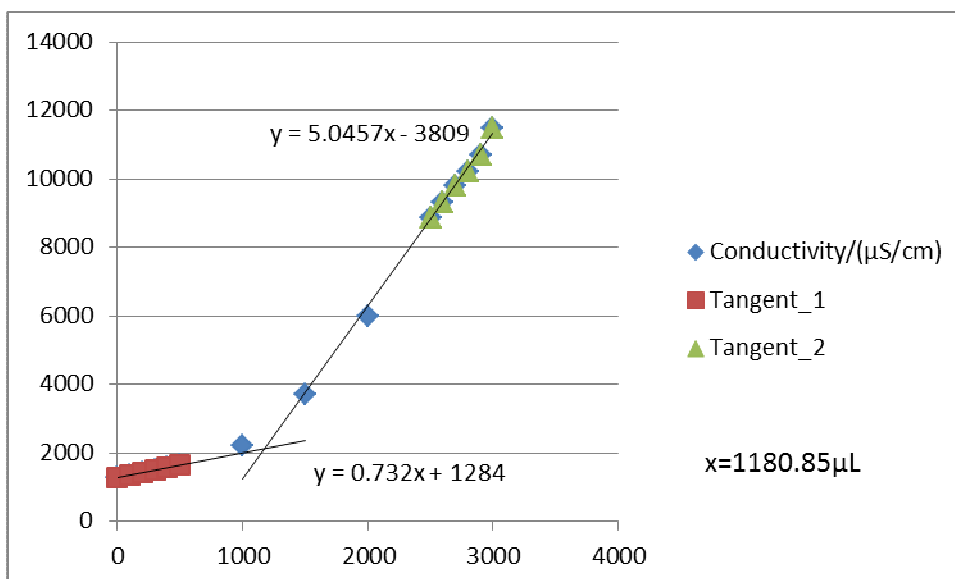**F51: Titration Curves for 0.1184 mol/L MEA Third Run at 313 K**
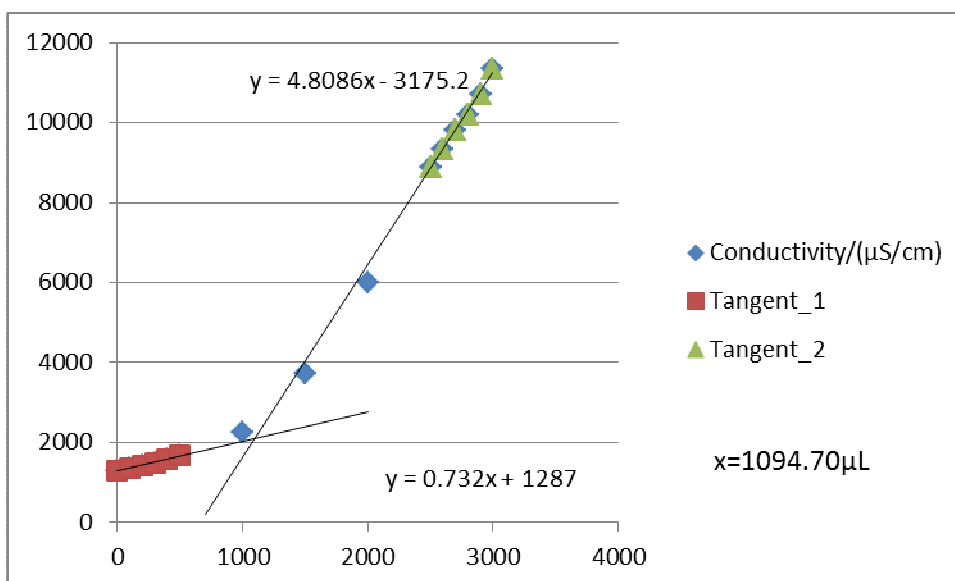

Figure F51-1: Titration 1 for 0.1184 mol/L MEA Third Run

Figure F51-2: Titration 2 for 0.1184 mol/L MEA Third Run

228

Figure F51-3: Titration 3 for 0.1184 mol/L MEA Third Run

F52: Titration Curves for 0.1575 mol/L MEA First Run at 313 K

Figure F52-1: Titration 1 for 0.1575 mol/L MEA First Run

229

Figure F52-2: Titration 2 for 0.1575 mol/L MEA First Run

Figure F52-3: Titration 3 for 0.1575 mol/L MEA First Run

F53: Titration Curves for 0.1575 mol/L MEA Second Run at 313 K

Figure F53-1: Titration 1 for 0.1575 mol/L MEA Second Run

Figure F53-2: Titration 2 for 0.1575 mol/L MEA Second Run

231

Figure F53-3: Titration 3 for 0.1575 mol/L MEA Second Run

F54: Titration Curves for 0.1575 mol/L MEA Third Run at 313 K

Figure F54-1: Titration 1 for 0.1575 mol/L MEA Third Run

232

Figure F54-2: Titration 2 for 0.1575 mol/L MEA Third Run

Figure F54-3: Titration 3 for 0.1575 mol/L MEA Third Run

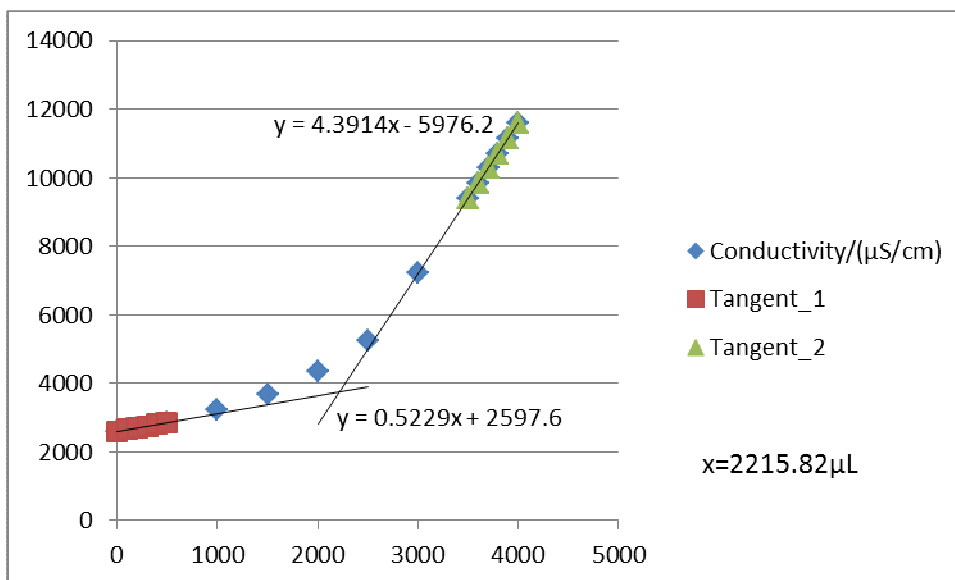**F55: Titration Curves for 0.1965 mol/L MEA First Run at 313 K**
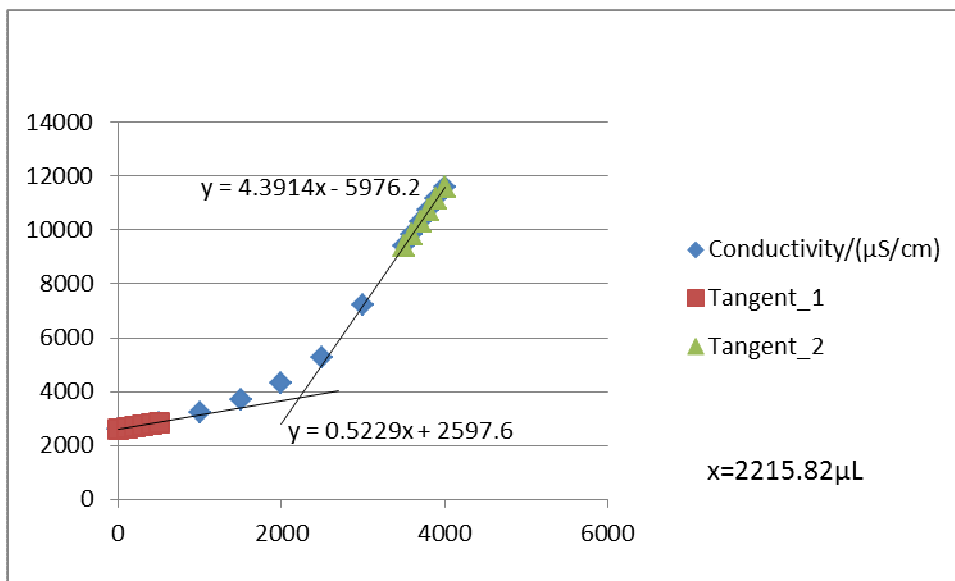

Figure F55-1: Titration 1 for 0.1965 mol/L MEA First Run
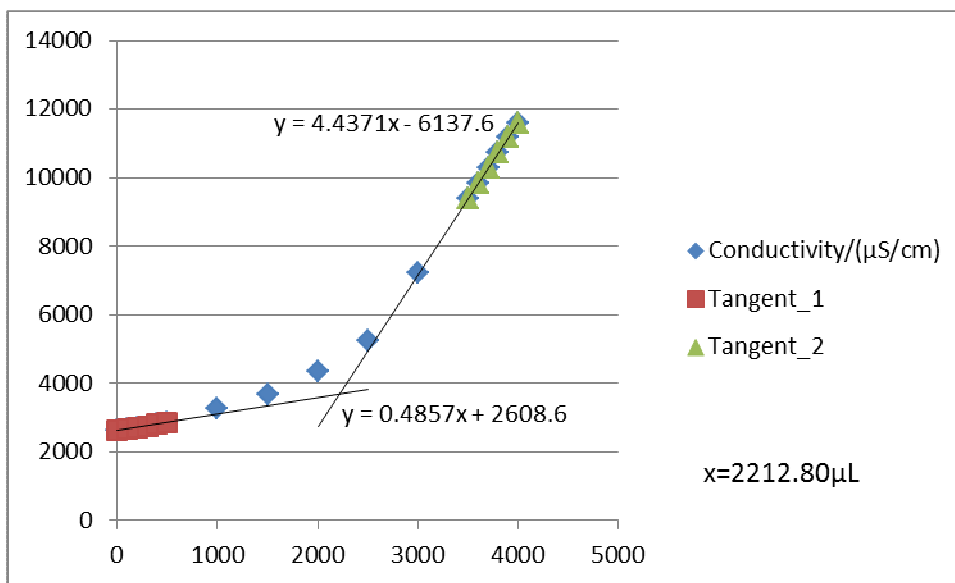

Figure F55-2: Titration 2 for 0.1965 mol/L MEA First Run

234

Figure F55-3: Titration 3 for 0.1965 mol/L MEA First Run

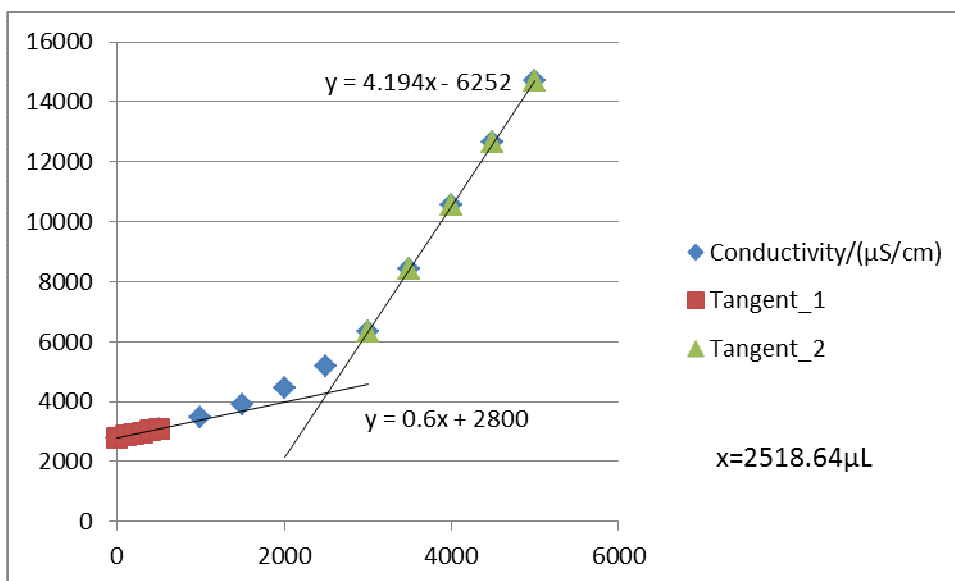**F56: Titration Curves for 0.1965 mol/L MEA Second Run at 313 K**

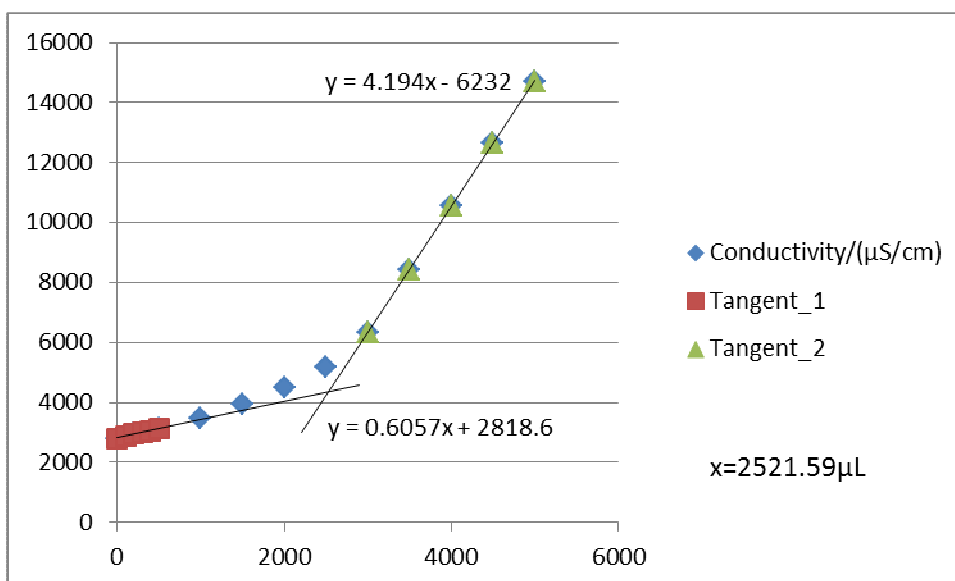

Figure F56-1: Titration 1 for 0.1965 mol/L MEA Second Run

235

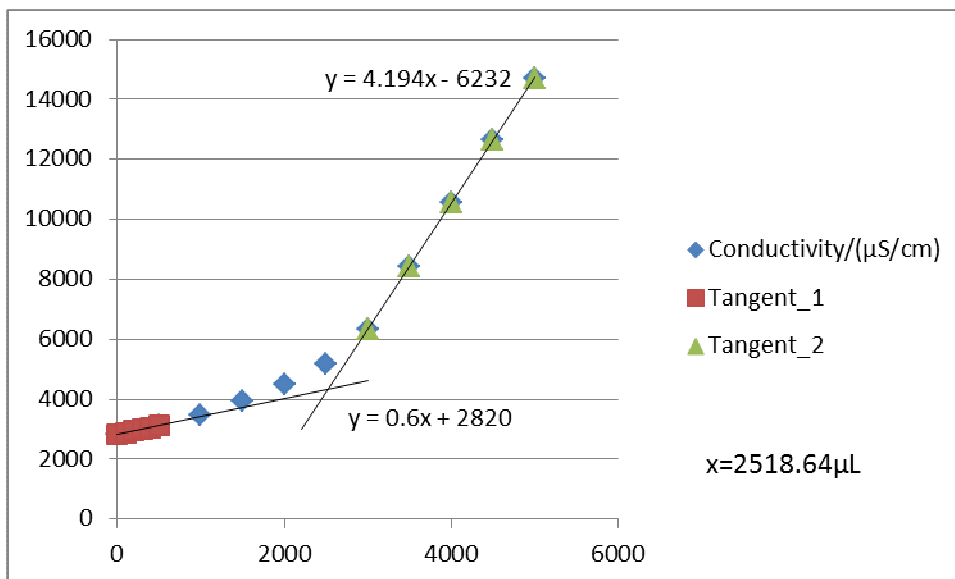Figure F56-2: Titration 2 for 0.1965 mol/L MEA Second Run

Figure F56-3: Titration 3 for 0.1965 mol/L MEA Second Run

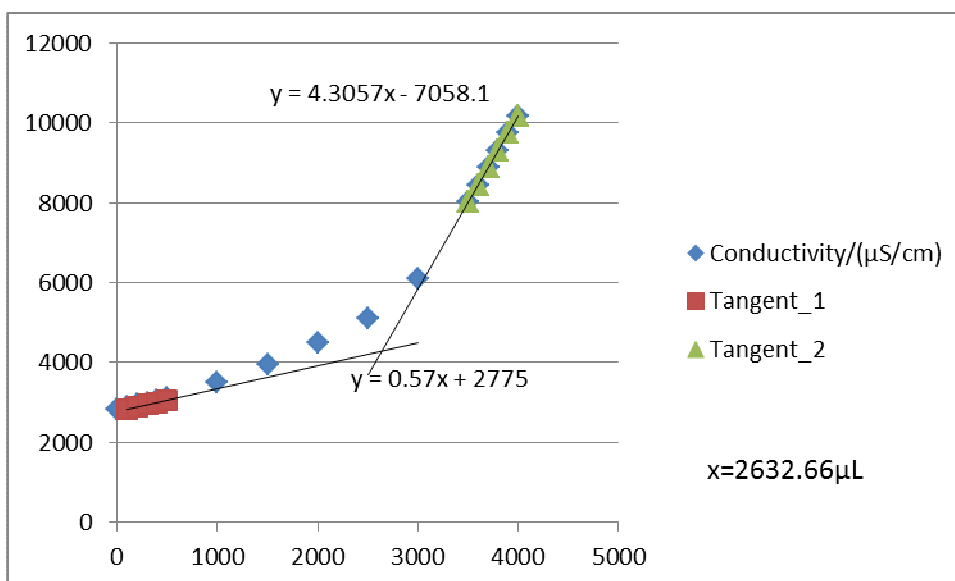**F57: Titration Curves for 0.1965 mol/L MEA Third Run at 313 K**

Figure F57-1: Titration 1 for 0.1965 mol/L MEA Third Run

Figure F57-2: Titration 2 for 0.1965 mol/L MEA Third Run

Figure F57-3: Titration 3 for 0.1965 mol/L MEA Third Run

F58: Titration Curves for 0.2609 mol/L MEA First Run at 313 K

Figure F58-1: Titration 1 for 0.2609 mol/L MEA First Run

Figure F58-2: Titration 2 for 0.2609 mol/L MEA First Run

Figure F58-3: Titration 3 for 0.2609 mol/L MEA First Run

F59: Titration Curves for 0.2609 mol/L MEA Second Run at 313 K

Figure F59-1: Titration 1 for 0.2609 mol/L MEA Second Run

Figure F59-2: Titration 2 for 0.2609 mol/L MEA Second Run

240

Figure F59-3: Titration 3 for 0.2609 mol/L MEA Second Run

F60: Titration Curves for 0.2609 mol/L MEA Third Run at 313 K
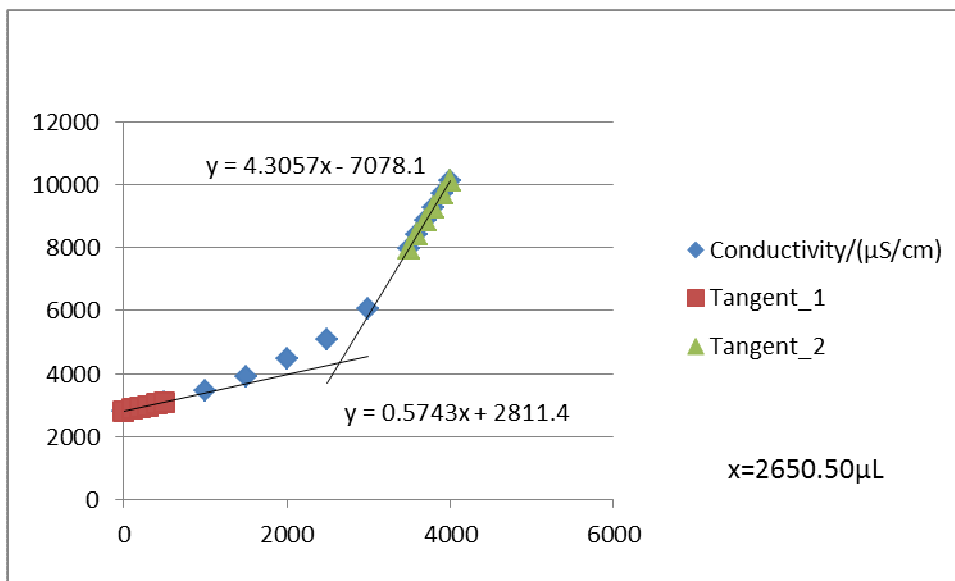

Figure F60-1: Titration 1 for 0.2609 mol/L MEA Third Run

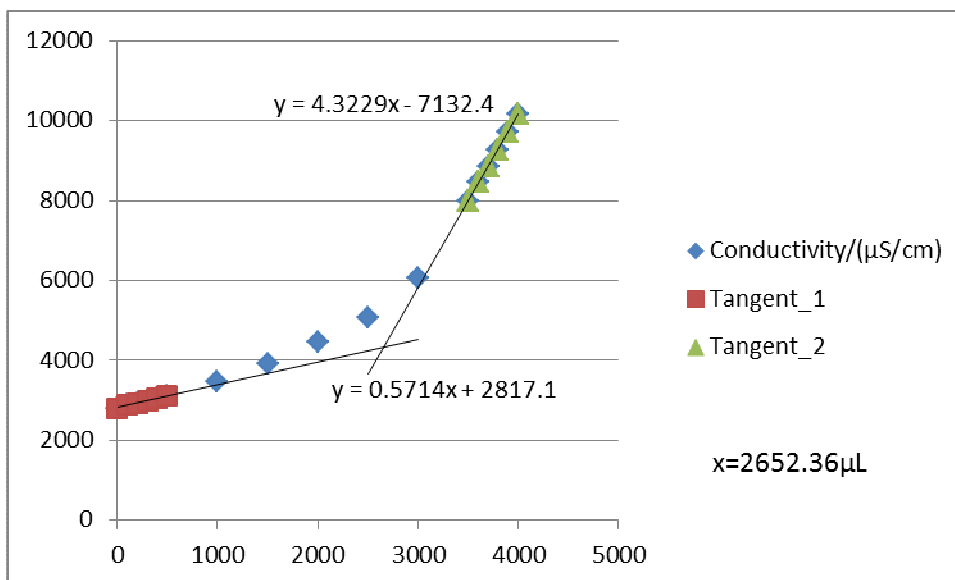Figure F60-2: Titration 2 for 0.2609 mol/L MEA Third Run

Figure F60-3: Titration 3 for 0.2609 mol/L MEA Third Run

APPENDIX G: TITRATION CURVES FOR SECOND SERIES RUNS

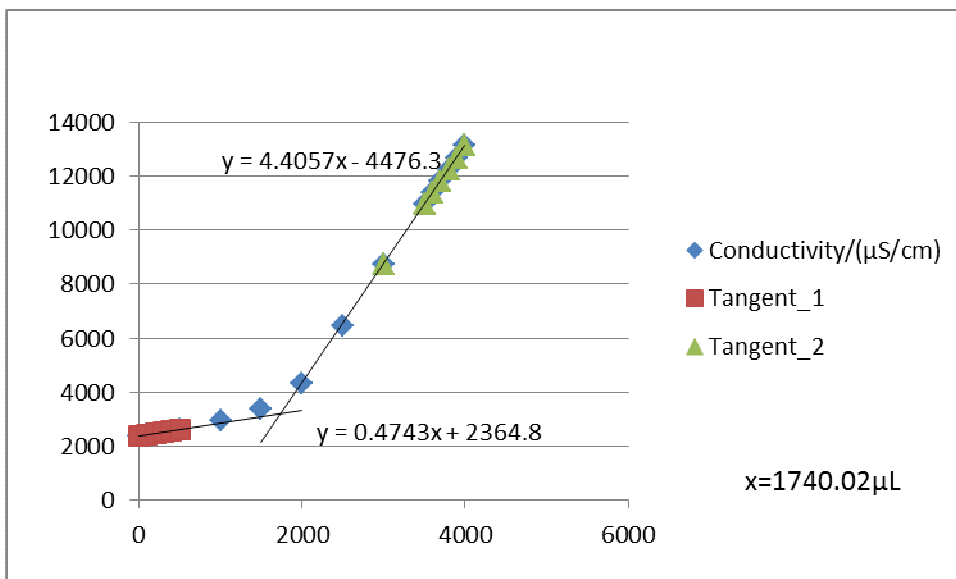## G1: Titration Curves for 0.01986 mol/L MEA First Run at 298 K

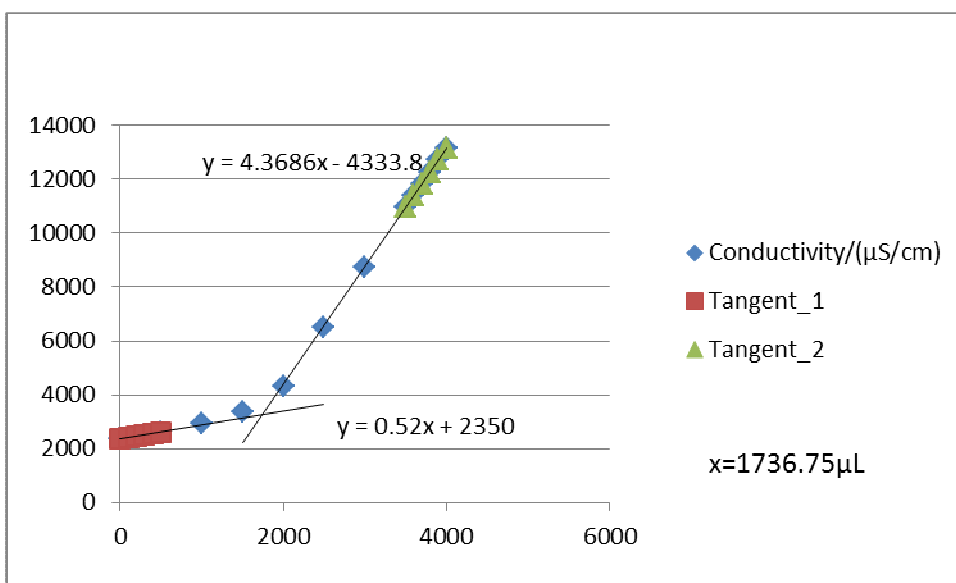
Figure G1-1 Titration 1 for 0.01986 mol/L MEA First Run
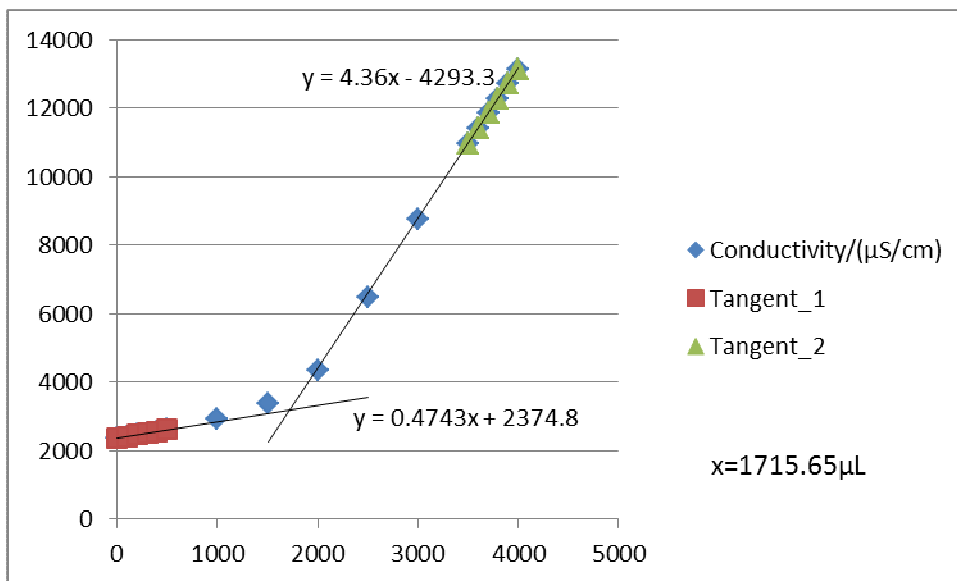

Figure G1-2 Titration 2 for 0.01986 mol/L MEA First Run

Figure G1-3 Titration 3 for 0.01986 mol/L MEA First Run

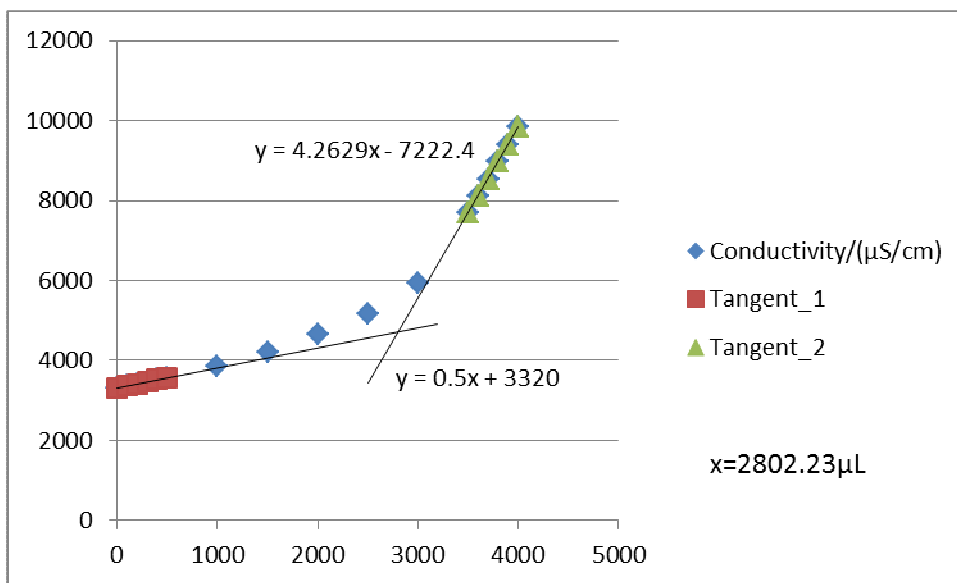## G2: Titration Curves for 0.01986 mol/L MEA Second Run at 298 K

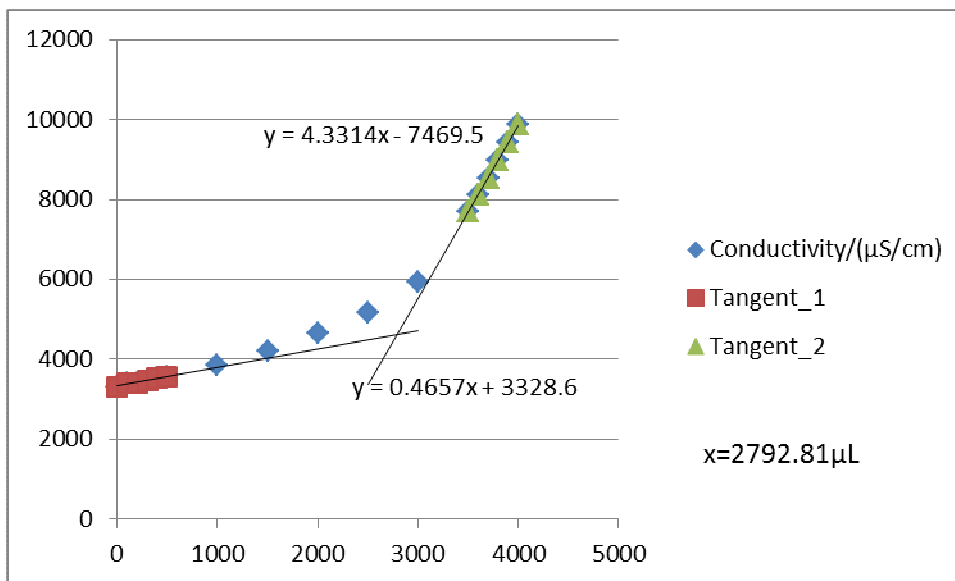Figure G2-1 Titration 1 for 0.01986 mol/L MEA Second Run

244

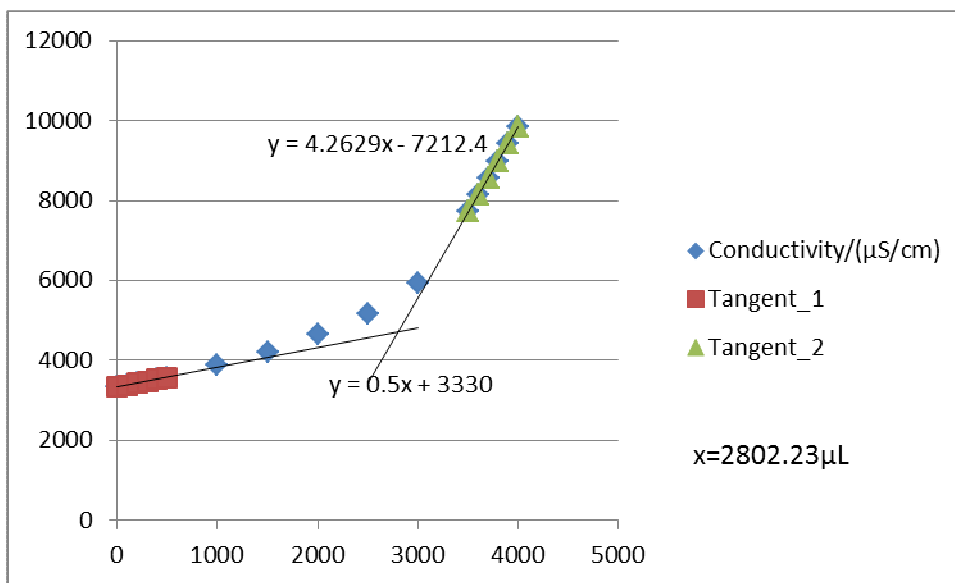Figure G2-2 Titration 2 for 0.01986 mol/L MEA Second Run
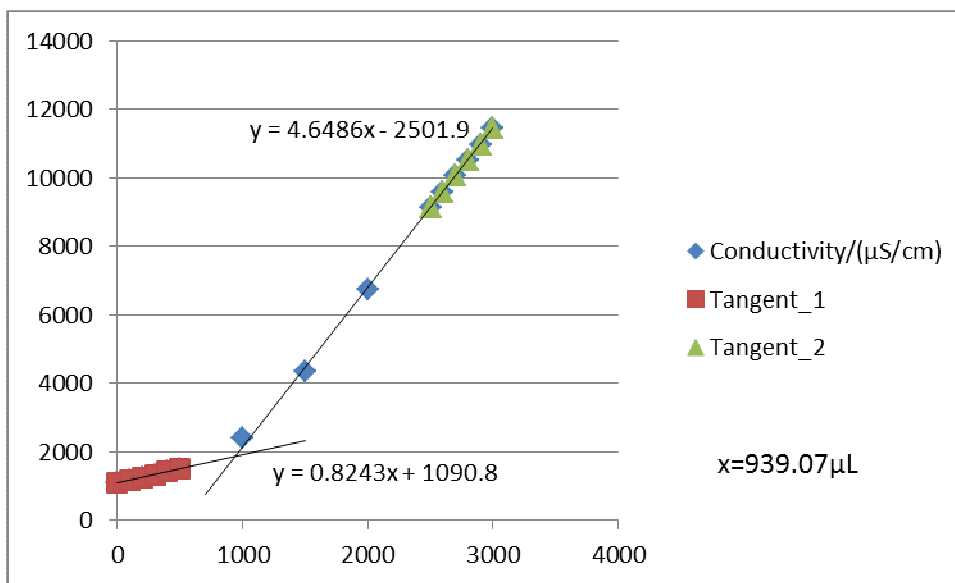
Figure G2-3 Titration 3 for 0.01986 mol/L MEA Second Run

G3: Titration Curves for 0.01986 mol/L MEA Third Run at 298 K

Figure G3-1 Titration 1 for 0.01986 mol/L MEA Third Run

Figure G3-2 Titration 2 for 0.01986 mol/L MEA Third Run

Figure G3-3 Titration 3 for 0.01986 mol/L MEA Third Run

G4: Titration Curves for 0.04956 mol/L MEA First Run at 298 K

Figure G4-1 Titration 1 for 0.04956 mol/L MEA First Run

247

Figure G4-2 Titration 2 for 0.04956 mol/L MEA First Run

Figure G4-3 Titration 3 for 0.04956 mol/L MEA First Run

G5: Titration Curves for 0.04956 mol/L MEA Second Run at 298 K

Figure G5-1 Titration 1 for 0.04956 mol/L MEA Second Run

Figure G5-2 Titration 2 for 0.04956 mol/L MEA Second Run

249

Figure G5-3 Titration 3 for 0.04956 mol/L MEA Second Run

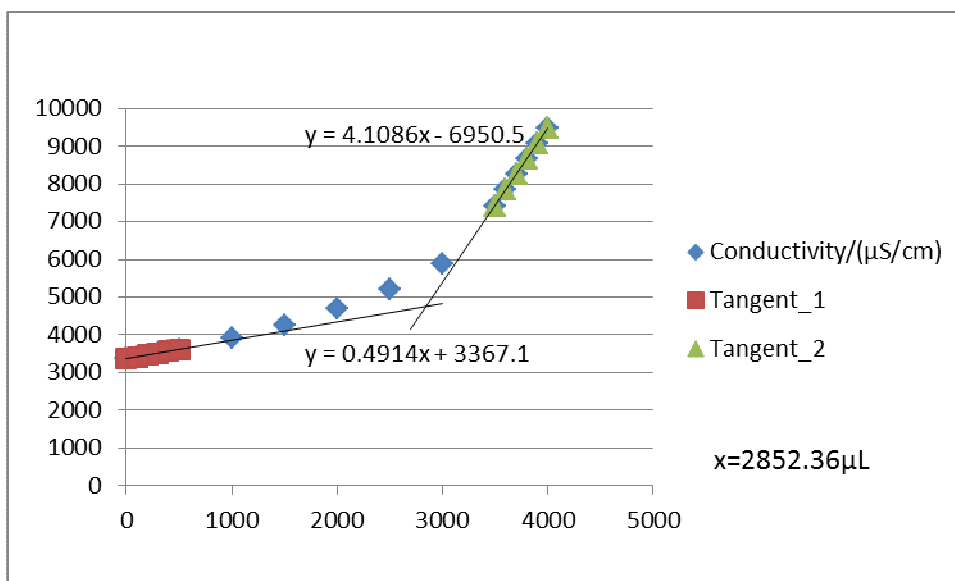## G6: Titration Curves for 0.04956 mol/L MEA Third Run at 298 K

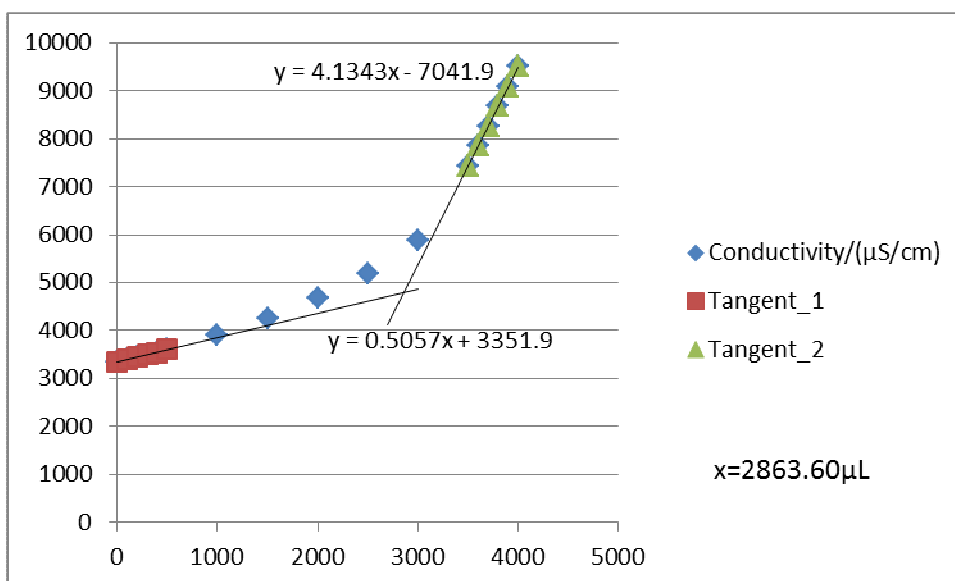
Figure G6-1 Titration 1 for 0.04956 mol/L MEA Third Run

250

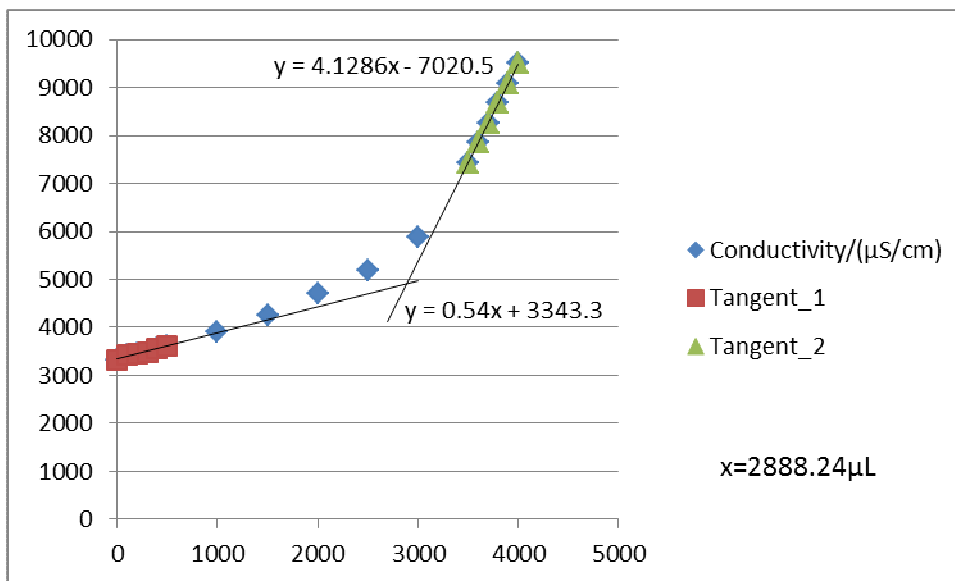Figure G6-2 Titration 2 for 0.04956 mol/L MEA Third Run

Figure G6-3 Titration 3 for 0.04956 mol/L MEA Third Run

251

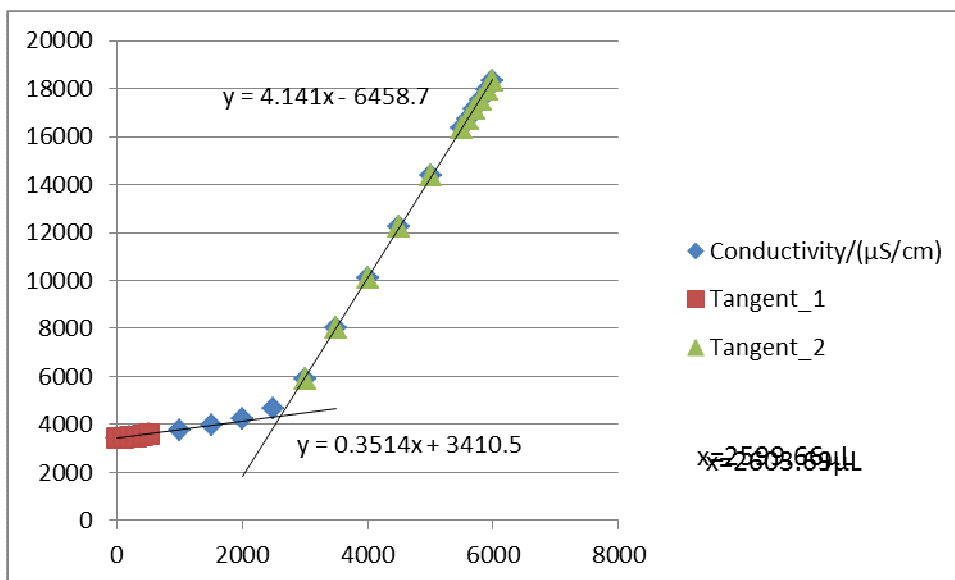**G7: Titration Curves for 0.07915 mol/L MEA First Run at 298 K**

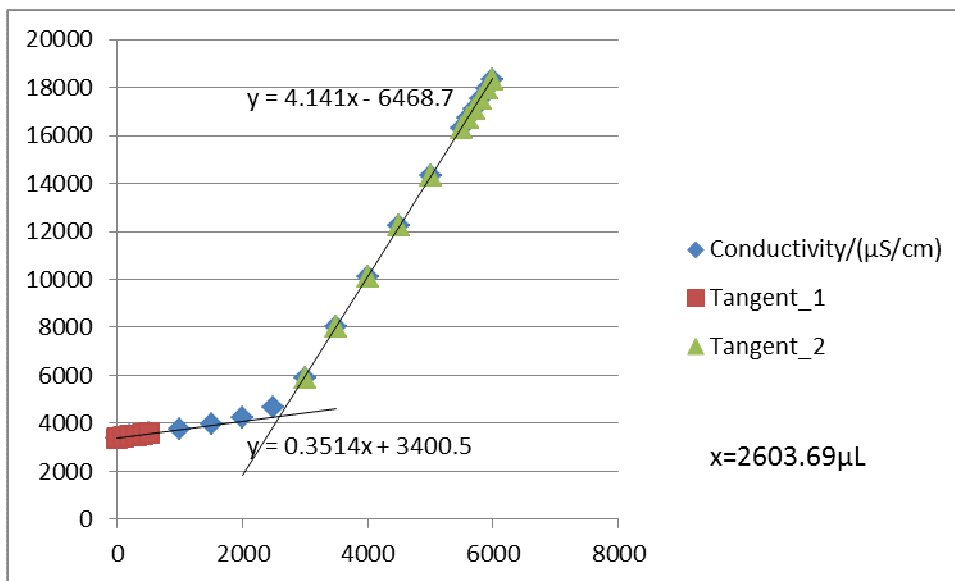Figure G7-1 Titration 1 for 0.07915 mol/L MEA First Run

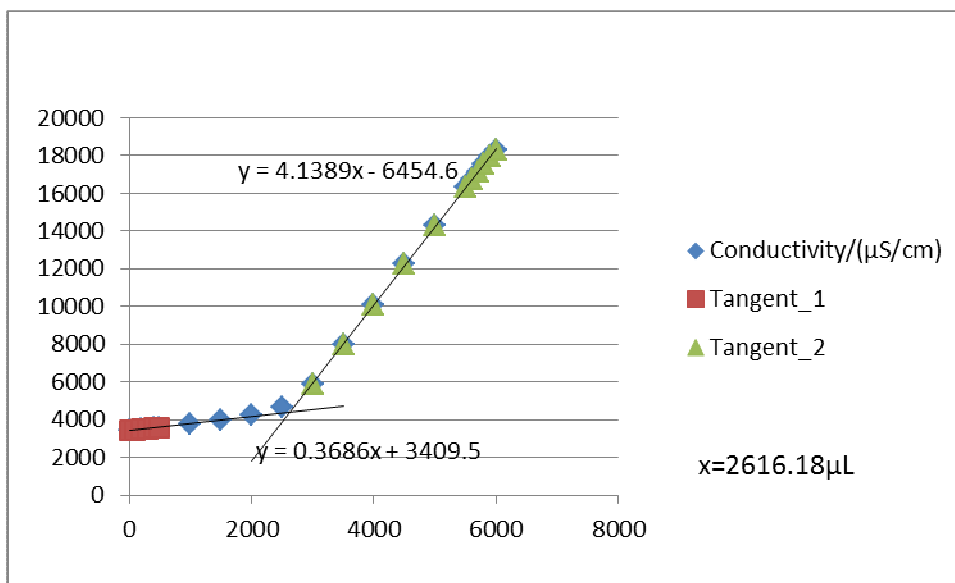Figure G7-2 Titration 2 for 0.07915 mol/L MEA First Run

252

Figure G7-3 Titration 3 for 0.07915 mol/L MEA First Run

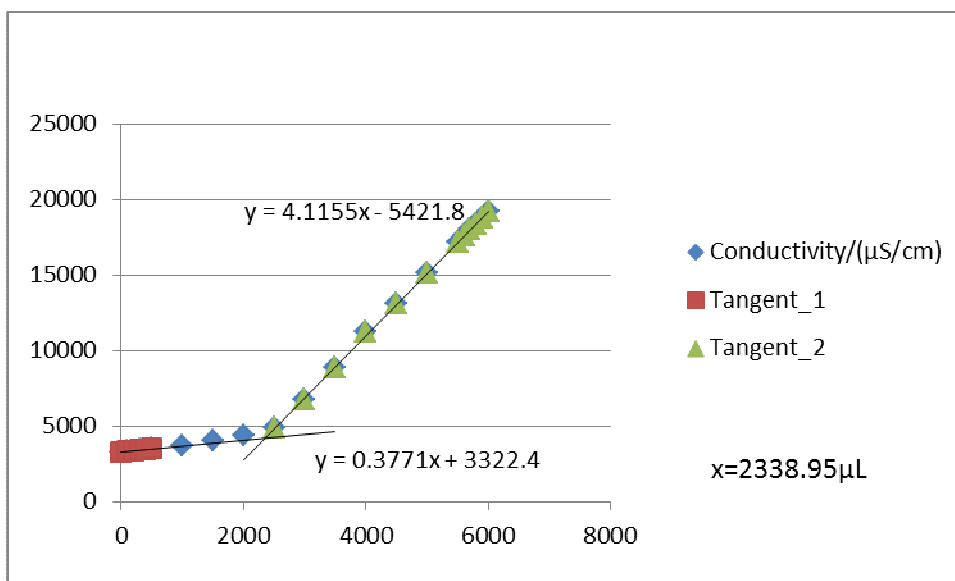**G8: Titration Curves for 0.07915 mol/L MEA Second Run at 298 K**

Figure G8-1 Titration 1 for 0.07915 mol/L MEA Second Run

253

Figure G8-2 Titration 2 for 0.07915 mol/L MEA Second Run

Figure G8-3 Titration 3 for 0.07915 mol/L MEA Second Run

254

G9: Titration Curves for 0.07915 mol/L MEA Third Run at 298 K

Figure G9-1 Titration 1 for 0.07915 mol/L MEA Third Run

Figure G9-2 Titration 2 for 0.07915 mol/L MEA Third Run

255

Figure G9-3 Titration 3 for 0.07915 mol/L MEA Third Run

G10: Titration Curves for 0.1184 mol/L MEA First Run at 298 K

Figure G10-1 Titration 1 for 0.1184 mol/L MEA First Run

256

Figure G10-2 Titration 2 for 0.1184 mol/L MEA First Run

Figure G10-3 Titration 3 for 0.1184 mol/L MEA First Run

G11: Titration Curves for 0.1184 mol/L MEA Second Run at 298 K

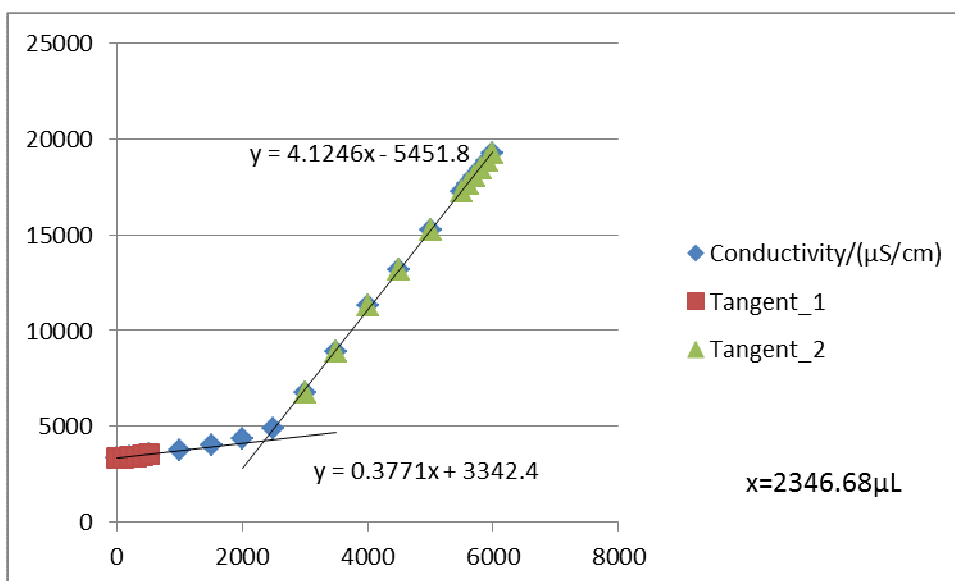Figure G11-1 Titration 1 for 0.1184 mol/L MEA Second Run

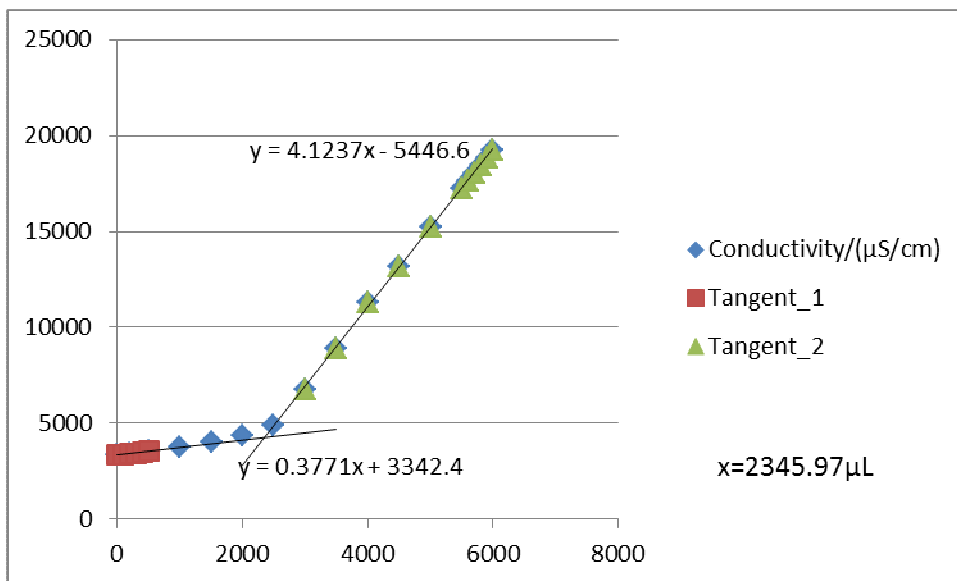Figure G11-2 Titration 2 for 0.1184 mol/L MEA Second Run

258
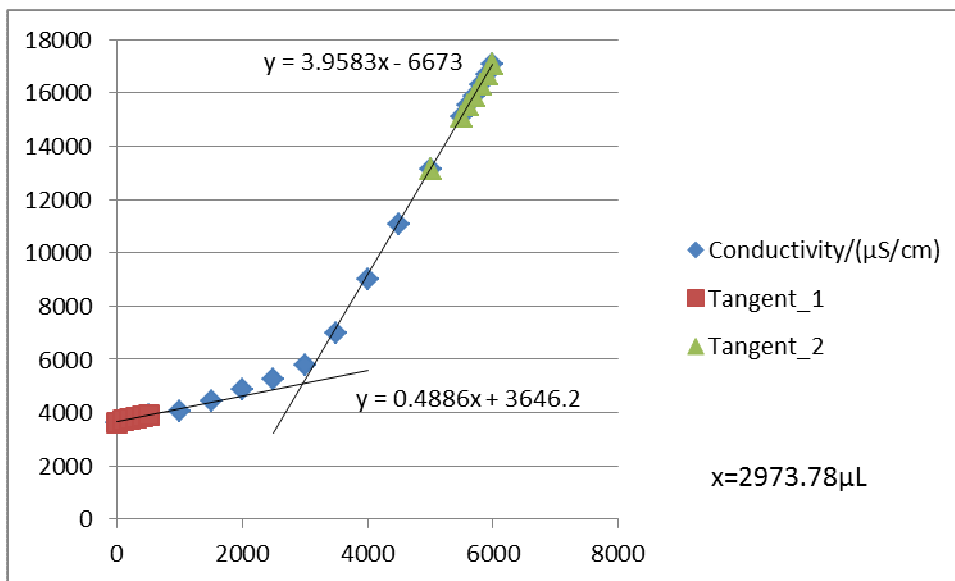
Figure G11-3 Titration 3 for 0.1184 mol/L MEA Second Run

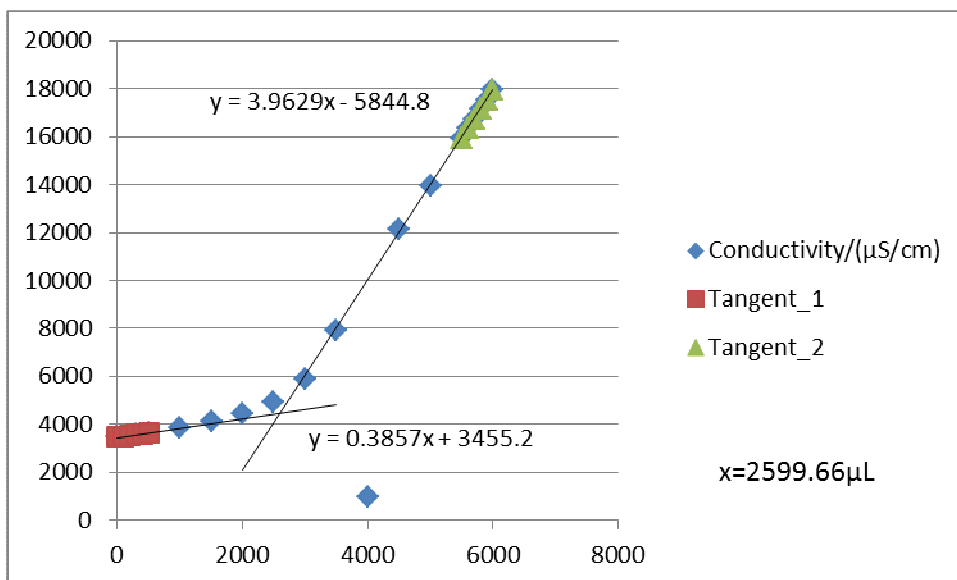**G12: Titration Curves for 0.1184 mol/L MEA Third Run at 298 K**

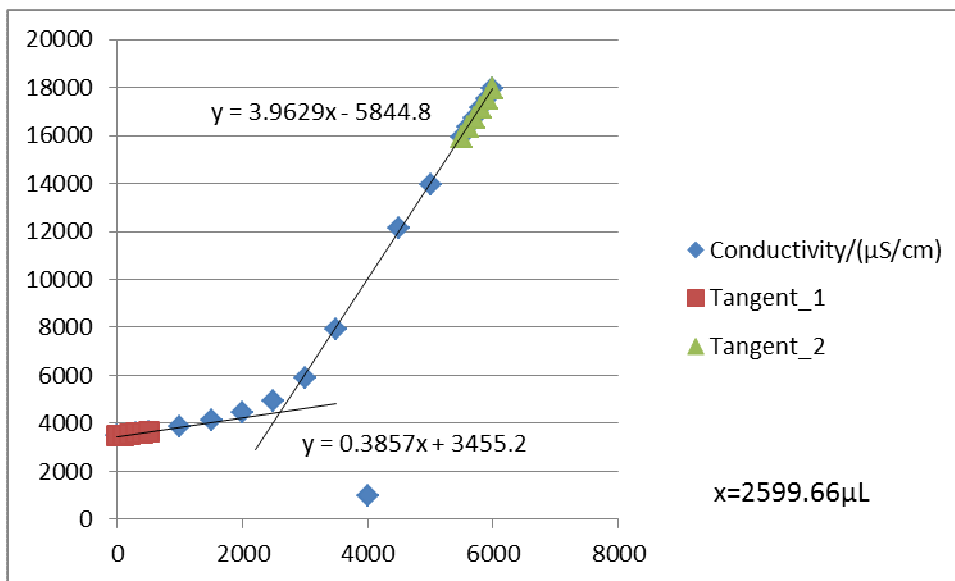

Figure G12-1 Titration 1 for 0.1184 mol/L MEA Third Run

259
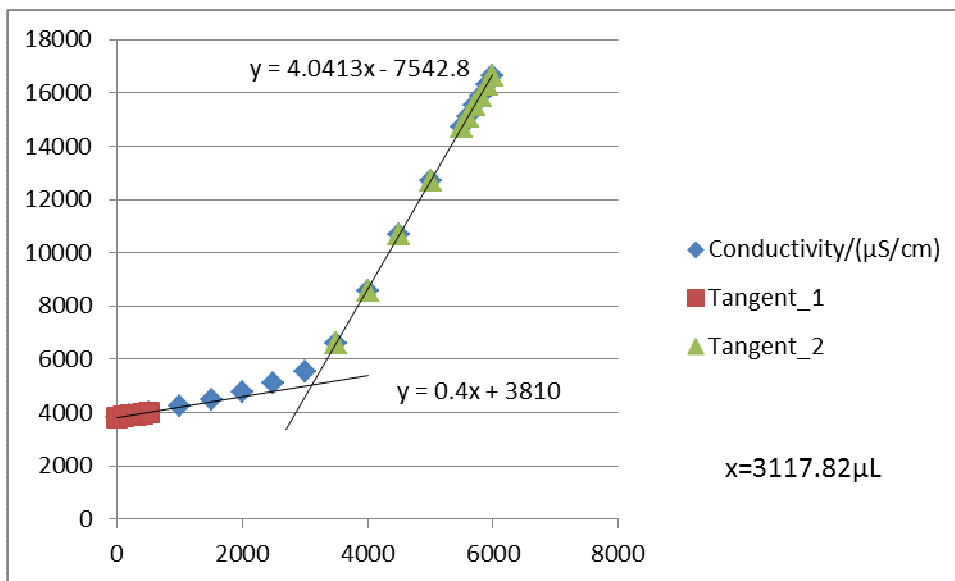
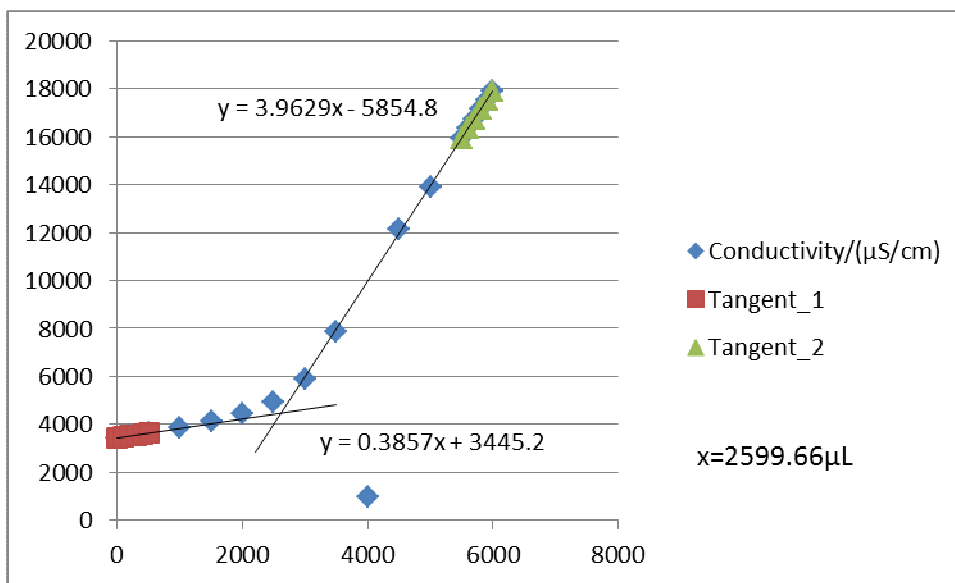Figure G12-2 Titration 2 for 0.1184 mol/L MEA Third Run

Figure G12-3 Titration 3 for 0.1184 mol/L MEA Third Run

260

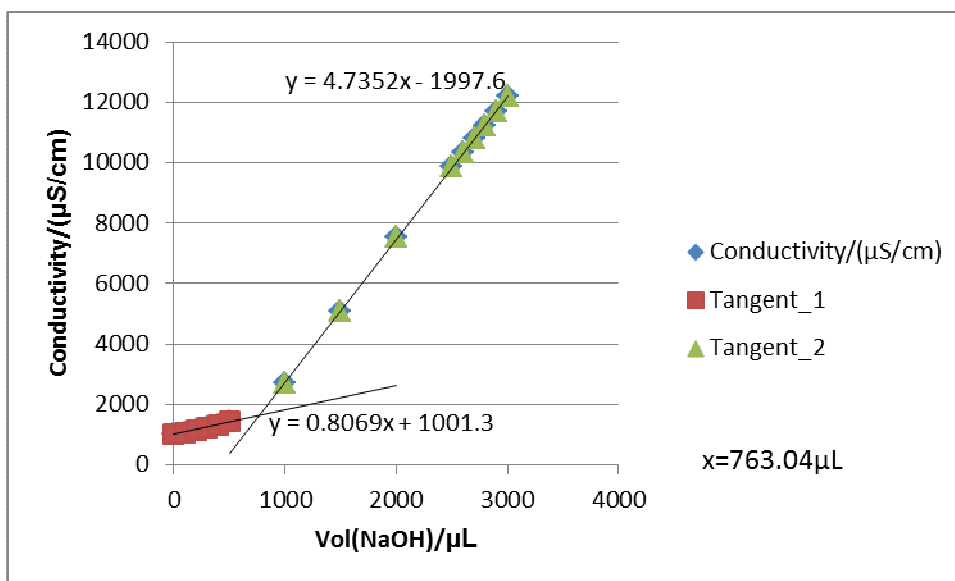**G13: Titration Curves for 0.01986 mol/L MEA First Run at 303 K**

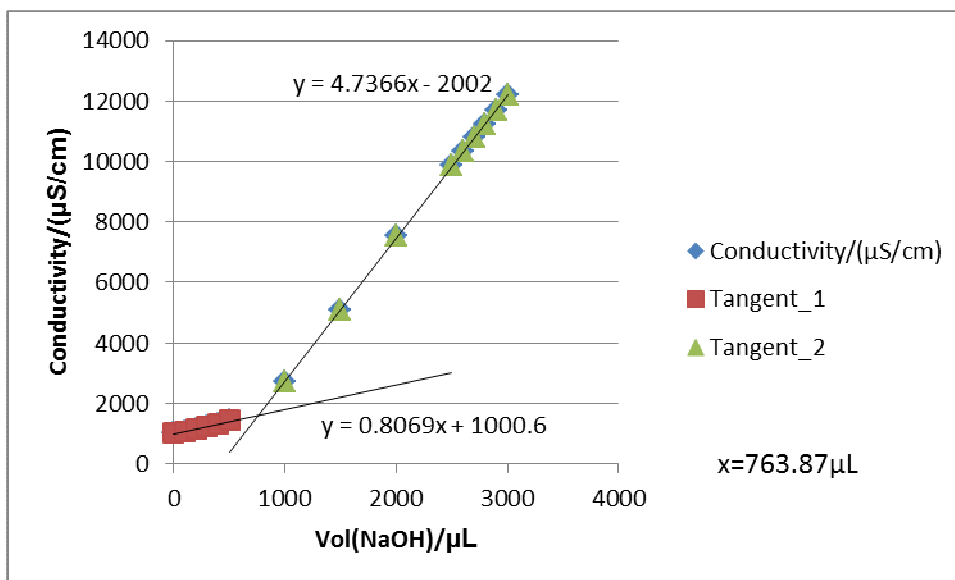Figure G13-1 Titration 1 for 0.01986 mol/L MEA First Run

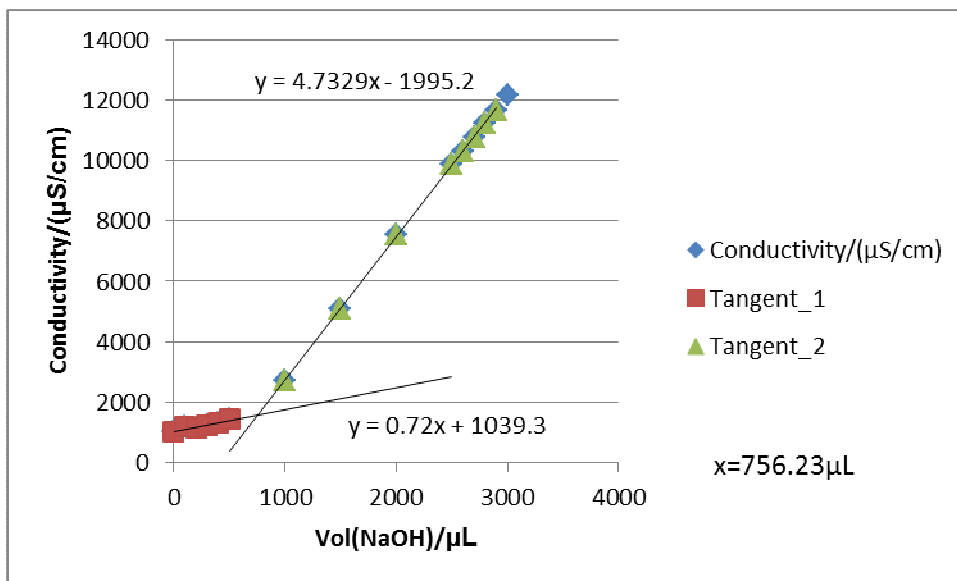Figure G13-2 Titration 2 for 0.01986 mol/L MEA First Run

Figure G13-3 Titration 3 for 0.01986 mol/L MEA First Run

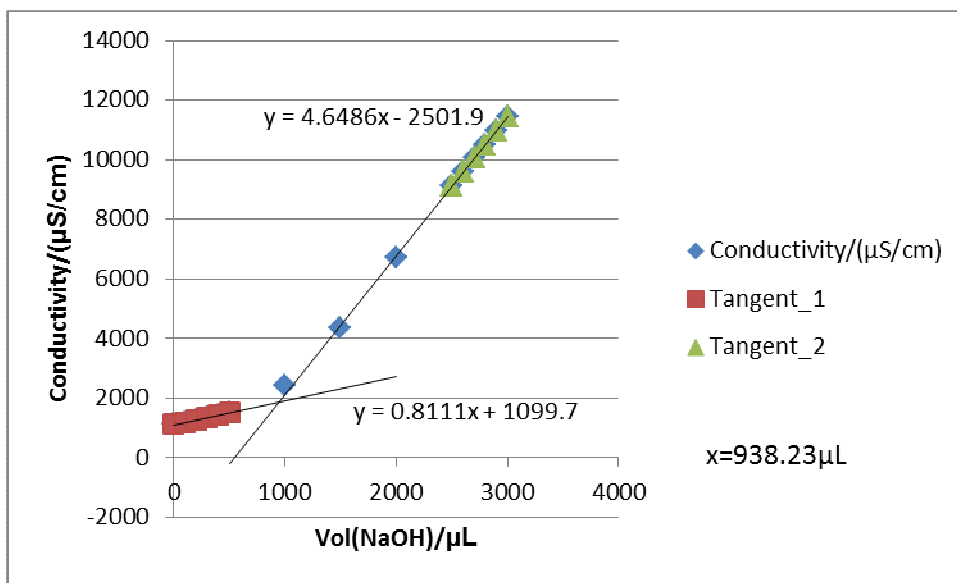**G14: Titration Curves for 0.01986 mol/L MEA Second Run at 303 K**

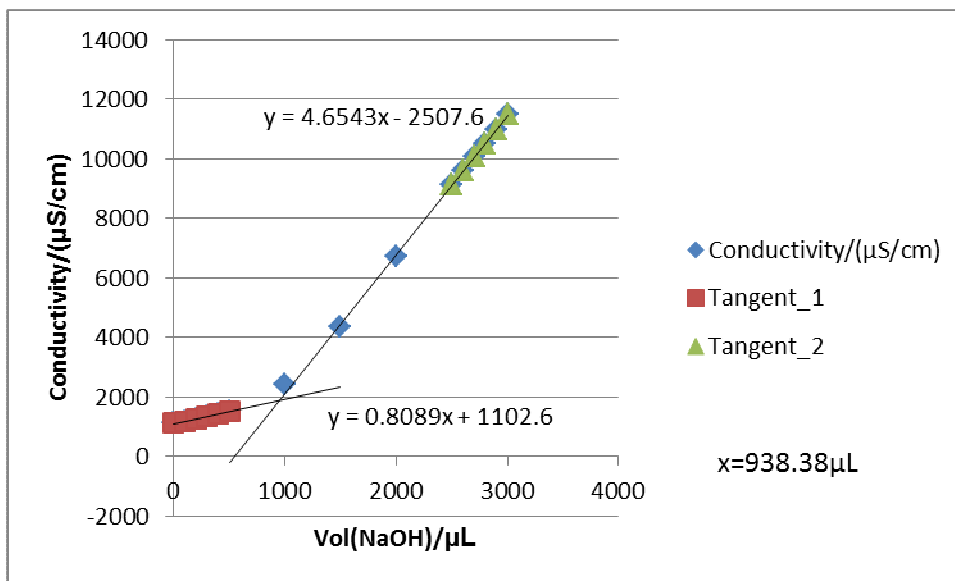Figure G14-1 Titration 1 for 0.01986 mol/L MEA Second Run

262

Figure G14-2 Titration 2 for 0.01986 mol/L MEA Second Run

Figure G14-3 Titration 3 for 0.01986 mol/L MEA Second Run

263

G15: Titration Curves for 0.01986 mol/L MEA Third Run at 303 K

Figure G15-1 Titration 1 for 0.01986 mol/L MEA Third Run

Figure G15-2 Titration 2 for 0.01986 mol/L MEA Third Run
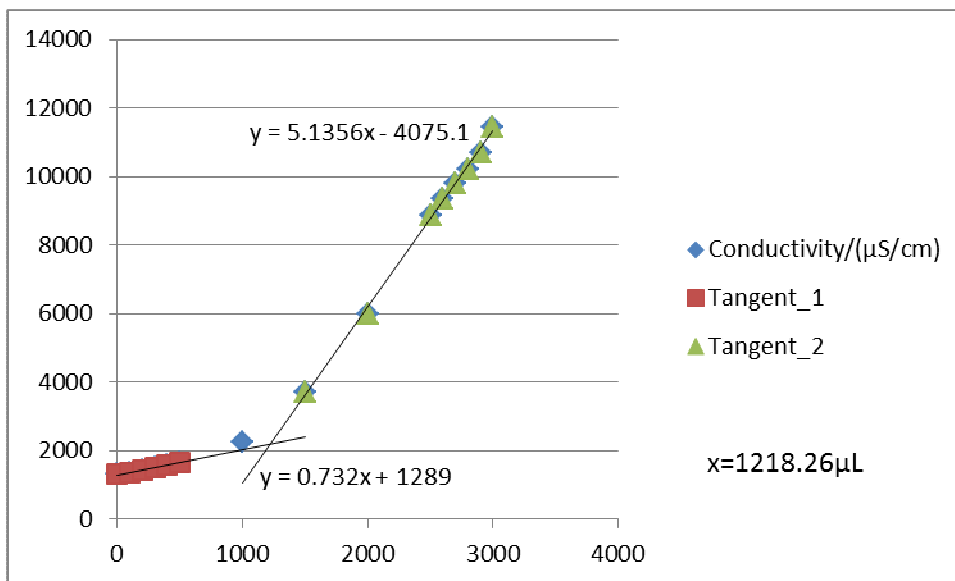
Figure G15-3 Titration 3 for 0.01986 mol/L MEA Third Run

G16: Titration Curves for 0.04956 mol/L MEA First Run at 303 K

Figure G16-1 Titration 1 for 0.04956 mol/L MEA First Run

265

Figure G16-2 Titration 2 for 0.04956 mol/L MEA First Run

Figure G16-3 Titration 3 for 0.04956 mol/L MEA First Run

G17: Titration Curves for 0.04956 mol/L MEA Second Run at 303 K

Figure G17-1 Titration 1 for 0.04956 mol/L MEA Second Run

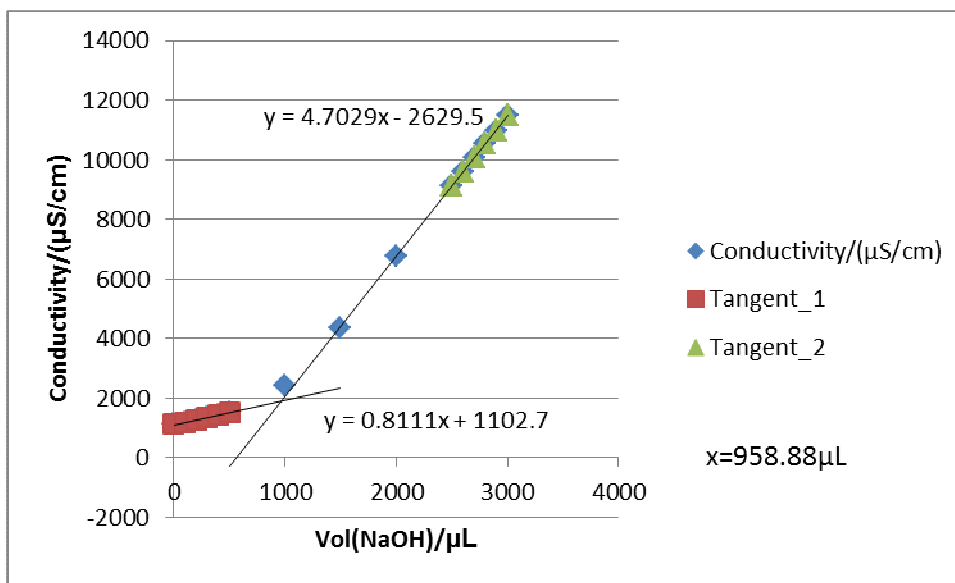
Figure G17-2 Titration 2 for 0.04956 mol/L MEA Second Run

267

Figure G17-3 Titration 3 for 0.04956 mol/L MEA Second Run

G18: Titration Curves for 0.04956 mol/L MEA Third Run at 303 K
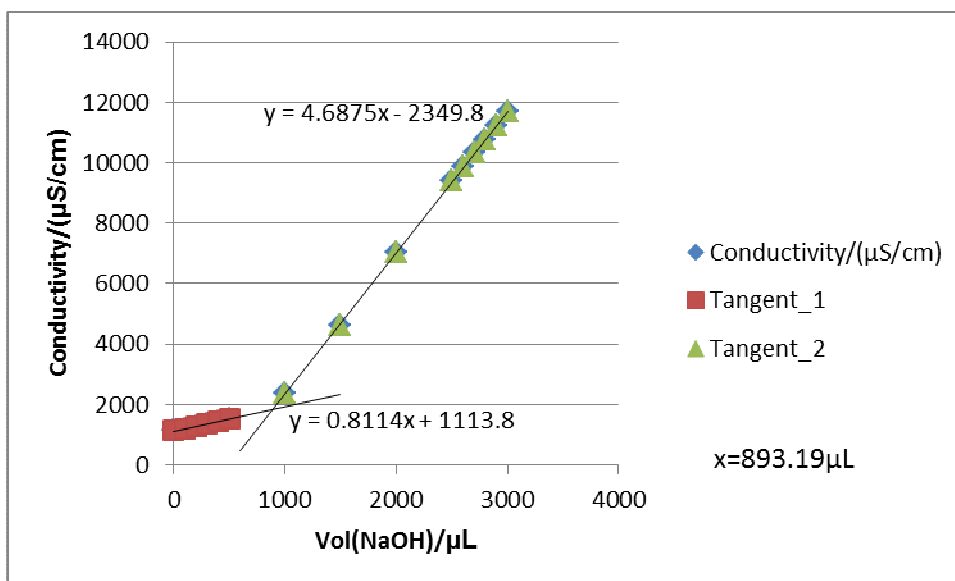

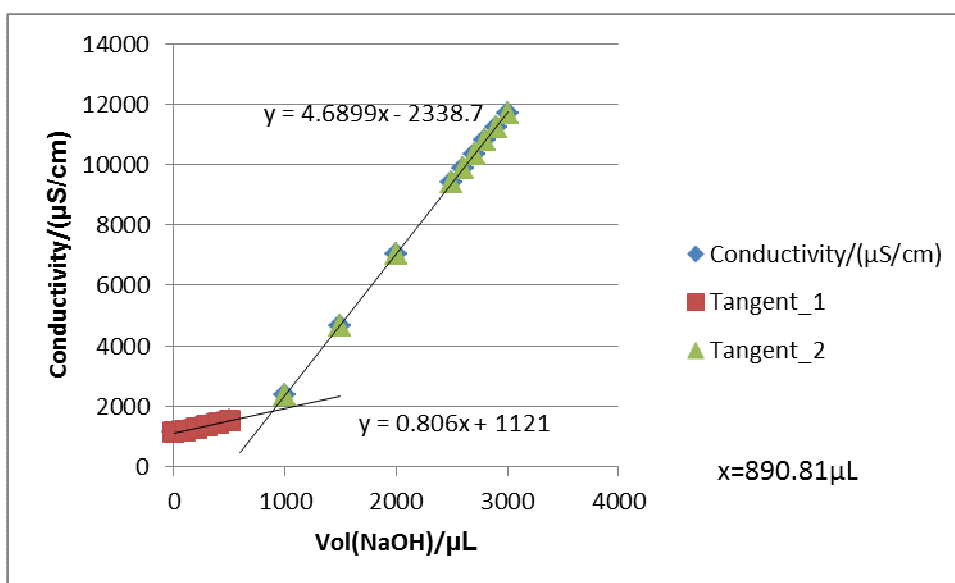Figure G18-1 Titration 1 for 0.04956 mol/L MEA Third Run

268

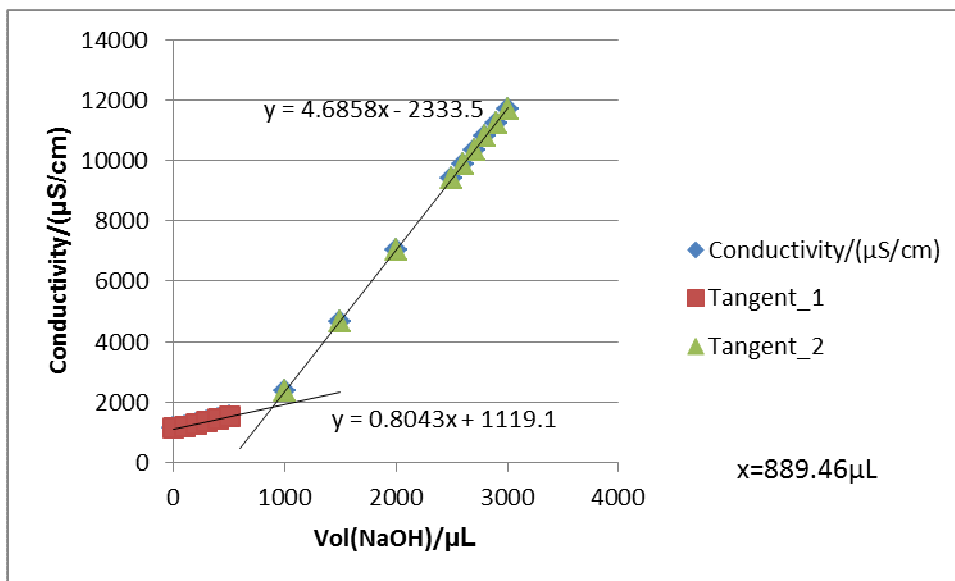Figure G18-2 Titration 2 for 0.04956 mol/L MEA Third Run

Figure G18-3 Titration 3 for 0.04956 mol/L MEA Third Run

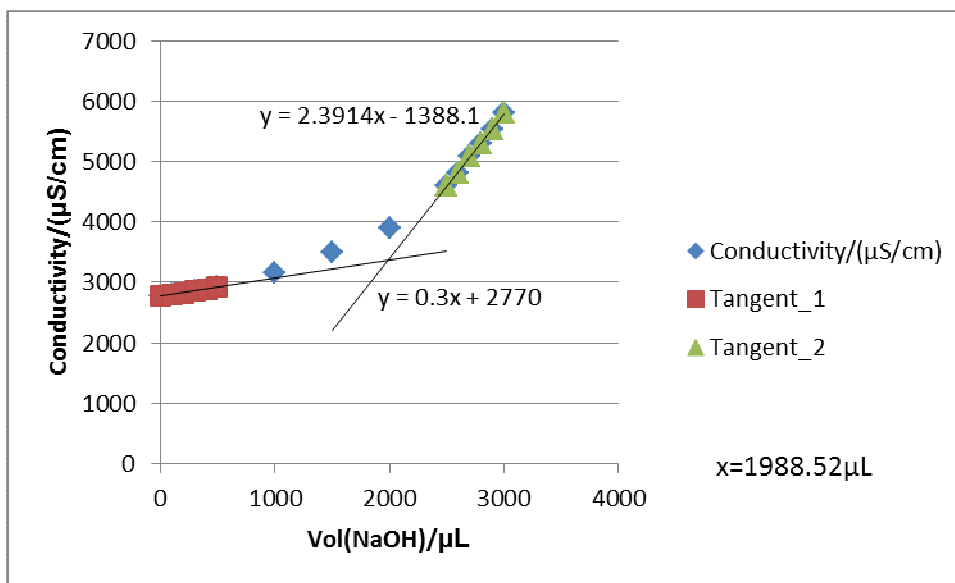**G19: Titration Curves for 0.07915 mol/L MEA First Run at 303 K**

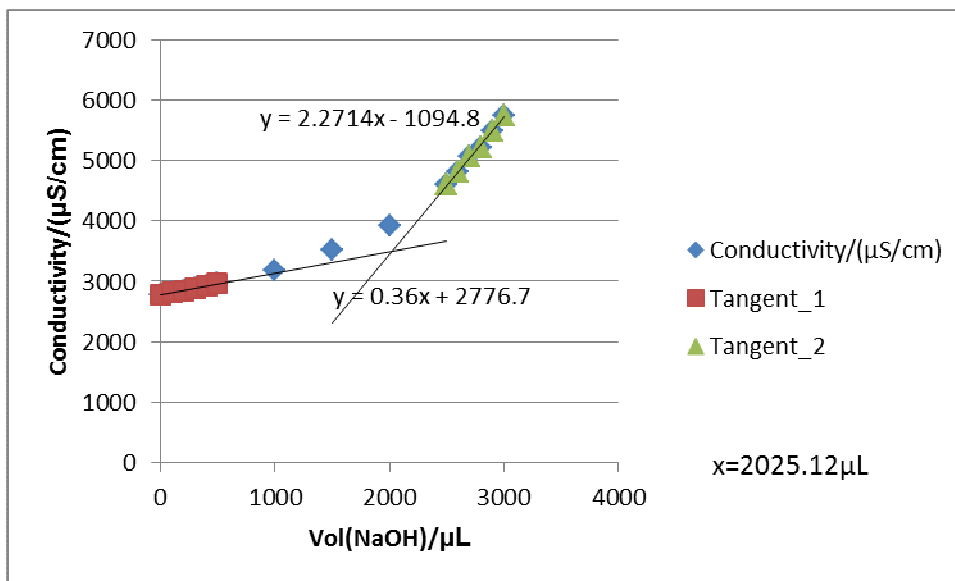Figure G19-1 Titration 1 for 0.07915 mol/L MEA First Run

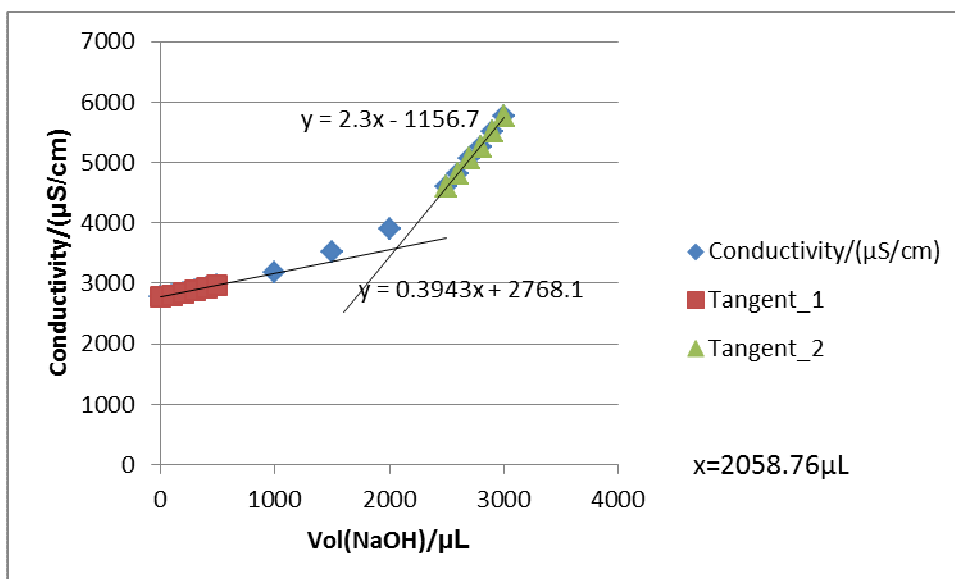Figure G19-2 Titration 2 for 0.07915 mol/L MEA First Run

Figure G19-3 Titration 3 for 0.07915 mol/L MEA First Run

G20: Titration Curves for 0.07915 mol/L MEA Second Run at 303 K
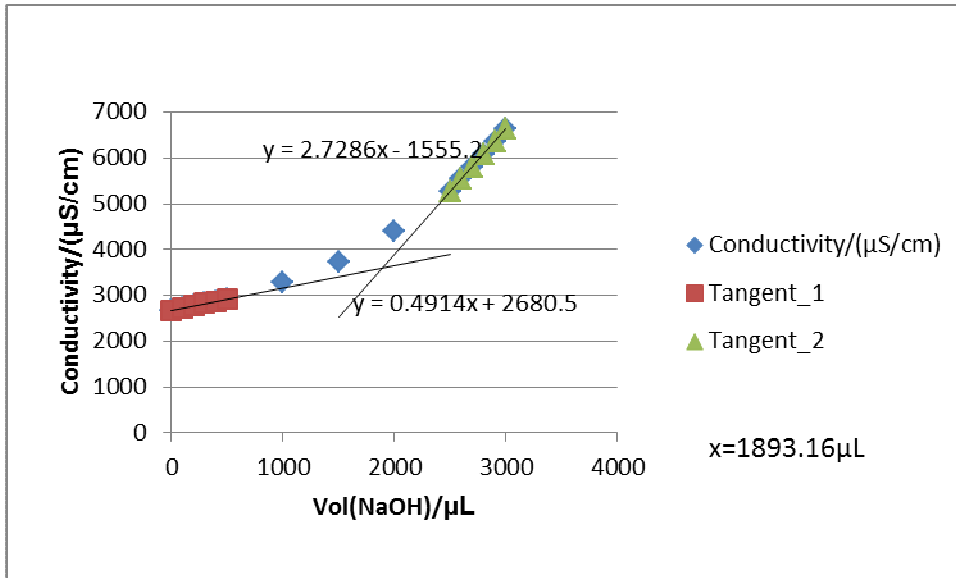

Figure G20-1 Titration 1 for 0.07915 mol/L MEA Second Run

271

Figure G20-2 Titration 2 for 0.07915 mol/L MEA Second Run

Figure G20-3 Titration 3 for 0.07915 mol/L MEA Second Run

272

G21: Titration Curves for 0.07915 mol/L MEA Third Run at 303 K

Figure G21-1 Titration 1 for 0.07915 mol/L MEA Third Run

Figure G21-2 Titration 2 for 0.07915 mol/L MEA Third Run

273

Figure G21-3 Titration 3 for 0.07915 mol/L MEA Third Run

G22: Titration Curves for 0.1184 mol/L MEA First Run at 303 K

Figure G22-1 Titration 1 for 0.1184 mol/L MEA First Run

274

Figure G22-2 Titration 2 for 0.1184 mol/L MEA First Run

Figure G22-3 Titration 3 for 0.1184 mol/L MEA First Run

G23: Titration Curves for 0.1184 mol/L MEA Second Run at 303 K

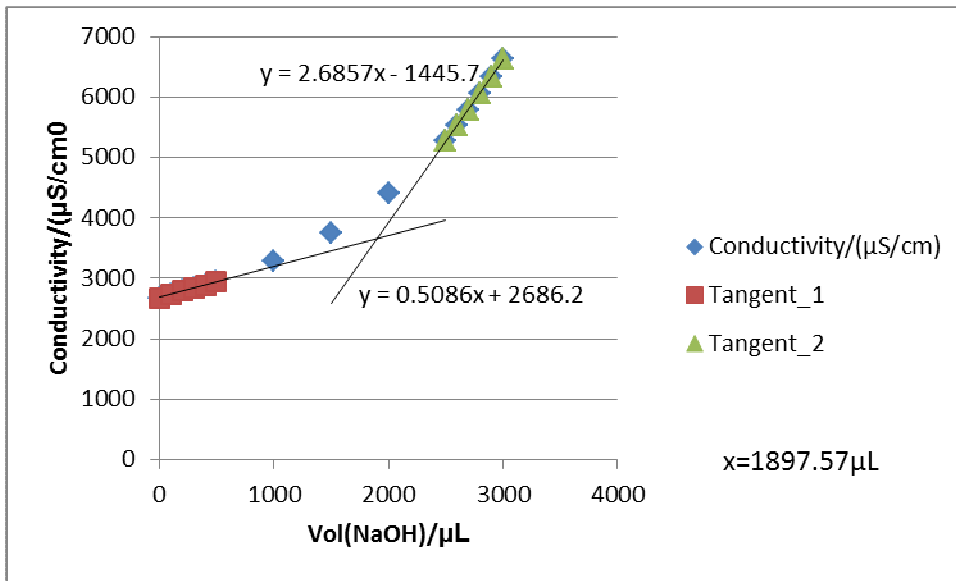Figure G23-1 Titration 1 for 0.1184 mol/L MEA Second Run

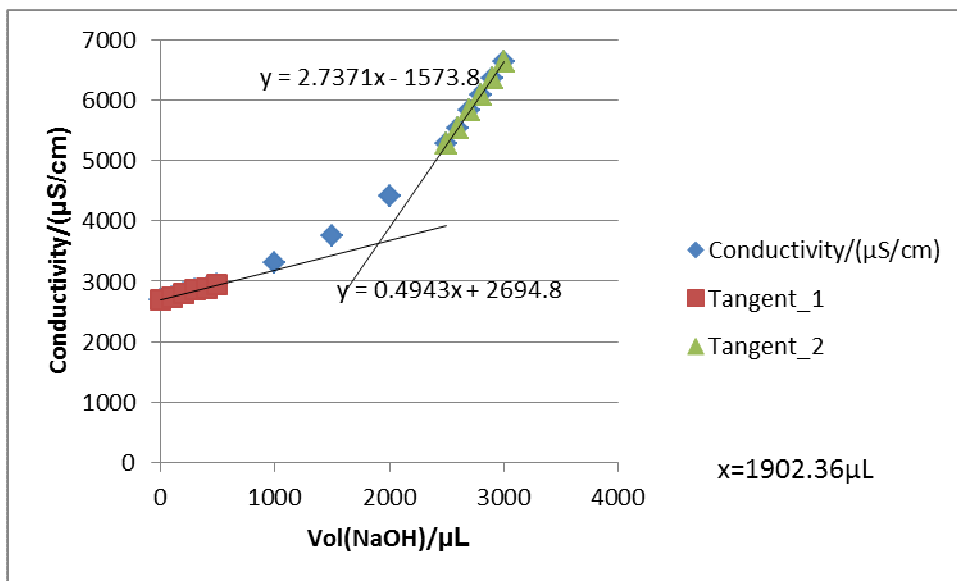

Figure G23-2 Titration 2 for 0.1184 mol/L MEA Second Run

Figure G23-3 Titration 3 for 0.1184 mol/L MEA Second Run

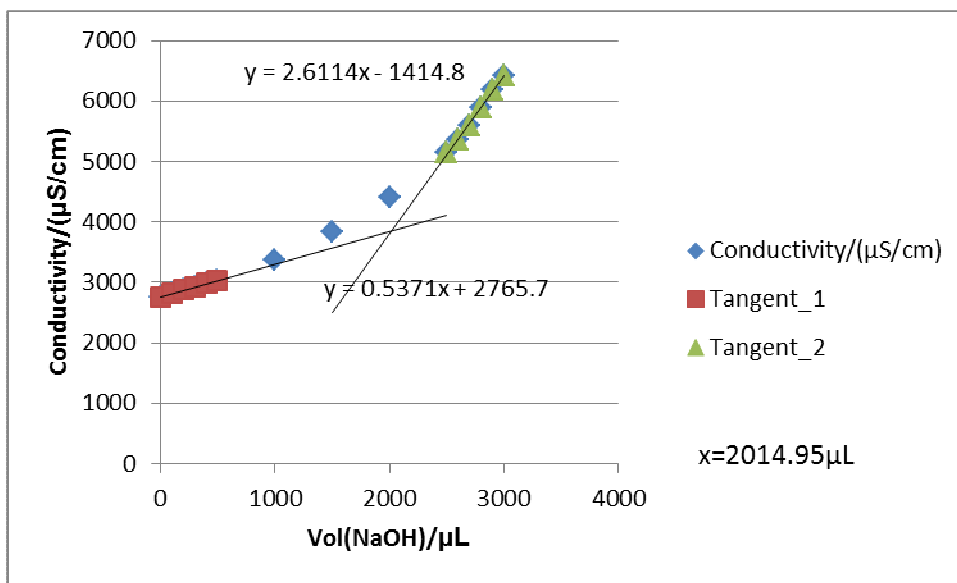## G24: Titration Curves for 0.1184 mol/L MEA Third Run at 303 K
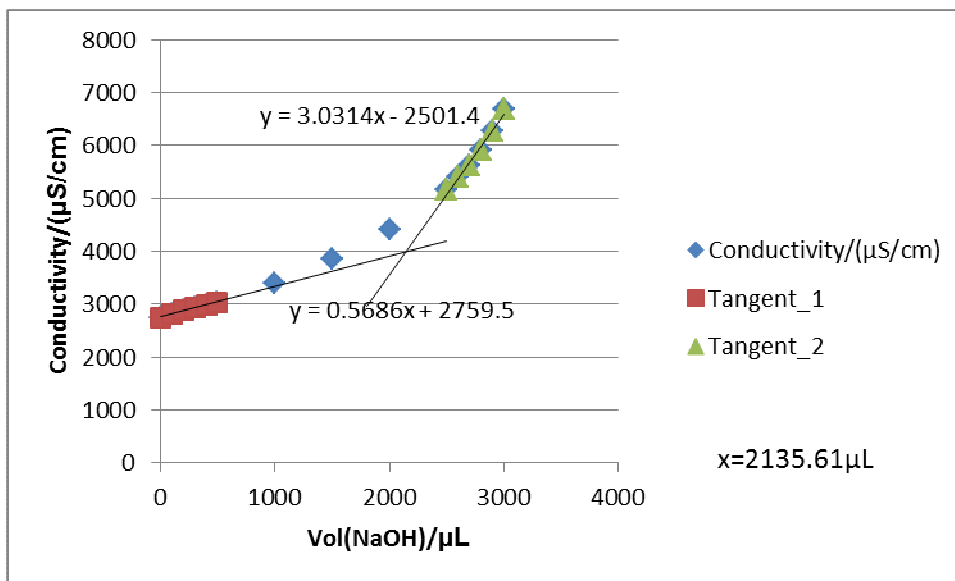

Figure G24-1 Titration 1 for 0.1184 mol/L MEA Third Run

Figure G24-2 Titration 2 for 0.1184 mol/L MEA Third Run

Figure G24-3 Titration 3 for 0.1184 mol/L MEA Third Run

278

G25: Titration Curves for 0.01986 mol/L MEA First Run at 308 K

Figure G25-1 Titration 1 for 0.01986 mol/L MEA First Run

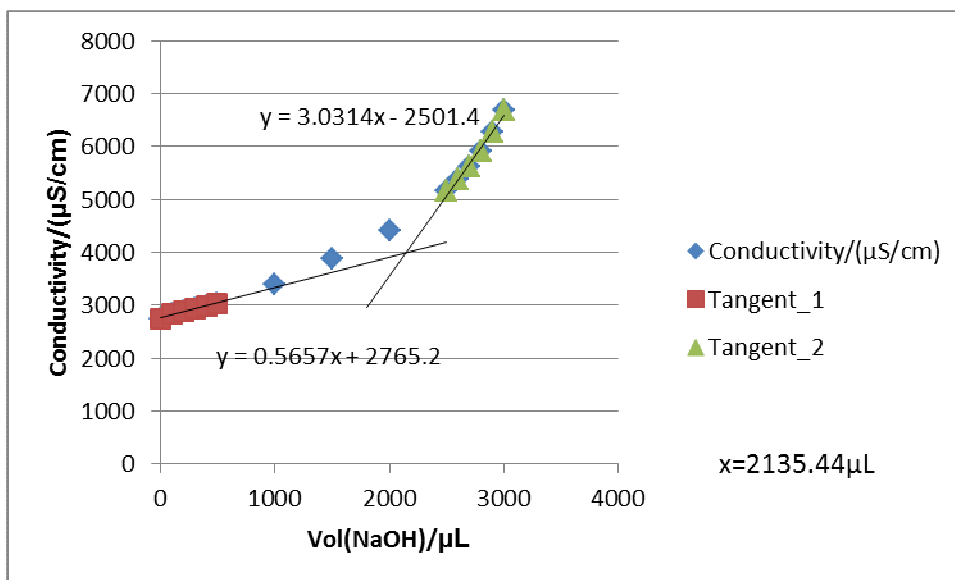

Figure G25-2 Titration 2 for 0.01986 mol/L MEA First Run

Figure G25-3 Titration 3 for 0.01986 mol/L MEA First Run

G26: Titration Curves for 0.01986 mol/L MEA Second Run at 308 K

Figure G26-1 Titration 1 for 0.01986 mol/L MEA Second Run

280

Figure G26-2 Titration 2 for 0.01986 mol/L MEA Second Run

Figure G26-3 Titration 3 for 0.01986 mol/L MEA Second Run

G27: Titration Curves for 0.01986 mol/L MEA Third Run at 308 K

Figure G27-1 Titration 1 for 0.01986 mol/L MEA Third Run

Figure G27-2 Titration 2 for 0.01986 mol/L MEA Third Run

Figure G27-3 Titration 3 for 0.01986 mol/L MEA Third Run

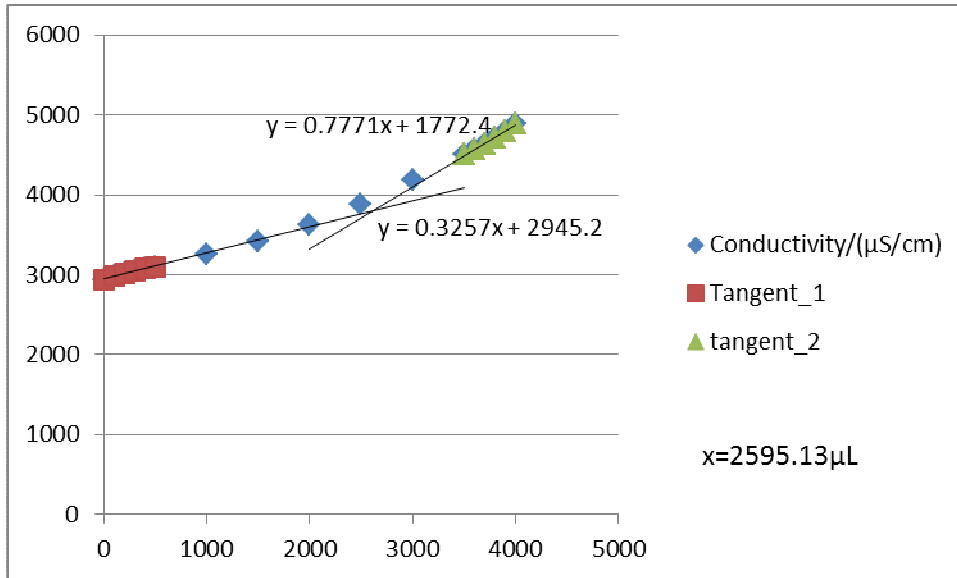## G28: Titration Curves for 0.04956 mol/L MEA First Run at 308 K

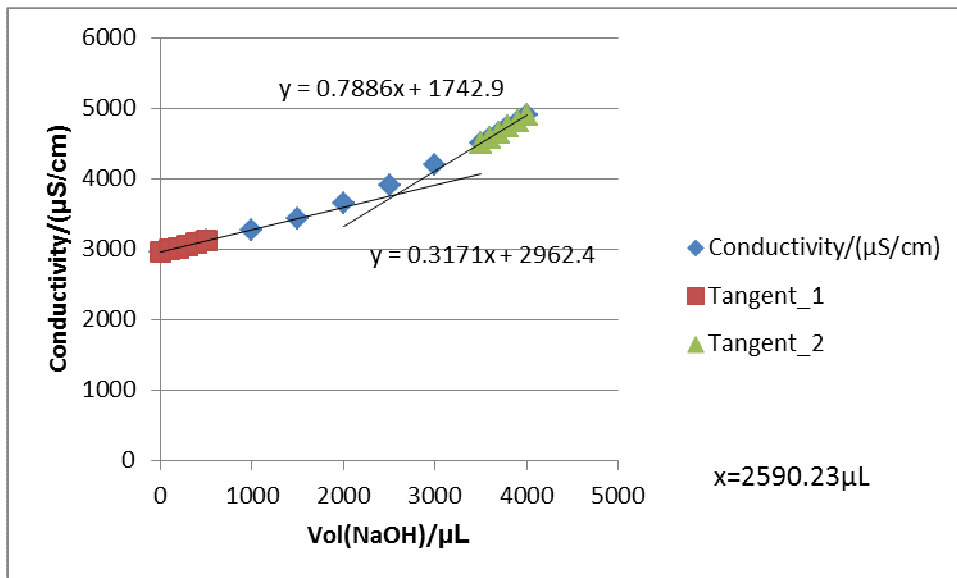

Figure G28-1 Titration 1 for 0.04956 mol/L MEA First Run

283

Figure G28-2 Titration 2 for 0.04956 mol/L MEA First Run
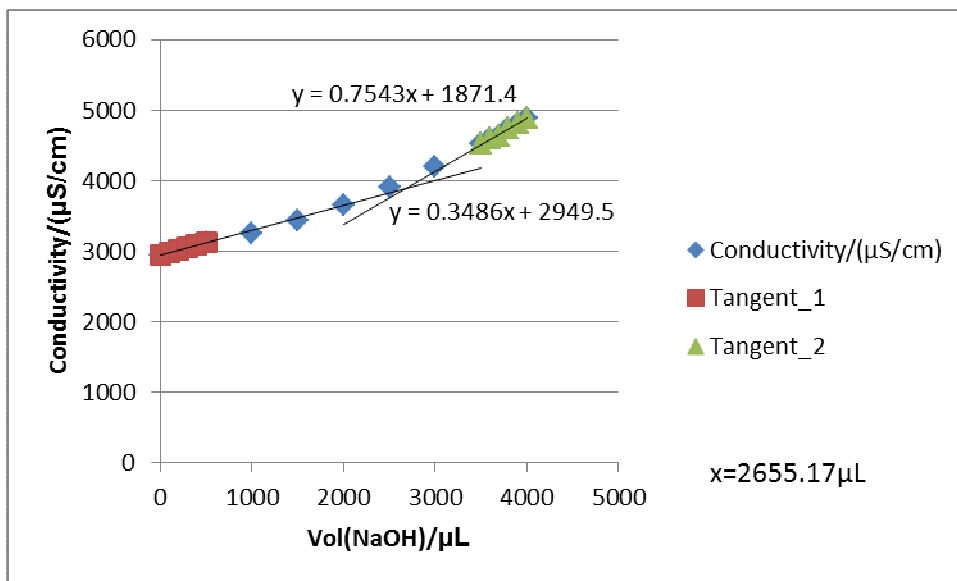

Figure G28-3 Titration 3 for 0.04956 mol/L MEA First Run

G29: Titration Curves for 0.04956 mol/L MEA Second Run at 308 K
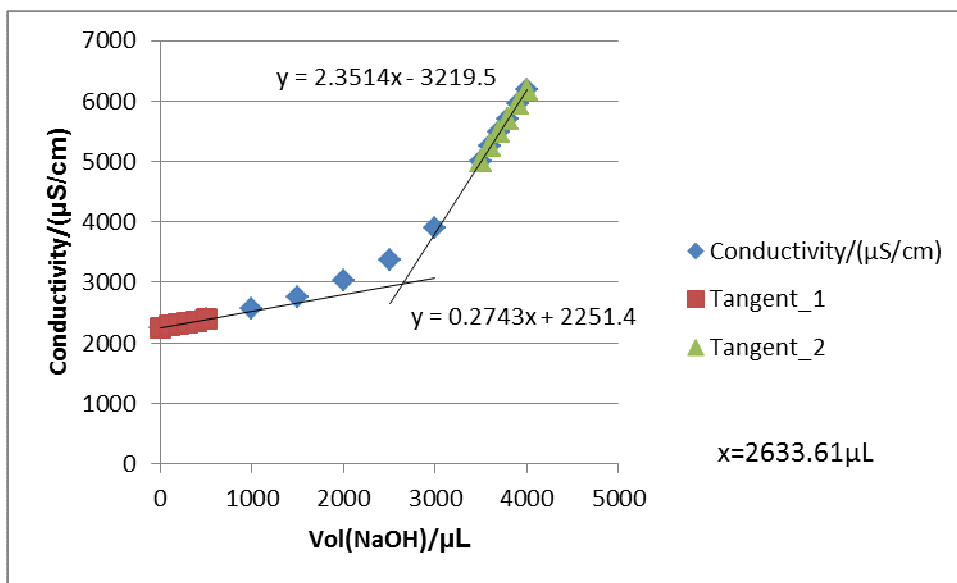

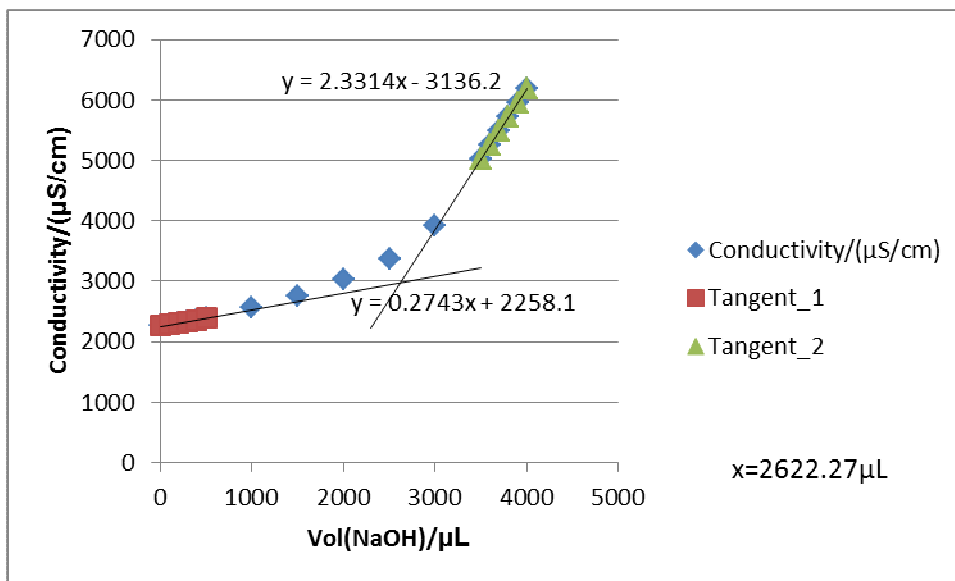
Figure G29-1 Titration 1 for 0.04956 mol/L MEA Second Run

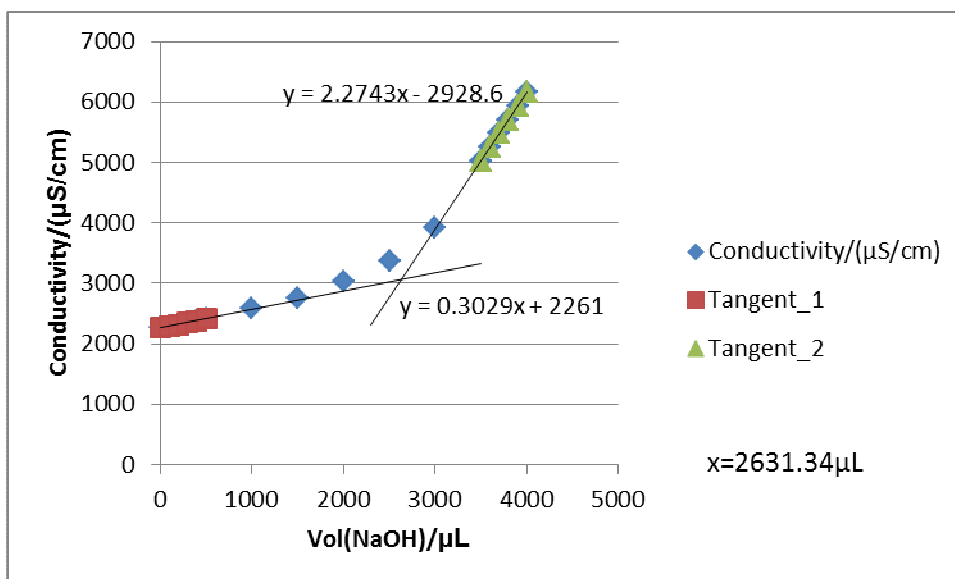Figure G29-2 Titration 2 for 0.04956 mol/L MEA Second Run

Figure G29-3 Titration 3 for 0.04956 mol/L MEA Second Run

G30: Titration Curves for 0.04956 mol/L MEA Third Run at 308 K
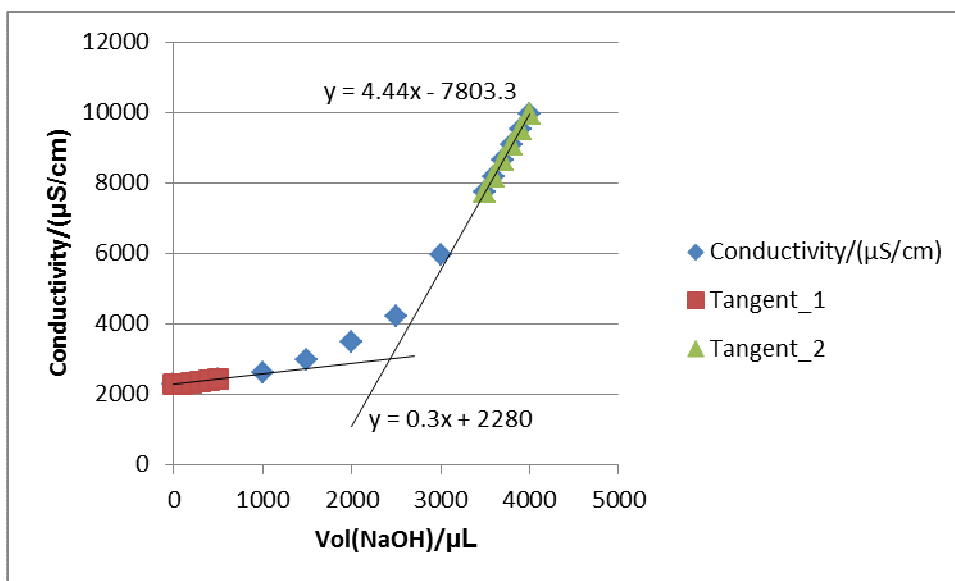

Figure G30-1 Titration 1 for 0.04956 mol/L MEA Third Run

286

Figure G30-2 Titration 2 for 0.04956 mol/L MEA Third Run

Figure G30-3 Titration 3 for 0.04956 mol/L MEA Third Run

287

G31: Titration Curves for 0.07915 mol/L MEA First Run at 308 K

Figure G31-1 Titration 1 for 0.07915 mol/L MEA First Run

Figure G31-2 Titration 2 for 0.07915 mol/L MEA First Run

288

Figure G31-3 Titration 3 for 0.07915 mol/L MEA First Run

G32: Titration Curves for 0.07915 mol/L MEA Second Run at 308 K

Figure G32-1 Titration 1 for 0.07915 mol/L MEA Second Run

Figure G32-2 Titration 2 for 0.07915 mol/L MEA Second Run

Figure G32-3 Titration 3 for 0.07915 mol/L MEA Second Run

290

G33: Titration Curves for 0.07915 mol/L MEA Third Run at 308 K

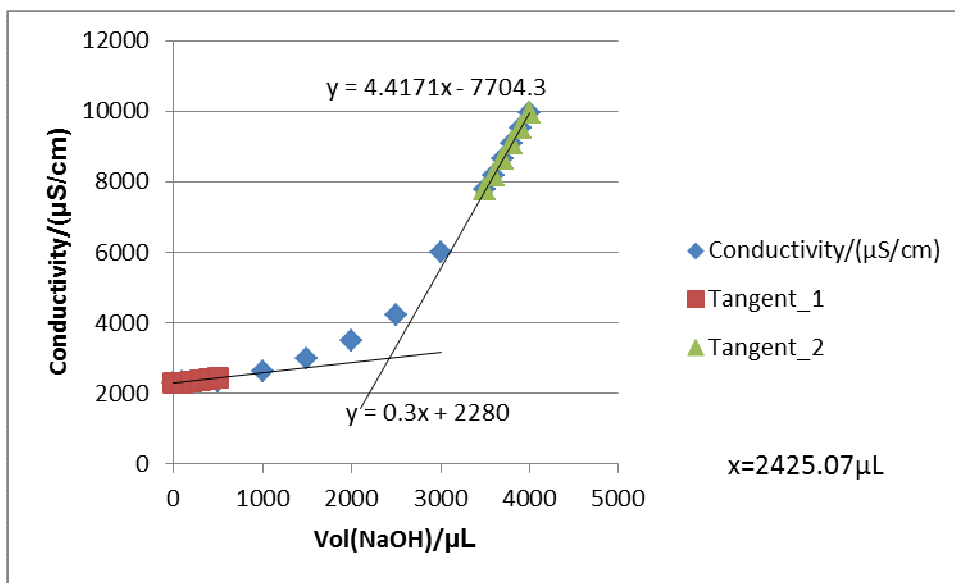Figure G33-1 Titration 1 for 0.07915 mol/L MEA Third Run

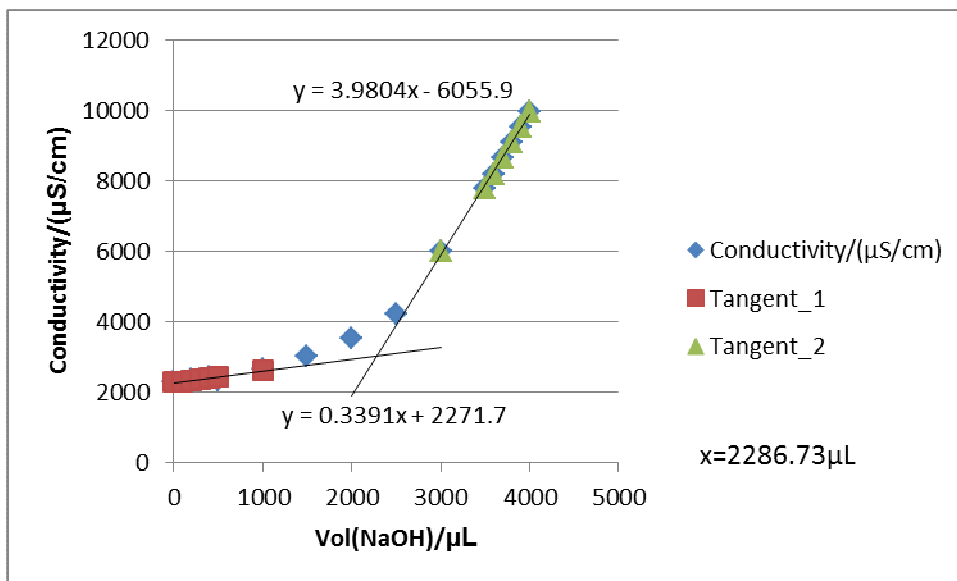Figure G33-2 Titration 2 for 0.07915 mol/L MEA Third Run

291

Figure G33-3 Titration 3 for 0.07915 mol/L MEA Third Run

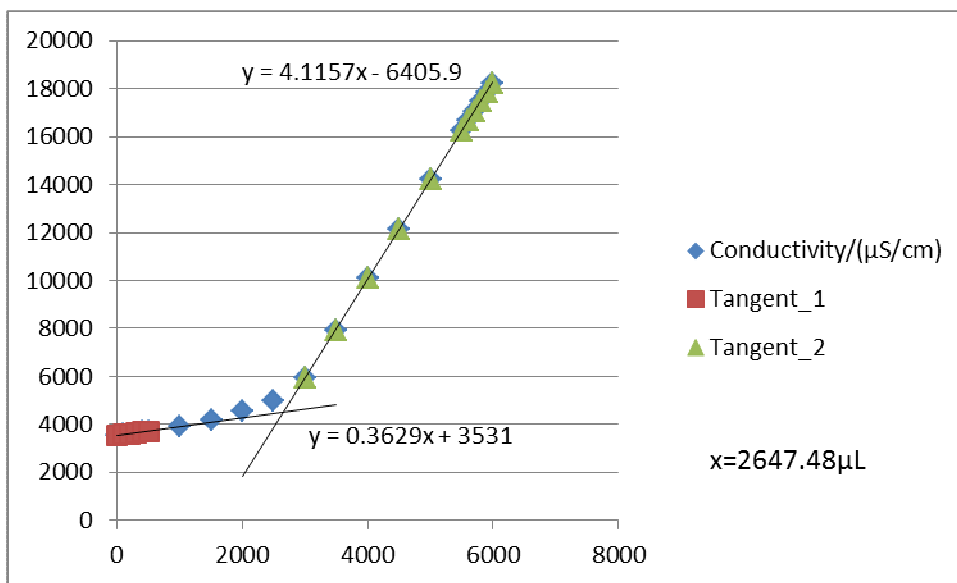## G34: Titration Curves for 0.1184 mol/L MEA First Run at 308 K

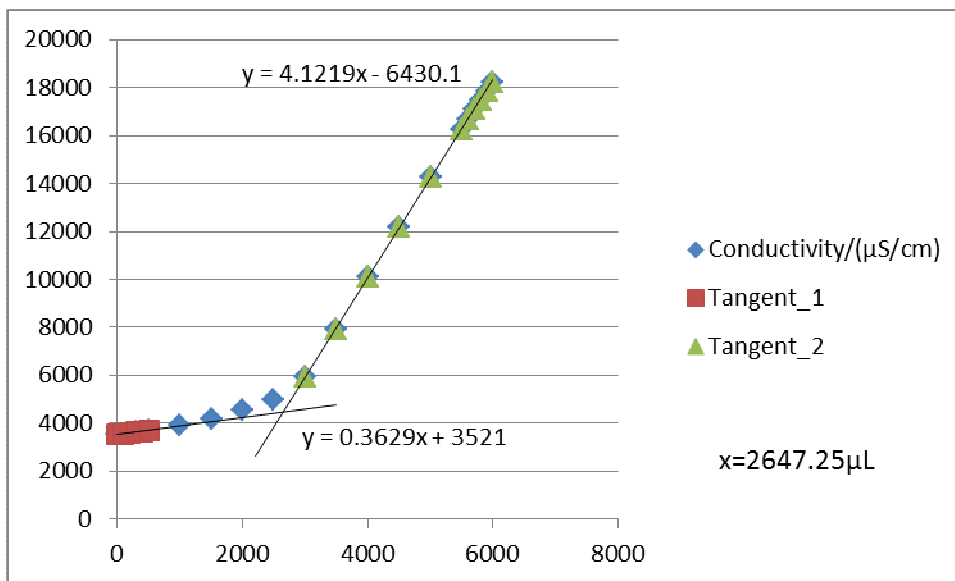
Figure G34-1 Titration 1 for 0.1184 mol/L MEA First Run

292

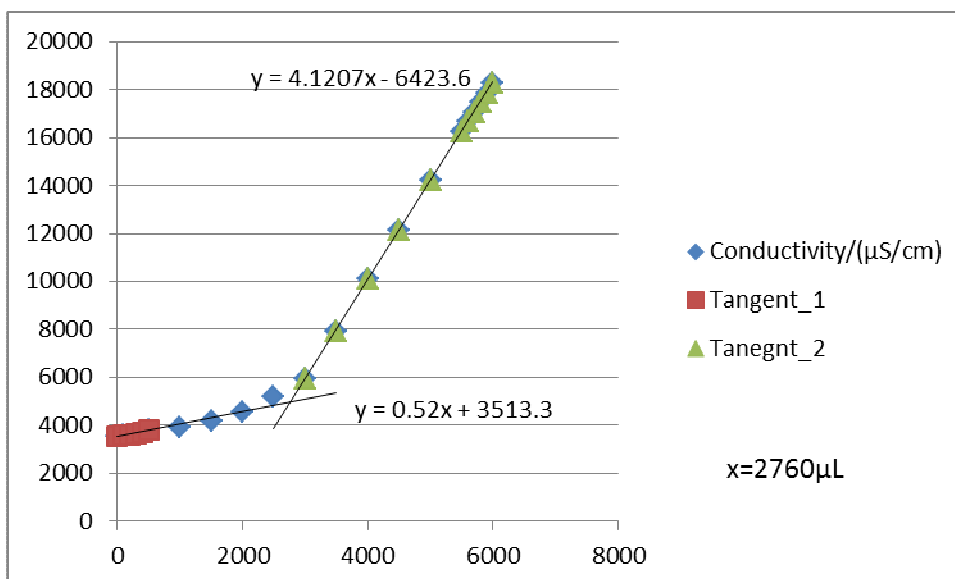Figure G34-2 Titration 2 for 0.1184 mol/L MEA First Run

Figure G34-3 Titration 3 for 0.1184 mol/L MEA First Run

293

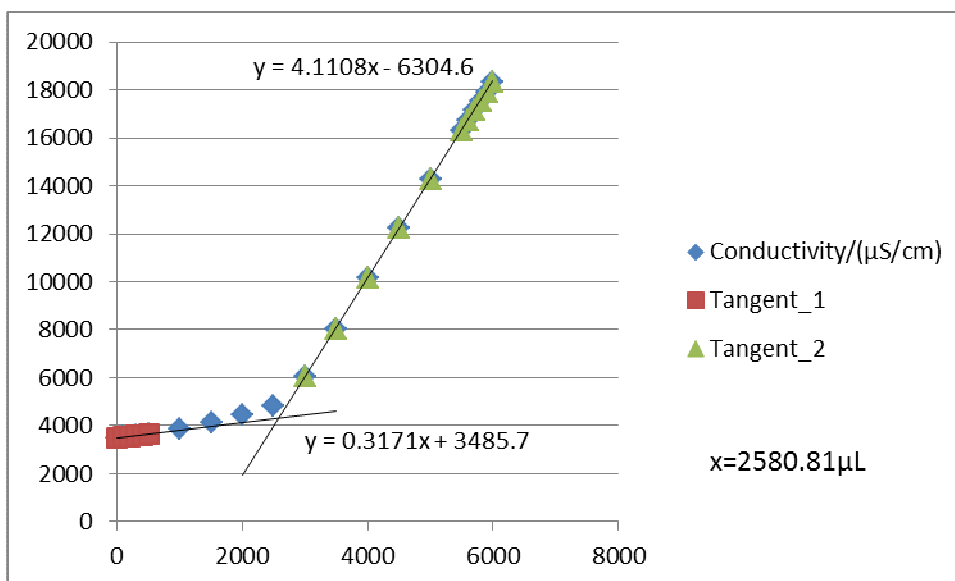**G35: Titration Curves for 0.1184 mol/L MEA Second Run at 308 K**

$y = 4.1108x - 6304.6$

$y = 0.3171x + 3485.7$

x=2580.81µL

Figure G35-1 Titration 1 for 0.1184 mol/L MEA Second Run

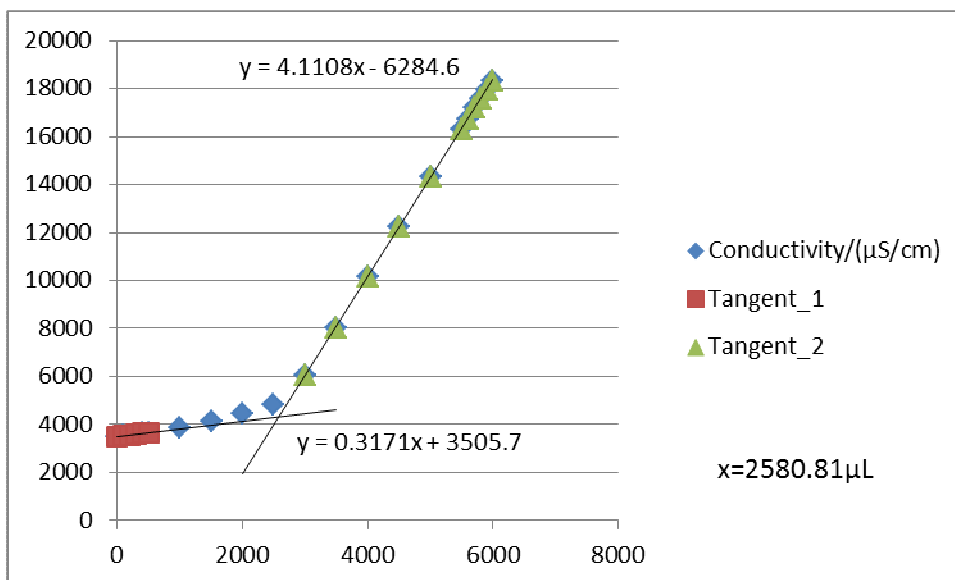$y = 4.1108x - 6284.6$

$y = 0.3171x + 3505.7$

x=2580.81µL

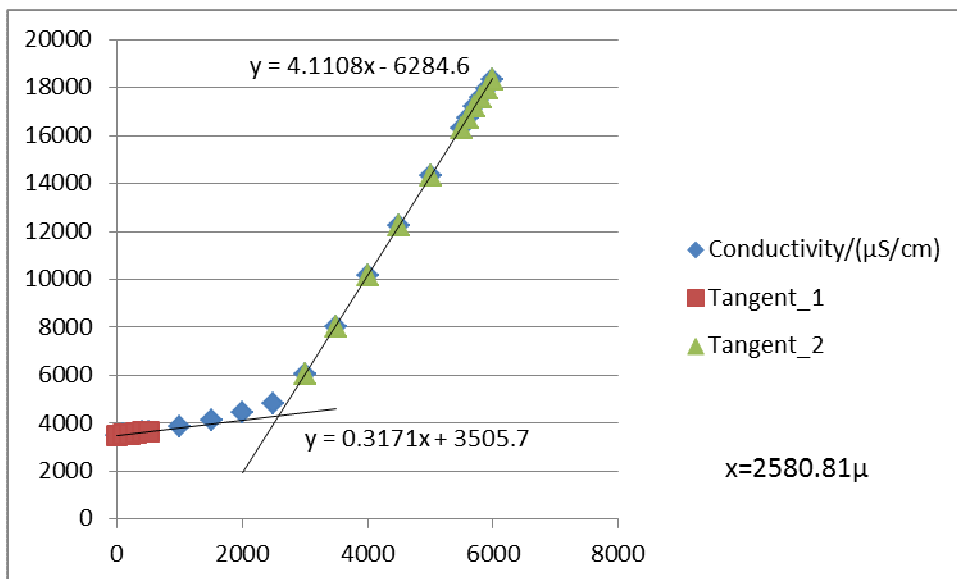Figure G35-2 Titration 2 for 0.1184 mol/L MEA Second Run

Figure G35-3 Titration 3 for 0.1184 mol/L MEA Second Run

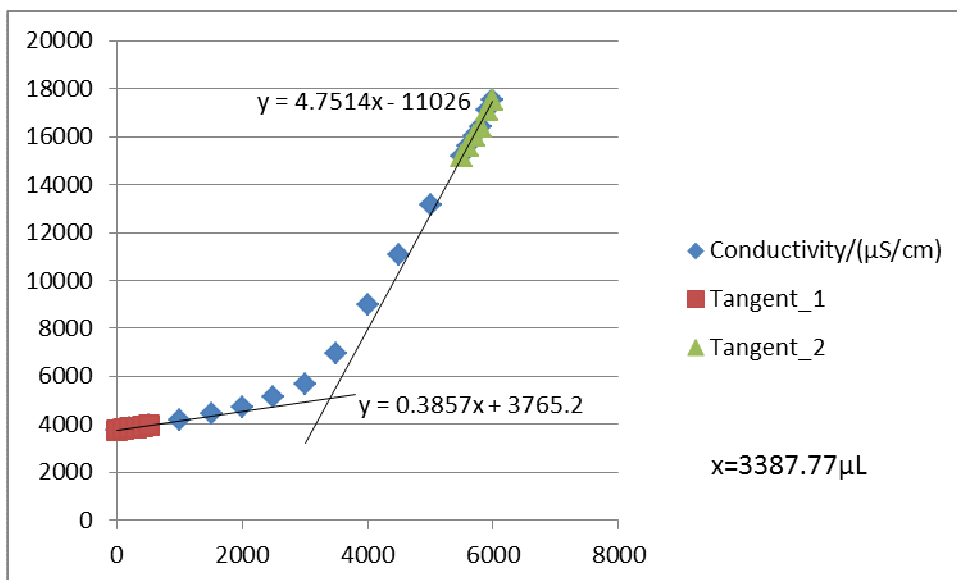**G36: Titration Curves for 0.1184 mol/L MEA Third Run at 308 K**

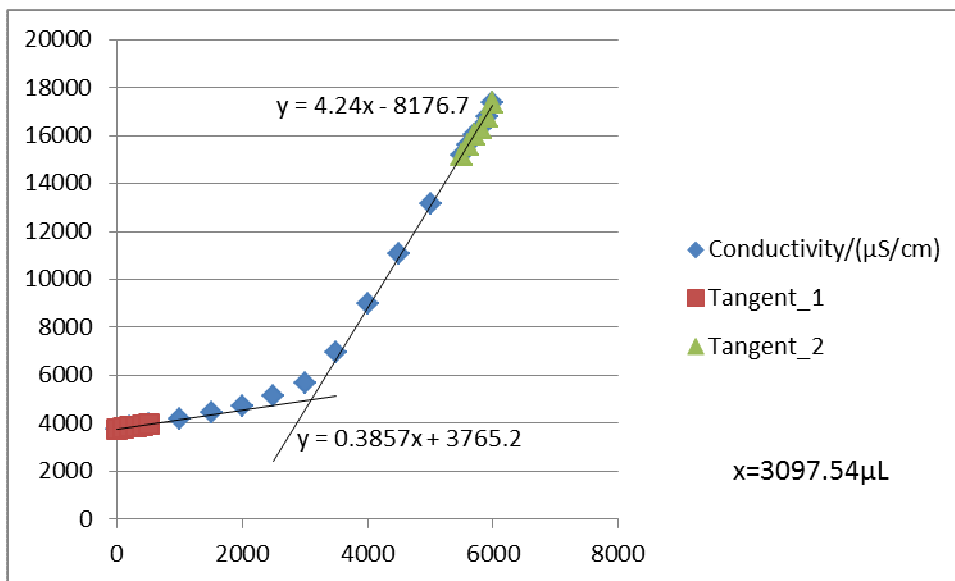Figure G36-1 Titration 1 for 3.6ml MEA Third Run

Figure G36-2 Titration 2 for 0.1184 mol/L MEA Third Run
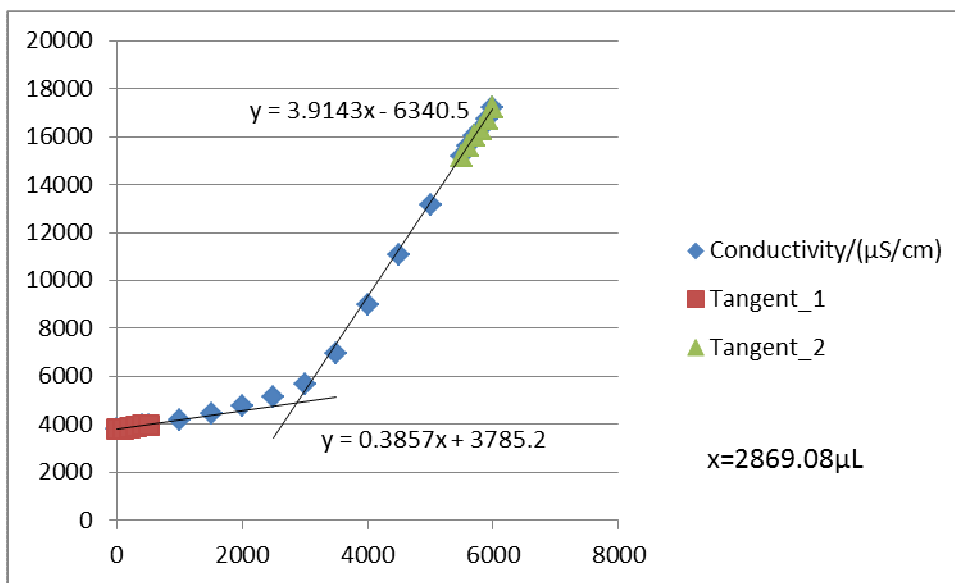

Figure G36-3 Titration 3 for 0.1184 mol/L MEA Third Run

296

G37: Titration Curves for 0.01986 mol/L MEA First Run at 313 K
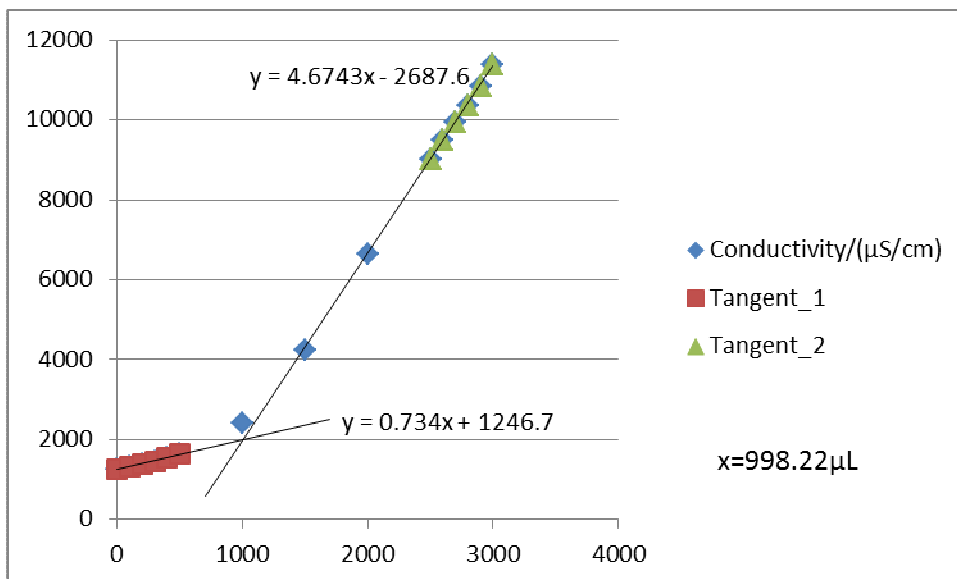

Figure G37-1 Titration 1 for 0.01986 mol/L MEA First Run
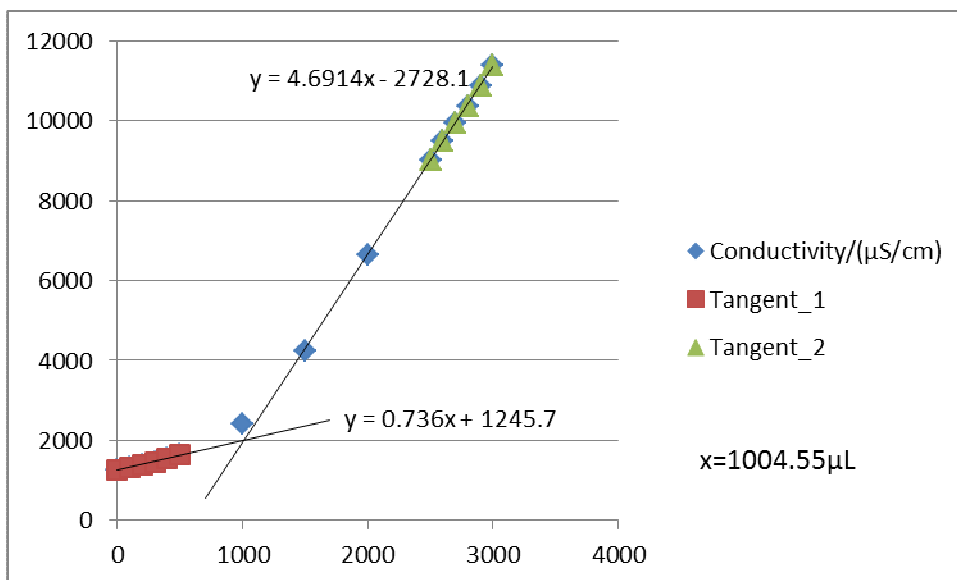

Figure G37-2 Titration 2 for 0.01986 mol/L MEA First Run

Figure G37-3 Titration 3 for 0.01986 mol/L MEA First Run

G38: Titration Curves for 0.01986 mol/L MEA Second Run at 313 K

Figure G38-1 Titration 1 for 0.01986 mol/L MEA Second Run

298

Figure G38-2 Titration 2 for 0.01986 mol/L MEA Second Run

Figure G38-3 Titration 3 for 0.01986 mol/L MEA Second Run

G39: Titration Curves for 0.01986 mol/L MEA Third Run at 313 K

Figure G39-1 Titration 1 for 0.01986 mol/L MEA Third Run

Figure G39-2 Titration 2 for 0.01986 mol/L MEA Third Run

Figure G39-3 Titration 3 for 0.01986 mol/L MEA Third Run

G40: Titration Curves for 0.04956 mol/L MEA First Run at 313 K
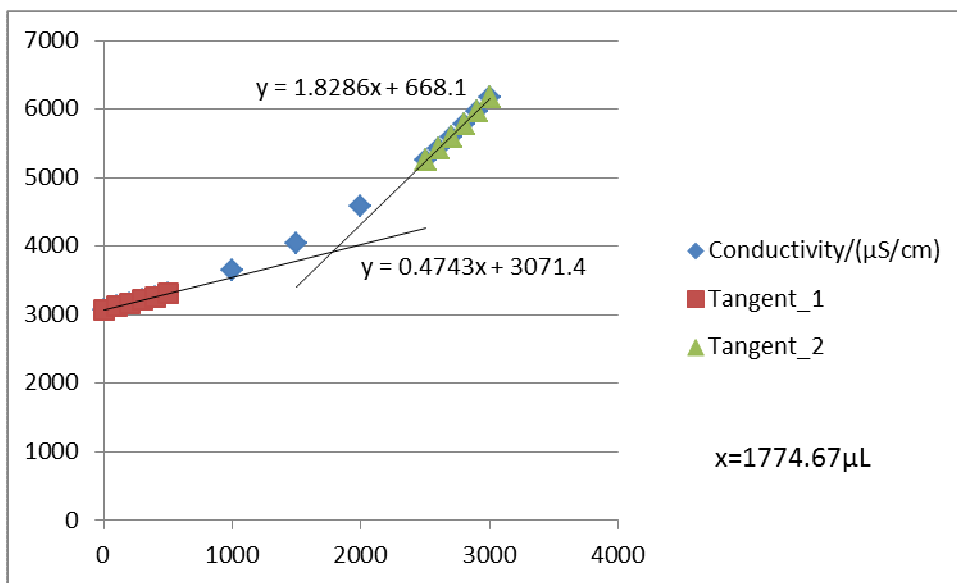
Figure G40-1 Titration 1 for 0.04956 mol/L MEA First Run

301

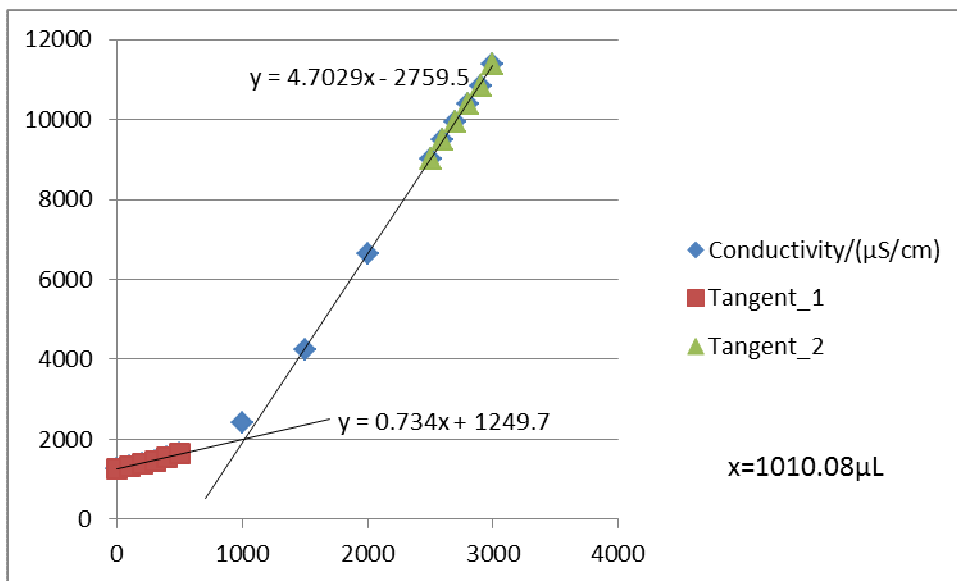Figure G40-2 Titration 2 for 0.04956 mol/L MEA First Run

Figure G40-3 Titration 3 for 0.04956 mol/L MEA First Run

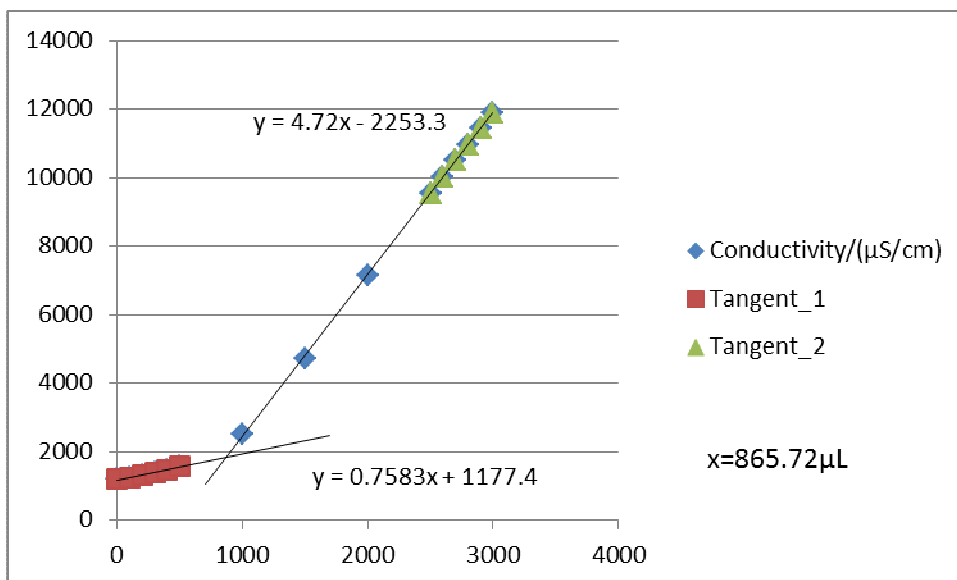**G41: Titration Curves for 0.04956 mol/L MEA Second Run at 313 K**

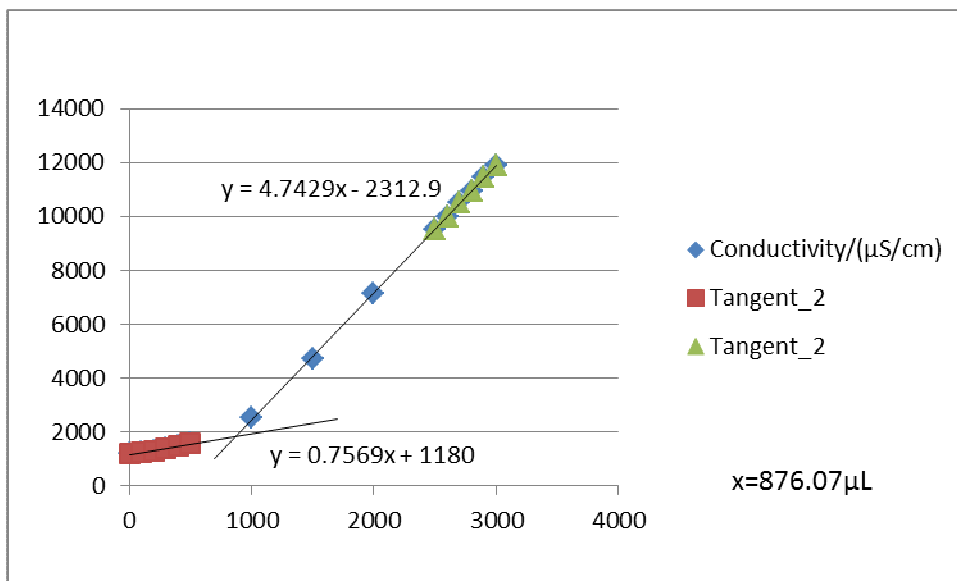
Figure G41-1 Titration 1 for 0.04956 mol/L MEA Second Run

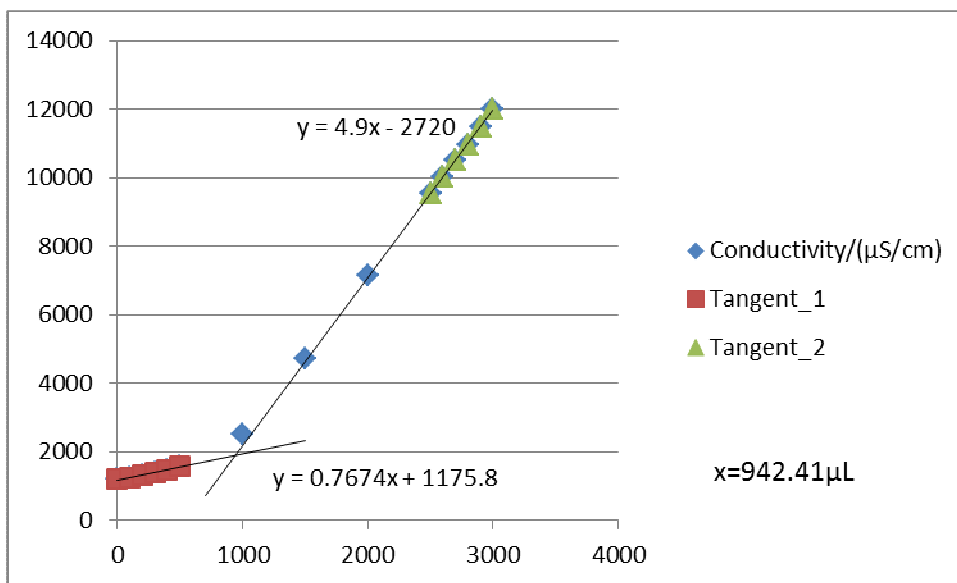
Figure G41-2 Titration 2 for 0.04956 mol/L MEA Second Run

Figure G41-3 Titration 3 for 1.5ml MEA Second Run

G42: Titration Curves for 0.04956 mol/L MEA Third Run at 313 K

Figure G42-1 Titration 1 for 0.04956 mol/L MEA Third Run

304

Figure G42-2 Titration 2 for 0.04956 mol/L MEA Third Run

Figure G42-3 Titration 3 for 0.04956 mol/L MEA Third Run

305

G43: Titration Curves for 0.07915 mol/L MEA First Run at 313 K
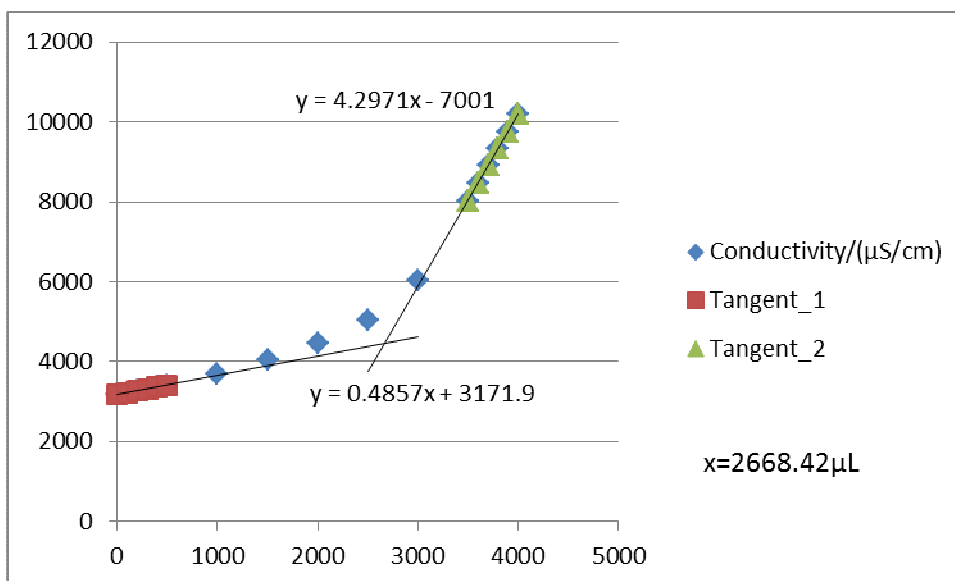
Figure G43-1 Titration 1 for 0.07915 mol/L MEA First Run
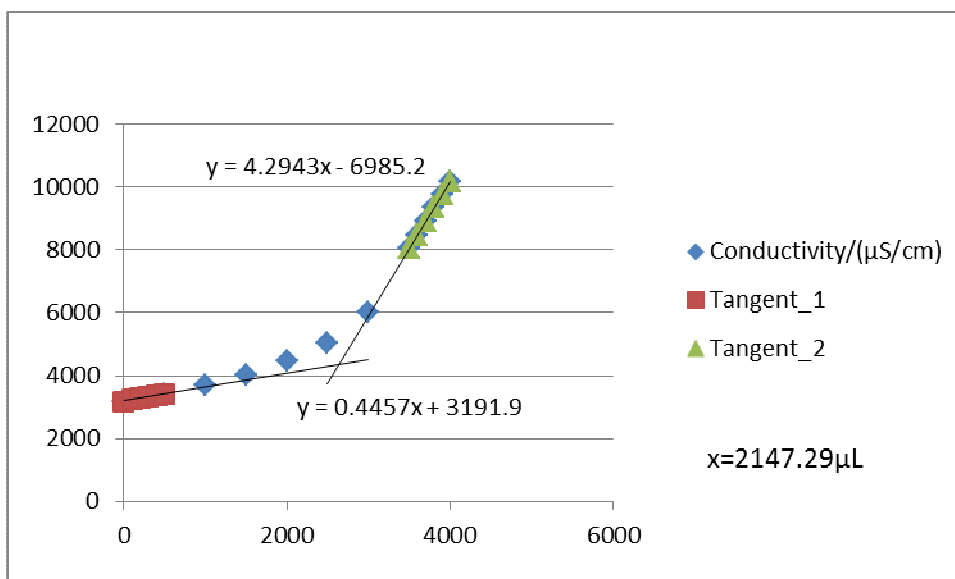
Figure G43-2 Titration 2 for 0.07915 mol/L MEA First Run

306
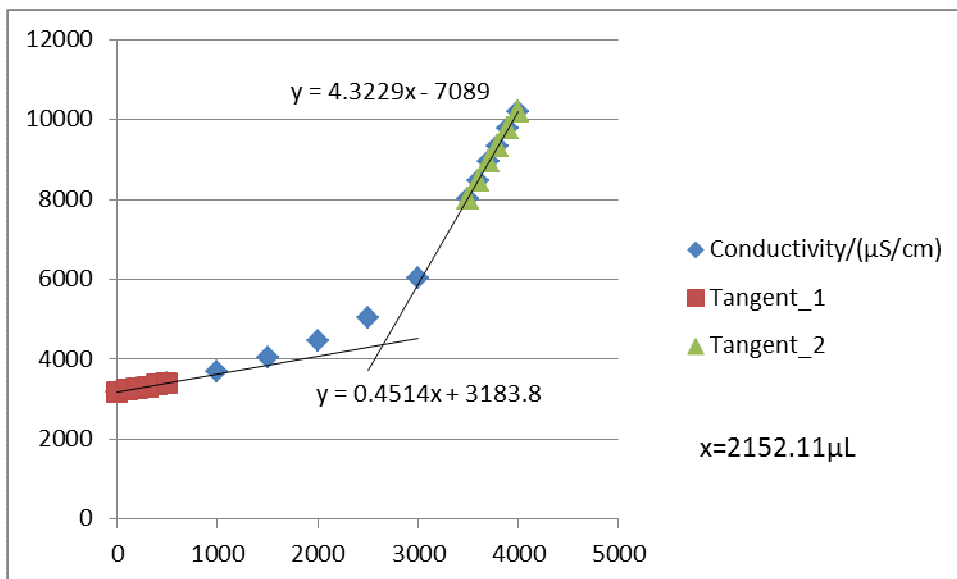
Figure G43-3 Titration 3 for 0.07915 mol/L MEA First Run

G44: Titration Curves for 0.07915 mol/L MEA Second Run at 313 K
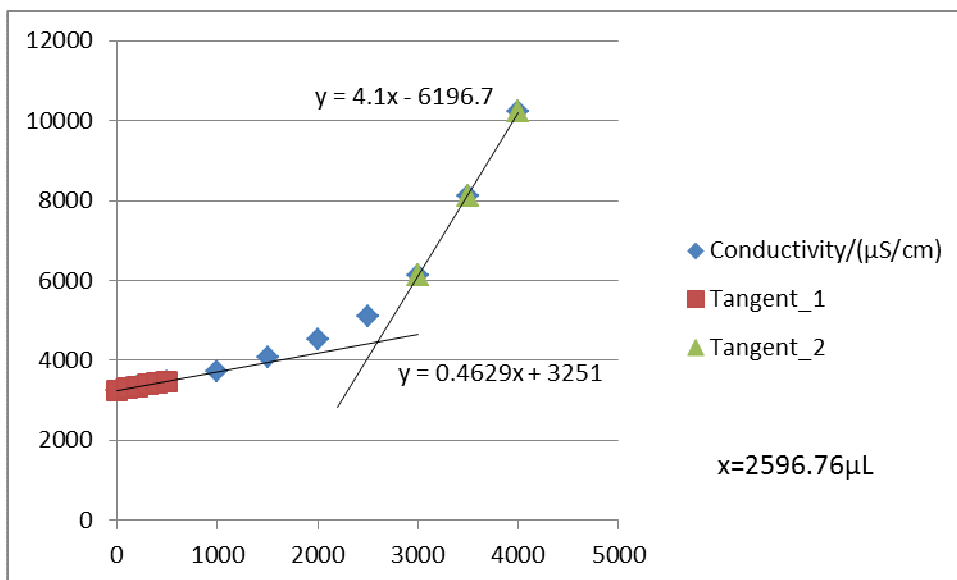
Figure G44-1 Titration 1 for 0.07915 mol/L MEA Second Run

307
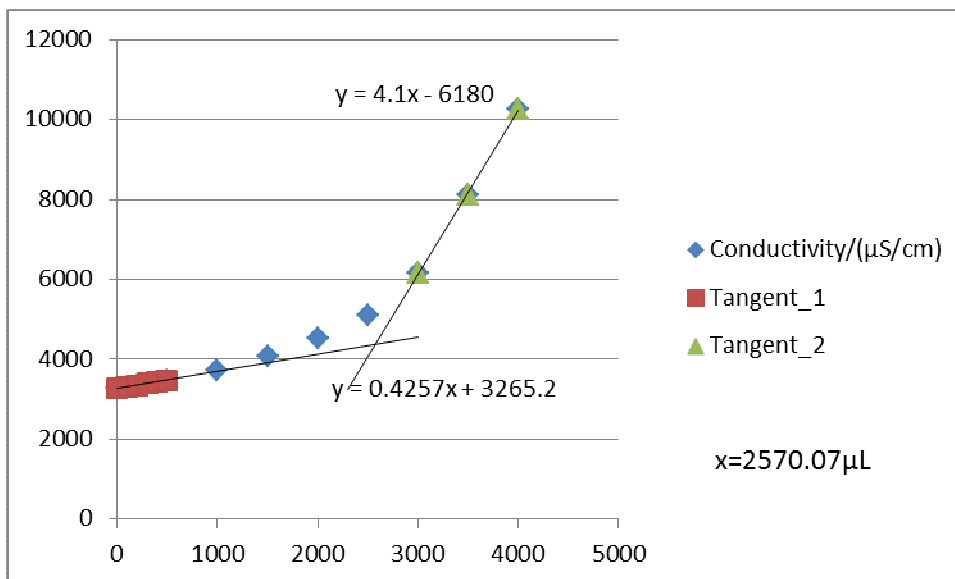
Figure G44-2 Titration 2 for 0.07915 mol/L MEA Second Run
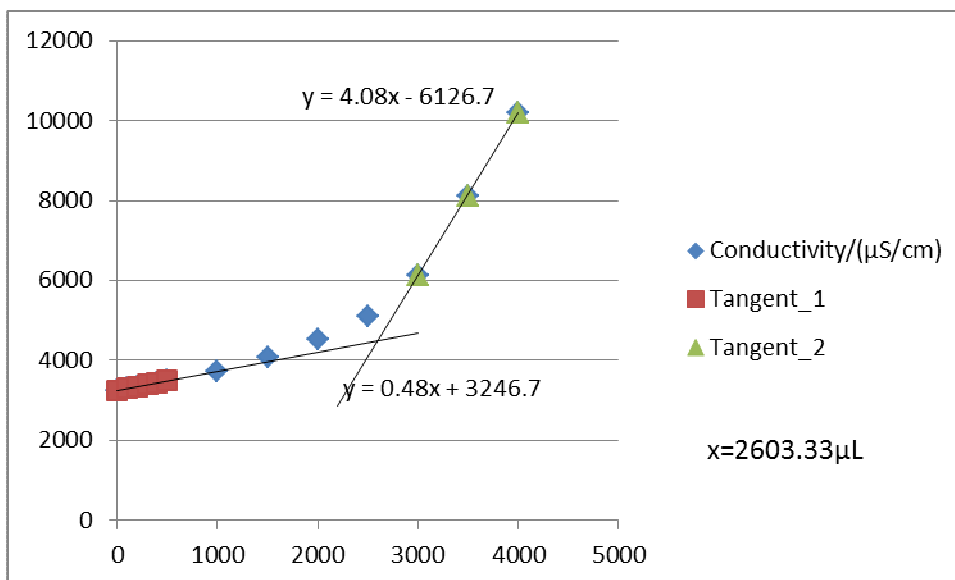
Figure G44-3 Titration 3 for 0.07915 mol/L MEA Second Run

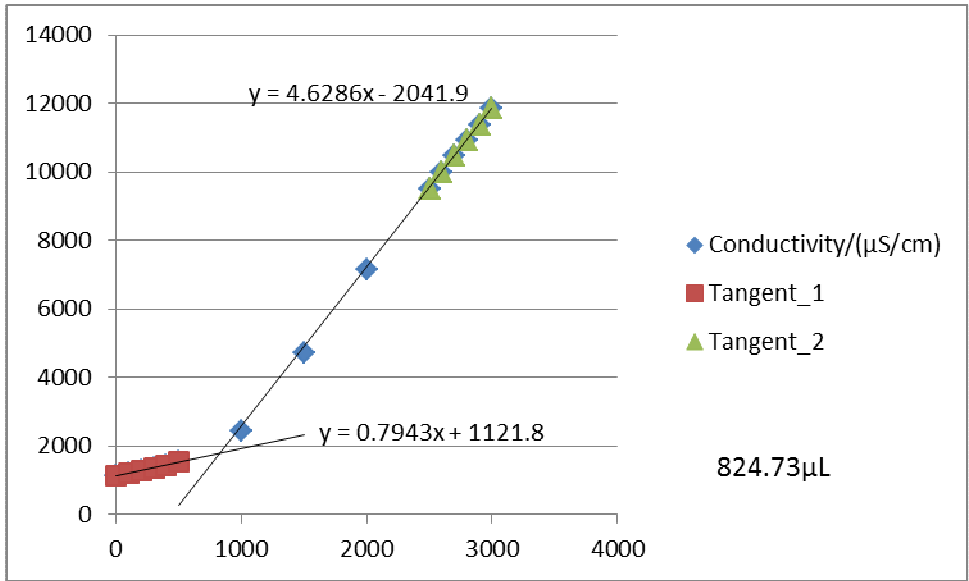**G45: Titration Curves for 0.07915 mol/L MEA Third Run at 313 K**
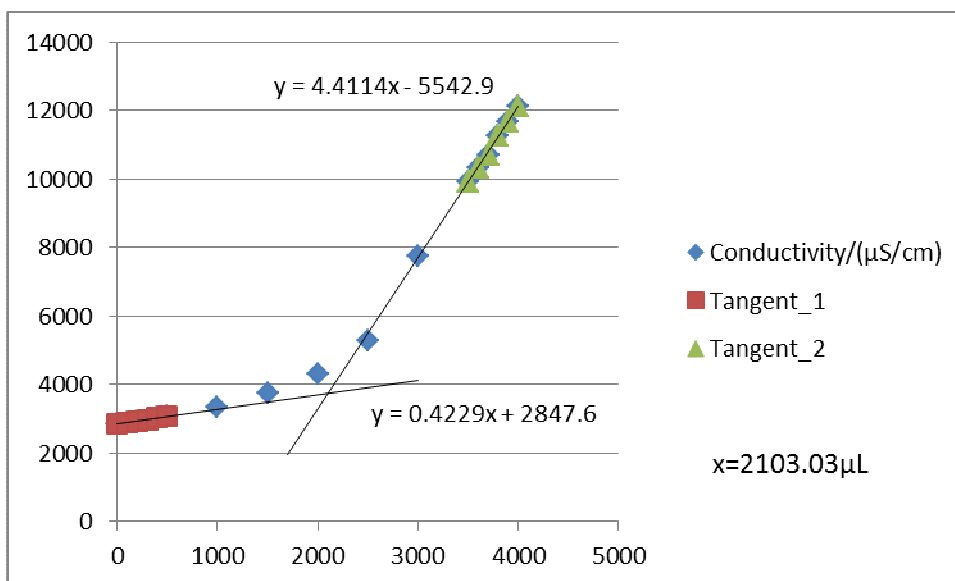
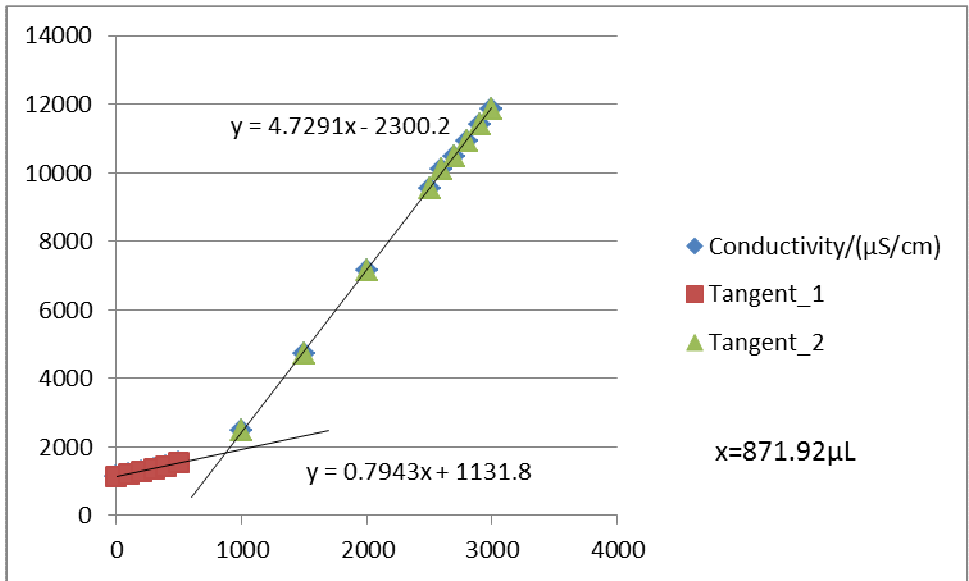

Figure G45-1 Titration 1 for 0.07915 mol/L MEA Third Run
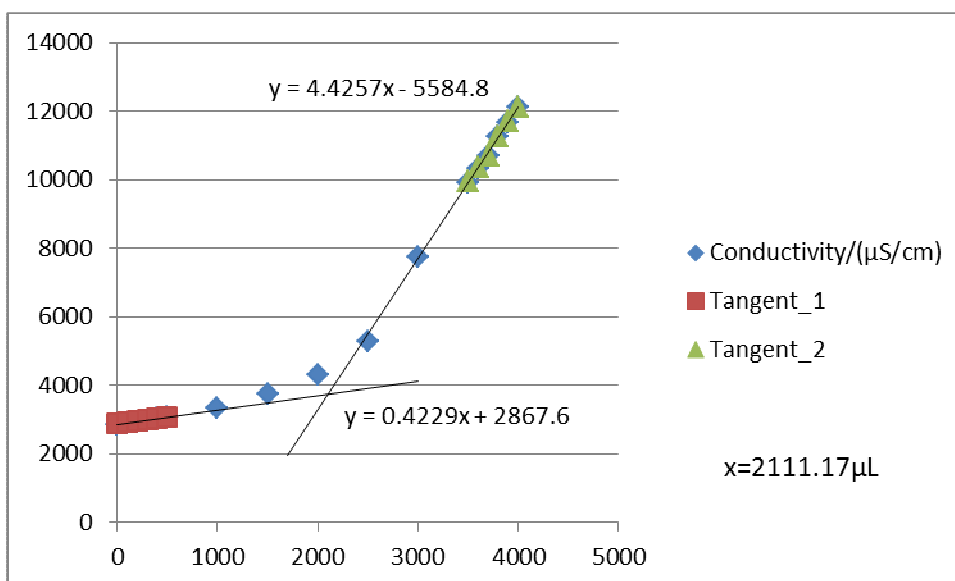
Figure G45-2 Titration 2 for 0.07915 mol/L MEA Third Run
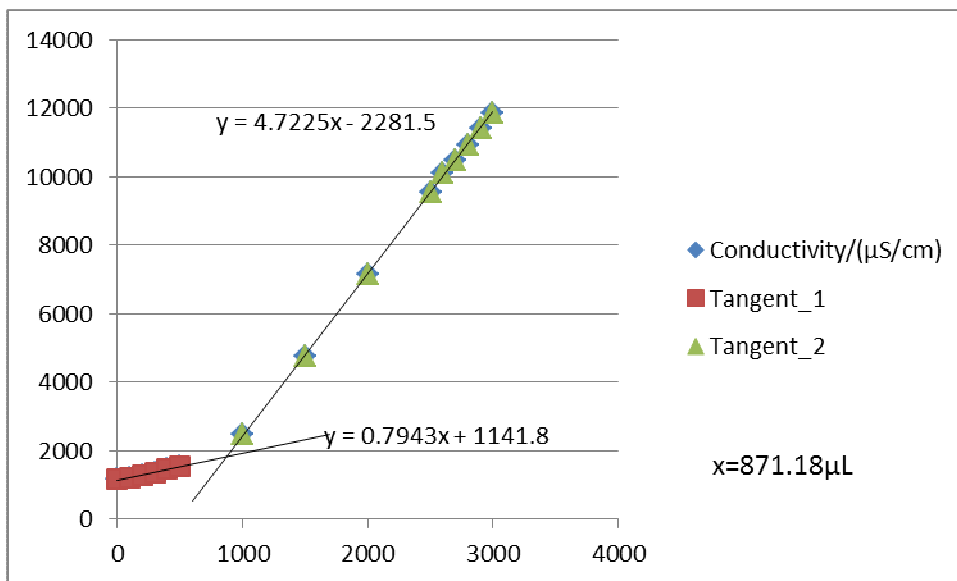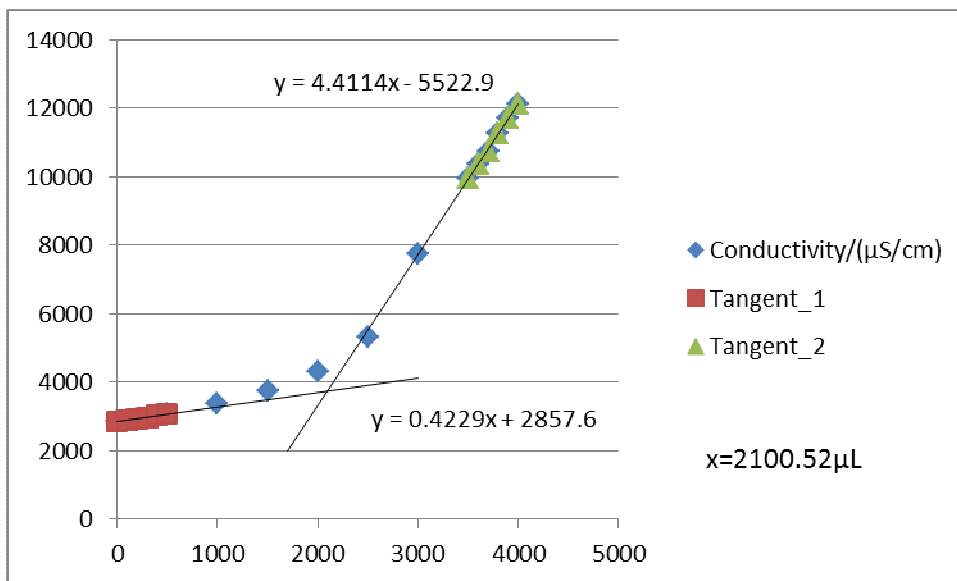
Figure G45-3 Titration 3 for 0.07915 mol/L MEA Third Run

G46: Titration Curves for 0.1184 mol/L MEA First Run at 40$^{\mathrm{o}}$C
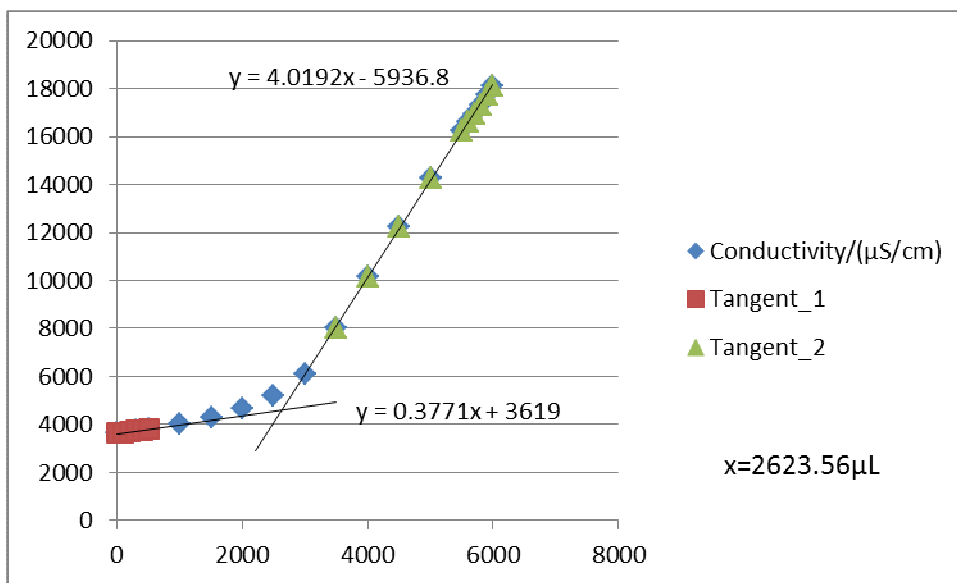
Figure G46-1 Titration 1 for 0.1184 mol/L MEA First Run

310
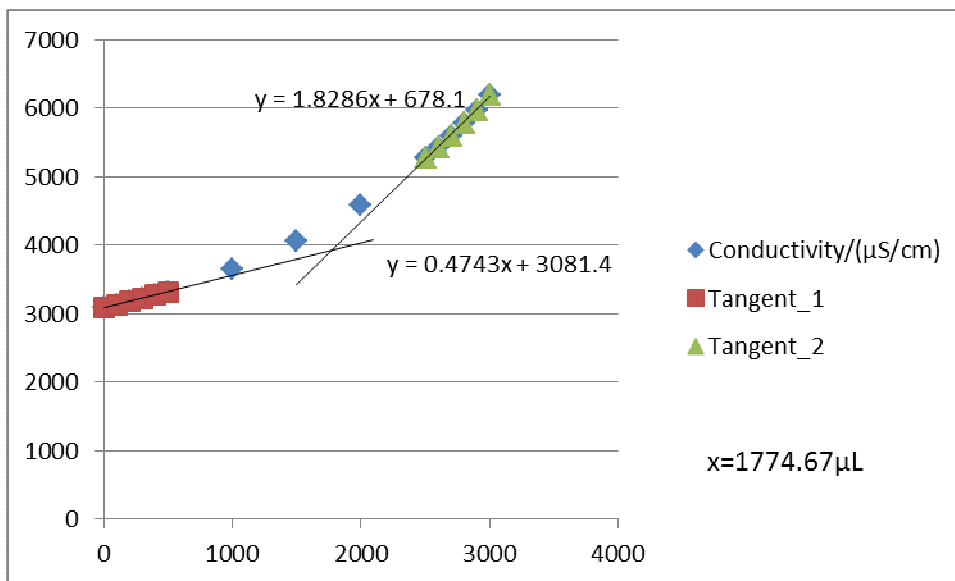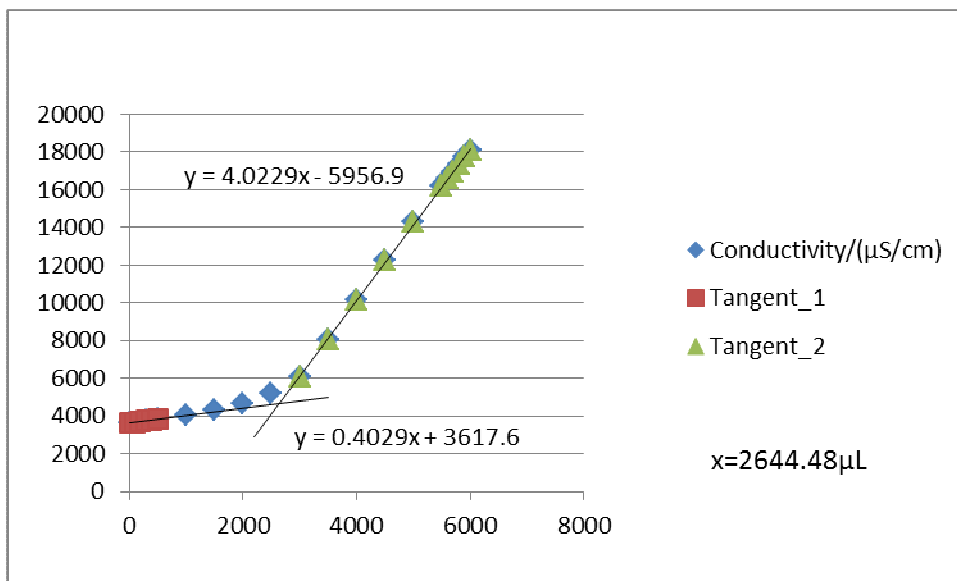
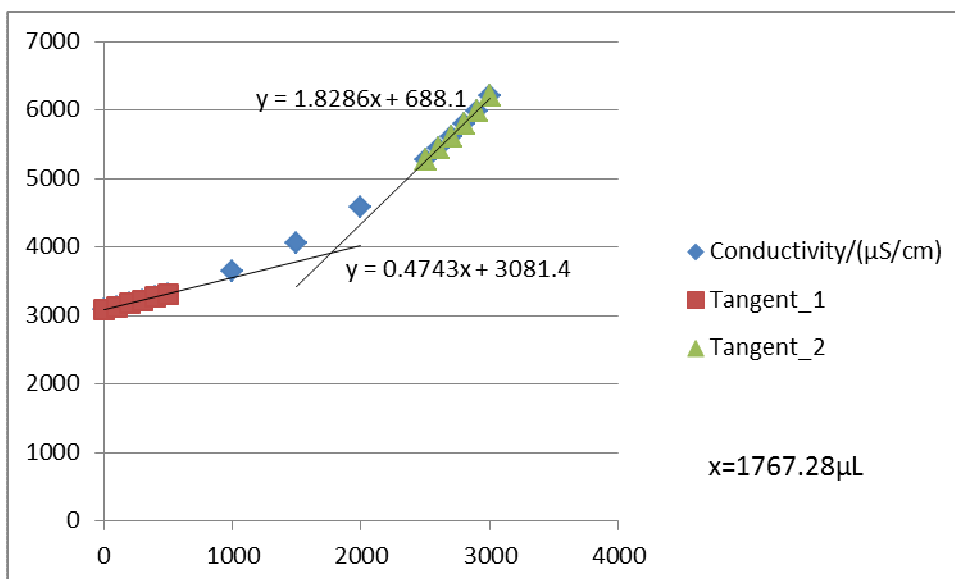Figure G46-2 Titration 2 for 0.1184 mol/L MEA First Run
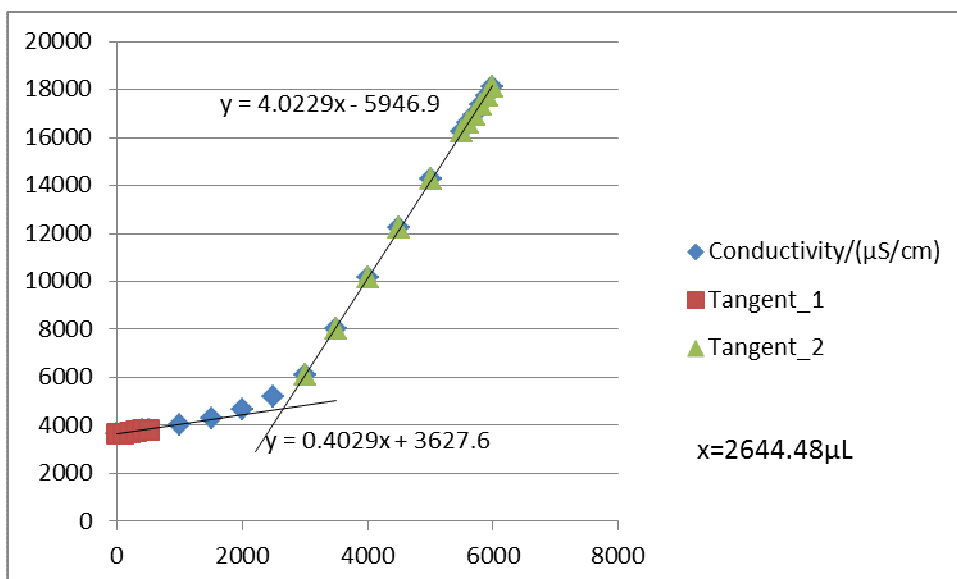
Figure G46-3 Titration 3 for 0.1184 mol/L MEA First Run

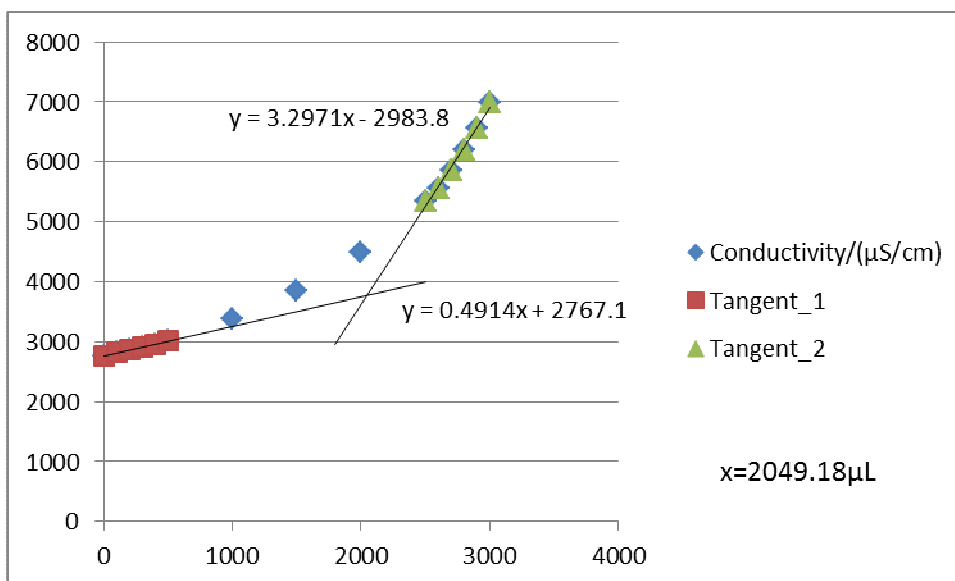**G47: Titration Curves for 0.1184 mol/L MEA Second Run at 40°C**
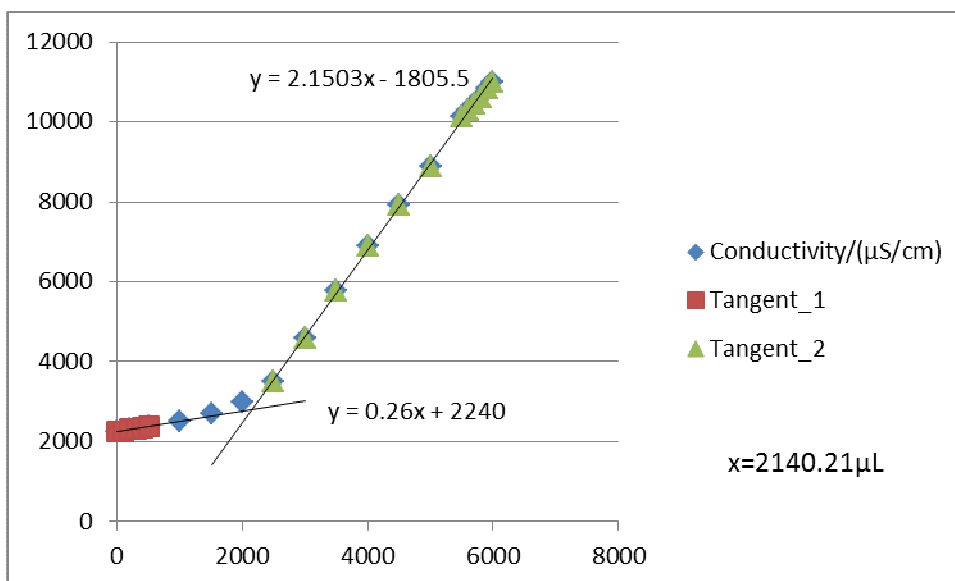
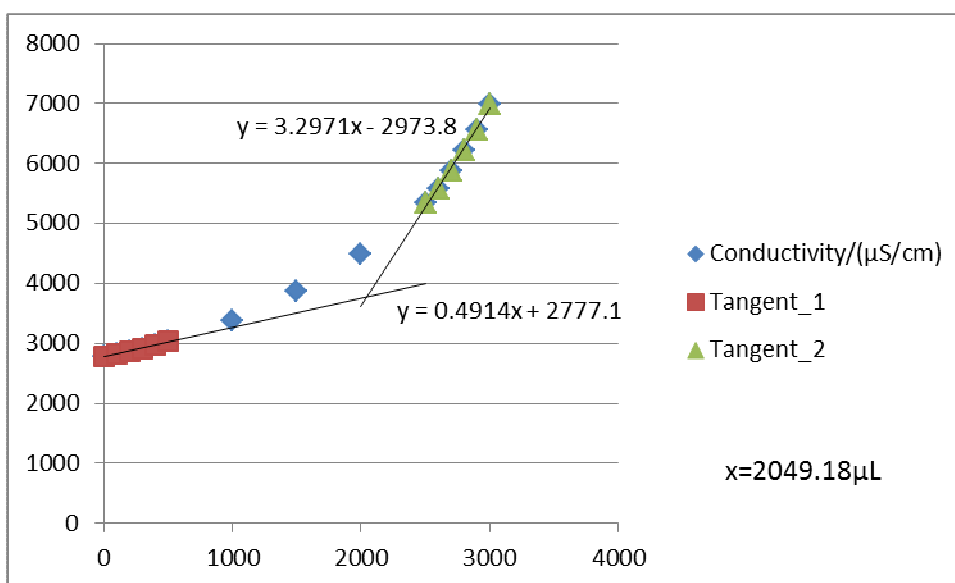
Figure G47-1 Titration 1 for 0.1184 mol/L MEA Second Run
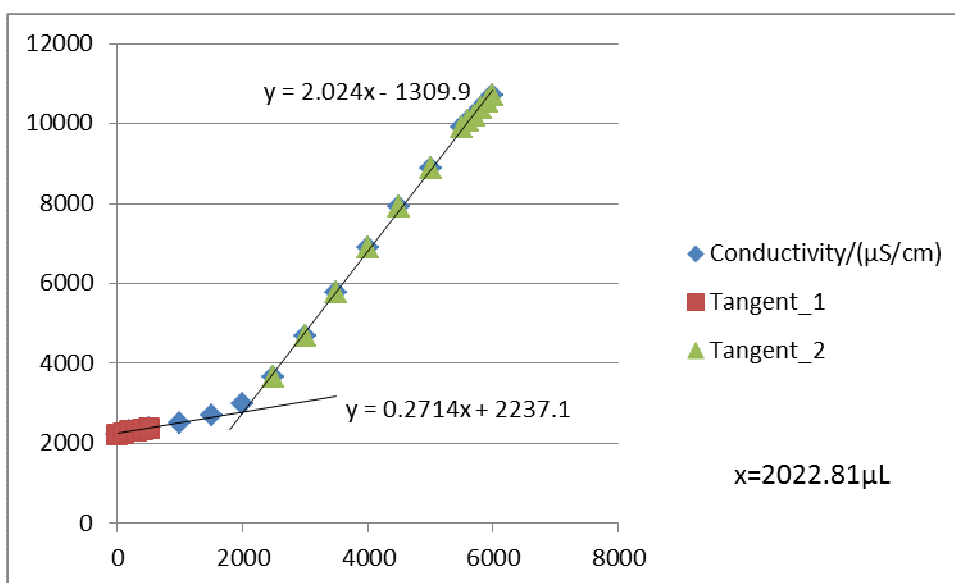
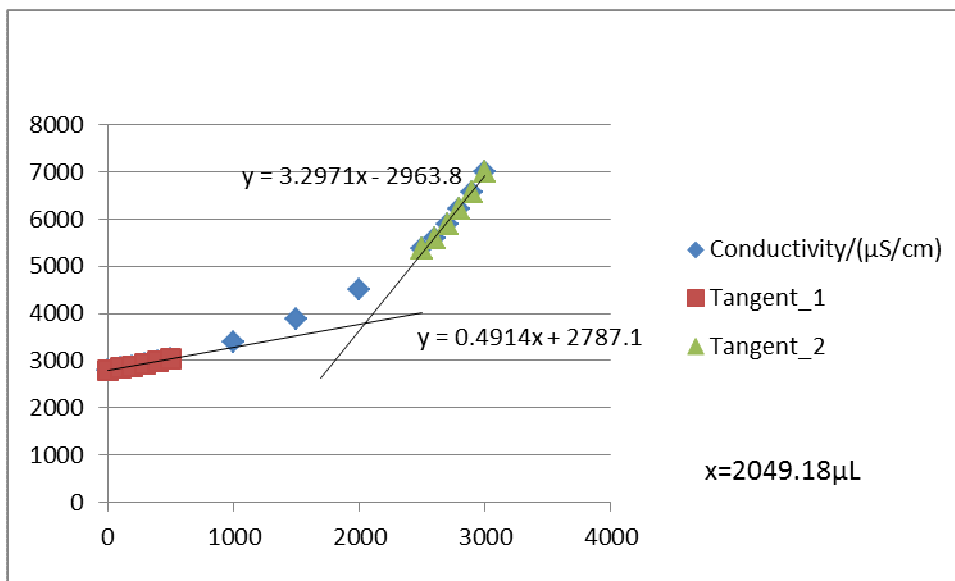
Figure G47-2 Titration 2 for 0.1184 mol/L MEA Second Run
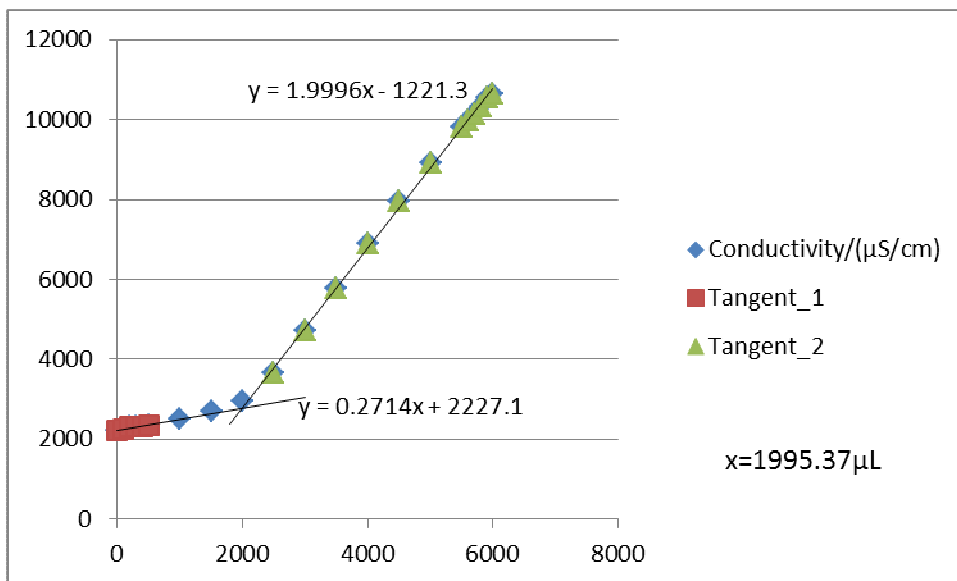
Figure G47-3 Titration 3 for 0.1184 mol/L MEA Second Run

G48: Titration Curves for 0.1184 mol/L MEA Third Run at 313 K
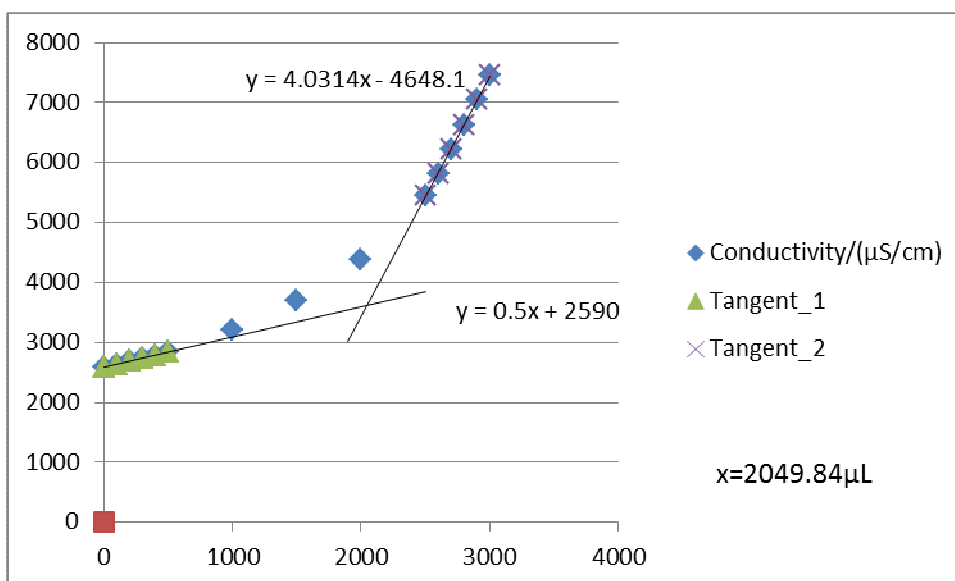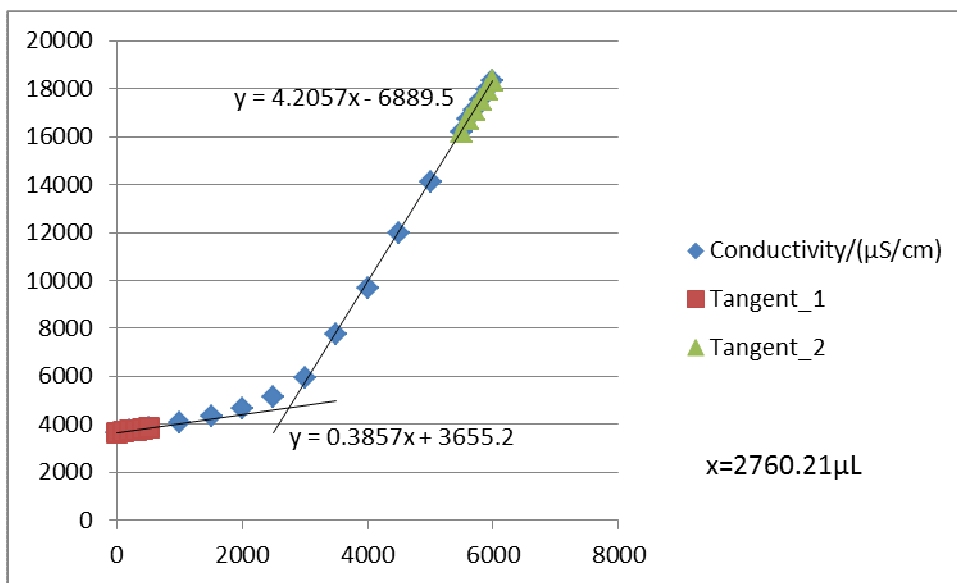
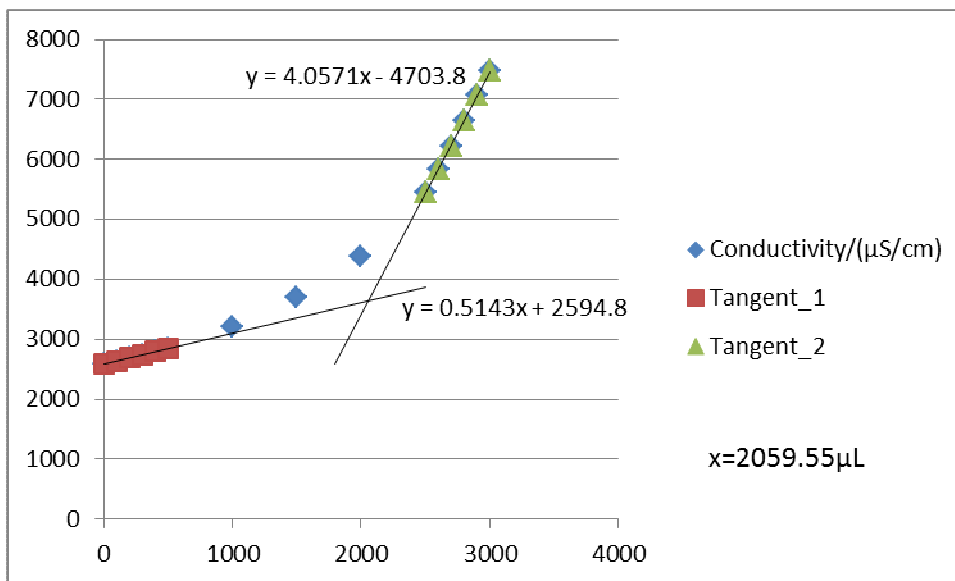

Figure G48-1 Titration 1 for 0.1184 mol/L MEA Third Run
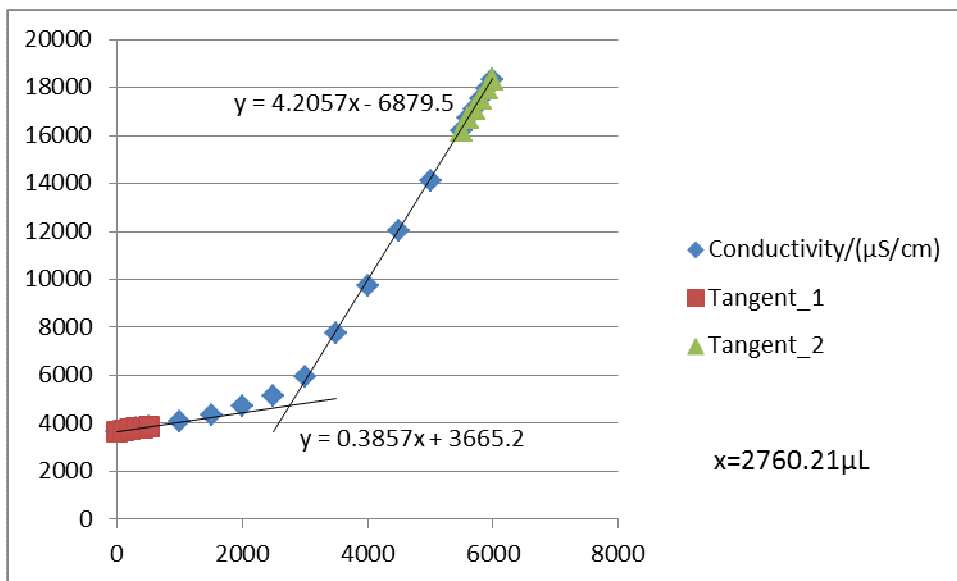
Figure G48-2 Titration 2 for 0.1184 mol/L MEA Third Run
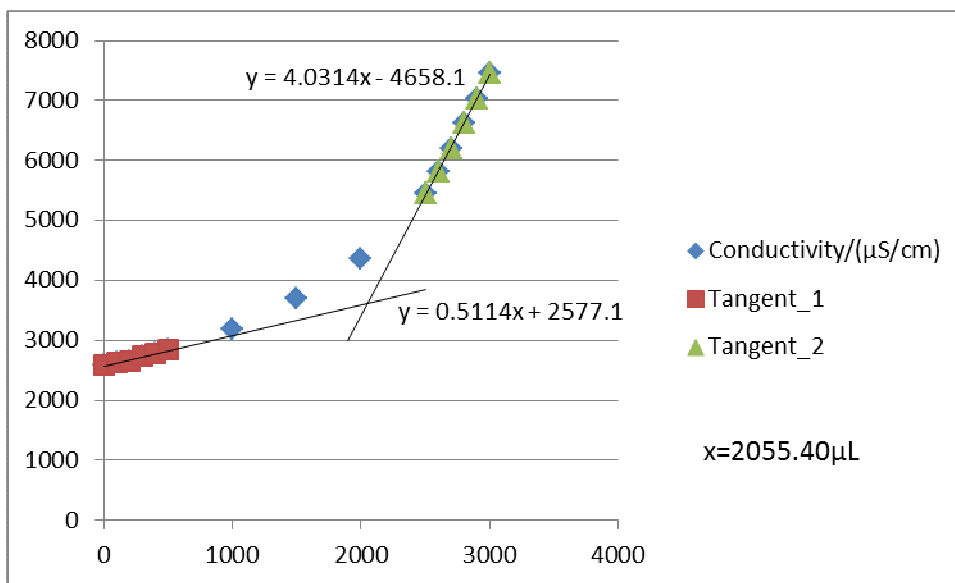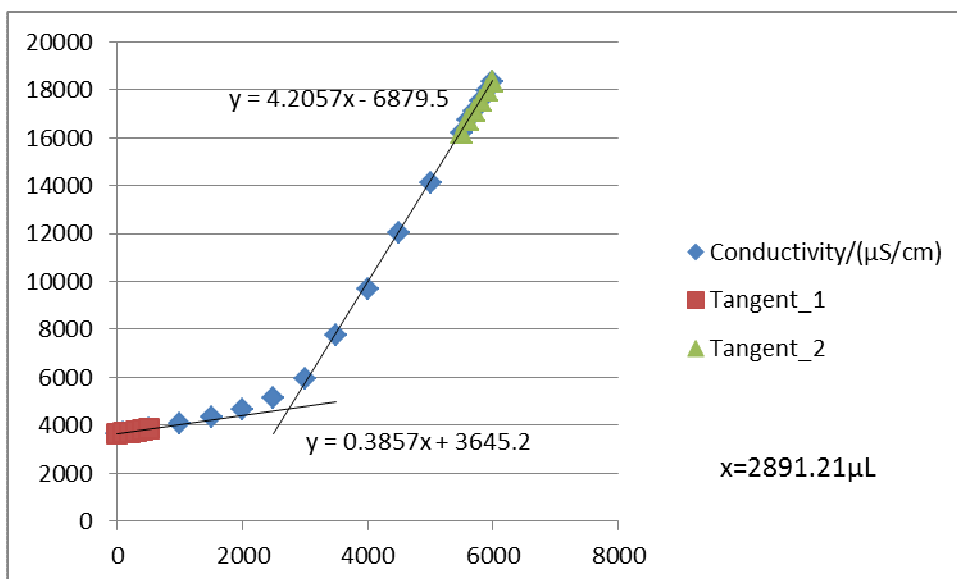

Figure G48-3 Titration 3 for 0.1184 mol/L MEA Third Run

314

APPENDIX H: MATLAB PROGRAM FOR SERIES 1

```matlab
function out = MEAfittinginfseries1(expdata)
%% Rate constant estimation
% Inputs:
% Experimental data (concentration-time profile): expdata
% Concentration equation (dC/dt = f_C(r)) [or conversion X, in this case]
% Rate equation (r = f_r(k))
% Lower and upper bounds for k


% Bounds for k
%%bounds = [6e-08 6e-06];  {Simplifying program}%


% Relevant time span
tspan = expdata(:,1);


% Experimental conversions
Xexp = expdata(:,2);


% Bounds and initial guess for k
%%lb = bounds(1);
%%ub = bounds(2);
k0 = [0 0 0 0]; %k0(1) = initial guess for rate constant; k0(2) = initial guess for equilibrium
const; ko(3)=water; k0(4)=amine;


% Wrapper function for minimization function
PredictionErrork = @(k) PredictionError(Xexp,ConversionPrediction(tspan,k));


% Minimization
%[out.kOpt,out.predErrOpt,out.exitflag,out.output] = fminsearch(PredictionErrork,k0);
options = optimset('largescale','off','display','off');
%[out.kOpt,out.predErrOpt,out.exitflag,out.output] =
fmincon(PredictionErrork,k0,[],[],[],[],zeros(1,3),20*ones(1,3),[],options);
```

```matlab
[out.kOpt,out.predErrOpt,out.exitflag,out.output] =
fminsearchbnd(PredictionErrork,k0,zeros(1,4),inf*ones(1,4),options);
% Calculute profile for optimimum k
% Wrapper to pass constant k value
ConversionEquationConstantk = @(t,X) ConversionEquation(t,X,out.kOpt);
[tpredOpt,XpredOpt] = ode45(ConversionEquationConstantk,[tspan(1) tspan(end)],0);


% Plots
figure;
% Predicted profile
plot(tpredOpt,XpredOpt,'-');
hold on;
% Actual data
plot(tspan,Xexp,'rx');


legend('Predicted profile','Actual data');


end


function dX = ConversionEquation(t,X,k)
% Change of conversion with time


% Constant parameters
CA0 = 0.123537; % mol/L
Th = 0.958419; % feed ratio


% Differential equation
dX = (CA0*((Th-X)*(1-X)-X.^2/k(2)))/(1/k(1)+1/(k(3)*55.5+k(4)*CA0*(Th-X)));


end


function Xpred = ConversionPrediction(tspan,k)
% Predicting the conversion values at specific time points (tspan),
% for a given choice of the rate constant k
```

```matlab
% Initial conditions for conversion
X0 = 0;


% Wrapper to pass constant k value
ConversionEquationConstantk = @(t,X) ConversionEquation(t,X,k);


% Ordinary differential equation solving
[tpred,Xpred] = ode45(ConversionEquationConstantk,tspan,X0);


end


function predErr = PredictionError(Xexp,Xpred)
% Sum of squared errors
% for prediction associated with a certain k value
predErr = sum((Xexp-Xpred).^2);


end
```

APPENDIX I: SPECIFICATIONS OF VALVES AND FITTINGS

I1: Valves and their specifications

Valve	Specifications				
	Valve type	Primary material	Valve size	Media temp.	Connection description
SS-20VM4	Needle	Stainless steel grade 316	0.25 inch	-54 to 232°C	Male NPT
SS-16DKF4	Needle	Stainless steel grade 316	0.25 inch	-29 to 93 ^{o}C	Female NPT
SS-14DKM4-S4	Needle	Stainless steel grade 316	0.25 inch	-29 to 93 ^{o}C	Male NPT

The SS-20VM4 is a stainless steel integral bonnet needle valve, 0.21 Cv, 0.25 in. MNPT, Vee stem while the SS-16DKF4 is a stainless steel integral bonnet non-rotating stem valve, 0.53 Cv, 0.25 in. FNPT. SS-14DKM4-S4 is also a stainless steel integral bonnet non-rotating stem valve but with a Cv value of 0.27. It is a 0.25 in. MNPT $\times$ 0.25 in. Swagelok tube fitting. A Cv value is the flow coefficient or flow capacity rating of a valve. It is the flow rate of pure water that passes through the valve when it is fully open at 15.6 ^{o}C and when the pressure difference between the ends of the valve is 6.9 kPa (**www.vizavalve.com**).

Valves SS-20VM4, SS-16DKF4 and SS-14DKM4-S4 were all needle valves. These types of valves have small openings. They also have plungers that are needle-shaped and it takes a number of turns to move the plunger thus making it possible to regulate the gas flow rate with great precision. Therefore, with a needle valve, one can control the flow of a gas that passes through the valve. This means that the gas flow rate can be easily adjusted to any specific amount. It is for this reason that the needles valves were chosen.

All of the three needle valves in table 7 had working temperatures and pressures of 38 ^{o}C and 20684 kPA respectively.

I2: Fittings and their specifications

Fitting	Specifications			
	Fitting style	**Connection type**	**Material**	**Dimensions**
SS-4-VCO-T	Tee	Face seal	Stainless steel grade 316	0.25 inch
SS-4-WVCO-7-4	-	Face seal; Threaded-female; Tapered thread	Stainless steel grade 316	0.25 inch
SS-4-WVCO-1-4	-	Face seal; Threaded-male; Tapered thread	Stainless steel grade 316	0.25 inch
SS-400-1-4	-	Threaded-male; Tapered thread	Stainless steel grade 316	0.25 inch

The SS-4-VCO-T fitting is a stainless steel VCO O-ring face seal fitting, 0.25 in. and it has a tee fitting style while the SS-4-WVCO-7-4 is a stainless steel VCO O-ring face seal fitting, female NPT connector, 0.25 in. Female VCO fitting × 0.25 in. FNPT. Fitting SS-4-WVCO-1-4 is stainless steel VCO O-ring face seal fitting, MNPT connector, 0.25 in. Female VCO fitting × 0.25 in. MNPT and fitting SS-400-1-4 is stainless steel Swagelok tube fitting, male connector, 0.25 in. tube OD × 0.25 MNPT respectively. There was also a 304L-HDF4-50, which was a 50ml CO_2 sample cylinder (gas bomb).

319

APPENDIX J: CELL CONSTANT DETERMINATION (CALIBRATION)

The calibration process was started by pressing the *CAL* button on the conductivity meter repeatedly until *CAL CELL* indicated on the display of the meter. The *OK* button was then pressed to confirm the selection of *CAL CELL*. The measuring cell was immersed in the control standard solution, 0.01mol/L KCl and the cell constant determination with stability control started by pressing the *OK* button. The auto read, *AR* display indicator flashed until there was a stable signal. An auto read measurement is carried out for stability control. The meter then stored the determined cell constant automatically and switched over to the measuring mode.

After the cell determination process, the meter then automatically evaluated the current status. A cell constant of 0.469 cm^{-1} and a conductivity reading of 1413 µS/cm were displayed and this shows that the meter was working with a correctly calibrated measuring cell. This is because a cell constant value of 0.469 cm^{-1} is within the range of 0.585 to 0.715 cm^{-1}.

APPENDIX K: STANDARDISATION OF ALKALINE NaOH SOLUTION

The following procedure was used to prepare 1 L of 1 mol/L standard NaOH,

- Weigh 1.00 g of potassium hydrogen phthalate.

- Using a volumetric flask, dissolve the potassium hydrogen phthalate to 1 L with freshly boiled distilled water.

- On the radiometer TIM 856 autotitrator, the end point titration settings were set as follows:

  - Burette volume: 25 ml
  - Stirring speed: 400 rpm
  - Working mode: pH
  - Number of end points: 1
  - End point: 8.55 pH
  - Sample unit: ml
  - Standard amount: 20
  - Standard concentration: 1 mol/L
  - Result: mol/L

- Using a 25 ml burette, and a 1 mol/L NaOH solution as titrant, prepare the titration system.

- Calibrate the pHC2401-8 electrode.

- Pipette 20 ml of 1 mol/L potassium phthalate.

- Fill up to 100 ml with distilled water.

- Dip the electrode and delivery tip in the solution and start the method by pressing RUN.

- The NaOH concentration was based on the following formula:

$$Vol(NaOH) * c(NaOH) = Vol(KHP) * c(KHP) \qquad \text{(K1)}$$

Where vol is volume in ml, c is concentration in mol/L and KHP is potassium phthalate.

APPENDIX L: MATLAB PROGRAM FOR SERIES 2

```matlab
function out = MEAfittinginfseries2(expdata)
%% Rate constant estimation
% Inputs:
% Experimental data (concentraction-time profile): expdata
% Concentration equation (dC/dt = f_C(r)) [or conversion X, in this case]
% Rate equation (r = f_r(k))
% Lower and upper bounds for k

% Bounds for k
%%bounds = [6e-08 6e-06];  {Simplifying program}%

% Relevant time span
tspan = expdata(:,1);

% Experimental conversions
Xexp = expdata(:,2);

% Bounds and initial guess for k
%%lb = bounds(1);
%%ub = bounds(2);
k0 = [0 0 0 0 0]; %k0(1) = initial guess for rate constant; k0(2) = initial guess for MEA rxn
order; k0(3)=CO2 rxn order; k0(4)=reverse rate constant; k0(5)=reaction order for the salt;


% Wrapper function for minimization function
PredictionErrork = @(k) PredictionError(Xexp,ConversionPrediction(tspan,k));

% Minimization
%[out.kOpt,out.predErrOpt,out.exitflag,out.output] = fminsearch(PredictionErrork,k0);
options = optimset('largescale','off','display','off');
%[out.kOpt,out.predErrOpt,out.exitflag,out.output] =
fmincon(PredictionErrork,k0,[],[],[],[],zeros(1,3),20*ones(1,3),[],options);
```

```matlab
[out.kOpt,out.predErrOpt,out.exitflag,out.output] =
fminsearchbnd(PredictionErrork,k0,zeros(1,5),[inf 2 2 inf 2],options); % inf*ones(1,5)
% Calculute profile for optimimum k
% Wrapper to pass constant k value
ConversionEquationConstantk = @(t,X) ConversionEquation(t,X,out.kOpt);
[tpredOpt,XpredOpt] = ode45(ConversionEquationConstantk,[tspan(1) tspan(end)],0);


% Plots
figure;
% Predicted profile
plot(tpredOpt,XpredOpt,'-');
hold on;
% Actual data
plot(tspan,Xexp,'rx');


legend('Predicted profile','Actual data');


end


function dX = ConversionEquation(t,X,k)
% Change of conversion with time


% Constant parameters
CA0 = 0.1184; % mol/L
Th = 1.04; % feed ratio


% Differential equation
dX = k(1)*CA0*(1-X).^k(2)*(Th-X).^k(3)-k(4)*(CA0*X).^k(5);


end


function Xpred = ConversionPrediction(tspan,k)
% Predicting the conversion values at specific time points (tspan),
% for a given choice of the rate constant k
```

323

```matlab
% Initial conditions for conversion
X0 = 0;


% Wrapper to pass constant k value
ConversionEquationConstantk = @(t,X) ConversionEquation(t,X,k);


% Ordinary differential equation solving
[tpred,Xpred] = ode45(ConversionEquationConstantk,tspan,X0);


end


function predErr = PredictionError(Xexp,Xpred)
% Sum of squared errors
% for prediction associated with a certain k value
predErr = sum((Xexp-Xpred).^2);


end
```

APPENDIX M: MATLAB PROGRAM USED FOR BOOSTRAP APPROACH

```matlab
% load data for a specified run
clear Ksim err
model = cell(5,1);

for m = 1:5,

    runs = ...
{'first_run36.txt','second_run36.txt','third_run36.txt'};

    for p = 1:length(runs),
        run = runs{p};
        Xall = load(sprintf('E:\\Modelling Results Inf\\First Series\\Runs @ 25\\3.6ml
MEA\\%s',run));

        sims = 20;
        switch m
            case 1
                Ksim{m,p} = zeros(sims,4); % change num
                err{m,p} = zeros(sims,1);
            case 2
                Ksim{m,p} = zeros(sims,5); % change num
                err{m,p} = zeros(sims,1);
            case 3
                Ksim{m,p} = zeros(sims,2); % change num
                err{m,p} = zeros(sims,1);
            case 4
                Ksim{m,p} = zeros(sims,4); % change num
                err{m,p} = zeros(sims,1);
            case 5
                Ksim{m,p} = zeros(sims,4); % change num
                err{m,p} = zeros(sims,1);
            otherwise
                % do nothing
        end


        for isim = 1:sims,
            %if mod(isim,5)==0,
                fprintf(1,'model: %d\t run: %s\t simulation:%d\n',m,run,isim);
            %end
            close all
            % random split of data into training and testing sets
            length_of_train_set = round(0.75*(size(Xall,1)));
            rind = randperm(size(Xall,1));
            train = sort(rind(1:length_of_train_set)); % sort enforces time relationship
            %test = sort(rind(length_of_train_set+1:end));
            switch m
                case 1
```

325

```matlab
            model{m} = MEAfittingmodel1(Xall(train,:));
        case 2
            model{m} = MEAfittingmodel2(Xall(train,:));
        case 3
            model{m} = MEAfittingmodel3(Xall(train,:));
        case 4
            model{m} = MEAfittingmodel4(Xall(train,:));
        case 5
            model{m} = MEAfittingmodel5(Xall(train,:));
        otherwise
            % do nothing
    end


    Ksim{m,p}(isim,:) = model{m}.kOpt;
    err{m,p}(isim,1) = model{m}.predErrOpt;
    end

end

end
```